VOLUME 117 NUMBER 1

THE ASTROPHYSICAL JOURNAL

AN INTERNATIONAL REVIEW OF SPECTROSCOPY AND ASTRONOMICAL PHYSICS

JANUARY 1953

THE F-TYPE COMPONENT OF CAPELLA . . . . . . *Otto Struve and S. M. Kung* 1
THE SPECTRUM OF 48 LIBRAE FROM 1944 TO 1952 . . . . . *Paul W. Merrill* 7
THE MAGNETICALLY VARIABLE STAR HD 153882 *Guro Gjellestad and Horace W. Babcock* 12
VARIATIONS IN LIGHT OF THE SPECTRUM VARIABLES 73 DRACONIS AND IOTA CASSIOPEIAE . . . *Sanford S. Provin* 21
THE SPECTRA OF CERTAIN STARS WHOSE ATMOSPHERES MAY BE DEFICIENT IN HYDROGEN . . . *William P. Bidelman* 25
THE SOLAR SPECTRUM FROM λ 2285 to λ 3000 A . . . . . *Harold E. Clearman* 29
TABLE OF INFRARED SOLAR LINES, 1.4–2.5 μ *Orren C. Mohler, A. Keith Pierce, Robert R. McMath, and Leo Goldberg* 41
EJECTION OF HYDROGEN AND IONIZED CALCIUM ATOMS WITH HIGH VELOCITY AT THE TIME OF SOLAR FLARES *Helen W. Dodson, E. Ruth Hedeman, and Joseph Chamberlain* 66
$H\alpha$ EMISSION STARS AND PECULIAR OBJECTS IN THE REGION OF THE ORION NEBULA . . . *Guillermo Haro* 73
THE TRANSFER OF THE NORTH POLAR STANDARDS TO THE SOUTHERN HEMISPHERE . . . *Arthur N. Cox* 83
ON THE SPATIAL DISTRIBUTION OF GALAXIES: A SPECIFIC MODEL *J. Neyman, E. L. Scott, and C. D. Shane* 92
THE ANALYSIS OF COUNTS OF THE EXTRAGALACTIC NEBULAE IN TERMS OF A FLUCTUATING DENSITY FIELD . . . *D. Nelson Limber* 134
FLUCTUATIONS IN BRIGHTNESS OF THE MILKY WAY . . . *D. Nelson Limber* 145
THE INTERSTELLAR STRUCTURES. I. GAS CLOUDS . . . . . *Eugene N. Parker* 169
MAGNETO-HYDRODYNAMIC SHOCK WAVES . . . . . . *H. Lawrence Helfer* 177
A GRAVITATIONALLY CONTRACTING STELLAR MODEL . . . . *Richard D. Levee* 200
THE VARIATIONAL METHOD FOR PROBLEMS OF RADIATIVE TRANSFER. I. ISOTROPIC SCATTERING WITH A CONSTANT NET FLUX . . . . *Su-Shu Huang* 211
THE VARIATIONAL METHOD FOR PROBLEMS OF RADIATIVE TRANSFER. II. THE FORMATION OF ABSORPTION LINES IN THE MILNE-EDDINGTON MODEL *Su-Shu Huang* 215
THE VARIATIONAL METHOD FOR PROBLEMS OF RADIATIVE TRANSFER. III. REFLECTION EFFECT . . . *Su-Shu Huang* 221
INFLUENCE OF DOPPLER EFFECT AND DAMPING ON LINE-ABSORPTION COEFFICIENT AND ATMOSPHERIC RADIATION TRANSFER *Gilbert N. Plass and Daniel I. Fivel* 225

NOTES

Radial Velocities of Five Southern Proper-Motion Stars . . . . . . *Jorge Sahade* 234
Observations of Helium in Diffuse Nebulae . . . . *Hugh M. Johnson* 235
Vibration Spectrum of $N^{14}N^{15}$ . . . . *David R. Bates* 236
A New Photograph of the *Mg* II Doublet at 2800 A in the Sun *F. S. Johnson, J. D. Purcell, R. Tousey, and N. Wilson* 238
REVIEWS 240

THE UNIVERSITY OF CHICAGO PRESS
CHICAGO, ILLINOIS, U.S.A.

January 1953 Vol. 117, No. 1

THE ASTROPHYSICAL JOURNAL

AN INTERNATIONAL REVIEW OF SPECTROSCOPY AND ASTRONOMICAL PHYSICS

Published in Collaboration with the American Astronomical Society

S. CHANDRASEKHAR
Managing Editor

GERARD P. KUIPER
Associate Editor

Yerkes Observatory of the University of Chicago

EDITORIAL BOARD

H. W. BABCOCK (1953-57)
Mount Wilson Observatory of the Carnegie Institution of Washington

G. HERZBERG (1952-56)
National Research Council, Ottawa

FRED L. WHIPPLE (1952-54)
Harvard College Observatory

C. D. SHANE (1952-55)
Lick Observatory, University of California

LYMAN SPITZER, JR. (1952-53)
Princeton University Observatory

6

The Astrophysical Journal is published bimonthly by the University of Chicago at the University of Chicago Press, 5750 Ellis Avenue, Chicago 37, Illinois, during January, March, May, July, September, and November. ¶Two volumes are published per year, one beginning with the January issue and the other beginning with the July issue. The subscription price is $6.00 per volume or $12.00 per year; the price of single copies is $3.00. (Orders for service of less than a volume will be charged at the single copy rate.) ¶Postage is prepaid by the publishers on all orders from the United States and its possessions. No extra charge is made for postage to countries in the Pan American Postal Union. ¶Postage is charged extra as follows: for Canada, 20 cents per volume, 40 cents per year (total $6.20 per volume, $12.40 per year); on single copies 5 cents (total $3.05); for all other countries in the Postal Union, 40 cents per volume, 75 cents per year (total $6.40 per volume, $12.75 per year), on single copies 10 cents (total $3.10). ¶Subscriptions are payable in advance. Please make all remittances payable to The University of Chicago Press, in United States currency or its equivalent by postal or express money orders or bank drafts.

The following is an authorized agent:

For the British Empire, except North America and Australasia: The Cambridge University Press, Bentley House, 200 Euston Road, London, N.W. 1, England. Prices of yearly subscriptions and of single copies may be had on application.

Claims for missing numbers should be made within the month following the regular month of publication. The publishers expect to supply missing numbers free only when losses have been sustained in transit, and when the reserve stock will permit.

Business correspondence should be addressed to The University of Chicago Press, Chicago 37, Illinois.

Communications for the editors and manuscripts should be addressed to: S. Chandrasekhar, Editor of THE ASTROPHYSICAL JOURNAL, Yerkes Observatory, Williams Bay, Wisconsin.

Line drawings and photographs should be made by the author, and all marginal notes such as co-ordinates, wave lengths, etc., should be included in the cuts. It will not be possible to set up such material in type.

One copy of the corrected galley proof should be returned as soon as possible to the editor, Yerkes Observatory, Williams Bay, Wisconsin. Authors should take notice that the manuscript will not be sent to them with the proof.

The cable address is "Observatory, Williamsbay, Wisconsin."

The articles in this journal are indexed in the *International Index to Periodicals*, New York, N.Y.

Applications for permission to quote from this journal should be addressed to The University of Chicago Press, and will be freely granted.

Microfilms of complete journal volumes are available to regular subscribers only and may be obtained at the end of the year. Orders and inquiries should be addressed to University Microfilms, 313 North First Street, Ann Arbor, Michigan.

Notice to subscribers: If you change your address, please notify us and your local postmaster immediately.

Entered as second-class matter, July 31, 1940, at the Post-Office at Chicago, Ill., under the Act of March 3, 1879.

Acceptance for mailing at special rate of postage provided for in United States Postal Act of October 3, 1917, Section 1103, amended February 28, 1925.

[PRINTED IN U.S.A.]

THE ASTROPHYSICAL JOURNAL

AN INTERNATIONAL REVIEW OF SPECTROSCOPY AND
ASTRONOMICAL PHYSICS

VOLUME 117 JANUARY 1953 NUMBER 1

THE F-TYPE COMPONENT OF CAPELLA*

Otto Struve and S. M. Kung
Berkeley Astronomical Department, University of California

Received August 6, 1952

ABSTRACT

The spectroscopic features of the F component of Capella are described, together with their peculiar influence upon the stronger lines of *Fe* I, *Ti* II, *Mg* I, *Al* II, etc., in the G component. The best available lines of the F star lead to a mass ratio of $\alpha = \mathfrak{M}_G/\mathfrak{M}_F = 0.90$ and to $\mathfrak{M}_G = 2.5\,\odot$; $\mathfrak{M}_F = 2.8\,\odot$.

The spectrum of the F-type component of Capella is so remarkable that a detailed description of it at this time is highly desirable. Brief accounts have already been published.[1] We now present a series of illustrations which clearly bring out the essential features of this object.

Figure 1 shows two Mount Wilson coudé spectrograms, obtained in 1938 by W. S. Adams and T. Dunham, Jr., with an original dispersion of 10 A/mm. The spectrum at the top, phase 97.5 days, taken on October 16, represents approximately the time of conjunction, the F star being behind and the G star in front. The spectrum at the bottom, phase 23.5 days, was taken on November 15 and represents approximately the time of largest negative velocity of the F star. The two strips have been mounted in such a way that the numerous sharp, faint lines coincide in position. These lines belong entirely to the G star. Hence any displaced features can be safely attributed to the F star.

We notice at once that some strong *Fe* I lines belong to the F spectrum. These lines—*Fe* I 4046, 4064, and 4072—are diffuse and strong. There is a strong indication that these lines are broadened by turbulence, an effect that tends to suppress the weak lines. It is for this reason that all the faint lines of *Fe* I are entirely due to the G star. The turbulence of the F star's atmosphere is larger than that of α Persei, and it may exceed that of δ Canis Majoris.[2]

Several other F lines, though badly blended with the numerous background lines of the G star, are clearly discernible. They are *Mn* I 4031, *Sr* II 4078, and $H\delta$. All are diffuse and appear only as a whitish haze on the background of the continuous spectrum. Finally, there are a number of regions, for example, between *Fe* I 4064 and *Fe* I 4072, where the presence of an F line makes itself felt only through an apparent strengthening of those faint and sharp G-type background lines which accidentally coincide with the F-type line.

Altogether, we conclude that the diffuse absorption lines approximately confirm their classification as type F. We notice, especially, in the case of *Fe* I 4046, that the corresponding line of the G star is either absent or greatly suppressed. This phenomenon is the most baffling one of the many puzzling features of this spectrum.

---

* The observational material used in this study was obtained at the Mount Wilson Observatory.

[1] *Proc. Nat. Acad. Sci.*, **37**, 327, 1951; *Sky and Telescope*, **10**, 135, 1951.

[2] S. S. Huang and Otto Struve, *Ap. J.*, **116**, 410, 1952.

The suppression of the strongest *Fe* I lines of the G star is so remarkable that an indiscriminately constructed curve of growth for this object would present a declining branch for large values of NHf. Lines of intermediate intensity, such as *Fe* I 4072, show a hazy undisplaced feature which we attribute to an intrinsically strong G-type line that is veiled by a large amount of emission. Undoubtedly, this emission is somehow connected with the fact that Capella is a binary consisting of two giant components.

The phenomenon of suppression of the strongest lines of *Fe* I and some other elements in the G component is particularly striking in the ultraviolet region. Figures 2–12 show a series of spectrograms of Capella, with Arcturus at the top and α Persei at the bottom. An attempt has been made to line up the absorption lines of Arcturus with those of the G component of Capella. The similarity between these two giant spectra is sufficient to demonstrate the suppression of the stronger lines in Capella G. The plates of Capella are as follows:

Phase 82.8 days: Dec. 31, 1950; max. vel. of F star
Phase 6.9 days: Jan. 28, 1951; av. vel. of F star
Phase 29.9 days: Feb. 20, 1951; min. vel. of F star
Phase 30.8 days: Feb. 21, 1951; min. vel. of F star
Phase 57.7 days: Mar. 20, 1950; av. vel. of F star

Figures 13 and 14 show two spectrograms of Capella each, again lined up in such a way that the faint, sharp G-type lines coincide. The dates are as follows:

Phase 82.8 days: Dec. 31, 1950; max. vel. of F star
Phase 25.3 days: Nov. 15, 1940; min. vel. of F star

Figure 15 shows the region of the *Na* I lines on two spectrograms of Capella taken on February 21, 1951, with Arcturus at the top. We see here that the strong lines of the G component are not greatly suppressed in *Na* I or *Fe* I. On the other hand, the lines of the F component not only are broad and diffuse but have small central intensities. Clearly, there is a pronounced diminution of the (uncorrected) equivalent widths with increasing wave length, and we reasonably attribute this to the difference in the temperatures of the two stars: the continuous spectrum of type F predominates in the ultraviolet region, that of the G star predominates in the red region. It is difficult to disentangle the F and G components in the yellow and green regions. Nevertheless, the high-dispersion Mount Wilson spectrograms (2.9 A/mm in the violet and blue regions; 4.3 A/mm in the yellow and red regions) show several strong lines of *Fe* I with both the sharp G component and the diffuse F component present. This agrees with the unpublished results of Emilio Krüger, to whom we are indebted for access to his work, and of K. O. Wright, who spoke of his Victoria observations at the 1952 meeting of the American Astronomical Society in Victoria, B.C. We believe that the effect of suppression, so conspicuous in the violet and ultraviolet regions, is still present but that the gradual tendency of the light of the G star to predominate in the longer wave lengths makes this phenomenon less conspicuous in the yellow and red parts of the spectrum. Presumably, the broad emission lines which we believe veil the strong G lines more effectively than the weak G lines (because the emission intensity is proportional to NHf, while the absorption intensity is more nearly proportional to $\sqrt{NHf}$) is independent of wave length. The continuous spectrum of the G star, on the other hand, increases rapidly with increasing wave length.

Figure 16 shows the region of $H\alpha$ on three dates: February 21, 1951; March 20, 1951; and March 23, 1951. The asymmetry of $H\alpha$ is not caused by the blending of the G and F components. This phenomenon has not been explained. Similarly, the variations in the

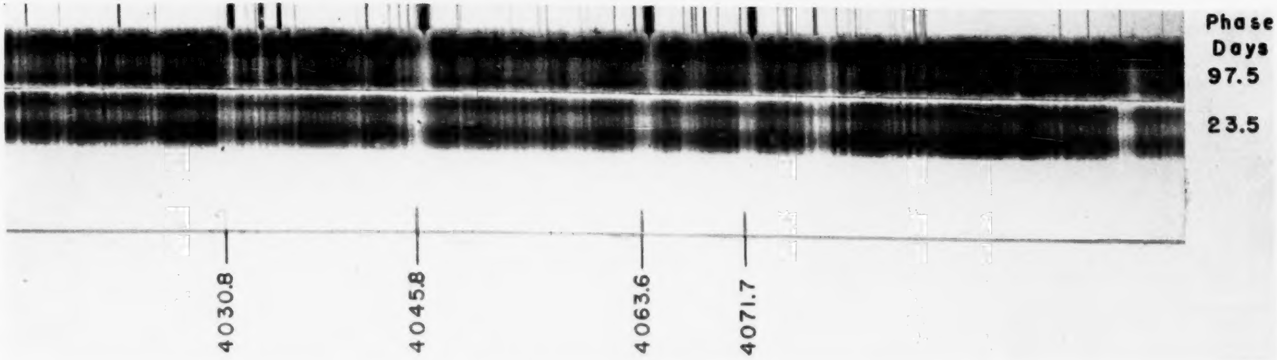
Phase
Days
97.5
23.5
4030.8
4045.8
4063.6
4071.7

FIG. 1.—Spectrum of Capella

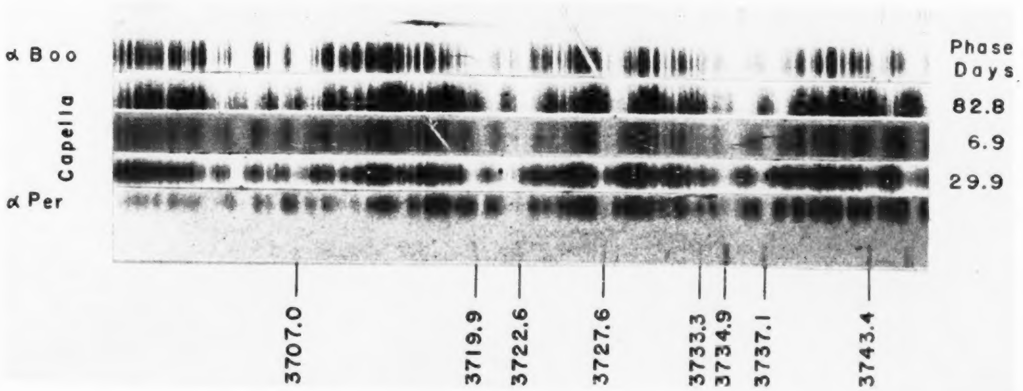
α Boo
Capella
α Per
Phase Days
82.8
6.9
29.9
3707.0
3719.9
3722.6
3727.6
3733.3
3734.9
3737.1
3743.4

FIG. 2.—Spectrum of Capella. (The comparison line marked 3707.0 should read 3709.2)

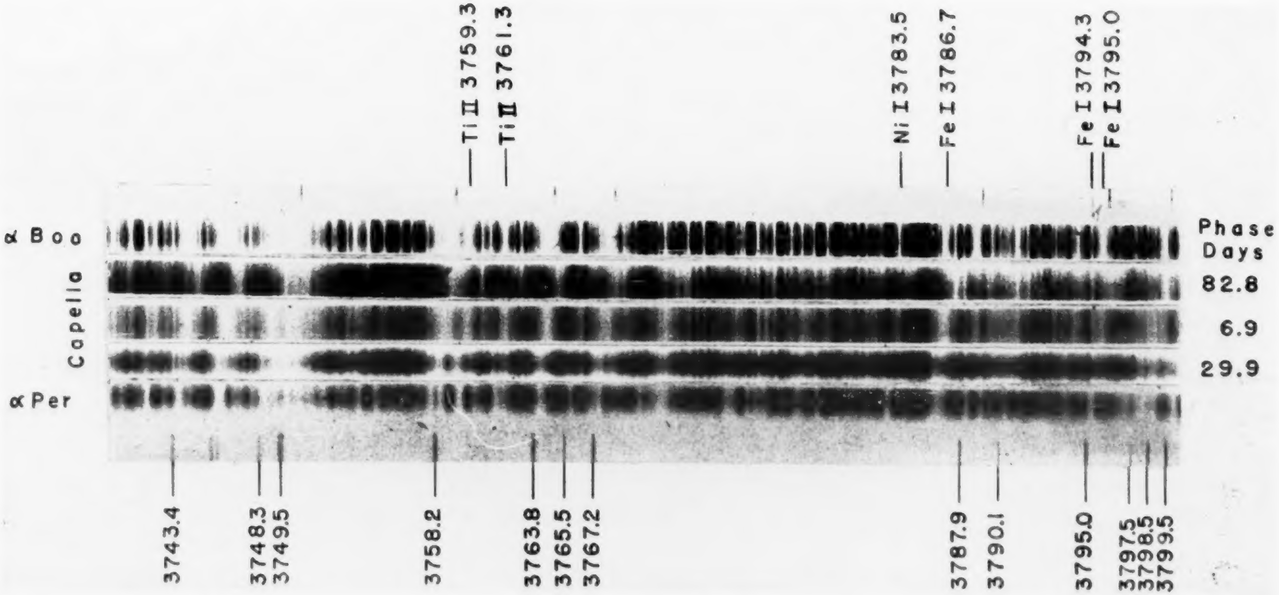

Ti II 3759.3
Ti II 3761.3
Ni I 3783.5
Fe I 3786.7
Fe I 3794.3
Fe I 3795.0
α Boo
Capella
α Per
Phase Days
82.8
6.9
29.9
3743.4
3748.3
3749.5
3758.2
3763.8
3765.5
3767.2
3787.9
3790.1
3795.0
3797.5
3798.5
3799.5

Fig. 3.—Spectrum of Capella

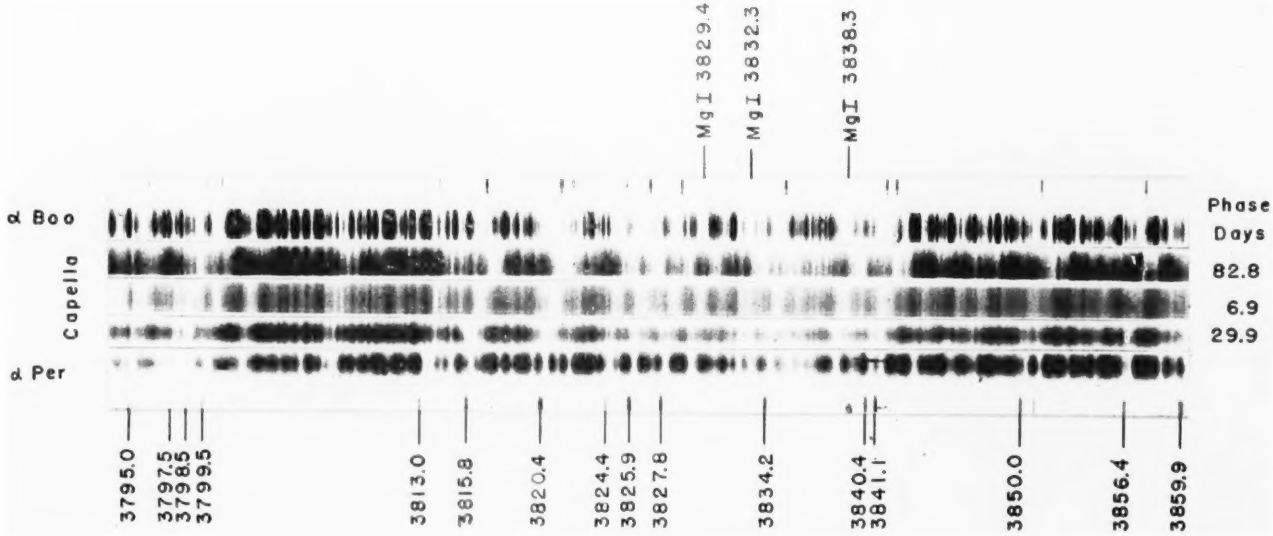

FIG. 4.—Spectrum of Capella

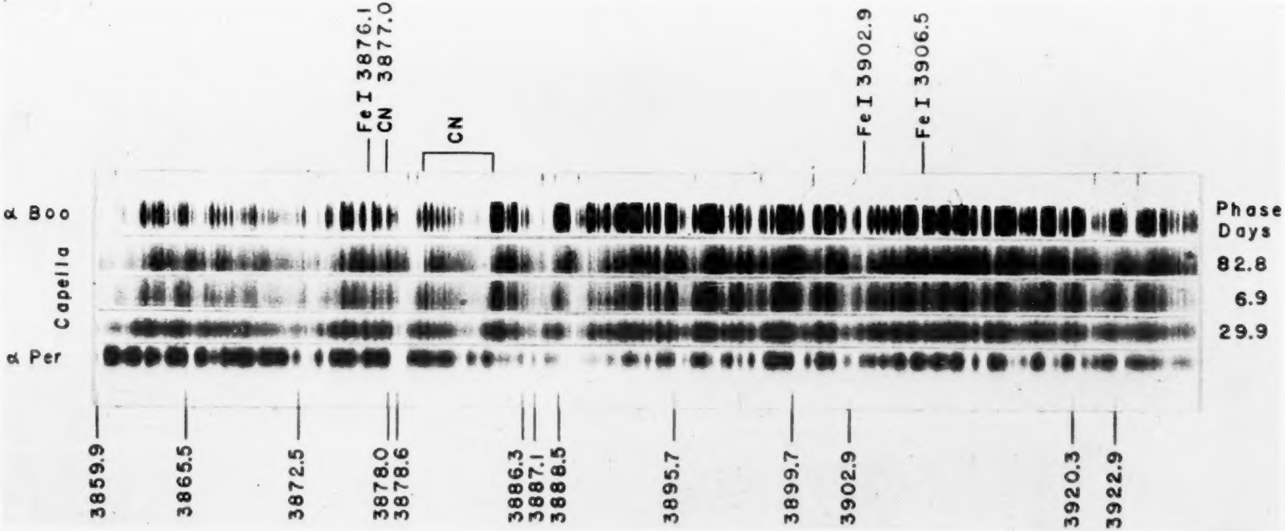
Fe I 3876.1
CN 3877.0
CN
Fe I 3902.9
Fe I 3906.5
α Boo
Capella
α Per
Phase
Days
82.8
6.9
29.9
3859.9
3865.5
3872.5
3878.0
3878.6
3886.3
3887.1
3888.5
3895.7
3899.7
3902.9
3920.3
3922.9

FIG. 5.—Spectrum of Capella. (The comparison line marked 3899.7 should read 3902.9. The comparison line marked 3902.9 should read 3906.5. Star line marked *Fe* I 3902.9 should read *Fe* I 3906.5 and Star line marked *Fe* I 3906.5 should read *Fe* I 3909.8.)

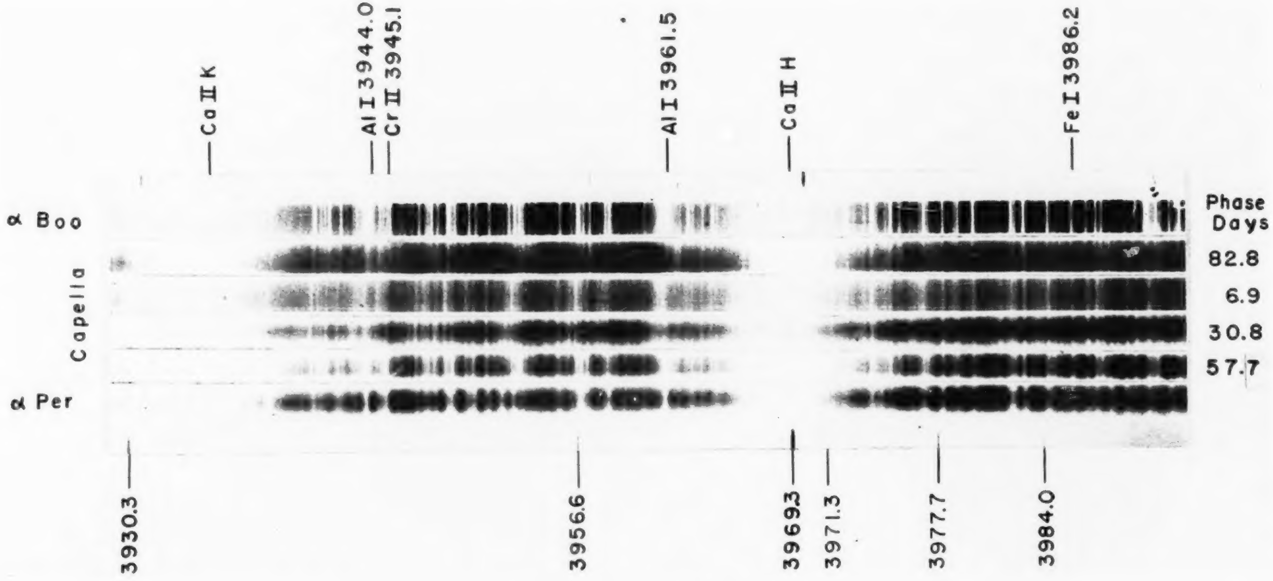
Ca II K
Al I 3944.0
Cr II 3945.1
Al I 3961.5
Ca II H
Fe I 3986.2
α Boo
Capella
α Per
Phase Days
82.8
6.9
30.8
57.7
3930.3
3956.6
39693
3971.3
3977.7
3984.0

FIG. 6.—Spectrum of Capella

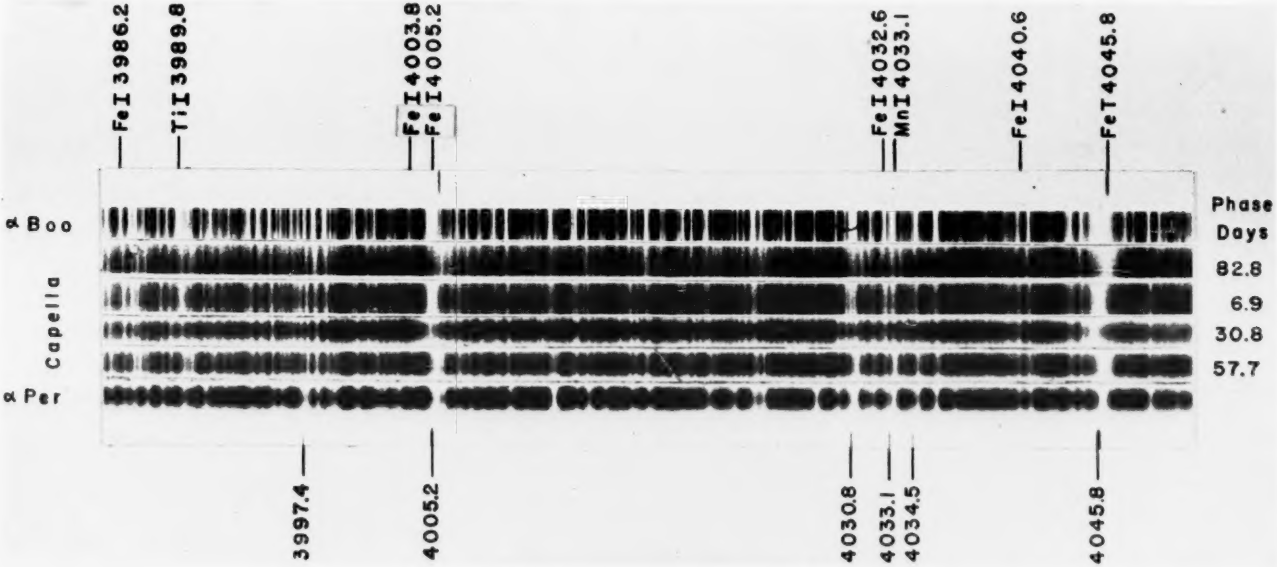

FeI 3986.2
TiI 3989.8
FeI 4003.8
FeI 4005.2
FeI 4032.6
MnI 4033.1
FeI 4040.6
FeI 4045.8
Phase
Days
82.8
6.9
30.8
57.7
α Boo
Capella
α Per
3997.4
4005.2
4030.8
4033.1
4034.5
4045.8

FIG. 7.—Spectrum of Capella

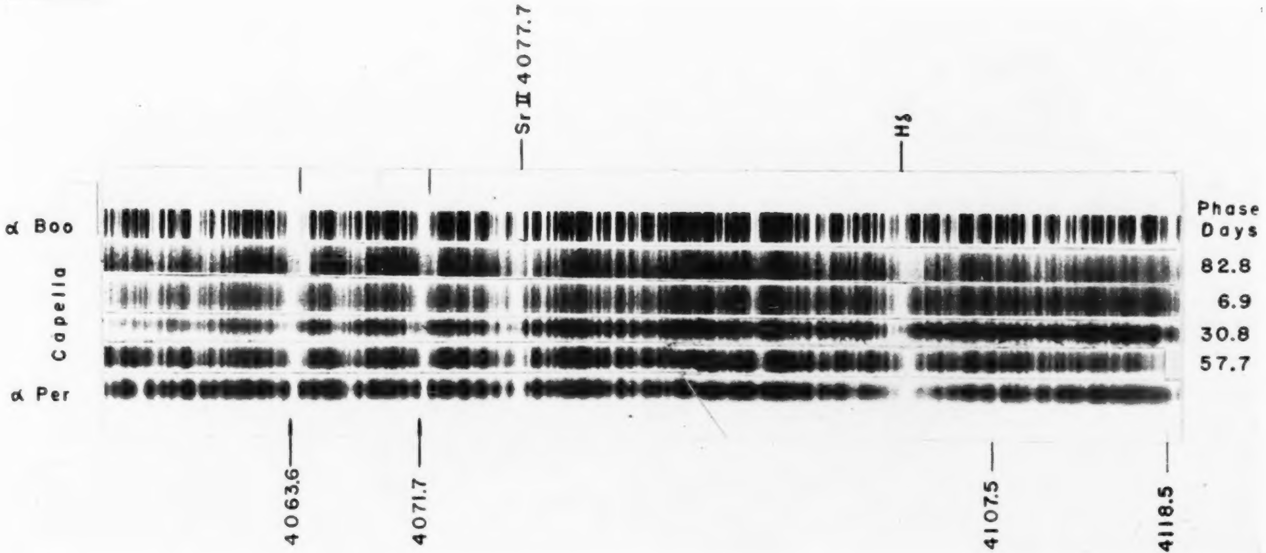
Sr II 4077.7
Hδ
α Boo
Capella
α Per
Phase
Days
82.8
6.9
30.8
57.7
4063.6
4071.7
4107.5
4118.5

FIG. 8.—Spectrum of Capella

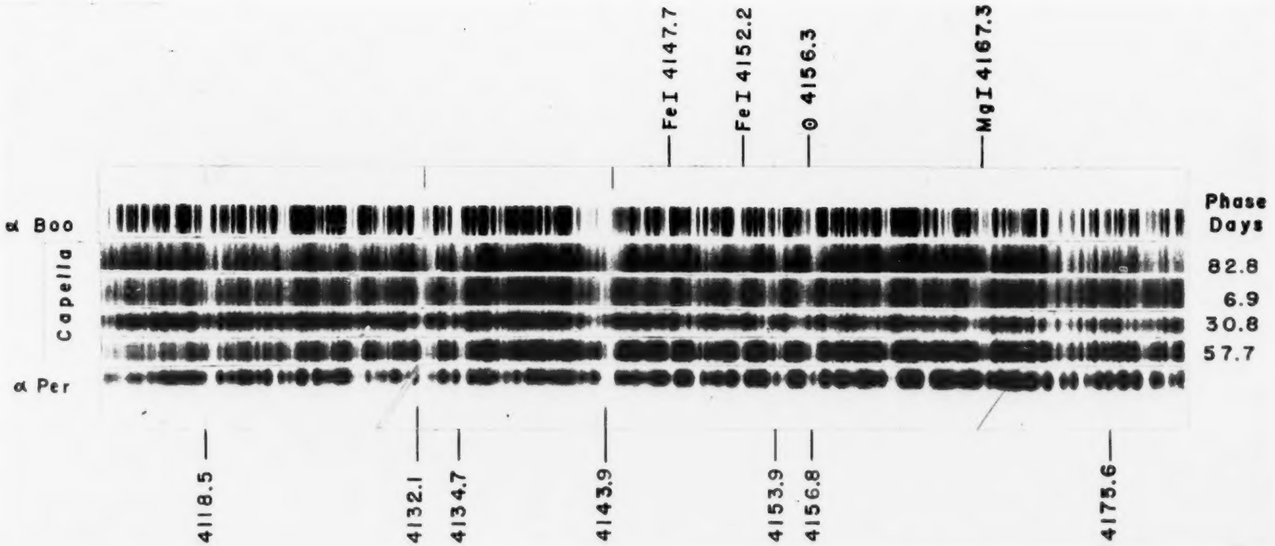
Fe I 4147.7
Fe I 4152.2
O 4156.3
Mg I 4167.3
α Boo
Capella
α Per
Phase Days
82.8
6.9
30.8
57.7
4118.5
4132.1
4134.7
4143.9
4153.9
4156.8
4175.6

FIG. 9.—Spectrum of Capella

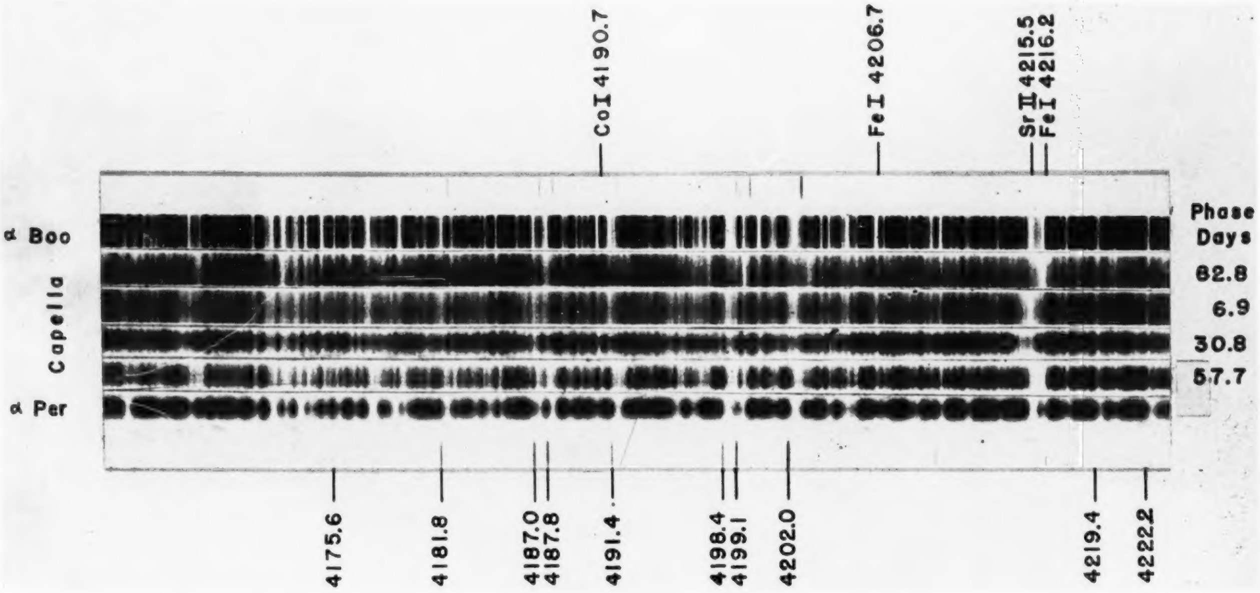

FIG. 10.—Spectrum of Capella

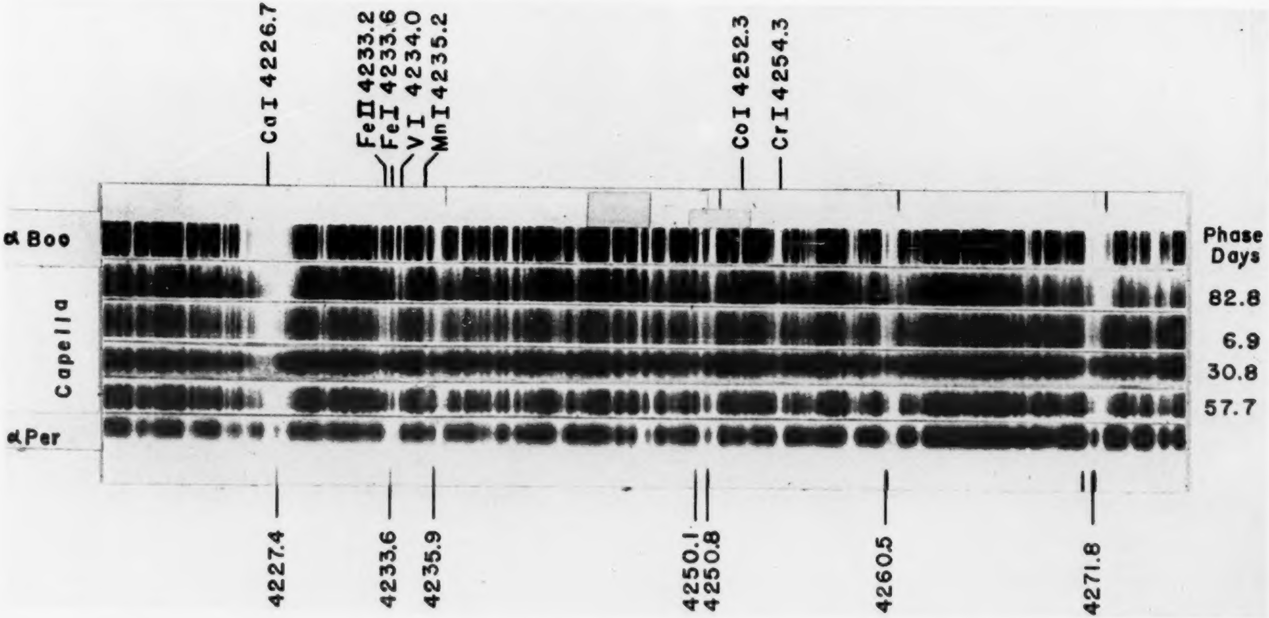
Ca I 4226.7
Fe II 4233.2
Fe I 4233.6
V I 4234.0
Mn I 4235.2
Co I 4252.3
Cr I 4254.3
α Boo
Capella
α Per
Phase Days
82.8
6.9
30.8
57.7
4227.4
4233.6
4235.9
4250.1
4250.8
4260.5
4271.8

FIG. 11.—Spectrum of Capella

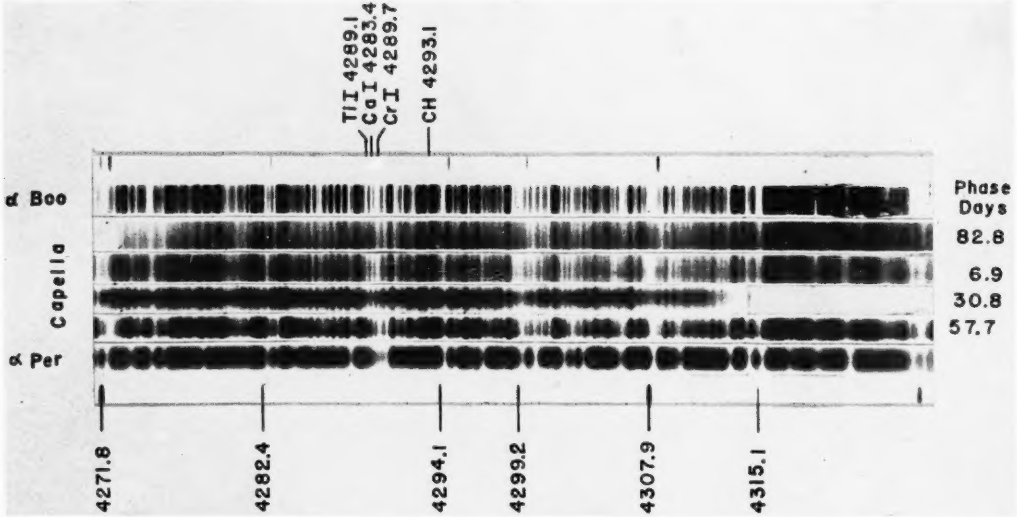

FIG. 12.—Spectrum of Capella. (The star line marked *Ca* I 4283.4 should read *Ca* I 4289.4)

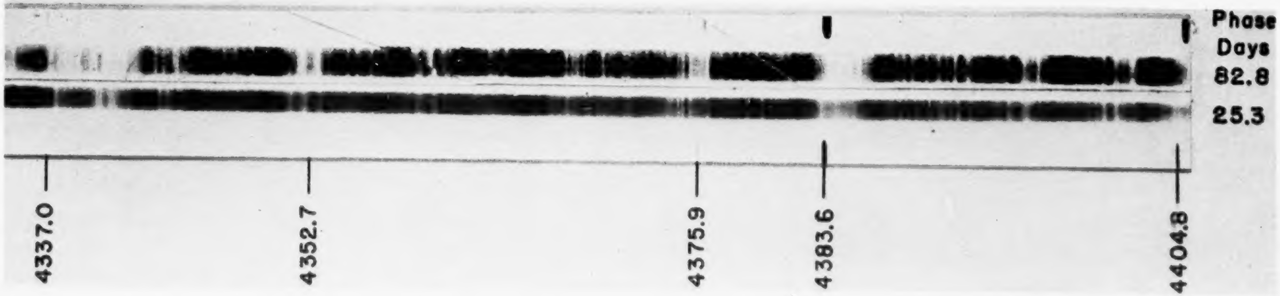

Phase
Days
82.8
25.3
4337.0
4352.7
4375.9
4383.6
4404.8

FIG. 13.—Spectrum of Capella

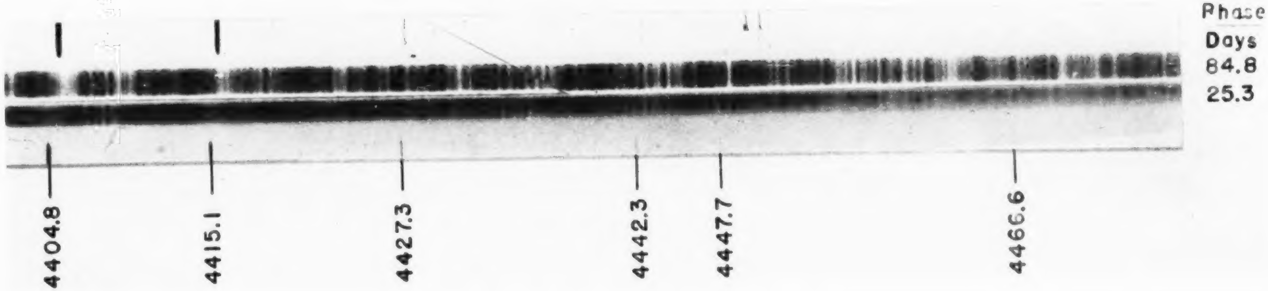
Phase
Days
84.8
25.3
4404.8
4415.1
4427.3
4442.3
4447.7
4466.6

Fig. 14.—Spectrum of Capella

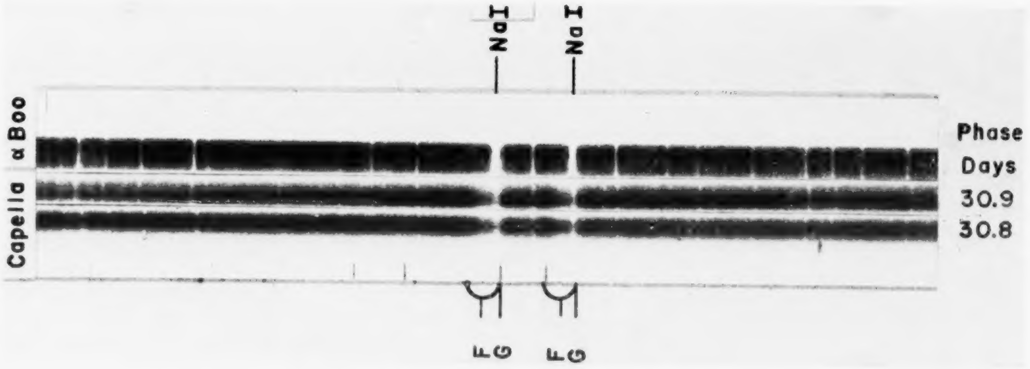
Na I
Na I
α Boo
Capella
Phase
Days
30.9
30.8
F
G
F
G

FIG. 15.—Spectrum of Capella

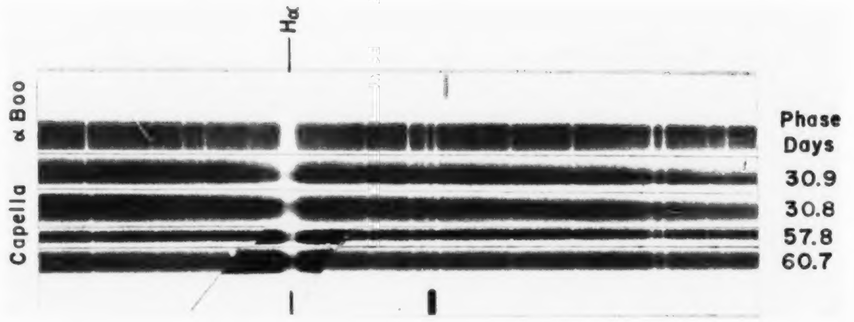

Hα
α Boo
Capella
Phase
Days
30.9
30.8
57.8
60.7

Fig. 16.—Spectrum of Capella

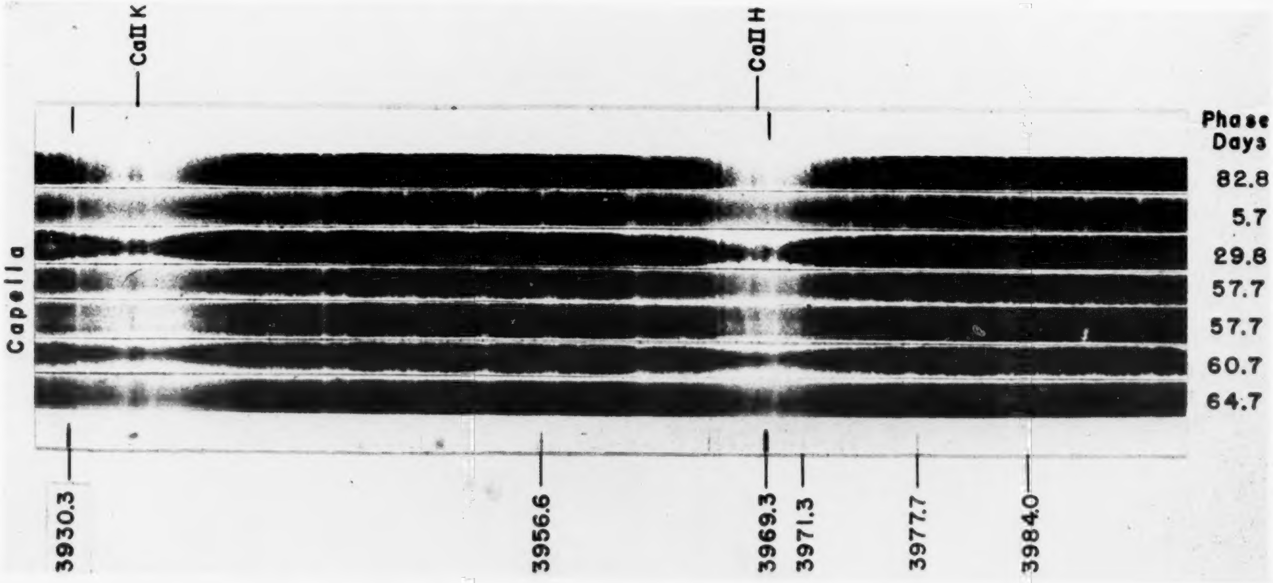
CaII K
CaII H
Phase
Days
82.8
5.7
29.8
57.7
57.7
60.7
64.7
Capella
3930.3
3956.6
3969.3
3971.3
3977.7
3984.0

FIG. 17.—Spectrum of Capella

relative intensities of the emission components of *Ca* II in Figure 17 are probably not directly related to the F component.[3]

In the ultraviolet region (Fig. 2) the F lines are very strong and numerous. The faint, sharp G lines are also numerous, but they are greatly influenced in intensity by the overlying, broad features of the F star. The suppression of the strong lines of the G component is remarkable, as in *Fe* I 3707, 3720, 3735, 3737, and 3743. A striking example of the strengthening of an accidentally present background line of the G star when it falls within a strong F line is shown immediately to the violet of *Fe* I 3727.6. This is the line *Cr* (?) 3726.9. It is very faint at phase 29.9 days. The effect is so pronounced that we can almost suspect the presence of real veiling by emission similar to that which suppresses the strong lines of the G component.

The lines of *Fe* I with high excitation potential show no systematic effect of veiling in the G component. But this is almost certainly due to the fact that these lines are weak. In Figure 3, *Fe* I 3795.0 ($a^5F-y^5F^\circ$; e.p. 1.0 volt) is normally a strong transition, and it is greatly suppressed in the G star at phases 82.8 and 29.9 days. An interesting case of suppression on the same plate is that of *Ti* II 3761.3.

In Figure 4 we find an outstanding case of suppression in the G lines of *Mg* I 3829, 3832, and 3838, and, of course, also in all the stronger lines of *Fe* I, such as 3815.8 and 3820 ($a^5F-y^5D^\circ$; e.p. 0.9 volt).

Figure 5 illustrates the behavior of *CN*. The weak band lines are entirely due to the G star and are normal throughout. But the strong band edge is apparently a blend of F and G: notice that at phase 29.9 days this edge falls to the violet of the position observed at phases 82.8 and 6.9 days. Undoubtedly, the strong edge of the G star, which at phase 29.9 should still be present in the position that corresponds to its location in Arcturus, is suppressed by the veiling effect. It should be noted that, while all strong lines of *Fe* I are influenced by the veiling effect, all weak lines are unaffected by it (except when these lines accidentally fall within the confines of an F line of appreciable strength). Thus *Fe* I 3906.5 ($a^5D-z^5D^\circ$; e.p. 0.1 volt) is normal, despite its low excitation potential, because this line corresponds to an intrinsically weak transition. Compare the behavior of this line with that of the pair *Fe* I 3878.0 and 3878.6, which is greatly influenced.

Figure 6 is interesting because of the suppression in the G star of the line *Al* I 3961.5. There is a blend in *Al* I 3944.0. The suppression of *Al* I 3961.5 at phase 82.8 days without the presence of a strong F line of the same element shows that there is no simple one-to-one relationship between the intensity of the F line and the degree of suppression.

The lines of *Ca* II are not well shown in Figure 6. However, Figure 17 shows that the G lines of *Ca* II are veiled to a considerable extent in their wings. Yet it seems remarkable that the central emission components of these lines and the general veiling effect are quite insufficient to suppress completely the strong absorption lines. This throws a doubt upon our interpretation of the veiling effect. In the case of *Fe* I, *Mg* I, *Al* I, *Ti* I, etc., the hypothetical emission feature which causes the veiling shares the velocity of the G star, has a spectral type close to G, and a line profile which is broadened by turbulent (or other motions) to agree approximately in width with the stronger *Fe* I absorption lines of the G star. Thus, in the case of *Ca* II, we could identify these emission features only with the central emission lines. These, however, are quite weak and would completely destroy our analogy to type G of the emitting source (in the solar flash spectrum the *Ca* II lines are by far the most intense features). There is no way to overcome this difficulty at the present time.

Figure 7 shows in a remarkable way the behavior of some *Fe* I lines. Thus the strong transition *Fe* I 4046 ($a^3F-y^3F^\circ$; e.p. 1.5 volts) is greatly affected, while *Fe* I 4032.6 ($a^3F-y^5P^\circ$; e.p. 1.5 volts) is quite normal. Notice also that the faint lines *Fe* I 3986.2

---

[3] Otto Struve, *Ann. d'ap.*, **14**, 2, May–June, 1951.

and 4040.6 ($a^3D - v^3F^\circ$; e.p. 3.3 volts) are normal, despite the fact that one of these lines is close to *Fe* I 4046.

Figure 8 shows that *Hδ* in the F star is surprisingly weak. Thus the F spectrum is certainly not normal. The weakness of the F star's hydrogen lines can be traced through the entire ultraviolet region. *Sr* II 4078 is present in the F star, but it is relatively weaker than in α Persei.

The strange tendency of *Mg* I toward suppression is illustrated by the relatively faint line *Mg* I 4167, in Figure 9. It is distinctly weak at phase 82.8 days.

In Figure 10 the presence of the F line of *Sr* II 4215.5 and its suppression in the G star is complicated by the presence of *Fe* I 4216.2. Notice that this line belongs to multiplet $a^5D - z^7P^\circ$; e.p. 0.0 volt. It certainly changes in character, and not all of this change can be attributed to *Sr* II. But the line *Fe* I 4206.7, also of multiplet $a^5D - z^7P^\circ$; e.p. 0.0 volt, is normal.

As we pass into the longer wave lengths, the effect of suppression or veiling of the G lines becomes less pronounced. In Figure 11, *Ca* I 4227 is a blend of F and G. The latter is not greatly suppressed. The line *Fe* I 4271.8 (also shown in Fig. 12) is peculiar. Notice how faint this line appears at phase 30.8 days. This effect has been confirmed on other spectrograms taken at similar phases. Both lines, *Fe* I 4272 and 4308 ($a^3F - z^3G^\circ$; e.p. 1.5 volts) are greatly suppressed in the G star, while the weaker transition, *Fe* I 4148, of the same multiplet (Fig. 9) is normal.

The very important question of the radial velocity of the F star, which yields the mass ratio of the system, and hence the individual masses of the two components, has already been discussed.[1] It is quite certain that the previously accepted mass ratio $\alpha = \mathfrak{M}_G/\mathfrak{M}_F = 1.2$ is too large. But it is very difficult to make an accurate determination. There are two distinct ways in which we can proceed: (1) to study the double lines of *Na* I and the few unblended pairs of *Fe* I in the yellow and red regions; (2) to measure those ultraviolet *Fe* I lines which belong to the F component and are not seriously affected by the suppressed G lines. The former is influenced by the presence of strong G lines, which may blend with the extreme edges of the F lines. Nevertheless, the previous measures[1] gave $K_G = 26.0$ km/sec; $K_F = 26.5$ km/sec; $\alpha = 1.0$.

We have now measured the best available F lines in the ultraviolet region. Two methods were used. In the first, the broad F lines were referred to suitably chosen faint G lines. Pairs of spectrograms were then formed, one near maximum velocity, the other near minimum. Let d be the difference in the wave lengths of the selected G line and an F line, θ_a and θ_i the phases of the two spectrograms, at maximum and minimum velocity, respectively. For the present purpose we can neglect the eccentricity of the orbit and write:

$$\Delta S_i = d + (K_G + K_F)\sin\theta_i \text{ (min. phase)},$$

$$\Delta S_a = d + (K_G + K_F)\sin\theta_a \text{ (max. phase)}.$$

Hence

$$K_F = \frac{\Delta S_i - \Delta S_a}{\sin\theta_i - \sin\theta_a} - K_G .$$

We adopt $K_G = 26.0$ **km**/sec.

In the second method we designate by d_0 the difference in wave length between the selected comparison line and an F line. Let V_i and V_a be the appropriate solar reductions. Then

$$\Delta S_i = d_0 + K_F \sin\theta_i - V_i ,$$

$$\Delta S_a = d_0 + K_F \sin\theta_a - V_a .$$

Hence

$$K_F = \frac{(\Delta S_i - \Delta S_a) + (V_i - V_a)}{\sin\theta_i - \sin\theta_a} .$$

Table 1 lists the spectrograms used in these measurements. Table 2 gives the results for the individual lines. The scatter is quite large. Nevertheless, the final value should have considerable weight:

$$K_F = 22.1 \text{ km/sec} , \qquad K_G = 26.0 \text{ km/sec} , \qquad \alpha = 0.85 .$$

Combining this with the result obtained from the double *Na* I lines, we adopt $\alpha = \mathfrak{M}_G/\mathfrak{M}_F = 0.90$. There is some slight uncertainty in the adopted value of K_G. Our own

TABLE 1

COUDÉ SPECTROGRAMS OF α AURIGAE (LINEAR DISPERSION 2.9 A/MM)
(Epoch = 1935 Sept. 4. 160 U.T. = J D 2428050.660; Period = 104.023 Days)

Plate Cd	Date	U.T.	JD 2430000+	E	Phase (Days)
6778.....	1950 Dec. 31	4:10	3646.674	53	82.795
6779.....	1950 Dec. 31	5:25	3646.726	53	82.847
6787.....	1951 Jan. 2	3:07	3648.630	53	84.751
7804.....	1952 Feb. 10	8:28	4052.853	57	72.882
7904.....	1952 Apr. 15	4:30	4117.688	58	33.694
7905.....	1952 Apr. 15	5:02	4117.710	58	33.716
7920.....	1952 Apr. 16	2:55	4118.622	58	34.628
7921.....	1952 Apr. 16	3:16	4118.636	58	34.642

TABLE 2

DETERMINATION OF K_F

F STAR λ	CD 7804 AND 7904 WITH RESPECT TO		CD 6787 AND 7905 WITH RESPECT TO		CD 6779 AND 7920 WITH RESPECT TO		CD 6778 AND 7921 WITH RESPECT TO	
	G Lines $\Delta S_i - \Delta S_a$ (Km/Sec)	Comp. Lines $\Delta S_i - \Delta S_a$ (Km/Sec)	G Lines $\Delta S_i - \Delta S_a$ (Km/Sec)	Comp. Lines $\Delta S_i - \Delta S_a$ (Km/Sec)	G Lines $\Delta S_i - \Delta S_a$ (Km/Sec)	Comp. Lines $\Delta S_i - \Delta S_a$ (Km/Sec)	G Lines $\Delta S_i - \Delta S_a$ (Km/Sec)	Comp. Lines $\Delta S_i - \Delta S_a$ (Km/Sec)
3720..........	....	....	....	....	....	11.0	....	....
3735..........	....	....	....	....	38.1	9.3	....	....
3737..........	....	18.1	....	....	45.1	....	....	....
3745..........	37.0	12.8	....	....	....	....	....	....
3764..........	45.0	18.6	....	....	50.0	11.4	....	....
3816..........	44.1	16.1	....	....	39.5	9.0	....	8.1
3838..........	....	15.6	....	....	....	8.0	....	7.6
3841..........	....	....	....	....	53.7	....	....	....
3856..........	42.9	19.4	....	0.7	43.0	8.8	39.9	8.2
3878..........	46.4	24.1	42.2	9.7	46.2	....	45.6	14.2
3887..........	....	....	....	....	....	8.9	....	....
4045..........	....	11.9	....	....	....	....	....	....
Average..	43.1	17.1	42.2	5.2	45.1	9.5	42.8	9.5
Corrected to ⊙.	....	16.3	....	19.2	....	23.9	....	24.0
For phase f....	46.7	17.7	46.6	21.2	49.4	26.2	46.9	26.3
K_F..........	20.7	17.7	20.6	21.2	23.4	26.2	20.9	26.3

final result[4] was $K_G = 26.4$ km/sec. Other determinations gave: Reese, $K_G = 25.8$ km/sec; Goos, $K_G = 26.5$ km/sec; W. Struve, $K_G = 26.0$ km/sec. The mean of all four determinations is 26.2 km/sec. The resulting change in a is insignificant.

Let us next see how our new determination of a affects the individual masses. We have

$$f(\mathfrak{M}) = \frac{\mathfrak{M}_G}{(1+a)^2}\sin^3 i = 0.198\odot .$$

Adopting Merrill's value of $i = 41°$, we have

$$\frac{\mathfrak{M}_G}{(1+a)^2} = 0.702 .$$

With $a = 0.90$, we find $\mathfrak{M}_G = 2.5\odot$; $\mathfrak{M}_F = 2.8\odot$. The currently adopted values were $\mathfrak{M}_G = 4.2\odot$; $\mathfrak{M}_F = 3.3\odot$.

The distance of Capella was determined originally from a comparison of Merrill's interferometric determination of $(a_F + a_G)\sin i$ and the corresponding spectrographic value. The latter is now also changed, and consequently not only the mass is shifted in the conventional $\mathfrak{M} - L$ relation but also its absolute magnitude. For example, in Eddington's diagram[5] the circle representing Capella G should be dropped about $\frac{1}{2}$ cm and moved to the left nearly 2 cm. In view of the remaining uncertainty of K_F, it is not profitable to specify the location more exactly.[6]

---

[4] Otto Struve and Ruth Kilby (in preparation).

[5] *The Internal Constitution of the Stars* (Cambridge, 1926), p. 153.

[6] Dr. D. Harris, Jr., has informed us that our new value of a brings into better accord the trigonometric parallax of Capella with the orbital value. Several among the earlier workers have been puzzled by the appearance of the F-type lines in Capella. H. M. Reese (*Lick Obs. Bull.*, **1**, 35, 1901) stated that "no very satisfactory determinations of the lesser component's velocities are at hand," and he did not even plot these velocities in his diagram illustrating the two curves. F. Goos (*Der spektroskopische Doppelstern Capella* [Bonn, 1908]), in discussing H. F. Newall's observations, refers to the spectrum as "sehr merkwürdig"; and W. Struve (*Zs. f. Ap.*, **17**, 61, 1939) speaks of "Eigentümlichkeiten die vielleicht . . . noch einer Klärung bedürfen." But it is quite obvious that the dispersion used in these investigations was not sufficient to unravel the truly remarkable features of the spectrum of Capella.

THE SPECTRUM OF 48 LIBRAE FROM 1944 TO 1952

PAUL W. MERRILL
MOUNT WILSON AND PALOMAR OBSERVATORIES
CARNEGIE INSTITUTION OF WASHINGTON
CALIFORNIA INSTITUTE OF TECHNOLOGY

Received September 1, 1952

ABSTRACT

The remarkable oscillation which began in the atmosphere of the shell star 48 Librae in 1935 has continued through 1952, although the second cycle had a smaller amplitude in velocity than the first. As in the first cycle, velocities derived from metallic lines and from hydrogen lines toward the limit of the series had greater amplitudes than those from the hydrogen lines near *H*6. Changes in the intensity and structure of the lines exhibit a complicated relationship to the velocity-curve.

The spectrum of the shell star 48 Librae[1] has been studied in considerable detail at the Yerkes and McDonald Observatories[2,3] and at the Mount Wilson Observatory.[4] The remarkable atmospheric oscillations which began about 1935 and were still in progress in 1943 called for continued observation.

The present paper describes numerous spectrograms (Table 1) obtained at the Mount Wilson and Palomar Observatories since 1943. Nearly all include the region from $H\beta$ shortward past the limit of the Balmer series, dispersion 10 A/mm. They were taken by me, with the exception of four by Arthur Abt; three by I. S. Bowen; two by R. F. Sanford; and one each by W. S. Adams and A. J. Deutsch. I am indebted to these observers for their spectrograms and to Miss Cora G. Burwell, Miss Sylvia Burd, and Miss Louise Lowen for their expert assistance in measuring and computing.

The dark lines have continued to exhibit slow systematic changes in intensity and structure similar to those previously observed.[4] The changes are not extreme and have relatively slight effects on the measured velocities recorded in Table 1. The values for *H*6 and *H*28 were read from smoothed progression-curves plotted for the individual plates. Regular changes from year to year in the positions and slopes of these curves are shown by the mean curves in Figure 1, which are in continuation of those in Figures 9 and 10 of *Mount Wilson Contribution*, No. 690.[4] Velocity-curves from both series of spectrograms are in Figure 2. The second minimum, in 1945, is considerably higher than the first minimum, in 1937; and the second maximum, in 1951, is slightly lower than the first maximum in 1941. These facts indicate that the atmospheric oscillations of 48 Librae are subject to damping. The curve for *H*28 has considerably greater amplitude than that for *H*6 and after 1939 seems to precede it in phase by about 100 days. It will be most interesting to see how future cycles behave.

The velocities derived from various metallic lines follow rather closely those of the Balmer lines toward the limit of the series. In the earlier series, displacements of *H*28 and of lines of ionized metals were treated together. In the present series, certain slight differences appear, to which attention may now be called. The lines of *Fe* II are more numerous than those of any other metal. The measured velocities in Table 1 are plotted in Figure 3. The detailed behavior with respect to the velocities from *H*28 is indicated in Table 2. Reference to the velocity-curve shows that the behavior at the two successive

---

[1] HD 142983, MWC 239; 1900 R.A. $15^{\mathrm{h}}52^{\mathrm{m}}6$; Dec. $-13°59'$; mag. 4.7.

[2] O. Struve, *McDonald Contr.*, No. 73; *Ap. J.*, **98**, 98, 1943.

[3] W. A. Hiltner, *McDonald Contr.*, No. 82; *Ap. J.*, **99**, 103, 1944.

[4] P. W. Merrill and R. F. Sanford, *Mt. W. Contr.*, No. 690; *Ap. J.*, **100**, 14, 1944.

TABLE 1

RADIAL VELOCITIES 1944–1952

PLATE	DATE	JD 243	RADIAL VELOCITY (KM/SEC)			NUMBER Fe II LINES MEASURED
			*H*6	*H*28	*Fe* II	
Ce 3420	1944 May 10	1221	−25	−30	−29.1	18
3454*	June 10	1252	−29	−30	−29.4	38
3737	1945 Mar. 24	1539	−40	−48	−47.1	18
3761	Apr. 28	1574	−41	−49	−48.0	4
3906	Aug. 20	1688	−41	−51	−48.5	8
4199†	1946 Mar. 21	1901	−18†	....	−44.0	10
4200	Mar. 21	1901	−43	−48	−45.7	14
4320	July 13	2015	−42	−46	−42.7	3
4613	1947 Mar. 8	2253	−38	−41	−38.6	7
4683	May 6	2312	−34	−36	−36.6	5
4697†	May 27	2333	−20†	....	....	....
4734	July 1	2368	−33	−34	−34.6	12
5130	1948 Mar. 22	2633	−24	−23	−22.1	2
5137	Mar. 23	2634	−23	−23	−22.0	8
5199	June 16	2719	−20	−19	−19.9	1
5204	June 17	2720	−20	−19	−19.8	10
5226	July 18	2751	−19	−16	−23.7	1
5229	July 19	2752	−17	−18	−17.2	11
5676	1949 June 11	3079	− 4	+ 3	+ 4.2	16
5677	June 11	3079	− 3	+ 6	+ 2.7	13
5685	June 13	3081	− 4	+ 3	+ 4.2	16
5745	July 12	3110	− 2	+ 7	+ 4.3	16
5753	July 14	3112	− 3	+ 6	+ 3.4	7
5805	Aug. 3	3132	− 3	+ 5	+ 5.6	10
5916	Sep. 9	3169	+ 1	+ 9	+ 7.9	14
6157a	1950 Feb. 21	3334	+ 9	+16	+16.2	3
6157b	Feb. 21	3334	+ 9	+17	+14.7	16
6164	Feb. 22	3335	+ 8	+16	+14.6	10
6165	Feb. 22	3335	+10	+17	+15.6	7
6233	May 23	3425	+13	+25	+16.3	1
6237	May 24	3426	+14	+22	+16.8	10
6243†	May 25	3427	−22†	....	....	....
6426	Aug. 4	3498	+14	+24	+19.9	3
6433	Aug. 5	3499	+16	+25	+21.6	15
6437	Aug. 6	3500	+14	+22	+17.9	11
6441	Aug. 7	3501	+15	+24	+20.5	14
6885	1951 Feb. 24	3702	+20	+24	+22.0	15
6886	Feb. 24	3702	+19	+24	+21.8	15
6962	Mar. 27	3733	+19	+22	+21.2	19
7012	May 14	3781	+20	+20	+20.6	20
7076	June 22	3820	+18	(+13)	+18.8	18
7081	June 23	3821	+18	+16	+17.9	9
7082†	June 23	3821	−12†	....	+17.2	4
7213	July 31	3859	+18	+14	+17.8	16
7214	July 31	3859	+14	+16	+17.0	13
7218	Aug. 1	3860	+14	+19	+18.2	16
Pc 196	Oct. 18	3938	+16	....	+11.0	17
Pc 257	1952 Feb. 1	4044	+10	+ 8	+ 8.1	46
Pc 302	Apr. 5	4108	+ 4	(− 1)	+ 2.7	57
Ce 8099	June 12	4176	− 1	− 4	− 0.7	36

* Dispersion 2.9 A/mm; dispersion for all other plates in blue-violet, 10 A/mm.

† Visual region: dispersion either 20 or 15 A/mm; velocity from $H\alpha$ entered in $H6$ column.

maxima is not the same. At the first maximum the *Fe* II curve departs farther from the *H*6 curve than does the *H*28 curve; at the second maximum it departs less.

On the whole, displacements of lines of various metals agree fairly well. In particular, the lines of *Ca* II appear to agree within errors of measurement with those of *Fe* II. Table 3 shows, however, that for certain elements systematic residuals of a few kilometers per second appear at times. The displacements of *Ti* II lines were algebraically greater than those of *Fe* II lines in 1941 and again in 1949–1950; they were algebraically less in 1944 and in 1951–1952. In 1944 and 1949, lines of *Ni* II had residuals opposite in sign to those of *Ti* II.

At the H and K lines, a narrow, extremely weak component measured on 15 plates

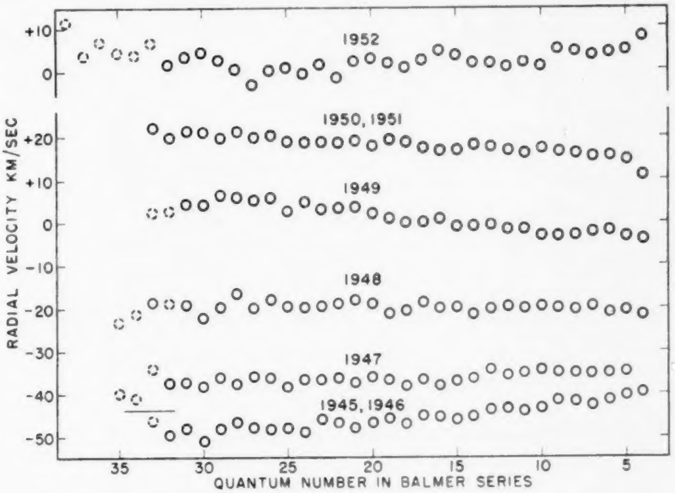

FIG. 1.—Mean progression-curves

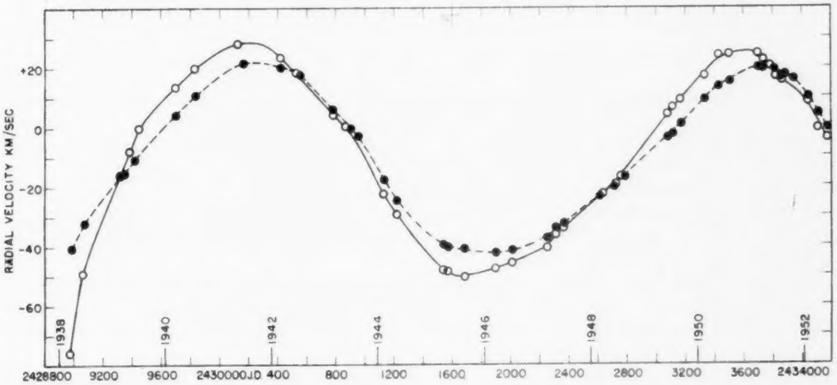

FIG. 2.—Velocity-curves from hydrogen lines. *Open circles and solid line*, velocities from *H*28; *filled circles and dashed line*, velocities from *H*6.

has a mean displacement of −9 km/sec. This value differs somewhat from the previous measurement of −15 km/sec, but, because of the difficulty of measurement, it is not certain that the difference is real.

The intensities of the metallic lines increased slowly from 1938 to a maximum in 1943. Thereafter, they decreased to a flat minimum in 1946 or 1947. The intensities increased decidedly from 1950 to 1952. The indications are that the maximum intensity occurs on the falling branch of the velocity-curve, with a flat minimum on the rising branch. The widths of the hydrogen lines followed about the same course, except that in 1952 the widths were no greater than in 1950, although the lines appeared somewhat stronger.

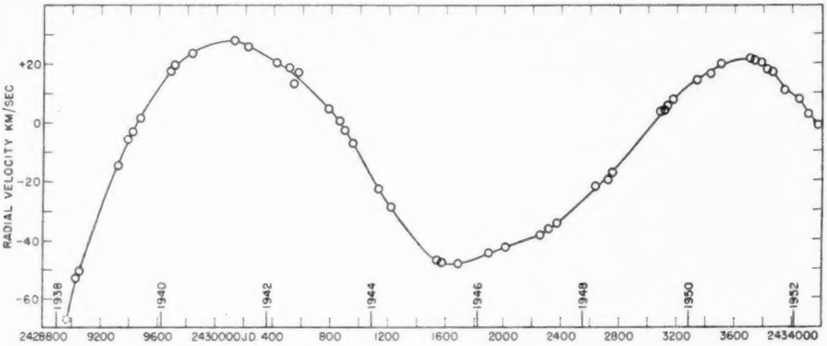

FIG. 3.—Velocity-curve from lines of *Fe* II

TABLE 2

DISPLACEMENTS OF *Fe* II LINES WITH RESPECT TO THOSE OF *H*28

JD	Remarks	JD	Remarks
2429000–9500	Agree closely	2432400–3200	Agree
9500–0100	Lie above	3200–3800	Lie below
2430100–1600	Agree	3800–4200	Agree (or above?)
1600–2400	Lie above		

The dark lines appeared nearly symmetrical during most of the time corresponding to the lower part of the velocity-curve and, curiously enough, also for a short interval near maximum velocity. Before maximum they were sharper on the shortward side; just after maximum they were sharper on the longward side. Thus the line shapes appear to be more directly related to the acceleration than to the velocity.

The curve formed by plotting the ratio of the intensity of the shortward emission component of *H*β to that of the longward component, as usual in shell stars, resembles the velocity-curve in shape and phase.

The foregoing data show how complicated the behavior of an extended stellar atmosphere can be. It is hoped that, in connection with similar data for other stars, they will lead to hypotheses that will eventually yield the correct physical interpretation of the remarkable phenomena involved.

In future observations, residuals in the displacements of various lines and especially the small but important asymmetries of the lines could be better studied with higher dispersion.

TABLE 3

RESIDUALS WITH RESPECT TO VELOCITIES FROM LINES OF *Fe* II
(Km/Sec)

Plate	*Ti* II	No.	*Cr* II	No.	*Ni* II	No.	*Si* II	No.	*Ca* II (H, K)	*Mg* I	No.
Ce 3420	(−11)*	8	−11	3	+3	3	(−14)	3	0	−10	2
3454	−13	18	−9	5	+6	2	−8	4	+2	−16	2
3737	−1	3	−11	1	+5	10	+2	2	0	−3	1
3761	...	...	...	...	+4	3	...	...	0	...	...
3906	...	...	...	...	+3	2	...	...	+1	...	...
4200	...	...	+10	1	+4	9	+4	1	−2	+2	1
4320	...	...	...	...	+4	3	...	...	−2	−2	1
4613	+6	1	+2	1	0	7	...	...	0		
4683	+4	1	−6	1	+4	6	...	...	+2	+1	2
4734	−1	3	−4	1	+2	5	...	...	−1		
5130	+4	2	...	...	0	1	...	...	0		
5137	0	2	...	...	0	4	+5	1	0		
5199	...	...	+2	1	+2	3	...	...	+1		
5204	+4	2	+4	2	0	4	...	...	+4	(+8)	2
5229	+6	1	−4	2	−3	3	...	...	+2	...	...
5676	+1	6	+1	2	−7	3	+1	1	−3	+6	2
5677	+2	4	+2	3	−4	7	...	...	−3	...	...
5685	+6	7	0	4	−8	2	+3	1	−4	+2	2
5745	+8	6	−1	1	−4	4	...	...	−1	+5	2
5753	+6	3	...	...	−4	6	...	...	−2	...	...
5805	+8	3	...	...	−7	3	...	...	−2	+2	2
5916	+6	3	−2	1	−3	1	...	...	−4	...	...
6157a	+6	2	...	...	−4	1	...	...	+1	+2	2
6157b	+7	5	−6	1	−4	5	...	...	−2	(+10)	2
6164	+5	4	...	...	−4	2	...	...	+5	...	...
6165	+6	5	...	...	−8	1	...	...	+1	...	...
6233	+9	3	...	...	−1	1	...	...	+7	...	...
6237	+6	4	...	...	−6	1	...	...	+1	+5	2
6426	+10	1	...	...	−5	3	...	...	+4	...	...
6433	+4	2	+2	1	0	1	+4	1	+2	+1	1
6437	...	...	−3	1	−2	1	...	...	+3	0	1
6441	+4	6	+2	1	0	1	...	...	+4	−1	3
6885	0	2	−5	3	0	3	...	...	+2	−4	2
6886	+2	6	−4	4	+1	1	...	...	+4	−3	3
6962	−3	9	−6	6	+1	2	−8	1	+1	−2	1
7012	0	12	+3	4	+5	2	−2	1	+1	−4	3
7076	−3	4	−6	1	+2	3	−4	2	+2	0	2
7081	−2	4	...	...	−3	1	...	...	+3	−1	3
7213	−5	4	+5	1	−2	1	−8	1	+1	−3	3
7214	−3	10	−6	1	−1	3	0	2	−2	−6	3
7218	−7	8	...	...	−2	3	−3	1	−1	−2	2
Pc 196	−5	12	+1	2	+2	1	...	...	−1	...	...
Pc 257	−4	17	−3	9	−1	7	−7	4	−1	−6	3
Pc 302	−8	19	−1	7	−2	3	−11	4	−3	−5	3
Ce 8099	−9	14	−4	7	−3	4	−12	3	−3	−10	3

---

* Parentheses indicate that velocities from individual lines agree poorly.

THE MAGNETICALLY VARIABLE STAR HD 153882

GURO GJELLESTAD*

INSTITUTE OF THEORETICAL ASTROPHYSICS, THE UNIVERSITY, BLINDERN, OSLO, NORWAY

AND

HORACE W. BABCOCK

MOUNT WILSON AND PALOMAR OBSERVATORIES
CARNEGIE INSTITUTION OF WASHINGTON
CALIFORNIA INSTITUTE OF TECHNOLOGY

Received August 25, 1952

ABSTRACT

The reversing magnetic field of the peculiar A-type star HD 153882 has been investigated on twenty spectrograms made with the double analyzer for circularly polarized light. The effective magnetic field intensity at the pole, H_p, as determined from measures of the Zeeman effect on about thirty lines on each plate, varies periodically between the limits +4500 gauss and −4000 gauss. The derived period is 6.005 days.

Measures of H_p and of radial velocity have been tabulated for elements at various phases. The mean velocity-curve is anharmonic, with a range of 5.3 km/sec. Systematic velocity differences between elements are small; this is probably related to the fact that the spectrum shows little or no variability in relative line intensities. The spectrum is peculiar in that *Cr* I, *Cr* II, and *Mn* I are strong, and the K line is sharp, but the star is not a typical spectrum variable.

A cross-over effect in the polarized line profiles, rather similar to that previously found in HD 125248 and in α^2 CVn, was observed at phases when the effective magnetic field is near zero.

According to the *Henry Draper Catalogue*, the star HD 153882 is of spectral type A0p and magnitude 6.16. It is remarked that "the K line is very faint. Lines (of *Si* II) λ 4128.1 and λ 4131.1 are strong, also several at about λ 4173." Since these peculiarities are characteristic of a star with a strong magnetic field, it was observed with the polarizing analyzer at the Mount Wilson Observatory in July, 1948. The first plate gave evidence of a magnetic field of a few kilogauss at the pole, and additional plates soon showed that the intensity and polarity of the field varied, probably with a period of a few days.[1] Observations were continued in the ensuing years.

All plates were taken with the double polarizing analyzer and the coudé spectrograph of the 100-inch telescope, with the exception of one plate of 1952 taken with the 200-inch telescope. The plates of 1948–1949 were all of dispersion 10.2 A/mm, while several of 1950–1951 have a dispersion of 4.5 A/mm, and the plate of 1952 is of 2.3 A/mm. The technique of observation and reduction of the spectrograms is essentially the same as that described for HD 125248.[2] The declination of HD 153882 is +15°, and the optical compensator for the phase shift of the oblique coudé flat mirror was therefore used as for α^2 Canum Venaticorum and other northern stars.

THE SPECTRUM

The spectrum of HD 153882 is in many respects similar to that of α^2 CVn near *Cr* maximum.[3] Both have a sharp, weak K line, and the hydrogen lines have rather strong central cores with broad wings. Metallic lines are fairly numerous, but the excitation of

---

* The investigation presented here was carried out while Miss Gjellestad was the holder of an International Study Grant 1951–1952 from the American Association of University Women (A.A.U.W.). Miss Gjellestad wishes to express her grateful thanks to A.A.U.W. for the fellowship and to the Mount Wilson and Palomar Observatories for the privilege of studying the observational material of magnetic stars as a guest investigator.

[1] H. W. Babcock, *Pub. A.S.P.*, **61**, 226, 1949.

[2] H. W. Babcock, *Ap. J.*, **114**, 1, 1951.

[3] H. W. Babcock and S. Burd, *Ap. J.*, **116**, 8, 1952. References to earlier work on the spectrum of α^2CVn will be found in this paper.

HD 153882 appears to be slightly lower, with stronger lines of *Fe* I and weaker lines of *Si* II. In this star, *Cr* I and *Cr* II are judged to be stronger than in α^2 CVn, but we have not identified in it with certainty any lines of the rare earths, so numerous in the latter near *Eu* II maximum. Lines of *Mn* I are fairly strong (more intense than in α^2 CVn) but are broader and shallower than most. *Ti* II is present with about the same intensity in the two stars. The unidentified line at approximately λ 4188.8, which has been found in α^2 CVn by Struve and Swings,[4] and in β CrB by W. A. Hiltner, [5] is also present in HD 153882. A questionable line at λ 4206.3 may be due to *Mn* II. Two lines at λ 4177.7 and λ 4384.3 appear to be predicted lines of *Fe* II.

The metallic lines are slightly less shallow in HD 153882 than in α^2 CVn but are of about the same width. A little rotational broadening is probably present. Measurements of line widths yield an approximate upper limit of 10 km/sec for $v_e \sin i$. If the star is rotating with an equatorial velocity v_e of the order of 100 km/sec, typical of type A0, the axis of rotation makes an angle i with the line of sight of about 6°.

HD 153882 is thus characterized by abnormal line intensities, and the spectrum is properly classified as peculiar. A careful visual comparison of the plates produced no evidence of changes in line intensities, however; this is particularly noteworthy, as the star exhibits alternating magnetic polarity of about the same amplitude and period as α^2CVn, an outstanding spectrum variable.

The plates of 1950–1951 with a dispersion of 4.5 A/mm were chosen for measurement, together with two plates having a dispersion of 10.2 A/mm, to give sufficient data for a magnetic curve. The first two plates of 1948, two of 1949, and the plate of 1952 were also measured later for refinement of the period. The best lines were measured for determination of the magnetic field-intensity and for radial velocity, blends being avoided as far as possible. Occasional measures of lines later identified as probable blends of the same element were retained for determination of the magnetic field, but not for velocity, and only if the z-values were nearly the same for the two contributors. Later the best plates were remeasured for identification of other elements represented by weaker and shallower lines.

Table 1 lists results of twenty spectrograms. The date of each observation (U.T.) is given, as well as phase in days and fraction of the period. Also the dispersion and the type of emulsion are given, when this was not the Eastman II*a*-O.

The polar magnetic field H_p is given for all plates by elements, but radial velocities are not listed for the plates of lower dispersion. Four plates (Ce 5242, 5250, 5656, and 5661) were measured for Zeeman effect only, and identification and reduction were made by comparison with the results obtained from Ce 6371 and 6386.

The probable error in the magnetic field-intensities is less than 500 gauss, and in radial velocities is between 0.2 and 0.4 km/sec, when a sufficient number of lines were available.

The mean magnetic field and the mean velocity given in the table are means from measurements of the best lines, mainly those of *Fe* I, *Fe* II, *Cr* I, *Cr* II, *Ca* II (K), *Mg* II λ 4481, and occasionally a single line of another element. The average number of thirty lines measured for Zeeman effect on each plate is less than for HD 125248 and α^2 CVn because of the quality of the spectrum, and the measuring was more difficult because of the width and shallowness of the lines.

All plates were measured and reduced by Miss Gjellestad.

THE MAGNETIC FIELD

The magnetic data of Table 1 indicate that the field of HD 153882 varies periodically. The following elements were derived:

$$\text{Maximum positive field} = \text{JD } 2432754.826 + 6.005E\,.$$

---

[4] *Ap. J.*, **98**, 361, 1943.

[5] *Ap. J.*, **102**, 438, 1945.

TABLE 1

Magnetic and Velocity Measurements at Various Phases

	No. of Lines	Element	H_p (Gauss)	No. of Lines	v (Km/Sec)
Coudé 5242					
1948 July 24.262	9	*Fe* I, II	−3500	…	…
1.936*d*, 0.32*P*	8	*Cr* I, II	−3450	…	…
	1	*Mg* II	−2650	…	…
10.2 A/mm	1	*Ca* II	−3850	…	…
	23	Mean	−3400	…	…
Coudé 5250					
1948 July 25.241	9	*Fe* I, II	−3400	…	…
2.915*d*, 0.49*P*	8	*Cr* I, II	−3800	…	…
	1	*Mg* II	−3550	…	…
10.2 A/mm	1	*Ca* II	−3850	…	…
	22	Mean	−3550	…	…
Coudé 5656					
1949 June 8.372	9	*Fe* I, II	−3850	…	…
2.781*d*, 0.46*P*	7	*Cr* I, II	−4150	…	…
	1	*Mg* II	−3550	…	…
10.2 A/mm	1	*Ca* II	−7700	…	…
	22	Mean	−3950	…	…
Coudé 5661					
1949 June 9.351	15	*Fe* I, II	−3350	…	…
3.760*d*, 0.63*P*	8	*Cr* I, II	−3950	…	…
	1	*Mg* II	−3550	…	…
10.2 A/mm	1	*Ca* II	−5800	…	…
	29	Mean	−3600	…	…
Coudé 6249					
1950 May 29.361	6	*Fe* I, II	−4200	5	−31.9
3.475*d*, 0.58*P*	8	*Cr* I, II	−3550	5	−33.2
	1	*Mg* II	−4650	1	−30.6
4.5 A/mm	1	*Ca* II	−3400	1	−31.4
	22	Mean	−3750	10	−32.5
Coudé 6256					
1950 May 30.378	1	*Mg* II	0	1	−30.9
4.492*d*, 0.75*P*	1	*Ca* II	+1700	1	−30.9
(cross-over)					
4.5 A/mm	12	Mean	+ 250	8	−33.4
Coudé 6264					
1950 May 31.387	11	*Fe* I	+3450	8	−36.2
5.501*d*, 0.92*P*	10	*Fe* II	+3100	8	−35.1
	12	*Cr* I, II	+3700	9	−35.7
4.5 A/mm	1	*Mg* II	+3900	1	−30.9
	1	*Ca* II	+4250	1	−33.8
	5	*Mn* I	+3350	5	−40.0
	46	Mean	+3450	30	−36.4
Coudé 6348					
1950 July 2.326	10	*Fe* I, II	−2500	7	−31.3
1.410*d*, 0.23*P*	7	*Cr* I, II	−2500	4	−31.7
(cross-over)	1	*Mg* II	−2350	1	−31.9
4.5 A/mm	1	*Ca* II	−2550	1	−29.9
	23	Mean	−2450	11	−31.4

TABLE 1—*Continued*

	No. of Lines	Element	H_p (Gauss)	No. of Lines	v (Km/Sec)
Coudé 6352					
1950 July 3.267	1	*Mg* II	−3900	1	−28.9
2.351*d*, 0.39*P*	1	*Ca* II	−3400	1	−29.2
4.5 A/mm	22	Mean	−3950	12	−32.4
Coudé 6367					
1950 July 26.281	14	*Fe* I, II	−2300	13	−31.7
1.345*d*, 0.22*P*	1	*Mg* II	−2700	1	−31.6
(cross-over)	1	*Ca* II	−2550	1	−28.2
4.5 A/mm	26	Mean	−2300	18	−31.9
Coudé 6371					
1950 July 27.285	14	*Fe* I, II	−3700	....	....
2.349*d*, 0.39*P*	7	*Cr* I, II	−4200	....	....
	1	*Mg* II	−3550	....	....
10.2 A/mm	1	*Ca* II	−3850	....	....
	27	Mean	−3800	....	....
Coudé 6376					
1950 July 28.288	12	*Fe* I	−2700	7	−31.3
3.352*d*, 0.56*P*	9	*Fe* II	−2850	10	−30.8
	16	*Cr* I, II	−3150	9	−32.3
4.5 A/mm	1	*Mg* II	−2350	1	−28.1
	1	*Ca* II	−2550	1	−31.0
	45	Mean	−2850	26	−31.4
Coudé 6386					
1950 July 30.280	20	*Fe* I, II	+3800	....	....
5.344*d*, 0.89*P*	8	*Cr* I, II	+3850	....	....
	1	*Mg* II	+3550	....	....
10.2 A/mm	1	*Ca* II	+3850	....	....
	33	Mean	+3850	....	....
Coude 7031					
1951 May 20.408	12	*Fe* I	+4300	11	−37.2
5.227*d*, 0.87*P*	6	*Fe* II	+3100	7	−36.1
	13	*Cr* I, II	+3650	8	−36.4
4.5 A/mm	1	*Mg* II	+3900	1	−30.1
	1	*Ca* II	+5100	1	−31.7
103-O					
	38	Mean	+3700	27	−36.7
Coudé 7060					
1951 May 27.417	13	*Fe* I	+4400	11	−32.7
0.226*d*, 0.04*P*	12	*Fe* II	+4500	11	−32.3
	12	*Cr* I, II	+4600	6	−32.6
4.5 A/mm	1	*Mg* II	+4700	1	−31.4
	1	*Ca* II	+5100	1	−30.7
103-O	4	*Mn* I	+3600	4	−34.2
	2	*Ti* II	+2650	3	−28.5
	1	*Si* II	+6800	2	−30.5
	47	Mean	+4400	28	−32.5
Coudé 7066					
1951 May 28.455	8	*Fe* I	− 100	6	−31.9
1.264*d*, 0.21*P*	12	*Fe* I, II	0	10	−31.7
(cross-over)	6	*Cr* I, II	−1300	5	−32.0
4.5 A/mm	1	*Mg* II	−1550	1	−32.4
	1	*Ca* II	0	1	−31.9
103-O					
	26	Mean	− 400	15	−31.8

TABLE 1—*Continued*

	No. of Lines	Element	H_p (Gauss)	No. of Lines	v (Km/Sec)
Coudé 7068					
1951 June 14.305	16	*Fe* I	+4700	10	−32.2
0.099*d*, 0.02*P*	10	*Fe* II	+4600	9	−32.2
	14	*Cr* I, II	+4600	7	−32.7
4.5 A/mm	1	*Mg* II	+5450	1	−30.8
	1	*Ca* II	+4250	1	−30.1
103-O	4	*Mn* I	+3050	4	−34.7
	2	*Si* II	+3200	2	−33.2
	3	*Ti* II	+2850	3	−27.4
	50	Mean	+4550	26	−32.3
Coudé 7072					
1951 June 15.310	7	*Fe* I, II	+1900	5	−30.7
1.104*d*, 0.18*P*	1	*Mg* II	0	1	−31.1
(cross-over)	1	*Ca* II	−2550	1	−31.5
4.5 A/mm	16	Mean	+ 900	7	−31.0
103-O					
Coudé 7129					
1951 July 21.262	1	*Mg* II	0	1	−29.7
1.026*d*, 0.17*P*	1	*Ca* II	0	1	−29.9
(cross-over)					
4.5 A/mm	11	Mean	+ 400	6	−30.1
Pa 345 a, b:					
1952 May 12.356	15	*Fe* I	−4000	15	−32.8
2.875*d*, 0.48*P*	9	*Fe* II	−4300	10	−31.8
	15	*Cr* I, II	−3750	15	−33.0
2.3 A/mm	1	*Mg* II	−2350	1	−30.8
	1	*Ca* II	− 450	1	−30.3
103-O	47	Mean	−3850	40	−32.6

In Figure 1 the mean magnetic field is plotted according to these elements. A smooth curve has been drawn in to represent these observations as closely as possible. This is subject to improvement when further observations become available. The relatively sharp positive and flat negative loops and the rapid change through zero mean field appear to be well established.

In Figure 2 the magnetic field as measured for different elements has been plotted in the period of 6.005 days. *Fe* I and *Fe* II have been plotted separately when sufficient lines were available, and together for plates with fewer lines. *Cr* I and *Cr* II have been plotted together. The smooth curve of Figure 1 has been reproduced for comparison. Results from other elements are of relatively low weight and therefore have not been plotted here.

RADIAL VELOCITIES

In Figure 3 a weighted mean of radial velocities, mainly for *Fe* I, *Fe* II, *Cr* I, and *Cr* II, for plates of dispersion 4.5 A/mm and for one plate of dispersion 2.3 A/mm has been plotted in the period of 6.005 days established by the magnetic measurements. The number of plates as well as number of lines measured on each plate is less than for the corresponding mean magnetic field. It is of significance that the elements mentioned are in good

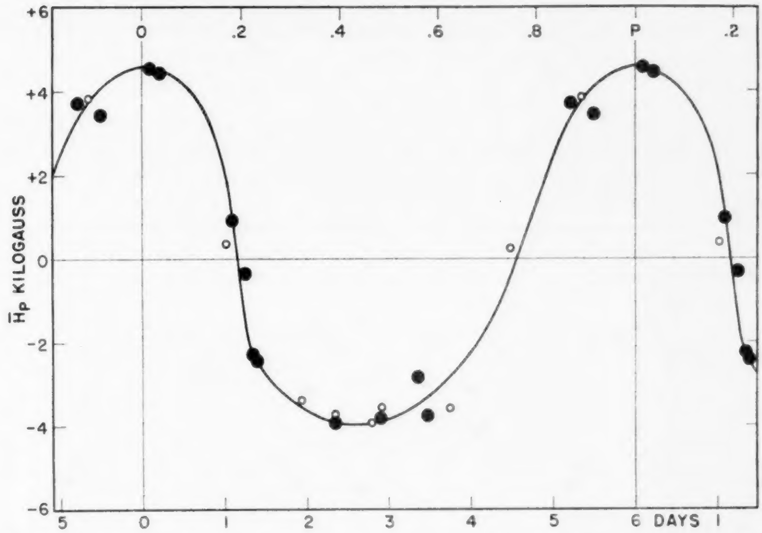

FIG. 1.—Magnetic field intensity at the pole, H_p, in kilogauss, plotted in the period of 6.005 days. The points are mean values mainly from *Fe* I, *Fe* II, *Cr* I, *Cr* II, *Ca* II (K) and *Mg* II λ 4481. Small open circles represent points of low weight.

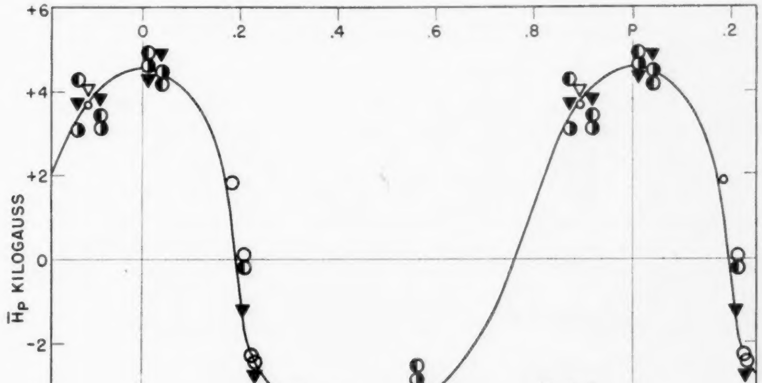

FIG. 2.—Similar results for the individual elements *Fe* I and *Fe* II (*Fe* I and II plotted together when fewer lines were available), and for *Cr* I and *Cr* II. The smooth curve from Fig. 1 has been reproduced for comparison.

accord as regards velocity. If any real systematic differences occur, they are only slightly larger than the probable error of measurement. It is quite possible that the velocities of *Ca* II, *Mg* II, and *Sr* II differ from the mean curve, but unfortunately each of these elements is represented by only one useful line.

The result that *Cr* and *Fe*, at least, give accordant velocities and that no variations in line intensities have been observed in HD 153882 is in interesting contrast to α^2 CVn, in which the elements (including *Cr*) that show the greatest fluctuations in line intensity show correspondingly peculiar velocity-curves.[4,3]

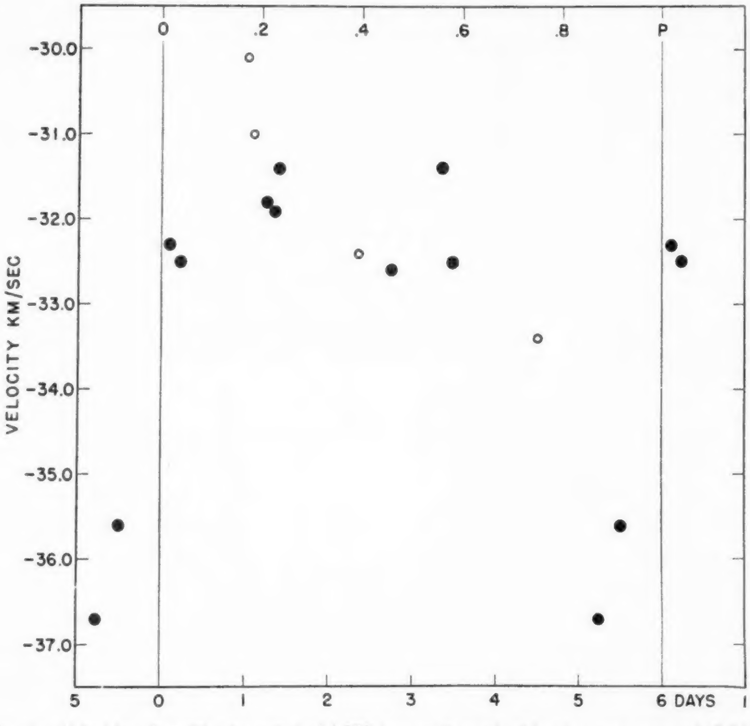

FIG. 3.—Velocities plotted in the period of 6.005 days as determined by the mean magnetic field. The points are values mainly from *Fe* I, *Fe* II, *Cr* I, and *Cr* II. Small open circles represent points of low weight.

LINE PROFILES—CROSS-OVER EFFECT

As has already been mentioned, a careful visual comparison of plates at various phases has revealed no definite changes in total intensity of any lines. The processes acting in HD 125248 and in α^2 CVn to produce the striking out-of-phase intensity changes of the rare-earth and chromium lines appear to be ineffective in HD 153882. Another smaller effect on line intensities must occur in this star, but it may be essentially constant. This is the small but perceptible Zeeman broadening of lines to a degree depending upon pattern width in a field of 4 kilogauss. Provided that the line is on the "flat" portion of the curve of growth, this broadening leads to an increase in total absorption.[6] Precise microphotometry of the spectrum at the cross-over phases and at maximum magnetic field should be carried out, to determine, if possible, whether the field is reversed by a systematic change in direction of the magnetic vector over the surface (the magnetic intensity remaining constant) or whether the field intensity of all points actually passes through zero and reverses.

---

[6] H. W. Babcock, *Ap. J.*, **110**, 126, 1949.

On spectrograms taken at phases apart from the two cross-over points, the profile of any given line is essentially identical in the two adjacent spectra analyzed for circular polarization of opposite sign. However, on six plates taken near phases 0.2 and 0.75, where the effective field in the line of sight is relatively small and is passing rapidly through zero, a cross-over effect rather similar to that previously found in HD 125248 and in α^2 CVn was noted. The effect, which takes slightly different forms in various lines, is best seen on Ce 6256 at phase 0.75. In many of the strong and intermediate lines, there is a tendency for the lines in the spectrum analyzed for left-handed circular polarization to split into two components, while the same lines in the dextrogyrate spectrum remain single but become slightly sharper and deeper. In other lines the effect takes the less extreme form, as described for HD 125248 and α^2 CVn, with a broadening but no splitting in the levogyrate spectrum. In Figure 4 is reproduced a direct-intensity tracing of Ce 6256 in the region λλ 4269–4277 which shows the doubling for *Fe* II λ 4273. Although the effect is not seen in all lines on this plate, it is rather systematic. While the existence and order of magnitude of the changes in the polarized line profiles are evident from the present series of plates, the proper analysis of these profiles will have to await microphotometry of superior spectrograms taken on fine-grain emulsions with the highest available dispersion.

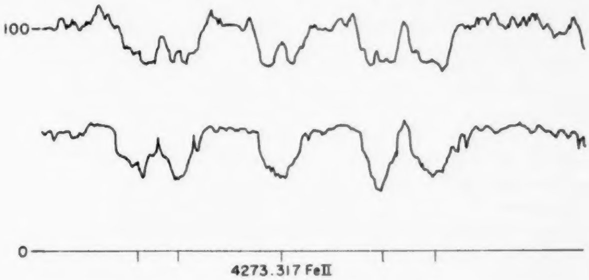

FIG. 4.—Direct-intensity tracing of Ce 6256 at phase 0.75 in the region λλ 4269–4277. Upper tracing is from the levogyrate polarized spectrum, while the lower tracing is from the dextrogyrate spectrum. The lines are, from left to right: *Fe* I λ 4271.159, *Fe* I λ 4271.764, *Fe* II λ 4273.317 (note doubling), *Cr* I λ 4274.803, and *Cr* II λ 4275.57. The base line for zero intensity refers to the upper tracing and shows the shallowness of the lines.

On five other plates, taken at phases 0.17–0.23, a similar effect of opposite sign is found. On some of these plates only a few lines are with certainty seen to be affected, but this may be due to the fact that not all were taken at the most favorable phase or under optimum conditions.

The cross-over effect can, in principle, be interpreted as proposed for HD 125248[2], i.e., as a combination of Doppler effect and Zeeman effect from two more or less distinct areas on the surface of the star that are characterized by a small difference in sight-line velocity and by opposite magnetic polarity. For maximum sharpness of the "narrow" profiles in the cross-over effect, we have the relation $H = 790\, v/z$ gauss, where z is the blended width of the Zeeman pattern in terms of the normal triplet. Whether the "broad" profiles observed with the analyzer are merely widened or actually doubled then depends upon z, H, and v, as well as on the intrinsic half-width.

The sign of the cross-over effect in HD 153882 is such that near the descending node of the magnetic curve (phase 0.2) the portion of the stellar surface characterized by positive magnetic polarity has, relative to the rest of the surface, a positive velocity in the line of sight. As in previous papers, positive magnetic polarity is taken to mean that the magnetic vector is directed toward the observer.

VARIATIONS IN LIGHT OF THE SPECTRUM VARIABLES 73 DRACONIS AND IOTA CASSIOPEIAE*

Sanford S. Provin
Yerkes Observatory

Received July 30, 1952

ABSTRACT

Photoelectric observations of the spectrum variables 73 Draconis and ι Cassiopeiae indicate that both vary in total light. For these stars, the amplitude at $\lambda_{\text{eff}} \sim 5500$ A is greater than the amplitude at $\lambda_{\text{eff}} \sim 4400$ A. The visual amplitudes are 0.04 and 0.03 mag., respectively.

Spectrum variables of type A belong to the group of peculiar A stars which have been the object of a number of investigations during the last forty years. In these studies the spectrum has been the main feature of investigation. However, the total light has also been examined in the case of three spectrum variables, viz., α^2 Canum Venaticorum,[1,2,3] HD 125248 = BD − 18°3789,[4] and ϵ Ursae Majoris.[5] At this time, in view of the discovery by Babcock that peculiar A stars usually have large magnetic fields associated with them, it is concluded that further study of the total light of peculiar A stars and, in particular, of spectrum variables should be undertaken. The present paper is concerned with results obtained, up to now, on the two spectrum variables, 73 Draconis and ι Cassiopeiae.

The observations presented here were made with the photometer of the 12-inch refractor of the Yerkes Observatory. The amplifier of this photometer is of the M.I.T. type.[6] An RCA 1P21 multiplier is the light-sensitive element.

Observations were made at two effective wave lengths: $\lambda \sim 5500$ A, isolated by a Corning 3384 filter, and $\lambda \sim 4400$ A, isolated by a Corning 5030 and a Schott GG-13 filter. The deflections during an observation were taken in the following order: blue, yellow, dark, yellow, blue. Two stars of approximately the same color as the variable were used for comparison. One comparison star was used for most of the observations in an evening, while the second comparison star was observed for approximately every fifth comparison.

In the reductions of the observations, mean extinction coefficients were used. This procedure was followed because of the uncertainties in the determination of extinction on any particular night. The mean extinction coefficients are:

$$f_B = 0.35 \text{ mag.}, \qquad f_Y = 0.24 \text{ mag.}, \qquad f_C = 0.11 \text{ mag.}$$

They were determined from extinction observations made on most of the nights on which the above stars were observed. Late B and early A stars were used for these determinations.

---

* Preliminary results were given at the Christmas meeting, 1951, of the American Astronomical Society (see *A.J.*, **57,** 24, 1952, for abstract of this report).

[1] Guthnick and Prager, *Veröff. Sternw. Berlin-Babelsberg*, **1,** 44, 1914.

[2] Tai, *M.N.*, **100,** 94, 1939–40.

[3] Nikonov and Brodskaya, *Bull. Abastumani Ap. Obs.*, **11,** 7, 1950.

[4] Stibbs, *M.N.*, **110,** 395, 1950.

[5] Guthnick, *Sitz. Preuss. Akad. Berlin*, No. 29, p. 657, 1931.

[6] See G. E. Valley, Jr., and H. Wallman, *Vacuum Tube Amplifiers* (New York: McGraw-Hill Book Co., Inc., 1948), p. 480, Fig 11.63, for the basic diagram of this amplifier.

73 DRACONIS

73 Draconis is designated as A2p in the *Henry Draper Catalogue*. Its visual magnitude is 5.18. The star is characterized by having *Sr* II λ 4077 strong, with lines of two groups of elements typified by *Cr* II and *Eu* II varying in intensity, out of phase, with a period of 20.27 days.[7,8]

Photoelectric observations were begun in September, 1951. Observations were made on thirteen nights between September 12, 1951, and November 27, 1951, with eight of the nights falling in one period. 76 Dra (A0; $5^{\mathrm{m}}69$) was used as the primary star for comparison with 73 Dra. It was chosen for its brightness and color, although it is about 8° from 73 Dra. During the period of the first eight observations, +75°778 (B9; $7^{\mathrm{m}}04$) was used as a second comparison star. It was chosen because of color and because the extinction correction between it and 76 Dra is approximately the same as between 73 Dra and 76 Dra. Beginning with the observation of October 25, HR 8112 (B9; $5^{\mathrm{m}}90$) was used as a second comparison star. The observations are given in Table 1. Only the comparison of visual magnitudes is given for 76 Dra and the other two comparison stars used. For the comparison of 73 Dra and 76 Dra, the visual, blue, and color-magnitude[9] differences are given, together with the date of observation and phase calculated according to the elements given by Durham.[8] The errors indicated are mean errors of the mean of the magnitude differences observed. The observations are plotted against phase in Figure 1.

TABLE 1

PHOTOMETRIC OBSERVATIONS OF 73 DRACONIS

DATE U.T. 1951	PHASE $P=20.27$	76 DRA − 73 DRA			+74°778 − 76 DRA	HR 8112 − 76 DRA
		Y	B	C		
Sept. 12.166	0.025	0.565 ± 0.003	0.491 ± 0.003	−0.075 ± 0.002	1.334	....
14.105	.120	.567 ± .006	.497 ± .008	− .069 ± .004	1.339	....
15.105	.170	.553 ± .003	.481 ± .006	− .073 ± .003	1.335	....
16.125	.220	.539 ± .007	.487 ± .007	− .057 ± .003	1.334	....
19.280	.376	.535 ± .003	.486 ± .004	− .049 ± .003	....	....
23.054	.562	.544 ± .005	.485 ± .004	− .057 ± .003	1.336	....
27.190	.766	.538 ± .003	.489 ± .007	− .047 ± .005	....	....
29.093	.860	.532 ± .003	.472 ± .003	− .060 ± .003	1.334	....
Oct. 25.043	.140	.557 ± .004	.483 ± .004	− .074 ± .004	1.339	0.147
Nov. 10.168	.936	.549 ± .003	.478 ± .005	− .073 ± .004	....	.144
11.222	.988	.561 ± .002	.486 ± .003	− .075 ± .002	....	.149
25.031	.669	.542 ± .003	.492 ± .004	− .049 ± .003	....	.144
27.030	0.768	0.533 ± 0.004	0.484 ± 0.005	−0.050 ± 0.003	....	0.145

The observations indicate that 73 Dra varies in visual light with an amplitude near 0.04 mag. There is also variation in blue light, but of smaller amplitude. The observations of color indicate a change in color amounting to 0.025 mag., with the star bluest at minimum light. Maximum light occurs near *Eu* II maximum intensity.

---

[7] Morgan, *Ap. J.*, **77**, 77, 1933.

[8] Geneva E. Durham, *Ap. J.*, **98**, 504, 1943.

[9] The colors referred to in this paper are natural photoelectric colors, i.e., the observed colors characteristic of our telescope, filter, and cell combination.

ι CASSIOPEIAE

In the *Henry Draper Catalogue*, ι Cassiopeiae ($4^{m}59$) is designated as A5p. In the spectrum of this star *Sr* II λ 4077 is strong. Variations in the intensity of the K line of *Ca* II were first pointed out by Morgan.[10] Deutsch[11] found the period of variation to be 1.740 days.

ι Cas has two companions, all three components having common proper motion. The nearer companion is at 2″, while the more distant companion is 7″ from the primary star. Both companions were included in the diaphragm when the observations were made. Their combined magnitude is 6.5.

Photoelectric observations were made on 20 nights (23 observational points), covering the period between September 12, 1951, and February 22, 1952. 48 Cas (A3; $4^{m}61$) was used as primary comparison star. This star is a $0''.7$ binary with no known peculiarities. As a second comparison star ω Cas (B8; $5^{m}03$) was used. This star is a known spectroscopic binary with a period of 69.9 days. It has turned out that the agreement between 48 Cas and ω Cas is not good over long periods.[12]

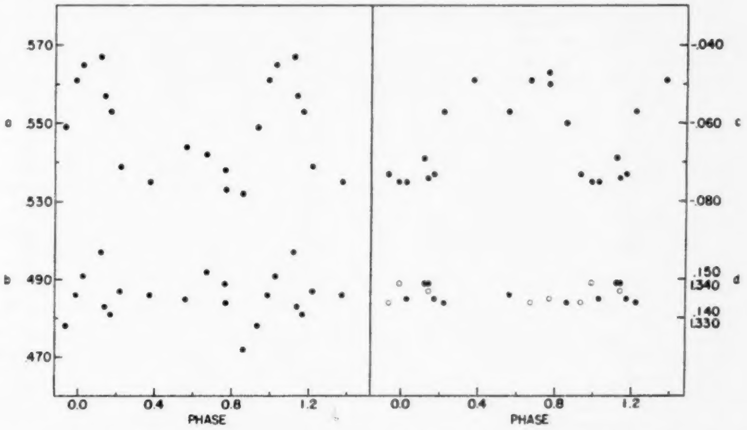

FIG. 1.—76 Dra–73 Dra: *a*, Comparisons at $\lambda_{\rm eff} \sim 5500$ A; *b*, comparisons at $\lambda_{\rm eff} \sim 4400$ A; *c*, comparisons of color; *d*, comparisons of 76 Dra with BD+75°778 (*filled circles*) and of 76 Dra with HR 8112 (*open circles*) at $\lambda_{\rm eff} \sim 5500$ A.

Table 2 gives the date of observation, together with the magnitude difference, 48 Cas *minus* ι Cas, for the visual, blue, and color observations. The comparisons of 48 Cas and ω Cas are also given for the visual magnitudes. Phases were calculated, using a period of 1.740 days, with the date of the first observation taken arbitrarily as zero phase. The observations are plotted against phase in Figure 2.

It is concluded that ι Cas varies in visual light with an amplitude of about 0.03 mag. In blue light the amplitude is approximately 0.015 mag.[13] The color change is 0.015 mag., and again the star is bluest at minimum light.

---

[10] *Pub. Yerkes Obs.*, **1**, 133, 1935.

[11] *Ap. J.*, **103**, 99, 1946.

[12] During those periods when the agreement is good, the same variation of ι Cas is indicated by the comparisons with both ω Cas and 48 Cas. It is therefore concluded that the magnitude of ω Cas is not constant.

[13] Since the two companions of ι Cas were included in the diaphragm, the true amplitudes are about 15 per cent larger.

TABLE 2

PHOTOMETRIC OBSERVATIONS OF ι CASSIOPEIAE

DATE U.T. 1951–52	PHASE P-1.740	48 CAS − ι CAS			(ω − 48)
		Y	B	C	
Sept. 12.264	0.000	0.026±0.004	0.054±0.005	0.029±0.004	....
15.229	.704	.042± .003	.056± .006	.014± .006	0.440
15.334	.764	.037± .005	.053± .006	.016± .005	.442
16.323	.332	.012± .004	.038± .006	.027± .004	.443
27.350	.670	.032± .006	.052± .006	.015± .003	.447
29.230	.751	.031± .002	.053± .006	.021± .006	.441
Oct. 10.375	.156	.023± .004	.043± .006	.022± .005	.436
Nov. 3.168	.830	.027± .004	.053± .008	.027± .008	.427
3.292	.901	.043± .003	.061± .005	.018± .005	.417
19.270	.084	.029± .002	.054± .002	.020± .003	.447
24.105	.437	.014± .002	.042± .003	.028± .002	.438
26.105	.587	.025± .002	.041± .005	.016± .002	.409
Dec. 10.092	.051	.045± .002	.058± .003	.014± .002	.450
Jan. 4.005	.368	.013± .002	.038± .003	.026± .002	.425
13.063	.574	.032± .002	.051± .002	.019± .002	.426
21.043	.160	.032± .002	.055± .002	.023± .002	.451
29.022	.746	.033± .001	.050± .001	.017± .001	.434
30.022	.321	.022± .001	.046± .002	.024± .002	.435
30.130	.383	.017± .001	.042± .002	.025± .001	.440
Feb. 9.042	.079	.039± .002	.053± .002	.014± .001	.436
12.034	.798	.031± .001	.050± .001	.019± .001	.434
17.083	.700	.036± .002	.052± .003	.014± .002	.439
22.038	0.548	0.024±0.001	0.045±0.001	0.021±0.001	0.433

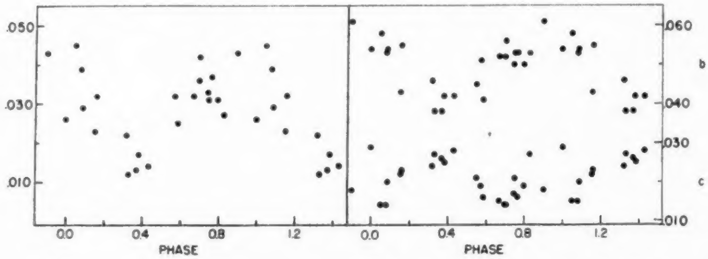

FIG. 2.—48 Cas − ι Cas: *a*, Comparisons at $\lambda_{\text{eff}} \sim 5500$ A; *b*, comparisons at $\lambda_{\text{eff}} \sim 4400$ A; *c*, comparisons of color.

At this time, the spectroscopic elements have not been checked, so that it is not known to what spectroscopic phase maximum light corresponds. However, the elements given by Deutsch[11] predict *Ca* II maximum intensity at phase 0.676, as given here.

In conclusion, I wish to thank Dr. W. A. Hiltner for a number of helpful suggestions and for supervising this work.

THE SPECTRA OF CERTAIN STARS WHOSE ATMOSPHERES MAY BE DEFICIENT IN HYDROGEN[*]

WILLIAM P. BIDELMAN
Yerkes and McDonald Observatories

Received August 27, 1952

ABSTRACT

Among the stars whose spectra show bands of the molecule C_2, there exist a number in whose spectra the hydrogen lines are abnormally weak or absent. These stars are of two types: the first consists of the variable stars of the R CrB class, while the second consists of stars of somewhat similar spectrum which have not yet been found to be variable. High-level lines of C I have long been known to be present in the spectrum of R CrB; a recent study of the visual region of the spectrum of that star at McDonald has shown that unusually strong high-level lines of O I and N I are also present. It is pointed out that the stars with abnormally weak hydrogen lines which have strong bands of C_2 show little or no evidence of the carbon isotope of mass 13; this contrasts with the ratio of $C^{12}:C^{13}$ of the order of 3:1 which McKellar has found to be common to the normal carbon stars. Two features in the spectrum of the R CrB variable star SV Sge are identified with "tail" bands of the Swan system of C_2.

I. INTRODUCTION

A number of peculiar stars are now known in whose spectra the lines of hydrogen are far weaker than in the spectra of normal stars of similar temperature, while the lines of other elements are not so affected. These objects are probably all of fairly high luminosity; in temperature they range from that of the hottest stars to approximately that of the sun, or somewhat cooler. The earliest in type of these apparently hydrogen-deficient stars are HD 160641[1] and HD 124448,[2] which show no indication of hydrogen lines in their spectra, although they are of O and B types, respectively. Other members of this group are the well-known peculiar star, υ Sgr,[3] and its lower temperature analogue, HD 30353.[4] Finally, the group contains a number of cooler objects which show molecular bands of C_2 in their spectra; these comprise the variable stars of the R CrB type and other stars of somewhat similar spectrum which are not known to be variable. The present paper concerns itself with certain features of the spectra of those apparently hydrogen-deficient stars which appear also to be rich in carbon.

II. THE "CARBON STARS" WHOSE ATMOSPHERES APPEAR TO BE DEFICIENT IN HYDROGEN

The stars observed by the writer which show an anomalous weakness of the hydrogen lines in their spectra and which also show C_2 bands are listed in Table 1. Apparent magnitudes (photographic when italic), galactic co-ordinates, radial velocities, and some notable spectroscopic characteristics of these stars are contained in the table.

The weakness of the hydrogen lines in the spectra of the stars of the R CrB type was first found in the case of the prototype by Ludendorff many years ago.[5] The absence of

[*] *McDonald Contributions*, No. 215.

[1] W. P. Bidelman, *Ap. J.*, **116**, 227, 1952.

[2] D. M. Popper, *Pub. A.S.P.*, **54**, 160, 1942; **58**, 370, 1946; and **59**, 320, 1947.

[3] J. L. Greenstein, *Ap. J.*, **91**, 438, 1940; and J. L. Greenstein and W. S. Adams, *Mt. W. Contr.*, No. 738; *Ap. J.*, **106**, 339, 1947.

[4] W. P. Bidelman, *Ap. J.*, **111**, 333, 1950.

[5] *A.N.*, **173**, 1, 1906.

*H*γ on his spectrograms represented the outstanding anomaly in its spectrum, which, in the region studied by him, otherwise resembled closely that of the F5 I*b* star α Persei. Some thirty years later Berman identified a number of strong lines in the photographic region of the spectrum of R CrB with lines of neutral carbon arising from 7.4 e.v. and concluded, on the basis of a curve-of-growth analysis of the spectrum, that carbon is by far the most abundant constituent of the atmosphere of that star.[6] Berman found no lines of oxygen or nitrogen in the region of the spectrum which he investigated and was consequently unable to determine the abundances of those elements. Recent observations at the McDonald Observatory of the visual region of the spectrum show that several lines of neutral oxygen arising from 10.7 e.v. are present in unusual strength in at least two stars of the R CrB type—R CrB itself and XX Cam.[7] Also present is the blend of *N* I lines near λ 6484 arising from 11.7 e.v., which is present in great strength in υ Sgr[8] and HD 30353. However, it is known that high-excitation lines of both *O* I and *N* I in the infrared region of the spectrum are greatly strengthened in the spectra of normal supergiant A- and F-type stars,[9] and undoubtedly a careful study by the method of model stellar atmospheres will be required to establish the true relative abundances of the elements *C*, *N*, and *O* in the R CrB stars.

TABLE 1

"CARBON STARS" APPARENTLY DEFICIENT IN HYDROGEN

Name	Apparent Magnitude	*l*	*b*	*V* (Km/Sec)	Spectroscopic Characteristics
R CrB[*]	5.8–<14	12	+50	+21	Weak C_2, strong *C* I, *O* I, and *N* I present; *He* I emission below maximum light[†]
XX Cam[*]	*8.7–10.3*	118	+ 2	+16	Weak C_2, strong *C* I, *O* I, and *N* I present[‡]
RY Sgr[*]	6.0–14.0	332	−21	......	Weak C_2, strong *C* I[§]
SU Tau[*]	9.5–16.0	157	− 3	......	Weak C_2, strong *C* I[§]
RS Tel[*]	*9.3–<13.0*	315	−15	......	Strong C_2, *CN*, and *C* I[‖]
HD 137613	7.4	310	+25	+55	Strong C_2, *CN*, and *C* I
HD 173409	9.2	331	−14	−65	Strong C_2, *CN*, and *C* I
HD 175893	9.3	335	−16	+42	Strong C_2, *CN*, and *C* I
HD 182040	7.0	354	−13	−47	Strong C_2, *CN*, and *C* I[#]
SV Sge[*]	*11.6–13.9*	18	+ 3	+ 4	Very strong C_2, strong *CN*

[*] Variable star of the R CrB type. Undoubtedly all of the R CrB stars show abnormally weak hydrogen lines.

[†] L. Berman, *Ap. J.*, **81,** 369, 1935; and G. H. Herbig, *Ap. J.*, **110,** 143, 1949.

[‡] W. P. Bidelman, *Ap. J.*, **107,** 413, 1948.

[§] C. P. Gaposchkin, *Harvard Bull.*, **903,** 35, 1936; and W. W. Morgan, *The Telescope*, **8,** 77, 1941.

[‖] Gaposchkin, *loc. cit.*

[#] W. C. Rufus, *Pub. Michigan Obs.*, **2,** 103, 1915; and A. McKellar and W. Buscombe, *Pub. Dom. Ap. Obs. Victoria*, **7,** 361, 1948.

The weak bands of C_2 which appear in the spectrum of R CrB have been considered as additional evidence of a high abundance of carbon in that star. Though these bands have not been found to strengthen appreciably when R CrB becomes fainter,[10] Espin's

---

[6] *Ap. J.*, **81,** 369, 1935.

[7] The writer has been informed by Dr. P. C. Keenan, of the Perkins Observatory, that he has also independently discovered strong high-excitation lines of neutral oxygen in the visual and infrared spectrum of R CrB.

[8] J. L. Greenstein, *Ap. J.*, **97,** 252, 1943.

[9] P. W. Merrill, *Mt. W. Contr.*, No. 486; *Ap. J.*, **79,** 183, 1934; see also P. C. Keenan and J. A. Hynek, *Ap. J.*, **111,** 1, 1950.

[10] G. H. Herbig, *Ap. J.*, **110,** 143, 1949.

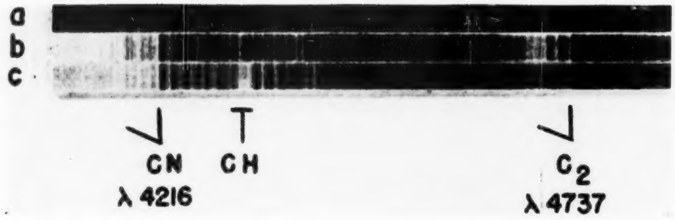

FIG. 1.—The photographic region of the spectrum of: *a*, R CrB; *b*, HD 182040; and *c*, the normal carbon star HD 156074. The absence of the *CH* bands in the spectrum of HD 182040 is evident.

visual observations indicate that considerable changes in their intensity can occur even during the maximum phase of this variable star.[11] In view of this fact, the existence of members of the R CrB class with considerably stronger C_2 bands than R CrB itself has is not surprising. RS Tel and SV Sge both show strong carbon bands, and also strong CN bands as well; in fact, the majority of the R CrB stars with known spectrum exhibit strong enough bands of C_2 and CN to be classified as of type R on low-dispersion spectrograms.

The four nonvariable stars of Table 1 make up an interesting group. These objects have spectra which resemble that of RS Tel. The temperature of these stars is probably somewhat lower than that of the stars showing the weaker carbon bands. Figure 1 shows the photographic region of the spectrum of one of these objects, HD 182040, along with that of R CrB, above, and that of the normal carbon star of type $C1_2$, HD 156074, below.[12] The absence of the CH bands in the spectrum of HD 182040 is very striking; it was first noted by R. H. Curtiss[13] and was later discussed at some length by Wurm.[14] Curtiss also first called attention to the abnormal weakness of the hydrogen lines in the spectrum of this star.[13] Recent McDonald observations show that the spectra of HD 137613, HD 173409, and HD 175893 are nearly identical with that of HD 182040. It may be significant that these four peculiar stars are all located in the general direction of the galactic center.

III. THE CARBON ISOTOPE RATIO IN THESE STARS APPARENTLY DEFICIENT IN HYDROGEN

Aside from the weakness or absence in their spectra of the hydrogen lines and the molecular bands of CH, the peculiar stars showing strong bands of C_2 appear to differ in another way from the normal carbon stars: this relates to the relative abundances of the carbon isotopes of masses 12 and 13. McKellar has found that the normal R-type stars show a surprisingly accordant value of the abundance ratio of C^{12} and C^{13} atoms, as inferred from the relative intensities of the $C^{12}C^{12}$, $C^{12}C^{13}$, and $C^{13}C^{13}$ molecular bands of the Swan system of C_2, of about 3 to 1.[15] Of fifteen stars studied by McKellar, only three objects gave an isotope ratio differing substantially from this value; all three of these stars are peculiar, two being members of the high-velocity group of carbon stars whose spectra are characterized by an excessive strength of the bands of CH,[16] while the other is HD 182040. In the case of these three stars, McKellar has found little or no evidence of the presence of the C^{13} isotope. For HD 182040 he has determined a lower limit of the ratio $C^{12}:C^{13}$ of 30:1.[15,17] Sanford has pointed out that another of the peculiar stars showing strong C_2 bands, HD 137613, also shows no evidence of the carbon isotope of mass 13.[18] Observations at McDonald of the other stars listed in Table 1 which show strong Swan bands are entirely in accordance with the results on these two stars. In no case are the isotope bands visible on spectrograms of dispersion 76 A/mm at $H\gamma$. The most striking example is that of the star SV Sge, in which the minimum isotope ratio may be estimated as of the order of 100:1.[19] For the peculiar stars which show weak carbon bands, it is not possible to give a value of the isotope ratio. However, it may be noted that Berman states that "there is no evidence that the bands due to the C_2 isotopes at 4745 and 4752 are present in the spectrum" of R CrB.[6]

---

[11] *M.N.*, **51**, 11, 1890.

[12] The type given is that in the system of Keenan and Morgan, *Ap. J.*, **94**, 501, 1941. In Sanford's catalogue (*Mt. W. Contr.*, No. 689; *Ap. J.*, **99**, 145, 1944) it is classified R0.

[13] *Pub. Michigan Obs.*, **2**, 182, 1916.

[14] *Naturwiss.*, **29**, 686, 1941.

[15] *Pub. Dom. Ap. Obs. Victoria*, **7**, 395, 1948.

[16] P. C. Keenan, *Ap. J.*, **96**, 101, 1942.

[17] A preliminary evaluation of this minimum ratio published by McKellar in *Pub. A.S.P.*, **48**, 216, 1936, was 43:1.

[18] *Pub. A.S.P.*, **52**, 203, 1940.

Further observations are desirable to check the generality of the high-isotope ratio indicated by these peculiar stars, but we may provisionally conclude that these stars differ from the normal carbon stars both in the apparent deficiency of hydrogen in their atmospheres and in the ratio of the numbers of carbon atoms of masses 12 and 13. The isotope ratio in these stars may equal, or even exceed, the terrestrial and meteoric value of about 90:1. We may note in passing that the value of this ratio in the solar atmosphere is also certainly larger than that found by McKellar for the normal carbon stars.[20]

IV. "TAIL" BANDS OF C_2 IN THE SPECTRUM OF SV SGE

The low-dispersion spectrogram of SV Sge obtained at the McDonald Observatory on September 19, 1951, shows in addition to very strong bands of the (1, 0) sequence of the Swan system of C_2, two fairly strong linelike features which have not been previously observed in stellar spectra. Their wave lengths have been measured as λ 4772.5 and λ 4839.0. It is probable that these two features are due to the (10, 9) and (11, 10) bands of the Swan system of C_2. These are two of the so-called "tail" bands of C_2 which have been studied in the laboratory by Phillips.[21] Their appearance in the spectrum of SV Sge is very similar to that in the laboratory spectra. According to the data given by Phillips, these bands arise from lower levels at 1.7 and 1.9 e.v.

These bands have not been certainly observed in cometary spectra; a possible occurrence of one of them is as the faint unidentified feature at λ 4772 in the extraordinary spectrum of Comet Morehouse as photographed by de la Baume Pluvinel and Baldet.[22] The vibrational temperature indicated by the C_2 molecules in this comet was exceptionally high, to judge from the relative intensities of the various bands of the (1, 0) sequence of the Swan system as estimated on the slit spectrograms obtained by Campbell and Albrecht.[23]

---

[19] The absence of the isotopic C_2 bands in the spectrum of SV Sge was first noted by the writer in the course of an examination of several spectrograms of R CrB stars which had been taken by members of the staff of the Mount Wilson Observatory. He is greatly indebted to Drs. I. S. Bowen and A. H. Joy for the privilege of examining these spectrograms.

[20] J. L. Greenstein, R. S. Richardson, and M. Schwarzschild, *Pub. A.S.P.*, **62**, 15, 1950.

[21] *Ap. J.*, **108**, 434, 1948.

[22] *Ann. Meudon*, **7**, 24, 1926.

[23] *Lick Obs. Bull.*, **5**, 58, 1908.

THE SOLAR SPECTRUM FROM λ 2285 TO λ 3000 A*

HAROLD E. CLEARMAN
Applied Physics Laboratory, Johns Hopkins University, Silver Spring, Maryland†

Received June 16, 1952

ABSTRACT

This paper presents measurements on the solar spectra previously obtained by Hopfield and Clearman. A complete wave-length list is given, together with a discussion of the element identifications. An intensity-curve is given covering the region λλ 2575–2900 A. Equivalent widths of several strong lines are estimated. A value of the *Mg/Ca* abundance ratio is calculated from a discussion of the emission lines in the center of the *Mg* II and *Ca* II resonance lines.

INTRODUCTION

The spectrum of the sun in the region below λ 3000 A has been obtained in "V-2" rocket flights by Hopfield and Clearman[1] and, independently, by a group of workers at the Naval Research Laboratory.[2] The present paper extends and revises the wave-length list given by Hopfield and Clearman. In addition, the present paper includes a detailed discussion of the identifications, element by element, intensity estimates of the lines, an intensity-curve of the spectrum, and a detailed discussion of the strongest *Mg* and *Si* lines. The apparatus used was described in the previous paper,[1] which also listed the spectra obtained and the corresponding altitudes.

WAVE-LENGTH MEASUREMENTS

The two films with best definition were remeasured on a large Gaertner comparator. The values agreed with the previous measurements to within 0.3 A. As in the previous work, iron lines in the solar spectrum itself were used as standards, an effort having been made to select the least blended lines. In plotting the correction-curve from the iron lines, an average scatter of 0.2 A was observed. This low precision is due to the combined effect of the low dispersion and the large amount of blending.

Table 1 lists the measured wave lengths of all absorption lines that could be measured in the solar spectrum. In addition to the wave lengths, listed in the first column, the second column gives eye estimates of the intensities; the third colume, the element or elements responsible for the lines; the fourth column, the laboratory wave length; and the fifth column, an arbitrary number designating the multiplet involved. The identifications will be fully described in a subsequent section.

On the films, the spectrum is detectable down to 2250 A, the shortest measurable wave length being 2284 A. In making the eye estimates, it was impossible to maintain a scale reliable over the entire range of wave lengths because of the great variation in over-all intensity. Therefore, these estimates are useful for comparing lines within a small range of wave length but are not to be considered as an extension of the Rowland scale into this wave-length region.

---

* Assisted by U.S. Navy Bureau of Ordnance under Contract NOrd 7386. Based on a dissertation submitted to the faculty of Princeton University in partial fulfilment of the requirements for the degree of Doctor of Philosophy.

† Present address: Hofstra College, Hempstead, N.Y.

[1] J. J. Hopfield and H. E. Clearman, *Phys. Rev.*, **73,** 877, 1948.

[2] W. A. Baum, F. S. Johnson, J. J. Oberly, C. C. Rockwood, C. V. Strain, and R. Tousey, *Phys. Rev.*, **70,** 781, 1946; E. Durand, J. J. Oberly, and R. Tousey, *Ap. J.*, **109,** 1, 1949.

TABLE 1

SOLAR LINES λλ 2280–3000 A

λ (Sun)	Int. (Sun)	Element	λ (Lab.)	Mul-tiplet No.
2284.9....	5w	*Fe* I	2284.1	26
			etc.	
2298.5....	5w	*Fe* I	2298.2	26
			etc.	
2313.3....	3	*Fe* I	2313.1	26
2316.3....	3	......	......	......
2320.1....	10w	*Fe* I	2320.4	26
2328.6....	5w	*Fe* II	2327.4	10
2332.2....	5w	*Fe* II	2331.3	9
		Fe II	2332.8	10
2338.2....	3w	*Fe* II	2338.0	10
2344.0....	3w	*Fe* II	2343.5	10
		Fe II	2344.0	9
		Fe II	2344.3	10
2348.2....	2	*Fe* II	2348.1	8
		Fe II	2348.3	10
2351.2....	1	*Fe* I	2350.4	27
2354.7....	3	*Fe* II	2354.5	......
		Fe II	2354.9	9
		Fe I	2355.3	27
2359.6....	10w	*Fe* II	2359.1	10
		Fe II	2360.0	9
		Fe II	2360.3	8
2364.3....	2	*Fe* II	2364.8	10
2367.2....	5	*Fe* II	2366.6	9
		Fe II	2366.9	11
		Fe II	2368.6	8
2370.4....	2	*Fe* II	2370.3	8
		Fe II	2370.5	9
		Fe I	2371.4	27
2374.0....	15w	*Fe* I	2373.6	27
		Fe II	2373.7	11
		Fe I	2374.5	27
		Fe II	2375.2	8
2377.8....	3	......	......	......
2382.1....	8	*Fe* I	2381.8	27
		Fe II	2382.0	11
		Fe II	2382.4	9
		Fe II	2383.1	11
		Fe II	2383.2	8
2384.5....	1	*Fe* II	2384.4	8
		Fe II	2385.0	9
2388.3....	3	*Fe* II	2388.6	11
2390.1....	0	*Fe* I	2390.0	27
2395.0....	8	*Fe* II	2395.4	11
		Fe II	2395.6	11
2399.2....	5	*Fe* II	2399.2	8, 11
2402.2....	1	*Fe* II	2402.6	8
2405.6....	8	*Fe* II	2404.4	11
		Fe II	2404.9	11
		Fe II	2406.7	11
2409.9....	3	*Fe* II	2410.5	11
2413.1....	3	*Fe* II	2413.3	11
2416.8....	2	......	......	......
2419.4....	1	......	......	......
2424.2....	10	*Fe* II	2424.1	......
2428.5....	5	......	......	......
2431.7....	5	......	......	......
2435.3....	10	*Fe* II	2434.9	......
		Si I	2435.2	7
2443.5....	3	*Fe* I	2443.9	......
2447.2....	5	*Fe* I	2447.7	10
2461.9....	10	*Fe* I	2462.6	10
2466.3....	1	*Fe* II	2466.7	......
		Fe II	2466.8	......
2469.5....	1	......	......	......
2472.6....	4	*Fe* I	2472.9	10
		Fe I	2472.9	10
		Fe I	2473.1	16
2475.7....	2w	......	......	......
2478.7....	5w	*C* I	2478.5	1
		Fe I	2479.8	10
2483.2....	5w	*Fe* I	2483.3	10
		Fe I	2484.2	10
2490.7....	10w	*Fe* I	2488.1	10
		Fe I	2489.8	10
		Fe I	2490.6	10
		Fe I	2491.2	10
2496.4....	1w	*Fe* I	2496.5	......
2498.4....	1w	*Fe* I	2498.9	16
2501.4....	5w	*Fe* I	2501.1	9
2506.3....	8w	*Si* I	2506.9	1
2508.9....	2	*Fe* II	2509.1	......
2511.4....	7	*Fe* I	2510.8	9
2514.1....	4	*Si* I	2514.3	1
2516.3....	4	*Si* I	2516.1	1
2519.3....	3	*Si* I	2519.2	1
2523.2....	5w	*Fe* I	2522.8	9
		Si I	2524.1	1
		Fe I	2524.3	9
2528.5....	5w	*Fe* I	2527.4	9
		Si I	2528.5	1
		Fe I	2529.1	9
		Fe I	2529.8	9
2532.3....	1w	*Si* I	2532.4	6
2541.2....	3w	*Fe* I	2541.0	9
2545.3....	3w	*Fe* I	2546.0	9
2549.1....	10w	*Fe* I	2549.6	9
2552.9....	2	*Fe* I	2552.6	16
		P I	2553.3	1
2555.5....	1	*P* I	2554.9	1
2557.3....	1	*Fe* II	2557.5	......
2560.3....	1w	*Fe* II	2560.3	......
2562.8....	8	*Fe* II	2562.5	6
		Fe II	2563.5	6
2567.8....	3d	*Fe* II	2566.9	6
		Al I	2568.0	2
		Si I	2568.6	5
2571.6....	3d	......	......	......

TABLE 1—*Continued*

λ (Sun)	Int. (Sun)	Element	λ (Lab.)	Multiplet No.
2575.6	10d	*Al* I	2575.1	2
		Al I	2575.4	2
		Fe I	2576.7	23
		Si I	2577.1	4
2582.6	3	*Fe* II	2582.6	6
2585.5	10w	*Fe* I	2584.5	23
		Fe II	2585.9	1
2588.2	2	......	......	......
2591.2	2	*Fe* II	2591.5	6
2593.8	3	*Fe* II	2593.7	6
		Na I	2593.8	3
		Na I	2593.9	3
		Fe I	2594.2	23
2598.9	20w	*Fe* II	2598.4	1
		Fe II	2599.4	1
		Fe I	2599.6	23
2606.3	15	*Fe* I	2605.7	22
		Fe I	2506.8	23
		Fe II	2507.1	1
2611.7	5	*Fe* I	2510.8	8
		Fe II	2611.1	6
		Fe II	2611.9	1
		Fe I	2612.8	8
2614.3	5	*Fe* II	2513.8	1
		Fe I	2614.5	23
2617.9	5	*Fe* II	2617.6	1
		Fe I	2618.0	23
		Fe I	2618.7	8
2620.6	1w	*Fe* II	2620.4	1
2622.2	1w	*Fe* II	2621.7	1
2623.7	1	*Fe* I	2623.4	8
		Fe I	2623.5	23
2625.8	3	*Fe* II	2625.7	1
2628.3	10	*Fe* II	2628.3	1
		Fe II	2628.6	......
2631.8	25	*Fe* II	2631.0	1
		Fe II	2631.3	1
		Ti I	2631.6	2
		Fe II	2631.6	......
2633.7	1	*Fe* II	2633.2	......
		V I	2633.6	3
2636.6	3w	*Fe* I	2635.8	23
		Fe I	2636.5	22
		Fe II	2636.7	......
2638.6	1	......	......	......
2641.1	10ws	*Ti* I	2641.1	2
		Fe II	2641.1	......
		Fe I	2541.6	21
2644.2	2	*Fe* I	2644.0	23
		Ti I	2644.3	2
2645.1	3	*V* I	2645.3	3
		Fe I	2645.4	8
2648.5	8w	*Fe* I	2647.6	8
		V I	2647.7	3
2651.4	3	*Fe* I	2651.7	22
		V I	2651.9	3
		Al I	2652.5	1
2653.8	2	......	......	......
2656.2	2w	*Fe* I	2656.1	......
		V I	2656.2	3
2658.4	3	*Fe* II	2658.3	......
2660.2	1	*Al* I	2660.4	1
		Fe I	2660.4	22
2661.8	3	*Fe* I	2661.2	21
		V I	2661.4	3
		Fe I	2662.1	21
2663.9	4	......	......	......
2666.6	5	*Fe* I	2666.4	21
		Fe II	2666.6	......
		Fe I	2666.8	14
2669.5	5	*Al* II	2669.1	1
2672.8	10	*Fe* I	2673.2	21
2675.5	0	*P* I	2675.3	2
2677.5	0	*P* I	2677.1	2
2678.9	10w	*Fe* I	2679.1	13
2680.7	2	*Na* I	2680.3	2
		Na I	2680.4	2
		Fe I	2680.5	21
2684.4	8w	*Fe* II	2684.8	......
		Fe I	2684.9	21
2688.0	1	*P* I	2688.0	2
2690.1	10w	*Fe* I	2689.2	14
		Fe I	2690.1	6
2692.7	3	*Fe* II	2692.6	......
		Fe I	2692.7	21
		Fe II	2692.8	5
2695.7	8	*Fe* I	2695.0	13
2697.8	3	*Fe* II	2697.5	......
2699.2	4	*Fe* I	2699.1	14
2701.9	5d	*Fe* I	2701.9	......
2704.0	5d	*Fe* II	2704.0	......
2705.8	2	......	......	......
2707.0	2	*Fe* I	2706.6	14
		Fe II	2707.1	......
2708.7	3	......	......	......
2710.2	1	......	......	......
2711.6	5	*Fe* I	2711.7	13
		Fe II	2711.8	......
2714.3	8	*Fe* II	2714.4	4
		Fe I	2714.9	14
		Fe II	2714.9	3
2716.0	2	*Fe* II	2716.2	......
		Fe II	2716.7	5

TABLE 1—*Continued*

λ (Sun)	Int. (Sun)	Element	λ (Lab.)	Multiplet No.
2719.1	5	*Fe* I *Fe* I	2718.4 2719.0	14 7
2721.0	5	*Fe* I *Fe* I	2720.5 2720.9	6 7
2723.7	4	*Fe* I	2723.6	7
2724.9	2	*Fe* II *Fe* I *Fe* I	2724.9 2725.0 2725.6	5 14 14
2727.8	8w	*Fe* II *Fe* II *Fe* I	2727.4 2727.5 2728.0	...... 4 13
2730.9	5w	*Fe* II *Fe* I	2730.7 2731.0	5 14
2733.8	10	*Fe* I *Fe* I *Fe* I	2733.6 2734.0 2734.6	12 14 13
2735.4	2	*Fe* I *Fe* I	2735.5 2735.6	12 ......
2737.2	10	*Fe* I *Fe* II *Fe* I	2737.0 2737.0 2737.3	15 4 7
2739.9	10	*Fe* II	2739.5	4
2742.3	8	*Fe* I *Fe* I *Fe* I *Fe* I	2742.0 2742.1 2742.3 2742.4	6 11 12 7
2743.9	10w	*Fe* II *Fe* I *Fe* I *Fe* I	2743.2 2743.6 2744.1 2744.5	5 13 7 12
2746.7	10w	*Fe* II *Fe* II *Fe* I	2746.5 2747.0 2747.0	5 4 11, 13
2749.9	15w	*Fe* II *Fe* II *Fe* II *Fe* I	2749.2 2749.3 2749.5 2750.1	4 5 4 7
2753.9	4	*Fe* I *Fe* I	2753.7 2754.0	12 13
2756.6	20	*Fe* II *Fe* I *Fe* I	2755.7 2756.3 2756.3	5 6 7
2759.9	8	*Fe* I	2759.8	13
2761.4	12	*Fe* I *Fe* II *Fe* I	2761.8 2761.8 2762.0	12 4 12
2764.3	3	*Fe* I	2764.3	......
2766.5	8	*Fe* I *Fe* I	2766.9 2767.5	13 12
2769.3	10	*Fe* II *Fe* I	2768.9 2769.7	4 20
2773.4	8	......	......	......
2774.9	1w	*Fe* II *Fe* I	2774.7 2774.7	 12
2776.6	2	*Mg* I	2776.7	3, 5
2778.3	1w	*Fe* I *Mg* I	2778.2 2778.3	20 3, 5
2779.9	1w	*Fe* II *Mg* I	2779.3 2779.8	 5
2781.3	2w	*Mg* I *Fe* I	2781.4 2781.8	3, 5 12
2783.5	3w	*Mg* I *Fe* II	2783.0 2783.7	5 ......
2785.7	2w	......	......	......
2788.8	1w	*Fe* I	2788.1	20
2791.1	1w	......	......	......
2792.5	1w	*Fe* I	2792.4	......
2795.6	10000	*Mg* II	2795.5	1
2802.9	5000	*Mg* II	2802.7	1
2813.3	3w	*Fe* I	2813.3	20
2817.5	5w	*Fe* I	2817.5	20
2820.0	1w	*Fe* I	2820.8	4
2822.7	3w	......	......	......
2825.8	4w	*Fe* I *Fe* I *Fe* I	2825.6 2825.7 2826.0	11 5 5
2828.3	2w	*Fe* I *Fe* I	2827.9 2828.8	5 11
2830.5	2	......	......	......
2832.3	3	*Fe* I	2832.4	20
2836.0	10	*Fe* I *Fe* II	2835.5 2835.7	4 ......
2838.3	3	*Fe* I	2838.1	20
2840.6	5w	*Fe* I *Fe* II *Fe* II	2840.4 2840.6 2840.8	4 ....
2843.5	8	*Fe* I *Fe* I *Fe* I	2844.0 2843.6 2843.9	20 19 4
2845.6	1	*Fe* I	2845.6	19
2847.9	1	*Fe* II	2848.0	......
2852.2	1000	*Mg* I	2852.1	1
2854.2	2	*V* I *V* I	2853.8 2854.1	2 2
2856.9	2	......	......	......
2858.8	3	*Ti* II *Fe* I *V* I	2858.4 2858.9 2859.0	3 4 2
2860.1	1	......	......	......
2861.0	2	*Fe* II	2861.2	3
2862.4	1	*V* I *Fe* I	2862.4 2862.5	2 19
2863.6	1	*Ni* II *Fe* I	2863.7 2863.9	1 4

TABLE 1—*Continued*

λ (Sun)	Int. (Sun)	Element	λ (Lab.)	Multiplet No.
2865.3	5	......	......	......
2867.4	5	*V* I *Fe* I	2867.0 2867.3	2 ......
2869.3	10s	*Ti* II *Fe* II *V* II *Fe* I	2868.7 2868.9 2869.0 2869.3	2 3 2 4
2871.0	1	*Fe* II	2871.1	......
2873.2	1	*Fe* II	2873.4	......
2873.9	5	*Fe* I	2874.2	4
2876.4	5	*O* I *Fe* II *Fe* I	2876.3 2876.8 2877.3	1 25
2879.0	5	*O* I *V* II	2879.0 2879.2	1 2
2881.7	500	*Si* I	2881.6	2
2883.9	4	*Fe* II *O* I *V* II	2883.7 2883.8 2884.8	...... 1 2
2886.2	1	*Fe* II *Fe* I	2886.2 2886.3	....
2888.0	1	*V* I *Fe* II *V* I *Ti* II	2887.7 2888.1 2888.5 2888.9	1 ...... 1 2
2889.6	1	*V* II *Fe* I	2889.6 2889.9	2 ......
2891.4	2	*Ti* II *Fe* I *V* II	2891.1 2891.4 2891.6	2 2
2893.1	2	*V* II *Fe* II *V* II *Fe* I	2892.7 2892.8 2893.3 2893.8	2 3 2 19
2894.7	4	*Fe* I *V* I *Fe* II	2894.5 2894.4 2894.8	...... 1 ......
2896.5	1	*Ti* II	2895.8	1
2897.8	2	......	......	......
2899.5	2	*V* I *Fe* I *V* I	2899.2 2899.4 2899.6	1 1
2900.3	1	......	......	......
2902.3	8	*Ti* II *Fe* II *Mg* I	2901.9 2902.3 2902.9	1 6
2904.2	1	*V* I	2904.1	1
2906.3	1	*V* I *Mg* I *V* II	2906.1 2906.4 2907.5	1 6 1
2908.1	1w	*Fe* II *V* II	2907.9 2908.8	2 2
2909.4	0	*Fe* I *Ti* II	2909.3 2909.9	 1
2910.8	1	*V* II	2911.1	1
2912.2	2	*Fe* I *Fe* I	2912.2 2912.3	2 25
2913.9	1w	*Ni* II *Fe* I	2913.6 2914.3	1 ......
2915.5	3	*V* I *Fe* II	2914.9 2916.2	1 2
2917.9	3	*Fe* II *Fe* I	2917.5 2818.0	3 ......
2919.5	1	......	......	......
2920.1	0	*V* II *Fe* I	2920.4 2920.7	1 ......
2921.0	1	......	......	......
2922.0	1	*Fe* II *Fe* I	2922.0 2922.4	 25
2923.5	2	*Fe* I *V* I *Fe* I	2923.3 2923.6 2923.9	...... 1 ......
2924.4	2	*V* II *V* II	2924.0 2924.6	1 1
2925.7	5s	*Mn* I *Fe* II	2925.6 2926.6	1 2
2928.9	8	*Mg* II *Fe* I	2928.6 2929.0	2 2
2930.5	2	*V* II	2930.8	1
2931.6	3	......	......	......
2933.2	3w	*Mn* II	2933.1	1
2934.6	2w	*V* II	2934.4	1
2937.0	10*l*	*Mg* II *Mg* I *Fe* I	2936.5 2936.7 2936.9	2 2 2
2939.3	5	*Mn* II *Fe* II	2939.3 2939.5	1 2
2941.5	10w	*Fe* I *V* II *V* II *Mg* I	2941.3 2941.4 2941.5 2942.0	2 1 1 2
2944.7	10w	*Ni* I *Fe* II *V* II *Fe* II	2943.9 2944.4 2944.6 2945.3	1 7 1 2
2947.9	10	*Fe* II *Fe* I	2947.7 2947.9	7 2
2949.4	8	*Fe* II *Mn* II	2949.2 2949.2	 1
2951.2	1w	*V* II	2950.3	1
2952.3	0	*V* II	2952.1	1

TABLE 1—*Continued*

λ (Sun)	Int. (Sun)	Element	λ (Lab.)	Multiplet No.
2954.0	10	*Fe* II	2953.8	2
		Fe I	2953.9	2
2957.3	10s	*Fe* I	2957.4	2
		V II	2957.5	1
2959.9	5	*Fe* II	2959.6	......
2961.4	4	*Fe* II	2961.3	2
2962.4	0	*Fe* I	2962.1	24
2963.7	1	......	......	......
2965.3	4	*Fe* II	2964.6	2
		Fe II	2965.0	7
		Fe I	2965.3	2
2966.9	10s	*Fe* I	2966.9	2
		Cr I	2967.7	1
2970.3	12s	*Fe* I	2969.5	17
		Fe I	2970.1	2, 3
		Si I	2970.4	3
		Ti I	2970.4	1
		Fe II	2970.5	2
2971.9	1	*Cr* I	2971.1	1
2973.3	10	*Fe* I	2973.1	2
		Fe I	2973.2	2
2976.3	5w	*Cr* I	2975.5	1
		Fe II	2975.9	2
2979.1	5wd	*Fe* II	2979.3	2
2981.5	8	*Ti* I	2981.4	1
		Fe I	2981.4	3
		Ni I	2981.7	1
2983.6	3	*Ti* I	2983.3	1
		Fe I	2983.6	1
2984.8	3	*Fe* I	2984.8	18
		Fe II	2984.8	7
2985.9	5	*Ti* I	2985.5	1
		Fe II	2985.5	7
		Cr I	2985.9 etc.	1
2987.6	5	*Fe* I	2987.2	17
		Si I	2987.7	3
2990.5	5d	*Fe* I	2990.4	......
2991.9	3w	*Cr* I	2991.9	1
2994.5	15	*Fe* I	2994.4	1
		Fe I	2994.5	3
2999.5	4	*Fe* I	2999.5	17
3000.9	8	*Ti* I	3000.7	1
		Ti I	3000.8	1
		Cr I	3000.9	1
		Fe I	3001.0	1

INTENSITY MEASUREMENTS

It was not practicable to impress photometric calibration exposures directly on the film used for the solar spectrum. Therefore, the calibration was made on a number of strips taken from the same roll of film. Calibration exposures were made with a medium quartz spectrograph using a mercury arc as source and a logarithmic sector disk. These exposures were made at the latest date possible before the spectrograph was shipped to the test station (about 10 days before the flight). The undeveloped calibration films were rolled up in the take-up spool of the spectrograph at the time it was loaded and were eventually developed at the same time as the solar spectrograms. It was hoped that this procedure would minimize differences in treatment between the two sets of film.

The film density was measured on a photoelectric microphotometer. It was found possible to obtain a useful curve down to a wave length of 2575 A. In the course of the measurements, it was found that the background density of the calibration films was slightly greater than that of the spectra. No explanation for this could be found, and in the reduction of the films it was approximately corrected by simply subtracting off the background intensity.

Calibration-curves were drawn for several wave lengths in the region covered by the films. It was found that there was no appreciable variation of γ with wave length, and therefore a mean calibration-curve was used. As will be seen from the intensity-curve of Figure 1, there is no point at which the undisturbed continuum can be located. This makes it impossible to plot intensities as a fraction of the intensity of the continuum, and therefore an approximate standardization was made to obtain true relative intensities.

For a standard source a carbon arc was used, the spectral energy distribution being

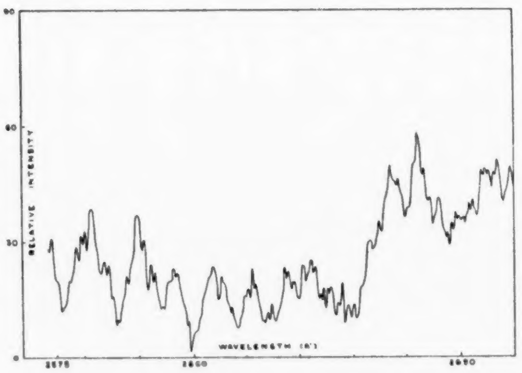

FIG. 1*A*.—Solar intensity-curve

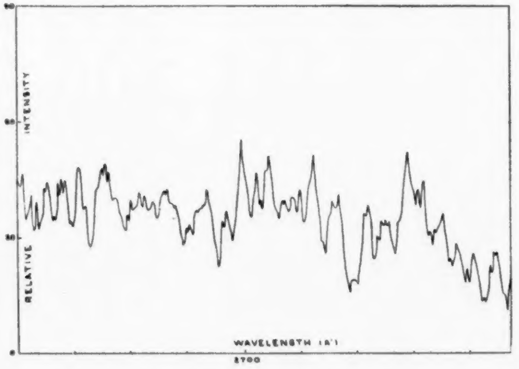

FIG. 1*B*.—Solar intensity-curve

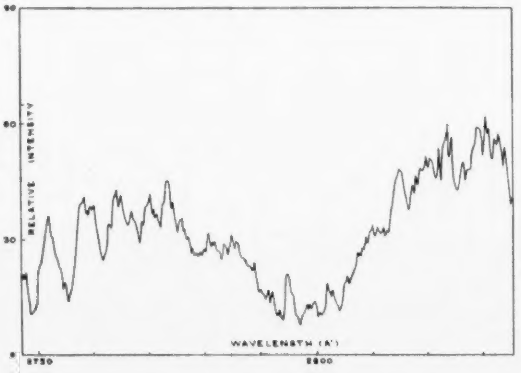

FIG. 1*C*.—Solar intensity-curve

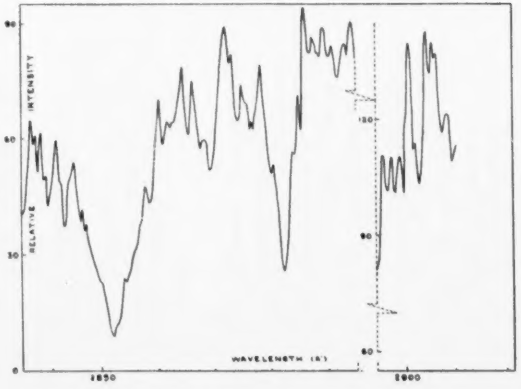

FIG. 1*D*.—Solar intensity-curve

taken from the paper by MacPherson.[3] As no spectrum of this arc had been obtained on the same lot of film used for the solar spectra, the following procedure was adopted for obtaining a standardization. An iron-arc spectrum had been obtained on this film. The carbon-arc spectrum was obtained, together with the spectrum of an iron arc running under the same conditions as the original iron arc. The sensitivity-curve of the film used for the carbon-arc spectrum was then obtained by measuring the intensities at suitable intervals and comparing with MacPherson's data. The relative sensitivity of the two films was obtained by comparing the intensities of about twenty iron lines distributed throughout the region. Combining these two curves gives the over-all sensitivity-curve of the film used for the spectra. It was found that the sensitivity of the film dropped about 35 per cent from 3000 A to 2600 A.

The final intensity-curve thus obtained is shown in Figure 1. In calculating this curve, an effort was made to reproduce all variations found in the original microphotometer traces. The intensities are in arbitrary units. The curve is limited at the long-wave-length end by overexposure of the plates and at the short-wave-length end by underexposure.

IDENTIFICATIONS

It proved possible to identify the element or elements responsible for 90 per cent of the 248 absorption lines listed in Table 1. In general, a line was assigned to an element only when all strong lines from a multiplet could either be found or accounted for as being masked by an extremely strong line of some other element. This work was greatly facilitated by a manuscript copy, very kindly furnished by Dr. Moore, of her *Ultraviolet Multiplet Table*.[4]

Inspection of the spectra showed that most of the lines were due to iron. Therefore, the first step in identifications was to search for lines belonging to the low-level multiplets of *Fe* I and *Fe* II. The excitation potential of all multiplets thus searched for was 1 volt or less. Following the search for iron lines, a search was made for low-level lines from other elements. Admittedly, this procedure discriminates against elements other than iron. In justification, it should be pointed out that, in the case of the elements in the first two periods, the spectra consist for the most part of a few strong lines, which were generally found. Also, because of the small dispersion of the instrument, it is to be expected that most of the lines of the elements in the first long period would be blended with iron or masked by it. For a final check after all identifications had been made, a search was made in the *MIT Wave-Length Tables* to see if any strong probable lines had been missed. Of course, many coincidences between solar wave lengths and wave lengths in these tables were noted, but none were probable, and no identifications from this source were added to Table 1.

In the following paragraphs the features of the spectrum will be discussed, element by element. In general, a line is identified as belonging to a particular element only when the multiplet to which it belongs is represented with reasonable completeness. For convenience, the multiplets are designated by arbitrary numbers in the last column of Table 1, and all multiplets identified are listed in Table 2.

B I.—This element has been identified in the sun only by its bands. The ultimate lines are at 2496 A and 2497 A. This region contains several strong *Fe* lines, so it is not surprising that the *B* I lines could not be found.

C I.—The only strong line of *C* I to be expected is 2479 A (multiplet 1). This region of the spectrum is occupied by the strong *Fe* I multiplet 10. The carbon line doubtless contributes to the solar line at 2478.7 A, but its intensity is, at most, comparable to the iron lines and may be less.

O I.—Although one multiplet is listed in Table 1, its excitation potential is high, and all its lines are blended with *Fe* and *V*. Therefore, this identification is to be regarded as uncertain.

---

[3] *J. Opt. Soc. America*, **30**, 189, 1940.

[4] C. E. Moore, *Ultraviolet Multiplet Table* (N.B.S. Circular, No. 488), Sec. 1 (1950).

Na I.—Several higher members of the principal series lie in this region of the spectrum. The first is masked by the very strong *Mg* I line, while the next two have been identified, although blended with iron. Higher members are too faint to be expected.

Mg I.—The resonance line and several other multiplets are to be expected. It is estimated that multiplets 2, 5, and 6 contribute appreciably to the strength of the solar feature.

Mg II.—Of the three low doublets, the ${}^2\mathrm{P}-{}^2\mathrm{D}$ is completely masked by the resonance doublet. The structure of the latter doublet will be discussed in the final section.

Al I.—Two doublets are expected and were found.

Al II.—One line is identified from a low singlet-triplet combination.

Si I.—Seven strong multiplets of low excitation potential, including the resonance multiplet, lie in this region. All the expected lines from these multiplets are accounted for.

TABLE 2

SOLAR MULTIPLETS

Element	Multiplet No.	Designation	Element	Multiplet No.	Designation
C I	1	$2\mathrm{p}^2\ {}^1\mathrm{S}-2\mathrm{p}3\mathrm{s}\ {}^1\mathrm{P}^\circ$	*Fe* I	1	$\mathrm{a}\ {}^5\mathrm{D}-\mathrm{y}\ {}^5\mathrm{D}^\circ$
O I	1	$3\mathrm{p}\ {}^3\mathrm{P}-3\mathrm{d}\ {}^3\mathrm{P}^\circ$		2	$\mathrm{a}\ {}^5\mathrm{D}-\mathrm{y}\ {}^5\mathrm{F}^\circ$
Na I	1–4	$3\mathrm{s}\ {}^2\mathrm{S}-m\mathrm{p}\ {}^2\mathrm{P}^\circ$		3	$\mathrm{a}\ {}^5\mathrm{D}-\mathrm{z}\ {}^5\mathrm{P}^\circ$
		$(m=5, 6, 7, 8)$		4	$\mathrm{a}\ {}^5\mathrm{D}-\mathrm{z}\ {}^5\mathrm{G}^\circ$
Mg I	1	$3\ {}^1\mathrm{S}-3\ {}^1\mathrm{P}^\circ$		5	$\mathrm{a}\ {}^5\mathrm{D}-\mathrm{z}\ {}^3\mathrm{G}^\circ$
	2	$3\ {}^3\mathrm{P}^\circ-6\ {}^3\mathrm{S}$		6	$\mathrm{a}\ {}^5\mathrm{D}-\mathrm{y}\ {}^3\mathrm{F}^\circ$
	3	$3\ {}^3\mathrm{P}^\circ-7\ {}^3\mathrm{S}$		7	$\mathrm{a}\ {}^5\mathrm{D}-\mathrm{y}\ {}^5\mathrm{P}^\circ$
	5	$3\ {}^3\mathrm{P}^\circ-3\mathrm{p}^2\ {}^3\mathrm{P}$		8	$\mathrm{a}\ {}^5\mathrm{D}-\mathrm{y}\ {}^5\mathrm{D}^\circ$
	6	$3\ {}^3\mathrm{P}^\circ-5\ {}^1\mathrm{D}$		9	$\mathrm{a}\ {}^5\mathrm{D}-\mathrm{x}\ {}^5\mathrm{D}^\circ$
Mg II	1	$3\ {}^2\mathrm{S}-3\ {}^2\mathrm{P}^\circ$		10	$\mathrm{a}\ {}^5\mathrm{D}-\mathrm{x}\ {}^5\mathrm{F}^\circ$
	2	$3\ {}^2\mathrm{P}^\circ-4\ {}^2\mathrm{S}$		11	$\mathrm{a}\ {}^5\mathrm{F}-\mathrm{z}\ {}^5\mathrm{H}^\circ$
Al I	1	$3\mathrm{p}\ {}^2\mathrm{P}^\circ-5\mathrm{s}\ {}^2\mathrm{S}$		12	$\mathrm{a}\ {}^5\mathrm{F}-\mathrm{w}\ {}^5\mathrm{D}^\circ$
	2	$3\mathrm{p}\ {}^2\mathrm{P}^\circ-4\mathrm{d}\ {}^2\mathrm{D}$		13	$\mathrm{a}\ {}^5\mathrm{F}-\mathrm{w}\ {}^5\mathrm{F}^\circ$
Al II	1	$3\ {}^1\mathrm{S}-3\ {}^3\mathrm{P}^\circ$		14	$\mathrm{a}\ {}^5\mathrm{F}-\mathrm{v}\ {}^5\mathrm{D}^\circ$
Si I	1	$3\mathrm{p}^2\ {}^3\mathrm{P}-3\mathrm{p}4\mathrm{s}\ {}^3\mathrm{P}^\circ$		15	$\mathrm{a}\ {}^5\mathrm{F}-\mathrm{y}\ {}^5\mathrm{S}$
	2	$3\mathrm{p}^2\ {}^1\mathrm{D}-3\mathrm{p}4\mathrm{s}\ {}^1\mathrm{P}^\circ$		16	$\mathrm{a}\ {}^5\mathrm{D}-\mathrm{y}\ {}^7\mathrm{P}^\circ$
	3	$3\mathrm{p}^2\ {}^1\mathrm{D}-3\mathrm{p}4\mathrm{s}\ {}^3\mathrm{P}^\circ$		17	$\mathrm{a}\ {}^5\mathrm{F}-\mathrm{x}\ {}^5\mathrm{F}^\circ$
	4	$3\mathrm{p}^2\ {}^1\mathrm{S}-3\mathrm{p}4\mathrm{d}\ {}^3\mathrm{D}^\circ$		18	$\mathrm{a}\ {}^5\mathrm{F}-\mathrm{y}\ {}^7\mathrm{P}^\circ$
	5	$3\mathrm{p}^2\ {}^1\mathrm{S}-3\mathrm{p}5\mathrm{s}\ {}^3\mathrm{P}^\circ$		19	$\mathrm{a}\ {}^5\mathrm{F}-\mathrm{x}\ {}^5\mathrm{P}^\circ$
	6	$3\mathrm{p}^2\ {}^1\mathrm{S}-3\mathrm{p}5\mathrm{s}\ {}^1\mathrm{P}^\circ$		20	$\mathrm{a}\ {}^5\mathrm{F}-\mathrm{y}\ {}^5\mathrm{G}^\circ$
	7	$3\mathrm{p}^2\ {}^1\mathrm{D}-3\mathrm{p}3\mathrm{d}\ {}^1\mathrm{D}^\circ$		21	$\mathrm{a}\ {}^5\mathrm{F}-\mathrm{x}\ {}^3\mathrm{D}^\circ$
P I	1	$3\mathrm{p}^3\ {}^2\mathrm{P}^\circ-3\mathrm{p}^24\mathrm{s}\ {}^2\mathrm{P}$		22	$\mathrm{a}\ {}^5\mathrm{F}-\mathrm{y}\ {}^3\mathrm{G}^\circ$
	2	$3\mathrm{p}^3\ {}^2\mathrm{P}^\circ-3\mathrm{p}^24\mathrm{s}\ {}^4\mathrm{P}$		23	$\mathrm{a}\ {}^5\mathrm{F}-\mathrm{x}\ {}^5\mathrm{G}^\circ$
Ti I	1	$\mathrm{a}\ {}^3\mathrm{F}-\mathrm{w}\ {}^3\mathrm{F}^\circ$		24	$\mathrm{a}\ {}^3\mathrm{F}-\mathrm{x}\ {}^5\mathrm{G}^\circ$
	2	$\mathrm{a}\ {}^3\mathrm{F}-\mathrm{u}\ {}^3\mathrm{D}^\circ$		25	$\mathrm{a}\ {}^3\mathrm{F}-\mathrm{y}\ {}^5\mathrm{D}^\circ$
Ti II	1	$\mathrm{a}\ {}^4\mathrm{F}-\mathrm{z}\ {}^2\mathrm{G}^\circ$		26	$\mathrm{a}\ {}^5\mathrm{D}-\mathrm{w}\ {}^5\mathrm{D}^\circ$
	2	$\mathrm{a}\ {}^4\mathrm{F}-\mathrm{y}\ {}^2\mathrm{D}^\circ$		27	$\mathrm{a}\ {}^5\mathrm{D}-\mathrm{x}\ {}^5\mathrm{P}^\circ$
	3	$\mathrm{a}\ {}^2\mathrm{F}-\mathrm{z}\ {}^2\mathrm{P}^\circ$	*Fe* II	1	$\mathrm{a}\ {}^6\mathrm{D}-\mathrm{z}\ {}^6\mathrm{D}^\circ$
V I	1	$\mathrm{a}\ {}^4\mathrm{F}-\mathrm{v}\ {}^4\mathrm{D}^\circ$		2	$\mathrm{a}\ {}^4\mathrm{D}-\mathrm{z}\ {}^6\mathrm{F}^\circ$
	2	$\mathrm{a}\ {}^4\mathrm{D}-\mathrm{u}\ {}^4\mathrm{P}^\circ$		3	$\mathrm{a}\ {}^4\mathrm{D}-\mathrm{z}\ {}^6\mathrm{P}^\circ$
	3	$\mathrm{a}\ {}^4\mathrm{F}-\mathrm{t}\ {}^4\mathrm{D}^\circ$		4	$\mathrm{a}\ {}^4\mathrm{D}-\mathrm{z}\ {}^4\mathrm{D}^\circ$
V II	1	$\mathrm{a}\ {}^5\mathrm{F}-\mathrm{z}\ {}^5\mathrm{F}^\circ$		5	$\mathrm{a}\ {}^4\mathrm{D}-\mathrm{z}\ {}^4\mathrm{F}^\circ$
	2	$\mathrm{a}\ {}^5\mathrm{F}-\mathrm{z}\ {}^5\mathrm{D}^\circ$		6	$\mathrm{a}\ {}^4\mathrm{D}-\mathrm{z}\ {}^4\mathrm{P}^\circ$
Cr I	1	$\mathrm{a}\ {}^5\mathrm{D}-\mathrm{y}\ {}^5\mathrm{D}^\circ$		7	$\mathrm{a}\ {}^4\mathrm{P}-\mathrm{z}\ {}^4\mathrm{P}^\circ$
Mn I	1	$\mathrm{a}\ {}^8\mathrm{P}-\mathrm{b}\ {}^8\mathrm{D}^\circ$		8	$\mathrm{a}\ {}^4\mathrm{F}-\mathrm{z}\ {}^4\mathrm{D}^\circ$
	2	$\mathrm{a}\ {}^6\mathrm{S}-\mathrm{b}\ {}^6\mathrm{P}^\circ$		9	$\mathrm{a}\ {}^4\mathrm{F}-\mathrm{z}\ {}^4\mathrm{F}^\circ$
Mn II	1	$4\mathrm{s}\ {}^5\mathrm{S}-4\mathrm{p}\ {}^5\mathrm{P}^\circ$		10	$\mathrm{a}\ {}^6\mathrm{D}-\mathrm{z}\ {}^6\mathrm{P}^\circ$
Ni I	1	$\mathrm{a}\ {}^3\mathrm{D}-\mathrm{y}\ {}^3\mathrm{D}^\circ$		11	$\mathrm{a}\ {}^6\mathrm{D}-\mathrm{z}\ {}^6\mathrm{F}^\circ$
Ni II	1	$\mathrm{a}\ {}^2\mathrm{D}-\mathrm{z}\ {}^2\mathrm{D}^\circ$			

P I.—This element has been identified in the sun only by a few infrared lines of high excitation potential. In the ultraviolet, two multiplets are to be expected. Of the seven expected lines, two are masked by strong lines due to *Si* and *Fe*, while the other five are present. No lines of other elements were found which could plausibly account for the solar lines. This identification is therefore judged to be reliable and confirms the presence of phosphorus in the sun.

Long-period elements (except Fe).—A large number of lines of these elements fall in this region. However, none is expected to be prominent. A relatively small number of lines can be ascribed to these elements with fair probability. More complete identification would require much higher dispersion.

Fe I and Fe II.—In both these spectra, many strong transitions from low states are expected, making iron very strong in this region. Not only is a very large portion of the identified lines attributed to iron but also most of the components of the low iron multiplets have been identified. The identification of these multiplets in the sun is remarkably complete, considering the small dispersion.

Since the iron spectrum is so completely represented, it was thought that a listing of other iron lines would be justified. Therefore, the solar-line list was compared with the complete lists of classified *Fe* I and *Fe* II lines.[5] A considerable number of solar lines, otherwise unidentified, coincided with lines from these lists. These lines are listed in Table 1 as identified, but with no multiplet number assigned. These identifications are to be regarded as much less certain than the others.

Bands.—A search was made for band heads of diatomic molecules, such as the compounds of the abundant light elements and the oxides and hydrides of the abundant metals. Although several coincidences in wave length between band heads and solar absorption were observed, in all cases only parts of band systems could be found, and other members of the systems, of comparable intensity, were definitely absent. Because of this, it was concluded that no bands could be identified on these plates.

Atmospheric lines.—A search for lines due to the earth's atmosphere was made by comparing two exposures of comparable intensity taken at altitudes of 95 and 155 km, respectively. These two plates were observed simultaneously in a comparator which brought the two images together in the field of view. No lines were found on the low-altitude plate that did not also appear on the other. Hence the portion of the atmosphere between 95 and 155 km produced no absorption that could be detected.

FEATURES OF THE SPECTRUM

As previously mentioned, there is no observable undisturbed continuum in the region below 3000 A. In this, the spectrum resembles the region just above 3000 A in a more exaggerated form, and the lack of a continuum is believed to be intrinsic and not due to the low dispersion. Many multiplets of very great strength are present. In addition to the obvious examples of *Si* I, multiplets 1 and 2, *Mg* I, multiplet 1, and *Mg* II, multiplet 1, there are many strong *Fe* I and *Fe* II multiplets. As an example, we may cite multiplet 1 of *Fe* II, which is the resonance multiplet. Because of its great strength, it apparently causes the sharp general drop in the intensity-curve at 2631 A. Several other strong iron multiplets produce a similar effect.

The greatest wave length to which the intensity curve has been plotted is about 2900 A. All the films were overexposed at longer wave lengths, and it proved impossible to obtain a reliable curve at any longer wave length. For the same reason, the sharp drop in intensity at about 2890 A is to be regarded with suspicion.

Any attempt to compare the spectrum with a black-body curve is complicated by the low precision of the intensities at wave lengths above 2900 A. If a black-body curve at

---

[5] H. N. Russell, C. E. Moore, and D. Weeks, *Trans. Amer. Phil. Soc.*, Vol. **34**, Part II, 1944; Dobbie, *Ann. Solar Phys. Obs. Cambridge*, Vol. **5**, Part I, 1938.

5000° K is fitted to the curve at 2900 A, then the solar intensity at shorter wave lengths is much less than that of the black body at that temperature. If it is assumed that the intensity drop near 2890 A is not real and the black-body curve be fitted at 2885 A, then most of the solar curve is below the black body, but the region near 2640 A nearly reaches the black-body intensity. In any case, there is certainly no excess solar intensity above the black body above 2300 A, and throughout most of the region the solar intensity is depressed by the strong absorption lines.

Because the undisturbed continuum was not apparent and also because of the large amount of blending, it was considered impractical to calculate the equivalent widths of all lines. However, the equivalent widths of four very strong lines were estimated.

The *Si* I line at 2881 A and the *Mg* I line at 2852 A are isolated lines far stronger than any others in their neighborhood. Therefore, their equivalent widths were estimated by sketching in a background by connecting the densest points on either side of these lines. The equivalent widths determined from this estimated background were found to be 2.8 A for the *Si* I line and 6.3 A for the *Mg* I line. In the region below 2630 A there are many very strong lines, such as *Si* I near 2510 A and several very strong *Fe* I and *Fe* II multiplets. Because of the low film density in this region, it was impractical to obtain their equivalent widths.

Because of its great importance, an attempt was made to estimate the equivalent width of the *Mg* II resonance doublet at 2796–2802 A. An inspection of the intensity-curve shows that the wings of this doublet extend an enormous distance away. It is very difficult to make any reasonable estimate of the background position or of the extent of these wings. By making two extreme assumptions, values for the equivalent widths of the two lines combined are found to be 16 A and 50 A. This is by far the strongest absorption feature in that portion of the sun's spectrum so far observed.

The *Mg* II resonance lines show emission at their centers. A similar effect is shown in the calcium H and K lines, although to a lesser extent. If we make the reasonable assumption that the same process is responsible for the emission in both cases, we can make a very simple calculation of the abundance ratio of these two elements. For this purpose we will consider the K line and the *Mg* II 2796 A line.

The strength of the emission lines can be expressed in terms of the equivalent width of a line as high as the continuum at the wave length in question. For the magnesium line, using the higher estimate of the continuum, as previously mentioned, the equivalent width was estimated to be 0.21 A. The equivalent width of the K emission was found from the profile taken from the Minnaert atlas. The value is estimated to be 0.0008 A. The energy of these emission lines can then be obtained by multiplying these equivalent widths by the black-body energy, using as a rough approximation a temperature of 5000° K. The black-body energy at 2796 A is 6.2×10^{13} erg-cm^{-3}-sec^{-1}, and at 3933 A it is 4.7×10^{14} erg-cm^{-3}-sec^{-1}. Multiplying these by the equivalent widths gives the emission energies of 1.3×10^{5} erg-cm^{-2}-sec^{-1} and 3.8×10^{3} erg-cm^{-2}-sec^{-1}, respectively. Taking the ratio of these quantities and multiplying by the ν^4 correction gives a ratio of magnesium to calcium abundance of 12. This may be compared with the values quoted by Strömgren,[6] which are: Strömgren, 23; Russell, 12; analysis of meteors, 15.

The experimental part of this work was performed in collaboration with J. J. Hopfield and greatly assisted by members of the staff of the Applied Physics Laboratory, Johns Hopkins University, Messrs. J. W. B. Barghausen, L. W. Fraser, A. V. Gagnes, R. S. Ostrander, and J. V. Smith. The author is greatly indebted to Dr. G. P. Kuiper, director of the Yerkes Observatory, for extending to him the privilege of spending three months there, and to members of the staff of Yerkes Observatory, especially Dr. Jesse Greenstein, for their help and criticism. The author also wishes to thank Dr. Leo Goldberg, of

---

[6] B. Strömgren, in *Festschrift für Elis Strömgren* (Copenhagen: Einar Munksgaard, 1940).

the University of Michigan Observatory, for his helpful discussion. The manuscript of the ultraviolet multiplet table, very kindly furnished by Dr. Moore, was invaluable in the work. Above all, the author feels deeply indebted to Dr. J. A. Van Allen, head of the high-altitude research group at the Applied Physics Laboratory, for his support and guidance.

TABLE OF INFRARED SOLAR LINES, 1.4–2.5μ*

Orren C. Mohler, A. Keith Pierce, Robert R. McMath,
and Leo Goldberg
McMath-Hulbert Observatory, University of Michigan

Received Sept. 2, 1952

ABSTRACT

Accurate wave lengths and measurements of equivalent width are given for 888 solar lines in the spectral region 1.4–2.5μ. The number of solar lines has been more than doubled, as compared with previous preliminary studies in this spectral region. The wave lengths of the solar lines are referred to those of the Fraunhofer lines in the visible and very near infrared spectrum by the method of overlapping orders. The root-mean-square errors of the infrared standard wave lengths, as derived from repeated measurements of individual lines, are ± 0.13 A for the 1.6μ region and ± 0.17 A for the 2.3μ region. The equivalent widths are preliminary. The estimated errors are between 10 and 100 per cent, depending upon the degree of blending.

About 470 infrared solar lines have been tentatively identified with atoms of *H*, *K*, *C*, *Al*, *Na*, *Si*, *Mg*, *Ca*, *Ni*, and *Fe* and with first overtone lines of *CO*. Comparisons between solar wave lengths and those measured in the laboratory or predicted from term values reveal somewhat closer agreement, on the average, between the solar and the predicted values than between the solar and the laboratory values.

I. INTRODUCTION

When the atlas of the infrared solar spectrum was published,[1] it was hoped that an accompanying table of wave lengths, intensities, and identifications of solar and telluric lines could be issued very soon thereafter. As the measurements progressed, it soon became apparent that the amount of labor involved was very much greater than had been anticipated, principally because of the development of more accurate, but also more time-consuming, methods of wave-length measurement. Since the solar lines in the region 1.4–2.5μ are much fewer in number than the telluric lines and since they are of greater immediate interest to astronomers and to laboratory spectroscopists, it was decided not to delay their publication until the completion of the much larger table. The more than 800 solar lines presented in this paper include all those that can be recognized in the published infrared atlas, together with a certain number of very faint lines whose appearance in the atlas is marginal but which can be clearly distinguished on more recent tracings with improved resolution.

The observations upon which the present paper are based were made with the infrared spectrometer and Cashman *PbS* cell attached to the Snow telescope on Mount Wilson. The instrumental details and observing procedure have been described in previous publications.[1,2] The observational data include not only the original tracings made for the infrared atlas but also a large number of additional tracings, including a new map of the spectrum of the solar disk made with improved resolution; tracings made with low sun; tracings of the east and west limbs, particularly in the spectral regions of heavy telluric absorption; and a series of tracings designed especially for the measurement of wave length. All measurements of wave length and intensity refer to the center of the sun's disk, except for a few lines for which equivalent widths were measured only at the limb, for reasons to be described below.

---

* Work supported in part by Contract N6-onr-232-V with the Office of Naval Research.

[1] O. C. Mohler, A. K. Pierce, R. R. McMath, and L. Goldberg, ***Photometric Atlas of the Near Infra-red Solar Spectrum*** ***λ 8465 to λ 25242*** (Ann Arbor: University of Michigan Press, 1950).

[2] R. R. McMath and O. C. Mohler, *J. Opt. Soc. America*, **39**, 903, 1949.

II. SEPARATION OF SOLAR AND TELLURIC LINES

The recognition of solar lines in the spectral region 1.4–2.5μ is complicated by the presence of extensive and complex molecular-band structures due to telluric H_2O, CO_2, and CH_4. Much weaker bands of N_2O also make their appearance at 2.13μ and 2.26μ at path lengths of 2 or 3 air masses.[3] Water vapor causes complete absorption at 1.4μ, 1.9μ, and 2.7μ; and from these band centers irregularly spaced lines of widely varying intensity stretch out over the intervening regions. Methane produces a regular band system with P, Q, and R branches at 1.66μ and irregular overlapping systems centered at 2.20μ, 2.32μ, and 2.37μ. Many of the lines of the CO_2 bands at 1.95μ, 2.01μ, and 2.05μ are strongly saturated. Weaker CO_2 bands are to be found at 1.54μ, 1.57μ, 1.60μ, and 1.65μ and still fainter isotope bands in the 2μ region.

Solar lines may be distinguished from those that originate in the earth's atmosphere by four differences in behavior. Solar lines show (1) no variation in intensity between high- and low-sun tracings; (2) Doppler shifts due to the sun's rotation on tracings made at east and west limbs; (3) enhancement or weakening at the limb when compared to intensity at the center of the disk; (4) Zeeman splitting of lines in sunspot spectra.

Since the beginning of solar observations with lead sulphide cells at the McMath-Hulbert Observatory in May, 1947, and at the Mount Wilson Observatory in May, 1949, a very large number of tracings have been made at various solar altitudes from sunrise to sunset. These records, made with path lengths varying from about 1 to 35 air masses, provide a substantial body of data for the separation of solar from telluric lines. Although the prominent solar lines are easily identified from high- and low-sun intercomparisons, the method has many uncertain features and must be applied with caution. For example, in regions of heavy telluric absorption the solar lines tend to become completely masked on low-sun tracings. Furthermore, low-sun tracings made on very dry days may exhibit weaker lines of water vapor than those made at noon on humid days.

Perhaps the most effective method for recognizing the solar lines is by comparison of the spectra of the east and west limbs. Tracings for this purpose have been made at the Snow telescope, with the spectrometer slit placed about 0.15 cm inside the limbs of the 17-cm image. The east-west displacements amount to 0.20 A at λ 15000 and 0.33 A at λ 25000, or about 1.2 and 2.0 mm, respectively, on the tracings. Even though there are irregularities in the tracings due to bad seeing, guiding errors, and small variations in the motions of grating and recording paper, nevertheless, when several pairs of east-west tracings are superimposed over an illuminated screen, the solar lines can be identified reliably by simple inspection. In many instances faint solar lines that lie in the wings of strong telluric lines are displaced into view by the solar rotation. One weakness of the east-west-limb method is that it will not reveal the blending of a strong solar line that coincides almost exactly in wave length with a weaker telluric line. The method also fails when no sharp telluric lines are present to serve as standards and when groups of faint solar lines are combined into a shallow, broad line with an ill-defined center.

Comparisons of intensities at the disk center and at the limb have been especially valuable in identifying the solar CO lines at 2.3μ, which enhance at the limb by a factor of 2–3. Tracings of infrared spot spectra show that certain solar atomic lines are widened by the unresolved Zeeman splitting, as is also the case in the photographic region. The widening is especially conspicuous in the infrared, since, by Preston's law, the Zeeman splitting is proportional to λ^2. To date, only small sections of the sunspot spectrum have been traced.

In addition to the foregoing methods, the solar origin of a line may be suggested by its appearance—e.g., the lines of hydrogen and magnesium display very broad wings—and by the coincidence of its wave length with that observed in the laboratory or predicted from tables of term values. All the procedures described above have been employed in selecting the solar lines arrayed in Table 1, but the chief criteria have been the east-west-limb and high-low-sun comparisons.

---

[3] R. R. McMath, A. K. Pierce, O. C. Mohler, L. Goldberg, and R. A. Donovan, *Phys. Rev.*, **78**, 65, 1950.

III. WAVE-LENGTH MEASUREMENTS

The wave lengths tabulated in the first column of Table 1 have been determined by linear interpolation between standard lines, separated, on the average, by 5–6 A and distributed more or less uniformly throughout the spectral region 1.4–2.5μ. The wave lengths of the standard lines have, in turn, been referred to those of the Fraunhofer lines in the visible and very near infrared spectrum by the method of overlapping orders. Thus the primary standards consist of the many thousands of highly accurate wave lengths contained in the *Revision of Rowland's Table of Solar Wave Lengths*[4] (as corrected further[5] in 1932) and in the *Infra-red Extension*.[6]

Two different procedures were followed in applying the method of overlapping orders. In the first, the positions of Fraunhofer lines in the overlapping third- or fourth-order spectrum were measured visually with respect to the position of the first-order infrared lines. In the second, both the first-order infrared spectrum and the overlapping second-order region were traced in alternate short sections with the Speedomax recorder, and the first-order wave lengths in each section were interpolated between the second-order standards on either side.

a) VISUAL METHOD

The instrumental arrangement for the application of the visual method is illustrated in Figure 1. It consists of a hinged mirror, to intercept and deflect the spectrum to a focus on the micrometer cross-wires, and a second flat mirror and viewing eyepiece. With the hinged mirror outside the beam, the entrance and exit slits of the spectrometer are opened to 0.001 inch, and the grating is rotated until the zero-order image is centered on the exit slit. The centering is accomplished by tracing the profile of the zero-order image with the Speedomax and stopping the grating at the point of maximum deflection. The hinged mirror is then turned to deflect the zero-order image into the micrometer eyepiece, and a reading is taken with the image centered on the cross-wires. Since the entrance slit has only one movable jaw, the micrometer reading must be corrected by subtracting half the slit width. The corrected reading, R_0, is the micrometer reading, for zero entrance-slit width, corresponding to a line exactly centered on the exit slit.

With the micrometer zero reading established, the spectrometer slits are adjusted to the width, W_2, normally employed for infrared recording, and the infrared line to be measured is centered on the exit slit. The mirror is then turned to deflect the spectrum to the micrometer, and the predispersing unit is adjusted so that the visible spectrum falls on the spectrometer entrance slit. The higher-order Fraunhofer spectrum is then visible in the eyepiece, but the entrance slit must be narrowed to W_1 in order to make the visible lines appear sharp. Micrometer readings, R_1 and R_2, are then taken on two lines with wave lengths λ_1 and λ_2, that fall on either side of the infrared line. The corresponding micrometer readings corrected for finite slit width are $R_1 - W_1/2$ and $R_2 - W_1/2$. If n is the order of the visible spectrum, the wave length, λ_0, of the infrared line is given by

$$\frac{\lambda_0/n - \lambda_1}{\lambda_2 - \lambda_1} = \frac{R_0 - (R_1 - W_1/2)}{R_2 - R_1} . \tag{1}$$

The higher-order standard wave lengths, λ_2 and λ_1, must be corrected to take account

---

[4] *Pub. Carnegie Inst. Washington*, No. 396, 1928.

[5] C. E. St. John and H. D. Babcock, *Trans. I.A.U.*, **4**, 60, 1932.

[6] H. D. Babcock and C. E. Moore, *Pub. Carnegie Inst. Washington*, No. 579, 1947.

TABLE 1

SOLAR LINES IN THE SPECTRAL REGION 1.4μ–2.5μ

WAVE LENGTH I.A.	EQUIV. WIDTH (MILLI-A)	IDENT.	WAVE LENGTH		MULTIPLET OR BAND	LOW E.P.	NOTES
			Meas.	Pred.			
14129.44	192 C	*Fe* I ?	28.70	28.5	$w^5D_3^\circ - f^7D_2$	5.44	1
14180.58	10 C						
14205.61	21 C						
14221.54	155 B	*Si* I		21.5	$4p^1P_1 - 5s^3P_1^\circ$	5.86	
14237.02	22 E		36.88				2, 3
14251.35	12 D	*Fe* I	51.12	51.3	$e^5D_4 - u^5P_3^\circ$	5.54	2
14293.34	?	*Fe* I	93.17				3
14300.01	11 B	*Ni* I		299.9	$y^3G_4^\circ - f^3F_3$	5.49	
14301.59	27 B						4
14309.12	118 D	*Fe* I	08.76	08.7	$c^3P_2 - z^3D_3^\circ$	3.02	1, 2
14331.79	32 C	*Fe* I	31.60	32.5	$a^3P_1 - z^5D_1^\circ$	2.42	
14354.85	8 C	*Fe* I	54.32				
14380.08	111 E	*C* I ?		80.0	$3p^3P_2 - 4s^1P_1^\circ$	8.85	
14429.00	57 B	*C* I ?		26.0	$3p^3P_2 - 3d^3D_3^\circ$	8.85	
14443.72	155 C	*Fe* I ?	42.90	41.6	$w^5F_2^\circ - e^7F_1$	5.49	
14461.36		*Fe* I	61.16				
14462.68	27 C						
14472.96	17 B						5
14475.91	18 B	*Fe* I		76.1	$x^5F_1^\circ - e^5F_2$	5.10	5
14480.42	36 C						
14486.34	10 B						
14498.21	96 D	*Fe* I	98.65				2
14512.50	366 C	*Fe* I	13.02				
14514.26	29 D						5
14523.84	44 C	*Fe* I	23.25	24.4	$e^5D_3 - u^5P_2^\circ$	5.58	
14542.52	332 B	*C* I ?		39.	$3s^1P^\circ - 3p^1P$	7.68	
14555.23	280 D	*Fe* I ?	55.74				
14577.09	4 D	*Fe* I		77.1	$x^3F_4^\circ - f^3D_3$	5.81	
14592.74	96 B	*Si* I		92.4	$4p^3D_1 - 5s^1P_1^\circ$	5.95	
14603.21	20 D	*Fe* I		3.7	$c^3P_0 - z^3D_1^\circ$	3.11	
14615.76	55 C	*Mg* I		15.0	$4p^1P^\circ - 6s^1S$	6.12	
14631.74	36 C	*Fe* I		32.1	$w^5F_3^\circ - f^7D_2$	5.47	5
14637.13	23 C	*Si* I		39.0	$3d^3P_2^\circ - 5p^3P_1$	6.26	5
14638.98	37 B						
14639.72	31 C						
14641.33	6 C						6
14641.79	9 C						6
14651.11	72 C	*Fe* I		50.8	$u^5D_3^\circ - f^5P_2$	5.79	
14652.98	115 B	*Fe* I	52.40				
14659.11	32 D	*Fe* I		59.0	$a^1P_1 - z^3P_1^\circ$	3.41	5
14683.14	23 B						
14740.82	10 A	*C* I ?		38.4	$3p^3P_1 - 4s^3P_2$	8.85	
14745.59	13 A	*Fe* I		45.5	$a^5P_2 - z^7P_2^\circ$	2.20	
14747.20	14 A	*Fe* I		47.5	$v^5D_1^\circ - e^7G_2$	5.99	
14750.01	186 B	*Fe* I ?	50.64	50.8	$x^3G_2^\circ - g^7D_2$	5.93	
14769.90	33 A	*Si* I		70.0	$4p^3D_2 - 5s^1P_1^\circ$	5.96	
14770.99	4 B						
14771.68	11 L						
14779.84	44 C	*Na* I *C* I		79.5 79.6	$4p^2P^\circ - 5d^2D$ $3p^3P_0 - 4s^3P_1^\circ$	3.75 8.84	
14781.91	12 B						
14783.00	28 A	*C* I *Si* I		83.0 83.0	$3p^3P_2 - 4s^3P_2^\circ$ $3d^3P_1^\circ - 5p^3P_1$	8.85 6.27	
14787.44	13 C						5
14806.97	30 B	*C* I		06.8	$3p^3P_1 - 4s^3P_1^\circ$	8.85	
14808.42	41 C						4
14810.57	26 L						7

TABLE 1—*Continued*

WAVE LENGTH I.A.	EQUIV. WIDTH (MILLI-A)	IDENT.	WAVE LENGTH		MULTIPLET OR BAND	LOW E.P.	NOTES
			Meas.	Pred.			
14821.08	10 L	...	...	...	...	...	5
14823.17	5 C	...	...	...	...	...	
14824.98	14 B	...	...	...	...	...	7
14833.55	4 B	*C* I	...	32.8	$3p\,^3P_1-4s\,^3P^\circ_0$	8.85	
14872.29	62 D	*Fe* I ?	...	71.2	$b\,^3D_2-z\,^3G^\circ_3$	3.64	
14878.07	296 D	*Mg* I	...	78.3	$3d\,^3D-4f\,^3F$	5.94	
14882.09	4 B	*Fe* I ?	...	84.5	$b\,^3D_3-z\,^3G^\circ_3$	3.64	5
14897.62	58 B	...	...	...	...	...	
14904.06	60 C	...	...	...	...	...	
14933.90	7 B	*Fe* I ?	...	32.8	$e\,^5D_3-7^\circ_2$	5.58	7
14938.27	59 C	...	...	...	...	...	
14943.44	17 C	...	...	...	...	...	4
14956.38	193 B	*Fe* I	55.99	56.0	$e\,^5D_4-t\,^5D^\circ_3$	5.54	
14973.69	28 C	...	...	...	...	...	
14974.66	8 C	...	...	...	...	...	7
14979.94	16 A	...	...	...	...	...	
14983.02	15 B	...	...	...	...	...	
15005.22	4 C	...	...	...	...	...	
15017.87	57 A	...	...	...	...	...	
15021.29	8 B	...	...	...	...	...	5
15025.19	698 C	*Mg* I	...	25.1	$4s\,^3S_1-4p\,^3P_2$	5.11	
15051.97	243 B	*Fe* I	52.05	52.0	$w\,^5F^\circ_3-f\,^7D_4$	5.47	
15059.40	6 C	...	...	...	...	...	
15067.13	18 B	...	...	...	...	...	
15077.55	54 B	*Fe* I	76.81	77.4	$e\,^5D_3-u\,^5P^\circ_3$	5.58	
15088.48	4 C	...	...	...	...	...	7
15089.05	5 C	...	...	...	...	...	7
15092.02	12 D	...	...	...	...	...	7, 8
15093.07	4 D	...	...	...	...	...	
15095.02	118 B	*Fe* I	95.39	...	...	...	
15096.16	92 B	...	...	...	...	...	
15099.42	11 C	*Fe* I	...	99.6	$t\,^5D^\circ_4-i\,^5D_4$	6.33	7
15102.64	4 B	...	...	...	...	...	
15106.79	12 L	*Ni* I	...	06.9	$y\,^3P^\circ_2-f\,^3D_3$	5.29	7
15116.93	11 B	*Ni* I	...	16.8	$e\,^3D_2-w\,^3P^\circ_1$	5.30	4, 7
15118.38	11 B	*Fe* I	...	18.3	$t\,^5D^\circ_3-i\,^5D_2$	6.47	
15120.75	5 D	*Fe* I	...	20.5	$w\,^5D^\circ_3-f\,^5D_3$	5.44	7
		Fe I	...	21.2	$e\,^5D_2-u\,^5P^\circ_2$	5.62	
15122.56	105 B	*Fe* I	22.37	...	...	...	
15136.32	25 D	...	...	...	...	...	
15153.95	15 B	...	...	...	...	...	
15160.75	34 C	...	...	...	...	...	
15163.30	47 B	*K* I ?	...	62.8	$3d\,^3D_{2\frac{1}{2}}-4f\,^2F$	2.67	
15165.53	2 C	...	...	...	...	...	5
15173.50	8 C	...	...	...	...	...	5
15176.80	32 A	*Fe* I	...	76.8	$z\,^3P^\circ_2-a\,^1F_3$	4.21	
15178.34	65 B	...	...	...	...	...	
15194.42	6 A	*Fe* I	...	94.5	$a\,^5P_1-z\,^7P^\circ_2$	2.22	
		Fe I	...	94.7	$x\,^3G_3-g\,^7D_3$	5.93	
15201.48	24 B	*Fe* I	...	01.8	$w\,^5F^\circ_2-f\,^7D_3$	5.49	
15207.50	227 A	*Fe* I	07.90	...	...	...	
15210.44	8 A	...	...	...	...	...	
15213.09	16 C	*Fe* I ?	...	14.0	$w\,^5G^\circ_4-f\,^5G_3$	5.90	
15217.72	104 A	...	...	...	...	...	
15219.67	174 A	*Fe* I	19.47	19.5	$e\,^5D_3-t\,^5D^\circ_2$	5.58	
15222.36	16 C	...	...	...	...	...	5, 9
15224.90	68 A	...	...	...	...	...	
15233.75	3 C	...	...	...	...	...	
15237.97	8 B	...	...	...	...	...	5

TABLE 1—*Continued*

Wave Length I.A.	Equiv. Width (Milli-A)	Ident.	Wave Length		Multiplet or Band	Low E.P.	Notes
			Meas.	Pred.			
15240.98	27 D	...	...	...	...	...	7
15243.75	10 C	...	...	...	...	...	
15245.14	192 C	*Fe* I	44.66	44.8	$e^5D_3-u^5F^{\circ}_3$	5.58	
15262.61	59 B	*Fe* I	...	62.5	$x^3F^{\circ}_2-f^3D_3$	5.85	
15267.19	16 A	*Fe* I	...	67.0	$X_3-1^{\circ}_2$	5.07	
15272.78	4 B	...	...	...	...	...	
15284.75	4 B	...	...	...	...	...	
15285.84	7 A	...	...	...	...	...	
15290.26	4 D	*Fe* I	...	90.4	$5^{\circ}_3-i^5D_2$	6.38	
15294.69	494 A	*Fe* I	95.10	94.8	$b^3D_1-z^5G^{\circ}_2$	3.63	
15296.37	6 C	*Fe* I		96.1	$x^5F^{\circ}_3-e^5F_4$	5.06	
15301.70	46 A	...		...	...	...	
15328.38	10 A	*Fe* I		28.1	$b^3P_1-z^5P^{\circ}_2$	2.84	
15335.44	267 B	*Fe* I		35.0	$x^3D^{\circ}_3-e^3D_2$	5.60	
15341.57	14 B	...		...	...	...	
15343.76	60 D	*Fe* I		45	$e^5D_0-u^5P^{\circ}_1$	5.65	10
15346.92	22 C	C I?		48.	$4s^1P^{\circ}-5p^1P$	9.71	7, 10
15348.82	20 C	...		...	...	...	
15361.35	23 C	*Si* I		61.8	$4p^3D_1-5s^3P^{\circ}_2$	5.95	7
15373.66	5 B	*Fe* I		73.3	$e^5D_2-t^5D^{\circ}_1$	5.62	
15375.47	28 C	*Fe* I *Si* I		76.3 76.8	$w^5F^{\circ}_1-f^5D_1$ $4p^1D_2-4d^3P^{\circ}_2$	5.50 6.22	
15377.01	169 A	...		...	...	...	
15382.17	51 A	*Fe* I		81.5	$b^3D_2-z^5G^{\circ}_2$	3.64	
15387.88	115 C	...		...	...	...	10
15394.72	174 B	*Fe* I	94.81	95.3	$e^5D_2-u^5F^{\circ}_2$	5.62	
15399.97	92 A	...		...	...	...	10
15403.89	99 B	...		...	...	...	10
15419.38	5 C	*Fe* I		19.1	$v^5F^{\circ}_4-g^7D_5$	5.94	
15422.44	109 A	...		...	...	...	
15451.45	29 C	...		...	...	...	
15459.32	56 B	...		...	...	...	
15469.94	58 A	...		...	...	...	
15478.63	109 B	...		...	...	...	
15485.60	16 A	...		...	...	...	
15490.99	39 D	*Fe* I		90.4	$a^5P_2-z^7P_3$	2.20	11
15496.92	46 A	*Si* I		96.5	$3d^3P^{\circ}_1-5p^3D_2$	6.27	
15499.70	41 A	*Si* I		99.4	$5p^1P_1-7d^3D_2$	6.99	
15501.41	189 D	*Fe* I	01.06	...	...	...	11
15509.12	19 C	...		...	...	...	
15514.45	25 C	...		...	...	...	
15519.46	51 A	*Fe* I	...	20.3	$a^3P_0-z^5D^{\circ}_1$	2.48	
15524.48	12 C	*Fe* I	...	24.5	$u^5D^{\circ}_4-f^5P_3$	5.79	5
15531.80	99 A	*Fe* I	...	31.6	$e^5D_1-u^5F^{\circ}_1$	5.64	
15534.31	107 A	*Fe* I	33.61	33.0	$e^5D_1-u^5P^{\circ}_2$	5.64	
15537.71	71 B	*Fe* I	...	37.6	$u^5D^{\circ}_4-h^5D_4$	5.79	
15540.57	25 A	...	...	...	...	...	
15542.15	93 B	*Fe* I	...	41.6	$e^5D_1-t^5D^{\circ}_0$	5.64	
15543.83	18 B	...		...	...	...	
15550.63	44 B	C I?	...	51.	$4p^3P_2-6d^3D_3$	10.08	
15551.60	49 B	...	...	...	...	...	
15555.46	119 A	*Ni* I?	...	56.1	$e^1D_2-w^1D_2$	5.49	
15557.97	208 A	*Si* I	...	58.7	$4p^3D_2-5s^3P^{\circ}_2$	5.96	
15560.96	50 B	C I?	...	58.	$4p^3P_1-6d^3D^{\circ}_2$	10.08	
15565.38	12 C	*Fe* I *Fe* I	...	64.4 65.1	$x^3D^{\circ}_2-f^5F_2$ $e^7D_1-w^3P^{\circ}_2$	5.61 5.42	7
15566.88	26 A	*Fe* I?		66.6	$e^5D_2-7^{\circ}_2$	5.62	
15571.86	25 A	...		...	...	...	12
15581.11	5 C	...		...	...	...	

TABLE 1—*Continued*

Wave Length I.A.	Equiv. Width (Milli-A)	Ident.	Wave Length		Multiplet or Band	Low E.P.	Notes
			Meas.	Pred.			
15588.37	104 A	*Fe* I	...	88.6	$w^5F_2^\circ-f^5D_2$	5.49	
15590.15	45 D	...	...	...	...	...	
15591.59	245 A	*Si* I	...	91.4	$3d^3P_1^\circ-5p^3D_1$	6.27	
		Fe I	90.52	...	...	...	
15593.71	32 C	*Fe* I	...	93.8	$x^5F_4^\circ-e^5F_5$	5.03	
15594.66	9 B	...	...	...	...	...	
15598.78	17 A	*C* I ?	...	601	$4p^3P_2-6d^3D_2^\circ$	10.08	
15604.24	176 A	...	...	...	...	...	
15605.66	40 B	*Fe* I ?	04.95	...	...	...	
15611.26	41 A	...	...	...	...	...	
15613.68 15614.01	82 A	...	...	...	...	...	
15621.68	256 A	*Fe* I	21.94	21.5	$e^5D_4-t^5D_4^\circ$	5.54	
15629.47	8 A	*Fe* I	...	29.8	$y^5P_3^\circ-e^7D_4$	4.56	
15632.04	247 A	*Fe* I	32.45	...	...	...	
15632.71	70 D	...	...	...	...	...	
15645.02	26 A	...	...	...	...	...	
15648.44	93 A	*Fe* I	48.85	...	...	...	
15652.84	90 A	*Fe* I	...	52.9	$z^7D_1^\circ-a^3D_1$	2.48	
15662.05	185 A	*Fe* I	62.09	61.3	$x^3D_3^\circ-f^5F_3$	5.60	
15665.27	64 A	*Fe* I	65.02	...	...	...	4, 7
15670.16	18 C	...	...	...	...	...	
15671.00	22 C	...	...	...	...	...	7
15671.86	14 C	...	...	...	...	...	7
15673.23	29 B	...	...	...	...	...	7
15677.57	152 C	...	...	...	...	...	13
15680.15	31 C	*Si* I	...	79.9	$3d^3P_0^\circ-5p^3D_1$	6.27	
15682.61	29 C	*Fe* I ?	...	81.6	$z^7F_4^\circ-b^3D_3$	2.85	
15686.25	208 D	...	...	...	...	...	14
15687.68	36 E	*Fe* I	86.94	87.3	$v^5F_2^\circ-g^7D_2$	5.98	
15691.90	166 C	...	...	...	...	...	10
15711.36	11 D	...	...	...	...	...	
15723.26	162 B	*Fe* I	23.35	23.7	$e^5D_2-u^5P_3^\circ$	5.62	
15726.88	8 C	*Fe* I	...	27.0	$e^5F_3-t^5P_2^\circ$	5.92	
15729.46	25 C	*Fe* I	...	29.7	$b^3F_2-z^5F_3^\circ$	2.61	
		Fe I	...	30.4	$w^5F_4-f^7D_5$	5.46	
15731.13	18 D	...	31.17	...	...	...	
15733.33	17 B	*Fe* I	...	32.8	$y^5P_2^\circ-e^5D_1$	4.61	
15740.66	391 B	*Mg* I	...	...	$4^3P_0^\circ-4^3D$	5.93	
15741.92	130 C	*Fe* I	42.00	41.8	$e^5D_0-u^5F_1^\circ$	5.65	
15749.05	715 A	*Mg* I	...	...	$4^3P_1^\circ-4^3D$	5.93	
15759.31	5 B	*C* I ?	...	59	$4p^3D_1-5d^3P_1^\circ$	9.94	
15765.84	767 E	*Mg* I	...	...	$4^3P_2^\circ-4^3D$	5.93	
15770.57	146 D	*Fe* I	69.03	69.3	$e^5D_4-u^5F_5^\circ$	5.54	10
15773.93	44 D	...	...	...	...	...	
15784.71	65 B	...	...	...	...	...	
15789.10	143 B	*Fe* I	89.12	...	...	...	
15797.44	7 C	*Fe* I	97.99	...	...	...	
15798.64	192 B	...	...	...	...	...	
15816.88	42 D	...	...	...	...	...	
15818.34	302 B	*Fe* I	17.55	17.8	$w^5F_1^\circ-f^5D_2$	5.50	
		Fe I	17.55	18.1	$e^5D_3-u^5F_4^\circ$	5.58	
15819.28	73 D	...	...	...	...	...	
15821.84	51 D	...	...	...	...	...	
15822.98	159 B	*Fe* I	21.92	22.4	$e^5D_1-u^5F_2^\circ$	5.64	
15824.67	11 B	...	...	...	...	...	
15827.26	44 C	...	...	...	...	...	
15829.34	6 B	...	...	...	...	...	
15833.66	249 B	...	...	...	...	...	

TABLE 1—*Continued*

Wave Length I.A.	Equiv. Width (Milli-A)	Ident.	Wave Length		Multiplet or Band	Low E.P.	Notes
			Meas.	Pred.			
15835.22	222 B	*Fe* I *Si* I	34.82	34.6	$4p^1D_2-4d^1D^\circ_2$	6.22	
15837.65	115 A	*Fe* I *Fe* I		37.2 37.4	$z^7D^\circ_2-a^3D_3$ $x^3G^\circ_4-g^7D_4$	2.47 5.93	
15840.14	36 A	*C* I ?		39	$4p^3D_2-5d^3P^\circ_2$	9.94	
15844.98	7 B						
15848.87	11 B						
15852.61	142 E						15
15854.41	7 B						
15860.20	24 A						
15863.84	117 B						
15864.73	26 D						
15868.67	179 A	*Fe* I	68.30	68.4	$e^5D_3-t^5D^\circ_3$	5.58	
15871.50	15 A						
15873.90	19 A						
15878.39	139 B	*Fe* I	78.19	78.3	$e^5D_2-t^5D^\circ_2$	5.62	
15879.45	168 A	*Mg* I		79.8	$3d^3D-5p^3P^\circ_2$	5.94	
15884.41	192 C	*Si* I		84.1	$4p^3D_1-5s^3P^\circ_1$	5.95	
15886.16	112 D						
15888.49	1118 A	*Si* I		87.7	$4s^1P^\circ_1-4p^1P_1$	5.08	
15891.31	20 E						
15892.58	285 D	*Fe* I *Fe* I	92.55	91.7 93.0	$x^3G^\circ_3-g^7D_4$ $v^5F^\circ_3-g^7D_3$	5.93 5.96	14
15895.20	190 C						
15896.68	19 D						
15899.40	74 C						
15901.64	67 A						
15904.57	157 A	*Fe* I	05.22	04.5	$v^5P^\circ_2-f^3D_1$	5.97	
15906.19	168 A	*Fe* I		05.9	$e^5D_2-u^5F^\circ_3$	5.62	
15909.38	42 A						
15911.46	143 B	*Fe* I	11.05	11.3	$e^5F_4-y^1F^\circ_3$	5.87	
15917.34	28 A	*C* I		17.	$4p^3D_3-5d^3P_2$	9.94	
15920.74	190 A	*Fe* I	20.00				4
15922.78	18 C						
15928.17	35 A						
15929.51	33 A						
15934.08	44 A						
15938.84	79 A						4
15941.80	69 A		42.60				
15943.78	14 A						
15945.18	19 A						4
15952.52	31 C						
15954.26	175 D	*Mg* I		54.6	$4d^1D_2-7f^1F^\circ_3$	6.59	8
15960.05	597 A	*Si* I		61.1	$4p^3D_3-5s^3P^\circ_2$	5.98	
15962.55	94 C						4
15965.00	111 B	*Fe* I	65.41	65.8	$5^\circ_3-i^5D_4$	6.38	
15971.39	36 A						
15973.13	51 B	*Fe* I		73.8	$a^1P_1-y^5D^\circ_2$	3.41	4
15974.32	2 D						
15980.90	316 A	*Fe* I *Fe* I	80.08	80.8 80.8	$e^3D_3-t^3F^\circ_4$ $z^1F^\circ_3-3_4$	6.36 6.27	
15982.20	43 E	*Fe* I		83.2	$b^3D_2-z^5G^\circ_3$	3.64	
15992.53	9 B						
15997.93	59 B	*Fe* I		98.3	$w^5F^\circ_2-f^5D_3$	5.49	
16006.97	229 B	*Fe* I		06.0	$z^5F^\circ-c^3F_3$	3.37	
16009.76	117 B						
16013.92	30 D	*Ni* I		13.4	$y^3G^\circ_5-e^3F_4$	3.83	
16015.52	4 C						

TABLE 1—*Continued*

WAVE LENGTH I.A.	EQUIV. WIDTH (MILLI-A)	IDENT.	WAVE LENGTH		MULTIPLET OR BAND	LOW E.P.	NOTES
			Meas.	Pred.			
16016.88	40 C	*Fe* I	....	16.7	$e^5D_0-t^5D^\circ_1$	5.65	
16018.90	2 C	*Fe* I	....	18.8	$x^3D^\circ_3-f^5F_4$	5.60	
16020.06	16 C	....	....	....	....	....	
16022.03	34 D	*Fe* I	....	21.8	$b^3D_3-z^5G^\circ_3$	3.64	
16029.65	20 B	....	....	....	....	....	
16038.06	116 C	*Fe* I	....	38.2	$b^3F_4-z^5F^\circ_5$	2.56	
16040.80	170 B	*Fe* I	41.07	....	....	....	
16049.18	8 A	....	....	....	....	....	
16051.83	10 A	....	....	....	....	....	
16070.42	30 D	*Fe* I	....	69.5	$X_3-x^3F^\circ_3$	5.07	
16071.66	98 C	....	....	....	....	....	
16072.47	31 E	*Fe* I	72.43	72.2	$v^5D^\circ_1-f^5D_0$	5.55	
16076.09	107 B	....	....	....	....	....	
16088.91	60 B	....	....	....	....	....	
16089.87	7 B	*Fe* I	....	90.8	$c^3F-x^5D^\circ_4$	4.14	
16094.95	399 A	*Si* I	....	94.7	$4p^3D_2-5s^3P^\circ_1$	5.96	
16100.43	47 C	....	....	....	....	....	
16102.47	211 B	*Fe* I	03.29	....	....	....	
16118.92	25 B	*C* I ?	....	15.	$4p^3D_2-5d^3D^\circ_3$	9.94	
16123.25	8 B	....	....	....	....	....	7
16129.26	59 *C*	*C* I	....	29.8	$4p^3D_1-5d^3D^\circ_2$	9.94	4
16136.35	99 C	*Ca* I	35.80	36.6	$5p^3P_0-5d^3D_1$	4.53	10
16150.89	70 A	*Ca* I	49.79	50.5	$5p^3P_1-5d^3D_2$	4.53	
16153.31	141 A	....	....	....	....	....	4
16155.31	30 C	*Fe* I	....	55.6	$x^3D^\circ_1-e^3D_2$	5.65	
16156.66	69 C	*Ca* I	56.04	57.3	$4p^1P_1-5d^1D_2$	4.55	
16157.47	74 B	....	....	....	....	....	16
16163.90	223 B	{*Fe* I {*Si* I	64.63	.... 63.4	.... $4p^3D_1-4d^3D^\circ_2$	.... 5.95	
16169.01	18 A	....	....	....	....	....	7
16170.39	26 A	....	....	....	....	....	4
16172.09	30 A	....	....	....	....	....	
16175.17	101 A	....	....	....	....	....	
16178.23	16 A	*Fe* I	....	78.1	$w^5F^\circ_5-f^5D_4$	5.48	
16179.81	90 B	*Fe* I	....	79.6	$w^5G^\circ_4-f^5G_4$	5.90	
16181.14	114 B	*C* I ?	....	80.0	$4p^3D_2-5d^3D^\circ_2$	9.94	
16184.11	8 A	....	....	....	....	....	
16185.92	94 B	....	....	....	....	....	
16195.27	116 A	*Ca* I	95.33	97.0	$5p^3P_2-5d^3D_3$	4.53	
16197.23	160 B	*C* I ?	....	96.	$4p^3D_3-5d^3D^\circ_3$	9.94	
16198.66	140 A	....	....	....	....	....	
16201.67	25 A	....	....	....	....	....	
16204.38	128 B	....	....	....	....	....	
16207.97	152 A	....	....	....	....	....	
16213.72	155 A	....	....	....	....	....	17
16215.92	217 A	*Si* I	....	16.2	$4p^3D_1-4d^3D^\circ_1$	5.95	
16225.75	82 A	*Fe* I	....	26.1	$a^5P_3-z^7P^\circ_4$	2.18	
16227.22	10 B	....	....	....	....	....	
16228.80	6 A	....	....	....	....	....	5
16231.74	139 A	....	....	....	....	....	
16236.08	79 A	....	....	....	....	....	
16241.86	203 A	*Si* I	....	42.5	$4p^3D_2-4d^3D^\circ_3$	5.96	
16246.61	86 B	*Fe* I	....	47.2	$x^3D^\circ_1-f^5F_2$	5.65	18
16252.61	34 A	*Ni* I	....	52.5	$y^3G^\circ-f^3F_4$	5.49	
16259.01	23 A	*C* I	....	59.5	$4p^3D_3-5d^3D^\circ_2$	9.94	
16272.64	37 A	....	....	....	....	....	
16277.68	39 A	....	....	....	....	....	
16280.83	5 B	....	....	....	....	....	
16284.76	82 A	....	....	....	....	....	

TABLE 1—*Continued*

Wave Length I.A.	Equiv. Width (Milli-A)	Ident.	Wave Length		Multiplet or Band	Low E.P.	Notes
			Meas.	Pred.			
16292.94	60 A	*Fe* I		93.0	$w^5F_5^{\circ}-e^7F_6$	5.48	
16310.44	72 A	*Ni* I		10.6	$e^3D_3-w^3P_2^{\circ}$	5.28	
16316.33	295 A	*Fe* I	16.26	15.3	$z^7F_2^{\circ}-b^3D_1$	2.87	
16318.68	68 B	*C* I ?		17.	$4p^3D_2-5d^3F_2^{\circ}$	9.94	
16320.04	22 B						4
16324.56	135 A	*C* I		24.2	$3d^1P_1^{\circ}-5p^1P$	9.76	
16331.51	58 A						
16333.16	19 C	*Fe* I		33.0	$e^5D_1-t^5D_2^{\circ}$	5.64	
16333.92	28 C						
16345.68	27 B	*C* I ?		43.8	$3p^1D_2-3d^1P_1^{\circ}$	9.00	
16347.09	29 B						
16356.42	16 A	*Ni* I ?		55.5	$w^3F_3^{\circ}-e^3G_3$	5.52	
16363.23	187 B						
16364.88	195 B	*Mg* I		64.4	$4d^3D-9f^3F^{\circ}$	6.72	19
16366.37	70 D						
16377.52	49 A	*C* I		77.7	$4p^3D_3-5d^3F_3^{\circ}$	9.94	
16380.22	220 B						
16381.62	349 C	*Si* I		81.0	$4p^1P-3d^1P^{\circ}$	5.86	
16382.26	75 D	*Si* I		81.6	$4p^3D_2-4d^3D_2^{\circ}$	5.96	20
16384.20	41 A	*Fe* I		83.5	$e^5D_2-5_3^{\circ}$	5.62	
16388.78	38 A	*Na* I		88.6	$4^2P_{1\frac{1}{2}}-6^2S_{\frac{1}{2}}$	3.75	4
16390.96	25 B						4
16394.54	131 A						
16396.26	14 C						5, 10
16404.79	128 B	*Fe* I ?	03.97	05.0	$v^5P_2^{\circ}-g^5F_2$	5.97	
16407.89	77 D						10
16410.34	6 C						
16412.29	6 D	*Fe* I		11.8	$d^3F_4-y^5G_3^{\circ}$	4.59	
16413.08	45 B						
16416.87	6 B						
16428.92	14 A						5
16435.22	92 A	*Si* I		35.9	$4p^3D_2-4d^3D_1^{\circ}$	5.96	10
16436.81	67 A	*Fe* I	37.28				
16440.68	49 A						
16445.02	278 B	*Fe* I	45.02	43.9	$e^7D_4-w^3F_3^{\circ}$	5.35	
16446.83	14 E						
16455.04	60 C	*Fe* I		54.4	$w^5G_3^{\circ}-f^5G_4$	5.91	4
16457.32	4 A						
16460.42	16 C	*Fe* I		60.4	$x^3D_3^{\circ}-e^3D_3$	5.60	7, 10
16464.19	9 C						5
16465.17	11 C						5
16467.01	99 A						
16468.67	6 B						
16471.95	22 C						
16474.20	46 A	*Fe* I	74.10				
16480.75	16 E	*Ni* I		80.6	$e^3D_3-v^3F_3^{\circ}$	5.28	
16481.42	36 D						
16486.80	316 B	*Fe* I	87.39				
16494.57	36 B	*C* I ?		94.7	$4p^1D_2-6d^1P_1^{\circ}$	10.13	
16506.47	100 C						
16515.84	127 B	*Fe* I		15.6	$v^5D_0^{\circ}-f^5D_1$	5.56	4
16517.36	199 B	*Fe* I	17.38				
16519.47	69 B						
16522.25	98 C						
16524.69	211 A	*Fe* I	23.69	25.0	$e^5F_1-t^5P_1^{\circ}$	5.98	
16530.56	45 B						4, 7
16538.05	36 B						
16539.36	64 B						
16541.56	140 C						21

TABLE 1—*Continued*

Wave Length I.A.	Equiv. Width (Milli-A)	Ident.	Wave Length		Multiplet or Band	Low E.P.	Notes
			Meas.	Pred.			
16544.82	41 A						
16546.26	17 A						
16550.42	16 B						
16552.02	76 A						
16553.90	27 A						
16557.20	45 D						21
16559.70	52 C	*C* I ?		60.	$4p^1D_2-6d^1F^\circ_3$	10.13	
16561.78	162 C						
16584.65	29 A						
16586.17	17 A	*Fe* I		85.9	$e^5D_2-t^5D^\circ_3$	5.62	
16587.33	16 A						
16593.21	16 B	*Ni* I		93.3	$y^3G^\circ_3-f^3F_3$	5.61	
16606.56	18 D						
16607.60	44 C						
16608.85	56 B						4
16612.83	86 B	*Fe* I		13.0	$X_3-x^3F^\circ_4$	5.07	
16614.62	18 A	*Fe* I		14.7	$X_3-u^5D^\circ_2$	5.07	5
16619.84	22 C	*Fe* I		19.6	$e^5D_3-t^5D^\circ_4$	5.58	5
16624.81	14 B						5
16626.89	16 C	*Ni* I		27.0	$w^3F^\circ_4-f^3D_3$	5.36	5
16632.51	53 B	*Fe* I *Mg* I		32.5 33.3	$e^5F_4-t^5P^\circ_3$ $5^3P^\circ-9^3D^3$	5.87 6.72	
16646.04	110 A	*Fe* I *Fe* I	46.43 46.43	45.9 46.6	$u^5P^\circ_3-i^5D_4$ $w^3G^\circ_5-e^5H_4$	6.41 5.98	
16658.49	29 D	*Fe* I		57.6	$v^5F^\circ_3-g^7D_4$	5.96	
16659.71	38 D						
16661.48	77 B	*Fe* I	62.23	60.6	$y^3F^\circ_3-e^7D_4$	4.61	
16665.66	95 B	*Fe* I		65.3	$X_2-u^5D^\circ_1$	5.10	
16673.80	57 A						19
16679.32	45 D						
16680.89	353 B	*Si* I		81.4	$4p^3D_3-4d^3D^\circ_3$	5.98	
16685.72	46 A						
16693.27	45 A	*Fe* I		93.5	$x^3G^\circ_4-g^7D_5$	5.93	
16707.82	40 B						
16713.04	51 A						4, 5
16719.08	364 A	*Al* I		19.0	$4^2P^\circ_{\frac{1}{2}}-4^2D_{1\frac{1}{2}}$	4.08	
16720.75	18 D						
16721.62	48 C						
16723.40	88 B	*Fe* I	22.66				
16724.68	26 C						
16748.03	25 C						
16750.57	490	*Al* I		50.6	$4^2P^\circ_{1\frac{1}{2}}-4^2D_{2\frac{1}{2}}$	4.09	4
16753.19	110 B	*Fe* I		52.6	$v^5P^\circ_1-g^5F_2$	5.99	
16757.70	10 B						
16760.26	71 A						
16763.46	165 B	*Al* I		63.4	$4^2P^\circ_{1\frac{1}{2}}-4^2D_{1\frac{1}{2}}$	4.09	
16775.26	8 A						
16779.88	40 A	*Fe* I		80.3	$X_2-w^3D^\circ_2$	5.10	5
16783.15	19 A						
16792.37	14 B						
16794.28	31 C						
16799.68	62 A	*Fe* I		99.6	$e^5F_4-9^\circ_4$	5.87	
16807.58	18 B						
16815.52	20 A	*Ni* I		15.6	$e^3D_2-w^3P^\circ_2$	5.30	
16818.78	46 B						
16820.66	108 A						
16822.85	6 B	*Fe* I		23.0	$a^1D_2-y^5F^\circ_2$	3.55	
16828.24	148 A	*Si* I		28.2	$4p^3D_3-4d^3D^\circ_2$	5.98	4

TABLE 1—*Continued*

Wave Length I.A.	Equiv. Width (Milli-A)	Ident.	Wave Length		Multiplet or Band	Low E.P.	Notes
			Meas.	Pred.			
16833.18	18 A	....	....	....	....	....	
16843.50	13 B	....	....	....	....	....	
16855.86	16 D	....	....	....	....	....	
16863.57	44 B	....	....	....	....	....	
16867.37	50 C	*C* I ?	....	67.	$4p^1P_1-5d^1P^\circ_1$	9.99	
16874.34	19 C	....	....	....	....	....	
16884.90	25 B	....	....	....	....	....	
16888.35	23 B	*C* I ?	....	87.	$3p^1D_2-3d^1F^\circ_3$	9.00	
16892.42	15 C	*Fe* I	....	92.0	$w^5G^\circ_6-f^5G_5$	5.87	
16895.29	11 B	....	....	....	....	....	
16899.02	18 B	*Ni* I	....	98.9	$w^3F^\circ_4-e^3G_4$	5.36	
16927.88	70 C	....	....	....	....	....	
16928.74	50 D	*Fe* I	....	28.5	$e^5F_3-y^1F^\circ_3$	5.92	
16929.94	26 C	....	....	....	....	....	
16945.42	17 A	*Ni* I	....	45.1	$w^3F^\circ_4-e^3G_5$	5.36	
16948.18	8 B	....	....	....	....	....	
16954.20	18 A	....	....	....	....	....	
16957.84	13 A	....	....	....	....	....	
16970.06	113 C	*Fe* I	70.74	70.5	$e^5F_1-t^5P^\circ_2$	5.98	
16996.40	141 A	*Ni* I	....	96.4	$e^3D_2-v^3F^\circ_3$	5.30	
17001.06	88 B	*Ni* I	....	01.3	$e^1D_2-w^1F^\circ_3$	5.49	
17005.41	57 D	*Fe* I	06.32	....	....	....	
17009.28	33 A	....	....	....	....	....	
17011.34	123 A	*Fe* I	11.54	....	....	....	
17027.84	26 A	....	....	....	....	....	4
17033.40	22 B	....	....	....	....	....	4
17037.84	56 B	....	....	....	....	....	
17045.20	67 A	*Fe* I	....	45.3	$z^1F^\circ_3-2$	6.27	
17052.13	31 C	*C* I ?	....	54.	$4p^1D_2-6d^1D^\circ_2$	10.13	
17061.35	11 D	....	....	....	....	....	
17065.12	34 C	....	....	....	....	....	
17067.68	60 A	....	....	....	....	....	
17075.12	28 A	....	....	....	....	....	
17088.85	33 C	*C* I ?	....	88.2	$4p^1P_1-6s^1P^\circ_1$	9.99	
17094.40	14 C	....	....	....	....	....	
17097.18	37 A	....	....	....	....	....	
17108.82	991 A	*Mg* I	....	08.1	$4s^1S_0-4p^1P^\circ_1$	5.39	
17112.60	42 D	....	....	....	....	....	
17131.12	28 B	....	....	....	....	....	
17144.40	12 A	....	....	....	....	....	
17152.37	14 C	*Si* I	....	52.6	$3d^1F^\circ_3-4f^3D_2$	6.61	
17161.18	106 A	*Fe* I	62.07	....	....	....	
17166.44	58 C	....	....	....	....	....	
17191.77	5 B	....	....	....	....	....	
17200.45	14 A	....	....	....	....	....	4
17204.38	108 B	....	....	....	....	....	
17205.82	64 D	*Si* I	....	05.7	$4p^3P_1-5s^1P^\circ_1$	6.08	
17225.77	259 A	*Fe* I *Si* I	....	25.1 25.8	$w^5P^\circ_1-g^5D_1$ $3d^1P^\circ_1-4f^3D_2$	5.75 6.62	
17232.37	30 D	....	....	....	....	....	
17233.37	39 D	....	....	....	....	....	
17234.56	132 B	....	....	....	....	....	
17262.14	9 B	*Fe* I	....	61.9	$x^5G^\circ_3-f^5F_2$	5.69	
17275.06	184 D	....	....	....	....	....	
17277.48	30 C	....	....	....	....	....	
17282.35	57 C	....	....	....	....	....	
17293.17 17293.69	37 D	*Fe* I	....	93.6	$v^5P^\circ_3-f^3D_3$	5.95	24
17302.34	140 B	*Fe* I	02.92	....	....	....	

TABLE 1—*Continued*

WAVE LENGTH I.A.	EQUIV. WIDTH (MILLI-A)	IDENT.	WAVE LENGTH		MULTIPLET OR BAND	LOW E.P.	NOTES
			Meas.	Pred.			
17306.66	25 B	*Fe* I		05.6	$v^5P^{\circ}_1-f^3D_2$	5.99	
17321.78	22 C						
17323.56	130 D	*Fe* I		23.6	$x^5G^{\circ}_4-f^5F_3$	5.68	
17325.82	62 E						
17327.48	429 A						
17338.65	282 A	*Fe* I		38.3	$t^5D^{\circ}_4-3_4$	6.33	4
17349.87	27 B						
17400.74	16 A						
17427.63	50 C	*Fe* I		28.4	$w^5P^{\circ}_2-g^5D_2$	5.74	
17433.83	35 A						
17448.78	161 A						
17451.19	37 A						
17454.08	22 B	*Fe* I		54.8	$a^3D_1-z^3F^{\circ}_2$	3.27	
17456.17	123 A	*C* I		56.	$3p^1D_2-4s^1P^{\circ}_1$	9.00	4
17473.55	12 B						
17474.42	4 C						
17476.05	53 A						7
17478.28	79 A						
17480.76	55 B						
17488.66	24 B						
17505.85	141 A						
17513.68	22 B						
17516.13	27 A						
17521.34	115 B						22
17524.32	25 D						
17526.54	27 D						
17531.30	23 C						
17534.90	37 D						
17538.72	31 B	*Fe* I		38.6	$w^5P^{\circ}_3-e^5P_3$	5.72	
17543.58	38 C						
17548.64	37 D						
17554.37	127 A						
17565.23	29 C	*Fe* I		64.8	$w^5G^{\circ}_4-f^5G_5$	5.90	
17580.61	142 B						
17582.06	47 C						
17592.64	50 A	*Si* I		93.5	$4p^3P_2-5s^1P^{\circ}_1$	6.10	
17608.14	109 B						
17611.68	25 C						
17612.66	50 D						
17617.21	288 A	*C* I ? *Si* I ?		16.0 17.6	$3d^3P^{\circ}_2-5p^3D_3$ $3d^1F^{\circ}_3-4f^3G_4$	9.83 6.61	
17622.46	34 C	*Ni* I		22.5	$x^3F^{\circ}_3-f^3D_2$	5.41	
17623.64	91 C	*Si* I		23.4	$3d^1F^{\circ}_3-4f^3G_3$	6.61	
17637.50	171 A	*Fe* I		36.9	$z^3F^{\circ}_4-d^3F_3$	3.88	
17644.24	25 C						
17672.43	60 C	*Fe* I		72.4	$w^5P^{\circ}_1-e^5P_2$	5.75	
17684.00	134 B	*Fe* I		84.9	$z^3D^{\circ}_3-d^3F_3$	3.88	
17694.28	36 D	*Fe* I		94.2	$e^7D_3-2^{\circ}_2$	5.38	
17698.05	11 B						
17711.10	11 A						
17712.97	31 A						
17714.71	22 A						
17717.40	17 A						
17718.80	4 B	*Fe* I		18.5	$a^5P_3-z^7F^{\circ}_2$	2.18	
17720.81 17721.02	119 D	*C* I ?		22.	$3d^3P^{\circ}_2-5p^3D_2$	9.83	25
17727.46	44 E	*Fe* I		27.6	$w^5P^{\circ}_1-g^5D_2$	5.75	
17728.28	123 B	*Fe* I		28.3	$x^5G^{\circ}_2-f^5F_3$	5.70	
17743.68	8 C						

TABLE 1—*Continued*

WAVE LENGTH I.A.	EQUIV. WIDTH (MILLI-A)	IDENT.	WAVE LENGTH		MULTIPLET OR BAND	LOW E.P.	NOTES
			Meas.	Pred.			
17747.48	41 A	*C* I ?		48	$3d^3P^\circ_1-5p^3D_2$	9.83	
17762.30	32 C	*Fe* I		62.0	$x^5G^\circ_4-f^5F_4$	5.68	
17769.08	132 B						
17771.22	156 A	*Fe* I ?	71.97				
17811.20	36 D						
17822.78	27 B	*Fe* I		22.8	$w^5P^\circ_1-e^5P_1$	5.75	
17826.58	216 C						
17861.83	22 D						
17880.66	42 C						
17889.51	87 A	*C* I ?		89.7	$3p^1D_2-3d^3F^\circ_2$	9.00	
17926.46	73 C						
17932.89	57 D	*Fe* I ?	31.06				
17938.98	52 D	*Fe* I	38.36	37.7	$e^5F_3-9^\circ_4$	5.92	
17952.11	21 A						
17979.61	78 C						
17982.57	86 A						
17986.90	99 C						
17988.87	15 B						
18014.68	20 L						
18027.16	19 C						
18066.85	56 C						
18077.22	17 B						
18078.34	16 B						
18093.14	27 D						
18137.82	119 A						
18140.02	42 B						
18190.34	51 C						5
19425.32	42 C	*Fe* I		25.8	$x^5G^\circ_4-e^5G_4$	5.68	7
19484.55	34 D						
19505.88	193 D	*Ca* I *Si* I	5.62 5.62	05.8 05.8	$4p^3P^\circ_1-3d^3D_1$ $4p^3P_2-5s^3P^\circ_1$	1.89 6.10	
19533.60	15 C						
19592.98	26 C	*Fe* I		92.8	$x^5D^\circ_2-e^5D_2$	4.99	
19613.39	27 E						
19685.61	39 D						
19722.74	618 C	*C* I ? *Si* I		20.8 23.2	$3p^1P_1-3d^1D_2$ $4p^3P_2-4d^3D^\circ_3$	8.53 6.10	
19728.65	4 C						7
19746.85	16 L	*Fe* I		47.1	$a^3D_2-z^3D^\circ_2$	3.30	
19758.88	6 C						
19759.47	6 C						7
19776.85	496 C	*Ca* I	76.67	76.8	$4p^3P^\circ_2-3d^3D_3$	1.90	
19815.43	263 A	*Ca* I	15.14	15.2	$4d^1D_2-4f^1F^\circ_3$	4.62	7
19853.40	289 A	*Ca* I	52.96	53.1	$5s^3S_1-5p^3P^\circ_2$	3.91	
19862.62	360	*Ca* I	61.70	...	$4p^3P^\circ_2-3d^3D_2$	1.90	
19917.57	123 B	*Ca* I	16.34	17.3	$4p^3P^\circ_2-3d^3D_1$	1.90	
19923.70	33 B	*Fe* I		23.4	$x^5D^\circ_0-e^5D_1$	5.02	
19929.27	391 C	*Si* I		28.7	$4p^3P_2-4d^3D_2$	6.10	
19934.04	256 C	*Ca* I	32.94	33.9	$5s^3S_1-5p^3P^\circ_2$	3.91	
19947.84	21 C	*Fe* I		47.7	$w^5P^\circ_3-e^5S_2$	5.72	7
19971.92	151 D	*Si* I ?		72.8	$4d^3D^\circ_1-4f^3D_1$	6.72	
20008.42	256 E	*Si* I ?		09.1	$4p^3P_2-4d^3D^\circ_1$	6.10	5
20219.46	39 C						
20301.94	95 D						
20344.31	88 B	*Si* I		43.5	$4p^3S_1-5s^3P^\circ_1$	6.12	
20471.80	33 B						
20480.87	31 B						
20485.42	15 C						
20530.54	196 D						

TABLE 1—*Continued*

WAVE LENGTH I.A.	EQUIV. WIDTH (MILLI-A)	IDENT.	WAVE LENGTH		MULTIPLET OR BAND	LOW E.P.	NOTES
			Meas.	Pred.			
20600.90	22 C						
20603.45	127 D	*Si* I		03.0	$4d^3D^\circ_3-4f^3D_3$	6.72	
20630.32	152 D						
20694.30	25 C						
20698.90	87 L						
20711.46	47 D						
20717.50	68 B						
20723.66	36 B						
20766.29	38 C	*Fe* I		65.9	$a^3P_2-z^7F^\circ_2$	2.28	7
20790.53	25 C						
20799.96	35 C	*Fe* I		99.1	$z^3F^\circ_2-d^3F_2$	3.98	
20861.48	11 B						
20875.60	14 A						
20890.50	26 A						
20917.28	360 C						
20920.29	147 C						5
20952.57	54 B						
20965.82	65 A						5
20967.62	26 D	*Fe* I		67.6	$z^7D^\circ_5-b^3G_4$	2.40	
21023.06	79 A						
21060.87	472 D						
21093.17	438 A	*Al* I		93.6	$4^2P^\circ_{1/2}-5^2S_{1/2}$	4.08	
21139.56	30 A						
21145.76	78 A						
21156.68	127 D						1
21163.83	325 A	*Al* I		64.3	$4^2P^\circ_{1\frac{1}{2}}-5^2S_{1/2}$	4.09	
21168.20	41 A						
21171.08	20 C						
21208.17	129 B						
21211.72	34 A						
21225.83	30 B	*Mg* I		26.1	$5p^3P^\circ-8s^3S$	6.72	
21260.00	165 A						22
21295.16	44 A						
21354.27	443 B	*Si* I		54.6	$4p^1D_2-5s^1P^\circ_1$	6.22	
21368.71	54 A						7, 22
21373.19	18 A						22
21389.08	50 B						
21428.76	100 E						23
21440.54	41 A						
21442.44	27 C						
21453.32	16 D						5
21459.11	46 A						
21469.55	14 B						
21515.34	12 B						7
21575.61	59 A						
21581.27	27 A						4
21593.07	26 C						
21613.58	50 A	*Si* I		13.4	$5p^3D_3-7s^3P^\circ_2$	7.09	
21616.32	10 B						
21655.	2875 B	*H* I		55.4	4−7	12.69	
21691.60	33 A						7
21721.01	35 D	*Si* I		21.7	$4d^3P^\circ_1-5f^1D_2$	7.03	5
21735.44	27 A						
21783.39	30 A						
21790.53	12 C						5
21791.24	19 C						
21816.63	22 A						
21819.68	238 B	*Si* I		20.1	$4d^3D^\circ_2-4f^3F_3$	6.72	
21833.36	12 B						

TABLE 1—*Continued*

Wave Length I.A.	Equiv. Width (Milli-A)	Ident.	Wave Length		Multiplet or Band	Low E.P.	Notes
			Meas.	Pred.			
21838.43	19 B	...	...	...	...	...	
21851.80	7 A	*Fe* I	...	51.5	$b^3D_3-z^3P^\circ_2$	3.64	
21858.22	30 A	...	...	...	...	...	
21874.26	90 C	*Si* I	...	74.3	$4d^3D^\circ_2-4f^3F_2$	6.72	
21879.38	300 C	...	...	...	...	...	
21883.01	30 A	...	...	...	...	...	
21895.07	82 A	...	...	...	...	...	
21897.45	20 C	...	...	...	...	...	
22056.56	307 A	*Na* I	...	56.1	$4^2S_{½}-4^2P^\circ_{1½}$	3.19	
22062.82	362 B	*Si* I	...	61.2	$4d^3D^\circ_3-4f^3F_4$	6.72	
22072.77	37 A	*Si* I	...	72.0	$4d^3D^\circ_3-4f^3F_3$	6.72	
22083.90	247 A	*Na* I	...	83.6	$4^2S_{½}-4^2P^\circ_{1½}$	3.19	
22257.15	145 A	*Fe* I	...	57.0	$x^5F^\circ_3-e^5D_2$	5.06	
22380.89	199 A	*Fe* I	...	81.0	$x^5F^\circ_4-e^5D_3$	5.03	
22392.90	55 B	*Fe* I	...	93.0	$x^5F^\circ_1-e^5D_0$	5.10	
22420.06	51 A	...	...	...	...	...	
22445.20	52 A	...	...	...	...	...	
22460.62	42 B	...	...	...	...	...	4
22473.47	209 B	...	...	...	...	...	
22493.86	12 A	...	...	...	...	...	7
22507.52	30 A	...	...	...	...	...	
22518.70	22 C	...	...	...	...	...	
22526.06	16 D	...	...	...	...	...	
22537.92	248 A	...	...	...	...	...	
22552.75	83 C	...	...	...	...	...	
22608.08	223 B	*Ca* I	08.39	08.1	$4d^3D_1-4f^3F_2$	4.68	
22619.81	240 B	*Fe* I	...	20.1	$x^5F^\circ_5-e^5D_4$	4.99	
22624.99	199 B	*Ca* I	25.51	25.2	$4d^3D_2-4f^3F_3$	4.68	
22626.62	67 D	*Ca* I	...	27.0	$4d^3D_2-4f^3F_2$	4.68	
22651.43	218 A	*Ca* I	51.30	51.4	$4d^3D_3-4f^3F_4$	4.68	
22653.82	56 B	*Ca* I	...	53.8	$4d^3D_3-4f^3F_3$	4.68	
22665.88	108 A	*Si* I	...	66.2	$3d^1P^\circ_1-5p^1D_2$	6.62	
22708.38	122 C	...	...	...	...	...	
22740.66	89 C	...	...	...	...	...	
22770.40	20 B	...	...	...	...	...	
22782.08	67 A	...	...	...	...	...	
22795.12	33 B	...	...	...	...	...	
22808.12	665 B	*Mg* I ?	...	07.2	$4d^3D-6f^3F^\circ$	6.72	
22846.44	49 C	*Fe* I	...	45.9	$e^5F_5-u^5F^\circ_4$	5.83	
22930.22	27 E	*CO*	...	30.49	2–0, *R* 53	...	
22934.57	111 C	*Si* I	...	34.8	$4p^3P_0-3d^1P^\circ_1$	6.08	
22937.28	15 D	*CO*	...	37.64	2–0, *R* 57	...	
22941.04	16 C	*CO*	...	41.12	2–0, *R* 43	...	
22944.31	54 C	*CO*	...	44.43	2–0, *R* 42	...	
22966.84	15 C	*CO*	...	66.89	2–0, *R* 37	...	
22972.64	16 D	*CO* *CO*	... ...	72.59 72.91	2–0, *R* 36 4–2, *R* 56	... ...	
22985.00	20 C	*CO* *CO*	... ...	85.21 84.68	2–0, *R* 34 2–0, *R* 67	... ...	
22991.88	49 A	*CO* *CO*	... ...	92.08 91.71	2–0, *R* 33 2–0, *R* 68	... ...	
23006.64	19 A	*CO*	...	07.11	2–0, *R* 31	...	
23023.79	26 B	*CO*	...	23.70	2–0, *R* 29	...	
23041.89	12 C	*CO*	...	41.95	2–0, *R* 27	...	
23044.71	9 B	...	...	...	...	...	
23072.05	24 A	*CO*	...	72.26	2–0, *R* 24	...	
23106.24	25 A	*Si* I *CO*	... ...	06.4 06.23	$4p^3P_1-3d^1P^\circ_1$ 2–0, *R* 21	6.08 ...	

TABLE 1—*Continued*

WAVE LENGTH I.A.	EQUIV. WIDTH (MILLI-A)	IDENT.	WAVE LENGTH		MULTIPLET OR BAND	LOW E.P.	NOTES
			Meas.	Pred.			
23118.41	23 B	*CO*	...	18.36	2–0, *R* 20	...	
23130.54	22 A	*CO*	...	30.88	2–0, *R* 19	...	
23141.44	88 C	*Si* I	...	42.6	$5^1sP^\circ_1-4f^3D_2$	6.80	
		CO	...	42.12	4–2, *R* 46	...	
23144.22	147 C	*Si* I	...	45.0	$5^1sP^\circ_1-4f^3D_1$	6.80	
		CO	...	43.83	2–0, *R* 18	...	
23199.71	15 D	*CO*	...	99.64	2–0, *R* 14	...	
23214.76	48 C	*CO*	...	14.56	2–0, *R* 13	...	
23222.27	19 C	*CO*	...	22.49	3–1, *R* 47	...	
		CO	...	22.00	3–1, *R* 53	...	
23228.19	16 B	*CO*	...	28.37	3–1, *R* 44	...	
23229.96	27 B	*CO*	...	29.93	2–0, *R* 12	...	
		CO	...	30.09	3–1, *R* 57	...	
23255.31	13 B	*CO*	...	54.90	3–1, *R* 63	...	
23256.68	20 B	*CO*	...	56.41	3–1, *R* 37	...	
23262.19	86 B	*CO*	...	62.63	3–1, *R* 36	...	
		CO	...	61.93	2–1, *R* 10	...	
23266.90	8 B	*CO*	...	66.64	3–1, *R* 65	...	
23269.49	33 A	*CO*	...	68.16	3–1, *R* 35	...	
		Fe I	...	69.5	$z^5P^\circ_2-c^3F_2$	3.65	
23273.26	16 C	*CO*	...	73.14	3–1, *R* 66	...	
23274.66	35 A	*CO*	...	74.66	3–1, *R* 34	...	
23281.57	31 C	*CO*	...	81.54	3–1, *R* 33	...	
23295.36	77 C	*CO*	...	95.54	2–0, *R* 8	...	
		CO	...	95.27	3–1, *R* 69	...	
23296.16	47 C	*CO*	...	95.54	2–0, *R* 8	...	
		CO	...	96.57	3–1, *R* 31	...	
23305.74	65 D	*CO*	...	04.72	3–1, *R* 30	...	
23341.56	48 D	*CO*	...	41.28	3–1, *R* 26	...	
23348.95	239 B	*Na* I	...	47.7	$4^2P^\circ_{\frac{1}{2}}-4^2D_{1\frac{1}{2}}$	3.75	
		CO	...	49.07	2–0, *R* 5	...	
23351.75	42 D	*CO*	...	51.53	3–1, *R* 25	...	
23362.31	102 B	*CO*	...	62.12	3–1, *R* 24	...	
23379.29	51 L	...	...	...	...	...	
23379.59	432 C	*Na* I	...	78.6	$4^2P^\circ_{1\frac{1}{2}}-4^2D$	3.75	
23385.12	75 C	*CO*	...	84.58	3–1, *R* 22	...	
23393.47	73 D	...	...	...	...	...	
23410.80	9 B	...	...	...	...	...	
23434.14	23 A	*CO*	...	34.29	3–1, *R* 18	...	
23445.39	47 L	...	...	...	...	...	
23487.92	45 B	...	...	...	...	...	
23506.39	17 A	*CO*	...	05.92	3–1, *R* 13	...	
23513.25	28 D	...	...	...	...	...	
23524.42	22 C	*CO*	...	24.12	4–2, *R* 55	...	
23531.10	26 C	*CO*	...	31.10	4–2, *R* 42	...	
23533.03	24 B	*CO*	...	32.81	4–2, *R* 58	...	
23534.60	62 B	*CO*	...	34.70	4–2, *R* 41	...	
23536.79	29 C	*CO*	...	36.58	4–2, *R* 59	...	
23538.54	16 D	*CO*	...	37.47	3–1, *R* 11	...	
		CO	...	38.57	4–2, *R* 40	...	
23547.70	40 B	*CO*	...	47.67	4–2, *R* 38	...	
23549.39	12 B	...	...	...	...	...	
23558.27	35 B	*CO*	...	58.54	4–2, *R* 36	...	
23564.52	50 C	*CO*	...	64.54	4–2, *R* 35	...	
23570.88	42 B	*CO*	...	70.93	4–2, *R* 34	...	
		CO	...	70.76	3–1, *R* 9	...	
23574.66	37 D	*CO*	...	75.32	4–2, *R* 66	...	

TABLE 1—*Continued*

WAVE LENGTH I.A.	EQUIV. WIDTH (MILLI-A)	IDENT.	WAVE LENGTH		MULTIPLET OR BAND	LOW E.P.	NOTES
			Meas.	Pred.			
23585.14	34 B	*CO*		85.11	4–2, *R* 32		
23588.19	21 A	*CO*		88.00	3–1, *R* 8		
23590.89	22 A	*CO*		90.34	4–2, *R* 68		
23592.91	43 A	*CO*		92.90	4–2, *R* 31		
23601.08	56 B	*CO*		01.03	2–0, *P* 6		
		CO		01.03	4–2, *R* 30		
23605.77	18 B	*CO*		05.72	3–1, *R* 7		
23618.38	41 B	*CO*		18.54	4–2, *R* 28		
23623.93	10 B	*CO*		23.79	3–1, R 6		
23625.07	23 B	*CO*		24.85	2–0, *P* 7		
23637.79	44 L	*CO*		37.70	4–2, *R* 26		
23648.19	58 D	*CO*		47.98	4–2, *R* 25		
		CO		49.05	2–0, *P* 8		
23658.88	54 B	*CO*		58.67	4–2, *R* 24		
23745.30	22 C	*CO*		45.21	4–2, *R* 17		
23750.44	20 A	*CO*		50.34	2–0, *P* 12		
23789.06	95 D	*CO*		88.77	4–2, *R* 14		
23803.70	50 D	*CO*		04.07	4–2, *R* 13		
		CO		03.50	2–0, *P* 14		
23811.74	5 B	*Si* I		11.2	$4p^3P_2-3d^1P^\circ_1$	6.10	
23841.63	132 C	*CO*		41.93	5–3, *R* 40		
23844.48	154 B						
23846.43	35 C	*CO*		46.25	5–3, *R* 39		
23859.50	145 E	*Mg* I		59.8	$5p^3P^\circ-6d^3D$	6.72	
23880.78	22 C	*CO*		80.83	5–3, *R* 33		
23887.94	22 C	*CO*		87.22	4–2, *R* 8		
		CO		88.53	5–3, *R* 32		
23898.53	17 A	*CO*		98.24	3–1, *P* 6		
23912.67	21 B	*CO*		12.76	5–3, *R* 29		
23915.43	17 A	*CO*		15.45	2–0, *P* 18		
23930.94	22 D	*CO*		31.08	5–3, *R* 27		
23953.67	65 C						
23973.07	17 B	*CO*		73.37	5–3, *R* 23		
23981.29	17 B	*CO*		81.31	4–2, *R* 3		
23984.80	28 D	*CO*		85.05	5–3, *R* 22		
24009.69	43 B	*CO*		09.53	5–3, *R* 20		
24022.22	88 B	*CO*		21.99	4–2, *R* 1		
		CO		22.51	5–3, *R* 19		
24023.64	38 D	*CO*		23.61	3–1, *P* 11		
24048.39	42 C						
24076.94	22 C	*CO*		76.95	3–1, *P* 13		
24078.16	27 A	*CO*		78.58	5–3, *R* 15		
24104.52	17 A	*CO*		04.24	3–1, *P* 14		
24125.23	13 A	*CO*		25.12	5–3, *R* 12		
24163.59	45 B	*CO*		62.73	6–4, *R* 60		
24172.11	25 B	*CO*		72.02	6–4, *R* 36		
24198.73	25 C	*CO*		98.55	6–4, *R* 32		
24202.90	20 C	*CO*		02.50	4–2, *P* 6		
24203.63	29 C						
24206.35	25 B	*CO*		06.28	6–4, *R* 31		
24218.48	18 A	*CO*		18.16	3–1, *P* 18		
24219.72	35 C						
24223.01	69 A	*CO*		23.08	6–4, *R* 29		
24227.55	27 B	*CO*		27.49	2–0, *P* 28		
		CO		27.08	4–2, *P* 7		
		CO		27.02	6–4, *R* 69		
24230.39	23 C	*CO*		30.31	5–3, *R* 6		
24241.54	49 B	*CO*		41.65	6–4, *R* 27		
24248.00	23 B	*CO*		47.82	3–1, *P* 19		

TABLE 1—*Continued*

Wave Length I.A.	Equiv. Width (Milli-A)	Ident.	Wave Length		Multiplet or Band	Low E.P.	Notes
			Meas.	Pred.			
24251.28	70 C						
24260.91	34 C	*CO*		61.30	2–0, *P* 29		
24277.80	59 A	*CO*		77.68	4–2, *P* 9		
		CO		77.97	3–1, *P* 20		
24283.69	44 B						
24295.36	70 A	*CO*		95.82	6–4, *R* 22		
		CO		95.61	2–0, *P* 30		
24307.49	42 D	*CO*		07.98	6–4, *R* 21		
24308.33	27 D	*CO*		08.55	3–1, *P* 21		
24333.79	50 B	*Fe* I		33.7	$c^3F_3-y^3F_2^\circ$	4.14	
		CO		33.65	6–4, *R* 19		
24371.24	42 A	*CO*		71.13	3–1, *P* 23		
24374.58	242 B						
24381.44	60 B						
24403.21	33 B	*CO*		03.13	3–1, *P* 24		
24405.25	21 B	*CO*		05.63	6–4, *R* 14		
24432.86	30 A						
24435.92	21 B	*CO*		35.70	3–1, *P* 25		
24438.50	39 D						
24440.58	31 B	*CO*		40.36	4–2, *P* 15		
24448.50	123 D						
24478.58							4
24479.33	16 B	*CO*		79.42	7–5, *R* 38		
24480.85	23 B						
24484.19	38 B	*CO*		84.43	7–5, *R* 37		
24485.95	12 C						
24488.16	50 C	*Fe* I		87.9	$x^5F_4^\circ-e^5D_4$	5.03	
24515.57	29 C	*CO*		16.31	7–5, *R* 32		
		CO		15.87	5–3, *P* 6		
24523.19	26 A	*CO*		24.05	7–5, *R* 31		
24535.72	33 B	*CO*		36.09	3–1, *P* 28		
24547.64	207 B						
24551.75	28 A	*Fe* I		51.0	$e^5F_3-u^5F_2^\circ$	5.92	
24553.89	19 B						
24556.21	114 B						
24566.26	256 B	*Mg* I		66.2	$4d^1D_2-5f^1F_3^\circ$	6.59	
24568.62	73 D						
24570.28	30 B	*CO*		70.59	3–1, *P* 29		
24574.35	115 A						
24601.50	30 A	*CO*		02.28	7–5, *R* 23		
24603.32	18 A						
24643.24	31 C	*CO*		43.45	5–3, *P* 11		
24648.57	87 A						
24651.74	50 B	*CO*		51.71	4–2, *P* 22		
		CO		52.31	7–5, *R* 19		
24665.38	34 B	*CO*		65.96	7–5, *R* 18		
		CO		65.82	2–0, *P* 40		
24677.08	23 C	*CO*		76.90	3–1, *P* 32		
24693.80	21 C	*CO*		94.63	7–5, *R* 16		
24729.08	107 D						
24739.99	27 B	*CO*		41.08	7–5, *R* 13		
24758.67	33 A	*CO*		58.73	6–4, *P* 3		
24848.98	85 D						
24851.32	63 B	*CO*		51.98	4–2, *P* 28		
24954.60	38 L						
24983.45	71 L	*CO*		83.08	3–1, *P* 40		
24998.89	70 L	*CO*		99.20	2–0, *P* 48		
25004.16	31 C	*CO*		03.89	5–3, *P* 23		

NOTES TO TABLE 1 ON FOLLOWING PAGE

NOTES TO TABLE 1

1. Blend atm H_2O.
2. Solar identification by coincidence.
3. Masked by atm H_2O, except when very dry.
4. Blend atm.
5. Solar origin very questionable.
6. Strongly enhanced at limb; may be of molecular origin.
7. Solar origin questionable.
8. Double line?
9. Double line, $\Delta\lambda = 0.7$ A.
10. Blend atm CO_2.
11. Double line, $\Delta\lambda = 0.5$ A.
12. Very broad.
13. Faint companions at 76.78 and 77.14.
14. Double line, $\Delta\lambda = 0.30$ A.
15. Several solar and atmospheric lines in close blend.
16. May be *Ca* I instead of preceding line.
17. Double lines at 13.31 and 14.02.
18. Faint solar line at 45.90.
19. Broad, shallow line.
20. *Si* I may be blended with preceding line.
21. Group of several faint lines.
22. Broad line.
23. Blend of several lines.
24. Equivalent width given for combined blend 93.17 and 93.69.
25. Equivalent width given for combined blend 20.81 and 21.02.

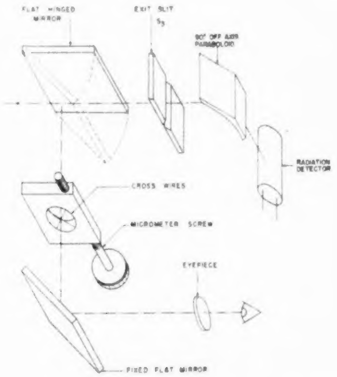

FIG. 1.—Schematic arrangement for visual measurement of wave lengths by overlapping orders

of deviations from standard atmospheric conditions[7] and for the radial velocity of the earth relative to the sun.

The visual method has the advantage that the infrared standards for all wave lengths longer than λ10000 may be related directly to a set of primary standards that are accurate to 1 part in 2–3 million. The method is also independent of errors in the grating drive, and two visual orders may generally be used for each infrared line. On the other hand, the visual procedure is exceedingly slow and laborious and is expensive in terms of telescope time. Appreciable errors may also arise from uncertainties in the centering of the infrared lines on the exit slit.

---

[7] H. D. Babcock and C. E. Moore, *Ap. J.*, **83**, 103, 1936; H. D. Babcock, *Ap. J.*, **111**, 60, 1950.

b) AUTOMATIC METHOD

Infrared wave-length standards may also be derived with reference to known standards in the second-order spectrum by a relatively rapid automatic method. The entrance and exit slits are first adjusted until the first- or second-order spectrum, whichever is the fainter, produces a usable deflection in the Speedomax recorder. The predispersing unit is then adjusted to shorter wave lengths, and a short section of the second-order spectrum is traced. Next, the predispersing unit is adjusted to longer wave lengths, and a short section of the first-order spectrum is traced. Alternate sections of the second- and first-order spectra are traced until the region to be measured has been covered. A neutral absorbing wedge, placed in front of the predispersing unit, serves to reduce the intensity of the brighter-order spectrum approximately to that of the fainter order. (A sample tracing of the first- and second-order spectra is shown in Fig. 2.) Finally, the wave lengths of the first-order lines are interpolated between those in the adjacent second-order tracings, which are taken from the *Infra-red Extension* to the *Revised Rowland*.[6]

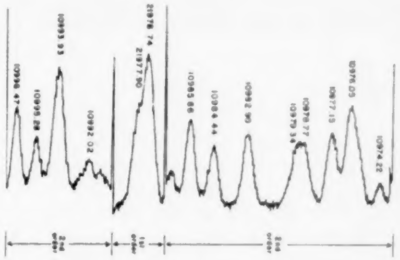

FIG. 2.—Tracings of first- and second-order infrared solar spectra, illustrating automatic method of wave-length determination. The wave length of the central first-order line, λ 21976.74, has been measured by interpolation between the overlapping second-order lines on either side.

The major advantage of the automatic method is its speed and efficient use of observing time. The line settings may be made without ambiguity by simple bisection of the profiles, and both spectrum orders are recorded with the same slit widths. On the other hand, the accuracy of the measures depends on the constancy of the grating and paper drives, and the slit widths are generally wider than the optimum for the second-order spectrum. Also, the wave lengths derived by this method for the 2μ region will be less accurate than those in the 1.6μ region because interferometric measures of wave lengths in the *Infra-red Extension* were not carried to wave lengths longer than about λ10600.

Both visual and automatic methods have been used to measure the wave lengths of about 1020 standard lines in the interval 1.4–2.5μ. On the average, the measured lines are spaced about 5–6 A apart, but the interval varies considerably, depending on the availability of suitable lines, and is much greater in regions of strong telluric absorption. The number of infrared standards has therefore been increased by a large factor as compared with those given in the infrared atlas,[1] which are separated by 30–40 A, on the average. The root-mean-square error of the standard wave lengths, as derived from repeated measurements of a single line, is ± 0.13 A for the 1.6μ region, ± 0.17 A for the 2.3μ region, and ± 0.16 A for both regions combined.

Wherever possible, the wave lengths of the solar lines given in Table 1 are direct measures with reference to overlapping orders. The wave lengths of the remaining lines have been interpolated linearly, an average of five standard lines being used for each interpolation. In the interpolation process, the standards derived by the visual and automatic methods have been assigned weights 1 and 2, respectively.

The solar wave lengths have been examined for scale and zero-point differences in comparison with those measured in the laboratory or predicted from term values. Laboratory measures with the lead sulphide cell have been made for *Fe* I in the region 1.0–1.9μ by Knopf and Fisher[8] at the Northwestern Technological Institute, for *Ca* I, by Humphreys[9] at the National Bureau of Standards, and for *CO* by Plyler, Benedict, and Silverman,[10] also at the Bureau of Standards. The differences, sun − lab, and sun − pred., are shown in Figure 3. The lines represented are those for which both laboratory and predicted wave lengths are available and which are believed to be unblended. For the *Fe* and *Ca* lines combined, the mean difference, solar − lab., is ±0.060 A ± 0.065. For the *CO* lines the mean difference, solar − pred., is ±0.005 A ± 0.022. The solar wave lengths of *Fe* and *Ca* lines, therefore, tend to agree with the predicted rather than with the laboratory wave lengths.

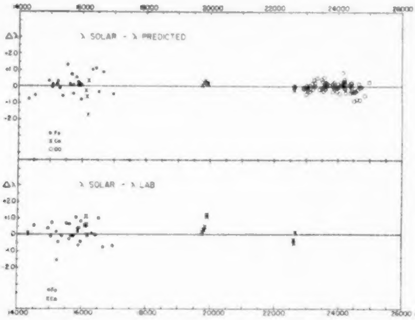

FIG. 3.—Wave-length differences in angstroms, solar − pred. (*upper*) and solar − lab. (*lower*).

IV. INTENSITY MEASUREMENTS

Some three thousand tracings, each about 80 A in length, were examined and intercompared in the search for solar lines. The best of these, many of which are of much better resolution than those in the infrared atlas, have been selected for the measurement of equivalent widths contained in the second column of Table 1. Four steps are involved in the measurement. First, the profiles must be converted to a linear intensity scale. Second, the dispersion must be established from the wave-length scale. Third, the continuum must be located and the effects of blending taken into account in the representation of the profile. Finally, the area under the profile must be measured and converted to units of equivalent width.

a) INTENSITY CALIBRATION

The calibration of the deflection of the Speedomax recorder in terms of true intensity has been accomplished as a result of extensive measurements of intensity with the Snow telescope installation by Mr. Dale Vrabec. The curve relating deflection to intensity, which is illustrated in Figure 2 of the infrared atlas,[1] was obtained by application of the inverse-square law. Inspection of the calibration-curve shows that the *PbS* cell and amplifier are very nearly linear over the range from 15 to 100 per cent of the deflection normally corresponding to the continuum. All the solar lines observed in the infrared are comparatively so weak that their observed profiles are always on the linear portion of the calibration-curve. Hence it is sufficient merely to extend the linear portion of the curve downward to its intercept on the deflection axis and to measure relative intensities directly from the depressed zero.

---

[8] Unpublished. We are indebted to Dr. Fisher for communicating the results in advance of publication.

[9] *J. Res. Nat. Bur. Stand.*, **47**, 262, 1951.

[10] *J. Chem. Phys.*, **20**, 175, 1952.

b) DISPERSION

The dispersion of the tracings in each region of the spectrum has been determined from the wave-length measurements described in the preceding section. For the purpose of equivalent width determinations, a mean dispersion-curve was derived from the plotted points in Figure 3 of the atlas.

c) CORRECTION FOR BLENDING

The solar lines are relatively so weak and infrequent that they are most often found blended with a telluric line rather than with another solar line. In the event of blending with a telluric line, the continuum is no longer a straight line parallel to the zero base but must be taken as the profile of the telluric line. When the variation in intensity of the telluric line over the profile of the solar line is small, the measuring procedure is relatively simple. The blended half of the telluric line is reconstructed by symmetry with the remainder of the line, and the area measured is that bounded by the sketched-in profile of the telluric line and the observed profile of the solar line. When the variation in intensity of the telluric line over the profile of the solar line is large, a more exact procedure is indicated. Let $i_\lambda(s)$ and $i_\lambda(t)$ be the percentage residual intensities at wave length λ of the solar and telluric lines, respectively, and let $i_\lambda(b)$ denote the intensity of the blended profile. Then

$$i_\lambda(b) = i_\lambda(s)\, i_\lambda(t) . \tag{2}$$

Since $i_\lambda(b)$ is known and $i_\lambda(t)$ may be found from the unblended half of the telluric line, $i_\lambda(s)$ may be computed.

The separation of the equivalent widths of two blended solar lines is more difficult and has been the subject of study by many investigators. The Utrecht workers,[11] for example, consider that the reconstructed wing of the stronger line defines the top of the area of the weaker line. An analysis of the transfer equation then leads to the preparation of tables relating the observed area to the undisturbed area. For close pairs they have used "model doublets" computed for a number of intensity ratios and separations. Inasmuch as the present intensity measurements are of a very preliminary nature and will undoubtedly be repeated in the near future with records of higher resolution, it was felt that the simplest possible procedure should be followed in the separation of blends. Accordingly, the blended profiles were separated merely by sketching in the blended wings of both lines from symmetry considerations. The equivalent widths so determined will be slightly too large.

In many instances the blending is so close that no reliable separation can be made. In order to indicate the extent of blending, each entry in the second column of Table 1 has beside it a letter with the following meaning:

---

[11] *Recherches Astr. Obs. Utrecht*, Vol. **12**, Part 2, 1951.

A. Indicates no blending, or so little that the wings and continuum are very well established.
B. Some blending, 50 per cent or less of the line involved; equivalent width uncertain by 10–25 per cent.
C. Strong blending; equivalent width uncertain by about 50 per cent.
D. Very strong blending; equivalent width uncertain by about 100 per cent.
E. Equivalent width hardly more than a rough guess.

d) MEASUREMENT OF AREAS

The areas of the profiles were obtained by one of two methods. For the stronger lines, the planimeter method was used, each profile being circumscribed a total of ten times. For the smaller areas, and as a check on the larger ones, the tracings were contact-printed on double-weight photographic paper, and the areas cut out and weighed with an accuracy of 2–3 per cent. The weights were then compared with those of standard areas, consisting of rectangular strips processed at the same time.

The equivalent widths listed in Table 1 refer to radiation from the center of the disk, except for relatively few lines for which only limb profiles were measurable. The limb values are denoted by the letter "L" and refer to the point on the disk for which $\cos\theta = 0.2$. Most of the values given in the table are averages from three tracings. Some of the strong lines have been measured on five tracings, and the values for about 10 per cent of the fainter lines are based on a single tracing.

V. IDENTIFICATIONS

Preliminary identifications of infrared solar lines have been reported previously for the regions 1.52–1.75μ and 1.95–2.49μ. The earlier lists contained about 400 solar lines, of which 140 were assigned identifications almost wholly on the basis of predicted wave lengths. In the present paper the number of solar lines has been more than doubled, and the number of identifications more than tripled through the tentative identification of about 470 lines. The increase in the percentage of identified lines results chiefly from the recent laboratory investigation of the infrared *Fe* I spectrum by Knopf and Fisher and from the discovery of *CO* in the sun.[12] For example, the *CO* molecule accounts for about 125 lines in the spectrum of the disk center from 2.3μ to 2.5μ.

The entries in Table 1 relevant to the identifications are given in the third to the seventh columns, inclusive. The third column gives the atom or molecule responsible for the line; the fourth column, the wave length measured in the laboratory; the fifth column, the predicted wave length; the sixth column, the term designation or, for the *CO* lines, the vibrational transition, the *J*-value of the lower level, and the membership of the line in either the positive *R* branch or the negative *P* branch; and the seventh column, the lower excitation potential. The measured wave lengths in the fourth column were taken from Knopf and Fisher[8] for *Fe* I and from Humphreys[9] for *Ca* I. The predicted wave lengths were computed from C. E. Moore's[13] tables of atomic term values or from the constants of the *CO* molecule derived by Plyler, Benedict, and Silverman.[10]

It is worth noting that every line of *Ca* I and *Fe* I that is observed in the laboratory appears in the solar spectrum or is masked by a telluric line. Additional fainter lines, especially of *Fe* I, are found in the sun and not in the laboratory. The absence of many *Fe* I lines from the laboratory is mainly an effect of temperature. The infrared lines are nearly all of excitation potential higher than 4 volts, and many of the weaker ones are enhanced by the high solar temperature. The absence of the fainter lines from the laboratory spectra is also to be explained in part as a consequence of somewhat lower resolving power. The great brightness of the sun in the infrared makes possible the use of very narrow spectrometer slits, as compared with those employed with laboratory spectra. For example, the 2–2 and 3–3 transitions of the *Ca* I multiplet $4d^3D-4f^3F^\circ$ reported by Humphreys as unresolved with respect to adjacent strong lines are clearly separated in the solar spectrum.

---

[12] L. Goldberg, R. R. McMath, O. C. Mohler, and A. K. Pierce, *Phys. Rev.*, **85**, 140, 1952. A detailed discussion of *CO* in the sun will appear shortly in *Ap. J.*

[13] *Nat. Bur. Stand. Circular*, No. 467, 1948.

Many of the solar-line identifications that are based on predicted wave lengths are highly tentative. It is especially difficult to be certain of the *Fe* I identifications, since the parity rule seems to be the only certain barrier to the appearance of the lines. Some of the coincidences given in Table 1 may therefore be due to chance. Also, the *C* I term values are uncertain, and many of the predicted wave lengths are not known to an accuracy of better than 1–3 A. It is to be hoped that further infrared studies of atomic spectra will soon be made in the laboratory. The atoms most urgently in need of investigation are carbon, magnesium, and silicon. The *Fe* I spectrum should also be explored further for fainter lines and extended beyond its present observed limit of 1.9μ.

The authors wish to express their appreciation to Dr. I. S. Bowen for making available the Snow telescope, to Mr. Dale Vrabec for obtaining many of the tracings, and to Mr. Russell A. Donovan for assistance in certain phases of the reductions.

EJECTION OF HYDROGEN AND IONIZED CALCIUM ATOMS WITH HIGH VELOCITY AT THE TIME OF SOLAR FLARES*

HELEN W. DODSON, E. RUTH HEDEMAN, AND JOSEPH CHAMBERLAIN†
McMath-Hulbert Observatory of the University of Michigan
Received September 6, 1952

ABSTRACT

High-velocity ejections of both hydrogen and ionized calcium atoms at the time of *onset* of five flares near the solar limb are described. For four of the five cases, reports of solar radiation at radio frequencies are available and indicate bursts or "outbursts" at the start of the flare and ejection. Consideration of time relationships and of the frequency of occurrence of 200 Mc/sec bursts with flares leads to the suggestion that the burst at radio frequencies is to be associated with the high-velocity ejection rather than with the *Hα* brightening.

Observational evidence for material particles moving outward from the sun with very high velocities at the time of solar flares is limited. The existence of such corpuscular ejections has been inferred from the onset of geomagnetic storms some 1–3 days after the occurrence of certain great flares near the central part of the solar disk. Faint absorption observed on the short-wave-length side of the H and K lines in the solar spectrum during geomagnetic storms[1, 2] and the detection of hydrogen emission in the aurora[3] with a high velocity of approach to the earth[4] tend to strengthen the above inference. Furthermore, an apparent weakening in the violet wing of *Hα* flare emission has been interpreted as indicating the presence of a rapidly ascending hydrogen absorption cloud above certain flares observed on the solar disk.[5]

This paper presents observations made at the McMath-Hulbert Observatory of hydrogen and ionized calcium atoms moving away from the sun with very high velocities at the time of the *onset* of five flares near the solar limb. Because of limitations inherent in the observations, the measured velocities represent minimum values. For the ejection of July 6, 1948, the outward velocity was at least 750 km/sec and thus was greater than the velocity of escape from the sun. The large motions outward from the sun and *across* the observer's line of sight were accompanied by large motions *along* the line of sight. The latter were indicated by Doppler shifts in *Hα* spectra recorded with the Stone spectroheliograph.[6] After each ejection some faint material fell back to the solar surface, but the fall was not comparable to the rise.

The high-velocity ejections here described are considered as differing in degree, if not in kind, from the often reported surge-type prominences (at the limb)[7] and "active dark flocculi" (on the disk)[8, 9] that accompany flares. The latter phenomena have smaller

---

* Work supported in part by Contract N6-onr-232-V with the Office of Naval Research.

† Now with the Air Force Cambridge Research Center.

[1] R. S. Richardson, *Trans. Amer. Geophys. Union*, p. 558, 1944.

[2] H. A. Bruck and F. Rutlant, *M.N.*, **106**, 130, 1946.

[3] C. W. Gartlein, *Trans. Amer. Geophys. Union*, **31**, 18, 1950.

[4] A. B. Meinel, *Phys. Rev.*, **80**, 1096, 1950.

[5] M. A. Ellison, *M.N.*, **103**, 3, 1943.

[6] R. R. McMath, *Pub. Michigan Obs.*, **8**, 141, 1942.

[7] R. R. McMath and Orren Mohler, *Observatory*, **68**, 110, 1948.

[8] H. W. Newton, *M.N.*, **102**, 2, 1942.

[9] M. A. Ellison, *M.N.*, **102**, 11, 1942.

velocities and are observed later in the course of the flare than the ejections here reported. It is possible that the type of prominence known as "ejection,"[10] for which the observed motion is outward only, may include examples of the type under consideration. The high-velocity prominence of January 12, 1926, photographed by Pettit,[11] and the great limbward ejection at the start of the flare of November 19, 1949, reported by Ellison and Conway,[12] appear to be phenomena similar to the high-velocity ejections described in this paper.

Records or reports of solar radiation at radio frequencies are available for the times of four of the five flares and ejections here considered. For each of the four cases there is evidence of a distinct burst of considerable magnitude at the time of the *start* of the flare and ejection. A general study of solar flares and 200 Mc/sec radiation[13] has shown that burstlike events occurred on 200 Mc/sec records near the commencement of only 40 per cent of the flares. The *Hα* brightening is therefore not "sufficient" for the emission of a burst at this radio frequency. The observations described in this paper suggest that the burst, or "outburst," observed on radio frequencies near the start of solar flares may be associated with the *high-velocity* ejections that accompany certain flares. This is consistent with the results of interferometric measures made in Australia on radio frequencies, which indicate that the sources of certain outbursts are in rapid motion.[14]

OBSERVATIONAL DATA[15]

July 6, 1948.—For this date, Ca^+ spectroheliograms (λ 3933) and *Hα* spectra and spectroheliograms photographed in the 50-foot solar tower of the McMath-Hulbert Observatory record the outbreak of a flarelike prominence at or near the west limb of the sun at least as early as $15^h03^m30^s$ U.T. It had not completely faded when, at 15^h24^m, it rose and brightened a second time. It had faded by 16^h00^m. A sudden ionospheric disturbance (SID) was recorded in Washington between 15^h03^m and 16^h00^m and in England from 15^h25^m to 15^h40^m.[16] The two reported starting times of the SID's represent the two different outbreaks of the flare and agree within 1 minute with the two observed brightenings of the flarelike prominence at the solar limb.

This flare of July 6, 1948, although rooted on the disk, extended outward into an intensely bright elevated phenomenon for which the height was 50,000 km. The intensity of the prominence-like flare cannot be compared directly to that of disk flares because the Ca^+ "limb and disk" spectroheliograms on which it is recorded were made through a semitransparent occulting disk of unknown transparency. *Hα* flare radiation was as much as 9 A wide and showed Doppler shifts of more than +5 A during the first rise and −3 A during the second elevation of the flare. Only minimum values of the Doppler shift are known, because the spectrum data are restricted to 13 A in the neighborhood of *Hα* and the flare emission extended beyond these limits. During the later phases of the activity, the flarelike prominence remained nearly fixed at a height of 35,000 km. At this time *Hα* was 5 A wide and relatively symmetrical.

Between 15^h10^m and 15^h25^m the flarelike prominence moved laterally about 50,000 km. This motion was so different from that usually recorded on our prominence films that the feature became known to us as "the walking ghost." It has been a curiosity in our film file.

---

[10] R. R. McMath and E. Pettit, *Ap. J.*, **88**, 244, 1938.

[11] *Ap. J.*, **84**, 319, 1936.

[12] *Observatory*, **70**, 77, 1950.

[13] Being prepared for publication by H. W. Dodson, E. R. Hedeman, and L. Owren.

[14] W. N. Christiansen, J. V. Hindman, A. G. Little, Ruby Payne-Scott, D. B. Yabsley, and C. Allen, *Australian J. Sci. Res.*, **4**, 51, 1951.

[15] All times recorded are U.T., Universal Time, or Greenwich Civil Time with the day starting at midnight.

[16] Central Radio Propagation Laboratory, National Bureau of Standards, F48, p. 38, 1948.

Two additional phenomena took place in the neighborhood of this prominence-like flare. The first was a high-velocity ejection observed between 15^h06^m and 15^h20^m. It could have started earlier than 15^h06^m and not have been observed because of Doppler shifts greater than 5 A or because the spectrograph slit did not cross its exact location. The ejection was at least as high as 25,000 km at $15^h06^m44^s$, and its line-of-sight velocity was at least as great as -200 km/sec. For the next $1\frac{1}{2}$ minutes it moved outward from the solar surface (across the observer's line of sight) with a velocity of the order of 750 km/sec. By 15^h12^m the ejection had reached a height of 190,000 km, and the observed outward velocity was reduced to 300 km/sec. During this time interval, the line-of-sight velocity also decreased slowly to about -100 km/sec, and $H\alpha$ was 2 A wide. The ejection was traced to 290,000 km above the sun's limb. It was very faint at heights greater than 200,000 km. At these heights some of the $H\alpha$ spectra continued to show negative line-of-sight velocities. Others had positive displacements, indicating that some material had started to fall back toward the sun. The path of this ejection was nearly linear and cut the tangent to the solar limb at an angle of 84°.

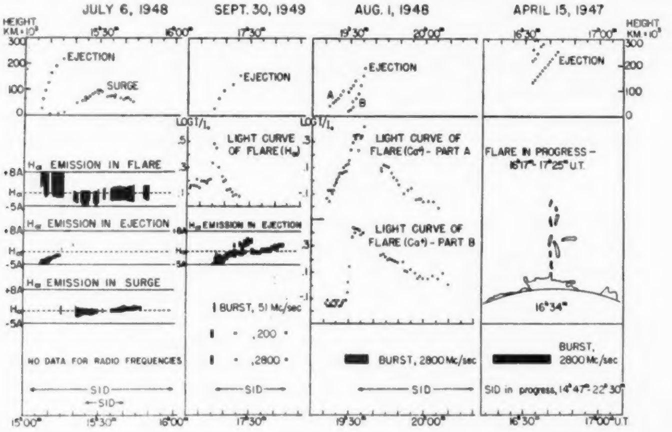

FIG. 1.—Diagram showing time relationships for ejections and surge, width and position of $H\alpha$ emission, intensity of flare, bursts at radio frequencies, and sudden ionospheric disturbances.

The second activity recorded in the neighborhood of the flare was a surge-type prominence that began its principal rise at 15^h15^m and reached a height of 95,000 km 15 minutes later. It faded as it sank back to the solar surface. The velocity across the line of sight did not exceed 200 km/sec. The maximum line-of-sight velocity was about 50 km/sec and changed from minus to plus as the motion of the surge changed from ascent to descent. In the surge $H\alpha$ was of the order of 2 A wide.

The time relationships, the changes in height, Doppler shifts, and widths and positions of $H\alpha$ are summarized in Figure 1 for the prominence-like flare, the high-velocity ejection, and the surge-type prominence. Spectra and spectroheliograms in Figures 2 and 3 show some of the phenomena here described. To a first degree of approximation, the features as recorded in $H\alpha$ and the K line of ionized calcium are remarkably similar; but closer examination, especially for the spectroheliograms for 15^h46^m, shows certain marked differences in the intensity distribution for the two elements. The surge remained as a distinct feature longer in *Hα* than in the K line of Ca^+. On the other hand, the central part of the loop was brighter in Ca^+. Both elements were present in the high-velocity ejection.

No records of solar radiation at radio frequencies are available to the writers for the time of this flare and ejection.

September 30, 1949.—On this date a high-velocity ejection of hydrogen atoms, very similar to the one described above, was observed at the east limb of the sun, at the time of the onset of a flare in a large *plage* and spot group. The photometric light-curve of the flare shows that the rapid brightening in *Hα* began between 17^h14^m and 17^h15^m U.T. An SID was reported as starting at 17^h17^m (see Figs. 1 and 2).[17]

TABLE 1

SUMMARY OF OBSERVATIONS

DATE	FLARE IMPORTANCE	TIME OF START (U.T.)			MAX. OBSERVED VELOCITY (KM/SEC)	BURST ON RADIO FREQUENCIES
		Flare	SID	Ejection		
Apr. 15, 1947	2	$<16^h17^m$	In prog.	$<<<16^h33^m$	500	16^h18^m–16^h41^m; 2800 Mc/sec
July 6, 1948	1	15 03.5	15^h03^m	<15 06.7	750	No data
Aug. 1, 1948 (a)	2	19 22	None	<19 22	>270	No burst on 2800 Mc/sec
Aug. 1, 1948 (b)		19 29.5	19 34	19 29	>570	19^h29^m–19^h38^m; 2800 Mc/sec
Sept. 30, 1949	1	17 14.5	17 17	<17 15.8	350	17^h15^m–17^h16^m; 200 Mc/sec; 2800 Mc/sec 17^h16^m–$17^h16^m.8$; 51 Mc/sec
May 8, 1951	2	15 05	15 06	≥15 08	500	$15^h08^m.5$–$15^h09^m.5$; 200 Mc/sec

The high-velocity ejection was first observed at $17^h15^m46^s$ at an elevation of at least 25,000 km. It moved outward from the sun with an initial velocity as great as 350 km/sec. The line-of-sight velocity exceeded −200 km/sec and *Hα* was 5 A wide. Prominence material was observed at a height of 150,000 km at 17^h26^m. The path of the nearly linear trajectory of this ejection cut the solar limb at an angle of 62°. Heights and velocities are again minimum values due to observational limitations.

Records of 200 Mc/sec solar radiation secured at Cornell University at the time of this ejection show a distinctive burst starting at 17^h15^m and lasting for 1 minute (see Fig. 4). A single burst of 1 minute's duration is reported for this same time on 2800 Mc/sec from the National Research Council, Ottawa, Canada.[18] The National Bureau of Standards in Washington, D.C., recorded a distinctive single burst on 51 Mc/sec at 17^h16^m, which lasted for 0.8 minute.[19] Since the radio burst at the start of this flare and high-velocity ejection was apparently observable over a wide range of radio frequencies, it falls into the category known as "outburst."

May 8, 1951.—The flare that occurred on the east limb of the sun at 15^h05^m U.T. on this date has already been fully described.[20] In addition to the flare, the spectra and *Hα* spectroheliograms show that a faint prominence with large Doppler shifts moved outward from the sun with a velocity across the line of sight of the order of 500 km/sec at about 15^h08^m. It reached a height of at least 216,000 km by 15^h14^m U.T. Detailed examination of the 200 Mc/sec records for this date shows a distinct burst of 1 minute's duration, superposed on the general activity and gradual increase in flux associated with this flare. The burst began at $15^{h}08^{m}.5$ (see Fig. 4).

---

[17] Central Radio Propagation Laboratory, National Bureau of Standards, F62, p. 32, 1949.

[18] A. E. Covington, *Pub. Nat. Res. Council of Canada, ERA-192*, p. 40.

[19] *Quart. Bull. Solar Activity*, No. 87, p. 84, 1949.

[20] H. W. Dodson, *Ap. J.*, **115**, 78, 1952.

August 1, 1948.—A flare of importance 2 took place at N. 12° W. 77° on this date. This flare and attendant limb activity are recorded on calcium spectroheliograms in which the photosphere is covered by a semitransparent occulting disk. A number of different regions brightened to flare intensity at slightly different times. Photometric light-curves show that the first brightenings began at $19^{h}22^{m}$ U.T., the later brightenings at $19^{h}29^{m}.5$. The onsets of both brightenings were accompanied by high-velocity ejections beyond the solar limb. The first ejection was in progress at $19^{h}22^{m}$. It attained an outward velocity of 270 km/sec by $19^{h}26^{m}$. The second ejection began at $19^{h}29^{m}$. Its velocity across the line of sight became as great as 570 km/sec at $19^{h}33^{m}$, when it moved out of the field of the spectroheliograph. The path of these ejections cut the solar limb at an angle of 75°. No *Hα* spectra are available for this date.

Reports from Ottawa[21] of 2800 Mc/sec solar radiation indicate that no burst occurred with the ejection at $19^{h}22^{m}$ but that a burst of 9 minutes' duration began at $19^{h}29^{m}$.

April 15, 1947.—Solar observations for this date at the McMath-Hulbert Observatory were interrupted by clouds between $16^{h}03^{m}$ U.T. and $16^{h}33^{m}$ U.T. A flare of importance 2 at S. 37° W. 90° was reported by the Meudon Observatory as being in progress between

---

[21] Covington, *op. cit.*, p. 36.

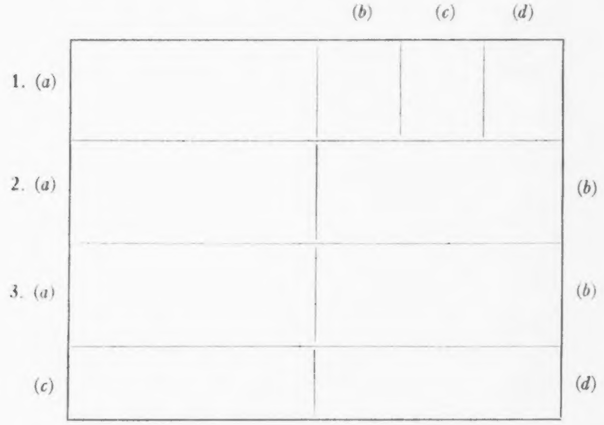

FIG. 2.—1. September 30, 1949. *a*, *Hα* spectroheliogram showing flare near limb, $17^{h}16^{m}$ U.T. *b*, *c*, *d*, Thirteen angstroms of spectrum showing *Hα* emission in the ejection for $17^{h}17^{m}$, $17^{h}20^{m}$, and $17^{h}25^{m}$ U.T., respectively. (Dispersion runs vertically, wave lengths increase upward. The dark *Hα* absorption line of scattered sunlight provides a reference wave length and indicates height of slit above solar limb.)

2. August 1, 1948. *a*, Ionized calcium (K line) spectroheliogram showing flare on disk and ejection at limb, $19^{h}38^{m}$ U.T. *b*, Thirteen angstroms of spectrum centered on *Hα* showing emission in the ejection, $19^{h}38^{m}$ U.T. (see description above).

3. July 6, 1948. *a*, Ionized calcium (K line) spectroheliogram of flare and ejection, $15^{h}13^{m}$ U.T. *b*, *c*, *d*, Thirteen angstroms of spectrum in neighborhood of *Hα* for $15^{h}13^{m}$, $15^{h}25^{m}$, and $15^{h}35^{m}$ U.T., respectively, showing *Hα* emission in ejection, flare, and surge (see description above).

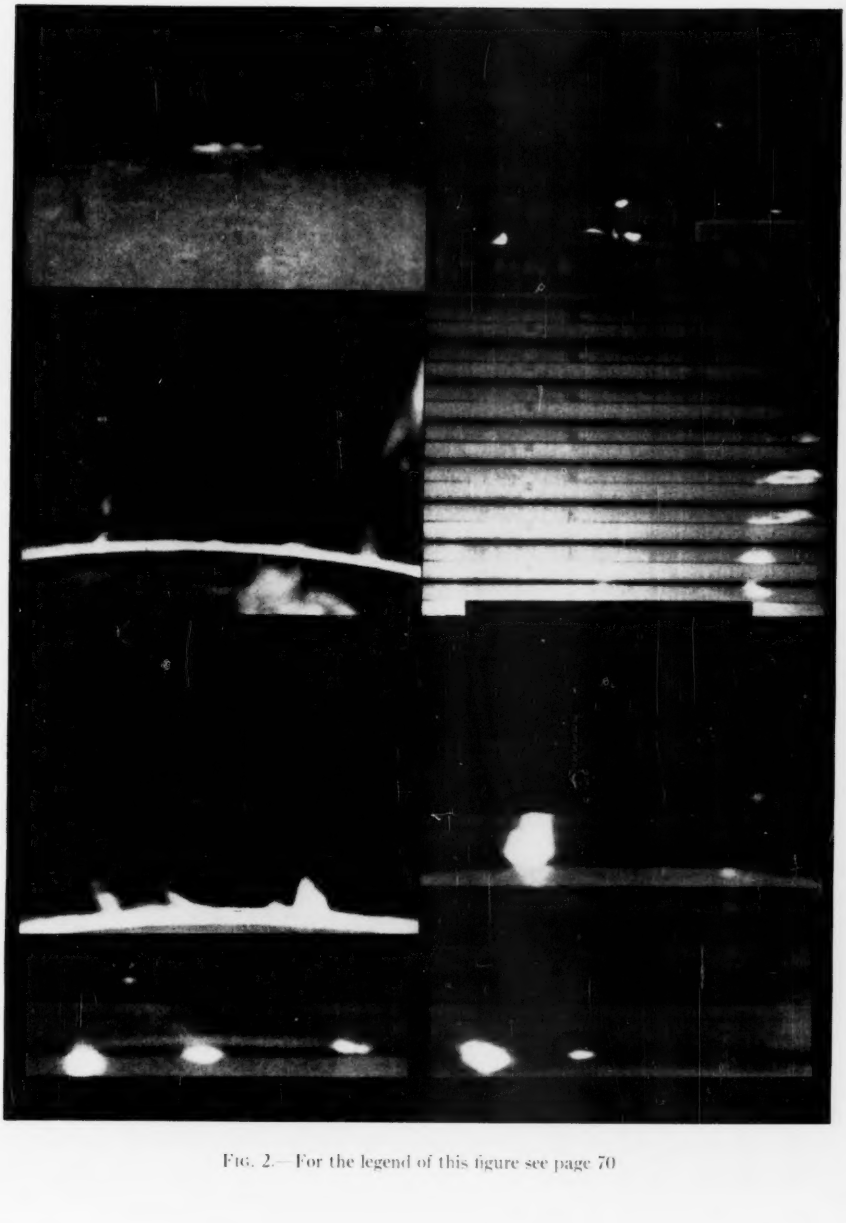

FIG. 2.—For the legend of this figure see page 70

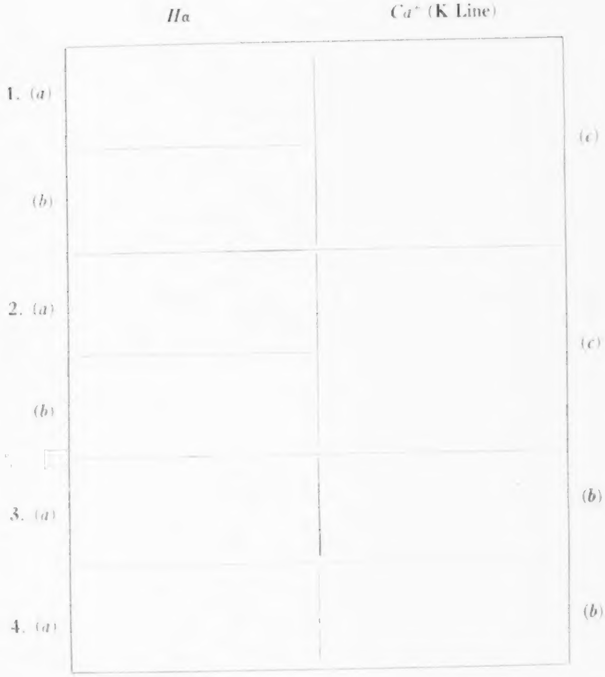
$H\alpha$
Ca^{+} (K Line)
1. (a)
(c)
(b)
2. (a)
(c)
(b)
3. (a)
(b)
4. (a)
(b)

FIG. 3.—Hydrogen and ionized calcium spectroheliograms showing ejection, flare, and surge, July 6, 1948.

1. *a*, $15^{h}10^{m}$ U.T.; *b*, $15^{h}13^{m}$ U.T.; *c*, $15^{h}13^{m}$ U.T.
2. *a*, $15^{h}15^{m}$ U.T.; *b*, $15^{h}22^{m}$ U.T.; *c*, $15^{h}22^{m}$ U.T.
3. *a*, $15^{h}38^{m}$ U.T.; *b*, $15^{h}38^{m}$ U.T.
4. *a*, $15^{h}46^{m}$ U.T.; *b*, $15^{h}46^{m}$ U.T.

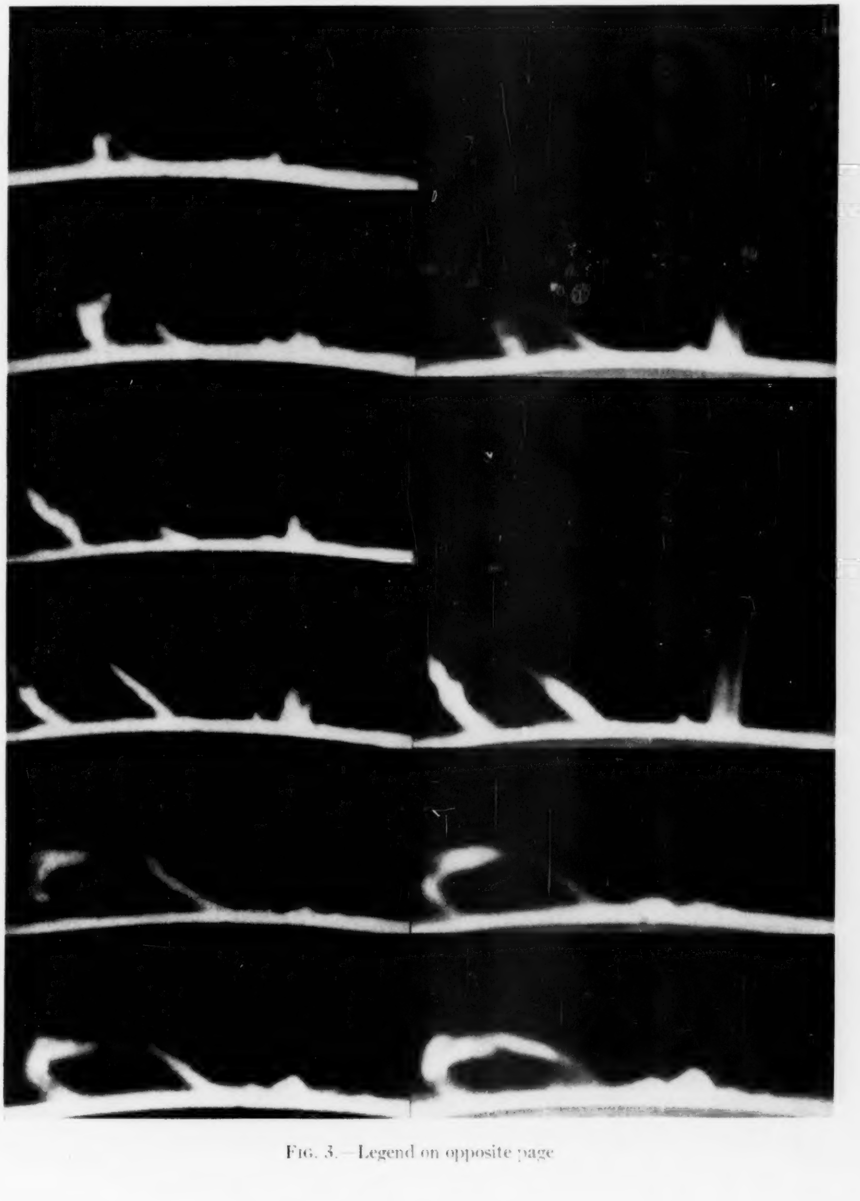

FIG. 3.—Legend on opposite page

16^h17^m and 17^h25^m.[22] The report from Ottawa[23] of 2800 Mc/sec solar radiation indicates a burst from 16^h18^m to 16^h41^m. The calcium and hydrogen spectroheliograms photographed from 16^h33^m onward show that a very great ejection had taken place prior to this time. Its path was almost radial, and it extended more than 300,000 km above the solar surface. At 16^h33^m it was still moving outward with velocities of 230–500 km/sec. Doppler shifts were positive and ranged from 2 to 4 angstroms. *Hα* was 1 to 3 angstroms wide.

SUMMARY

The above observations indicate that high-velocity ejections take place at the time of *onset* of certain flares. Atoms of both hydrogen and ionized calcium are present in the ejections. The ejection may originate from a region on the solar disk relatively close to

---

[22] *Quart. Bull. Solar Activity*, No. 78, p. 77, 1947.

[23] Covington, *op. cit.*, p. 34.

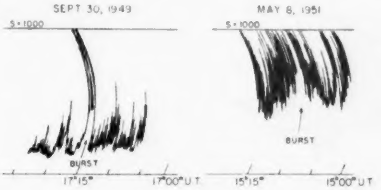

FIG. 4.—Distinct bursts of 200 Mc/solar radiation recorded at Cornell University at time of start of ejections; September 30, 1949, and May 8, 1951.

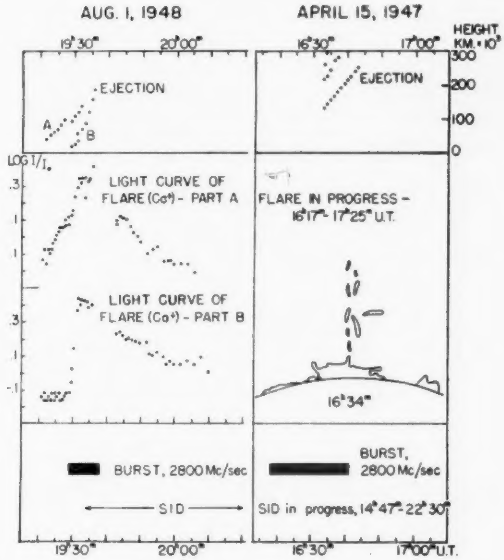

FIG. 5

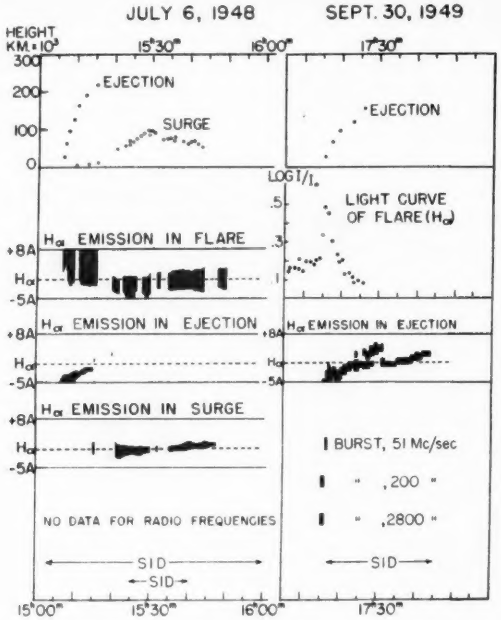

Fig. 6

the observed *Hα* brightening (September 30, 1949) or from an area some 100,000 km distant (July 6, 1948). The apparent trajectories are nearly linear and cut the solar limb in directions that deviate from the radial by as much as 30°. Distinctive bursts occurred on radio frequencies at the start of the high-velocity ejections.

The authors wish to express their appreciation to all members of the staff of the McMath-Hulbert Observatory who assisted in securing the observational material here presented and to the Department of Electrical Engineering of Cornell University for providing the 200 Mc/sec solar records.

Hα EMISSION STARS AND PECULIAR OBJECTS IN THE REGION OF THE ORION NEBULA

GUILLERMO HARO
Tonantzintla and Tacubaya Observatories, Mexico

Received May 9, 1952

ABSTRACT

Two hundred and fifty-five stars showing emission in *Hα* have been observed in an area of 3.5 square degrees which contains the brightest part of the Orion Nebula. The distribution and frequency of these emission stars seem to be correlated with the general shape and differing intensity of the bright nebulosities of this region. At the same time the existence of a dense stellar group—provisionally called the "Orion Nebula Cluster"—centered at the Trapezium stars is strikingly revealed. Fourteen peculiar objects, most of them stars imbedded in nebulous material, have been found in the same area. One of these is probably a new faint cometary nebula. The apparent coexistence and concentricity observed between the Nebula and the densest group of emission stars suggests a tentative hypothesis of the formation of late-type dwarf stars from the Orion nebular material.

At the American Astronomical Society meeting held in Tucson, Arizona, in December, 1949, the writer presented his preliminary results on faint stars with strong emission in and around the Orion Nebula.[1] At that time it was stated that 37 of the Orion variables listed in Kukarkin and Parenago's variable-star catalogue had been found to show conspicuous bright *Hα* in their spectrum, while 100 other stars, not listed in that catalogue, also showed emission characteristics. Soon thereafter Herbig's[2] independent investigation of 11 Orion variables with spectra showing emission lines appeared. Both Herbig's and the writer's observations pointed out the weakness of previous speculations which were based on the apparent absence of stars with spectacular emission spectra in the Orion Nebula.

In the present investigation the writer's former results have been summarized and considerably extended by new observations. These results may be stated as follows: (1) A large number of emission stars and evidence of change in some of the characteristics of many have been found. (2) The presence of a strong stellar concentration, probably a star cluster, centered approximately at the Trapezium stars and extending over practically the whole area covered by the main body of the Nebula is indicated. (3) Some peculiar objects found during this investigation are discussed in further detail.

I. OBSERVATIONAL DATA

The observational material was secured with the Tonantzintla Schmidt telescope, and 81 plates centered on the Trapezium were obtained. Of these, 31 were taken with the 4° objective prism, using 103*a*-E plates and a red filter; the remaining 50 were direct photographs on plates sensitized for different wave lengths. All the spectral plates were taken from 1949 to the beginning of 1952 with exposure times of 5–120 minutes. Most of the direct plates were obtained during the same period of time. The limiting photographic magnitude reached for emission stars is approximately 17.5.

a) STARS WITH *Hα* IN EMISSION

Table 1 gives the list of 255 stars with emission *Hα* found in an area of 3.5 square degrees covering the main body of the Orion Nebula. The first column gives the serial number by which the stars are identified in the included charts. The second and third col-

---

[1] *A.J.*, **55**, 72, 1950.

[2] *Ap. J.*, **111**, 15, 1950.

TABLE 1

STARS WITH $H\alpha$ IN EMISSION

No.	R.A. (1900)	Dec. (1900)	Name	Brun's No.	Max.	Min.	Int. Br't $H\alpha$	Light-Variation	Figure	Notes
1	...	...	...	...	...	...	4–1	V	3	
2	...	...	...	...	...	...	4–0	V	3	
3	...	...	...	150	...	...	3–0	V	3	
4	...	...	...	...	...	...	3–0	V	3	
5	$5^h30^m46^s$	−4°28′.8	BO	810	13.6	15.4	5–0	V	3	1
6	5 30 13	−4 31.6	SY	515	13.9	16.0	5–5	V	3	
7	...	...	...	509	...	...	4–3	V	3	
8	...	...	...	...	...	...	5–3	V	3	
9	...	...	...	...	...	...	5–4	V	3	2
10	...	...	...	554	...	...	3–0	V	3	
11	...	...	...	...	...	...	4–2	V	3	
12	...	...	...	392	...	...	2–0	V	3	
13	...	...	...	264	...	...	4–1	V	3	2
14	...	...	...	...	...	...	4–2	V	3	
15	...	...	...	...	...	...	3–3	...	3	
16	5 31 12	−4 45.3	CH	942	14.6	16.5	3–0	V	3	
17	...	...	...	...	...	...	2–0	V	3	
18	...	...	...	140	...	...	3–1	V	3	
19	5 30 26	−4 46.1	CD	648	14.2	15.7	3–0	V	3	
20	...	...	...	878	...	...	5–5	...	3	
21	...	...	...	222	...	...	4–0	V	3	
22	...	...	...	756	...	...	5–2	V	3	
23	...	...	...	571	...	...	3–0	V	3	1
24	5 30 58	−4 51.2	AS	898	15.0	17.0	4–1	V	3	1
25	...	...	...	754	...	...	5–3	V	3	
26	...	...	...	768	...	...	4–4	...	3	
27	...	...	...	739	...	...	5–2	V	3	1
28	...	...	...	507	...	...	5–2	V	3	2
29	5 29 33	−4 49.0	BV	256	15.2	17.2	5–3	V	3	3
30	5 28 38	−4 47.5	VX	106	15.1	16.6	4–4	V	3	
31	5 28 38	−4 48.1	BS	104	15.3	16.5	4–3	V	3	4
32	5 30 49	−4 52.0	...	842	14.0	15.0	4–0	V	3	
33	...	...	...	668	...	...	5–5	...	3	
34	5 28 59	−4 52.0	SU	156	14.2	(16.8	5–0	V	3	5
35	...	...	...	956	...	...	4–2	V	3	
36	...	...	...	...	...	...	5–5	...	3	2
37	...	...	...	723	...	...	3–0	V	3	
38	...	...	...	475	...	...	5–3	V	3	
39	...	...	...	...	...	...	3–0	V	3	
40	...	...	...	941	...	...	2–0	V	3	
41	...	...	...	267	...	...	5–5	...	3	
42	...	...	...	675	...	...	5–5	...	3	
43	5 30 07	−4 54.9	BY	469	14.9	16.8	4–0	V	3	1
44	...	...	...	...	...	...	4–4	...	3	2
45	5 29 15	−4 54.1	BT	200	14.8	16.9	4–4	V	3	
46	...	...	...	...	...	...	5–5	...	3	
47	...	...	...	...	...	...	5–5	...	3	
48	...	...	...	...	...	...	3–0	V	3	
49	...	...	...	...	...	...	4–4	...	3	2
50	...	...	...	654	...	...	2–0	V	3	
51	5 30 35	−4 59.2	AL	737	14.7	15.8	5–5	V	3	
52	...	...	...	800	...	...	4–4	...	3	
53	...	...	...	699	...	...	3–0	V	3	
54	...	...	...	743	...	...	3–0	V	3	6
55	...	...	...	...	...	...	4–4	...	3	2
56	...	...	...	...	...	...	3–3	...	3	
57	5 29 31	−5 01.4	...	258	13.9	14.5	4–1	V	3	
58	5 29 30	−5 01.4	...	249	13.6	14.1	4–2	V	3	

TABLE 1—*Continued*

No.	R.A. (1900)	Dec. (1900)	Name	Brun's No.	Max.	Min.	Int. Br't *Hα*	Light-Variation	Figure	Notes
59	.....	.....	.....	.....	.....	.....	4–2	V	3	
60	.....	.....	.....	323	.....	.....	4–4	.....	3	
61	.....	.....	.....	918	.....	.....	2–0	V	3	
62	.....	.....	.....	496	.....	.....	3–1	V	3	
63	.....	.....	.....	.....	.....	.....	4–2	V	3	
64	.....	.....	.....	964	.....	.....	3–0	V	4	
65	.....	.....	.....	.....	.....	.....	4–4	.....	6	
66	$5^h30^m52^s$	−5°05′.5	CE	856	15.6	16.9	4–4	V	4	
67	5 30 41	−5 05.2	TV	785	13.4	15.6	3–0	V	4	
68	.....	.....	.....	.....	.....	.....	3–3	.....	6	
69	.....	.....	.....	860	.....	.....	3–0	V	4	1
70	.....	.....	.....	1043	.....	.....	5–0	V	4	5–6
71	5 28 41	−5 06.1	VY	112	14.9	16.0	5–5	V	5	
72	5 30 59	−5 08.1	AR	901	14.0	(15.6	4–4	V	4	
73	.....	.....	.....	788	.....	.....	4–2	V	4	
74	5 29 58	−5 07.5	YZ	422	15.1	15.8	3–3	V	4	
75	.....	.....	.....	.....	.....	.....	2–2	.....	4	2
76	5 30 49	−5 09.6	AO	839	15.0	(16.8	2–2	V	4	
77	.....	.....	.....	752	.....	.....	4–4	.....	4	
78	.....	.....	.....	382	.....	.....	4–4	.....	4	
79	.....	.....	.....	662	.....	.....	2–1	?	4	
80	.....	.....	.....	1038	.....	.....	3–0	V	6	
81	.....	.....	.....	850	.....	.....	3–3	.....	4	
82	.....	.....	.....	368	.....	.....	3–1	V	4	
83	.....	.....	.....	947	.....	.....	2–0	V	4	
84	.....	.....	.....	757	.....	.....	4–4	.....	4	
85	.....	.....	.....	559	.....	.....	2–0	V	4	
86	.....	.....	.....	863	.....	.....	3–3	.....	4	
87	.....	.....	.....	.....	.....	.....	5–3	V	4	
88	5 32 39	−5 16.3	.....	1110	14.0	14.3	5–5	V	6	
89	5 30 32	−5 15.1	AI	708	13.2	15.5	4–3	V	4	
90	5 29 49	−5 14.8	XZ	367	14.9	17.0	4–1	V	4	
91	.....	.....	.....	445	.....	.....	3–0	V	4	6
92	.....	.....	.....	704	.....	.....	4–4	.....	4	
93	.....	.....	.....	347	.....	.....	4–0	V	4	
94	.....	.....	.....	280	.....	.....	4–1	V	4	
95	.....	.....	.....	185	.....	.....	3–0	V	4	
96	.....	.....	.....	869	.....	.....	2–0	V	4	
97	5 28 38	−5 16.3	RZ	109	15.2	16.8	3–3	V	5	
98	.....	.....	.....	.....	.....	.....	3–0	V	5	
99	.....	.....	.....	.....	.....	.....	3–3	.....	5	2
100	5 29 12	−5 17.9	WX	189	13.8	16.5	3–0	V	4	
101	.....	.....	.....	133	.....	.....	4–2	V	5	
102	.....	.....	.....	.....	.....	.....	2–0	V	4	
103	5 31 38	−5 21.8	.....	1005	14.0	(14.3	4–0	V	4	
104	5 30 58	−5 20.3	.....	889	12.9	(15.5	4–2	V	4	
105	.....	.....	.....	.....	.....	.....	3–0	V	4	
106	.....	.....	.....	965	.....	.....	4–1	V	4	
107	.....	.....	.....	.....	.....	.....	4–4	.....	6	
108	.....	.....	.....	97	.....	.....	4–1	V	5	
109	.....	.....	.....	753	.....	.....	4–2	V	4	
110	5 30 56	−5 25.0	.....	879	15.8	16.5	4–3	V	4	
111	5 30 40	−5 25.4	AM	789	14.1	15.7	4–3	V	4	
112	.....	.....	.....	154	.....	.....	3–3	.....	5	
113	.....	.....	.....	.....	.....	.....	3–0	.....	6	
114	.....	.....	.....	919	.....	.....	4–2	V	4	
115	5 29 46	−5 26.8	.....	340	12.1	12.7	3–3	V	4	
116	5 28 27	−5 26.1	VW	82	15.2	16.8	4–1	V	5	
117	.....	.....	.....	.....	.....	.....	3–3	.....	4	
118	.....	.....	.....	.....	.....	.....	4–4	.....	5	2

TABLE 1—*Continued*

No.	R.A. (1900)	Dec. (1900)	Name	Brun's No.	Max.	Min.	Int. Br't *Hα*	Light-Variation	Figure	Notes
119	5h31m43s	−5°30′.2	BC	1014	15.0	16.1	5–5	V	4	
120				904	...	...	4–2	V	4	
121							3–0	V	5	
122							2–2	...	5	
123	5 30 56	−5 32.5	T	884	9.5	12.1	4–4	V	4	7
124				42	...	...	3–3	...	5	
125							3–0	V	4	
126							3–3	...	4	
127	5 29 29	−5 35.0	WZ	234	15.0	16.5	4–4	V	4	
128				561	...	...	3–3	V	4	
129							3–3	...	4	
130				533	...	...	5–0	V	4	
131	5 28 51	−5 35.2	VZ	136	14.0	15.6	5–3	V	5	
132				...	...	...	5–2	V	4	1
133				794	...	...	4–4	...	4	
134				525	...	...	4–4	...	4	
135	5 29 20	−5 38.0		214	13.2	14.1	5–3	V	4	
136				108	...	...	3–0	V	5	6
137	5 30 27	−5 38.7	AG	673	14.2	(15.6	5–5	V	4	
138				1054	...	...	5–3	V	6	
139	5 29 43	−5 39.0		321	14.1	14.6	4–3	V	4	
140				305	...	...	4–0	V	4	
141				301	...	...	4–0	V	4	
142				314	...	...	3–0	V	4	
143	5 30 13	−5 41.1		524	14.0	15.0	4–0	V	4	
144				...	...	...	3–0	V	4	
145				...	...	...	3–0	V	5	
146				...	...	...	5–2	V	4	
147				...	...	...	3–0	V	4	2
148	5 29 09	−5 41.1	WW	178	14.4	15.5	4–2	V	4	
149				572	...	...	3–2	?	4	
150				563	...	...	5–5	...	4	
151				385	...	...	3–3	...	4	
152							4–3	V	4	2
153				954	...	...	3–0	V	4	
154				339	...	...	3–0	V	4	
155	5 27 53	−5 44.0	UZ	16	15.6	(16.0	4–0	V	5	
156				611	...	...	3–3	...	4	2
157	5 30 2	−5 45.7		451	13.4	14.0	5–5	V	4	
158				327	...	...	3–0	V	4	
159	5 29 0	−5 45.8		160	13.2	14.1	3–0	V	5	
160				680	...	...	5–3	V	4	
161				634	...	...	5–5		4	
162				...	...	...	5–1	V	4	2
163				953	...	...	5–5		4	
164				758	...	...	4–1	V	4	
165				635	...	...	4–4		4	
166	5 29 55	−5 46.4		404	13.2	14.0	5–1	V	4	
167				...	...	...	4–1	V	4	
168							3–1	V	5	
169	5 30 20	−5 47.3	AB	574	14.2	15.2	5–5	V	4	
170				553	...	...	4–0	V	4	
171				316	...	...	4–0	V	4	
172					...	...	4–4	...	4	2
173				473	...	...	4–1	V	4	
174					...	...	5–0	V	4	1
175				514	...	...	3–0	V	4	
176				423	...	...	5–3	V	4	
177	5 29 47	−5 50.2	XY	364	15.0	17.0	4–0	V	4	1
178				409	...	...	3–1	V	4	

TABLE 1—*Continued*

No.	R.A. (1900)	Dec. (1900)	Name	Brun's No.	Max.	Min.	Int. Br't *Hα*	Light Variation	Figure	Notes
179	$5^{h}30^{m}01^{s}$	$-5^{\circ}50'.8$	ZZ	446	14.7	15.6	3–0	V	4	
180	5 30 16	−5 50.5	AA	543	13.6	15.7	4–2	V	4	
181							4–4		4	2
182	5 30 53	−5 53.3	CF	877	14.7	16.1	5–4	V	4	
183				640			3–0	V	4	
184							3–0	V	4	
185				1061			3–1	V	7	
186	5 30 20	−5 56.1	BZ	586	14.8	16.4	3–0	V	7	
187							4–4		7	
188	5 30 05	−5 58.5	BX	459	15.0	16.2	4–1	V	7	
189	5 31 04	−6 01.2	AU	927	14.5	16.0	5–5	V	7	
190				197			4–2	V	7	
191							4–4	V	7	2
192							3–1	V	7	
193				637			5–5		7	
194							4–4		7	
195							4–0	V	7	
196	5 29 54	−6 02.0	YY	408	13.9	15.7	5–3	V	7	
197							3–3		7	
198				709			4–0	V	7	8
199							5–4	V	7	2
200	5 29 43	−6 09.6	XX	319	14.2	16.3	5–1	V	7	
201				134			5–5		7	
202							3–3		7	2
203							5–3	V	7	1
204							5–3	V	7	1
205							4–0	V	7	1
206							3–0	V	7	
207				891			5–3	V	7	
208							4–2	V	7	
209	5 31 13	−6 18.3	AX	955	14.0	15.8	5–3	V	7	
210							3–3		7	
211							3–3			9
212	5 31 22	−6 21.5	BB		14.5	16.0	3–2	V	7	
213							5–2	V	7	
214							3–3		7	
215							5–5		7	2
216							4–2	V	7	
217							5–5		7	
218							4–0	V	7	
219	5 30 02	−6 28.0	BW		13.9	15.9	5–4	V	7	
220							3–1	V		9
221							3–1	V	7	
222							3–0	V	7	
223							5–5	V	7	2
224							4–4	V	7	2
225							4–4		7	2
226	5 32 08	−6 37.1	BE		13.2	(16.4	5–3	V	7	
227							3–3		7	
228							3–0	V	7	
229	5 32 21	−6 38.7	BF		9.5	12.5	5–5	V	7	
230							5–5		7	
231							5–3	V	7	
232							4–0	V	7	
233							5–2	V	7	
234							3–0	V	8	
235			BD-6°1253				4–4	V	8	
236	5 31 08	−6 46.4	AV		14.5	16.4	5–3	V	8	
237							4–1	V	8	
238							5–5	?	8	10

TABLE 1—*Continued*

No.	R.A. (1900)	Dec. (1900)	Name	Brun's No.	Max.	Min.	Int. Br't $H\alpha$	Light-Variation	Figure	Notes
239	$5^h30^m39^s$	$-6^\circ49'.3$	TW	.....	14.8	16.1	5–3	V	8	
240							4–4	.....	8	
241							4–4	.....	8	
242							5–1	V	8	
243							4–4	.....	8	2
244	5 30 59	−6 54.6	AT		14.8	16.5	4–0	V	8	
245							5–1	V	8	
246							3–1	V	8	
247							3–0	V	8	1
248							4–0	V	8	
249							4–4	.....	8	
250							4–1	V	8	1
251							4–4	.....	8	
252							4–4	.....	8	
253							3–0	V	8	
254							2–0	V	8	
255							4–4	.....	8	11

NOTES TO TABLE 1

1. The highest relative intensity of $H\alpha$ in emission was observed at the star's maximum light.
2. A very faint star.
3. At the star's minimum light only $H\alpha$ in emission was observed and no continuum.
4. The variable BS Orionis appears in Brun's list as No. 76, but owing to its position, star No. 104 of the same list corresponds to the BS Orionis position given by Kukarkin and Parenago.
5. The relative intensity of $H\alpha$ in emission varies conspicuously in less than 24 hours.
6. $H\alpha$ in emission was observed only once.
7. The variable T Orionis shows, on a blue-sensitive spectral plate, two more emission lines at approximately λ 4471 and λ 4144. Even though two more bright lines are suspected in the photographic region of the spectrum, it is not possible, on this plate, to notice any emission components of the blue hydrogen lines. Because of the strong infrared color observed for this variable, it seems that the bright star of spectral type A3 is associated with a fainter late-type star.
8. This star varies rapidly. A variation in light of more than 2 mag. was observed in 19 hours.
9. Star not included in the charts.
10. This star is very near the position given for ST Orionis and possibly is the same.
11. Star imbedded in a minute nebulosity mainly of the reflection type.

umns give the right ascension and declination of the variable stars contained in Kukarkin and Parenago's catalogue and those listed by A. Brun;[3] at the same time, these objects can be used as reference stars to identify the others. The name of the variable is in the fourth column, while the fifth column contains the star number in Brun's maps. The sixth and seventh columns indicate the magnitude of the variables; Kukarkin and Parenago's data are used preferentially. The eighth column gives on an arbitrary scale the provisional estimated intensities of the $H\alpha$ emission lines with respect to the underlying stellar continuous spectra: $H\alpha$ very strong $=5$, $H\alpha$ strong $= 4$, $H\alpha$ medium $=3$, $H\alpha$ weak $= 2$, $H\alpha$ doubtful $= 1$, $H\alpha$ not present as a bright line $= 0$. In this column the number at the left corresponds to the maximum estimated intensity of $H\alpha$, and the number at the right to the minimum in all the cases where some changes have been observed. The ninth column indicates with a "V" the stars suspected of light variation. The tenth column gives the number of the figures wherein the stars can be identified. Notes are referred to in the eleventh column.

Figure 1 shows the region of highest intensity of the Orion Nebula; Figures 2–7 chart

---

[3] *Pub. Obs. Lyon*, Vol. 1, Ser. I, Fasc. 12, 1935.

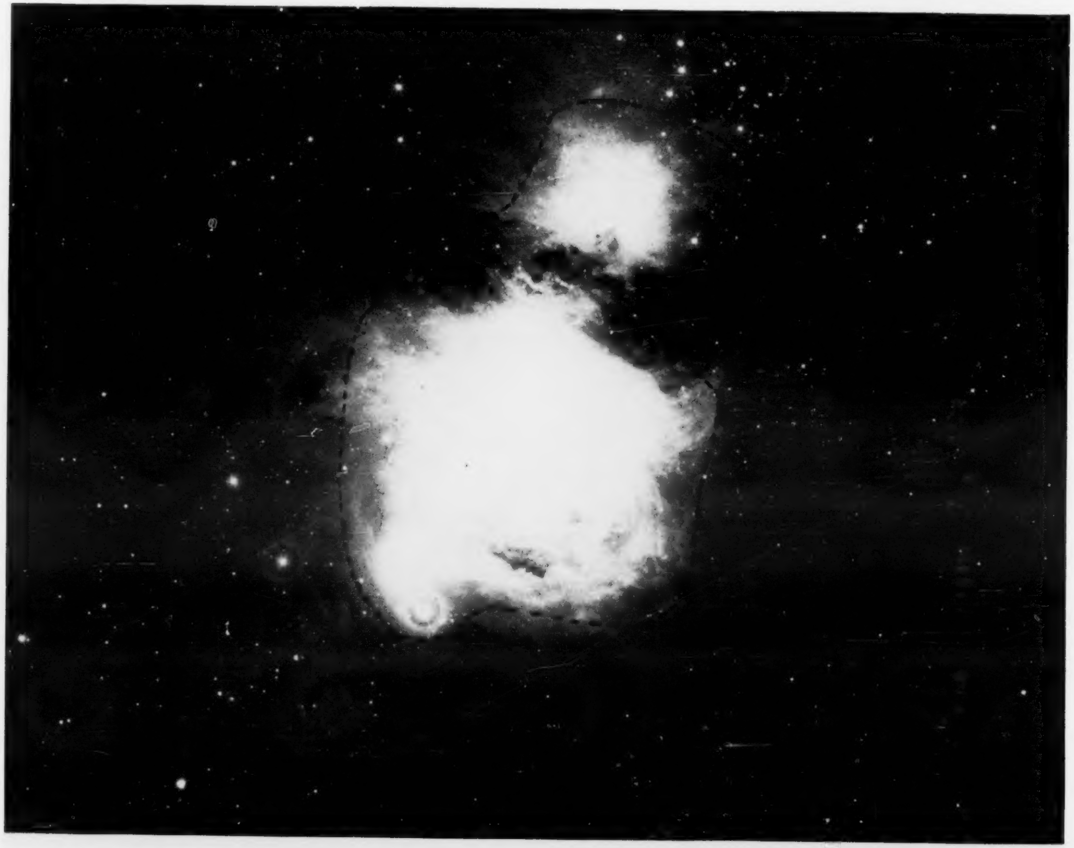

Fig. 1.—The dashed line encircles the brightest part of the Orion Nebula, covering an approximate area of 1.2 square degrees. Within this area 180 emission stars were found.

FIG. 2.—Two spectral plates taken with a difference of 23 hours. At the right, star No. 70 shows a conspicuous strong $H\alpha$ in emission.

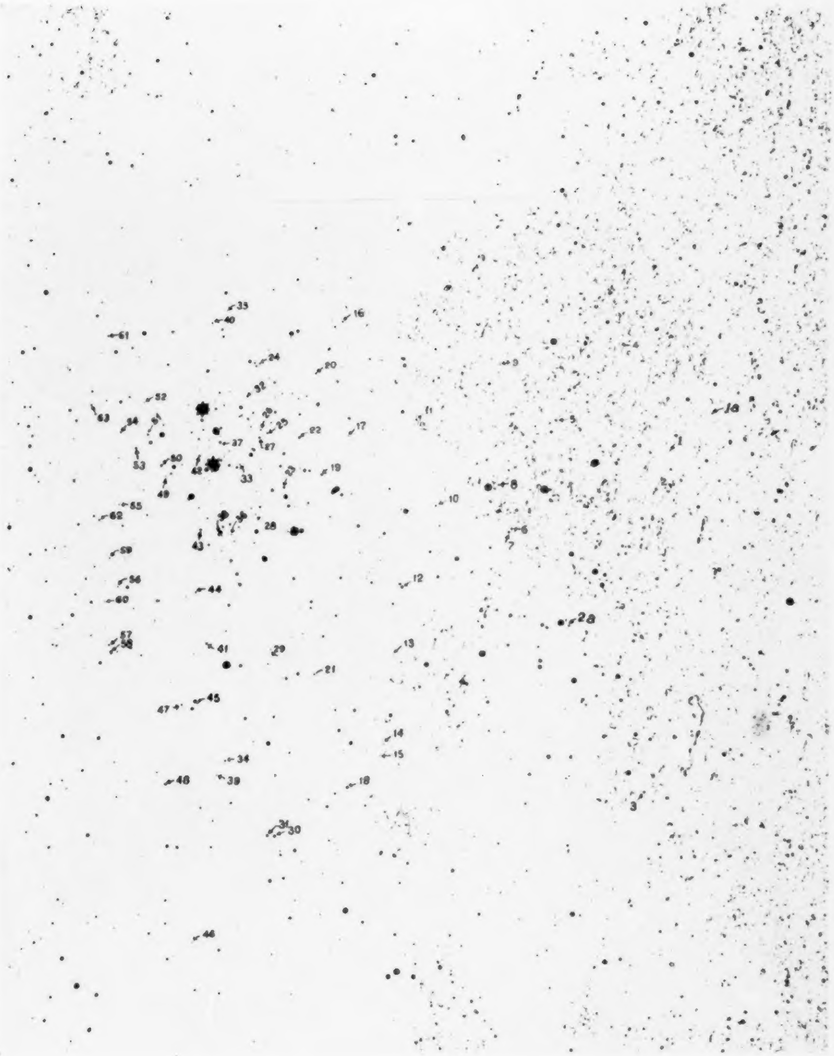
35
40
16
61
24
20
52
63
54
37
27
22
17
53
50
42
33
19
49
65
62
28
43
59
56
60
44
57
58
41
29
21
47
45
34
39
48
18
14
15
31
30
46
9
11
1a
1
2
2a
3
5
6
7
8
10
12
13

FIG. 3.—Identification chart for emission-line objects

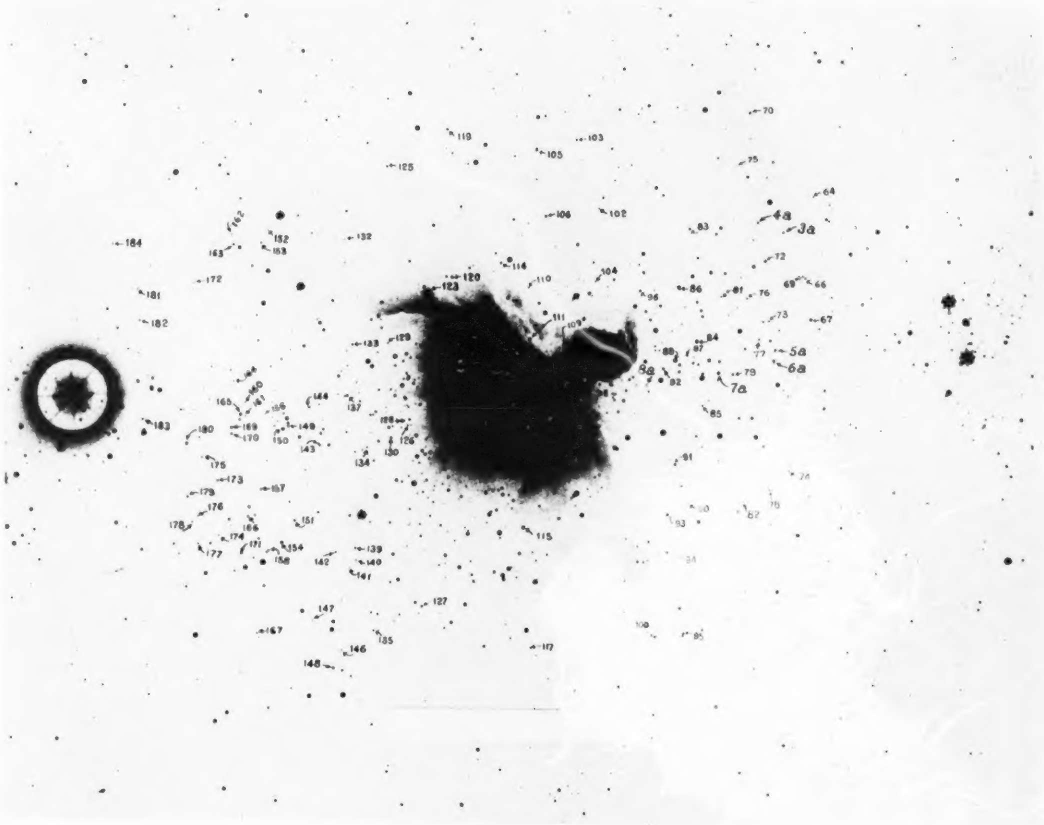
70
119
103
105
125
75
64
106
102
4a
3a
83
184
132
162
152
163
153
72
114
104
120
110
123
172
86
81
76
69
66
181
96
73
67
182
111
109
133
129
84
87
88
77
5a
6a
8a
92
79
7a
144
137
165
160
161
156
85
183
180
169
170
149
150
143
128
126
130
134
91
175
173
167
179
176
178
74
90
82
75
93
166
151
115
174
171
154
139
177
158
142
140
141
94
127
147
167
100
95
135
146
117
148

FIG. 4.—Identification chart for emission-line objects

112
101
99
159
131
118
121
98
71
97
136
122
108
116
168
124
145

FIG. 5.—Identification chart for emission-line objects

68
107
65
88
138
113
80

FIG. 6.—Identification chart for emission-line objects

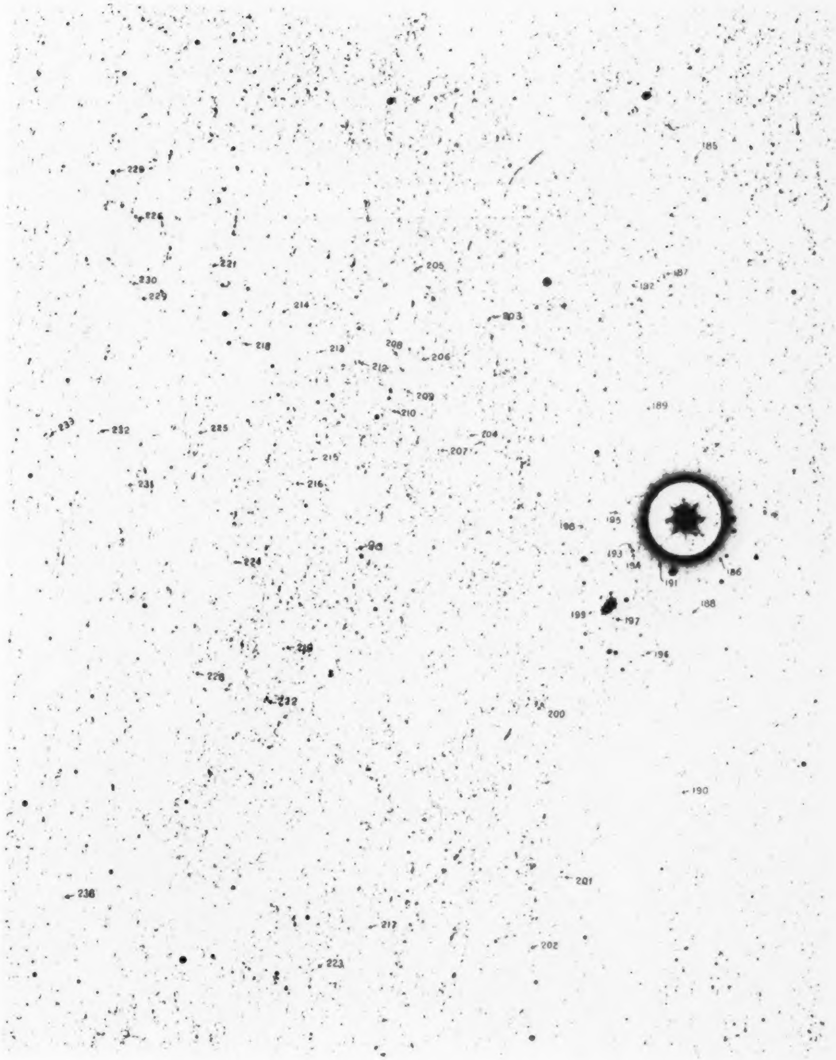
185
229
226
221
205
187
192
230
229
214
203
218
213
208
206
212
209
210
189
233
232
225
204
207
215
216
231
198
195
220
193
224
194
186
191
188
199
197
219
196
226
222
200
190
236
201
217
202
223

FIG. 7.—Identification chart for emission-line objects

252
255
243
254
253
249
245
240
13a
248
250
14a
251
246
242
234
247
12a
235
11a
10a
236
237
244
238
241

FIG. 8.—Identification chart for emission-line objects

the positions of the emission-line objects. The charts are reproductions of a I-N plate taken behind an infrared filter, Wratten No. 87. Some of the peculiar objects listed in Table 2 do not show images on the infrared plates; in such cases a dot, corresponding to the object's position, has been marked.

From the results given in Table 1 and observations that are not contained in it, the following points may be mentioned with regard to the emission stars found in the Orion Nebula region:

1. There is an obvious and striking concentration of emission stars in and near the Orion Nebula. The distribution and the frequency of the emission stars seems to be correlated with the apparent shape and intensities of the emission nebula. In the region covered by the brightest part of the nebula (Fig. 1), and which comprises an area of approximately 1.2 square degrees, there have been found 180 stars with emission. In the remaining part of the 3.5 square degrees area (2.3 square degrees), which still continues to be characterized by the presence of less bright nebular material, there are 75 emission stars; for comparison, in a 20 square degree region surrounding the 3.5 square degrees area only 30 emission stars have been found.

TABLE 2

PECULIAR OBJECTS IN THE ORION NEBULA REGION

No.	Figure	Brun's No.	Description
1*a*	3		This object is possibly a small bright nebula; the spectral Schmidt plates just show a bright $H\alpha$ without continuum, and it does not appear on the infrared plates
2*a*	3	328[a]	Possibly a white dwarf
3*a*	4		Small nebulous objects showing a bright $H\alpha$ and a relatively broad emission corresponding to the position of the [O I] lines at λ 6300 and λ 6363
4*a*	4		The same as No. 3*a*
5*a*	4		Small nebulosity of the reflection type
6*a*	4		The same as No. 5*a*
7*a*	4		A pair of infrared stars immersed in a faint and minute nebulosity, probably of the reflection type
8*a*	4		An infrared star imbedded in a minute nebulosity
9*a*	7		The same as No. 3*a*
10*a*	8		The same as No. 3*a*
11*a*	8		Small nebulous object showing $H\alpha$ and the [O I] lines at λ 6300 and λ 6363 in emission
12*a*	8		This object is composed of three nuclei scarcely separated on the Schmidt plates, showing $H\alpha$ and the [O I] lines at λ 6300 and λ 6363 in emission
13*a*	8		Probably a new faint cometary nebula with an infrared star at the apex
14*a*	8		The same as No. 3*a*

2. Notwithstanding that near the Trapezium stars it has not been possible, in this investigation, to discover stars with emission because of the interference of the nebula itself, all the observational data at hand seem to indicate that the number of variable stars, possibly with emission characteristics, increases as the distance to the Trapezium decreases.

3. The individual characteristics of each emission star—its apparent magnitude, its emission-line intensity, and its variability in light and in spectrum—do not appear to be correlated with the distance from the brightest part of the nebula.

4. Approximately 68 per cent of the emission stars show a permanently bright $H\alpha$, even if this emission varies in intensity, at least during my three years of observation.

5. Of the stars listed as variables by A. Brun[3] which were observed during this study, 70 per cent show emission in *Hα*.

6. Some stars show emission only occasionally. A typical example is the star listed as No. 70. This star appears invariable on all plates that were taken, with the exception of the one exposed on November 27, 1951, in which it shows an exceedingly strong *Hα* in emission without any apparent change in the continuous spectrum (Fig. 8); 23 hours before, its spectrum had appeared normal, and 22 hours later there remained only a dubious trace of emission in *Hα*. This type of star is strongly suggestive of the "flare" stars. Star No. 198 is another conspicuous example of rapid variation in light and in spectral characteristics, except that in this case the observed rapid variations have been multiple. In this star a variation in light larger than 2 mag. in a period of 19 hours has been observed.

7. In some cases the intensity of the emission may vary, without any apparent change in the intensity of the continuous spectrum. In other cases it seems as if the continuum varies without any apparent change in the intensity of the emission line.

8. In most cases it seems as if the highest intensity of the emission is at the star's maximum light, but some stars that probably are at their minima show an emission that appears to be at its maximum.

9. In many cases the intensity of the *Hα* emission varies from very strong to near invisibility.

10. The intensity of the continuum and emission in some stars does not appear to have changed in the three years of observation.

11. Owing to the color index of the stars showing emission and their characteristics in the spectral region of the red and near infrared, it may provisionally be supposed that the large majority of these stars have spectral types G, K, and early M. Possibly very few can be classified as being of late M type.

b) THE ORION NEBULA CLUSTER

It is interesting to point out that, on the *I-N* plates taken during this investigation, an outstanding dense stellar group is revealed. It has as an approximate center the Trapezium stars and extends over an area at least 20′ in diameter. Most of the stars that form this group have a large infrared color index, the brightest on the *I-N* plates being those near and around the Trapezium stars. The Trapezium cluster discussed by Baade and Minkowski[4] happens to be just the center of this stellar group that could be tentatively called the "Orion Nebula Cluster." The latter calls for a future and separate study.

c) PECULIAR OBJECTS

In Table 2, 14 objects are listed which show in one way or another certain peculiarities. In the first column numbers and letters are given by which these objects have been listed; in the second column the number of the figures on which they are identified; in the third column the corresponding number in Brun's maps; and in the fourth column a short description. In the following some of these objects are described in slightly more detail:

Object *2a* is possibly a white dwarf. This star does not appear on the infrared plates, despite the fact that the stars surrounding it, even the faintest ones on the blue plates, appear conspicuous in the infrared. Two direct plates were taken of this particular star, one immediately after the other; the first was a hypersensitized *I-N* plate with a Wratten No. 87 filter with a 60-minute exposure, and the other was a 103*a*-O plate with 10-minute exposure. This procedure was used to attempt to avoid a possible confusion, within a certain reasonable degree, between a variable star which could appear in its maximum light on a blue plate and in its minimum light on the infrared plate, and a star of negative color index.

---

[4] *Ap. J.*, **86**, 119, 1937.

Nebulous objects *3a*, *4a*, *9a*, *10a*, *11a*, *12a*, and *14a* are characterized in the spectral red plates of Tonantzintla by a strong emission in *Hα* and, furthermore, by an intense emission at λ 6300 and λ 6363, the continuous spectra on these plates not being observed. Because of the low dispersion used and the faintness of these objects, only in the case of the two brightest, *11a* and *12a*, was it possible to distinguish separately the two [*O* I] lines, while in the other cases these two lines appeared as a single one which was noticeably broad. In the case of the nebulous objects Nos. *3a* and *4a*, the two unresolved [*O* I] lines appear as intense as the *Hα* emission. Herbig[5] and the writer[6] have published information on this type of object.

The stars listed as *7a*, *8a*, and *13a* are objects with a considerable color index (blue-infrared), apparently associated with nebulosities mainly of the reflection type that also have a strong infrared color. Among these latter objects the most interesting, to the writer, are *7a* and *13a*. Object *7a* consists of a pair of infrared stars which the Tonantzintla Schmidt scale scarcely separates. These two stars are enveloped in a faint and minute nebulosity, probably of the reflection type. Object *13a* has all the appearance of a cometary nebula; the star at the apex of this fan-shaped nebula does not appear on the long-exposure Schmidt blue-sensitive plates and very doubtfully on the red plates, whereas on the *I-N* plates it appears fairly bright. The fan-shaped nebula by itself also shows peculiar characteristics: in blue and red light it is considerably brighter than the star and also in infrared light, even though here the difference is smaller; furthermore, the side of the fan near the star shows a spectrum mainly of the reflection type, while the farther extension of the "tail" has an emission spectrum and does not appear on the infrared plates. If this object is really a new cometary nebula and is roughly at the distance of the Orion Nebula, the star imbedded in the fan-shaped nebulosity will undoubtedly be a very red dwarf of insufficient radiation to attribute to it the formation of the comet-shaped nebula, as has been suggested by R. Minkowski[7] in similar cases. The writer is compelled to consider the possibility of a process radically opposed to the one suggested by Minkowski. In this new case the star would not be responsible for the fan-shaped nebula formation, but the star itself would be the result of a condensation of the nebular material at the apex of the fan.

II. SOME FINAL REMARKS

The observational results that have been presented here show that the Orion Nebula's physical conditions are not adverse to the presence of late-type stars with spectra which strongly indicate some interaction between the nebula and the stars. In fact, as far as the writer knows, the Orion Nebula is the most striking observed example of interaction between a diffuse nebula and dwarf stars of late spectral type.

The observed correlations between the form and difference of brightness in the main body of the Orion Nebula and the distribution and frequency of emission late-type dwarf stars suggest the two following possibilities: Either this star group has drifted into the nebula without any primary genetic connection with it, or these stars have originated from the nebula itself.

Owing to the coexistence and concentricity observed between the nebula and the densest group of emission stars, it does not seem plausible to the writer that the latter originally formed a dense and independent star group which simply happened to drift into the nebula, since such a morphological interdependent organization—as we observe at present—can hardly be accidental.

As a consequence of an observational approach, the writer suggests a tentative hypothesis for the formation of low-luminosity infrared stars as a direct effect of continuously growing nebular condensation nuclei. Possibly these infrared stars continue their evolutive process, growing in mass, temperature, and luminosity through the accretion of internebular matter. To this last stage may correspond the type of dwarf stars with emission spectral characteristics that are observed in the Orion Nebula.

---

[5] *Ap. J.*, **113,** 697, 1951.

[6] *Ap. J.*, **115,** 572, 1952.

[7] *Pub. A.S.P.*, **54,** 190, 1942.

The striking association of emission-line late-type dwarf stars with the Orion Nebula and the presence of 48 similar stars in an area of no more than 1 square degree in and around NGC 2264 suggest the possibility that this type of association may be a general characteristic of certain kinds of diffuse nebulae.

I am indebted to Mrs. Gladys Learn Haro for her valuable aid in the preparation of this article.

THE TRANSFER OF THE NORTH POLAR STANDARDS TO THE SOUTHERN HEMISPHERE*

ARTHUR N. COX
Goethe Link Observatory, Indiana University

Received July 31, 1952

ABSTRACT

Magnitudes on the Southern (S') system, defined by stars in the Harvard Standard E Regions, have been compared with the NPS, using four Harvard Standard C Regions as an intermediate step. The photoelectric comparison makes use of transfers made with the 24-inch Victoria telescope at the Royal Observatory, Cape of Good Hope, and with the 10-inch wide-angle camera at the Goethe Link Observatory. Magnitudes of stars in the NPS, C12, C2, C3, C4, E2, E3, E4, and E5 are given. The S' magnitudes can be converted to the system of Stebbins, Whitford, and Johnson by the linear relations: $\mathbf{P} = S'Pg + 0.10$; $\mathbf{V} = S'Pv + 0.10\, S'CI - 0.06$; $(\mathbf{P}-\mathbf{V}) = 0.90\, S'CI + 0.16$.

I. INTRODUCTION

One of the important problems in modern astronomy is the establishment of accurate magnitude sequences in numerous regions of the sky. It is desirable to have magnitudes with identical zero point, scale, and color system in all parts of the sky, in order that uniform conclusions can be drawn, regardless of the source of the standards. This work is an attempt to derive corrections to the magnitudes and colors of the stars in the Harvard Standard E Regions at −45° declination that have magnitudes on the so-called S' system.[1] Since the time of the original establishment of the magnitudes for the E region stars on a uniform system by Miss H. S. Leavitt,[2] photographic ties to other standard regions have been made by Miss C. H. Payne,[3] R. H. Stoy,[4] R. H. Stoy and A. Menzies,[5] and F. H. Seares and M. C. Joyner.[6] These ties need to be checked by a number of independent photoelectric observers. During the author's five-month stay at the Royal Observatory at the Cape of Good Hope, an unusual opportunity existed for making a comparison of the S' system with the Harvard Standard C Regions at +15° declination, using a 1P21 photoelectric photometer attached to the 24-inch Victoria telescope. The C region magnitudes were then compared directly with the North Polar Sequence, using the same photometer on the 10-inch wide-angle camera at the Goethe Link Observatory. The ties were made to derive corrections to the zero point and color system of the S' magnitudes, and no special attempt was made to detect scale errors.

The apparatus used with both telescopes included a 1P21 photoelectric photometer, a d.c. amplifier similar to the design of G. E. Kron,[7] and an Esterline-Angus 0–1 ma recording milliammeter. Except for the telescopes, identical apparatus was used at the Cape and at Link. Both the 24-inch and the 10-inch refractors were corrected for light in the photographic region. The 1P21 photometer contained (in order of increasing distance from the telescope objective) a 1.1-mm diaphragm, filters, a Fabry lens of 38 mm focal length, and the photomultiplier tube. The diaphragm diameter corresponded to 34 seconds of arc and 2 minutes of arc with the Victoria and the Link telescopes, respectively. The Corning glass filters used in the photometer for the yellow light are: 9780 one-half standard thickness cemented to 3384 one-quarter standard thickness; for the blue light the filters are: 3850 two-fifths standard thickness cemented to 5850 one-third standard thickness. Color-sensitivity data for the photomultiplier and filter-photomultiplier combination are given in Table 1 and in Figure 1. The spectral sensitivity of the 1P21 photomultiplier tube was determined at the Washburn Observatory with a mono-

---

* *Publications of the Goethe Link Observatory, Indiana University*, No. 10.

[1] *Cape Mineogram*, 1948. The original S system described in this reference has recently been revised to the more homogeneous S' system.

[2] *Harvard Ann.*, **71**, 233, 1917.

[3] *Harvard Ann.*, **89**, 1, 1931.

[4] *M.N.*, **103**, 288, 1943; **104**, 317, 1944.

[5] *M.N.*, **104**, 298, 1944.

[6] *Ap. J.*, **102**, 281, 1945.

[7] *Electronics*, **21**, 98, August, 1948.

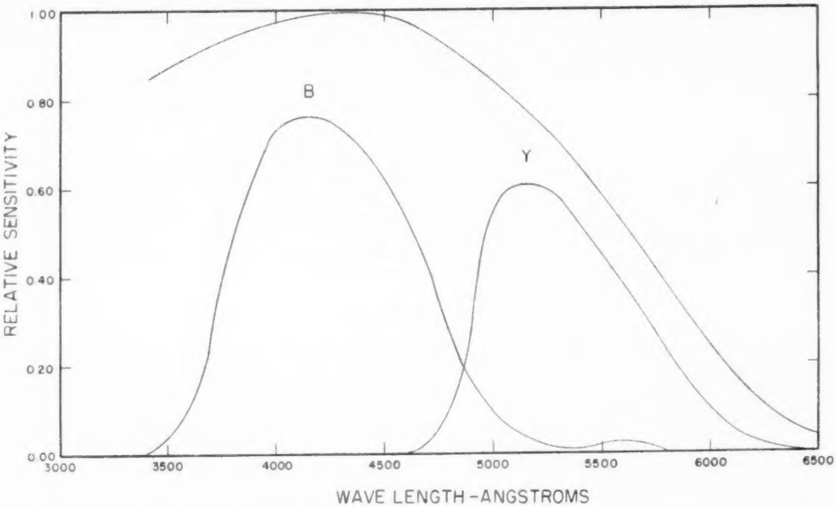

FIG. 1.—Sensitivity of the photomultiplier and filter-photomultiplier combination to equal energy at all wave lengths.

TABLE 1

COLOR SENSITIVITY OF THE PHOTOMULTIPLIER AND FILTER-PHOTOMULTIPLIER COMBINATION

λ	Photo-multi-plier	Blue	Yellow	λ	Photo-multi-plier	Blue	Yellow
3400	0.86	0.00	.....	5000	0.84	0.11	0.56
3500	0.88	.02	.....	5100	.79	.05	.62
3600	0.90	.11	.....	5200	.75	.03	.61
3700	0.92	.30	.....	5300	.70	.02	.58
3800	0.94	.50	.....	5400	.64	.01	.52
3900	0.95	.64	.....	5500	.59	.02	.46
4000	0.98	.73	.....	5600	.52	.02	.38
4100	0.99	.77	.....	5700	.46	.02	.30
4200	0.99	.76	.....	5800	.40	0.00	.23
4300	1.00	.74		5900	.32	.....	.15
4400	1.00	.69	.....	6000	.26	.....	.10
4500	0.99	.63	.....	6100	.18	.....	.05
4600	0.98	.55	0.00	6200	.12	.....	.02
4700	0.94	.42	.02	6300	.08	.....	.01
4800	0.91	.28	.09	6400	.05	.....	.01
4900	0.88	0.17	0.32	6500	0.04	.....	0.00

chromater, through the kindness of the director, Dr. A. E. Whitford. Diameters of the images of the telescope objectives produced on the sensitive surface by the Fabry lens were 3.4 and 5.6 mm with the Victoria and Link telescopes, respectively. The amplifier and recorder combination have been tested and found to be linear to within 1 per cent for all but very small deflections on the recording milliammeter. An independent test of the linearity of this apparatus has been made by J. Cuffey.[8] Weekly calibrations of the amplifier sensitivity steps were made at the Cape. The sensitivity resistors were sufficiently stable so that such frequent calibrations proved unnecessary. Only monthly calibrations were made at Link.

II. OBSERVATIONS

At the Cape, four E regions were tied to four C regions. These same C regions were later tied to the NPS at the Link Observatory. All observations were made at about the same zenith distance. The secant of the zenith distance was always greater than 1.3 and less than 1.8. The average values of sec z were 1.55 and 1.57 at the Cape and at Link, respectively. Owing to the rather poor western sky directly over the city of Capetown, all but two of the seventeen transfers made with the Victoria telescope were made with the E region in the southeast and the C region in the north. Sixteen NPS transfers at Link were made with the C region in the southwest, while fifteen other such transfers were made with the C region in the southeast. Only four stars were observed in each E region; five stars were observed in each of the C regions. Seventeen NPS stars were observed, but the fundamental standards were NPS 6, 2r, 4r, and 10. Only these latter four stars were used directly in the ties with the C regions. The magnitudes of the stars involved in the transfers lie between 7.0 and 10.5 mag.; their color indices range from -0.25 to $+1.54$. As an example of the observing routine, the procedure for the tie of E2 and C12 was: C12 F, G, L, F, N, O, F; E2 B, G, H, K, B; C12 F, G, L, F, N, O, F. This particular C region was tied to the NPS by a similar pattern: NPS 6, 2r, 4r, 10, 6; C12 F, G, L, F, N, O, F; NPS 6, 2r, 4r, 10, 6. All the standard stars were chosen from *Harvard Annals*, Volume **71.** Each transfer was assigned either unit or one-half weight according to the quality of the sky during the transfer. A single observation consisted of starlight deflections of 20 seconds duration in the following order: dark, yellow, blue, dark, blue, yellow, and dark. Frequent measures were made of the sky brightness.

Corrections for atmospheric extinction were obtained from the formula $m - m_0 = k(\sec z - \sec z_0)$, where k depends on the color of the star being observed. Here m is the observed magnitude at a zenith distance z, and m_0 is the magnitude corrected to the zenith distance z_0. The following linear equations express approximately the theoretically determined change in the yellow and blue extinction coefficients with the color of the star being observed:[9] $k_y = k_{0y} - 0.01C$; $k_b = k_{0b} - 0.05C$. The quantities k_{0y} and k_{0b} are the yellow and blue extinction coefficients for stars of zero color ($C = 0$) on the color system of the photometer. In no case, however, was the color of the star taken into account when computing extinction corrections.

Extinction measures at the Cape were usually made by reobserving the E region at a higher altitude after each transfer. All Cape observations were corrected with extinction coefficients that were determined on the night the observations were made. The much poorer weather at the Link Observatory made it almost impossible to measure extinction accurately and still have time to make an adequate transfer. Mean extinction coefficients were used, therefore, to correct all data taken at Link. The values 0.2 and 0.3, based on previous photoelectric experience at the Link Observatory, were adopted as average coefficients for the yellow and blue magnitudes, respectively. The reduction error of any individual observation taken at a zenith distance differing radically from the mean zenith distance would probably not be more than 0.03 mag. because of the assumption of the mean extinction coefficients. *Larger* uncertainties were always present at both observatories, because the extinction varied with azimuth in a manner impossible to determine. The Cape observations were corrected to a sec z_0, which was the mean of all the observations (about 1.55) involved in each transfer. All Link observations were corrected to the altitude of the pole (sec $z_0 = 1.57$).

---

[8] *Pop. Astr.*, **59**, 361, 1951.

[9] The method used to determine these coefficients is due to I. R. King and will soon be published by him.

III. REDUCTIONS

The reductions were made by treating the data as blue magnitudes and colors. Yellow magnitudes were reduced simultaneously to be used as a partial check. After extinction and amplifier sensitivity corrections had been applied, the data were analyzed to obtain the relative magnitudes of the stars in each standard region. With the adopted mean values of the relative magnitudes of the stars in a region on the natural color system of the apparatus, it was possible to determine the difference in magnitude between the brightest stars in each of the two regions being compared. A weighted average of the determinations of this difference in magnitude that were made on different nights was adopted as final.

Relations between the natural color system of the photometer and the S' system defined by the E region stars were derived by A. W. J. Cousins, using observations made with the same photometer of many other E region stars. His observations were taken at zenith distances which have an average sec z of less than 1.10. The relations are: $S'Pg = B + 0.05C$; $S'Pv = Y - 0.20C$; $S'CI = 1.25C$; and suitable zero-point corrections. Using the above values of the change of the extinction coefficient with color of the star (due to the change of effective wave length with color of the star), the appropriate formulae to be used for observations taken at, or corrected to, sec $z = 1.55$ are: $S'Pg = B + 0.07C$; $S'Pv = Y - 0.20C$; $S'CI = 1.27C$; and zero-point corrections. It is found, however, that the tie to the S' system is better represented by the equations $S'Pg = B + 0.08C$; $S'Pv = Y - 0.21C$; and $S'CI = 1.29C$. The discrepancy between the observed and computed color coefficients is probably due to accidental errors. In these expressions, B, Y, and C are the raw blue and yellow magnitudes and color of the star after extinction corrections have been applied. By comparing observations of eighteen C region stars made both at the Cape and at Link, it is concluded that the color systems of the photometer on the two telescopes were essentially the same. This fact could have been expected, inasmuch as the filters and photomultiplier tube were the same in both cases. Observations taken at both stations were corrected to about the same zenith distance, and extinction was not appreciably different.

Seventeen stars in the North Polar Sequence were observed to check the linearity of the apparatus and to derive color relations between the natural color system and the system of Stebbins, Whitford, and Johnson.[10] While only four stars are bright enough to be observed in common with the above observers, the best linear tie was obtained as follows: $\mathbf{P} = B + 0.084C$; $\mathbf{V} = Y - 0.081C$; $(\mathbf{P} - \mathbf{V}) = 1.165C$; and zero-point corrections. With these linear color relations and those given above, one can *derive* the relations between the S' system and the system of Stebbins, Whitford, and Johnson: $\mathbf{P} = S'Pg + \delta_1$; $\mathbf{V} = S'Pv + 0.10S'CI + \delta_2$; $(\mathbf{P} - \mathbf{V}) = 0.90S'CI + \delta_1 - \delta_2$. The $S'Pg$ magnitudes are at the same effective wave length as the $\mathbf{P}$ system magnitudes, while the $S'Pv$ magnitudes apply to an effective wave length redder than the $\mathbf{V}$ system magnitudes by about 10 per cent of the southern color base line.

It should be strongly emphasized that the conversion from the homogeneous (B, Y) system to the $(\mathbf{P}, \mathbf{V})$ system is essentially based on only four NPS stars. Therefore, all the $\mathbf{P}$ and $(\mathbf{P} - \mathbf{V})$ values will perhaps need revision when more of the seventeen NPS stars are available on this system. The relations between the S' and $(\mathbf{P}, \mathbf{V})$ systems will perhaps also be affected.

---

[10] *Ap. J.*, **112**, 469, 1950.

IV. SOURCES OF ERROR

Accidental and night-to-night errors are represented in Table 2. The table lists the regions compared, the directions involved in the transfer, the order of the transfers in time, the weight of the transfer as judged by the quality of the sky, and the blue, yellow, and color residuals for each individual transfer. These residuals are the differences between the observed and the final adopted magnitude difference between the brightest stars in each of the two regions being compared. The zero-point residuals are given only

TABLE 2

MAGNITUDE ZERO-POINT RESIDUALS

Regions	Directions	Order	Weight	$B-\bar{B}$	$V-\bar{V}$	$C-\bar{C}$
E2, C12	SE.-N.	4	1	−0.010	−0.005	−0.005
		6	1	− .015	− .015	.000
		8	1	− .020	− .005	− .015
		9	1	+ .025	+ .015	+ .010
E3, C2	SE.-N.	1	1	+ .025	+ .005	+ .020
		2	1	− .015	− .030	+ .015
		10	1	− .010	+ .010	− .020
		11	1	+ .010	+ .010	.000
E4, C3	SE.-N.	3	1	− .005	− .005	.000
		5	1	− .005	− .005	.000
		7	1	.000	− .005	+ .005
		12	1	.000	+ .005	− .005
E2, C4	SW.-N.	14	1	.000	+ .005	− .005
		16	1	− .005	.000	− .005
E5, C4	SE.-N.	13	1	− .010	.000	− .010
		15	1	− .010	− .010	.000
		17	½	+ .050	+ .030	+ .020
NPS, C2	N.-E.	4	1	+ .015	+ .020	− .005
	N.-E.	5	1	+ .020	.000	+ .020
	N.-E.	7	½	− .055	− .060	+ .005
	N.-E.	9	½	.000	+ .015	− .015
	N.-E.	10	½	− .005	− .005	.000
	N.-W.	11	1	+ .045	+ .030	+ .015
	N.-E.	14	1	+ .015	+ .015	.000
	N.-W.	18	1	+ .010	+ .005	+ .005
	N.-W.	21	1	− .025	− .025	.000
	N.-W.	23	1	+ .005	+ .010	− .005
NPS, C3	N.-E.	8	½	− .010	− .005	− .005
	N.-W.	12	1	− .025	− .015	− .010
	N.-W.	13	½	+ .015	+ .015	.000
	N.-E.	15	1	− .020	− .020	.000
	N.-W.	19	1	− .010	.000	− .010
	N.-W.	26	1	+ .035	+ .030	+ .005
	N.-W.	28	1	.000	+ .010	− .010
NPS, C4	N.-E.	16	1	− .010	− .020	+ .010
	N.-W.	20	1	+ .010	− .005	+ .015
	N.-E.	22	1	+ .005	.000	+ .005
	N.-E.	24	1	+ .010	.000	+ .010
	N.-E.	25	½	− .020	− .010	− .010
	N.-W.	27	1	− .050	− .040	− .010
	N.-W.	29	1	+ .010	.000	+ .010
	N.-W.	30	1	+ .015	.000	+ .015
	N.-W.	31	1	+ .005	+ .015	− .010
NPS, C12	N.-E.	1	1	+ .005	− .010	+ .015
	N.-E.	2	½	− .065	− .035	− .030
	N.-E.	3	1	− .025	+ .005	− .030
	N.-W.	6	½	+ .055	+ .060	− .005
	N.-W.	17	1	+0.030	+0.015	+0.015

to the nearest 0.005 mag. The probable error of a single Cape transfer as inferred from these residuals is ±0.011 mag. in the blue, ±0.008 in the yellow, and ±0.007 in the color. The corresponding probable errors for the Link transfers are ±0.017 mag. in the blue, ±0.014 in the yellow, and ±0.008 in the color.

While the small size of these errors shows that the night-to-night consistency is reasonably good, in a program such as this one, large, undetermined systematic errors could completely invalidate the results. To examine possible systematic errors, the transfers were divided into those made in the eastern and western sky, respectively. In the Northern Hemisphere the data show that the western sky gives systematically fainter magnitudes for some of the C regions. This systematic error is 0.06 mag. in the blue, 0.04 in the yellow, and 0.02 in the color zero points for the C12 stars. For the stars in C3 this systematic error between the eastern and western transfers amounts to 0.02 mag. in the blue, 0.02 in the yellow, and no change in the color zero point. The magnitudes of stars in C2 and C4 show no perceptible difference in zero point when they are tied to the NPS from either the eastern or the western sky. Except for the C12 transfers, which are of relatively low weight, these systematic east-west errors are satisfactorily small.

To test errors caused by orientation of the telescope, light-sources were set up in front of the objectives of the Victoria and Link telescopes. No orientation errors greater than 0.005 mag. existed with the photometer in normal operating position of the 10-inch Link telescope as determined from two independent tests with different light-sources. This result is confirmed by the small systematic east-west errors.

Two separate tests made with the uniformly illuminated objective of the Victoria telescope showed a definite orientation effect. By directly comparing the light-source when measured with the telescope pointed in the directions of the C and E regions, respectively, a systematic error of 0.02 mag. was discovered. This effect was traced to a small flexure of the mounting of the photometer on the telescope. Because of this flexure, the optical axis of the photometer was inclined at varying angles to the optical axis of the telescope. The flexure caused a shift in position of the circular spot of starlight on the sensitive surface of the photomultiplier tube. The Fabry lens insures that the spot will remain on the same region of the sensitive surface, provided that the star appears anywhere in the diaphragm and that the optical system is rigid. The above systematic correction was applied to all the transfers from the E regions to the C regions.

This flexure correction is confirmed by two transfers made from E2 in the western sky at the Cape. These two transfers and three from E5 made to the same C4 region from the eastern sky show that the magnitudes of the C4 region stars are 0.02 mag. brighter in the yellow, show no difference in the blue, and are 0.02 mag. redder in color zero point when tied to the E2 region in the western sky than when they are tied to E5 in the eastern sky. If no flexure corrections had been applied, the C4 magnitudes resulting from the ties to E2 in the west would have been 0.06 mag. brighter in the yellow, 0.04 brighter in the blue, and 0.02 redder in zero point than the magnitudes determined from the E5 region in the east. It does not seem reasonable that these latter discrepancies can be explained by a differing zero point from E2 to E5, and therefore the flexure correction is approximately confined.

Observations made with both refracting telescopes were made at a compromise focus between the yellow and blue foci. In the case of the 10-inch Cooke Triplet telescope, the focal setting varies with temperature. In order to test the stability of the color system with focus for this telescope, observations were made of the four standard pole stars at focal settings which differed much more from the compromise focus than any temperature change could produce. Within the errors of observation (±0.02 mag.), it was not possible to detect any definite change in effective wave length or even any change in the zero point of the yellow and blue magnitude systems. The stability of the color system is further confirmed by the identical color systems obtained with the same photometer on both the Victoria and the Link telescopes.

V. RESULTS

The raw magnitudes and colors of the North Polar Sequence stars and those referred to the system of Stebbins, Whitford, and Johnson are given in Table 3. In Table 4 the raw magnitudes of the C region stars are given, as well as the magnitudes on this same (***P*, *V***) system and on the *S′* system as compared with the NPS and the E regions, respec-

TABLE 3

NORTH POLAR SEQUENCE MAGNITUDES AND COLORS

Star	*B*	*C*	***P***	***P−V***
1	0.00	0.00	4.18	−0.14
2	0.88	−0.03	5.06	−0.17
3	1.45	+0.22	5.65	+0.12
4	1.62	+0.19	5.82	+0.08
5	2.24	+0.08	6.43	−0.05
6	2.93	+0.15	7.12	+0.04
7	3.14	−0.03	7.32	−0.17
8	4.18	+0.34	8.39	+0.26
9	4.82	+0.28	9.02	+0.18
10	5.00	+0.24	9.20	+0.14
1r	2.30	+1.46	6.60	+1.56
2r	3.59	+1.44	7.89	+1.54
3r	4.58	+1.31	8.87	+1.39
4r	4.99	+0.99	9.25	+1.02
5r	5.88	+1.48	10.19	+1.59
2s	2.27	+0.29	6.48	+0.20
3s	2.41	+0.37	6.62	+0.29

TABLE 4

MAGNITUDES AND COLORS OF C REGION STARS

Star	*B*	*C*	***P***	***P−V***	*S′Pg*	*S′CI*
C12 F	4.26	+0.29	8.46	+0.20	8.37	+0.06
G	4.33	+0.27	8.53	+0.18	8.45	+0.04
L	5.36	+0.45	9.58	+0.38	9.47	+0.24
N	5.92	+0.44	10.14	+0.37	10.04	+0.27
O	5.90	+0.98	10.16	+1.00	10.09	+0.98
C2 E	4.17	+0.57	8.40	+0.53	8.28	+0.39
F	4.62	+0.96	8.88	+0.98	8.74	+0.88
G	4.94	+0.42	9.15	+0.35	9.04	+0.20
H	5.13	+0.44	9.35	+0.37	9.20	+0.21
M	6.07	+0.58	10.30	+0.54	10.17	+0.39
C3 E	3.71	+0.10	7.90	−0.02	7.79	−0.20
F	3.78	+0.12	7.97	0.00	7.88	−0.17
G	4.05	+0.18	8.24	+0.07	8.13	−0.11
H	4.27	+0.74	8.51	+0.72	8.38	+0.63
M	4.88	+1.04	9.15	+1.07	9.01	+1.02
C4 E	4.03	+0.49	8.25	+0.43	8.16	+0.30
F	4.24	+1.04	8.51	+1.07	8.40	+1.00
G	4.48	−0.03	8.66	−0.17	8.54	−0.39
K	5.40	+1.06	9.67	+1.10	9.49	+0.98
L	5.62	+0.47	9.84	+0.41	9.73	+0.26

tively. The *B*, *C*, ***P***, and (***P*** − ***V***) values in Table 4 depend only on Link observations, while the *S′* magnitudes are from Cape data alone. The observed raw magnitudes of the E region stars and those referred to the (***P***, ***V***) system and the *S′* system are given in Table 5. Raw magnitudes for the E region stars were tied to the most recent values on the *S′* system, kindly supplied by Cousins before publication. The raw magnitudes listed in all the tables are on the natural color system of the photometer with a common zero point.

In the course of the work a slight variability of C3 M and C4 K was noted. The former star shows night-to-night residuals which average 0.03 mag., while the latter star seemed to be getting fainter by several hundredths of a magnitude from December, 1951, through February, 1952. C4 K is almost 0.1 mag. fainter as observed at Link compared to its magnitude determined at the Cape one year before. NPS 2r showed large night-to-night residuals; its variability was originally found by Johnson.[11] The variations are irregular but not rapid, for during a night the constancy was good. The extremes of the brightness of this star may be as much as 0.08 mag. apart. Since this star was observed at least several times each night, its mean magnitude on any night was used in the reductions for that night. The value given in Table 3 is the mean of the magnitudes of the star on all the nights that it was observed.

TABLE 5

MAGNITUDES AND COLORS OF E REGION STARS

Star	*B*	*C*	***P***	***P***−***V***	*S′Pg*	*S′CI*
E2 B	3.47	+0.20	7.67	+0.09	7.57	−0.06
G	4.31	+0.44	8.53	+0.37	8.43	+0.25
H	4.44	+1.12	8.71	+1.16	8.61	+1.12
K	4.61	+0.10	8.80	−0.02	8.70	−0.19
E3 E	3.64	−0.10	7.81	−0.26	7.70	−0.47
H	4.60	+0.23	8.80	+0.13	8.69	−0.04
L	5.25	+0.51	9.47	+0.45	9.36	+0.32
M	5.27	+0.92	9.53	+0.93	9.41	+0.84
E4 C	3.67	+0.05	7.85	−0.08	7.75	−0.26
F	3.86	+0.17	8.05	+0.06	7.95	−0.11
I	5.08	+0.19	9.28	+0.08	9.17	−0.08
O	5.49	+0.88	9.74	+0.89	9.64	+0.81
E5 D	3.53	−0.09	7.70	−0.24	7.61	−0.45
F	3.74	+0.50	7.96	+0.44	7.87	+0.31
H	4.36	+0.15	8.55	+0.04	8.46	−0.14
M	5.70	+1.38	9.99	+1.47	9.90	+1.45

It is possible to compare these results with those published by other photoelectric observers. There are overlaps with Eggen[12] in C12 and with Bok and Eggen in C4. Bok's C4 data is given by van Wijk,[13] and Eggen's is given by Kron and Smith.[14] Results of the comparisons are given in Table 6. From these data it appears that Eggen's ***P*** magnitudes are systematically 0.04 mag. brighter and 0.04 mag. bluer than those in this paper. There is only a slight difference between the color systems. The variable C4 K, which was omitted in the Eggen comparison, prevents any good comparison with the Bok results.

A comparison of the C region magnitudes as obtained from the NPS and from the E regions yields the zero-point corrections to the *S′* system which are given in Table 7.

---

[11] *Ap. J.*, **114**, 522, 1951.

[12] *Ap. J.*, **114**, 143, 1951.

[13] *A.J.*, **57**, 28, 1952.

[14] *Ap. J.*, **113**, 336, 1951.

Also given are the zero-point corrections found by comparing the (***P*, *V***) system and ***S′*** system magnitudes for the E region stars. The disagreement of the zero-point corrections to the *S′* system from one transfer to the next could possibly be due to a differing zero point in the various E regions. However, the agreement is satisfactory without assuming that the zero point changes between the E regions. The differences between the values of δ_1 and δ_2 determined by the independent ties are small in view of the many sources of accidental and systematic errors. The average value of δ_1 is $+0.10$ and of δ_2 is -0.06, giving a color zero-point correction of $+0.16$ mag. The stars C3 M and C4 K were omitted from the determinations of color coefficients and zero points.

TABLE 6

COMPARISONS OF C REGION MAGNITUDES WITH BOK AND EGGEN

Star	$P_{\text{Cox}}-P_{\text{Eggen}}$	$(P-V)_{\text{Cox}}-(P-V)_{\text{Eggen}}$	$P_{\text{Cox}}-Pg_{p\text{Bok}}$	$(P-V)_{\text{Cox}}-C_{p\text{Bok}}$	$(P-V)$
C12 F	+0.02	+0.03	......	......	+0.20
G	+ .04	+ .03	......	......	+0.18
L	+ .04	+ .06	......	......	+0.38
N	+ .05	+ .04	......	......	+0.37
O	+ .03	+ .02	......	......	+1.00
C4 E	+ .07	+ .06	......	......	+0.43
F	......	......	......	......	+1.07
G	+ .03	+ .02	+0.04	+0.16	−0.17
K	+ .13	+ .06	+ .14	+ .07	+1.10
L	+0.07	+0.07	+0.08	+0.14	+0.41

TABLE 7

ZERO-POINT CORRECTIONS TO THE S′ SYSTEM

TRANSFER	C REGION COMPARISONS			WEIGHTS		E REGION COMPARISONS		
	δ_1	δ_2	$\delta_1-\delta_2$	Link	Cape	δ_1	δ_2	$\delta_1-\delta_2$
NPS-C12-E2	+0.09	−0.05	+0.14	4	4	+0.10	−0.05	+0.15
NPS-C 2-E3	+ .13	− .05	+ .18	8½	4	+ .11	− .06	+ .17
NPS-C 3-E4	+ .11	− .05	+ .16	6	4	+ .10	− .06	+ .16
NPS-C 4-E5	+ .11	− .07	+ .18	8½	2½	+ .09	− .08	+ .17
NPS-C 4-E2	+0.11	−0.05	+0.16	8½	2	+0.10	−0.05	+0.15

This investigation has been supported in part by a number of grants from the Indiana University Graduate School. Some of the photoelectric equipment was constructed under a grant from Research Corporation. It is a great pleasure to thank H. M. Astronomer at the Cape of Good Hope, Dr. R. H. Stoy, Mr. A. W. J. Cousins, and the entire staff at the Royal Observatory for their very generous hospitality and co-operation. I also wish to thank Dr. John B. Irwin and Dr. James Cuffey for their assistance and for their many helpful discussions. I am indebted to Dr. Frank K. Edmondson for his active support in allotting me the necessary telescope time.

ON THE SPATIAL DISTRIBUTION OF GALAXIES
A SPECIFIC MODEL*

J. Neyman and E. L. Scott
Statistical Laboratory
and C. D. Shane
Lick Observatory, University of California

Received August 19, 1952

ABSTRACT

Counts of galaxies in 1° × 1° squares obtained at the Lick Observatory are used to test whether the serial correlations between these counts are compatible with the hypotheses that (i) galaxies occur only in clusters; (ii) the spatial distribution of cluster centers is quasi-uniform and, to be specific, follows a Poisson law; (iii) the number of ν of galaxies per cluster is a variable following an unspecified probability law with mean ν_1 and standard deviation σ_ν; (iv) the distribution of position of galaxies within a cluster follows a symmetric normal distribution with standard deviation σ. The outcome of the test is favorable to the hypotheses enumerated.

We note that the parameter σ measures, in a sense, the dimensions of the cluster. In order to obtain the most probable distance of the galaxy farthest from the cluster center, σ should be multiplied by a factor usually between 3 and 4, depending on the number of galaxies in the cluster. Numerical results include estimates of σ varying from 3×10^5 to 14×10^5 parsecs, according to the assumptions concerning the distribution of absolute magnitudes of the galaxies with $\sigma = 3.7 \times 10^5$ parsecs as the tentative best-fitting estimate.

Further numerical results, combined with certain plausible hypotheses, imply that ν_1, the average number of galaxies per cluster, is less than 287; that the standard deviation σ_ν of the number of galaxies per cluster is less than 144 and more than (probably much more than) 17; and that λ, the average number of cluster centers per cubic parsec, is between 0.12×10^{-18} and 34×10^{-18}. Tentative computations based on the assumption that $\nu - 1$ follows a negative binomial distribution show that the theory is compatible with the fact that within the area studied there are identified a number of very small clusters and, at the same time, a few giant clusters.

The best agreement between the theoretical and empirical serial quasi-correlations is obtained on the assumption that the standard deviation of the absolute magnitude of galaxies is $\sigma_M = 1.25$ mag.

I. INTRODUCTION

An examination of the distribution of the numbers of galaxies recorded on photographic plates shows that it does not conform to the Poisson law and indicates the presence of a factor causing "contagion." Two kinds of hypotheses have been advanced to explain this phenomenon: (i) the actual spatial distribution of galaxies is clustered, and (ii) the apparent clustering of galaxies is due to the effects of galactic interstellar clouds.

Hypothesis (i) is supported by the fact that many galaxies are obviously associated in clusters, some of which are now well identified and studied per se. Also, there is very substantial evidence in favor of hypothesis (ii). However, there are regions in the sky, particularly those close to the galactic poles, where the influence of interstellar clouds may be small or nonexistent. For this reason, we propose to study the hypothesis that, at least in certain regions of the sky where the effect of interstellar extinction is small, all the patchiness in the observable distribution of galaxies is due solely to the fact that the unobservable spatial distribution of galaxies is clustered. More specifically, the study will be directed to the probabilistic model of the spatial distribution of galaxies developed by two of the present authors in a recent paper[1] (hereafter referred to as "Paper I").

---

* All computations for this paper were performed at the Statistical Laboratory, University of California, with the partial support of the Office of Naval Research. Counts of galaxies were made at the Lick Observatory by C. D. Shane and C. A. Wirtanen. This paper is a joint publication of the Statistical Laboratory and of the Lick Observatory, *Contributions from the Lick Observatory*, Ser. II, No. 45.

This theory is based on several postulates that were described as structural. Briefly, the structural postulates are: (i) Galaxies occur only in clusters. (ii) The number ν of galaxies varies from cluster to cluster, subject to a probabilistic law with probability generating function $G_\nu(t)$. However, the postulates impose no restriction on the nature of the function $G_\nu(t)$. (iii) The distribution of galaxies within a cluster also is subject to a probabilistic law, characterized by a continuous probability density function $f(\eta)$, depending on the argument

$$\eta = \{(x-u)^2+(y-v)^2+(z-w)^2\}^{1/2}, \tag{1}$$

but otherwise free from restrictions. Here (x, y, z) are the co-ordinates of a given galaxy and (u, v, w) those of the corresponding cluster. (iv) The distribution of cluster centers in space is subject to a probabilistic law, described as quasi-uniform. According to this law, (*a*) to each region R in space there corresponds a random variable $\gamma(R)$ representing the number of cluster centers falling within R; and (*b*) the probability generating function $G_\gamma(t|\mathfrak{V})$ of $\gamma(R)$ depends on the volume $\mathfrak{V}$ of R but not on the shape or on the location of this region. Furthermore, (*c*) if R_1 and R_2 are two disjoint regions, then the variables $\gamma(R_1)$ and $\gamma(R_2)$ are independent. Paper I gives the most general form of the probability generating function $G_\gamma(t|\mathfrak{V})$ but otherwise leaves this function unspecified. Also, it was shown that, whatever the true distributions of ν and of $\gamma(R)$ may be, provided that the latter is consistent with the postulated quasi-uniformity, there is no change in the spatial distribution of galaxies if the probability generating function $G_\gamma(t|\mathfrak{V})$ is replaced by that of a Poisson law, say,

$$G^*_\gamma(t|\mathfrak{V}) = \exp\{\lambda\mathfrak{V}(t-1)\}, \tag{2}$$

and the probability generating function $G_\nu(t)$ by an appropriately adjusted probability generating function $G^*_\nu(t)$. In other words, it was shown[2] in Paper I that, without any restriction on the spatial distribution of galaxies other than that the distribution of cluster centers is quasi-uniform, one may assume that the distribution of $\gamma(R)$ is Poisson.

(v) If ξ is the distance of a galaxy from the observer and m_1 an arbitrary number, then there exists a function $\theta(\xi, m_1)$ representing the probability that the apparent magnitude m of the particular galaxy will be less than m_1. However, the exact nature of $\theta(\xi, m_1)$ is left unspecified.

The main result of Paper I is represented by the joint probability generating function $G_{N_1,N_2}(t_1, t_2)$ of the number N_1 of galaxies that have apparent magnitude less than a specified number m_1 and are included in an arbitrarily located solid angle ω_1, and of the number N_2 of galaxies located in an equally arbitrary solid angle ω_2 (which may coincide with ω_1, may overlap ω_1, or may be disjoint with ω_1) that have apparent magnitudes less than a specified number m_2 (which may be equal to or different from m_1). The probability generating function $G_{N_1,N_2}(t_1, t_2)$ is expressed in terms of the four unspecified functions, $G_\nu(t)$, $f(\eta)$, $G_\gamma(t|\mathfrak{V})$, and $\theta(\xi, m_1)$, and thus represents a characteristic of the general model of the distribution of galaxies consistent with the postulates adopted.*

---

[1] J. Neyman and E. L. Scott, *Ap. J.*, **116**, 144, 1952.

[2] Strictly speaking, the statement proved in Paper I is somewhat weaker and is to the effect that the joint probability generating function $G_{N_1,N_2}(t_1, t_2)$ of the numbers N_1 and N_2 of galaxies visible within any two solid angles ω_1 and ω_2 will not change if $G_\gamma(t|\mathfrak{V})$ is replaced by $G^*_\gamma(t|\mathfrak{V})$ and $G_\nu(t)$ by $G^*_\nu(t)$. However, it is easy to see that the proof applies to the stronger statement given in this paper. For this purpose it is sufficient to notice that, if the solid angles ω_1 and ω_2 are replaced by two arbitrary regions R_1 and R_2 and if one substitutes unity for $\theta(\xi)$, then formulae (40) and (41) of Paper I will represent the joint frequency function of the numbers, say N^*_1 and N^*_2 of galaxies present (though not necessarily visible) in the regions R_1 and R_2, respectively. The reasoning given in Paper I then proves that, whatever R_1 and R_2, the joint distribution of N^*_1 and N^*_2 is not altered by the substitutions indicated.

The purpose of the present paper is (*a*) to supplement the foregoing structural postulates by four additional postulates, described as secondary; (*b*) to apply the theory to actual counts of galaxies performed at the Lick Observatory; and (*c*) to obtain numerical values of the several constants involved in the specialized model characterizing the spatial distribution of galaxies.

The purpose of the secondary postulates is to provide at least interpolatory forms for the four functions $G_\nu(t)$, $f(\eta)$, $G_\gamma(t|\mathfrak{P})$, and $\theta(\xi, m_1)$, each depending upon a few parameters that can be adjusted to fit the observations. In selecting the particular forms of these functions, the authors were guided by the principle of avoiding unnecessary restrictions on the model, by the relevant opinions found in the literature (in particular, this applies to $\theta[\xi, m_1]$) and by considerations of simplicity and flexibility. Specifically, the numerical work involved in the estimation of the adjustable parameters proved so heavy that, with the present facilities, it was found impossible to let $G_\nu(t)$, $f(\eta)$, and $G_\gamma(t|\mathfrak{P})$ depend on more than one parameter each. With this limitation, efforts were made to select flexible formulae so that one could hope to approximate the distributions of the relevant random variables.

As already mentioned, no generality is lost by assuming that the number $\gamma(R)$ of cluster centers falling within any specified region R is Poisson-wise distributed with probability generating function (2), where λ stands for the average number of cluster centers per unit volume. Accordingly, formula (2) is postulated throughout the present paper, and λ is treated as an adjustable parameter. It will be noticed that (2) is not an interpolation formula. On the other hand, an interpolation formula had to be selected to replace the function $f(\eta)$. The form $f(\eta|\sigma)$ actually adopted depends upon a single adjustable parameter σ. The authors wish it to be clearly understood that this form is no more than a tentative interpolation formula and that no other significance is attached to it.

As to the function $G_\nu(t)$, the only assumption made is that the moments of ν exist. The authors are very reluctant to adopt any particular form for $G_\nu(t)$ because no one-parameter formula which the authors could think of presents sufficient flexibility to fit the qualitative impressions that they obtained from handling observational data. The formulae characterizing the observable distribution of galaxies are such that, within the limits of the computational facilities, it is possible to estimate the quotient c of the two first moments of ν, say ν_1 and ν_2, which are the mean number and the mean square of the number of galaxies per cluster, respectively. This quotient, then, is treated as an adjustable parameter characterizing the distribution of ν. It will be seen that, although regrettably insufficient, this characterization, combined with certain other considerations, does give a qualitative picture of what the actual distribution of the number of galaxies per cluster might be.

The unfortunate circumstance connected with leaving the function $G_\nu(t)$ unspecified is that the equations amenable to our present computational facilities determine the value of the product $\lambda\nu_1$ = expected number of galaxies per unit volume, but not of either of the two factors λ and ν_1 taken separately.

Thus, adopting the form of $\theta(\xi, m_1)$ currently discussed in the literature, the whole specialized model depends on the three parameters $\lambda\nu_1$, σ, and $c = \nu_2/\nu_1$. Following the indications of the concluding section of Paper I, a method is developed for estimating the three parameters from counts of galaxies in regularly placed nonoverlapping squares, all made to the same limiting magnitude.

While there seems to be some agreement (see Postulate S4 below) as to the form of the function $\theta(\xi, m_1)$, there are varying opinions as to the values of the constants involved. For this reason, the evaluation of the parameters $\lambda\nu_1$, σ, and c in the present model of the distribution of galaxies is made on several alternative hypotheses regarding $\theta(\xi, m_1)$, which, it is believed, cover the whole range of possibilities contemplated in the literature.

---

* *Note added in proof.*—The original proof of the formula giving $G_{N_1, N_2}(t_1, t_2)$ contains a mistake. Specifically, formula (22) is wrong. Nevertheless, the authors of Paper I were able to show that this mistake in the argument does not affect the final result and that the expression for $G_{N_1, N_2}(t_1, t_2)$ as given in Paper I is correct.

The estimates are based on a comparison between the theoretical values of the so-called "serial quasi-correlations," defined in equation (68) of Paper I, and their empirical counterparts obtained from counts of galaxies. It will be noticed that all the formulae of Paper I are concerned with numbers N_1 and N_2 of galaxies that have apparent magnitudes less than a specified quantity. Unfortunately, the empirical data do not involve the numbers N_1 and N_2 but the related numbers, say,

$$X_i = N_i \text{ plus the error of plate plus the error of counting,}$$

with $i = 1, 2$. Naturally, the correlations and also the quasi-correlations between X_1 and X_2, affected by errors of technique and of counting, must be less than those of N_1 and N_2. The evaluation of these errors and the method of correcting for them will be found in the Appendix. The Appendix also contains a description of the method used to allow for the effects of general galactic extinction.

The main results of this paper are contained in Section V, giving empirical values of the serial correlations and quasi-correlations computed from the Lick Observatory counts of galaxies in regularly spaced 1° × 1° squares. These empirical correlations and quasi-correlations are compared with their theoretical counterparts based on trial values of the parameters $\lambda\nu_1$, σ, and c, combined with several alternative combinations of constants in the function $\theta(\xi, m_1)$. It is found that, with appropriately selected constants, the theoretical correlations and quasi-correlations closely fit the figures found empirically.

II. SECONDARY POSTULATES

Postulate S1.—In Paper I it was shown that, out of the whole family of probability generating functions characterizing a quasi-uniform distribution, the simplest is that of the Poisson law, namely,

$$G_\gamma(t \mid \mathfrak{V}) = \exp\{-\lambda\mathfrak{V}(1-t)\}, \tag{3}$$

where λ is an adjustable parameter representing the average or the expected number of cluster centers per unit volume. Furthermore, as mentioned in the preceding section, if there are no limitations on the distribution of ν, the number of galaxies in a cluster, then the adoption of equation (3) represents no restriction on the spatial distribution of galaxies. Formula (3) is, then, adopted in this paper.

Postulate S2.—Considerations of simplicity also dictated the adoption of the symmetric normal probability density for the function $f(\eta)$,

$$f(\eta \mid \sigma) = \left(\frac{1}{\sigma\sqrt{2\pi}}\right)^3 \exp\left\{-\frac{1}{2\sigma^2}\left[(x-u)^2 + (y-v)^2 + (z-w)^2\right]\right\}. \tag{4}$$

Here σ is an adjustable parameter measuring, in a sense, the dimensions of a typical cluster.

In what follows, formula (4) will, then, be treated as the conditional probability density of the co-ordinates (X, Y, Z) of a galaxy, given that this galaxy belongs to a cluster with its center at (u, v, w). According to the postulates of Paper I, the positions of all the galaxies of a particular cluster are completely independent.

Postulate S3.—Throughout this paper it is assumed that the distribution of the number ν of galaxies per cluster has finite moments $\nu_1, \nu_2, \ldots$. Otherwise the probability generating function $G_\nu(t)$ is left unspecified. The ratio $c = \nu_2/\nu_1$ is treated as an adjustable parameter, an estimate of which is obtained from the observations.

In certain discussions it is interesting to have before one's eyes a specific formula that might conceivably represent the distribution of ν. Because of simplicity, one is tempted to consider either a Poisson or a negative binomial distribution. Since these two distributions have positive probabilities of the value zero and since in a real cluster the number of galaxies is at least equal to unity, it will be considered that the Poisson distribution or the negative binomial apply not to ν itself but to $\nu - 1$. Thus, as very tentative possibilities, we shall discuss either

$$G_\nu(t) = t\, e^{(\nu_1 - 1)(t-1)}\,, \tag{5}$$

which is the Poisson case, or

$$G_\nu(t) = \frac{t}{[1 - \beta(t-1)]^\alpha}\,, \tag{6}$$

which is the negative binomial case, where α and β are two positive adjustable parameters.

It is easy to see that equation (5) implies

$$\nu_1 = \frac{c-1}{2}\left\{1 + \left[1 + \left(\frac{2}{c-1}\right)^2\right]^{1/2}\right\} = \sigma_\nu^2 + 1\,, \tag{7}$$

where σ_ν^2 denotes the variance of ν. Thus, if c is a substantial number, which is found empirically to be the case, then $c - 1$ represents, approximately, the average number of galaxies per cluster.

On the other hand, formula (6) implies

$$\nu_1 = 1 + \alpha\beta \tag{8}$$

and

$$\begin{aligned} \alpha &= \frac{(\nu_1 - 1)^2}{1 + \nu_1(c-1) - \nu_1^2}\,, \\ \beta &= \frac{\alpha(c-3) + [(\alpha c - \alpha + 2)^2 + 4(\alpha^2 - 1)]^{1/2}}{2\alpha(\alpha + 1)}\,, \end{aligned} \tag{9}$$

while the definition of $c = \nu_2/\nu_1$ implies

$$\sigma_\nu^2 = \nu_1(c - \nu_1)\,. \tag{10}$$

The advantage of formula (5) is its familiarity and the fact that it depends upon a single adjustable parameter that is easily expressed in terms of c. The disadvantage of formula (5) is that it imposes a very limited variability on the random variable ν; so limited is the variation of ν implied by formula (5) that it is not likely to correspond to the observed variation in the number of galaxies in different clusters.

Formula (6) has the advantage that the variation it implies [see eq. (10)] may be as large as desired, provided that c is sufficiently large. Also, as is well known, the negative binomial distribution may be regarded as a particular weighted average of an infinity of Poisson distributions with indefinitely increasing expectations. Thus, assuming (6), one may have in mind the possibility that there is an infinity of different categories of clusters of galaxies such that within each category the number $\nu - 1$ varies according to a Poisson law and such that the expectation ν_1 varies, ranging from unity to infinity, from one category of clusters to another. Unfortunately, knowledge of c alone is not sufficient to determine the distribution (6).

POSTULATE S4.—The adopted form of the function $\theta(\xi, m_1)$ is based on studies of Hubble[3] regarding the distribution of the absolute magnitude of the galaxies. Hubble's

[3] *Mt. W. Contr.*, No. 548; *Ap. J.*, **84**, 158, 1936.

results suggest assuming that the distribution of absolute magnitude M of a galaxy is normal,[4] with probability density, say,

$$\frac{1}{\sigma_M\sqrt{2\pi}}\exp\left\{-\frac{1}{2\sigma_M^2}(M-M_0)^2\right\}. \tag{11}$$

Hubble's estimates are $M_0 = -14.2$ and $\sigma_M = 0.85$ mag. As to the apparent magnitude m of a galaxy distant from the observer by ξ parsecs, in the absence of interstellar extinction, the studies of Hubble and Humason suggest the formula[5]

$$m = M - 5 + 5\log\xi + 5.15\times 10^{-9}\xi\,, \tag{12}$$

where the last term on the right-hand side represents the effect of red shift. Combining these results, we easily obtain the following formula for the conditional probability density of the apparent magnitude of a galaxy, given that its distance from the observer is ξ, say,

$$p_m(m\mid\xi) = \frac{1}{\sigma_M\sqrt{2\pi}}\exp\left\{-\frac{1}{2\sigma_M^2}(m - M_0 + 5 - 5\log\xi - 5.15\times 10^{-9}\xi)^2\right\}. \tag{13}$$

Upon adopting (13), the probability $\theta(\xi, m_1)$ is

$$\begin{aligned}\theta(\xi, m_1) &= \int_{-\infty}^{m_1} p_m(m\mid\xi)\,dm\\ &= \mathfrak{G}\left(\frac{m_1 - M_0 + 5 - 5\log\xi - 5.15\times 10^{-9}\xi}{\sigma_M}\right),\end{aligned} \tag{14}$$

where, for every number x, the symbol $\mathfrak{G}(x)$ means

$$\mathfrak{G}(x) = \frac{1}{\sqrt{2\pi}}\int_{-\infty}^{x} e^{-t^2/2}\,dt\,. \tag{15}$$

We note that formula (14) contains two parameters, thus far unspecified, for which it is necessary to substitute numerical values before the formula can be used in actual computations. The first of these parameters is the difference $m_1 - M_0$ between the limiting apparent magnitude of the plates and the mean absolute magnitude of the galaxies. A considerable amount of computation was done, using the presumed[6] value $m_1 = 18.3$ and Hubble's estimate $M_0 = -14.2$. Since both these estimates appear somewhat uncertain, the computations were performed for three alternative values of the difference $m_1 - M_0$, namely, 31.5, 32.5, and 33.5 mag.

The second parameter left unspecified in formula (14) is σ_M, the standard deviation of the absolute magnitudes of the galaxies. Hubble's original estimate is $\sigma_M = 0.85$.

---

[4] Contrary to this assumption of a normal distribution, studies of the absolute magnitude of the members of the local group by Baade (*Mt. W. Contr.*, No. 697, 3; *Ap. J.*, **100**, 139, 1944), Holmberg (*Medd. Lunds. Obs.*, Ser. II, No. 128, 1950), and Hubble (*Mt. W. Contr.*, No. 548, 3; *Ap. J.*, **84**, 160, 1936) indicate that, for this cluster at least, the distribution of absolute magnitudes is somewhat skewed. See also Zwicky (*Pub. A.S.P.*, **63**, 61, 1951) for consideration of the Coma cluster. However, all these indications are not yet specific enough to be used in the present study.

[5] Hubble finds (*Mt. W. Contr.*, No. 557; *Ap. J.*, **84**, 517, 1936) the empirical increase in apparent magnitude with apparent velocity, $m = 2.94\,d\lambda/\lambda$. Also (*Mt. W. Contr.*, No. 549; *Ap. J.*, **84**, 270, 1936), the velocity of recession in km/sec is 526 times the distance in million parsecs. Solving for $d\lambda/\lambda$ and substituting, we obtain the last term in (12).

[6] The value of the limiting magnitude m_1 has not been determined directly for the counts made at the Lick Observatory. Interpolation from the regression equation given by Hubble (*Mt. W. Contr.*, No. 557, 13; *Ap. J.*, **84**, 529, 1936) with the average observed number of galaxies per square degree gives $m_1 = 18.25$ mag. Correction of the counts for the effects of general galactic extinction (see appendix) increases m_1 to 18.5, while correction also for errors in counting according to error model 2 provides $m_1 = 18.6$ mag.

However, since the dispersion in absolute magnitude is sometimes completely neglected and since different estimates have been given in the literature, for example, by Holmberg,[7] the computations were performed using four hypothetical values of σ_M, namely, $\sigma_M = 0.00, 0.85, 1.25$, and 2.00 mag. Each value of σ_M was combined with each value of the other parameter $m_1 - M_0$ so that the computations were carried out in parallel with twelve specializations of the function $\theta(\xi, m_1)$.

III. SOME IMPLICATIONS OF THE SECONDARY POSTULATES

The three formulae (3), (4), and (14) assumed to represent the distributions involved in the model of the spatial distribution of galaxies are used frequently in astronomical work and are very familiar. However, the implications of assuming these functions in this paper need not be so clear. The purpose of this section is, then, to illustrate some of these implications and to compare them qualitatively with the visual impressions that one has of the observable distribution of galaxies.

Our first comments refer to the assumptions that galaxies occur only in clusters and that the number ν of galaxies per cluster is a random variable (at least equal to unity), following a distribution with an unspecified probability generating function $G_\nu(t)$. The question that presents itself is: How do these assumptions compare, qualitatively, with what is actually observed?

The predominant impression that one obtains from the existing data regarding galaxies is that of an irregular "background" composed of galaxies that either are "single" or appear to be in small groups of perhaps a dozen members and, standing out from the general background, a few large clusters, such as those in Virgo, Coma, Corona Borealis, each containing hundreds of galaxies. The question then is whether the assumption of no single galaxies other than those implied by the assumed distribution $G_\nu(t)$, combined with the foregoing postulates regarding $f(\eta \mid \sigma)$ and $\theta(\xi, m_1)$, can account for the observed character of the background. The interest in this question depends very much on the nature of the distribution of ν. For example, if this distribution implies that $P\{\nu = 1\} = 0.99$, so that about 99 per cent of all "clusters" are composed of single galaxies, then the predominance of single galaxies in the background would need no other explanation and the postulate "all galaxies occur in clusters" would require additional quotation marks around the word "clusters." For this reason, the question raised is interesting only if one contemplates a distribution of ν of a more, so to speak, conservative type, with a reasonably large average for ν, so that it could account for clusters of several hundred galaxies each and a relatively small variation.

In order to throw some light on the situation, Figure 1 was constructed,[8] assuming what might be an ultra-conservative distribution of ν, namely, the Poisson law (5). For purposes of illustration here, we have chosen the distribution of ν itself rather than $\nu - 1$ to be Poisson. This distribution allows the slight possibility of clusters of zero members but does not alter the character of Figure 1. The three graphs in the top row represent three hypothetical Poisson distributions of the number ν with $\nu_1 = 6$, $\nu_1 = 60$, and $\nu_1 = 600$. The last of these values approximates the first estimate of ν_1 obtained in the preliminary computations based on the data from the Lick Observatory. Also, it is interesting in connection with the known large clusters, such as Coma. It will be seen that if $\nu_1 = 600$, then the occurrence of a cluster with more than 700 or less than 500 galaxies would be extremely rare. Similarly, if $\nu_1 = 60$, then the occurrence of clusters with hundreds of galaxies and with less than 20 would be practically impossible. This is what we mean by describing the Poisson distribution as "ultra-conservative."

The second and third rows of Figure 1 give graphs of probabilities $P\{n = k \mid n \geq n'\}$

---

[7] *Medd. Lunds. Obs.*, Ser. II, No. 128, 1950.

[8] The authors are indebted to Mrs. Roxie Hollander for the computation of probabilities illustrated in the two lower rows of Fig. 1.

that the number n of "visible" galaxies (that is, galaxies with apparent magnitude less than the limiting magnitude m_1 of the plate), all belonging to the same cluster, will equal k, given that this cluster contains at least n' visible galaxies. In the second row $n' = 1$, while in the third row $n' = 5$. All these probabilities were computed assuming the Poisson distributions of ν illustrated in the first row of graphs. Also, it was assumed that $m_1 - M_0 = 32.5$, $\sigma_M = 0.85$, and $\sigma = 5 \times 10^5$ parsecs, the latter value being within the plausible limits of the parameter involved in $f(\eta | \sigma)$. The formula for the probability $P\{n = k | n \geqq n'\}$ will appear in a later publication.

In order to explain these graphs more clearly, we shall interpret in detail the values of the ordinates of the first few points in the last graph in the second row. Since the graph corresponds to $n' = 1$, we visualize all the clusters that contain at least one visible galaxy. The value $P\{n = 1 | n \geqq 1\} = 0.279$ means, then, that, out of all these clusters, approximately 28 per cent will contain only one visible galaxy. Similarly, the value $P\{n = 2 | n \geqq 1\} = 0.114$ means that about 11.4 per cent of the same clusters (those with at least one visible galaxy) will contain exactly two visible galaxies, etc. Adding up the ordinates of the fifteen points given in the graph, we obtain the probability of 0.702 that a cluster with at least one visible galaxy will contain not more than 15 that are visible. Beyond $k = 15$, the probabilities continue to decrease at a slower and slower rate.

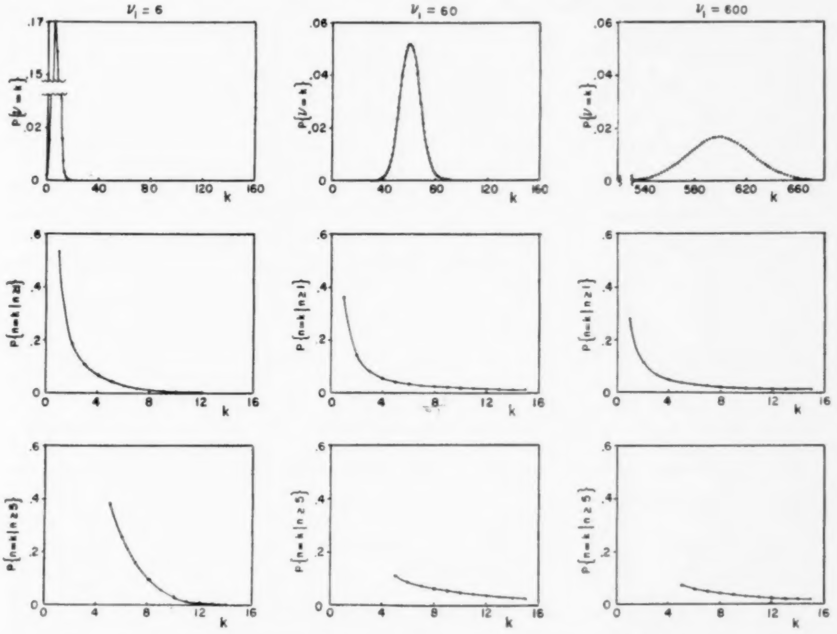

FIG. 1.—Consistency of predominance of apparently single visible galaxies with the assumption that galaxies occur only in concentrated clusters. *Top row:* Three hypothetical Poisson distributions of the actual number ν of galaxies per cluster, with mean $\nu_1 = 6$, $\nu_1 = 60$, and $\nu_1 = 600$. *Middle row:* The three corresponding conditional probability distributions $P\{n = k | n \geqq 1\}$ of the number n of "visible" galaxies (galaxies with $m < 18.3$) per cluster, given that this cluster contains at least *one* visible galaxy. *Bottom row:* The probabilities $P\{n = k | n \geqq 5\}$ that the number n equals k, given that the cluster contains at least *five* visible galaxies.

Therefore, the remaining probability of 0.298 is distributed over a long range of approximately equiprobable values of n. It is well known that in many cases clusters containing 100 or less visible galaxies may escape detection. For this reason Figure 1 seems to indicate, at least qualitatively, that, even if the number ν of galaxies per cluster had the ultra-conservative Poisson distribution with expectation $\nu_1 = 600$, the predominance of the chaotic background of apparently single galaxies would have been a perfectly natural phenomenon implied by the hypotheses assumed.

However, as already emphasized, the authors do not contemplate the Poisson law as a plausible approximation to the actual distribution of ν. The reason is that several relatively small groups of perhaps a dozen galaxies are known that seem to have only bright members. Consequently, these groups of galaxies cannot be very distant; yet, should they be part of a cluster of several hundred galaxies, then many more of these galaxies would also be visible on the plates. Thus, one must assume that small clusters of galaxies are not at all so uncommon as the Poisson law with $\nu_1 = 600$ would indicate. On the other hand, if one assumed a Poisson distribution with a low value of the expectation ν_1, so as to account for the not infrequent occurrence of small clusters, then this assumption would be difficult to reconcile with the existence of such rich clusters as those in Coma, Virgo, and Corona Borealis. As a result, when thinking of a plausible distribution of the number ν of galaxies per cluster, rather than visualizing a Poisson law, the authors have in mind a distribution with a much broader variation, perhaps a negative binomial distribution, representing a weighted average of an infinity of Poisson laws. Reverting again to Figure 1, it is easy to visualize that such a weighted average would (i) fit well with the general idea that all the galaxies belong to real clusters, each with at least several members; (ii) account for the photographs showing an observed chaotic background composed of apparently single galaxies; and (iii) be consistent with the existence of a few very large and of a few rather small clusters that are now identified.

Unfortunately, as will be illustrated below, the problem of identifying clusters with only a few visible galaxies presents very considerable difficulties, and it is doubtful that any reliable statistics of the number of clusters with a specified number of visible galaxies will be compiled in the foreseeable future. Therefore, the theoretical distributions in the two lower rows of Figure 1 may serve for qualitative comparisons only.

The phenomenon, illustrated in Figure 1, of the rareness of clusters that contain many visible galaxies is of sufficient interest to justify a further illustration of the machinery behind it. At the same time, we shall attempt to illustrate the observable implication of the two assumptions (i) that the function (4) represents the probability density of the co-ordinates of a galaxy within a cluster and (ii) that, when the cluster center is fixed, the positions of all the galaxies in this cluster are completely independent (see Paper I).

Figures 2 and 3 were constructed with these purposes in mind. The two columns of Figure 2 correspond to two different assumptions regarding σ_M, the standard deviation of the absolute magnitude of galaxies. The first column corresponds to the view that, for purposes of the study of the distribution of galaxies, so to speak in the large, the differences in absolute magnitudes from one galaxy to another could be neglected, so that $\sigma_M = 0$. The second column of Figure 2 corresponds to $\sigma_M = 1.0$, which is close to Hubble's estimate.

Each row of Figure 2 corresponds to a stated distance of the cluster center from the observer, 2×10^7, 3×10^7, 4×10^7, and 5×10^7 parsecs. Each of the eight graphs of Figure 2 represents the same cluster, centered at the mid-point of each graph, as it would be "seen" from the four distances indicated if the dispersion in absolute magnitude were characterized by $\sigma_M = 0$ and $\sigma_M = 1$, respectively. This cluster is purely hypothetical and was constructed synthetically in strict conformity with the postulates adopted in this paper. Assuming the tentative value of $\sigma = 5 \times 10^5$ parsecs as the value of the parameter in the distribution of the positions of galaxies within the cluster, tables[9] of independent normal deviates were used to obtain the three-dimensional co-ordinates of 60 galaxies (the choice of 60 is for illustration only; this point is discussed below) with respect to the cluster center. The graphs in the first column, corresponding to $M_0 = -14.2$ and $\sigma_M = 0$, were constructed on the assumption that the absolute magnitude of each galaxy is exactly $M = -14.2$. On the other hand, in the graphs of the second column, the absolute magnitudes of particular galaxies vary according to the distribution (11). The tables of the random normal deviates were used again in the second column to

---

[9] P. C. Mahalanobis, *Sankhyā*, 1, 1, 1933; and H. Wold, *Tracts for Computers*, No. 25, p. 1, 1948.

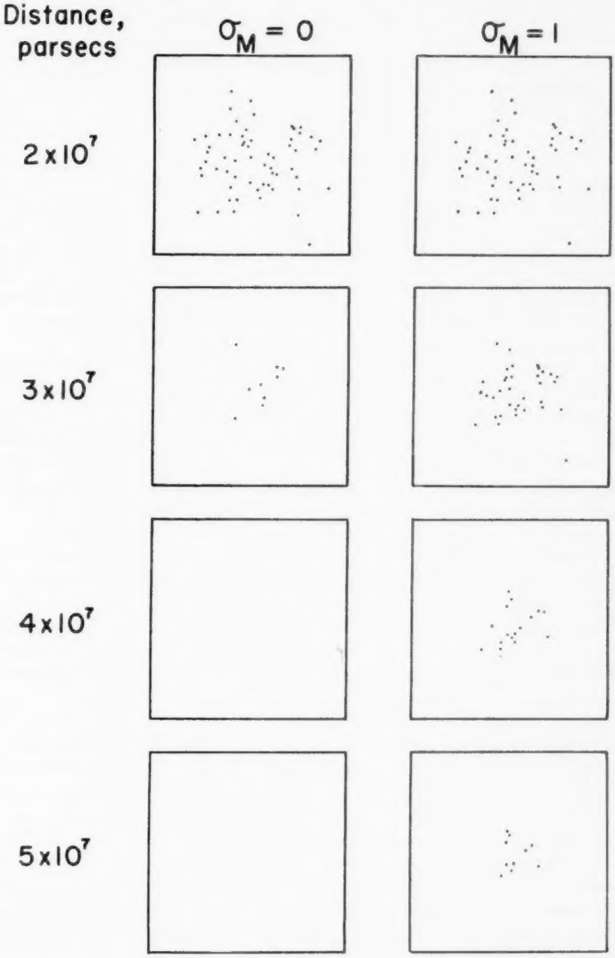

FIG. 2.—Effect of distance and of dispersion in absolute magnitude on appearance of a cluster. The same synthetic cluster of 60 galaxies as it would be "seen" from each of four distances. Plots on left assume all galaxies have some absolute magnitude, so that $\sigma_M = 0$. Plots on right assume dispersion in absolute magnitude is $\sigma_M = 1$ mag.

determine the absolute magnitude separately and independently for each galaxy, letting $\sigma_M = 1$. Now that we have the three co-ordinates with respect to the cluster center and the absolute magnitude of each of the galaxies in the cluster obtained synthetically, we can compute the apparent magnitude and apparent position of each galaxy for each of the four assumed distances to the cluster center. All those galaxies for which $m < 18.3$ were plotted.

In the first column, corresponding to $\sigma_M = 0$, the variation in the apparent magnitude of galaxies results solely from the variation in the distances of these galaxies. In the second column the variation in apparent magnitude is larger and results both from the variation in distance and from the variation in absolute magnitude. It so happens that the top picture in the first column shows the whole hypothetical cluster. This is because the variation in the distances of the galaxies was not sufficient to dim even a single one of the galaxies present to an apparent magnitude beyond the limit of 18.3 mag. when the cluster center is only 2×10^7 parsecs distant. On the other hand, with the variation in absolute magnitude of $\sigma_M = 1$, at the cluster distance of 2×10^7 parsecs, seven galaxies become "invisible," as illustrated in the top plot of the second column.

Upon examining the consecutive graphs from the top of each column to its bottom, we see that, as expected, the greater the distance of the cluster, the fewer galaxies remain visible. However, this process of losing sight of galaxies is much faster in the first column than in the second, so that, for the cluster distance of 4×10^7 parsecs and beyond, not a single galaxy of the cluster remains visible. This difference between the two columns suggests that the variability in absolute magnitude of galaxies must be an important element characterizing the observable distribution of galaxies.

The graphs of Figure 2 exhibit the following interesting details. First, the authors were a little surprised by the apparent lack of regularity in the distribution of dots, which shows little resemblance to the circular contours that one is accustomed to visualize in connection with the symmetric normal distribution. Second, as the distance between the observer and the cluster increases, so that a portion of the galaxies become invisible, the original cluster shows a tendency to disintegrate. Thus, if the model studied resembles the actual facts, one should not be surprised to find that several adjoining, but seemingly disconnected, groupings of galaxies are in reality parts of a single cluster.

These last remarks apply directly to clusters for which the total number of galaxies is 60. In addition, we must remember that the tentative conclusions drawn are based on only one synthetic cluster. Figure 3 gives, for $\sigma_M = 1$, three more similarly constructed clusters supposedly observed from a distance of 4×10^7 parsecs. It is seen that these are roughly the same in character as the one given in the second column of Figure 2. However, in spite of the fact that they were constructed with identical distributions, the four clusters appear to differ in their degree of concentration.

In connection with the discussion of Figure 1 and since clusters of about 600 members are probably not infrequent, it was decided to produce a synthetic plot of such a cluster as it would appear viewed from several distances. Two plots of such a cluster of galaxies observed at distances 4×10^7 and 5×10^7 parsecs are exhibited at the bottom of Figure 3. It is seen that these plots are more regular than those of clusters with only 60 galaxies and that they approximate the intuitive idea of a normal distribution. Also, one might say that, if the first of the two graphs represents a typical cluster distant 4×10^7 parsecs, then it is rather surprising that so few of these clusters have been identified. However, on closer examination of the general circumstances, the rareness of known clusters of this kind appears quite natural. The reason is that, even if one counts the number of galaxies in a 1° × 1° square with one corner at the center of the cluster, the average number of visible galaxies exhibited in the lower left graph of Figure 3 is only 25. On the other hand, the average number of galaxies per 1° × 1° square counted in the Lick Observatory data in the 1060 squares in the quadrant closest to the galactic pole is 68.6. Furthermore, the standard deviation of the counts in particular 1° × 1° squares is 25.3. Thus, excesses and deficiencies of 25 galaxies per square degree are of most common occurrence, and it should not be surprising that a cluster of the type visualized at the bottom of Figure 3 just sinks into the general rough background without standing out. The machinery behind this roughness is easy to visualize by contemplating layers of clusters occurring at increasing distances with correspondingly decreasing angular distances between component galaxies.

Figure 3 was constructed using the probability density (4) with the value of the parameter σ as estimated from the first computations on the Lick Observatory data. It will be realized that similar graphs would result from assuming any other symmetric probability density with a maximum at the center. As to the particular function (4), the authors are not certain that it will prove a satisfactory approximation[10] to the true distribution of galaxies within a cluster, and there are some observational facts that appear inconsistent with the properties of (4). One such fact is that the clusters plotted in Figures 2 and 3 exhibit relatively weak central concentrations. On the other hand, among the identified clusters there exist some, such as the Coma cluster, in which the central concentrations are much more pronounced. At the present moment it is difficult to be sure whether this observed considerable concentration is a more or less general rule or an ex-

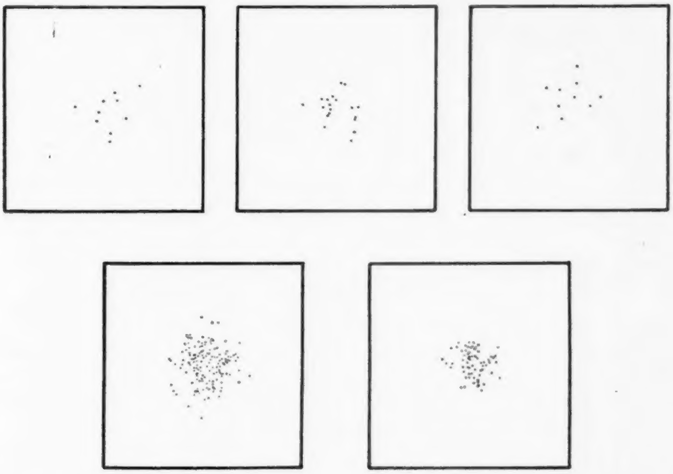

FIG. 3.—*Top row:* Implications of the assumption that the internal structure of a cluster is governed by the normal distribution. Three different synthetic clusters of 60 galaxies each, as viewed from a distance of 4×10^7 parsecs. Change from one cluster to the next is due to chance only. *Bottom row:* One cluster of 600 galaxies, as viewed from 4×10^7 and 5×10^7 parsecs, respectively.

---

[10] The authors are inclined to think that further studies of the same numerical material or, perhaps, of several sets of data corresponding to different limiting magnitudes will indicate the impossibility of assuming that a *unique* function $f(\eta)$ represents the internal structure of all the clusters. Contrary to this, they expect that the totality of clusters can be divided into a number of categories and that each category may be characterized by a particular probability density $f(\eta)$, perhaps combined with a corresponding distribution of ν. Should this actually be the case, then the unique parameter σ, for which an estimate is obtained in this paper, would be a certain weighted average of similar parameters referring to the particular categories of clusters. While thinking of these possibilities, the authors limit their present study to the simplifying postulates enumerated in Sec. II. If a theory involves too many adjustable parameters, then it ceases to possess the character of a structural model and becomes a complicated interpolation procedure.

ception, making the clusters in question conspicuous and easy to identify. The question of whether or not the function (4) yields a satisfactory approximation to the actual distribution of galaxies can be tested, and such a test is contemplated.

Our last comments refer to the function $\theta(\xi, m_1)$. As already mentioned, its general form is based on studies by Hubble and Humason, and it takes into account the effect of red shift. Because the red-shift term prevented us from obtaining explicit forms of certain integrals, its inclusion proved very troublesome. Figure 4 illustrates the difference between the function $\theta(\xi, m_1)$ as adopted in this paper and the alternative form neglecting the red shift. In both cases, it was assumed that $m_1 - M_0 = 32.5$ and $\sigma_M = 0.85$. This difference was considered substantial enough to warrant the extra computational difficulties connected with including the effects of red shift.

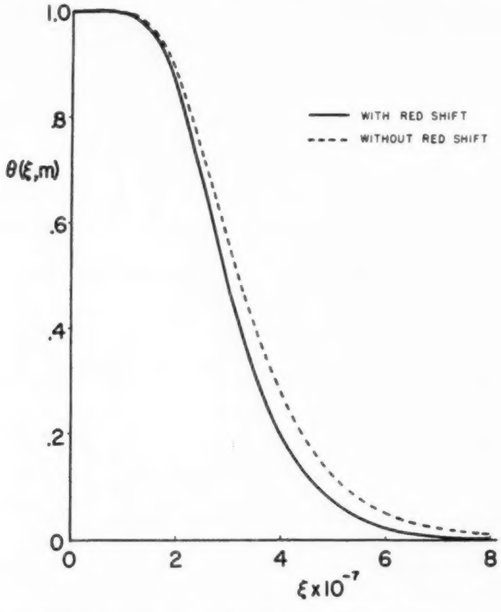

FIG. 4.—Effect of red shift on the probability $\theta(\xi, m_1)$ that a galaxy distant by ξ parsecs will be visible (will have $m < 18.3$ mag.).

IV. SPECIALIZATION OF CERTAIN FORMULAE OF PAPER I

To meet the purposes of the present paper, the theory of Paper I needs specialization in two respects. First, in accordance with the secondary postulates adopted, we must replace the originally unspecified functions $G_\gamma, f(\eta)$, and $\theta(\xi, m_1)$ by the particular selected forms (3), (4), and (14). Second, we must adapt the general theory so that it can be applied to actual counts performed at the Lick Observatory. These counts extend over a rectangular area 63° × 46° divided into 2898 squares 1° × 1° each, and the data represent the numbers of galaxies counted separately in each such square. The apparent limiting magnitude of each count is approximately the same and is believed to be $m_1 = 18.3$ mag.

All the computations in this paper refer to counts in pairs of 1° × 1° squares, exactly k degrees apart, for $k = 1, 2, 3, 4, 5, \ldots$. Since the theory of Paper I refers to numbers N_1 and N_2 of galaxies visible in two arbitrary solid angles ω_1 and ω_2, overlapping or not, with arbitrary limiting magnitudes m_1 and m_2, respectively, for the purposes of this paper we set $m_1 = m_2$ mag. and interpret ω_1 and ω_2 as two nonoverlapping 1° × 1° solid angles, similarly oriented, with their centers distant by k degrees in the direction of one of their sides.

It is easily seen that, with all the specializations indicated, the basic formulae of Paper I, namely, formulae (40) and (41) giving the probability generating function of N_1 and N_2, reduce to

$$\begin{aligned} G_{N_1, N_2}(t_1, t_2) &= \exp\left\{ \lambda \iiint_{-\infty}^{+\infty} [G_\nu\{1 - p_1(1-t_1) - p_2(1-t_2)\} - 1]\, du\, dv\, dw \right\} \\ &= \exp\{-\lambda I(t_1, t_2)\}, \qquad \text{say}, \end{aligned} \tag{16}$$

where, for $i = 1, 2$,

$$p_i = \iiint_{\omega_i} \theta(\xi, m_1)\, f(\eta \mid \sigma)\, dx\, dy\, dz\,. \tag{17}$$

Here, as just mentioned, ω_1 and ω_2 stand for two similarly oriented 1° × 1° solid angles with their centers distant by exactly k degrees in the direction of one of their sides, and $f(\eta \mid \sigma)$ is given by (4) and $\theta(\xi, m_1)$ by (14).

It was pointed out in Paper I that if the integral in the right-hand side of (16) is divergent for any t_1 and t_2, $0 \leqq t_1, t_2 \leqq 1$, then the probability that $N_i = \infty$ is equal to unity. Since this conclusion is contrary to the facts, it was decided to limit the study of the distribution of galaxies to such systems of secondary postulates for which the integral in the exponent of the expression representing $G_{N_1, N_2}(t_1, t_2)$ is convergent for all combinations of t_1 and t_2 with $0 \leqq t_1, t_2 \leqq 1$. For this reason, it is now necessary to show that, with the particular secondary postulates adopted, the integral $I(t_1, t_2)$ is convergent for the above values of t_1 and t_2. In so doing, we shall use the postulate that the moments of the variable ν exist and, therefore, the function $G_\nu(t)$ can be differentiated at $t = 1$. The proof is independent of the particular form (4) of the function $f(\eta)$ and is valid on condition that it is a probability density and depends only on the argument η.

Since every probability generating function is nondecreasing when its arguments are increased, we have

$$\begin{aligned} I(t_1, t_2) &= \iiint_{-\infty}^{+\infty} \{1 - G_\nu[1 + p_1(t_1 - 1) + p_2(t_2 - 1)]\}\, du\, dv\, dw \\ &\leqq \iiint_{-\infty}^{+\infty} \{1 - G_\nu[1 - p_1 - p_2]\}\, du\, dv\, dw = I^*, \qquad \text{say}. \end{aligned} \tag{18}$$

Using the differentiability of $G_\nu(t)$ and also the fact $G_\nu(1) = 1$, we have

$$\begin{aligned} I^* &= \iiint_{-\infty}^{+\infty} [G_\nu(1) - G_\nu(1 - p_1 - p_2)]\, du\, dv\, dw \\ &= \iiint_{-\infty}^{+\infty} (p_1 + p_2) \frac{dG_\nu[1 - \vartheta(p_1 + p_2)]}{dt}\, du\, dv\, dw\,, \end{aligned} \tag{19}$$

where $0 \leqq \vartheta \leqq 1$. But the derivative of a probability generating function is never negative and is nondecreasing, tending to the first moment as the argument tends to unity. Therefore, denoting the first moment of ν by ν_1, we have

$$I^* \leqq \nu_1 \iiint\limits_{-\infty}^{+\infty} (p_1 + p_2)\, du\, dv\, dw\,. \tag{20}$$

Using (17) and changing the order of integration, the integral in the right-hand side can be written as

$$\iiint\limits_{\omega_1 \cup \omega_2} \left[\theta(\xi, m_1) \iiint\limits_{-\infty}^{-\infty} f(\eta \mid \sigma)\, du\, dv\, dw \right] dx\, dy\, dz\,, \tag{21}$$

where $\omega_1 \cup \omega_2$ stands for the union of the solid angles ω_1 and ω_2. However, because of the particular property that the function $f(\eta \mid \sigma)$ depends only on the argument η and is a probability density, the inside integral in (21) is equal to unity. Thus there now remains to show that the integral

$$\iiint\limits_{\omega_1 \cup \omega_2} \theta(\xi, m_1)\, dx\, dy\, dz \tag{22}$$

is convergent. Since the integrand depends only upon ξ, it is convenient to introduce polar co-ordinates. Because of the particular shape of ω_1 and ω_2, the integral (22) then reduces to

$$8\alpha \sin \alpha \int_0^\infty \xi^2 \theta(\xi, m_1)\, d\xi\,, \tag{23}$$

where α stands for the arc of 30′.

Obviously, in order to prove the convergence of (23), it is sufficient to show that the integral of the same function taken from unity to infinity is convergent. Referring to (14), we see that, for $1 \leqq \xi$,

$$\theta(\xi, m_1) < \frac{1}{\sqrt{2\pi}} \int_{-\infty}^{a-b\xi} e^{-t^2/2} dt\,, \tag{24}$$

where a and $b > 0$ are numbers obtainable from (14). It follows that

$$\begin{aligned} \int_1^\infty \xi^2 \theta(\xi, m_1)\, d\xi &< \frac{1}{\sqrt{2\pi}} \int_1^\infty \left(\xi^2 \int_{-\infty}^{a-b\xi} e^{-t^2/2} dt \right) d\xi \\ &= \frac{1}{\sqrt{2\pi}} \left[\frac{\xi^3}{3} \int_{-\infty}^{a-b\xi} e^{-t^2/2} dt \,\Big|_{\xi=1}^{\xi=\infty} + \frac{b}{3} \int_1^\infty \xi^3 e^{-(a-b\xi)^2/2} d\xi \right], \end{aligned} \tag{25}$$

which is obviously convergent.

This completes the proof that the integral in (16) is convergent for all values of the arguments $0 \leqq t_1, t_2 \leqq 1$. Furthermore, for $t_1 = t_2 = 1$, this integral vanishes, which implies $P\{N_i = \infty\} = 0$, in accordance with the observed facts. By a similar method it is easy to show that the existence of the moment of ν of $(n+1)$st order [that is, the existence of the $(n+1)$st derivative of $G_\nu(t)$ at $t = 1$] implies the existence of the expectations $E(N_1^r N_2^s)$ for $r + s \leqq n$.

In order to obtain formulae for estimating the three parameters $\lambda\nu_1$, σ, and c involved in the present specialized model, formula (16) is used to obtain the expressions for the moments of the two variables N_1 and N_2 corresponding to counts in squares k degrees apart. Combining formulae (49) and (53) with (48) of Paper I and using the secondary postulates of the present paper, we obtain the following expressions for the expectations:

$$\bar{N} = E(N_1) = E(N_2) = \lambda \nu_1 R_{10} , \tag{26}$$

$$\sigma_{20} = E(N_1 - \bar{N})^2 = \bar{N} + \lambda(\nu_2 - \nu_1) R_{20} = \bar{N} + \lambda \nu_1 (c-1) R_{20} , \tag{27}$$

$$\sigma_{11}(k) = E[(N_1 - \bar{N})(N_2 - \bar{N})] = \lambda(\nu_2 - \nu_1) R_{11}(k) = \lambda \nu_1 (c-1) R_{11}(k) , \tag{28}$$

where $c = \nu_2 / \nu_1$ and, generally,

$$R_{mn}(k) = \iiint\limits_{-\infty}^{+\infty} p_1^m p_2^n du\, dv\, dw . \tag{29}$$

With reference to (20) it is easy to see that (29) is convergent. Formulae (27) and (28) yield

$$\frac{\sigma_{11}(k)}{\sigma_{20} - \bar{N}} = \frac{R_{11}(k)}{R_{20}} = Q_k \qquad \text{(say)} . \tag{30}$$

The numerator on the left-hand side represents the covariance of the numbers N_1 and N_2, and the denominator is the difference between their common variance and their expectation. The whole fraction on the left can be estimated from the empirical data. As to the middle term, perusal of formulae (17) and (29) indicates that, if one takes for granted not only the general form of the function $\theta(\xi, m_1)$ but also the two constants involved, then Q_k depends only upon the value of σ.

Thus, if one substitutes in the expression for Q_k trial values of σ and performs the computations, then the comparison between the numbers so obtained with those calculated from the data may be used to select or to interpolate an estimate of σ. Once such an estimate of σ is obtained, it can be substituted into the expressions for R_{10} and R_{20}, and thereupon the estimates of c and of the product $\lambda\nu_1$ are given by

$$c = 1 + \frac{\sigma_{20} - \bar{N}}{\bar{N}} \frac{R_{10}}{R_{20}} \tag{31}$$

and

$$\lambda \nu_1 = \frac{\bar{N}}{R_{10}} , \tag{32}$$

easily obtained from formulae (26)–(28). The main difficulty of the problem of estimation consists in computing R_{20} and $R_{11}(k)$ for several trial values of σ. In order to do so, it is necessary to develop formula (29) in full detail.

Denote generally by 2α the dimensions in radians of the squares in which the numbers N_1 and N_2 of "visible galaxies" are to be established. In the data of the Lick Observatory α is the arc of 30′. Further, denote by 2β the distance in radians between the centers of the two squares to which the numbers N_1 and N_2 refer. Thus, if we compare adjoining 1° × 1° squares, then β is the arc of 30′. In particular, if we take $\beta = 0$, then the two squares coincide.

Now consider the two integrals (17) and change from rectangular to polar co-ordinates ξ_i, φ_i, and ψ_i, with $i = 1, 2$. Then the integrals p_1 and p_2 can be written in the form

$$p_1 = \int_{-\alpha}^{+\alpha} \cos \varphi_1 d\varphi_1 \int_{-\beta-\alpha}^{-\beta+\alpha} d\psi_1 \int_0^{\infty} \xi_1^2 f(\eta_1 \mid \sigma)\, \theta(\xi_1, m_1)\, d\xi_1 , \tag{33}$$

$$p_2 = \int_{-\alpha}^{+\alpha} \cos \varphi_2 d\varphi_2 \int_{\beta-\alpha}^{\beta+\alpha} d\psi_2 \int_0^{\infty} \xi_2^2 f(\eta_2 \mid \sigma)\, \theta(\xi_2, m_1)\, d\xi_2 . \tag{34}$$

We shall use the symbol $R(\beta)$ to denote the integral

$$R(\beta) = \iiint_{-\infty}^{+\infty} p_1 p_2 \, du \, dv \, dw \, . \tag{35}$$

It is obvious that $R(0)$ coincides with R_{20}. Further, if $R_{11}(k)$ denotes the integral of the form (29) referring to two squares of angular dimensions $2a \times 2a$, which are k degrees apart, then, ascribing to β the value of the arc of $k/2$ degrees, we shall obtain $R(\beta) = R_{11}(k)$ for $k = 2\beta$. Thus the evaluation of (35) will lead to the evaluation of both R_{20} and $R_{11}(k)$. Unfortunately, the authors were not able to reduce $R(\beta)$ to an easily computable expression, and their results are limited to the following. Treating (35), with p_1 and p_2 given by (33) and (34), as a ninefold integral, changing the origin of measuring ψ_1 and ψ_2, and changing the order of integration, we have

$$R(\beta) = \int_{-a}^{+a} \cos \varphi_1 d\varphi_1 \int_{-a}^{+a} d\psi_1 \int_{-a}^{+a} \cos \varphi_2 d\varphi_2 \int_{-a}^{+a} J(\varphi_1, \psi_1, \varphi_2, \psi_2, \beta) \, d\psi_2 \, , \tag{36}$$

where

$$J(\varphi_1, \psi_1, \varphi_2, \psi_2, \beta) = \int_0^\infty \xi_1^2 \theta(\xi_1, m_1) \, d\xi_1 \int_0^\infty \xi_2^2 \theta(\xi_2, m_1) \, d\xi_2 \times \iiint_{-\infty}^{+\infty} f(\eta_1 \mid \sigma) \, f(\eta_2 \mid \sigma) \, du \, dv \, dw \, , \tag{37}$$

with

$$\eta_i^2 = (x_i - u)^2 + (y_i - v)^2 + (z_i - w)^2 \qquad \text{for} \qquad i = 1, 2 \, . \tag{38}$$

Referring to formula (4), the triple integral in the right-hand side of (37) can be written as

$$\left(\frac{1}{\sigma \sqrt{2\pi}} \right)^6 \iiint_{-\infty}^{+\infty} e^{-(\eta_1^2 + \eta_2^2)/2\sigma^2} du \, dv \, dw \, , \tag{39}$$

which has the value

$$\left(\frac{1}{\sigma \sqrt{2\pi}} \right)^3 e^{-(\xi_1^2 - 2A\xi_1\xi_2 + \xi_2^2)/4\sigma^2} \, , \tag{40}$$

with

$$A = \cos \varphi_1 \cos \varphi_2 \cos (2\beta - \psi_1 + \psi_2) + \sin \varphi_1 \sin \varphi_2 \, . \tag{41}$$

From now on, there is little that the authors accomplished toward the numerical evaluation of $R(\beta)$ other than by tedious numerical calculations. One method used consists in replacing the fourfold integral with respect to φ_1, ψ_1, φ_2, and ψ_2 by a sum of $5 \times 5 \times 5 \times 5 = 625$ terms, corresponding to a lattice of equidistant combinations of values of these variables. For each such combination the value of (37) was found by quadratures. Fortunately, not all the 625 points of the lattice lead to different values of A. Even so, however, the labor involved forced us to limit the computational program to a minimum. The alternative method used in computing $R(\beta)$ consists in replacing (40) by

$$\left(\frac{1}{\sigma \sqrt{2\pi}} \right)^3 e^{-(\xi_1^2 + \xi_2^2)/4\sigma^2} \sum_{n=0}^{\infty} \frac{(A/2)^n}{n!} \frac{\xi_1^n \xi_2^n}{\sigma^{2n}} \tag{42}$$

and putting $R(\beta)$ into the form of a series,

$$R(\beta) = \left(\frac{\sigma}{2\sqrt{\pi}} \right)^3 \sum_{n=0}^{\infty} \frac{B_n(\beta)}{2^n n!} K_n^2(\sigma) \, , \tag{43}$$

with

$$B_n(\beta) = \int_{-a}^{+a}\int_{-a}^{+a}\int_{-a}^{+a}\int_{-a}^{+a} A^n \cos\varphi_1 \cos\varphi_2 d\varphi_1 d\varphi_2 \tag{44}$$

and

$$K_n(\sigma) = \int_0^{\infty} t^{n+2}\theta(\sigma t, m_1)\, e^{-t^2/4}dt . \tag{45}$$

The advantage of (43) is that it is possible to compute the integrals $B_n(\beta)$ for all the contemplated values of the argument (for high values of n, numerical integration was used) and then to use them for all values of σ for which the values of (45) are available. The disadvantage of (43) is that the series in the right-hand side converges extremely slowly. Formula (43) was used throughout the computational program. Some of the numbers obtained were computed independently, using (36), and then checked.

As already mentioned, either method of computation is laborious to the extreme. Luckily, when the values of $R(\beta)$ were plotted against σ on a log-log scale, they formed smooth curves with features changing gradually from one system of values of β, $m_1 - M_0$, and σ_M to another. This circumstance was used to reduce the computations somewhat and to obtain a number of values of $R(\beta)$ by interpolation.

V. NUMERICAL RESULTS

The present study is based on the data selected from the set accumulated at the Lick Observatory so as to avoid, as far as possible, the interference of interstellar clouds. Actually, the data available refer to the area reproduced in Figure 5, and the area selected is that west of right ascension 16^h. It will be convenient to describe the total area reproduced in Figure 5 as the total *available area* and its section covered by the first investigation as the total *area used*.

Figure 5, prepared by one of the present authors for another publication,[11] gives contours of equal density of galaxies counted. It will be seen that the density generally decreases toward the lower left corner of the available area, that is, toward the galactic equator. In addition to this regular decrease, which might be ascribed to extinction caused by a uniform layer of absorbing matter, there are apparent patchy areas of low density of galaxies, one of which makes a substantial inroad into the lower left corner of the area used. Although there is no direct evidence, the authors are inclined to think that this particular decrease in the density of visible galaxies might be due to the effects of interstellar clouds rather than to gaps in the spatial distribution of clusters. The appendix gives a theory which, it is hoped, is adequate to provide corrections for a uniform layer of absorbing material within the local galaxy. However, no attempt was made to account for the extinction of light by irregular galactic clouds of random distribution.

For the above reasons, the authors decided to base the estimates of the three parameters involved in the model of the distribution of galaxies not on the whole *area used* but rather on its roughly rectangular part, described as the upper right *quadrant*, which is close to the galactic pole and is presumed to be less affected by galactic clouds than the other sections of the area available.

Actually, the area used was divided into four symmetrically placed, slightly overlapping, subareas that we describe as "quadrants," and all the computations were performed separately for each of them. The reason for this multiple computation of the same estimates was that the authors hoped to obtain an indirect confirmation of the hypothesis that the quasi-correlations computed for the upper right quadrant reflect the phenomena developing outside rather than inside of the local galaxy. Of the four quadrants studied,

---

[11] C. D. Shane and C. A. Wirtanen, in preparation.

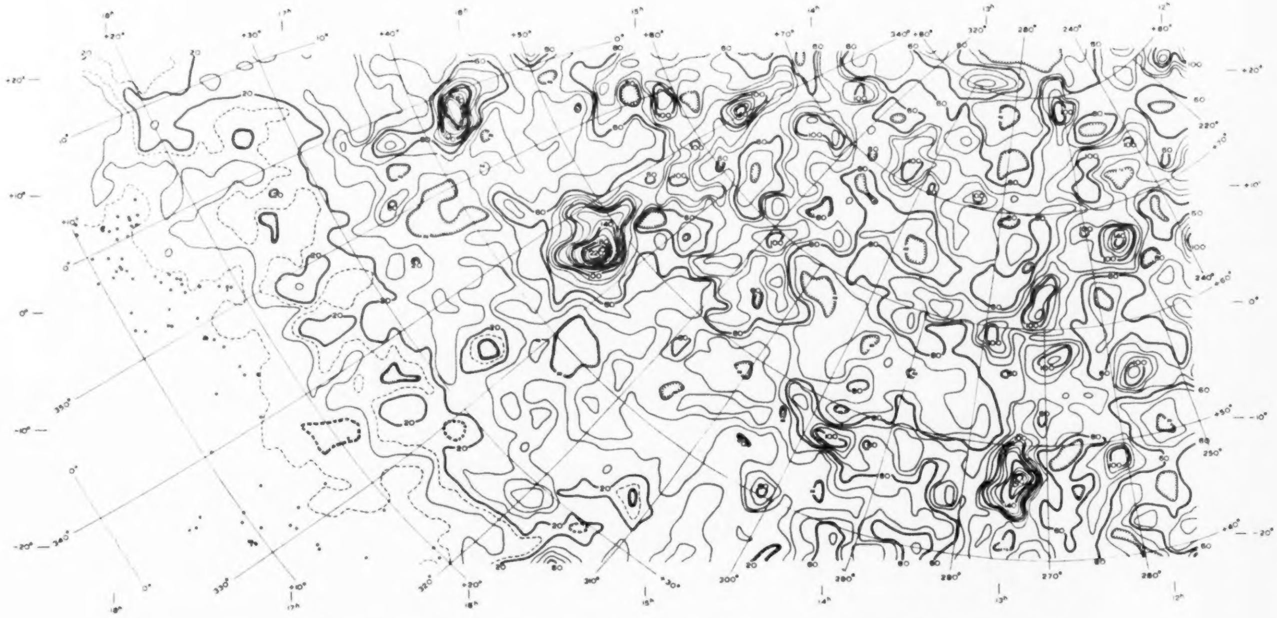
18h
17h
16h
15h
14h
13h
12h
+20°
+10°
0°
-10°
-20°
20
60
80
100

FIG. 5.—Total area available. Contour map, showing smoothed numbers of galaxies per square degree

the least reliable seems to be the one on the lower left; there appears to be not much difference between the upper left and the lower right quadrants.[12]

For these reasons it was expected that the sequences of the quasi-correlations computed for the lower right and the upper left quadrant should come out either in agreement with that corresponding to the upper right quadrant or be intermediate between the latter and the sequence corresponding to the lower left quadrant. Should there be agreement between the quasi-correlations for the upper right quadrant and those corresponding to at least one of the quadrants, either the upper left or the lower right, then this agreement would suggest to the authors that the approximately coinciding values of serial quasi-correlations can probably be considered as more or less independent measurements of the same phenomenon of clustering of galaxies in space.

The overlaps between the four quadrants were introduced in order to increase the number of observations on which each correlation or quasi-correlation is based. Referring to Section II of the appendix, it must be clear that, essentially, the numerator of the quasi-correlation Q_k depends on the average of products $X'X''$, where X' stands for the actual count of galaxies in any particular square within the area for which the computations are made, and X'' for the count in a square exactly k degrees away from the first. In order to satisfy this condition, the second square must be either in the same row or in the same column as the first. Thus the products $X'X''$ can be divided into two categories, those where both squares are in the same row of the area ("row products") and those where both squares are in the same column ("column products").

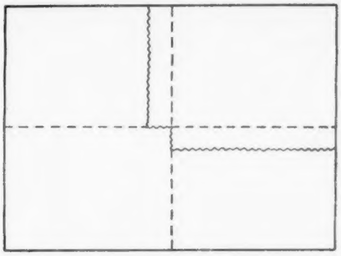

FIG. 6.—Schematic diagram of *area used*, four *quarters*, and the upper right *quadrant*

The overlaps of the upper right quadrant over the upper left and the lower right quarters of the area used are illustrated in Figure 6. The rectangle, divided vertically and horizontally into four "quarters," represents the area used. These "quarters" are not to be confused with the "quadrants." The upper right quadrant is the area bounded by the wavy line. It contains the whole upper right quarter and, in addition, two rectangular strips overlapping the upper left and the lower right quarters, respectively. The width of these strips is 6°.

The strip overlapping the upper left quarter was used when computing the "row products" $X'X''$. In fact, for each value of k, the sum of the "row products" was computed for the rectangle representing the upper right quarter combined with the 6° strip overlapping the upper left quarter of the area used. Similarly, the strip overlapping the lower right quarter appeared in computations of the "column products," which were obtained for the rectangle composed of the upper right quarter with the 6° strip overlapping the lower right quarter.

The delimitations and computations relating to the other three quadrants were analogous.

---

[12] However, some of the present authors have a slight a priori preference for the lower right quadrant as compared with the upper left quadrant.

Figure 7 gives the observed serial quasi-correlations, computed separately for each of the four quadrants and then for the entire area used. The figure is divided into ten separate graphs. The graphs on the left give curves computed without attempting to correct for the extinction by a uniform sheet of matter within the local galaxy. The graphs on the right were obtained by the method described in the appendix, allowing for general galactic extinction. In each graph there are three sequences of points, connected by straight lines. One sequence gives the quasi-correlations computed without attempting to correct for the errors of counting. The other two incorporate the corrections based on either error model 1 or error model 2 developed in the appendix.

The quasi-correlations uncorrected for uniform galactic absorption were computed for $k = 1, 2, \ldots, 23$, but they are shown on the graphs for $k \leq 10$ only. The reason for this omission is that for the four quadrants the quasi-correlations computed for larger values of k do not exhibit such regularity as shown in Figure 7, but vary chaotically about zero. This behavior may be due to the fact that, with increasing k, the number of observations on which a quasi-correlation is based is correspondingly decreased. All this applies to particular quadrants. On the other hand, the quasi-correlations relating to the total area

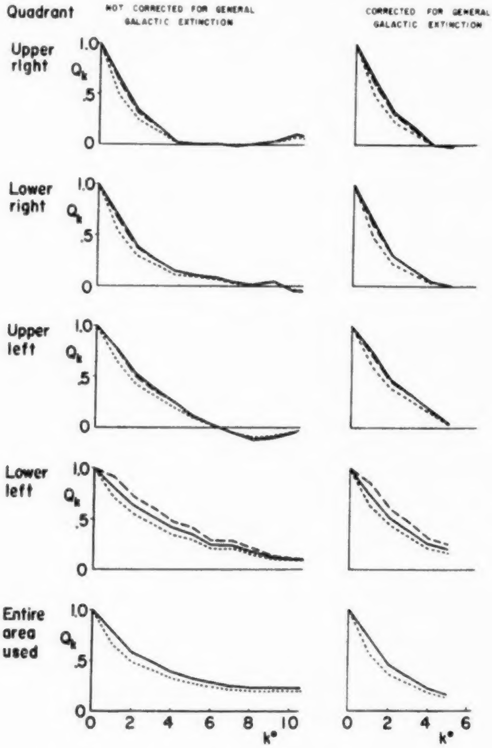

FIG. 7.—Empirical serial quasi-correlations plotted against k, the distance between 1° × 1° squares. *Dotted lines:* not corrected for errors in counting; *dashed lines:* corrected according to error model 1; *solid lines:* corrected according to error model 2. *Left column:* Not corrected for effects of general galactic extinction. *Right column:* Corrected for general galactic extinction.

continue to vary smoothly, reaching 0.063 at $k = 20$ and 0.008 at $k = 23$, and they show a plateau, as indicated in Figure 7.

Upon examining the formulae for the theoretical value of the quasi-correlation Q_k between the idealized counts N_1 and N_2, it is easy to see that Q_k is always positive and decreases with increasing k. Since the corrected quasi-correlations computed for the upper right quadrant reach zero before $k = 5$ and since the corrections for uniform galactic extinction are very laborious, the graphs in the right half of Figure 7 extend only to $k = 5$.

As might be expected, the correction for uniform galactic extinction invariably decreases the quasi-correlation, and its effect is the more marked, the closer the area concerned is to the galactic equator. The correction for errors of counting always increases the quasi-correlation. It is interesting that, with the exception of the lower left quadrant, the computations according to the two widely different error models lead to practically the same results. The reason for the substantial divergence of the results relating to the lower left quadrant is not clearly understood.

Turning the attention to the right-hand side of Figure 7, particularly to the graphs corresponding to error model 2, the authors were gratified to find that the quasi-correlations corresponding to the two right quadrants practically coincide. This coincidence, then, suggests to the authors not only that the two sets of figures represent (practically independent) measurements of the same phenomenon but also that these measurements are reasonably precise.

As expected, the quasi-correlations relating to the lower left quadrant are substantially higher than those corresponding to the two right quadrants, and the quasi-correlations of the upper left quadrant are intermediate. This increase in the quasi-correlations relating to the left-hand quadrants is due to some cause affecting, simultaneously and in the same direction, the counts of galaxies in both members of each pair of the 1° × 1° squares, this cause being additional to those operating in the two right-hand quadrants.

The authors believe that the correlations observed in the two right-hand quadrants are almost entirely due to clusters. For this reason they believe that only a very negligible proportion of these clusters have angular dimensions exceeding 4°. On the other hand, the increase in quasi-correlations in the left-hand quadrants is probably due to galactic clouds, with diameters occasionally much greater than 5°.

Numerical values of the quasi-correlations corrected for uniform galactic absorption and for errors in counting according to error model 2 are given in Table 1.

After this discussion of the purely empirical section of the results obtained, we proceed to the collation of these results with the theory, leading to the estimates of the three parameters involved in the model.

As already mentioned, when the two constants in the function $\theta(\xi, m_1)$ are fixed, the theoretical value of Q_k depends on the parameter σ only. Since the constants in $\theta(\xi, m_1)$ are somewhat uncertain, the computations were performed for twelve tentative combinations of values $\sigma_M = 0.00$, 0.85, 1.25, and 2.00 mag., with $m_1 - M_0 = 31.5$, 32.5, and 33.5 mag. For every such combination, the theoretical values of Q_k were computed with five trial values of $\sigma = 2 \times 10^5$, 4×10^5, 10^6, 2×10^6 and 10^7 parsecs. Next, these quasi-correlations were plotted against k on graphs exhibiting at once five curves, each corresponding to a separate value of σ. These theoretical curves were then compared with the empirical quasi-correlations, computed for the upper right quadrant, with corrections for the general galactic extinction and for the errors of counting, according to error model 2. Figure 8 represents a sample of such graphs, that corresponding to $\sigma_M = 0.85$ and $m_1 - M_0 = 32.5$. Open circles mark theoretical points actually computed. Filled circles indicate the empirical quasi-correlations. Each curve is marked by a number representing the tentative value of σ in units of 10^5 parsecs.

A glance at Figure 8 is sufficient to disqualify four of the five curves as possible theoretical counterparts of the empirical quasi-correlations. On the other hand, the second curve from the bottom, corresponding to the tentative value $\sigma = 4 \times 10^5$ parsecs, appears to be a reasonable possibility. Figures 9*a* and 9*b* give graphs, similar to that in Figure 8, corresponding to all the twelve systems of tentative combinations of values of $m_1 - M_0$ and σ_M. However, for the sake of clarity, the graphs of Figures 9*a* and 9*b* give only three theoretical curves each. Two of these curves (*dashed*) correspond to the original tentative values of σ and are selected to bracket the empirical points. The middle curve (*solid*) corresponds to a value of σ interpolated to give the best visual fit to the empirical points. The values of σ (in units of 10^5 parsecs) to which the curves correspond are indicated on the graphs. Also, to each tentative value of σ of the original set there corresponds a fixed style in drawing the curves, so that all the curves corresponding, for example, to $\sigma = 4 \times 10^5$ are drawn by means of the same system of dashes.

Following the curves corresponding to the same σ from one graph to another, we see that the quasi-correlations depend substantially on both $m_1 - M_0$ and σ_M, and decrease as either of the two arguments is increased.

As far as the agreement with the empirical quasi-correlation is concerned, it will be seen that, for each of the twelve systems of tentative values of $m_1 - M_0$ and σ_M, it was possible to find a value of σ, to be described as the estimate of σ, with which the theoretical curve fits the empirical points very reasonably. It is only while examining the particular graphs in turn that one observes that even the "best fitting" curve has some

TABLE 1

EMPIRICAL SERIAL QUASI-CORRELATIONS CORRECTED FOR UNIFORM GALACTIC EXTINCTION AND ERRORS IN COUNTING (MODEL 2)

k	QUADRANT				ENTIRE AREA USED
	Upper Right	Lower Right	Upper Left	Lower Left	
0°	+1.000	1.000	1.000	1.000	1.000
1	+0.637	0.635	0.753	0.744	0.724
2	+0.316	0.293	0.469	0.524	0.461
3	+0.166	0.163	0.321	0.387	0.343
4	−0.006	0.038	0.175	0.254	0.225
5	−0.018	0.003	0.034	0.200	0.161

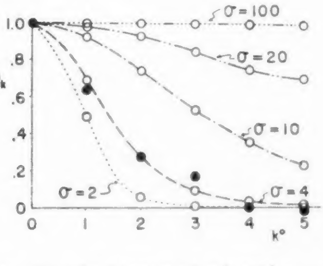

FIG. 8.—Process of estimating σ for a fixed system of values of $m_1 - M_0$ and σ_M. Filled circles show values of empirical quasi-correlations for upper right quadrant; open circles show theoretical quasi-correlations computed by assuming $m_1 - M_0 = 32.5$, $\sigma_M = 0.85$ mag., and five particular tentative values of σ indicated in the figure in units of 10^5 parsecs.

characteristics different from the sequence of points computed from observations. Since the precision of the empirical points is unknown, except that they agree with those of the lower right quadrant (although, as k increases, the number of square degrees used decreases), it is a matter of opinion which of the twelve systems of tentative values of $m_1 - M_0$ and σ_M yields the best of the "best fitting" curves of serial quasi-correlations.

Nevertheless, the authors feel that the curves corresponding to $\sigma_M = 0.85$ and particularly those corresponding to $\sigma_M = 0$ are too steep to fit the data as well as the curves corresponding to higher values of σ_M. As to the final choice, the authors are substantially more hesitant and fluctuate between

$$m_1 - M_0 = 31.5\ , \qquad \sigma_M = 1.25 \qquad \text{with} \qquad \sigma = 3.7 \times 10^5 \text{ parsecs}$$

and

$$m_1 - M_0 = 33.5\ , \qquad \sigma_M = 1.25 \qquad \text{with} \qquad \sigma = 7.5 \times 10^5 \text{ parsecs}\ .$$

Curiously, the serial quasi-correlations corresponding to $m_1 - M_0 = 32.5$ with $\sigma_M = 1.25$ do not seem to fit so well. It is hoped that similar analyses of other sets of data will lead to a more precise discrimination among all the possibilities contemplated.

The choice of the best fitting sequence of theoretical quasi-correlations consists, in effect, in estimating not only σ but also, simultaneously, the two parameters $m_1 - M_0$ and σ_M. In this connection it should be mentioned that, while the estimates of both $m_1 - M_0$ and σ_M are poorly determined, that of $m_1 - M_0$ appears more shaky than that of σ_M.

Once the estimate of σ is obtained for any given system of tentative values of $m_1 - M_0$ and σ_M, formula (31) gives the corresponding estimate of c, which is the ratio ν_2/ν_1 of the moments of ν. Table 2 gives the estimates of σ and c so obtained. In addition, the same table gives the estimates of the product $\lambda\nu_1$, which is the average number of galaxies per cubic parsec according to formula (32). Referring to formula (60) in Paper I, it will be recalled that the estimate of $\lambda\nu_1$ depends on $m_1 - M_0$ and on σ_M but not on σ or c.

Figure 10 was drawn to show the dependence of the estimates of σ and of c on $m_1 - M_0$ and on σ_M. It is emphasized that all these estimates are based on the same data, those relating to the upper right quadrant corrected for the effects of general galactic extinction and of errors in counting. It is seen that the dependence is very substantial. The conclusion is that, perhaps a little unexpectedly, in studies of the spatial distribution of galaxies precise estimates of $m_1 - M_0$ and of σ_M are quite important.

Another purpose of Figure 10 is to draw attention to the lack of precision in the estimates of σ and c, indicated above. The authors believe that for every combination of tentative values of $m_1 - M_0$ and σ_M the estimate of the best-fitting σ is good to one and one-half significant figures. However, this precision is only apparent and is ruined by the lack of precise information on $m_1 - M_0$ and σ_M. In fact, even after ruling out $\sigma_M = 0.00$ and $\sigma_M = 0.85$, there remains a very broad range of possible values of σ_M, say between 1.00 and 2.00 mag., which, combined with the range $31.5 \leqq m_1 - M_0 \leqq 33.5$(perhaps beyond), determines what appears to be a tremendous region of possible values of σ and c, as indicated in Figure 10.

One may presume that the estimates of σ and c depend not only on the values of $m_1 - M_0$ and σ_M but, more generally, on the assumptions regarding the probability density of absolute magnitude. Thus, if we abandon the assumption that the absolute magnitude is normally distributed, then the estimates of σ and c may be affected substantially. A similar remark applies to the assumptions regarding the red shift.

The reader will notice that, although serial correlations between the counts of galaxies are mentioned occasionally in this paper, their numerical values are not given. The reason is that the serial *correlations*, say, ρ_k, are simply proportional to the serial *quasi-correlations* Q_k, so that

$$\rho_k = Q_k \frac{\sigma_{20} - N}{\sigma_{20}} = Q_k F \qquad \text{(say)} \tag{46}$$

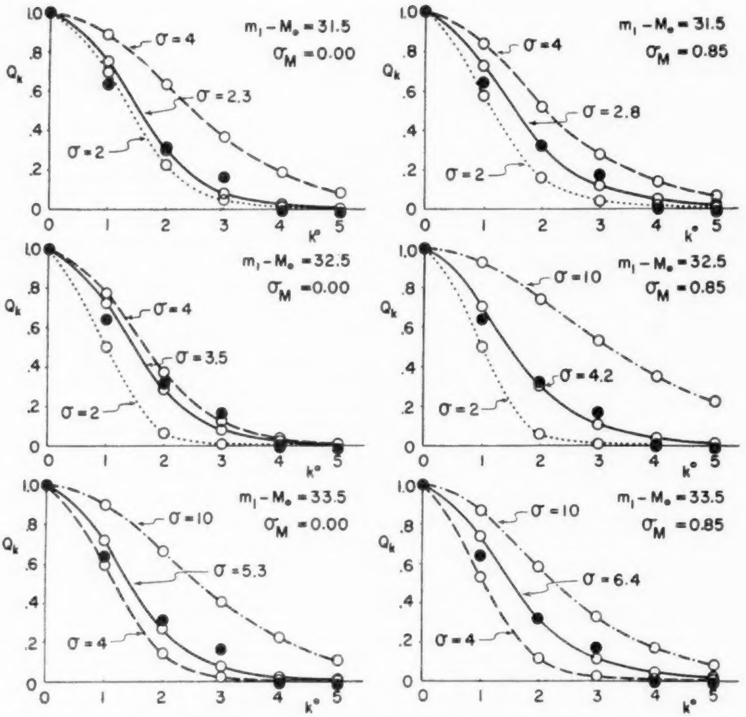

FIG. 9a.—Search for the best-fitting combination of values of the three parameters $m_1 - M_0$, σ_M, and σ. Filled circles show empirical quasi-correlations for the upper right quadrant. All open circles show theoretical serial quasi-correlations computed by assuming specified values of $m_1 - M_0$, σ_M, and σ. Open circles connected by solid lines correspond to the best-fitting value of σ; those connected by dashed lines correspond to the two "bracketing" values of σ from the original set. Each row of graphs corresponds to a fixed value of $m_1 - M_0$, left column corresponds to $\sigma_M = 0.00$, right column to $\sigma_M = 0.85$ mag.

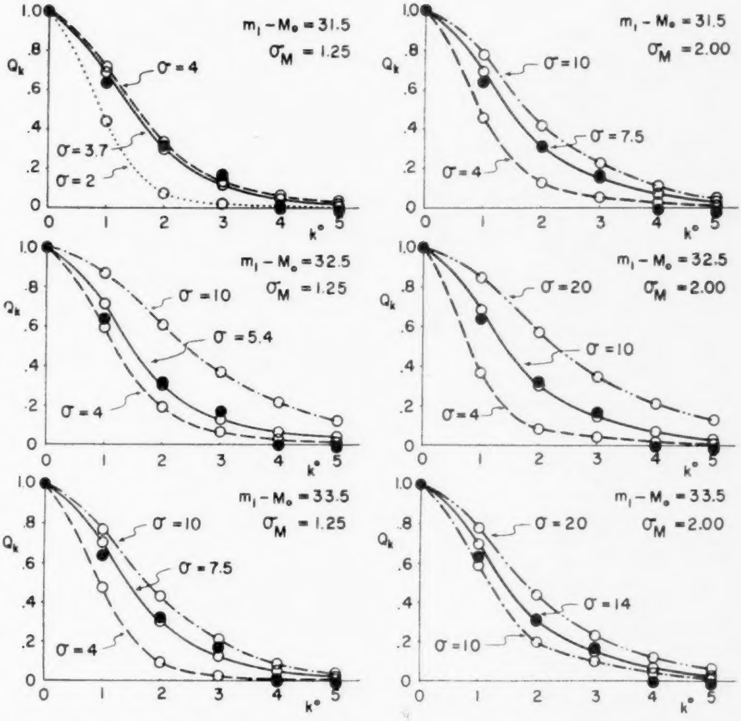

FIG. 9*b*.—Search for the best-fitting combination of values of the three parameters $m_1 - M_0$, σ_M, and σ. Filled circles show empirical quasi-correlations for the upper right quadrant. All open circles show theoretical quasi-correlations computed by assuming specified values of $m_1 - M_0$, σ_M, and σ. Open circles connected by solid lines correspond to the best-fitting value of σ, those connected by dashed lines correspond to the two "bracketing" values of σ from the original set. Each row of graphs corresponds to a fitted value of $m_1 - M_0$, left column corresponds to $\sigma_M = 1.25$, right column to $\sigma_M = 2.00$ mag.

with a constant factor of proportionality $F = 0.847$ for this study. One might perhaps think that, since the value of the correlation depends not only on σ but also on the distribution of cluster centers and on the distribution of the number of galaxies per cluster, while the quasi-correlation depends only on σ, a comparison between the empirical and the theoretical serial correlations would provide some sort of test of the theory. Regretfully, this presumption is wrong. The reason is that, since c is obtained from the same data as the quasi-correlations, the theoretical value of the factor F coincides with its empirical value. Thus a comparison of the empirical serial correlation, say ρ_k^*, with the the-

TABLE 2

ESTIMATES OF σ, OF c, AND OF $\lambda\nu_1$ CORRESPONDING TO VARIOUS ASSUMPTIONS REGARDING σ_M AND $m_1 - M_0$

σ_M (Mag.)	$m_1 - M_0$ (Mag.)	$\sigma \times 10^{-5}$ Parsecs	c	$\lambda\nu_1 \times 10^{18}$ (Gal/Psc^3)
0.00	31.5	2.3	66	120.7
	32.5	3.5	66	32.7
	33.5	5.3	65	9.2
0.85	31.5	2.8	162	65.9
	32.5	4.2	159	18.5
	33.5	6.4	147	5.7
1.25	31.5	3.7	288	34.2
	32.5	5.4	246	10.1
	33.5	7.5	195	3.2
2.00	31.5	7.5	687	7.1
	32.5	10.0	584	2.5
	33.5	14.0	499	0.9

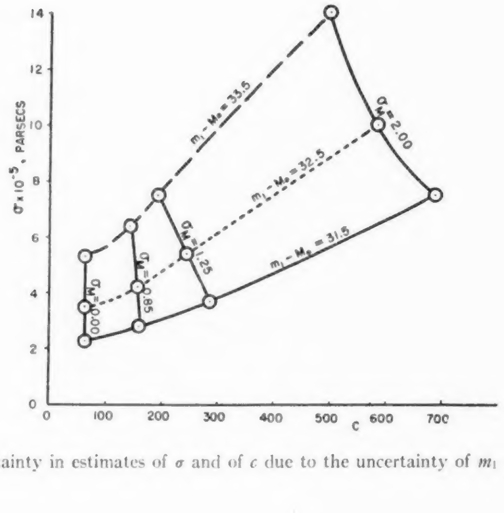

FIG. 10.—Uncertainty in estimates of σ and of c due to the uncertainty of $m_1 - M_0$ and of σ_M

oretical ρ_k would amount to a comparison of the product Q_k^*F with the product Q_kF and, consequently, would lead to no conclusions other than those obtainable from the foregoing comparisons of Q_k^* and Q_k.

VI. CONCLUDING REMARKS

The main results obtained are summarized in the upper right part of Figure 7, in Figures 9*a* and 9*b*, and in Table 2.

The very near coincidence of the empirical quasi-correlations obtained for the two right quadrants of the Lick Observatory data suggests that these quasi-correlations represent (practically independent) measurements of phenomena outside the local galaxy. However, it is not impossible that the same calculations, applied to data referring to another area of the sky, equally close to the galactic pole, will contradict this conclusion.

Figures 9*a* and 9*b* show that the quasi-correlations computed from the data of the upper right quadrant are consistent with the model of the spatial distribution of galaxies developed in Paper I. In particular, they are also consistent with the secondary postulates of the present paper on which they depend, namely, Postulate S2 that the internal structure of clusters is governed by the symmetric normal probability density (4) and Postulate S4 that the probability that a galaxy at distance ξ will be "visible" is $\theta(\xi, m_1)$, as given by formula (14). While noting this consistency, the authors wish to emphasize that it applies solely to one particular characteristic of the spatial distribution of galaxies, namely, to the serial quasi-correlations computed from the data now available at the Lick Observatory. It is quite possible that other studies of, for example, the quasi-correlations between counts made to two different limiting magnitudes will reveal the inadequacy of the model.

Proceeding on the tentative assumption of the general validity of the theory studied, we obtain the estimates of the three adjustable parameters $\lambda\nu_1$, σ, and $c = \nu_2/\nu_1$, as given in Table 2. It is noted that these estimates depend strongly on the presumed values of $m_1 - M_0$ and σ_M. The general shape of the curves representing the theoretical quasi-correlations also depends on these quantities. The comparisons exhibited in Figures 9*a* and 9*b* seem to indicate that probably the correct value of the dispersion σ_M exceeds 0.85 mag. The authors' very tentative final choice is $m_1 - M_0 = 31.5$ and $\sigma_M = 1.25$ mag. Referring to Table 2, we find that the tentative best estimates of the parameters involved in the present model are

$$\lambda\nu_1 = 3.42 \times 10^{-17} \text{ galaxies per cubic parsec} \tag{47}$$

$$\sigma = 3.7 \times 10^5 \text{ parsecs ,} \tag{48}$$

$$c = \frac{\nu_2}{\nu_1} = 288 \, . \tag{49}$$

The adoption of any particular value of $m_1 - M_0$ combined with a hypothesis regarding either m_1 or M_0 determines the value of the other parameter, M_0 or m_1, respectively. Thus, for example, if we adopt $m_1 - M_0 = 31.5$ and act on the presumption that the limiting apparent magnitude of the Lick Observatory counts is $m_1 = 18.3$ (or 18.6), then this would imply $M_0 = -13.2$ (or -12.9) mag., which is similar to the values suggested in the recent literature. On the other hand, if we adopt Hubble's estimate of $M_0 = -14.2$, then, with the same value of $m_1 - M_0 = 31.5$, the limiting magnitude of the Lick Observatory counts would be 17.3 mag., which seems too bright. In interpreting these figures, we must remember that $m_1 - M_0 = 31.5$ is not well determined, since 32.5 and 33.5 give almost as good a fit to the serial quasi-correlations.

In this connection we should recall that the theoretical quasi-correlations depend on the function $f(\eta | \sigma)$ selected to represent the probability density $f(\eta)$ of the co-ordinate of a galaxy within a cluster. As already mentioned, there is no certainty that the present selection is satisfactory. It is possible, therefore, that a revision of the interpolation formula used to approximate $f(\eta)$ would lead to a change in the estimate of $m_1 - M_0$.

It is most regrettable that the present study yields so little about the distribution of the number ν of galaxies per cluster. In order to obtain some specific information on how ν varies from cluster to cluster, it is necessary to calculate theoretical and empirical moments and product moments of the third order at least, the complexity of which is beyond the present computational means at the disposal of the authors and is likely to require the use of electronic computers.

All that the present work can yield is a pair of inequalities that we may supplement by some speculations. The inequalities in question result from equation (10), which is valid for any distribution of ν, since it follows from the definition of $c = \nu_2/\nu_1$. This equation gives the variance

$$\sigma_\nu^2 = \nu_1 (c - \nu_1) > 0 \tag{50}$$

of the number ν of galaxies per cluster in terms of its mean number ν_1 and of the quotient $c = \nu_2/\nu_1$, for which we have the estimated value $c = 288$. Formula (50) implies that the mean value ν_1 cannot be greater (and from general considerations must be smaller) than c. In other words, using the estimate of c obtained in this paper, we have to assume that the average number of galaxies per cluster is less, probably substantially less, than 288.

A further consequence of equation (50) is that the maximum value of σ_ν^2 is attained when $\nu_1 = c/2$. Thus, with the present estimate of c, the standard deviation of the number of galaxies per cluster is

$$\sigma_\nu \leqq \frac{c}{2} = 144 . \tag{51}$$

As discussed in Section II, the observed variability of the number of galaxies per cluster is much greater than that implied by the Poisson law, so that we can use the Poisson law to obtain a lower bound on σ_ν. If $\nu - 1$ followed the Poisson distribution, we would have

$$\nu_1 = \sigma_\nu^2 + 1 , \tag{52}$$

which, combined with (7), gives

$$\nu_1 = \sigma_\nu^2 + 1 = c - 1 = 287 . \tag{53}$$

In this way, the standard deviation σ_ν appears to be bounded on both sides:

$$\left[c - 2 \right]^{1/2} = \sqrt{286} = 16.9 < \sigma_\nu \leqq \frac{c}{2} = 144 . \tag{54}$$

The corresponding bounds on the mean number ν_1 are

$$1 \leqq \nu_1 < c - 1 = 287 , \tag{55}$$

which is not substantially shorter than the interval $1 \leqq \nu_1 < 288$ obtained from (50) alone.

Accordingly, using (47), the limits on λ, the average number of cluster centers per cubic parsec, are

$$\frac{\lambda \nu_1}{c - 1} = 1.19 \times 10^{-19} < \lambda \leqq \lambda \nu_1 = 342 \times 10^{-19} . \tag{56}$$

All these bounds are consequences of the estimate of c obtained and of the very probable assumption that the actual variability of ν is greater than that implied by the Poisson law.

It is now interesting to speculate a little and to obtain at least a qualitative check as to whether even the maximum variability of ν implied by the foregoing findings can account for the existence of a number of small clusters and, at the same time, of the several apparently giant clusters suggested by the equal density contours exhibited in Figure 5. It will be seen that within the area used (roughly 6 per cent of the sky) there are several large apparent concentrations of galaxies. At the present time there is no precise information as to the number of large clusters present in the area used or as to the distance of these clusters. However, it seems safe to presume that this area includes at least one and probably not more than five big clusters, of several hundred members each, which are at favorable distances so that they stand out from the general background. Just what the limits on the distance should be can be judged roughly from the fact that the Virgo cluster, 2 million parsecs away, is contained in the area used and yet it does not stand out from the background enough to be noticeable. On the other hand, the Coma cluster (just outside the area used), 14 million parsecs distant, is clearly visible on a contour diagram similar to Figure 5. Also, as determined by Mayall,[13] one of the conglomerations of galaxies clearly visible in the area used is 21 million parsecs distant. Taking all these figures into consideration, we assume that the lower limit on the distance of easily distinguished clusters is 4 millon parsecs. As to the upper limit, we shall assume alternatively 30 and 40 million parsecs.

We now supply answers to the following problems:

a) Assuming the maximum (or nearly maximum) variability of the number ν of galaxies per cluster consistent with the best-fitting estimates of the parameters obtained in this paper, determine the number of giant clusters—say, the number of those with more than 500 members—to be expected in an area equal to 6 per cent of the sky and with their distances (i) between 4 and 30 million parsecs and (ii) between 4 and 40 million parsecs.

b) On the same assumptions, estimate the probabilities that a cluster will have a very small number of galaxies, say, 1, 2, 3, 4, 5.

In accordance with the speculative character of the present discussion, we shall answer these questions on the assumption that the distribution of $\nu - 1$ is the negative binomial distribution as defined by formula (6) in Section II. As already mentioned, this distribution depends on two parameters α and β, and, as seen from (8) and (9), knowledge of the quotient c is insufficient to determine both. However, if the value of $c = 288$ is combined with the assumption that ν has the greatest possible variance σ_ν^2, then the negative binomial distribution is determined.

As already mentioned, the maximum value of σ_ν^2 is attained when $\nu_1 = c/2$. Thus, substituting $c = 288$ and $\nu_1 = 144$ in the first of formulae (9), we find that the maximum variability of ν is attained when $\alpha = 0.993$. Since this value is close to unity and since the computations with the negative binomial are greatly simplified when $\alpha = 1$, we shall base the following computations on $\alpha = 1$. The second formula in (9) then gives $\beta = 143.5$ and the probability generating function (6) reduces to

$$G_\nu(t) = \frac{t}{1 - \beta(t-1)} = \frac{1}{\beta+1} \sum_{n=1}^{\infty} t^n \left(\frac{\beta}{\beta+1}\right)^{n-1}, \tag{57}$$

so that, for $n = 1, 2, \ldots,$

$$P\{\nu = n\} = \frac{1}{\beta+1} \left(\frac{\beta}{\beta+1}\right)^{n-1}. \tag{58}$$

It is also easy to find that

$$P\{\nu > n\} = \left(\frac{\beta}{\beta+1}\right)^{n} \tag{59}$$

for $n = 0, 1, 2, \ldots.$

---

[13] C. D. Shane and C. A. Wirtanen, *Proc. Am. Phil. Soc.*, **94**, 17, 1950.

In order to provide an answer to problem *a* we start with (59) and substitute $\beta = 143.5$ and $n = 500$. The result is

$$P\{\nu > 500\} = 0.0311 \,. \tag{60}$$

Using the estimate of $\lambda = 2.38 \times 10^{-19}$ cluster centers per cubic parsec, we compute the expected number of cluster centers within the (i) 4—30 million-parsec shell and within the (ii) 4–40-million parsec shell in an area extending over 6 per cent of the sky. We find that the expected total number of cluster centers is 1611 and 3824, respectively. Multiplying these numbers by $P\{\nu > 500\}$, we find that the expected number of giant clusters is 50 and 119, respectively. Since there are between one and five giant clusters that may be identified within the area used, we conclude that the bounds on the variability of ν indicated in (54) are ample to account for the presence of these few giants. In fact, it is clear that, by reducing the variability of ν to a more moderate value rather than the extreme of largest possible variability, we can easily make the expected number of giant clusters in the area used agree with the observed number.

Turning now to problem *b*, we use formula (58) with $\beta = 143.5$ and $n = 1, 2, \ldots$. Easy arithmetic gives Table 3. It is seen that the hypothesis of a negative binomial distribution with (almost) the largest possible variation of ν implies an appreciable proportion of very small clusters. The final conclusion is, then, that the bounds on the variability of the number of galaxies per cluster are consistent with the general impressions suggested by a qualitative study of the distribution of galaxies.

TABLE 3

PROBABILITIES THAT A CLUSTER WILL CONTAIN EXACTLY n GALAXIES*

n	$P\{\nu=n\}$	n	$P\{\nu=n\}$
1	0.00692	4	0.00678
2	0.00687	5	0.00673
3	0.00682		

* The probabilities are computed on the assumptions that $m_1 - M_0 = 31.5$, $\sigma_M = 1.25$; that the variance σ_ν^2 of ν has the largest possible value compatible with the estimated value of $c = 288$; and that the actual distribution of $\nu - 1$ is negative binomial.

The foregoing tentative computations were performed using the best-fitting parameters for the distribution of absolute magnitude of galaxies. Since the distribution of absolute magnitude is poorly determined, the computations were performed for all the twelve tentative combinations of values of $m_1 - M_0$ and σ_M, combined with the corresponding best-fitting value of σ. The results are compiled in Tables 4 and 5 and in Figure 11.

Table 4 gives the bounds on σ_ν, ν_1, and λ corresponding to the different hypotheses regarding $m_1 - M_0$ and σ_M. Table 5 compiles the expected value $\mathrm{E}[\gamma(R) \mid \nu > 500]$ of the number of giant clusters within the total area used, distant from the observer alternatively between 4 and 30 and between 4 and 40 million parsecs, and corresponding to the greatest possible variability of ν. Finally, Figure 11 gives plots of the probabilities that the number ν of galaxies within a cluster will have any specified value n corresponding to the four different assumptions regarding σ_M and, again, corresponding to (almost) the largest possible variability of ν. Since the dependence on $m_1 - M_0$ is not marked, the curves are drawn for the intermediate case $m_1 - M_0 = 32.5$ only.

One particular detail of this material requires comment. Since it may be confidently estimated that the total area used contains at least one giant cluster, it appears plausible

TABLE 4

BOUNDS ON ν_1, σ_ν, AND λ CORRESPONDING TO TWELVE ALTERNATIVE HYPOTHESES REGARDING σ_M AND $m_1 - M_0$

σ_M (MAG.)	$m_1 - M_0$ (MAG.)	BOUNDS ON σ_ν (GAL/CLUSTER)		UPPER BOUND ON ν_1 (GAL/CLUSTER)	BOUNDS ON λ CLUSTERS/PSC^3	
		Lower	Upper		Lower $\times 10^{18}$	Upper $\times 10^{18}$
0.00......	31.5	8	33	65	1.85	121
	32.5	8	33	65	0.50	33
	33.5	8	33	64	0.14	9.2
0.85.......	31.5	13	81	161	0.41	66
	32.5	13	80	158	0.12	19
	33.5	12	74	146	0.039	5.7
1.25.......	31.5	17	144	287	0.12	34
	32.5	16	123	245	0.041	10
	33.5	14	98	194	0.016	3.2
2.00.......	31.5	26	344	686	0.010	7.1
	32.5	24	292	583	0.004	2.5
	33.5	22	250	498	0.002	0.9

TABLE 5

$E[\gamma(R) | \nu > 500]$ = EXPECTED NUMBER OF GIANT CLUSTERS ($\nu > 500$) IN AREA R OF 6% OF SKY, CORRESPONDING TO NEGATIVE BINOMIAL DISTRIBUTION OF $\nu - 1$ WITH LARGEST σ_ν

(Case i: Distant by 4–30 Million Parsecs;
Case ii: Distant by 4–40 Million Parsecs)

σ_M (MAG.)	$m_1 - M_0$ (MAG.)	$E[\gamma(R) \| \nu > 500]$	
		Case i	Case ii
0.00......	31.5	0.007	0.016
	32.5	0.002	0.004
	33.5	0.0004	0.0010
0.85......	31.5	11	27
	32.5	3	7
	33.5	0.6	1.4
1.25......	31.5	50	119
	32.5	10	23
	33.5	1.3	3
2.00......	31.5	32	77
	32.5	10	25
	33.5	3	8

that the computations based on the assumption of the *greatest possible variability* of ν should imply a value of $E[\gamma(R) \mid \nu > 500]$ substantially larger than a few units. If this be so, then the figures in Table 5 seem to rule out quite a few combinations of hypothetical values of $m_1 - M_0$ and σ_M, namely, all combinations with $\sigma_M = 0$, the combination $\sigma_M = 0.85$ with $m_1 - M_0 = 33.5$, and probably the combination $\sigma_M = 1.25$ with $m_1 - M_0 = 33.5$.

While the foregoing speculations appear suggestive, they are obviously deficient. In order to have an actual estimate of the distribution of ν (rather than the bounds on its variability) and to obtain an estimate of the parameter λ, we must await the time when it will be possible to perform the computations relating to formulae (55)–(59) of Paper I.

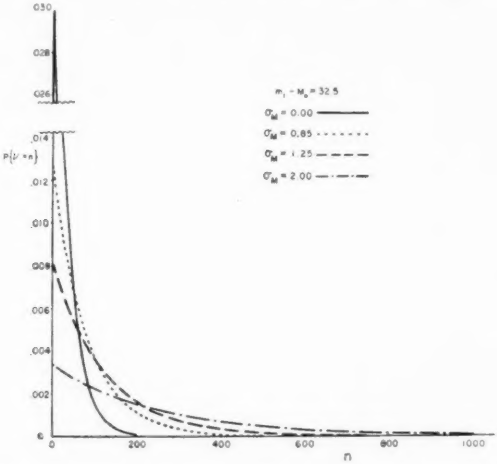

FIG. 11.—Consistency of theory with the existence of several identified very small clusters. Four graphs represent probabilities that the number ν of galaxies in a cluster will equal n computed on four alternative hypotheses regarding σ_M and on the assumption that ν has greatest possible variance and that $\nu - 1$ follows a negative binomial distribution.

Note added in proof.—In connection with the suggestion by W. Baade, made at the Rome meeting of the International Astronomical Union, 1952, to the effect that the distance scale requires revision, it may be useful to indicate the effect that such a revision would have on the constants estimated in the present paper. Suppose that all the present estimates of the distances to objects outside the Milky Way system should be multiplied by a factor a, with a corresponding correction for brightness. We shall be concerned with the values, say, $\sigma(a)$, $\lambda(a)$, $\nu_k(a)$, $m_1(a) - M_0(a)$, $\sigma_M(a)$, of the constants σ, λ, ν_k, $m_1 - M_0$, and σ_M discussed in the present paper that would have to be adopted as a result of such a change in scale. It is easy to see that

$$\sigma(a) = a\sigma,$$

$$\lambda(a) = \lambda / a^3,$$

$$\nu_k(a) = \nu_k,$$

$$m_1(a) - M_0(a) = m_1 - M_0 + 5 \log a,$$

$$\sigma_M(a) = \sigma_M.$$

The authors wish to acknowledge their deep indebtedness to several persons in the Statistical Laboratory, who, for about nine months, labored incessantly over the computations involved in the present paper. In particular, we are grateful to Mrs. Jeanne Lovasich, Mrs. Eloise Putz, and Mrs. Margaret Swanson, whose care, precision of work, and help to less experienced computers were very valuable.

APPENDIX

Idealized and Actual Counts of Galaxies

I. INTRODUCTION

The theory developed in Paper I is concerned with what was described as "idealized" plates or counts. This idealization included the postulates (*a*) that we count in two squares the numbers N_1 and N_2 of *all* the galaxies that have apparent magnitude less than the fixed limit m_1 and that we count nothing but such galaxies, and (*b*) that the apparent magnitude of a galaxy depends only on its absolute magnitude and on its distance as specified in equation (12) of the present paper. It is clear that neither of these postulates is satisfied by the actual counts which are now available or may become available in the future. Thus, in order to have any hope of obtaining realistic estimates of the three parameters $\lambda\nu_1$, σ, and c involved in the model studied, it is necessary to distinguish between the idealized counts N_i and their empirical counterparts, say, X_i, for $i = 1, 2$, and to establish relations between the frequency constants of N_1 and N_2, on the one hand, and of X_1 and X_2, on the other. The purpose of the present appendix is to establish these relations. This will be done by assuming a simplified model of general interstellar extinction and two alternative mechanisms of what we shall describe as errors of counting.

II. EFFECT OF GENERAL INTERSTELLAR EXTINCTION

The existence of interstellar extinction is a well-established fact. However, the exact nature of the distribution of the light-absorbing matter is a subject of discussion, although it is known that the two galactic polar regions are less affected by it than is the vicinity of the galactic equator. Originally, it was hoped that the region of the sky covered by the present investigation (with $\alpha = 11^h48^m$ to 16^h and $\delta = -23°$ to $+23°$) or at least its quadrant closest to the galactic pole could be assumed to be reasonably free from the effects of interstellar absorption. Figure A-1 flatly contradicts this assumption.

Each of the points exhibited in this figure has for its abscissa the latitude of the center of a photographic plate in Lick Observatory data covering a square of $6° \times 6°$. The ordinate of each point is the average number of galaxies counted on the plate per $1° \times 1°$ square. It is seen that, while there is substantial fluctuation, the correlation between the density of galaxies and the galactic latitude is quite distinct. Since this correlation is consistent with the generally accepted idea of the local galaxy as a flattish body containing absorbing matter, it was decided to base the present study on the simplifying assumption that the general absorption is of a deterministic character connected with the assumed shape of the galaxy. Specifically, it is assumed that, if a given $1° \times 1°$ square contains N galaxies with their distance ξ and their absolute magnitude M satisfying the relation

$$M - 5 + 5 \log \xi + 5.15 \times 10^{-9}\xi < m_1 ,$$

then the number of those galaxies in the same square whose apparent magnitude is less than the same limit m_1 will be only

$$N \times 10^{-k(\csc b - 1)} = N\mathcal{A}(b) \qquad \text{(say)}, \tag{A-1}$$

due to the effects of general interstellar extinction. Here b is the galactic latitude of the $1° \times 1°$ square considered and k is an appropriate constant related to the optical thickness of the absorbing layer.

Using the data exhibited in Figure A-1, the value of k was estimated to be $k = 0.37$. The continuous curve in Figure A-1 corresponds to formula (A-1) with this particular value of k.

The authors realize that the present assumption regarding the effect of general interstellar extinction is somewhat discordant with the theory in Paper I and represents an attempt at a heuristic interpolation rather than part of a probabilistic model. Also, a close study of data summarized in Figure A-1 shows a substantial dependence of the number of galaxies on the galactic longitude. To what extent this dependence is due to interstellar clouds or to clustering of galaxies is debatable. It must be clear, however, that the present study is based on the assumption of a uniform interstellar extinction, the intensity of which depends only on the length of the path traveled by light within the local galaxy.

The numbers N_1 and N_2 defined above will be described as the numbers of *visible* galaxies. The corresponding numbers $N_i \times \mathcal{A}(b)$ will be referred to as the numbers of ***apparently visible*** galaxies. In the further sections we shall deal with numbers X_1 and X_2 of *galaxies actually counted.*

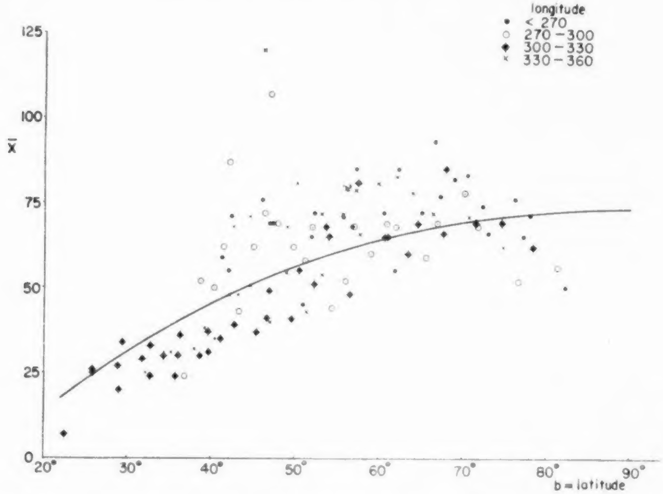

FIG. A-1.—Dependence of counts of galaxies on galactic latitude. Each point represents the average of counts in 36 squares 1° × 1° on a single plate, plotted against galactic latitude of the center of the plate. Solid curve corresponds to equation (A-1) with $N = 73$.

III. FIRST ERROR MODEL OF COUNTING GALAXIES

The simplest assumption regarding the relationship between the number X of galaxies actually counted in a 1° × 1° square and the corresponding number $N\mathcal{A}(b)$ of apparently visible galaxies is that

$$X = N\mathcal{A}(b) + \epsilon\,, \tag{A-2}$$

where ϵ is the "error of counting," a random variable with zero expectation and an unknown variance σ_ϵ^2, independent of N and independent of similar errors of counting in other 1° × 1° squares.

The set of these assumptions constitutes our first error model. It will be noticed that what we describe as the error of counting covers not only such errors in the strict sense of the word but also the effect of variation in the limiting magnitude of the plate, the effects of changing atmospheric conditions, faults in the emulsion, counting a star as a galaxy, and so forth.[14]

Simple calculations give

$$E(X) = \mathcal{A}(b)E(N)\,, \tag{A-3}$$

$$E(X^2) = \mathcal{A}^2(b)E(N^2) + \sigma_\epsilon^2\,, \tag{A-4}$$

---

[14] It is true that the counts X_i actually used in the present study were previously corrected for a number of the effects enumerated, as described in a forthcoming publication by C. D. Shane and C. A. Wirtanen. It is known, however, that, in spite of these corrections, some residual errors persist.

and, with reference to two different squares and the corresponding numbers X_1, X_2, N_1, N_2, b_1, and b_2,

$$E(X_1X_2) = \mathcal{A}(b_1)\mathcal{A}(b_2)E(N_1N_2)\,. \tag{A-5}$$

Formulae (A-3) and (A-4) apply to any particular square of the region of the sky covered by the investigation. Suppose now that this region contains n squares 1° × 1°, and let the subscript i refer to the ith square. Writing equation (A-3) for the ith square, summing, and solving for $E(N)$, we have

$$E(N) = \frac{E\left(\sum_{i=1}^{n} X_i\right)}{\sum_{i=1}^{n} \mathcal{A}(b_i)}\,. \tag{A-6}$$

Similarly, from formula (A-4),

$$E(N^2) = \frac{E\left(\sum_{i=1}^{n} X_i^2\right) - n\sigma_\epsilon^2}{\sum_{i=1}^{n} \mathcal{A}^2(b_i)}\,. \tag{A-7}$$

It follows that the expectation of N can be estimated by the quotient, say,

$$\frac{\bar{X}}{\bar{\mathcal{A}}} = \text{estimate of } E(N)\,, \tag{A-8}$$

of the arithmetic mean of the actual counts of galaxies in n squares of the region studied, divided by the arithmetic mean $\bar{\mathcal{A}}$ of the numbers $\mathcal{A}(b_i)$ corresponding to these squares. Similarly,

$$\frac{\frac{1}{n}\sum_{i=1}^{n} X_1^2 - \sigma_\epsilon^2}{\frac{1}{n}\sum_{i=1}^{n} \mathcal{A}^2(b_i)} = \text{estimate of } E(N^2) \tag{A-9}$$

can be taken as an estimate of $E(N^2)$. Here, however, we need the estimate of σ_ϵ^2, the origin of which will be described presently. Returning to (A-5), we consider pairs of similarly located squares in the region covered by the study, for example, all the pairs of squares exactly k degrees apart, either both in the same column or both in the same row. Let $n(k)$ denote the number of such pairs and let X_i', X_i'', b_i', and b_i'' denote the numbers X and latitude b referring to squares of the ith pair. It is easy to see that

$$\frac{\sum_{i=1}^{n(k)} X_i' X_i''}{\sum_{i=1}^{n(k)} \mathcal{A}(b_i')\mathcal{A}(b_i'')} = \text{estimate of } E(N_1N_2)\,, \tag{A-10}$$

where N_1 and N_2 in the right-hand side are understood to represent the numbers of galaxies visible in two similarly oriented squares, k degrees apart.

It will be seen that formulae (A-8), (A-9), and (A-10) give the estimates of all the frequency constants of N_1 and N_2 needed in the main part of the present paper. In order to be able to obtain the numerical values of these estimates, it is necessary to estimate σ_ϵ^2. Such an estimate is obtained from the Lick Observatory counts in 1° × 1° squares in the border rows and columns of each plate. The photographs were so adjusted that any two adjoining plates have an overlap of 1° × 6°. Thus the data contain double independent counts on different plates, for a total of 1248 squares. Of these, there are 96 corner squares for which there are independent counts on four different plates.

The square of the difference between two such counts relating to the same square, say $X - Y$, has expectation equal to $2\sigma_\epsilon^2$. Thus one-half of the average of the numbers $(X - Y)^2$ gives an estimate of σ_ϵ^2.

Numerical values of the various elements involved in the first error model are given in Section V, below.

IV. SECOND ERROR MODEL

If the assumptions of the first-error model were strictly satisfied, then the sums $X + Y$ and $X - Y$ of two independent counts in the same 1° × 1° square would be noncorrelated. Figure A-2 gives the plot of the differences $|X - Y|$ against the mean $(X + Y)/2$.

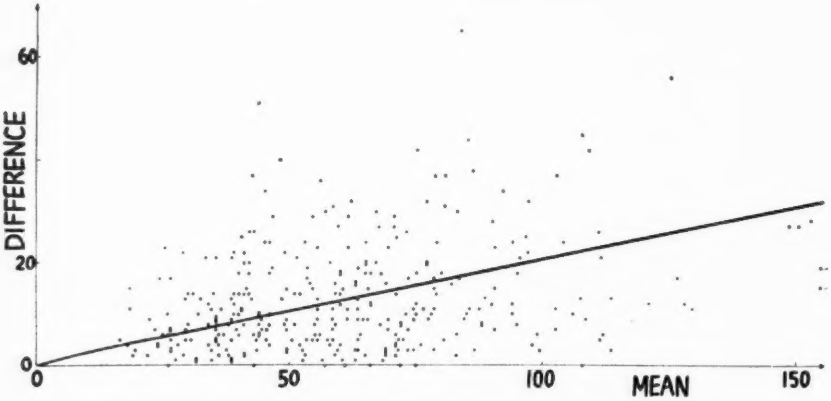

FIG. A-2.—Dependence of variability of duplicate counts X and Y of galaxies in 1° × 1° squares upon the average of these counts. The duplicate counts were made on two different plates covering the same square. Each point represents $|X - Y|$ plotted against $(X + Y)/2$. The scatter diagram is based on one-fourth of available data taken over the entire area used. The curve represents the relation predicted by error model 2.

It is seen that, although weak, a correlation between $|X - Y|$ and $X + Y$ exists, indicating the possibility that, when the common expectation of X and Y is large, the variability of X and Y is large, and vice versa. With this empirical fact in mind, the second error model was constructed. It is based on the following assumptions.

To each combination of the plate and of the 1° × 1° square, there corresponds a probability δ that an apparently visible galaxy will be counted. The counting of any particular apparently visible galaxy is independent of that of any other, so that the number X of galaxies actually counted is a binomial variable, with frequency function

$$P\{X = k \mid \delta, N\mathcal{A}(b)\} = C^k_{N\mathcal{A}(b)}\,\delta^k(1-\delta)^{N\mathcal{A}(b)-k}. \qquad \text{(A-11)}$$

Remark.—The attention of the reader is called to the flaw in the above construction due to the fact that, in most cases, the number $N\mathcal{A}(b)$ will not be an integer.

It is further assumed that the probability δ varies from one square to another in random fashion, with probability density[15]

$$p_\delta(x) = \frac{x^{\alpha-1}(1-x)^{\beta-1}}{B(\alpha,\beta)}, \tag{A-12}$$

where α and β are positive adjustable parameters.[16]

It is known that the density (A-12) is very flexible and, therefore, is likely to approximate the unknown distribution of δ.

The above assumptions, combined with another that the values of δ assumed for different squares are mutually independent and independent of the number N, constitute the second error model. The disadvantage of this model is that it does not allow for the possibility of counting as a galaxy either a star or a fault in the emulsion. Also, with the second model the interpretation of the limiting apparent magnitude may be expected to vary from one plate to another and even from one section of a given plate to another section. From the point of view of the first error model, the limiting apparent magnitude m_l is considered as some sort of average of the values varying from plate to plate, and the occasional excesses in recorded numbers of galaxies are ascribed to errors. With the second error model, denying the possibility of actual counts exceeding the number of apparently visible galaxies, the limiting apparent magnitude m_l must be interpreted as the faintest limiting magnitude of all those characterizing all the plates.

Closer examination of both models will reveal many other defects. However, the authors believe that further complication of the error model in an effort to make it more realistic is not justified at the present time.

In further work we shall need the expressions for moments of δ. Using (A-12), it is easy to find that

$$E(\delta^k) = \frac{\alpha(\alpha+1)(\alpha+2)\dots(\alpha+k-1)}{\gamma(\gamma+1)(\gamma+2)\dots(\gamma+k-1)} = \delta_k \qquad (\text{say}), \tag{A-13}$$

with $\gamma = \alpha + \beta$.

Returning to the actual counts X of galaxies in a 1° × 1° square and performing easy computations, we have

$$E(X) = E\{E[X \mid \delta, N\mathcal{A}(b)]\} = E\{\delta N\mathcal{A}(b)\} = \delta_1\mathcal{A}(b)E(N); \tag{A-14}$$

$$\begin{aligned} E(X^2) &= E\{E[X^2 \mid \delta, N\mathcal{A}(b)]\} \\ &= E\{\delta^2 N^2 \mathcal{A}^2(b) + (\delta - \delta^2) N\mathcal{A}(b)\} \\ &= \delta_2\mathcal{A}^2(b)E(N^2) + (\delta_1 - \delta_2)\mathcal{A}(b)E(N). \end{aligned} \tag{A-15}$$

Finally, if X_i', N_i', b_i', δ_i', and X_i'', N_i'', b_i'', δ_i'' refer to two squares k degrees apart,

$$\begin{aligned} E(X_i'X_i'') &= E\{E[X_i'X_i' \mid \delta_i', \delta_i'', N_i', N_i'', \mathcal{A}(b_i'), \mathcal{A}(b_i'')]\} \\ &= E\{\delta_i'\delta_i''\mathcal{A}(b_i')\mathcal{A}(b_i'')N_i'N_i''\} = \delta_1^2\mathcal{A}(b_i')\mathcal{A}(b_i'')E(N_1N_2). \end{aligned} \tag{A-16}$$

Proceeding in a manner exactly similar to that of Section III, we obtain the following estimates of the three expectations $E(N)$, $E(N^2)$, and $E(N_1N_2)$,

$$\frac{\bar{X}}{\delta_1\mathcal{A}} = \text{estimate of } E(N), \tag{A-17}$$

---

[15] Originally, a simpler model was considered, such that δ is a constant and has the same value for all squares. However, the implications of this model are contradicted by the data.

[16] The reader will perceive that the parameters α and β used here in the distribution of δ have no connection with the parameters α and β used in the generating function (6) of the number ν of galaxies per cluster.

$$\frac{\sum_{i=1}^{n} X^2 - \left(1 - \frac{\delta_2}{\delta_1}\right)\sum_{i=1}^{n} X_i}{\delta_2 \sum_{i=1}^{n} \mathcal{A}^2(b_i)} = \text{estimate of } E(N^2)\,, \tag{A-18}$$

$$\frac{\sum_{i=1}^{n(k)} X_i' X_i''}{\delta_1^2 \sum_{i=1}^{n(k)} \mathcal{A}(b_i')\,\mathcal{A}(b_i'')} = \text{estimate of } E(N_1 N_2)\,. \tag{A-19}$$

These formulae are, of course, analogous to formulae (A-8), (A-9), and (A-10) relating to the first error model.

In order to apply the results just obtained, it is now necessary to use the counts in overlapping squares of contiguous plates in order to estimate the parameters α and β in the density (A-12). Thereafter, formula (A-13) will determine δ_1 and δ_2 appearing in (A-17), (A-18), and (A-19).

As in Section III, the symbols X and Y will be used to denote two actual counts of galaxies performed independently within the same 1° × 1° square, the center of which has the galactic latitude b. These counts, then, are obtained from two overlapping plates. In order to obtain estimates of α and β in (A-12) we shall deal with factorial product moments of X and Y, say

$$M_{rs}(b) = E\left\{\frac{X!}{(X-r)!}\,\frac{Y!}{(Y-s)!}\right\} \tag{A-20}$$

for values of r and s such that $r + s \leqq 3$. Using (A-14), (A-15), and (A-20), we have

$$M_{01}(b) = M_{10}(b) = \delta_1 \mathcal{A}(b) E(N)\,, \tag{A-21}$$

$$M_{02}(b) = M_{20}(b) = \delta_2 [\mathcal{A}^2(b) E(N^2) - \mathcal{A}(b) E(N)]\,, \tag{A-22}$$

$$M_{11}(b) = \delta_1^2 \mathcal{A}^2(b) E(N^2)\,. \tag{A-23}$$

Further,

$$\begin{aligned} M_{03}(b) &= M_{30}(b) = E\{X(X-1)(X-2)\} \\ &= E\{E[X(X-1)(X-2) \mid \delta', N\mathcal{A}(b)]\} \\ &= E\{\delta'^3 [N^3\mathcal{A}^3(b) - 3N^2\mathcal{A}^2(b) + 2N\mathcal{A}(b)]\} \\ &= \delta_3 [\mathcal{A}^3(b)E(N^3) - 3\mathcal{A}^2(b)E(N^2) + 2\mathcal{A}(b)E(N)]\,, \end{aligned} \tag{A-24}$$

$$\begin{aligned} M_{21}(b) = M_{12}(b) &= E\{X(X-1)Y\} = E\{E[X(X-1)Y \mid \delta', \delta'', N\mathcal{A}(b)]\} \\ &= E\{\delta'^2\delta'' N^2\mathcal{A}^2(b)[N\mathcal{A}(b) - 1]\} \\ &= \delta_1\delta_2 [\mathcal{A}^3(b)E(N^3) - \mathcal{A}^2(b)E(N^2)]\,. \end{aligned} \tag{A-25}$$

Equations of this kind can be written for every 1° × 1° square in the region covered by investigation for which there are two independent counts of galaxies. Let, generally, M_{rs} and $\mathcal{A}_k$ stand for averages of $M_{rs}(b)$ and $\mathcal{A}^k(b)$ taken over all such squares. Then the last five formulae yield the following system of equations that must be satisfied by three first moments of N and by the unknown numbers α and β:

$$\begin{aligned} \delta_1 \mathcal{A}_1 E(N) &= M_{10} , \\ -\delta_2 \mathcal{A}_1 E(N) + \delta_2 \mathcal{A}_2 E(N^2) &= M_{20} , \\ \delta_2^1 \mathcal{A}_2 E(N^2) &= M_{11} , \\ 2\,\delta_3 \mathcal{A}_1 E(N) - 3\,\delta_3 \mathcal{A}_2 E(N^2) + \delta_3 \mathcal{A}_3 E(N^3) &= M_{30} , \\ -\delta_1 \delta_2 \mathcal{A}_2 E(N^2) + \delta_1 \delta_2 \mathcal{A}_3 E(N^3) &= M_{21} . \end{aligned} \tag{A-26}$$

These equations are nonhomogeneous linear in $\mathcal{A}_k E(N^k)$ for $k = 1, 2, 3$. Equating to zero the determinants of fourth order of two independent groups of these equations, we eliminate the products $\mathcal{A}_k E(N^k)$ and obtain two equations to be satisfied by α and β. Taking the first four equations (A-26), we obtain by this method

$$\frac{M_{10}}{\delta_1} + \frac{M_{20}}{\delta_2} - \frac{M_{11}}{\delta_1^2} = 0 . \tag{A-27}$$

The same method applied to the last four equations of the set (A-26) yields

$$2\,\frac{M_{20}}{\delta_2} - \frac{M_{21}}{\delta_1 \delta_2} + \frac{M_{30}}{\delta_3} = 0 . \tag{A-28}$$

Using (A-13), the last two equations are transformed into the system

$$\frac{\gamma}{\alpha} = \frac{\alpha M_{10} + M_{20} + M_{10}}{M_{11} - \alpha\,(M_{20} - M_{11})} = 2\,\frac{\alpha M_{20} + M_{30} + 2M_{20}}{2M_{21} - \alpha\,(M_{30} - M_{21})} . \tag{A-29}$$

The second of these equations reduces to a quadratic in α,

$$\begin{aligned} \alpha^2\,[2M_{20}\,(M_{20} - M_{11}) - M_{10}\,(M_{30} - M_{21})] + \alpha\,\{ 2\,[(M_{30} + 2M_{20})\,(M_{20} - M_{11}) \\ + M_{10}M_{21} - M_{20}M_{11}] - (M_{20} + M_{10})\,(M_{30} - M_{21}) \} + 2\,[M_{21}\,(M_{20} + M_{10}) \\ - M_{11}\,(M_{30} + 2M_{20})] = 0 . \end{aligned} \tag{A-30}$$

At the same time, the first equation gives

$$\gamma = \alpha\,\frac{\alpha M_{10} + M_{20} + M_{10}}{M_{11} - \alpha\,(M_{20} - M_{11})} . \tag{A-31}$$

The empirical evaluation of α and γ begins by estimating the factorial moments,

$$\begin{aligned} &\text{Estimate of } M_{10} = \tfrac{1}{2}\,(\bar{X} + \bar{Y}) , \\ &\text{Estimate of } M_{20} = \tfrac{1}{2}\,[\overline{X^2} + \overline{Y^2} - \bar{X} - \bar{Y}] , \\ &\text{Estimate of } M_{30} = \tfrac{1}{2}\,[\overline{X^3} + \overline{Y^3} - 3\,(\overline{X^2} + \overline{Y^2}) + 2\,(\bar{X} + \bar{Y})] , \\ &\text{Estimate of } M_{11} = \overline{XY} , \\ &\text{Estimate of } M_{21} = \tfrac{1}{2}\,[\overline{X^2 Y} + \overline{X Y^2}] - \overline{XY} , \end{aligned} \tag{A-32}$$

where the bar over each symbol indicates averaging over all available pairs X and Y. The estimates so obtained are substituted in (A-30). When the value of $\alpha > 0$ is obtained from this equation, the estimate of $\gamma = \alpha + \beta$ is obtained from (A-31). Then formula (A-13) gives δ_1 and

δ_2, which are to be used to obtain the corrected frequency constants of N_1 and N_2 in formulae (A-17)–(A-19).

V. NUMERICAL VALUES INVOLVED IN CORRECTIONS FOR GENERAL GALACTIC EXTINCTION AND FOR ERRORS IN COUNTING

The fundamental data used are summarized in Table A-1 for each quadrant and for the entire area used. Table A-1 also contains the sums of the extinction factors $\mathcal{A}(b)$ corresponding to the same five areas.

Since the number of terms entering the sums decreases as k increases, it is necessary to tabulate n_k for each value of k. This is done in Table A-2. The n_k's corresponding to different quadrants differ somewhat because it is not feasible to divide the entire area used into equal quarters.

The data relating to overlapping squares are summarized in the left half of Table A-3, while the corresponding estimates of the parameters involved in error models 1 and 2 are listed in the right half of this table.

TABLE A-1

SUMS OF OBSERVED COUNTS X AND SUMS OF CROSS-PRODUCTS $X'X''$ OF COUNTS IN 1° × 1° SQUARES k° APART (COMPUTED FROM LICK OBSERVATORY DATA) AND CORRESPONDING SUMS OF $\mathcal{A}(b) = 10^{-0.37}(\text{Csc } b - 1)$ FOR EACH QUADRANT AND FOR THE ENTIRE AREA USED

SUM OF n_k TERMS	QUADRANT				ENTIRE AREA USED
	Upper Right	Lower Right	Upper Left	Lower Left	
ΣX	121,590	116,195	113,913	75,803	341,932
ΣX^2	9,468,512	8,716,039	8,842,005	4,209,961	25,002,624
$\Sigma X'X''$					
for $k=1$	8,531,106	7,875,763	8,024,096	3,676,442	22,754,349
$k=2$	8,032,731	7,396,781	7,551,133	3,353,380	21,633,398
$k=3$	7,705,062	7,090,264	7,230,369	3,090,655	20,966,972
$k=4$	7,352,687	6,788,299	6,906,157	2,875,081	20,263,019
$k=5$	7,087,358	6,563,206	6,569,053	2,742,741	19,715,947
$k=6$	6,841,713	6,328,838	6,254,902	2,578,332	19,196,787
$k=7$	6,552,008	6,061,173	5,966,275	2,472,149	18,663,198
$k=8$	6,322,969	5,811,098	5,722,652	2,330,867	18,230,024
$k=9$	6,081,284	5,595,290	5,548,379	2,218,091	17,855,040
$k=10$	5,843,573	5,318,999	5,345,695	2,134,844	17,445,676
$k=11$	5,567,205	5,103,907	5,128,807	2,054,914	17,049,927
$k=12$	5,254,987	4,908,397	4,867,130	1,979,354	16,624,695
$k=13$	4,960,970	4,674,170	4,613,702	1,906,364	16,155,206
$k=14$	4,694,044	4,468,868	4,344,354	1,809,576	15,679,418
$k=15$	4,438,652	4,221,040	4,060,372	1,718,254	15,226,337
$k=16$	4,194,108	3,969,583	3,787,443	1,605,617	14,767,004
$k=17$	3,944,527	3,737,511	3,501,792	1,492,557	14,257,023
$k=18$	3,645,305	3,487,489	3,182,511	1,405,781	13,704,002
$k=19$	3,389,134	3,249,003	2,890,703	1,305,018	13,206,106
$k=20$	3,140,737	2,999,886	2,584,738	1,211,356	12,734,571
$k=21$	2,922,060	2,727,807	2,335,582	1,121,987	12,296,026
$k=22$	2,719,264	2,441,068	2,117,822	1,049,714	11,892,937
$k=23$	2,511,045	2,149,361	1,912,379	956,032	11,463,757
$\Sigma\mathcal{A}$	1657.6	1392.4	1449.2	1130.0	4480.8
$\Sigma\mathcal{A}^2$	1552.9	1088.3	1184.4	734.1	3613.5
$\Sigma\mathcal{A}'\mathcal{A}''$					
for $k=1$	1507.7	1060.2	1150.2	712.7	3554.4
$k=2$	1462.2	1028.7	1115.5	691.0	3493.8
$k=3$	1416.2	996.5	1080.5	668.9	3431.9
$k=4$	1369.8	964.5	1045.2	646.6	3369.1
$k=5$	1323.2	931.8	1009.5	624.0	3304.9

TABLE A-2

n_k, THE NUMBER OF TERMS OVER WHICH THE SUMS IN TABLE A-1 ARE TAKEN

k	n_k				
	QUADRANT				ENTIRE AREA USED
	Upper Right	Lower Right	Upper Left	Lower Left	
0°	1773	1804	1802	1834	5796
1	1719	1750	1747	1779	5687
2	1665	1696	1692	1724	5578
3	1611	1642	1637	1669	5469
4	1557	1588	1582	1614	5360
5	1503	1534	1527	1559	5251
6	1449	1480	1472	1504	5142
7	1395	1426	1417	1449	5033
8	1341	1372	1362	1394	4924
9	1287	1318	1307	1339	4815
10	1233	1264	1252	1284	4706
11	1179	1210	1197	1229	4597
12	1125	1156	1142	1174	4488
13	1071	1102	1087	1119	4379
14	1017	1048	1032	1064	4270
15	963	994	977	1009	4161
16	909	940	922	954	4052
17	855	886	867	899	3943
18	801	832	812	844	3834
19	747	778	757	789	3725
20	693	724	702	734	3616
21	639	670	647	679	3507
22	585	616	592	624	3398
23	531	562	537	569	3289

TABLE A-3

BASIC SUMS RELATING TO DUPLICATE COUNTS IN 1° × 1° SQUARES OF OVERLAPPING PLATES AND ESTIMATES OF FREQUENCY CONSTANTS INVOLVED IN THE TWO ERROR MODELS

(X is right or lower plate; Y is left or upper overlapping plate)

	Sum of 1248 Terms	Frequency Constant	Estimate
ΣX	72,619	σ_e^2	120.68
ΣX^2	5,234,169	M_{10}	58.51162
ΣX^3	460,054,417	M_{20}	4208.153
ΣY	73,426	M_{30}	369,070.1
ΣY^2	5,415,426	M_{11}	4145.983
ΣY^3	492,801,160	M_{21}	359,798.8
ΣXY	5,174,187	α	4.12256
ΣX^2Y	448,860,977	γ	4.77777
ΣXY^2	459,545,267	δ_1	0.862863
$\Sigma(X-Y)^2$	301,221	δ_2	0.765013

THE ANALYSIS OF COUNTS OF THE EXTRAGALACTIC NEBULAE IN TERMS OF A FLUCTUATING DENSITY FIELD

D. NELSON LIMBER
Yerkes Observatory

Received August 11, 1952

ABSTRACT

In this paper a method is developed for analyzing the counts of the extragalactic nebulae in terms of a fluctuating density field for the nebulae in space. It is shown how such an analysis can lead to a determination of the parameters characterizing the distribution of the nebulae. It is shown that the effects of galactic absorption, which may well be appreciable, can be taken quite simply into account on the recent theory of Chandrasekhar and Münch for the fluctuations in brightness of the Milky Way. The necessary expressions for analyzing the counts are developed for four separate cases so that the effects of a dispersion in the absolute magnitudes of the nebulae and of fluctuations in galactic absorption can be either included or neglected as the situation demands.

I. INTRODUCTION

The counts of the extragalactic nebulae undertaken by Professor Shane at the Lick Observatory will soon make available a wealth of material for statistical investigations of the distribution of the nebulae in space. The material consists of counts of the nebulae to a limiting apparent magnitude of approximately 19. These counts per unit area of the sky are given as a function of position. It appears that an analysis of these counts in terms of a fluctuating nebular density field along the lines of the recent theory of Chandrasekhar and Münch[1] for the fluctuations in brightness of the Milky Way might provide a comprehensive method which is mathematically tractable. This method of analysis seems to require a minimum of assumptions as to the parameters describing the distribution and can be readily extended so as to take into account fluctuations in galactic absorption.

II. THE THEORETICAL FORMULATION OF THE PROBLEM

Let $\rho(r)$ be the number of nebulae per unit volume in a given direction and at a distance r. Then, ignoring galactic absorption for the present, the number of nebulae within a small solid angle ω in the chosen direction and within a distance r' will be

$$N(r') = \omega \int_0^{r'} \rho(r)\, r^2 dr\,. \tag{1}$$

The assumption is now made that we can write

$$\rho(r) = \bar{\rho}\,[1 + D(r)]\,, \tag{2}$$

where $\bar{\rho}$ is a constant and where

$$\overline{D(\boldsymbol{r})} = 0\,, \qquad \overline{D^2(\boldsymbol{r})} \equiv \beta^2 = \text{Constant}\,, \tag{3}$$

and

$$\overline{D(\boldsymbol{r}_1)\, D(\boldsymbol{r}_2)} \equiv \beta^2 \Gamma(|\boldsymbol{r}_1 - \boldsymbol{r}_2|)\,. \tag{4}$$

---

[1] S. Chandrasekhar and G. Münch, *Ap. J.*, **115,** 103, 1952; this paper will be referred to as "Paper V" throughout the present paper.

In equation (4), $\Gamma(|\mathbf{r}_1-\mathbf{r}_2|)$ is the correlation coefficient describing the fluctuating density field of the nebulae.

If we assume a Gaussian form for the luminosity function of the nebulae, then the number of the nebulae with absolute magnitudes between M and $M+dM$ will be given by

$$N(M)\,dM=\rho(\mathbf{r})\,\frac{1}{\sigma\sqrt{[2\pi]}}\,e^{-(M-M_0)^2/2\sigma^2}\,dM\,, \tag{5}$$

where M_0 is a mean absolute magnitude. Using these results, together with the defining relationship for the absolute magnitude, we obtain the following expression for the number of nebulae in ω to a limiting apparent magnitude m':

$$\begin{gathered}N(m')=\frac{\omega\bar{\rho}}{\sigma\sqrt{[2\pi]}}\int_{-\infty}^{+\infty}dM\,e^{-(M-M_0)^2/2\sigma^2}\int_0^{r'}d\mathbf{r}\,r^2\,[1+D(\mathbf{r})]\,,\\ r'\equiv 10^{(1/5)(m'-M+5)}\,.\end{gathered} \tag{6}$$

Inverting the order of the integrations and introducing the error function defined for both positive and negative t by

$$\Phi(t)\equiv\frac{2}{\sqrt{\pi}}\int_0^t dt\,e^{-t^2}\,, \tag{7}$$

we obtain

$$N(m')=\tfrac{1}{2}\omega\bar{\rho}\int_0^{\infty}d\mathbf{r}\,r^2\,[1+D(\mathbf{r})]\left[1+\Phi\left(\frac{1}{\sigma\sqrt{2}}\{m'-M_o+5-5\log_{10}r\}\right)\right]. \tag{8}$$

Now the effect of galactic absorption of optical thickness $\tau(s)$ upon an extragalactic object which would have an apparent magnitude m in the absence of absorption is such that

$$m_{\text{observed}}\equiv m_o=m+2.5\,\tau(s)\log_{10}e\,. \tag{9}$$

Using this result in equation (8), we obtain, for the number of nebulae in ω to a limiting observed apparent magnitude m_o',

$$\begin{aligned}N(m_o')=\tfrac{1}{2}\omega\bar{\rho}\int_0^{\infty}&d\mathbf{r}\,r^2\,[1+D(\mathbf{r})]\\ &\times\left[1+\Phi\left(\frac{1}{\sigma\sqrt{2}}\{m_o'-M_0+5-2.5\,\tau(s)\log_{10}e-5\log_{10}r\}\right)\right].\end{aligned} \tag{10'}$$

On the other hand, if we should assume that all the extragalactic nebulae are of the same absolute magnitude, M_0, then the corresponding expression for $N(m_o')$ is

$$\begin{gathered}N(m_o')=\omega\bar{\rho}\int_0^{r'}d\mathbf{r}\,r^2\,[1+D(\mathbf{r})]\,,\\ r'\equiv 10^{(1/5)[m_o'-M_0+5-2.5\tau(s)\log_{10}e]}\,.\end{gathered} \tag{10''}$$

We shall obtain the formulae necessary to analyze the observed distribution for both of these cases.

In order to take into account the effects of galactic absorption, we find it most convenient to analyze the counts by means of strip correlations taken along parallels of galactic latitude. For such an analysis we require expressions for $\overline{N(m_o')}$ and $\overline{N(m_o')^2}$, where the mean is that taken over a range in galactic longitude for a given galactic latitude. We shall also need an expression for the angular correlation, $\overline{N(m_o')N(m_o')_\phi}$. The subscript ϕ is used to signify that the directions of the two counts are separated by an angle $\phi/\cos b$ in galactic longitude, the galactic latitude, b, being held the same for both.

In those cases in which account is taken of the fluctuations in galactic absorption, we shall assume that we can write[2]

$$\tau(s) = \bar{\tau}(s) + \int_0^{\bar{\tau}(s)} \delta(t)\, dt\,, \tag{11}$$

where $\delta(\boldsymbol{t})$ is a chance variable such that

$$\overline{\delta(\boldsymbol{t})} = 0\,, \qquad \overline{\delta^2(\boldsymbol{t})} = \alpha^2 = \text{Constant}\,,$$

and

$$\overline{\delta(\boldsymbol{t}_1)\,\delta(\boldsymbol{t}_2)} = \alpha^2 R(|\boldsymbol{t}_1 - \boldsymbol{t}_2|)\,. \tag{12}$$

Here $R(|\boldsymbol{t}_1 - \boldsymbol{t}_2|)$ is the correlation coefficient describing the distribution of the galactic absorbing matter.

III. THE EXPRESSIONS FOR $\overline{N(m_o')}$, $\overline{N(m_o')^2}$, AND $\overline{N(m_o')N(m_o')_\phi}$

We shall consider four situations.

Case I.—All the nebulae are of a given constant absolute magnitude, and the galactic absorption remains constant for a given galactic latitude. We shall find it convenient to define

$$\log_{10} A \equiv \tfrac{1}{5}\,[m_o' - M_0 + 5 - 2.5\,\tau \log_{10} e]\,, \tag{13}$$

where τ is the optical thickness of the galactic absorbing matter for the galactic latitude being considered. Since $\overline{D(\boldsymbol{r})} = 0$ by assumption, we find from equation (10″) that

$$\overline{N} = \tfrac{1}{3}\omega\bar{\rho}A^3\,, \qquad \overline{N^2} = \tfrac{1}{9}\omega^2\bar{\rho}^2A^6\left(1 + \frac{9}{A^6}Z_0\right), \tag{14}$$

and

$$\overline{NN_\phi} = \tfrac{1}{9}\omega^2\bar{\rho}^2A^6\left(1 + \frac{9}{A^6}Z_\phi\right), \tag{15}$$

where Z_0 and Z_ϕ are defined by

$$Z_0 \equiv \int_0^A\!\!\int_0^A d r_1 d r_2 r_1^2 r_2^2 \overline{D(r_1)\,D(r_2)}\,,$$

and

$$Z_\phi \equiv \int_0^A\!\!\int_0^A d r_1 d r_2 r_1^2 r_2^2 \overline{D(\boldsymbol{r}_1)\,D(\boldsymbol{r}_2)}\,. \tag{16}$$

We have written $\boldsymbol{r}_1$ and $\boldsymbol{r}_2$ for the arguments of D in the Z_ϕ expression in order to emphasize that the fluctuations in two different directions are considered; in the Z_0 expression the two fluctuations which occur refer to the same direction. We shall use these same means in order to emphasize this difference for the galactic absorption expressions as well. In Section IV we shall obtain analytical expressions for Z_0 and Z_ϕ in terms of the correlation coefficient.

Case II.—All the nebulae are of a given constant absolute magnitude, and there are fluctuations in the galactic absorption for a given galactic latitude. Under these assumptions we can express the upper limit of integration in equation (10″) as follows:

$$\begin{aligned} r' &= 10^{(1/5)[m_o' - M_0 + 5 - 2.5\tau(s)\log_{10} e]} \\ &= A\,\exp\left\{-\frac{1}{2}\int_0^{\tau}\delta(t)\,dt\right\}, \end{aligned} \tag{17}$$

---

[2] *Ibid.*

where A is the A defined by equation (13) when τ of that expression is now understood to be the mean value of $\tau(s)$ at the particular galactic latitude considered. If we now expand the term in equation (17) containing the chance variable $\delta(t)$ in a power series and retain only the first three terms—as was done in the analysis of the fluctuations in brightness of the Milky Way—we obtain

$$r' = A\left\{1 - \frac{1}{2}\int_0^\tau dt\,\delta(t) + \frac{1}{8}\int_0^\tau\int_0^\tau dt_1 dt_2\,\delta(t_1)\,\delta(t_2)\right\}. \tag{18}$$

In order to simplify our notation, we define

$$(1 - \epsilon) \equiv 1 - \frac{1}{2}\int_0^\tau dt\,\delta(t) + \frac{1}{8}\int_0^\tau\int_0^\tau dt_1 dt_2\,\delta(t_1)\,\delta(t_2). \tag{19}$$

We can then express equation (10″) as

$$N(m_0') = \omega\bar{\rho}\left\{\int_0^A dr\,r^2[1 + D(r)] - \int_{A(1-\epsilon)}^A dr\,r^2[1 + D(r)]\right\}. \tag{20}$$

In taking the mean of this expression, we encounter no difficulty in the evaluation of the first term. Since $\overline{D(r)}$ and $\overline{\delta(t)}$ vanish by assumption, the second term can also be readily evaluated. We obtain, to the order of approximation in which we are working,

$$\overline{N} = \tfrac{1}{3}\omega\bar{\rho}A^3\left(1 + \tfrac{9}{8}T_0\right), \tag{21}$$

where

$$T_0 \equiv \int_0^\tau\int_0^\tau dt_1 dt_2\,\overline{\delta(t_1)\,\delta(t_2)}. \tag{22}$$

We next consider $\overline{NN_\phi}$. From equation (10″):

$$\begin{aligned}\overline{NN_\phi} = \omega^2\bar{\rho}^2\Big\{&\int_0^A\int_0^A dr_1 dr_2\,r_1^2 r_2^2\left[1 + \overline{D(r_1)\,D(r_2)}\right]\\ &- 2\int_0^A\int_{A(1-\epsilon)}^A dr_1 dr_2\,r_1^2 r_2^2\left[1 + \overline{D(r_1)\,D(r_2)}\right]\\ &+ \int_{A(1-\epsilon)}^A\int_{A(1-\epsilon)}^A dr_1 dr_2\,r_1^2 r_2^2\left[1 + \overline{D(r_1)\,D(r_2)}\right]\Big\}^*,\end{aligned} \tag{23}$$

where the asterisk is to be understood as meaning a proper average over the τ variations. Proceeding as in case I and neglecting terms containing the product $\overline{D(r_1)D(r_2)}\;\overline{\delta(t_1)\delta(t_2)}$, we obtain

$$\overline{NN_\phi} = \tfrac{1}{9}\omega^2\bar{\rho}^2A^6\left\{1 + 9\frac{Z_\phi}{A^6} + \tfrac{9}{4}(T_0 + T_\phi)\right\}, \tag{24}$$

where

$$T_\phi \equiv \int_0^\tau\int_0^\tau dt_1 dt_2\,\overline{\delta(t_1)\,\delta(t_2)}. \tag{25}$$

Finally, from equation (24)

$$\overline{N^2} = \tfrac{1}{9}\omega^2\bar{\rho}^2A^6\left\{1 + 9\frac{Z_0}{A^6} + \tfrac{9}{2}T_0\right\}. \tag{26}$$

The evaluation of T_0 and T_ϕ is carried out for two forms of the correlation coefficient in Section IV.

Case III.—The distribution of the absolute magnitudes of the nebulae is Gaussian, and *the galactic absorption remains constant for a given galactic latitude.* From equation (10′) we have

$$N(m_o') = \tfrac{1}{2}\omega\bar{\rho}\int_0^\infty d\,r\,r^2\,[1+D(r)]\,[1+\Phi(x)]\,, \tag{27}$$

where we have written

$$x \equiv \frac{1}{\sigma\sqrt{2}}\,[m_o' - M_0 + 5 - 2.5\,\tau\,\log_{10} e - 5\,\log_{10} r]\,. \tag{28}$$

Hence,

$$\overline{N} = \tfrac{1}{2}\omega\bar{\rho}\int_0^\infty d\,r\,r^2\,[1+\Phi(x)]\,, \tag{29}$$

$$\overline{N N_\phi} = \tfrac{1}{4}\omega^2\bar{\rho}^2\int_0^\infty\int_0^\infty d\,r_1 d\,r_2\,r_1^2 r_2^2\,[1+\overline{D(r_1)\,D(r_2)}\,] \times [1+\Phi(x_1)\,\Phi(x_2)+\Phi(x_1)+\Phi(x_2)]\,, \tag{30}$$

and

$$\overline{N^2} = \tfrac{1}{4}\omega^2\bar{\rho}^2\int_0^\infty\int_0^\infty d\,r_1 d\,r_2\,r_1^2 r_2^2\,[1+\overline{D(r_1)\,D(r_2)}\,] \times [1+\Phi(x_1)\,\Phi(x_2)+\Phi(x_1)+\Phi(x_2)]\,. \tag{31}$$

To evaluate the integral of the expression for $\overline{NN_\phi}$ in terms of the correlation coefficient, we let

$$r^2 \equiv r_1^2 + r_2^2 - 2\,r_1 r_2\cos\phi \tag{32}$$

and obtain

$$\begin{aligned}\overline{N N_\phi} = \tfrac{1}{2}\omega^2\bar{\rho}^2\int_0^\infty d\,r_1\,r_1^2\int_{r_1\sin\phi}^{r_1} d\,r\,\frac{r}{\sqrt{[r^2 - r_1^2\sin^2\phi]}}\\ \times [r_1\cos\phi - \sqrt{(r^2 - r_1^2\sin^2\phi)}\,]^2\,[1+\overline{D(r_1)\,D(r_2)}\,]\\ \times [1+\Phi(x_1)+\{1+\Phi(x_1)\}\Phi\{x(r = r_1\cos\phi - \sqrt{[r^2 - r_1^2\sin^2\phi]})\}]\,,\end{aligned} \tag{33}$$

where $\overline{D(r_1)D(r_2)}$ is a function of r.

Case IV.—The distribution of the absolute magnitudes of the nebulae is Gaussian, and there are fluctuations in the galactic absorption for a given galactic latitude. Under these conditions equation (10′) becomes

$$N(m_o') = \tfrac{1}{2}\omega\bar{\rho}\int_0^\infty d\,r\,r^2\,[1+D(r)]\Big[1+\Phi\Big\{x - W\int_0^\tau dt\,\delta(t)\,,\Big\}\Big] \tag{34}$$

where

$$W \equiv \frac{2.5}{\sigma\sqrt{2}}\log_{10} e \tag{35}$$

and where x has the same meaning as in equation (28), with τ now standing for the mean value of the optical depth for the galactic latitude considered. In obtaining the desired formulae, we shall need expressions for the appropriate mean values of $\Phi(t)$ and $\Phi(t_1)\Phi(t_2)$. In order to obtain these, we first expand the function $\Phi(t)$ in these expressions about x in a Taylor's series and then take the required means of the resulting series. In this manner we obtain, on the scheme of approximation of equation (18),

$$\Big[\Phi\Big\{x - W\int_0^\tau dt\,\delta(t)\Big\}\Big]_{\text{mean}} \simeq \Phi(x) + \tfrac{1}{2}W^2\frac{d^2\Phi}{dx^2}\int_0^\tau\int_0^\tau dt_1 dt_2\,\overline{\delta(t_1)\,\delta(t_2)} \tag{36}$$

and

$$\left[\Phi\left\{x_1 - W\int_0^{\tau} dt_1\,\delta(t_1)\right\}\Phi\left\{x_2 - W\int_0^{\tau} dt_2\,\delta(t_2)\right\}\right]_{\text{mean}} \simeq \Phi(x_1)\,\Phi(x_2)$$
$$+ W^2\,\frac{d\Phi(x_1)}{dx_1}\,\frac{d\Phi(x_2)}{dx_2}\,T_\phi + \tfrac{1}{2}W^2\sum_{\substack{i=1\\ i\neq j}}^{2}\Phi(x_i)\,\frac{d^2\Phi(x_j)}{dx_j^2}\,T_0\,, \tag{37}$$

where we have let $[d^i\Phi(t)/dt^i]_{t=x}$ be denoted by $d^i\Phi(x)/dx^i$. We shall continue to use this notation in the work to follow. Using equations (36) and (37) in equation (34), we have

$$\overline{N} = \tfrac{1}{2}\omega\bar{\rho}\int_0^{\infty} d\,r\,r^2\left[1 + \Phi(x) + \tfrac{1}{2}W^2\,\frac{d^2\Phi(x)}{dx^2}\,T_0\right], \tag{38}$$

$$\overline{NN_\phi} = \tfrac{1}{4}\omega^2\bar{\rho}^2\int_0^{\infty}\int_0^{\infty} d\,r_1 d\,r_2\,r_1^2 r_2^2\,[1 + \overline{D(\boldsymbol{r}_1)\,D(\boldsymbol{r}_2)}\,]$$
$$\times\Big[1 + \Phi(x_1) + \Phi(x_2) + \Phi(x_1)\,\Phi(x_2)$$
$$+ \tfrac{1}{2}W^2\sum_{\substack{i=1\\ i\neq j}}^{2}\{1 + \Phi(x_j)\}\,\frac{d^2\Phi(x_i)}{dx_i^2}\,T_0 + W^2\,\frac{d\Phi(x_1)}{dx_1}\,\frac{d\Phi(x_2)}{dx_2}\,T_\phi\Big], \tag{39}$$

and

$$\overline{N^2} = \tfrac{1}{4}\omega^2\bar{\rho}^2\int_0^{\infty}\int_0^{\infty} d\,r_1 d\,r_2\,r_1^2 r_2^2\,[1 + \overline{D(r_1)\,D(r_2)}\,]$$
$$\times\Big[1 + \Phi(x_1) + \Phi(x_2) + \Phi(x_1)\,\Phi(x_2)$$
$$+ \tfrac{1}{2}W^2\sum_{\substack{i=1\\ i\neq j}}^{2}\left(\{1 + \Phi(x_j)\}\,\frac{d^2\Phi(x_i)}{dx_i^2} + \frac{d\Phi(x_i)}{dx_i}\,\frac{d\Phi(x_j)}{dx_j}\right)T_0\Big]. \tag{40}$$

The expression here for $\overline{NN_\phi}$ is evaluated in the same manner as was described for case III (cf. eqs. [32] and [33]).

IV. THE EVALUATION OF T_0, T_ϕ, Z_0, AND Z_ϕ

We shall express the integrals for T_0, T_ϕ, Z_0, and Z_ϕ in terms of the correlation coefficients, $\Gamma(\boldsymbol{r})$ and $R(t)$, and reduce the resulting expressions as far as possible in the general case. The following forms for the correlation coefficient are then inserted:

$$\text{(i)}\qquad \Gamma(\boldsymbol{r}) = e^{-r/r_0}\,, \qquad R(t) = e^{-t/\tau_0}\,,$$
and
$$\text{(ii)}\qquad \Gamma(\boldsymbol{r}) = e^{-r^2/r_0^2}\,, \qquad R(t) = e^{-t^2/\tau_0^2}\,; \tag{41}$$

and the resulting expressions are evaluated explicitly in terms of elementary functions except in the cases of T_ϕ and Z_ϕ, where one of the integrations must be performed numerically for certain of the terms.

The integral T_0.—From equations (12) and (22),

$$T_0 = \alpha^2\int_0^{\tau}\int_0^{\tau} dt_1 dt_2\,R(|t_1 - t_2|)\,. \tag{42}$$

Making use of symmetry, changing variables, and inverting the order of integration, we find that

$$T_0 = 2\alpha^2 \int_0^{\bar\tau} dt R(t)(\bar\tau - t) . \tag{43}$$

Inserting the two forms for $R(t)$ of equation (41), we obtain

$$T_0 = 2\alpha^2 \tau_0 \{ \bar\tau - \tau_0 (1 - e^{-\bar\tau/\tau_0}) \} \qquad \text{(for i)} \tag{44}$$

and

$$T_0 = \alpha^2 \{ \sqrt{[\pi]}\, \bar\tau \tau_0 \Phi\left(\frac{\bar\tau}{\tau_0}\right) - \tau_0^2 (1 - e^{-\bar\tau^2/\tau_0^2}) \} \qquad \text{(for ii)} , \tag{45}$$

respectively.

The integral T_ϕ.—From equations (12) and (25),

$$T_\phi = \alpha^2 \int_0^{\bar\tau} \int_0^{\bar\tau} dt_1 dt_2 R(|t_1 - t_2|) . \tag{46}$$

Changing variables and proceeding in the manner of Paper V, we arrive at the following expression

$$T_\phi = 2\alpha^2 \left\{ \frac{1}{\epsilon} \left[\tfrac{1}{2}\pi \int_0^{\bar\tau\epsilon} dt R(t)\, t + \int_{\bar\tau\epsilon}^{\bar\tau} dt R(t)\, t \sin^{-1}\left(\frac{\tau\epsilon}{t}\right) \right] - \int_0^{\bar\tau} dt R(t)\, t \right\} , \tag{47}$$

where we have assumed that ϕ is so small that we may write

$$\sin\phi \simeq 2 \sin\frac{\phi}{2} \simeq \phi \equiv \epsilon . \tag{48}$$

If we now substitute for $R(t)$ from equation (41), we obtain

$$\begin{aligned} T_\phi = 2\alpha^2 \Bigg\{ \frac{1}{\epsilon} \Bigg[\tfrac{1}{2}\pi\tau_0^2 \left(1 - \left\{\frac{\bar\tau\epsilon}{\tau_0} + 1\right\} e^{-\bar\tau\epsilon/\tau_0}\right) \\ + \int_{\bar\tau\epsilon}^{\bar\tau} dt\, e^{-t/\tau_0} t \sin^{-1}\left(\frac{\bar\tau\epsilon}{t}\right) \Bigg] - \tau_0^2 \left[1 - \left\{\frac{\bar\tau}{\tau_0} + 1\right\} e^{-\bar\tau/\tau_0} \right] \Bigg\} \end{aligned} \qquad \text{(for i)} \tag{49}$$

and

$$\begin{aligned} T_\phi = 2\alpha^2 \Bigg\{ \frac{1}{\epsilon} \Bigg[\tfrac{1}{4}\pi\tau_0^2 (1 - e^{-\bar\tau^2\epsilon^2/\tau_0^2}) \\ + \int_{\bar\tau\epsilon}^{\bar\tau} dt\, e^{-t^2/\tau_0^2} t \sin^{-1}\left(\frac{\bar\tau\epsilon}{t}\right) \Bigg] - \tfrac{1}{2}\tau_0^2 [1 - e^{-\bar\tau^2/\tau_0^2}] \Bigg\} , \end{aligned} \qquad \text{(for ii)} \tag{50}$$

respectively.

The integral Z_0.—From equations (4) and (16),

$$Z_0 = \beta^2 \int_0^A \int_0^A d r_1 d r_2 r_1^2 r_2^2 \Gamma(|r_1 - r_2|) . \tag{51}$$

Upon changing variables and inverting the order of integration, we are able to integrate once and obtain:

$$\begin{aligned} Z_0 = \beta^2 \Big\{ \tfrac{2}{5} A^5 \int_0^A d r \Gamma(r) - A^4 \int_0^A d r\, r \Gamma(r) \\ + \tfrac{2}{3} A^3 \int_0^A d r\, r^2 \Gamma(r) - \tfrac{1}{15} \int_0^A d r\, r^5 \Gamma(r) \Big\} . \end{aligned} \tag{52}$$

Substituting for $\Gamma(r)$ from equation (41), we have, after some reductions,

$$\begin{aligned} Z_0 = \beta^2 \{ [-8 r_0^6 + \tfrac{4}{3} A^3 r_0^3 - A^4 r_0^2 + \tfrac{2}{5} A^5 r_0] & \\ + [8 A r_0^5 + 4 A^2 r_0^4 + 8 r_0^6] \, e^{-A/r_0} \} & \end{aligned} \qquad \text{(for i)} \quad (53)$$

and

$$\begin{aligned} Z_0 = \beta^2 \{ [-\tfrac{1}{15} r_0^6 - \tfrac{1}{2} A^4 r_0^2] + [\tfrac{1}{5} \sqrt{(\pi)} \, A^5 r_0 + \tfrac{1}{6} \sqrt{(\pi)} \, A^3 r_0^3] \, \Phi\left(\frac{A}{r_0}\right) & \\ + [\tfrac{1}{15} r_0^6 + \tfrac{1}{15} A^2 r_0^4 + \tfrac{1}{5} A^4 r_0^2] \, e^{-A^2/r_0^2} \} , & \end{aligned} \qquad \text{(for ii)} \quad (54)$$

respectively.

The integral Z_ϕ.—From equations (4) and (16),

$$Z_\phi = \beta^2 \int_0^A \int_0^A d r_1 d r_2 r_1^2 r_2^2 \Gamma (| r_1 - r_2 |) . \qquad (55)$$

We first perform a change of variables and invert the order of the integrations as in the case of T_ϕ. The resulting expression is

$$\begin{aligned} Z_\phi = 2\beta^2 \{ \int_0^{A\epsilon} d r \, r \Gamma(r) \int_r^{r/\epsilon} d r_1 \left(\frac{r_1^4 \cos^2 \phi}{\sqrt{[r^2 - r_1^2 \epsilon^2]}} + r_1^2 \sqrt{[r^2 - r_1^2 \epsilon^2]} - 2 r_1^3 \cos \phi \right) & \\ + \int_{A\epsilon}^A d r \, r \Gamma(r) \int_r^A d r_1 \left(\frac{r_1^4 \cos^2 \phi}{\sqrt{[r^2 - r_1^2 \epsilon^2]}} + r_1^2 \sqrt{[r^2 - r_1^2 \epsilon^2]} - 2 r_1^3 \cos \phi \right) \} . & \end{aligned} \qquad (56)$$

The integration of the second and third terms of the two integrands is straightforward. The first term can be put into the form of a standard integral by means of an appropriate change of variables. Integrating once, we then obtain, in the scheme of approximation represented by equation (48),

$$\begin{aligned} Z_\phi = \beta^2 \int_{A\epsilon}^A d r \, r \Gamma(r) \{ - A^4 + \frac{r^4}{4\epsilon^5} \Big[+ 3 \sin^{-1} \frac{A\epsilon}{r} - 5 \frac{A\epsilon}{r} \left(1 - \frac{A^2\epsilon^2}{r^2} \right)^{1/2} & \\ + 2 \frac{A\epsilon}{r} \left(1 - \frac{A^2\epsilon^2}{r^2} \right)^{3/2} \Big] \} + \beta^2 \frac{1}{\epsilon^5} \left(\frac{3\pi}{8} - \epsilon \right) \int_0^{A\epsilon} d r \, r^5 \Gamma(r) . & \end{aligned} \qquad (57)$$

Two terms of this expression can be integrated explicitly for the two forms for the correlation coefficient, $\Gamma(r)$, of equation (41); the evaluation of the integrals containing the other terms can be obtained by numerical methods. Upon carrying out the two integrations which can be performed explicitly, we have

$$\begin{aligned} Z_\phi = \beta^2 \{ - A^4 [(r_0^2 - A\epsilon r_0) \, e^{-A\epsilon/r_0} - (r_0^2 - A r_0) \, e^{-A/r_0}] & \\ + \frac{1}{4\epsilon^5} \int_{A\epsilon}^A d r \, r^5 e^{-r/r_0} \Big[+ 3 \sin^{-1} \frac{A\epsilon}{r} - 5 \frac{A\epsilon}{r} \left(1 - \frac{A^2\epsilon^2}{r^2} \right)^{1/2} & \\ + 2 \frac{A\epsilon}{r} \left(1 - \frac{A^2\epsilon^2}{r^2} \right)^{3/2} \Big] \} + \beta^2 \frac{1}{\epsilon^5} \left(\frac{3\pi}{8} - \epsilon \right) \{ + 120 r_0^6 & \\ + [- A^5 \epsilon^5 r_0 - 5 A^4 \epsilon^4 r_0^2 - 20 A^3 \epsilon^3 r_0^3 - 60 A^2 \epsilon^2 r_0^4 & \\ - 120 r_0^5 (A\epsilon + r_0)] \, e^{-A\epsilon/r_0} \} & \end{aligned} \qquad \text{(for i)} \quad (58)$$

and

$$Z_\phi = \beta^2 \Big\{ -\frac{A^4 r_0^2}{2}\left(e^{-A^2\epsilon^2/r_0^2} - e^{-A^2/r_0^2}\right) + \frac{1}{4\epsilon^5}\int_{A\epsilon}^{A} d\,r\, r^5 e^{-r^2/r_0^2}$$
$$\times\left[+3\sin^{-1}\frac{A\epsilon}{r} - 5\,\frac{A\epsilon}{r}\left(1-\frac{A^2\epsilon^2}{r^2}\right)^{1/2} + 2\,\frac{A\epsilon}{r}\left(1-\frac{A^2\epsilon^2}{r^2}\right)^{3/2}\right]\Big\} \qquad \text{(for ii)} . \tag{59}$$
$$+\beta^2\frac{1}{\epsilon^5}\left(\frac{3\pi}{8}-\epsilon\right)\Big\} + r_0^6 + \left[-\tfrac{1}{2}A^4\epsilon^4 r_0^2 - r_0^4\left(A^2\epsilon^2 + r_0^2\right)\right] e^{-A^2\epsilon^2/r_0^2}\Big\}$$

V. THE METHOD OF ANALYSIS

The extragalactic nebulae must be viewed through the absorbing matter of our own galaxy, which, according to various estimates, has a half-thickness of the order of 0.30 mag. In view of the observed highly irregular distribution of the interstellar matter in the lower latitudes, it seems rather probable that similar fluctuations in optical thickness occur in the higher latitudes as well. It follows that such fluctuations alone could account for at least a part of any observed irregularities in the counts of the extragalactic nebulae. Since it is not at all obvious that these effects will be unimportant, it would seem desirable to take them into account, if at all possible. Otherwise the parameters derived from any analysis of these counts may not be truly representative of the actual space distribution of the nebulae. In the absence of detailed knowledge concerning the optical thickness of the galaxy as a function of direction, it seems that the foregoing developments for either case II or case IV offer as satisfactory a method for including such effects as can be hoped for.

The investigations of the fluctuations in brightness of the Milky Way which have been carried out by Chandrasekhar and Münch[3] and by the writer[4] provide the values of the interstellar absorption parameters required in removing these effects. These parameters were determined from observations in and near the plane of the galaxy, so that one must either assume that the parameters remain the same for all galactic latitudes or make an appropriate extrapolation assumption. In view of the fact that no pronounced changes were noted by the writer in the range from 0° to 15° in galactic latitude, it seems reasonable to assume—at least as a first approximation—that these parameters are independent of latitude.

With the values of the absorption parameters derived in these Milky Way investigations, the integrals T_0 and T_ϕ can be computed as functions of τ. Using these values, we can then proceed to analyze the counts of the nebulae for the nebular parameters $\bar{\rho}$, β^2, and r_0.

The determination of $\bar{\rho}$, $\bar{\tau}(b)$, β^2, *and* r_0 *for cases I and II.*—We shall now outline a method for analyzing counts of the nebulae for $\bar{\rho}$, β^2, and r_0 for case II; the necessary modifications for the analysis according to case I will be evident.

From equation (21) we have, for a given galactic latitude, b_1,

$$\frac{\overline{N(b_1)}}{\frac{1}{3}\omega\left[1+{}^{9}T_0(b_1)\right]} = \bar{\rho}A^3 . \tag{60}$$

Dividing this by the corresponding expression for another galactic latitude, b_2, and using equation (13), we obtain

$$\frac{1}{1.5\log_{10} e}\log_{10}\left[\frac{\overline{N(b_1)}}{N(b_2)}\,\frac{\left\{1+\frac{9}{8}T_0(b_2)\right\}}{\left\{1+\frac{9}{8}T_0(b_1)\right\}}\right] = \bar{\tau}(b_2) - \tau(b_1) . \tag{61}$$

Since $T_0(b_1)$ and $T_0(b_2)$ are of the nature of corrections, we can use approximate values for $\bar{\tau}$ in their evaluation. The quantities on the left-hand side are then either known or observed. If we now assume a general cosecant law for the galactic mean absorption, we are able to determine the half-thickness, $\bar{\tau}_{1/2}$, of the galactic absorbing matter. We have

---

[3] *Ibid.*

[4] D. N. Limber, *Ap. J.*, **117**, 145, 1953.

$$\bar{\tau}\,(b_i) = \bar{\tau}_{1/2} \operatorname{cosec} b_i \,, \tag{62}$$

and thus

$$\bar{\tau}_{1/2} = \frac{\bar{\tau}\,(b_1) - \bar{\tau}\,(b_2)}{\operatorname{cosec} b_1 - \operatorname{cosec} b_2} \,. \tag{63}$$

A best value for $\tau_{1/2}$ can be obtained from an analysis of the observed counts for different pairs of galactic latitudes, b_1 and b_2, by means of equation (63). With the half-thickness so determined, we can obtain $\bar{\tau}(b)$ by means of equation (61) or (62). If the resulting values of $\bar{\tau}(b)$ differ significantly from those used in the preliminary evaluation of $T_0(b)$, then the new results should be used in re-evaluating this latter function. Using these improved values in equation (61) and repeating the above process, we can obtain a second approximation to both $\bar{\tau}(b)$ and $\bar{\tau}_{1/2}$. This iteration process can be expected to give the required numerical result after only a few iterations. Paving determined $\bar{\tau}(b)$, we then analyze the observations by means of equation (21) and determine $\bar{\rho}$.

Next, we have, from equations (21), (24), and (26),

$$\frac{(\overline{N^2} - \overline{N}\,\overline{N_\phi}) - (T_0' - T_\phi')}{(\overline{N^2} - \overline{N}^2) - T_0'} = \frac{Z_0 - Z_\phi}{Z_0} \equiv f\,(r_0,\, A\,,\, \phi)\,, \tag{64}$$

where we have defined

$$T_0' \equiv \tfrac{1}{4}\omega^2 \bar{\rho}^2 A^6 T_0 \qquad \text{and} \qquad T_\phi' \equiv \tfrac{1}{4}\omega^2 \bar{\rho}^2 A^6 T_\phi \,. \tag{65}$$

Since the left-hand side of equation (64) contains only known and observable quantities and the right-hand side is a known function of arguments among which only r_0 is unknown, we can determine r_0 by means of this equation. This should then be independent of the particular galactic latitude and ϕ used in its determination, and the deviations from such a condition will provide a valuable measure of the accuracy of the r_0 determination. Having determined $\bar{\tau}(b)$, $\bar{\rho}$, and r_0, we are able to evaluate the final parameter, β^2, by means of equation (26).

The determination of $\bar{\rho}$, $\bar{\tau}(b)$, β^2, and r_0 for cases III and IV.—Here we shall restrict our remarks to case IV; the modifications which are required in applying this method to case III will be apparent.

We must first evaluate the expressions for $T_0[\bar{\tau}(b)]$ (cf. eqs. [44] and [45]). In order to do this, we make use of the values of $\bar{\tau}(b)$ which have been determined from an analysis according to case II. Since the function $T_0(b)$ is of the nature of a correction term, the errors introduced by this approximation may be expected to be small. From equation (38),

$$\frac{\overline{N\,(b_1)}}{\overline{N\,(b_2)}} = \frac{f\,(M_0,\, m_o',\, \bar{\tau}\,[\,b_1]\,,\, T_0\,[\,b_1]\,)}{f\,(M_0,\, m_o',\, \bar{\tau}\,[\,b_2]\,,\, T_0\,[\,b_2]\,)} \,. \tag{66}$$

Hence, knowing M_0 and m_o' and assuming a cosecant law, we can determine a second approximation to $\bar{\tau}(b)$. Using these results, we can correct the $T_0[\bar{\tau}(b)]$ values and repeat the process, obtaining a still higher approximation to $\bar{\tau}(b)$. However, if the values of $\bar{\tau}(b)$ of the second approximation do not differ appreciably from those of the case II solution, then such an iteration will not be necessary, and we can immediately go on to obtain $\bar{\rho}$ from equation (38).

We must next determine r_0 by analyzing the expression (cf. eqs. [38], [39], and [40]):

$$\frac{\overline{N^2} - \overline{N}\,\overline{N_\phi}}{\overline{N^2} - \overline{N}^2} = f\,(M_0,\, m_o',\, \phi,\, \bar{\tau}\,[\,b\,]\,,\, r_0)\,, \tag{67}$$

the β^2 factors having canceled. Using the value for $\bar{\tau}(b)$ determined earlier, we obtain a best value for r_0 by a numerical process of trial and error—appropriate trial values being selected on the basis of the r_0 results of the case II solution. Having $\bar{\rho}$ and r_0, we can then determine β^2 from equation (40).

VI. CONCLUDING REMARKS

The relative importance of the galactic absorption terms can be readily determined by simply analyzing the observations by means of both case I and case II. A comparison of the resulting two sets of parameters characterizing the distribution of the nebulae will then show clearly whether or not these effects are significant. Independent of the importance of galactic absorption, it is felt that the analysis of the nebular counts in terms of a fluctuating density field will prove valuable, at least as a first step. The resulting parameters may be expected to describe the essential nature of the distribution of the nebulae with a minimum of assumptions.

In concluding, I should like to acknowledge my indebtedness and gratitude to Professor Chandrasekhar, who suggested that such a treatment of the problem would prove useful.

FLUCTUATIONS IN BRIGHTNESS OF THE MILKY WAY

D. Nelson Limber
Yerkes Observatory

Received August 11, 1952

ABSTRACT

In this paper the recent Chandrasekhar-Münch theory of fluctuations in the brightness of the Milky Way in terms of a fluctuating field of absorbing matter is extended to systems of finite extent. The theoretical extensions necessary for the analysis of observational material are developed, and the analysis of Pannekoek's isophotal charts of the Southern Milky Way is carried out. The latitude dependence of the brightness correlations given by the theory is found to give satisfactory agreement with the observations for: (1) a microscale of the fluctuations of 0.01 in units of the mean optical thickness; (2) a root mean square of the fluctuations in the density of $5\bar{\rho}$; and an "effective" half-thickness of the relevant galactic absorbing matter of $0^{m}_{\cdot}20$.

1. *Introduction.*—In a recent paper[1] S. Chandrasekhar and G. Münch have proposed a new picture for the distribution of the interstellar matter. They assume that the coefficient of general absorption, κ, and the density of the interstellar medium, ρ, are continuous functions[2] of position, $\boldsymbol{r}$, which are subject to fluctuations. They then write

$$\kappa\rho(\boldsymbol{r}) = \overline{\kappa\rho}\,[1+\delta(\boldsymbol{r})]\,, \tag{1}$$

where the mean coefficient of volume absorption, $\overline{\kappa\rho}$, is assumed to remain constant throughout the medium and where $\delta(\boldsymbol{r})$ is a chance variable whose expectation value is zero:

$$\overline{\delta(\boldsymbol{r})} = 0\,. \tag{2}$$

The following further assumptions are made concerning $\delta(\boldsymbol{r})$:

$$\overline{\delta^2(\boldsymbol{r})} = \alpha^2\,. \tag{3}$$

and

$$\overline{\delta(\boldsymbol{r}_1)\,\delta(\boldsymbol{r}_2)} = \alpha^2 R(|\boldsymbol{r}_1-\boldsymbol{r}_2|)\,, \tag{4}$$

where α^2 is a constant independent of position and $R(\boldsymbol{r})$ is the correlation coefficient of the fluctuations $\delta(\boldsymbol{r})$ at the two points. It is assumed that the correlation coefficient depends only upon the separation of the two points considered.

It seems reasonable to suppose that the variation in the mass-absorption coefficient with position will be outweighed by that in the density, so that we may write equation (1) in the following way:

$$\kappa\rho(\boldsymbol{r}) = \kappa\bar{\rho}\,[1+\delta\rho]\,, \tag{5}$$

where $\delta\rho$ is a function of $\boldsymbol{r}$. In this case the parameter α^2 has the simple interpretation

$$\alpha^2 = \frac{\overline{\delta^2\rho}}{\rho^2} \tag{6}$$

---

[1] S. Chandrasekhar and G. Münch, *Ap. J.*, **115**, 103, 1952; this paper will be referred to hereafter as "Paper V."

[2] There is actually no reason why these functions must be so restricted as to be continuous. They can have discontinuities of various kinds without introducing any essential changes into the method of analysis given. Of course, the analysis might well be more complicated if the most general kind of discontinuities admissible is considered.

and is thus the mean square of the fluctuations in the density in units of the square of the mean density itself.

Chandrasekhar and Münch have applied this new picture to the problem of fluctuations in brightness of the Milky Way. Restricting themselves to the case of a system of infinite extent in the direction analyzed, they developed the necessary formulae for the analysis of the observational data. Using material selected from Pannekoek's isophotal charts of the Southern Milky Way for galactic latitudes from +2° to −2°, they then carried out an analysis for the following assumed forms for the correlation coefficient:

$$R(t) = e^{-t/\tau_0} \quad \text{and} \quad R(t) = e^{-t^2/\tau_0^2}, \tag{7}$$

where τ_0 is the microscale of the density distribution. In this way values of the parameters $\mathfrak{a}^2$ and τ_0 were obtained.

2. *The extension of the Chandrasekhar-Münch development to the case of a system of finite extent.*

i) *The fundamental expression for the brightness of the Milky Way in a direction in which the extent of the system is S.*—From equation (5) it follows that the true optical depth, $\tau(s)$, corresponding to a distance s can be expressed in terms of the mean optical depth, $\bar{\tau}(s)$, and the density fluctuation, $\delta\rho$, in the following way:

$$\tau(s) = \bar{\tau}(s) + \int_0^{\bar{\tau}(s)} \delta(t)\, dt, \tag{8}$$

where

$$\bar{\tau}(s) \equiv \bar{\kappa}\bar{\rho}\int_0^s ds' = \bar{\kappa}\bar{\rho}s \tag{9}$$

and where

$$\delta(t) \equiv \bar{\kappa}\bar{\rho}\,\delta\rho\,. \tag{10}$$

Let us now assume that the star density is constant within the system and zero outside. We assume, further, that the interstellar matter, statistically, is distributed uniformly throughout the stellar system. We shall then have for the brightness, u, of the Milky Way, in appropriate units, in a direction in which the extent of the system is S:

$$u = \int_0^T e^{-\tau(s)}\, d\bar{\tau}, \tag{11}$$

where for convenience we have let $\bar{\tau}(S)$ be denoted by T. Substituting for $\tau(s)$ from equation (8), we perform a series expansion upon the term containing the integral with $\delta(t)$ as integrand. If we then retain powers of this integral up to and including the second—in keeping with the scheme of approximation of Paper V—we obtain the fundamental relation

$$u = \int_0^T d\tau\, e^{-\tau}\left\{1 - \int_0^\tau dt\,\delta(t) + \frac{1}{2}\int_0^\tau\int_0^\tau dt_1 dt_2\,\delta(t_1)\,\delta(t_2)\right\}, \tag{12}$$

where we have suppressed the bar on $\bar{\tau}(s)$ for simplicity. We shall continue to suppress the bars in the work to follow whenever there is no danger of confusion.

From equation (12) we readily obtain for the mean value of the brightness in a direction in which the extent of the system is S the expression

$$\bar{u} = \int_0^T d\tau\, e^{-\tau}\left\{1 + \frac{1}{2}\int_0^\tau\int_0^\tau dt_1 dt_2\,\overline{\delta(t_1)\,\delta(t_2)}\right\}. \tag{13}$$

Substituting for $\overline{\delta(t_1)\delta(t_2)}$ from equation (4), we obtain

$$\bar{u} = \int_0^T d\tau\, e^{-\tau}\left\{1 + \tfrac{1}{2}\mathfrak{a}^2\int_0^\tau\int_0^\tau dt_1 dt_2 R(|t_1 - t_2|)\right\}. \tag{14}$$

The integration of the first term presents no difficulties. Making the substitution

$$t = t_2 - t_1 \, , \tag{15}$$

we can invert the order of integration and carry out two of the three integrations arising from the second term. The resulting expression is

$$\bar{u} = 1 + \alpha^2 \int_0^T dt R(t) \, e^{-t} + e^{-T} \Big[-1 - \alpha^2 (T+1) \int_0^T dt R(t) + \alpha^2 \int_0^T dt R(t) \, t \Big] \, . \tag{16}$$

ii) *The expression for* $\overline{u^2(S)}$.—We first square the expression for u given in equation (12),

$$\begin{aligned} u^2 = \int_0^T \int_0^T d\tau_1 d\tau_2 e^{-\tau_1 - \tau_2} \Big\{ 1 - \int_0^{\tau_1} dt \, \delta(t) + \frac{1}{2} \int_0^{\tau_1} \int_0^{\tau_1} dt_1 dt_2 \, \delta(t_1) \, \delta(t_2) \Big\} \\ \times \Big\{ 1 - \int_0^{\tau_2} dt \, \delta(t) + \frac{1}{2} \int_0^{\tau_2} \int_0^{\tau_2} dt_1 dt_2 \, \delta(t_1) \, \delta(t_2) \Big\} \, . \end{aligned} \tag{17}$$

Upon expanding the quantities on the right-hand side, taking the mean, inserting the correlation function for $\overline{\delta(t_1)\delta(t_2)}$, and retaining only those terms consistent with the scheme of approximation we are using, we obtain

$$\begin{aligned} \overline{u^2} = \int_0^T \int_0^T d\tau_1 d\tau_2 e^{-\tau_1 - \tau_2} \Big\{ 1 + \tfrac{1}{2} \alpha^2 \int_0^{\tau_1} \int_0^{\tau_1} dt_1 dt_2 R(|t_1 - t_2|) \\ + \tfrac{1}{2} \alpha^2 \int_0^{\tau_2} \int_0^{\tau_2} dt_1 dt_2 R(|t_1 - t_2|) + \alpha^2 \int_0^{\tau_1} \int_0^{\tau_2} dt_1 dt_2 R(|t_1 - t_2|) \Big\} \, . \end{aligned} \tag{18}$$

We shall consider the four terms of this integral in turn.

The first term presents no difficulty:

$$\int_0^T \int_0^T d\tau_1 d\tau_2 e^{-\tau_1 - \tau_2} = 1 - 2 e^{-T} + e^{-2T} \, . \tag{19}$$

In reducing the second term, we first carry out the integration over τ_2. Then, introducing the change of variables of equation (15) and inverting the order of integration twice, we obtain, after some reductions,

$$\begin{aligned} \tfrac{1}{2} \alpha^2 \int_0^T \int_0^T d\tau_1 d\tau_2 e^{-\tau_1 - \tau_2} \int_0^{\tau_1} \int_0^{\tau_1} dt_1 dt_2 R(|t_1 - t_2|) = \alpha^2 \Big\{ \int_0^T dt R(t) \, e^{-t} \\ + e^{-T} \Big[\int_0^T dt R(t) \, t - \int_0^T dt R(t) \, e^{-t} - (T+1) \int_0^T dt R(t) \Big] \\ + e^{-2T} \Big[(T+1) \int_0^T dt R(t) - \int_0^T dt R(t) \, t \Big] \Big\} \, . \end{aligned} \tag{20}$$

Since the third term is identical with the second, it, too, gives the expression on the right-hand side of equation (20). The fourth term can be simplified by inverting the order of integration twice; we obtain

$$\begin{aligned} \int_0^T \int_0^T d\tau_1 d\tau_2 e^{-\tau_1 - \tau_2} \int_0^{\tau_1} \int_0^{\tau_2} dt_1 dt_2 R(|t_1 - t_2|) = \alpha^2 \int_0^T \int_0^T dt_1 dt_2 R(|t_1 - t_2|) \\ \times \left[e^{-t_1 - t_2} - e^{-T - t_1} - e^{-T - t_2} + e^{-2T} \right] \, . \end{aligned} \tag{21}$$

We next introduce the change of variables of equation (15) and perform the indicated inversions in the order of integration. We are then able to carry out one of the two integrations for each of the terms. After some simplification it is found that

$$\alpha^2 \int_0^T \int_0^T d\tau_1 d\tau_2 e^{-\tau_1-\tau_2} \int_0^{\tau_1} \int_0^{\tau_2} dt_1 dt_2 R(|t_1-t_2|) = \alpha^2 \Big\{ \int_0^T dt R(t)\, e^{-t}$$

$$+ e^{-T}\Big[-2\int_0^T dt R(t) - 2\int_0^T dt R(t)\, e^{-t}\Big] \tag{22}$$

$$+ e^{-2T}\Big[\int_0^T dt R(t)\, e^{+t} - 2\int_0^T dt R(t)\, t + 2(T+1)\int_0^T dt R(t)\Big]\Big\}.$$

Upon combining the results of equations (19), (20), and (22)—the second of these to be multiplied by a factor of 2—we have

$$\overline{u^2} = 1 - 2e^{-T} + e^{-2T} + \alpha^2\Big\{3\int_0^T dt R(t)\, e^{-t}$$

$$+ e^{-T}\Big[2\int_0^T dt R(t)\, t - 2(T+2)\int_0^T dt R(t) - 4\int_0^T dt R(t)\, e^{-t}\Big] \tag{23}$$

$$+ e^{-2T}\Big[\int_0^T dt R(t)\, e^{+t} + 4(T+1)\int_0^T dt R(t) - 4\int_0^T dt R(t)\, t\Big]\Big\}.$$

iii) *The expression for the angular correlation* $\overline{uu_\phi}$.—In the following work the notation $\overline{uu_\phi}$ will be used to denote the product of the values for the brightness of the Milky Way in two directions which are separated by an angle ϕ. If the extent of the system in one of these two directions is S_1 and its extent in the other is S_2, we then obtain, from equation (12),

$$\overline{uu_\phi} = \int_0^{T_1}\int_0^{T_2} d\tau_1 d\tau_2 e^{-\tau_1-\tau_2}\Big\{1 + \tfrac{1}{2}\alpha^2\int_0^{\tau_1}\int_0^{\tau_1} dt_1 dt_2 R(|t_1-t_2|)$$

$$+ \tfrac{1}{2}\alpha^2\int_0^{\tau_2}\int_0^{\tau_2} dt_1 dt_2 R(|t_1-t_2|) + \alpha^2\int_0^{\tau_1}\int_0^{\tau_2} dt_1 dt_2 R(|\mathbf{t}_1-\mathbf{t}_2|)\Big\} \tag{24}$$

$$= A + B + C + D \qquad \text{(say)},$$

where T_1 and T_2 are used to denote $\bar{\tau}(S_1)$ and $\bar{\tau}(S_2)$, respectively. The case in which the two directions considered are not collinear has been distinguished from that in which they are collinear by writing $\mathbf{t}_1$ and $\mathbf{t}_2$ in the former case and t_1 and t_2 in the latter for the arguments of the correlation coefficient. Hence $|\mathbf{t}_1 - \mathbf{t}_2| \neq |t_1 - t_2|$. As in the case of $\overline{u^2}$, we shall consider each of the four terms of the integrand in turn.

The first of these terms gives

$$A \equiv \int_0^{T_1}\int_0^{T_2} d\tau_1 d\tau_2 e^{-\tau_1-\tau_2} = 1 - e^{-T_1} - e^{-T_2} + e^{-T_1-T_2}. \tag{25}$$

The second and third terms are just the corresponding terms of the $\overline{u^2}$ development when we take into account the fact that the two limits are now different. Thus, substituting T_1 and T_2 for T in the appropriate places in that solution, we arrive at the following:

$$B \equiv \tfrac{1}{2}\alpha^2\int_0^{T}\int_0^{T_2} d\tau_1 d\tau_2 e^{-\tau_1-\tau_2}\int_0^{\tau_1}\int_0^{\tau_1} dt_1 dt_2 R(|t_1-t_2|)$$

$$= \boldsymbol{\alpha}^2 \Big\{ \int_0^{T_1} dt R(t)\, e^{-t} + e^{-T_1} \Big[\int_0^{T_1} dt R(t)\, t - (T_1+1) \int_0^{T_1} dt R(t) \Big] \tag{26}$$
$$- e^{-T_2} \int_0^{T_1} dt R(t)\, e^{-t} + e^{-T_1-T_2} \Big[(T_1+1) \int_0^{T_1} dt R(t) - \int_0^{T_1} dt R(t)\, t \Big] \Big\}$$

and

$$C \equiv \tfrac{1}{2} \boldsymbol{\alpha}^2 \int_0^{T_1} \int_0^{T_2} d\tau_1 d\tau_2\, e^{-\tau_1-\tau_2} \int_0^{\tau_2} \int_0^{\tau_2} dt_1 dt_2 R(|t_1-t_2|)$$
$$= \boldsymbol{\alpha}^2 \Big\{ \int_0^{T_2} dt R(t)\, e^{-t} + e^{-T_2} \Big[\int_0^{T_2} dt R(t)\, t - (T_2+1) \int_0^{T_2} dt R(t) \Big] \tag{27}$$
$$- e^{-T_1} \int_0^{T_2} dt R(t)\, e^{-t} + e^{-T_1-T_2} \Big[(T_2+1) \int_0^{T_2} dt R(t) - \int_0^{T_2} dt R(t)\, t \Big] \Big\} .$$

The reduction of the fourth term is somewhat more lengthy. Inverting the order of integration twice, we have

$$D \equiv \boldsymbol{\alpha}^2 \int_0^{T_1} \int_0^{T_2} d\tau_1 d\tau_2\, e^{-\tau_1-\tau_2} \int_0^{\tau_1} \int_0^{\tau_2} dt_1 dt_2 R(|\mathbf{t}_1-\mathbf{t}_2|)$$
$$= \boldsymbol{\alpha}^2 \Big\{ \int_0^{T_1} \int_0^{T_2} dt_1 dt_2 R(|\mathbf{t}_1-\mathbf{t}_2|)\, e^{-t_1-t_2}$$
$$- e^{-T_1} \int_0^{T_1} \int_0^{T_2} dt_1 dt_2 R(|\mathbf{t}_1-\mathbf{t}_2|)\, e^{-t_2} \tag{28}$$
$$- e^{-T_2} \int_0^{T_1} \int_0^{T_2} dt_1 dt_2 R(|\mathbf{t}_1-\mathbf{t}_2|)\, e^{-t_1}$$
$$+ e^{-T_1-T_2} \int_0^{T_1} \int_0^{T_2} dt_1 dt_2 R(|\mathbf{t}_1-\mathbf{t}_2|) \Big\} .$$

We shall denote the four terms which make up D by D_1, D_2, D_3, and D_4, respectively, and consider each in turn.

In equation (28)

$$|\mathbf{t}_1-\mathbf{t}_2| \equiv t = \sqrt{[t_1^2+t_2^2-2t_1t_2\cos\phi]} . \tag{29}$$

or

$$t_2 = t_1\cos\phi \pm \sqrt{[t^2-t_1^2\sin^2\phi]} . \tag{30}$$

We shall be interested only in values of ϕ which are so small that we can write

$$\sin\phi \simeq \phi \equiv \epsilon \qquad \text{and} \qquad \cos\phi \simeq 1 . \tag{31}$$

In keeping with this degree of approximation, we shall neglect powers of ϵ higher than the first in the further analysis.

There is no loss of generality in assuming that

$$T_1 \geqslant T_2 . \tag{32}$$

Making use of the symmetry of the integrand, we can write the integral D_1 as follows:

$$D_1 = \boldsymbol{\alpha}^2 \Big\{ 2 \int_0^{T_2} dt_1 \int_0^{t_1} dt_2 R(|\mathbf{t}_1-\mathbf{t}_2|)\, e^{-t_1-t_2}$$
$$+ \int_{T_2}^{T_1} dt_1 \int_0^{T_2} dt_2 R(|\mathbf{t}_1-\mathbf{t}_2|)\, e^{-t_1-t_2} \Big\} . \tag{33}$$

We shall denote the first of these terms by $D_{1,1}$ and the second by $D_{1,2}$. Since t_1 and t_2 are not collinear, we introduce the change of variables (cf. eq. [30]):

$$t_2 = t_1 - \sqrt{[t^2 - t_1^2\epsilon^2]}\,, \tag{34}$$

the negative sign being taken because $t_2 \leqslant t_1$ in equation (33). We then obtain

$$D_{1,1} = 2\alpha^2 \int_0^{T_2} dt_1 \int_{t_1\epsilon}^{t_1} dt R(t)\, t\, \frac{\exp(-2t_1 + \sqrt{[t^2 - t_1^2\epsilon^2]})}{\sqrt{[t^2 - t_1^2\epsilon^2]}} \tag{35}$$

and

$$D_{1,2} = +\alpha^2 \int_{T_2}^{T_1} dt_1 \int_{\sqrt{[t_1^2 + T_2^2 - 2t_1T_2 \cos\phi]}}^{t_1} dt R(t)\, t\, \frac{\exp(-2t_1 + \sqrt{[t^2 - t_1^2\epsilon^2]})}{\sqrt{[t^2 - t_1^2\epsilon^2]}}\,. \tag{36}$$

Upon inverting the order of integration in equation (35), we find that

$$\begin{aligned} D_{1,1} = 2\alpha^2 \Big\{ & \int_0^{T_2\epsilon} dt R(t)\, t \int_t^{t/\epsilon} dt_1 \frac{\exp(-2t_1 + \sqrt{[t^2 - t_1^2\epsilon^2]})}{\sqrt{[t^2 - t_1^2\epsilon^2]}} \\ & + \int_{T_2\epsilon}^{T_2} dt R(t)\, t \int_t^{T_2} dt_1 \frac{\exp(-2t_1 + \sqrt{[t^2 - t_1^2\epsilon^2]})}{\sqrt{[t^2 - t_1^2\epsilon^2]}} \Big\}\,. \end{aligned} \tag{37}$$

When we invert the order of the integrations in equation (36), we must distinguish between the two cases (cf. Fig. 1):

$$t^* \leqslant T_2 \quad \text{(I)} \qquad \text{and} \qquad t^* \geqslant T_2 \quad \text{(II)}\,, \tag{38}$$

where

$$t^* \equiv \sqrt{[T_1^2 + T_2^2 - 2T_1T_2 \cos\phi]}\,. \tag{39}$$

Here and in the work to follow we shall denote case I by means of a single prime affixed to the *second* subscript in our notation for the D terms; case II will be denoted by means of a double prime affixed to this subscript. Later we shall encounter a further pair of cases to be distinguished (cf. eq. [54]). In marking the distinctions of both equation (38) and equation (54) we shall consistently use *single* and *double primes* to denote the situations referred to as cases I and II, respectively. There is no danger of confusing the two pairs of distinctions marked by these equations when this notation is used, since the distinctions of equation (38) arise only in connection with the second subscript in the notation adopted, whereas those of equation (54) arise only in connection with the third subscript.

In this notation we obtain for $D_{1,2}$:

$$\begin{aligned} D_{1,2'} = \alpha^2 \Big\{ & \int_{T_2\epsilon}^{t^*} dt R(t)\, t \int_{T_2}^{T_2 + \sqrt{[t^2 - T_2^2\epsilon^2]}} dt_1 \frac{\exp(-2t_1 + \sqrt{[t^2 - t_1^2\epsilon^2]})}{\sqrt{[t^2 - t_1^2\epsilon^2]}} \\ & + \int_{t^*}^{T_2} dt R(t)\, t \int_{T_2}^{T_1} dt_1 \frac{\exp(-2t_1 + \sqrt{[t^2 - t_1^2\epsilon^2]})}{\sqrt{[t^2 - t_1^2\epsilon^2]}} \\ & + \int_{T_2}^{T_1} dt R(t)\, t \int_t^{T_1} dt_1 \frac{\exp(-2t_1 + \sqrt{[t^2 - t_1^2\epsilon^2]})}{\sqrt{[t^2 - t_1^2\epsilon^2]}} \Big\} \end{aligned} \tag{40}$$

and

$$D_{1,2''} = \alpha^2 \left\{ \int_{T_2\epsilon}^{T_2} dt R(t)\, t \int_{T_2}^{T_2+\sqrt{[t^2-T_2^2\epsilon^2]}} dt_1 \frac{\exp(-2t_1+\sqrt{[t^2-t_1^2\epsilon^2]})}{\sqrt{[t^2-t_1\epsilon^2]}} \right.$$

$$+ \int_{T_2}^{t^*} dt R(t)\, t \int_{t}^{T_2+\sqrt{[t^2-T_2^2\epsilon^2]}} dt_1 \frac{\exp(-2t_1+\sqrt{[t^2-t_1^2\epsilon^2]})}{\sqrt{[t^2-t_1^2\epsilon^2]}} \tag{41}$$

$$\left. + \int_{t^*}^{T_1} dt R(t)\, t \int_{t}^{T_1} dt_1 \frac{\exp(-2t_1+\sqrt{[t^2-t_1^2\epsilon^2]})}{\sqrt{[t^2-t_1^2\epsilon^2]}} \right\} .$$

We now introduce ψ, defined by

$$t \sin(\psi + \tfrac{1}{2}\epsilon) \equiv t_1\epsilon . \tag{42}$$

and let

$$\sin\psi \equiv y . \tag{43}$$

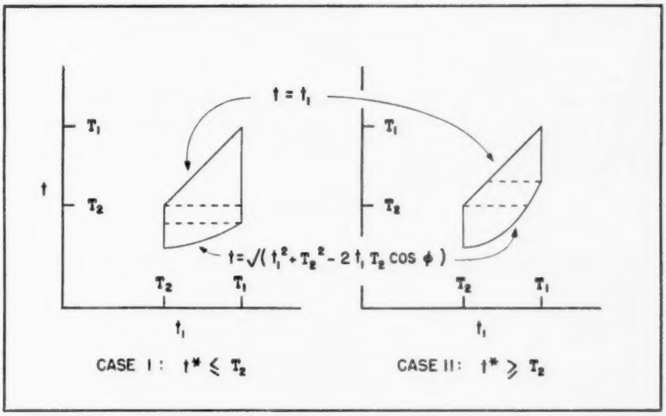

FIG. 1.—The cases to be distinguished upon inverting the order of integration in equation (36)

Retaining only those terms which are consistent with our scheme of approximation, we obtain, upon inverting the order of integration once more,

$$D_{1,1} = 2\frac{\alpha^2}{\epsilon} \left\{ \int_{\epsilon/2}^{1} \frac{dy}{\sqrt{[1-y^2]}} \int_{0}^{T_2\epsilon} dt R(t)\, t\, e^{-2ty/\epsilon} \right.$$

$$\left. + \int_{\epsilon/2}^{1} \frac{dy}{\sqrt{[1-y^2]}} \int_{T_2\epsilon}^{T_2\epsilon/(y+(1/2)\epsilon\sqrt{[1-y^2]})} dt R(t)\, t\, e^{-2ty/\epsilon} \right\} . \tag{44}$$

It will greatly simplify our notation if we introduce the following:

$$X(x, y) \equiv \frac{x\epsilon}{y+\frac{1}{2}\epsilon\sqrt{[1-y^2]}} \quad \text{and} \quad X'(x, y) \equiv \frac{x\epsilon}{y+\epsilon\sqrt{[1-y^2]}} . \tag{45}$$

Certain implicit relationships are encountered in our work. For convenience we shall denote

$$y+\tfrac{1}{2}\epsilon\sqrt{[1-y^2]} - \epsilon\left\{\frac{x}{z}+\sqrt{\left[1-\frac{x^2\epsilon^2}{z^2}\right]}\right\} = 0 \quad \text{by} \quad Y(x, y, z) , \tag{46}$$

$$y+\epsilon\sqrt{[1-y^2]}-\epsilon\left\{\frac{x}{z}+\sqrt{\left[1-\frac{x^2\epsilon^2}{z^2}\right]}\right\}=0 \qquad \text{by} \qquad Y'(x,\,y,\,z)\,, \tag{47}$$

$$y+\tfrac{1}{2}\epsilon\sqrt{[1-y^2]}-\frac{x\epsilon}{z}=0 \qquad \text{by} \qquad Z(x,\,y,\,z)\,, \tag{48}$$

and

$$y+\epsilon\sqrt{[1-y^2]}-\frac{x\epsilon}{z}=0 \qquad \text{by} \qquad Z'(x,\,y,\,z)\,. \tag{49}$$

Finally, we shall let

$$I_i \equiv I\,(M_i'',\,M_i';\,N_i'',\,N_i') \equiv \int_{M_i''}^{M_i'} \frac{dy}{\sqrt{[1-y^2]}} \int_{N_i''}^{N_i'} dtR\,(t)\,t\,e^{-2ty/\epsilon} \tag{50}$$

and

$$I_i' \equiv I_i'\,(M_i'',\,M_i';\,N_i'',\,N_i') \equiv \int_{M_i''}^{M_i'} \frac{dy}{\sqrt{[1-y^2]}} \int_{N_i''}^{N_i'} dtR\,(t)\,t\,e^{-ty/\epsilon}\,. \tag{51}$$

The I_i integrals arise from the D_1 terms, while the I_i' integrals appear in the reduction of the terms for D_2 and D_3. The integration limits for the I_i integrals are given in Table 1; those for the I_i' integrals are given in Table 2.

Equation (44) can now be written

$$D_{1,\,1}=2\,\frac{\alpha^2}{\epsilon}\,(I_1+I_2)\,. \tag{52}$$

The term $D_{1,\,2'}$ gives rise to three further terms. The first of these is

$$D_{1,\,2',\,1}=\frac{\alpha^2}{\epsilon}\,(I_3+I_4)\,. \tag{53}$$

In the reduction of $D_{1,\,2',\,2}$ we must distinguish between two further cases (cf. Fig. 2):

$$\frac{T_1}{T_2}\geqslant\frac{T_2}{t^*} \quad \text{(I)} \qquad \text{and} \qquad \frac{T_1}{T_2}\leqslant\frac{T_2}{t^*} \quad \text{(II)}\,. \tag{54}$$

As stated in the discussion following equation (39), we shall mark this distinction by affixing either a single or a double prime to the *third* subscript in our notation for the D terms. Then

$$D_{1,\,2',\,2'}=\frac{\alpha^2}{\epsilon}\,(I_5+I_6+I_7) \qquad \text{and} \qquad D_{1,\,2',\,2''}=\frac{\alpha^2}{\epsilon}\,(I_8+I_9+I_{10})\,. \tag{55}$$

For the last of the $D_{1,\,2'}$ terms we obtain

$$D_{1,\,2',\,3}=\frac{\alpha^2}{\epsilon}\,I_{11}\,. \tag{56}$$

The $D_{1,\,2''}$ expression gives the following three terms:

$$D_{1,\,2'',\,1}=\frac{\alpha^2}{\epsilon}\,(I_{12}+I_{13})\,, \qquad D_{1,\,2'',\,2}=\frac{\alpha^2}{\epsilon}\,(I_{14}+I_{15})\,, \tag{57}$$

and

$$D_{1,\,2'',\,3}=\frac{\alpha^2}{\epsilon}\,I_{16}\,. \tag{58}$$

TABLE 1

INTEGRATION LIMITS FOR THE I_i INTEGRALS

i	M'_i	M''_i	N'_i	N''_i
1	1	$\epsilon/2$	$T_2\epsilon$	0
2	1	$\epsilon/2$	$X(T_2, y)$	$T_2\epsilon$
3	$Y(T_2, y, t^*)$	$Z(T_2, y, t^*)$	t^*	$X(T_2, y)$
4	1	$Y(T_2, y, t^*)$	$Y(T_2, y, t)$	$X(T_2, y)$
5	$Z(T_2, y, t^*)$	$\epsilon/2$	T_2	$X(T_2, y)$
6	$Z(T_1, y, T_2)$	$Z(T_2, y, t^*)$	T_2	t^*
7	$Z(T_1, y, t^*)$	$Z(T_1, y, T_2)$	$X(T_1, y)$	t^*
8	$Z(T_1, y, T_2)$	$\epsilon/2$	T_2	$X(T_2, y)$
9	$Z(T_2, y, t^*)$	$Z(T_1, y, T_2)$	$X(T_1, y)$	$X(T_2, y)$
10	$Z(T_1, y, t^*)$	$Z(T_2, y, t^*)$	$X(T_1, y)$	t^*
11	$Z(T_1, y, T_2)$	$\epsilon/2$	$X(T_1, y)$	T_2
12	$\frac{3}{2}\epsilon$	$\epsilon/2$	T_2	$X(T_2, y)$
13	1	$\frac{3}{2}\epsilon$	$Y(T_2, y, t)$	$X(T_2, y)$
14	$\frac{3}{2}\epsilon$	$Y(T_2, y, t^*)$	$Y(T_2, y, t)$	T_2
15	$Y(T_2, y, t^*)$	$\epsilon/2$	t^*	T_2
16	$Z(T_1, y, t^*)$	$\epsilon/2$	$X(T_1, y)$	t^*

TABLE 2

INTEGRATION LIMITS FOR THE I'_i INTEGRALS

i	M_i	M'_i	N_i	N''_i
1	1	0	$T_2\epsilon$	0
2	1	0	$X'(T_2, y)$	$T_2\epsilon$
3	1	ϵ	$T_2\epsilon$	0
4	1	ϵ	$Y'(T_2, y, t)$	$T_2\epsilon$
5	$Y'(T_2, y, t^*)$	$Z'(T_2, y, t^*)$	t^*	$X'(T_2, y)$
6	1	$Y'(T_2, y, t^*)$	$Y'(T_2, y, t)$	$X'(T_2, y)$
7	$Z'(T_2, y, t^*)$	0	T_2	$X'(T_2, y)$
8	$Z'(T_1, y, T_2)$	$Z'(T_2, y, t^*)$	T_2	t^*
9	$Z'(T_1, y, t^*)$	$Z'(T_1, y, T_2)$	$X'(T_1, y)$	t^*
10	$Z'(T_1, y, T_2)$	0	T_2	$X'(T_2, y)$
11	$Z'(T_2, y, t^*)$	$Z'(T_1, y, T_2)$	$X'(T_1, y)$	$X'(T_2, y)$
12	$Z'(T_1, y, t^*)$	$Z'(T_2, y, t^*)$	$X'(T_1, y)$	t^*
13	$Z'(T_1, y, T_2)$	0	$X'(T_1, y)$	T_2
14	ϵ	0	T_2	$X'(T_2, y)$
15	1	ϵ	$Y'(T_2, y, t)$	$X'(T_2, y)$
16	$Y'(T_2, y, t^*)$	0	t^*	T_2
17	ϵ	$Y'(T_2, y, t^*)$	$Y'(T_2, y, t)$	T_2
18	$Z'(T_1, y, t^*)$	0	$X'(T_1, y)$	t^*
19	$Z'(T_2, y, t^*)$	$Y'(T_2, y, t^*)$	t^*	$Y'(T_2, y, t)$
20	1	$Z'(T_2, y, t^*)$	$X'(T_2, y)$	$Y'(T_2, y, t)$
21	$Y'(T_1, y, T_2)$	ϵ	$Y'(T_1, y, t)$	T_2
22	$Y'(T_2, y, t^*)$	ϵ	T_2	$Y'(T_2, y, t)$
23	$Y'(T_1, y, T_2)$	$Y'(T_2, y, t^*)$	T_2	t^*
24	$Y'(T_1, y, t^*)$	$Y'(T_1, y, T_2)$	$Y'(T_1, y, t)$	t^*
25	$Y'(T_1, y, T_2)$	ϵ	T_2	$Y'(T_2, y, t)$
26	$Y'(T_2, y, t^*)$	$Y'(T_1, y, T_2)$	$Y'(T_1, y, t)$	$Y'(T_2, y, t)$
27	$Y'(T_1, y, t^*)$	$Y'(T_2, y, t^*)$	$Y'(T_1, y, t)$	t^*
28	2ϵ	ϵ	T_2	$Y'(T_2, y, t)$
29	1	2ϵ	$X'(T_2, y)$	$Y'(T_2, y, t)$
30	$Z'(T_2, y, t^*)$	ϵ	t^*	T_2
31	2ϵ	$Z'(T_2, y, t^*)$	$X'(T_2, y)$	T_2
32	$Y'(T_1, y, t^*)$	ϵ	$Y'(T_1, y, t)$	t^*

Let us consider next the D_2 integral of equation (28). We first introduce the variable t of equation (34) and invert the order of integration. Then introducing Σ and y, defined by

$$t \sin(\Sigma + \epsilon) \equiv t_1\epsilon \qquad \text{and} \qquad \sin\Sigma \equiv y\,, \tag{59}$$

we again invert the order of integration. Using the previous notation for the cases to be distinguished, we finally obtain

$$D_{2,1} = -e^{-T_1}\frac{\alpha^2}{\epsilon}(I'_1 + I'_2)\,, \qquad D_{2,2} = -e^{-T_1}\frac{\alpha^2}{\epsilon}(I'_3 + I'_4)\,, \tag{60}$$

$$D_{2,3',1} = -e^{-T_1}\frac{\alpha^2}{\epsilon}(I'_5 + I'_6)\,, \tag{61}$$

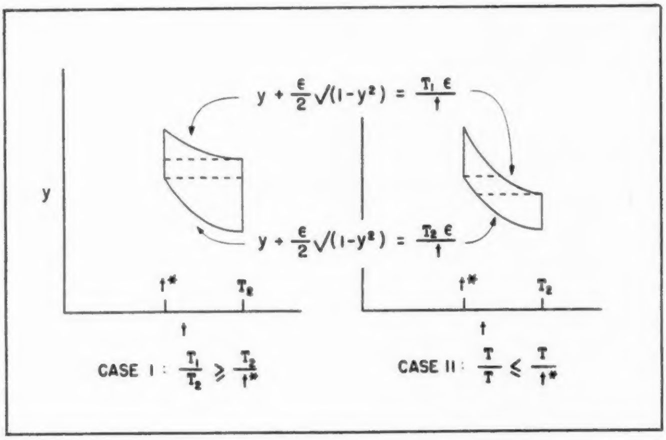
$y + \frac{\epsilon}{2}\sqrt{(1-y^2)} = \frac{T_1\,\epsilon}{t}$
$y + \frac{\epsilon}{2}\sqrt{(1-y^2)} = \frac{T_2\,\epsilon}{t}$
y
t*
T₂
t
t*
T₂
t
CASE I : $\frac{T_1}{T_2} \geqslant \frac{T_2}{t^*}$
CASE II : $\frac{T}{T} \leqslant \frac{T}{t^*}$

FIG. 2.—The cases to be distinguished upon inverting the order of integration in the $D_{1,2',2}$ reduction

$$D_{2,3',2'} = -e^{-T_1}\frac{\alpha^2}{\epsilon}(I'_7 + I'_8 + I'_9)\,, \qquad D_{2,3',2''} = -e^{-T_1}\frac{\alpha^2}{\epsilon}(I'_{10} + I'_{11} + I'_{12})\,, \tag{62}$$

$$D_{2,3',3} = -e^{-T_1}\frac{\alpha^2}{\epsilon}I'_{13}\,, \tag{63}$$

and

$$D_{2,3''} = -e^{-T_1}\frac{\alpha^2}{\epsilon}(I'_{14} + I'_{15} + I'_{16} + I'_{17} + I'_{18})\,. \tag{64}$$

The $D_{3,1}$ and $D_{3,2}$ terms of the D_3 integral are identical with those of the D_2 integral if we replace the factor e^{-T_1} in front of the integral by e^{-T_2}. Thus

$$D_{3,1} = -e^{-T_2}\frac{\alpha^2}{\epsilon}(I'_1 + I'_2) \qquad \text{and} \qquad D_{3,2} = -e^{-T_2}\frac{\alpha^2}{\epsilon}(I'_3 + I'_4)\,. \tag{65}$$

In reducing $D_{3,3}$, we perform the change of variables of equation (34) with t_1 and t_2 interchanged and invert the order of integration. Next, applying the transformations

$$t \sin(\Sigma - \epsilon) \equiv t_2\epsilon \qquad \text{and} \qquad y \equiv \sin\Sigma\,, \tag{66}$$

the order of integration is once more inverted. We then obtain

$$D_{3,3',1} = -e^{-T_2}\frac{\alpha^2}{\epsilon}(I'_{19}+I'_{20})\,, \qquad D_{3,3',3} = -e^{-T_2}\frac{\alpha^2}{\epsilon}I'_{21}\,, \tag{67}$$

$$D_{3,3',2'} = -e^{-T_2}\frac{\alpha^2}{\epsilon}(I'_{22}+I'_{23}+I'_{24})\,, \tag{68}$$

$$D_{3,3',2''} = -e^{-T_2}\frac{\alpha^2}{\epsilon}(I'_{25}+I'_{26}+I'_{27})\,, \tag{69}$$

and

$$D_{3,3''} = -e^{-T_2}\frac{\alpha^2}{\epsilon}(I'_{28}+I'_{29}+I'_{30}+I'_{31}+I'_{32})\,. \tag{70}$$

The D_4 integral of equation (28) is first transformed by applying the change of variables of equation (34). Inverting the order of integration and applying the further transformation,

$$t\sin\lambda \equiv t_1\epsilon\,, \tag{71}$$

we are able to integrate the resulting expression directly. In this manner we find that

$$\begin{aligned} D_{4,1} = e^{-T_1-T_2}\alpha^2\Big\{\frac{2}{\epsilon}\Big[\int_{T_2\epsilon}^{T_2} dtR(t)\,t\,\sin^{-1}\Big(\frac{T_{2\epsilon}}{t}\Big) \\ +\tfrac{1}{2}\pi\int_0^{T_2\epsilon} dtR(t)\,t\Big] - 2\int_0^{T_2} dtR(t)\,t\Big\}\,, \end{aligned} \tag{72}$$

and

$$\begin{aligned} D_{4,2} = e^{-T_1-T_2}\alpha^2\Big\{\frac{1}{\epsilon}\Big[\int_{T_2\epsilon}^{t^*} dtR(t)\,t\,\sin^{-1}\Big(\epsilon\Big\{\frac{T_2}{t}+\sqrt{\Big[1+\frac{T_2^2\epsilon^2}{t^2}\Big]}\Big\}\Big) \\ -\int_{T_2\epsilon}^{T_2} dtR(t)\,t\,\sin^{-1}\Big(\frac{T_{2\epsilon}}{t}\Big)+\int_{t^*}^{T_1} dtR(t)\,t\,\sin^{-1}\Big(\frac{T_{1\epsilon}}{t}\Big)\Big] - \int_{T_2}^{T_1} dtR(t)\,t\Big\}\,. \end{aligned} \tag{73}$$

3. *The reduction of the expressions of § 2 for the case $T_1 = T_2$.*—In the application of the foregoing theoretical development to be carried out in the present paper, we analyze the brightness of the Milky Way along parallels of galactic latitude. For this case we shall have

$$T_1 = T_2 \equiv T \qquad \text{(say)}\,, \tag{74}$$

and the expressions for $\overline{uu_\phi}$ of §2 simplify greatly.

The A integral of equation (25) becomes

$$A = 1 - 2\,e^{-T} + e^{-2T}\,. \tag{75}$$

The B and C integrals of equations (26) and (27) are now identical and are just the corresponding terms of the $\overline{u^2}$ development (cf. eq. [20]). Hence we have

$$\begin{aligned} B+C = 2\alpha^2\Big\{\int_0^T dtR(t)\,e^{-t} + e^{-T}\Big[\int_0^T dtR(t)\,t - (T+1)\int_0^T dtR(t) \\ -\int_0^T dtR(t)\,e^{-t}\Big] + e^{-2T}\Big[(T+1)\int_0^T dtR(t) - \int_0^T dtR(t)\,t\Big]\Big\}\,. \end{aligned} \tag{76}$$

In equations (52) through (58) for the D_1 integral, only the $D_{1,1}$ term is relevant. Thus

$$D_1 = 2\,\frac{\alpha^2}{\epsilon}\Big\{I\Big(1\,,\frac{\epsilon}{2};\,T\epsilon\,,0\Big)+I\Big(1\,,\frac{\epsilon}{2};\,X\,[T,\,y]\,,T\epsilon\Big)\Big\}\,. \tag{77}$$

The expressions for D_2 and D_3 are now identical, and only the $D_{2,1}$, $D_{2,2}$, $D_{3,1}$, and $D_{3,2}$ terms contribute. Hence, from equations (60) through (70), we have

$$\begin{aligned} D_2 + D_3 = -2e^{-T}\frac{\alpha^2}{\epsilon}\{ & I'(1, 0; T\epsilon, 0) + I'(1, 0; X'[T, y], T\epsilon) \\ & + I'(1, \epsilon; T\epsilon, 0) + I'(1, \epsilon; Y'[T, y, t], T\epsilon)\}. \end{aligned} \tag{78}$$

In the D_4 integral, only the $D_{4,1}$ term is relevant, so that we obtain, from equation (72),

$$D_4 = e^{-2T}\alpha^2\Bigl\{\frac{1}{\epsilon}\Bigl[2\int_{T\epsilon}^{T} dtR(t)\,t\sin^{-1}\Bigl(\frac{T\epsilon}{t}\Bigr) + \pi\int_0^{T\epsilon} dtR(t)\,t\Bigr] - 2\int_0^T dtR(t)\,t\Bigr\}. \tag{79}$$

Upon collecting the results of equations (75) through (79), we at last obtain the desired expression for $\overline{uu_\phi}$:

$$\begin{aligned} \overline{uu_\phi} = 1 + 2\alpha^2\Bigl[& \int_0^T dtR(t)\,e^{-t} + \frac{1}{\epsilon}\Bigl(\int_{\epsilon/2}^1 \frac{dy}{\sqrt{[1-y^2]}}\int_0^{T\epsilon} dtR(t)\,t\,e^{-2ty/\epsilon} \\ & + \int_{\epsilon/2}^1 \frac{dy}{\sqrt{[1-y^2]}}\int_{T\epsilon}^{X(T,y)} dtR(t)\,t\,e^{-2ty/\epsilon}\Bigr)\Bigr] + e^{-T}\Bigl\{-2 + 2\alpha^2\Bigl[-(T+1) \\ & \times\int_0^T dtR(t) + \int_0^T dtR(t)\,t - \int_0^T dtR(t)\,e^{-t} - \frac{1}{\epsilon}\Bigl(\int_0^1 \frac{dy}{\sqrt{[1-y^2]}} \\ & \times\int_0^{T\epsilon} dtR(t)\,t\,e^{-ty/\epsilon} + \int_0^1 \frac{dy}{\sqrt{[1-y^2]}}\int_{T\epsilon}^{X'(T,y)} dtR(t)\,t\,e^{-ty/\epsilon} \\ & + \int_\epsilon^1 \frac{dy}{\sqrt{[1-y^2]}}\int_0^{T\epsilon} dtR(t)\,t\,e^{-ty/\epsilon} + \int_\epsilon^1 \frac{dy}{\sqrt{[1-y^2]}} \\ & \times\int_{T\epsilon}^{Y'(T,y,t)} dtR(t)\,t\,e^{-ty/\epsilon}\Bigr)\Bigr]\Bigr\} + e^{-2T}\Bigl\{1 + 2\alpha^2\Bigl[(T+1)\int_0^T dtR(t) \\ & - 2\int_0^T dtR(t)\,t + \frac{1}{\epsilon}\Bigl(\tfrac{1}{2}\pi\int_0^{T\epsilon} dtR(t)\,t + \int_{T\epsilon}^T dtR(t)\,t\sin^{-1}\Bigl\{\frac{T\epsilon}{t}\Bigr\}\Bigr)\Bigr\}. \end{aligned} \tag{80}$$

4. *The evaluation of $\bar{u}$, $\overline{u^2}$, and $\overline{uu_\phi}$ for two particular forms of the correlation coefficient and for selected values of the parameters ϵ, τ_0, and T.*—The expressions to be used in the analysis of the observational material are developed for the following two forms for the correlation coefficient:

$$R(t) = e^{-t/\tau_0} \quad \text{and} \quad R(t) = e^{-t^2/\tau_0^2}. \tag{81}$$

An examination of the expressions for $\bar{u}$, $\overline{u^2}$, and $\overline{uu_\phi}$—equations (16), (23), and (80)—shows that we must deal with integrals containing the following integrands:

(1) $R(t)$, (2) $R(t)\,e^{-t}$, (3) $R(t)\,e^{+t}$,

(4) $R(t)\,t$, (5) $R(t)\,t\,e^{-ty/\epsilon}$, (6) $R(t)\,t\,e^{-2ty/\epsilon}$,

(7) $R(t)\,t\sin^{-1}\Bigl(\dfrac{T\epsilon}{t}\Bigr)$.

Each of the corresponding integrations except the last can be evaluated in terms of known functions for both forms for the correlation coefficient; the last must be evaluated numerically. Since the fifth and sixth of these integrands occur in double integrals (cf.

eq. [80]), we must perform a further integration in these cases. This has been done numerically.

Theoretical values for $\bar{u}$, $\overline{u^2}$, and $\overline{uu_\phi}$ have been computed by these means for both forms for the correlation coefficient and for the values of the parameters ϵ, τ_0, and T given in Table 3. The values for $\bar{u}^2$ have then been calculated from those for $\bar{u}$. In keeping with the present scheme of approximation, we have neglected the α^4 terms in this latter calculation. Tables 4, 5, and 6 give these computed values for $\bar{u}^2$, $\overline{u^2}$, and $\overline{uu_\phi}$.

TABLE 3

VALUES OF THE PARAMETERS τ_0, T, AND ϵ FOR WHICH THE COMPUTATIONS HAVE BEEN CARRIED OUT

τ_0	T	Corresponding Galactic Latitudes for Effective Galactic Half-thickness of: $0^{\mathrm{m}}20$	Corresponding Galactic Latitudes for Effective Galactic Half-thickness of: $0^{\mathrm{m}}25$	ϵ ×10² Radians	ϵ Degrees
0.008				1.0	0°53′
.010				2.0	1°10′
0.012				3.0	1°43′
	0.75	15°28′	19°28′	4.0	2°20′
	1.00	11°32′	14°29′	5.0	2°53′
	1.50	7°40′	9°36′	6.0	3°28′
	3.00	3°49′	4°47′	7.0	4°02′
	6.00	1°55′	2°23′	8.0	4°35′
				9.0	5°10′

TABLE 4

THEORETICAL VALUES OF $\bar{u}^2$ FOR TWO FORMS FOR THE CORRELATION COEFFICIENT

τ_0	T: 0.75	1.00	1.50	3.00	6.00
	$R=e^{-t/\tau_0}$				
	0.278+	0.400+	0.604+	0.903+	0.995+
0.008	0.00143 α^2	0.00262 α^2	0.00542 α^2	0.01206 α^2	0.01555 α^2
.010	.00177 α^2	.00326 α^2	.00675 α^2	.01504 α^2	.01940 α^2
0.012	0.00212 α^2	0.00390 α^2	0.00808 α^2	0.01801 α^2	0.02324 α^2
	$R=e^{-t^2/\tau_0^2}$				
0.008	0.00128 α^2	0.00234 α^2	0.00483 α^2	0.01073 α^2	0.01383 α^2
.010	.00159 α^2	.00292 α^2	.00603 α^2	.01340 α^2	.01727 α^2
0.012	0.00190 α^2	0.00349 α^2	0.00722 α^2	0.01605 α^2	0.02069 α^2

Table 7 gives the corresponding values for $(\overline{u^2} - \overline{uu_\phi})/(\overline{u^2} - \bar{u}^2)$ which are used in the subsequent analysis.

5. *The analysis of the observational material and the evaluation of the parameters characterizing the density distribution.*—The isophotal charts of the Southern Milky Way published by Pannekoek and Koelbloed[3] have been analyzed by means of the above theoretical development. These charts have been discussed in the light of this type of application in Paper V.

Since the aim of the present work is to determine the latitude dependences of the correlations, it has been felt that the inhomogeneities and the end-point errors introduced by any process of selection or restriction in the galactic longitudes would outweigh any advantages to be gained thereby. As a result, values of $\bar{u}^2$, $\overline{u^2}$, and $\overline{uu_\phi}$ have been obtained from an analysis of the entire galactic-longitude range from 170° to 10° for the galactic latitudes $\pm 2\overset{\circ}{.}5$, $\pm 5°$, $\pm 10°$, and $-15°$. Owing to limitations in the observational material, the galactic longitudes were restricted to the range from 210° to 340° for galactic latitude $+15°$. (The general agreement of those results of the present study which pertain to the region near the galactic plane with those of Chandrasekhar and Münch, who made use of selected regions, indicates that no major changes have been introduced into the τ_0 determination by reason of this method of treatment.) The readings were taken along parallels of galactic latitude at intervals of $\frac{1}{2}°$ for the integral values of ϕ from 1° to 5°, inclusive. These readings are plotted in Figures 3 and 4.

TABLE 5

THEORETICAL VALUES OF $\bar{u}^2$ FOR TWO FORMS FOR THE CORRELATION COEFFICIENT

τ_0	T				
	0.75	1.00	1.50	3.00	6.00
	$R=e^{-t/\tau_0}$				
	0.278+	0.400+	0.604+	0.903+	0.995+
0.008	0.00232 a^2	0.00423 a^2	0.00864 a^2	0.01859 a^2	0.02341 a^2
.010	.00289 a^2	.00527 a^2	.01076 a^2	.02319 a^2	.02920 a^2
0.012	0.00345 a^2	0.00630 a^2	0.01287 a^2	0.02794 a^2	0.03498 a^2
	$R=e^{-t^2/\tau_0^2}$				
0.008	0.00209 a^2	0.00379 a^2	0.00770 a^2	0.01665 a^2	0.02082 a^2
.010	.00261 a^2	.00473 a^2	.00961 a^2	.02065 a^2	.02600 a^2
0.012	0.00313 a^2	0.00566 a^2	0.01150 a^2	0.02474 a^2	0.03115 a^2

Since the observed intensities, I, given by the charts include both starlight—of intensity u—and diffuse galactic light, the analysis has been patterned after that of Paper V, where it is shown that the effect of the diffuse galactic light can be removed if one analyzes the quantity

$$\Sigma_\phi \equiv \frac{\overline{I^2} - \overline{I I_\phi}}{\overline{I^2} - \bar{I}^2} \qquad (82)$$

---

[3] A. Pannekoek and D. Koelbloed, *Pub. Astr. Inst. Amsterdam*, No. 9, 1949.

TABLE 6

THEORETICAL VALUES OF $\overline{uu_\phi}$ FOR TWO FORMS FOR THE CORRELATION COEFFICIENT

i) $R=e^{-t/\tau_0}$

$\phi\times10^2$ (RADIANS)	T				
	0.75	1.00	1.50	3.00	6.00
	$\tau_0=0.008$				
	0.278+	0.400+	0.604+	0.903+	0.995+
1	0.00231 a^2	0.00418 a^2	0.00824 a^2	0.01730 a^2	0.02164 a^2
2	.00219 a^2	.00390 a^2	.00777 a^2	.01625 a^2	.02030 a^2
3	.00212 a^2	.00374 a^2	.00743 a^2	.01542 a^2	.01937 a^2
4	.00203 a^2	.00361 a^2	.00714 a^2	.01489 a^2	.01876 a^2
5	.00196 a^2	.00350 a^2	.00692 a^2	.01450 a^2	.01830 a^2
6	.00191 a^2	.00340 a^2	.00676 a^2	.01420 a^2	.01796 a^2
7	.00187 a^2	.00332 a^2	.00661 a^2	.01396 a^2	.01767 a^2
8	.00183 a^2	.00325 a^2	.00651 a^2	.01378 a^2	.01747 a^2
9	0.00180 a^2	0.00320 a^2	0.00641 a^2	0.01362 a^2	0.01729 a^2
	$\tau_0=0.010$				
1	0.00288 a^2	0.00524 a^2	0.01045 a^2	0.02201 a^2	0.02754 a^2
2	.00282 a^2	.00498 a^2	.00992 a^2	.02074 a^2	.02594 a^2
3	.00272 a^2	.00479 a^2	.00950 a^2	.01984 a^2	.02482 a^2
4	.00263 a^2	.00465 a^2	.00918 a^2	.01913 a^2	.02401 a^2
5	.00254 a^2	.00451 a^2	.00890 a^2	.01861 a^2	.02340 a^2
6	.00247 a^2	.00439 a^2	.00868 a^2	.01820 a^2	.02294 a^2
7	.00241 a^2	.00429 a^2	.00849 a^2	.01787 a^2	.02256 a^2
8	.00236 a^2	.00421 a^2	.00835 a^2	.01760 a^2	.02226 a^2
9	0.00230 a^2	0.00414 a^2	0.00821 a^2	0.01737 a^2	0.02200 a^2
	$\tau_0=0.012$				
1	0.00345 a^2	0.00628 a^2	0.01257 a^2	0.02671 a^2	0.03327 a^2
2	.00340 a^2	.00604 a^2	.01201 a^2	.02535 a^2	.03152 a^2
3	.00331 a^2	.00584 a^2	.01156 a^2	.02431 a^2	.03025 a^2
4	.00322 a^2	.00568 a^2	.01119 a^2	.02352 a^2	.02930 a^2
5	.00313 a^2	.00552 a^2	.01087 a^2	.02289 a^2	.02856 a^2
6	.00304 a^2	.00538 a^2	.01062 a^2	.02239 a^2	.02799 a^2
7	.00297 a^2	.00527 a^2	.01039 a^2	.02198 a^2	.02748 a^2
8	.00290 a^2	.00517 a^2	.01020 a^2	.02164 a^2	.02712 a^2
9	0.00286 a^2	0.00507 a^2	0.01004 a^2	0.02136 a^2	0.02679 a^2

TABLE 6—*Continued*

ii) $R=e^{-t^2/\tau_0^2}$

$\phi\times10^3$ (RADIANS)	T				
	0.75	1.00	1.50	3.00	6.00
	$\tau_0=0.008$				
	0.278+	0.400+	0.604+	0.903+	0.995+
1	0.00208 α^2	0.00367 α^2	0.00720 α^2	0.01504 α^2	0.01863 α^2
2	.00191 α^2	.00337 α^2	.00660 α^2	.01377 α^2	.01713 α^2
3	.00180 α^2	.00317 α^2	.00622 α^2	.01306 α^2	.01632 α^2
4	.00172 α^2	.00303 α^2	.00596 α^2	.01263 α^2	.01582 α^2
5	.00166 α^2	.00293 α^2	.00578 α^2	.01233 α^2	.01548 α^2
6	.00162 α^2	.00285 α^2	.00565 α^2	.01211 α^2	.01524 α^2
7	.00158 α^2	.00280 α^2	.00555 α^2	.01195 α^2	.01506 α^2
8	.00154 α^2	.00274 α^2	.00547 α^2	01188 α^2	.01492 α^2
9	0.00152 α^2	0.00270 α^2	0.00541 α^2	0.01172 α^2	0.01481 α^2
	$\tau_0=0.010$				
1	0.00261 α^2	0.00472 α^2	0.00914 α^2	0.01916 α^2	0.02384 α^2
2	.00246 α^2	.00440 α^2	.00851 α^2	.01754 α^2	.00205 α^2
3	.00232 α^2	.00411 α^2	.00803 α^2	.01667 α^2	.02094 α^2
4	.00222 α^2	.00393 α^2	.00770 α^2	.01606 α^2	.02024 α^2
5	.00215 α^2	.00378 α^2	.00745 α^2	.01563 α^2	.01973 α^2
6	.00209 α^2	.00368 α^2	.00726 α^2	.01532 α^2	.01941 α^2
7	.00204 α^2	.00360 α^2	.00712 α^2	.01509 α^2	.01915 α^2
8	.00199 α^2	00352 α^2	.00700 α^2	.01489 α^2	.01894 α^2
9	0.00196 α^2	0.00348 α^2	0.00691 α^2	0.01474 α^2	0.01877 α^2
	$\tau_0=0.012$				
1	0.00313 α^2	0.00565 α^2	0.01109 α^2	0.02325 α^2	0.02903 α^2
2	00302 α^2	00532 α^2	.01041 α^2	.02156 α^2	.02695 α^2
3	.00286 α^2	.00505 α^2	.00985 α^2	.02043 α^2	.02562 α^2
4	.00275 α^2	.00484 α^2	.00945 α^2	.01966 α^2	.02474 α^2
5	.00266 α^2	.00467 α^2	.00915 α^2	.01911 α^2	02412 α^2
6	.00258 α^2	.00454 α^2	.00890 α^2	.01870 α^2	.02365 α^2
7	.00252 α^2	.00443 α^2	.00871 α^2	.01839 α^2	.02330 α^2
8	.00246 α^2	.00434 α^2	.00856 α^2	.01814 α^2	.02302 α^2
9	0.00242 α^2	0.00426 α^2	0.00844 α^2	0.01794 α^2	0.02279 α^2

TABLE 7

THEORETICAL VALUES OF $(\overline{u^2} - \overline{uu_\phi})/(\overline{u^2} - \bar{u}^2)$ FOR TWO FORMS FOR THE CORRELATION COEFFICIENT

i) $R = e^{-t/\tau_0}$

$\phi \times 10^2$ (RADIANS)	T				
	0.75	1.00	1.50	3.00	6.00
	$\tau_0 = 0.008$				
1	0.013	0.032	0.125	0.198	0.225
2	.142	.202	.268	.358	.395
3	.230	.303	.376	.485	.514
4	.323	.385	.465	.567	.592
5	.402	.456	.534	.626	.650
6	.461	.518	.585	.672	.693
7	.507	.562	.630	.709	.731
8	.552	.613	.661	.737	.756
9	0.585	0.638	0.693	0.761	0.779
	$\tau_0 = 0.010$				
1	0.004	0.017	0.078	0.145	0.169
2	085	.142	.210	.301	.333
3	156	.233	.314	.411	.447
4	.240	.310	.395	.498	.530
5	.311	.378	.466	.562	.592
6	.376	.438	.518	.612	.639
7	.425	.485	.566	.653	.678
8	.474	.527	.602	.686	.708
9	0.511	0.565	0.636	0.714	0.735
	$\tau_0 = 0.012$				
1	0.000	0.008	0.063	0.124	0.146
2	.040	.107	.179	.261	.295
3	.100	.190	.273	.366	.403
4	.172	.261	.351	.445	.484
5	.242	.326	.417	.509	.547
6	.310	.383	.470	.559	.595
7	.360	.430	.518	.600	.634
8	.409	.471	.557	634	.669
9	0.447	0.510	0.591	0.663	0.698

TABLE 7—*Continued*

ii) $R = e^{-t^2/\tau_0^2}$

$\phi \times 10^2$ (RADIANS)	*T*				
	0.75	1.00	1.50	3.00	6.00
	$\tau_0 = 0.008$				
1	0.006	0.082	0.176	0.272	0.313
2	.216	.291	.382	.486	.528
3	.354	.427	.515	.606	.644
4	.451	.524	.607	.679	.716
5	.524	.597	.668	.730	.764
6	.584	.646	.716	.767	.798
7	.632	.685	.749	.794	.824
8	.672	.723	.778	.806	.844
9	0.700	0.750	0.798	0.833	0.860
	$\tau_0 = 0.010$				
1	0.000	0.006	0.131	0.214	0.249
2	.155	.214	.308	.422	.456
3	.284	.346	.440	.549	.580
4	.379	.443	.533	.633	.660
5	452	522	601	692	714
6	.513	.579	.656	.735	.755
7	.565	.624	.695	767	785
8	.608	.665	.727	794	809
9	0.640	0.695	0.754	0.815	0.828
	$\tau_0 = 0.012$				
1	0.000	0.005	0.096	0.171	0.203
2	.094	.155	.255	.366	401
3	.217	.283	.385	.496	.529
4	.319	.378	.479	.585	.613
5	.382	.456	.549	.648	.672
6	.443	.518	.607	.695	.717
7	.496	.566	.651	.731	.750
8	.542	.610	.687	.759	.777
9	0.577	0.644	0.715	0.782	0.799

rather than either $\overline{\Pi}_\phi/\overline{I^2}$ or $\overline{\Pi}_\phi/\bar{I}^2$. It is shown in Paper V that we have, to a high degree of approximation,

$$\Sigma_\phi = \frac{\overline{u^2} - \overline{u u_\phi}}{\overline{u^2} - \bar{u}^2}\,. \tag{83}$$

From the observational material we have obtained Σ_ϕ for both the northern and the southern galactic latitudes, and the results are given in Table 8. In the work to follow it will become evident that in the present considerations the galaxy can be considered infinite in extent up to a galactic latitude of about 3°. In view of this, the results of the present observational analysis for $b = \pm\, 2\overset{\circ}{.}5$ have been combined with those of Paper V to give a mean curve of still greater weight for the important region in and near the galactic plane. (Since the material of Paper V refers to selected regions, some inhomogeneity is introduced when we compare this mean curve for the region of the galactic plane with the observational curves for the higher latitudes; nevertheless, the increased weight of the mean curve so obtained and the rather smooth galactic-latitude trend which results when this mean curve is used seem to justify this procedure in the present case.) These weighted means are given in Table 9, and the results given in Tables 8 and 9 are combined and plotted in Figure 5. The corresponding theoretical curves are given in Figures 6, 7, and 8, where the solid curves refer to the five selected values of T for the e^{-t/τ_0}

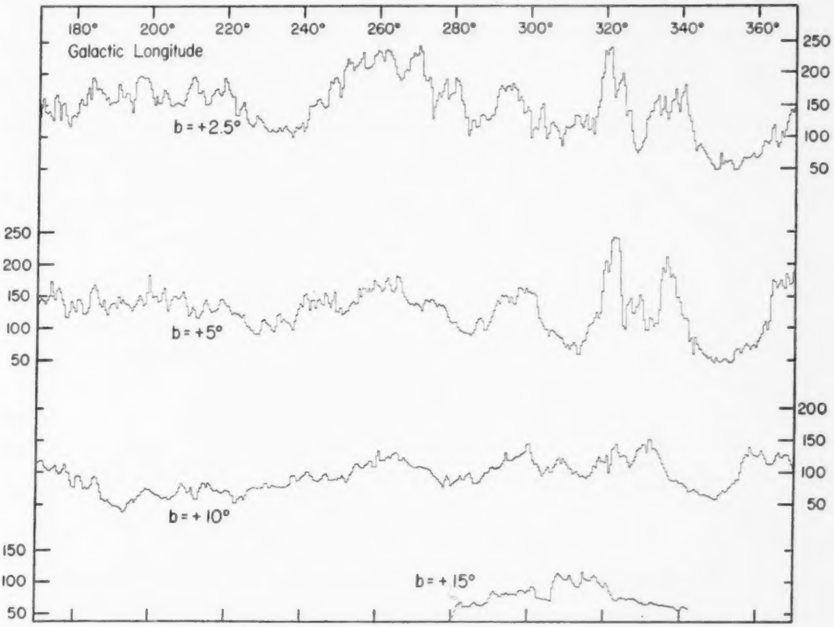

FIG. 3.—The dependence on galactic latitude and longitude of the surface brightness of the Milky Way, along arcs of constant galactic latitude, b, for the latitudes $+2\overset{\circ}{.}5$, $+5°$, $+10°$, and $+15°$ as read from Pannekoek's charts. The ordinates represent the intensity in the unit: brightness of one star of photographic magnitude 10 per square degree.

form for the correlation coefficient and the dashed curves refer to the extreme values, $T = 6.00$ and $T = 0.75$, for the $e^{-\rho^2/\tau_0^2}$ form.

In determining the best τ_0, we must restrict ourselves to those galactic latitudes for which T is effectively infinite; otherwise, the as yet undetermined "effective" half-thickness, $\bar{\tau}_{1/2\,\mathrm{eff}}$, of the absorbing matter in the galaxy will enter into the result. Since a comparison with the results of Paper V shows that the theoretical curves for $T = 6.00$ and $T = \infty$ differ only insignificantly, we are able to make use of the material for the latitudes $0° \leqslant |b| \leqslant 2.5°$ in the determination. From a comparison of the observational data for this range with the theoretical curves for $T \geqslant 6.00$, we find that the value

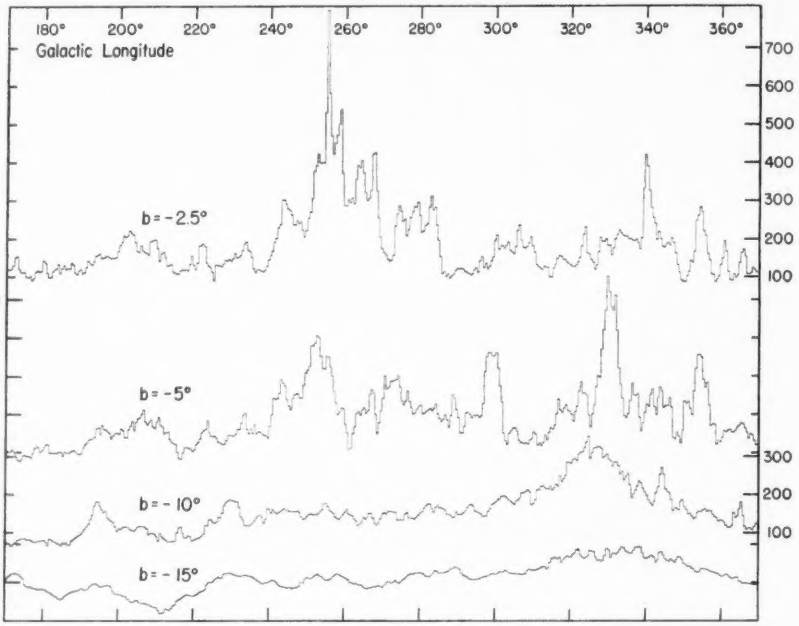

FIG. 4.—The dependence on galactic latitude and longitude of the surface brightness of the Milky Way, along arcs of constant galactic latitude, b, for the latitudes $-2.5°$, $-5°$, $-10°$, and $-15°$. Otherwise the legend of Fig. 3 applies to this figure also. (Note that the intensity scale here is three-fifths that of Fig. 3.)

$$\tau_0 \simeq 0.011 \tag{84}$$

provides quite satisfactory agreement.

With this τ_0 we can determine from the observations the "effective" half-thickness of the absorbing matter which is relevant to the fluctuations in brightness of the Milky Way. This relevant absorbing matter is that between the plane of the galaxy and the height z_l above the plane at which the star density has become appreciably smaller than its value in the galactic plane; i.e., z_l is the "effective" half-thickness of the stellar system. Hence any absorption farther above the plane than z_l will not be included in the "effective" half-thickness so determined. For this reason, we should expect $\bar{\tau}_{1/2\,\mathrm{eff}}$ to be somewhat smaller than the value obtained from studies of the counts of the extragalactic nebulae if the absorbing matter extends in appreciable quantities above z_l. From a comparison of the latitude dependence given by the theory with that from the observations, we find that satisfactory agreement is obtained for

$$\bar{\tau}_{1/2\,\mathrm{eff}} \simeq 0.20\ ; \tag{85}$$

it is definitely indicated that $\bar{\tau}_{1/2\,\mathrm{eff}}$ is less than 0.25. Upon using the value given in equation (85), the observational results for the higher latitudes are found to be quite consistent with the τ_0 value obtained from the data nearer the galactic plane. It should be emphasized, however, that the present theoretical development is based upon an idealized system in which the star density is constant within the system and zero beyond (cf. § 2). The effect of the roughly exponential falling-off in star density with height above the galactic plane is not as yet known with certainty, although it would seem that this effect must be of the second order.

Using the τ_0 value of equation (84), the writer has analyzed the observational mate-

TABLE 8

ANGULAR CORRELATIONS, Σ_ϕ, OF THE BRIGHTNESS OBSERVED IN THE SOUTHERN MILKY WAY

ϕ	2.5°	5°	10°	15°
	Northern Latitudes			
0°	0.000	0.000	0.000	0.000
1	.169	.105	.140	.101
2	.307	.193	.284	.220
3	.462	.259	.420	.284
4	.583	.349	.567	.387
5	0.699	0.576	0.711	0.474
	Southern Latitudes			
0°	0.000	0.000	0.000	0.000
1	.218	.164	.140	.081
2	.375	.412	.290	.171
3	.460	.574	.424	.257
4	.574	.739	.521	.340
5	0.657	0.887	0.581	0.489

TABLE 9

ANGULAR CORRELATIONS, Σ_ϕ, OF THE BRIGHTNESS OBSERVED IN THE SOUTHERN MILKY WAY FOR $-2.^\circ 5 \leqslant b \leqslant +2.^\circ 5$

	ϕ					
	0°	1°	2°	3°	4°	5°
Σ_ϕ	0.000	0.257	0.479	0.615	0.726	0.800

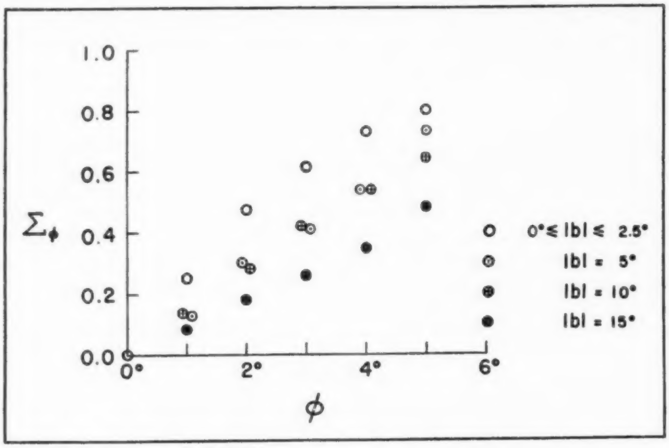

FIG. 5.—The normalized correlation function, $\Sigma_\phi(b)$, derived from the observational material for both northern and southern galactic latitudes for $0^\circ \leqslant |b| \leqslant 2^\circ\!.5$; $|b| = 5^\circ$; $|b| = 10^\circ$; and $|b| = 15^\circ$

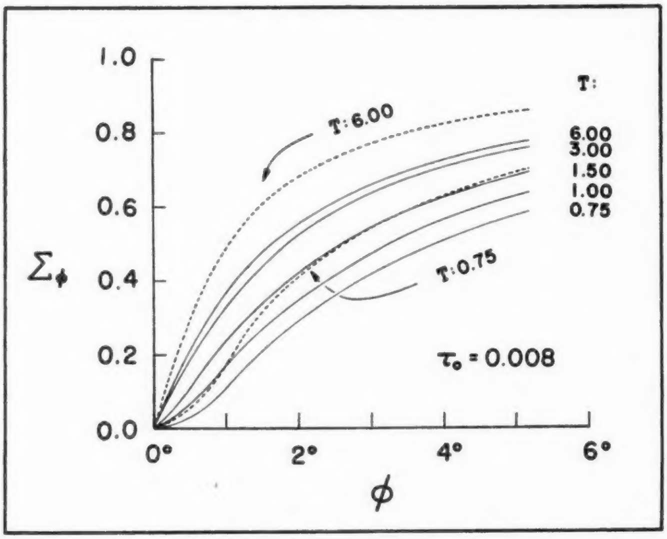

FIG. 6.—The normalized correlation function, $\Sigma_\phi(b)$, derived from the theory for a micro-scale, τ_0, of 0.008. The solid curves are derived for the correlation coefficient $R = e^{-t/\tau_0}$, while the dashed curves are derived for $R = e^{-t^2/\tau_0^2}$.

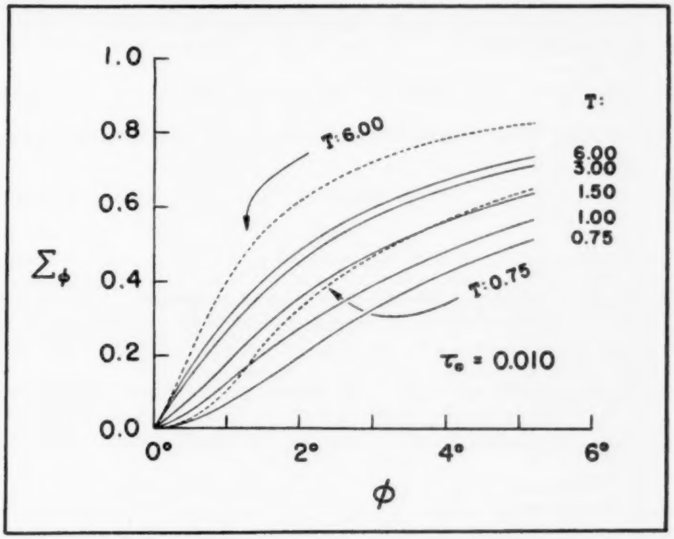

FIG. 7.—The normalized correlation function, $\Sigma_\phi(b)$, derived from the theory for a micro-scale, τ_0 of 0.010.

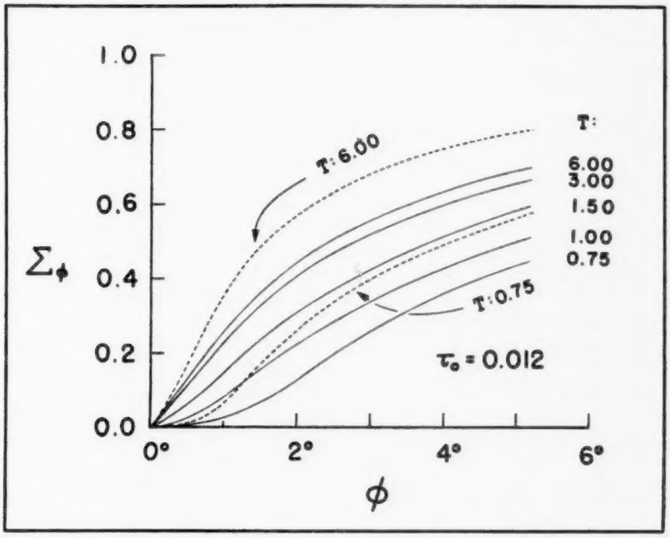

FIG. 8.—The normalized correlation function, $\Sigma_\phi(b)$, derived from the theory for a micro-scale, τ_0, of 0.012.

rial for $b = +2\overset{\circ}{.}5$ and $b = -2\overset{\circ}{.}5$ in the manner of Paper V, in order to determine the parameter $\mathfrak{a}^2$. Assuming, as in Paper V, that the albedo for interstellar matter is 0.4, we obtain

$$\mathfrak{a}^2 = 16 \qquad \text{(north)} \qquad \text{and} \qquad \mathfrak{a}^2 = 45 \qquad \text{(south)} . \tag{86}$$

Hence, from equation (6) we obtain for the root mean square of the fluctuations in the density

$$\sqrt{[\overline{\delta^2 \rho}]} = 4.0 \bar{\rho} \qquad \text{(north)} \tag{87}$$

and

$$\sqrt{[\overline{\delta^2 \rho}]} = 6.7 \bar{\rho} \qquad \text{(south)} . \tag{88}$$

The result for the northern galactic latitudes is in good agreement with the results of Paper V, while that for the southern latitudes is somewhat larger because of the brighter and more irregular structure in the southern portion which has been included in this analysis (cf. Figs. 3 and 4).

6. *Concluding remarks.*—The results of § 5 indicate that the observed fluctuations in the brightness of the Milky Way are consistent with an interpretation in terms of the distribution of the interstellar matter postulated by Chandrasekhar and Münch in Paper V.

In closing, I should like to express my very sincere thanks to Professor Chandrasekhar, who not only suggested this investigation but also has given generously of his time during the course of its development.

THE INTERSTELLAR STRUCTURES. I. GAS CLOUDS

EUGENE N. PARKER
Norman Bridge Laboratory of Physics, California Institute of Technology*

Received September 2, 1952

ABSTRACT

In an effort to arrive at a dynamical model for the interstellar medium, its mechanical properties are discussed. Using a polytrope relation between the temperature and density within a gas cloud, the mechanical and then the statistical properties of an idealized model of the interstellar clouds are developed. One finds that the collision rate of clouds, computed in an elementary fashion from their diameters and random translational velocities, leads to several difficulties. First, the very inelastic nature of head-on collisions would rapidly reduce the translational velocities, and it would be difficult to explain the observed radial velocities. Second, there would be a strong tendency toward statistical equilibrium of the internal state of the clouds. The equilibrium is investigated, and the cloud is found to be either in a collapsed condition or completely dispersed, again contrary to observation. Ordering of the translational velocities is proposed as one means of circumventing these difficulties. In any case, the tendency of clouds to collapse, possibly to form clusters of stars, is shown to be intrinsic in their nature.

I. MECHANICAL PROPERTIES OF THE INTERSTELLAR MEDIUM

This is the first of a series of papers attempting to investigate theoretically the mechanical and statistical state of the interstellar medium. This paper is devoted to the gas structures because they contain the great preponderance of matter, and the motion of such things as dust and smoke depend greatly upon the motion of the gas. We begin with a discussion of the mechanical properties of the gas, so that later we may consider its dynamical state.

Observation shows that the interstellar gas is clumped rather than homogeneous. The clump or cloud diameters are often assumed to be of the order of 10–20 psc, and the interval between cloud centers of the order of 20–40 psc. Densities within the clouds usually range from 5 to 1000 hydrogen atoms per cubic centimeter. The gas density[1, 2] outside the clouds is of the order of 10^{-1} or 10^{-2} hydrogen atoms per cubic centimeter, so that the over-all mean density is of the order of one hydrogen atom per cubic centimeter. We see, then, that the density within the clouds is 10^2 to 10^4 times greater than outside the clouds, and the clouds may be regarded as individual entities. The clouds apparently have more or less random translational velocities of the order of 5 km/sec.[3, 4, 5] There is some indication of equipartition of translational energy between clouds of different masses.[5] The escape velocity for atoms from a given cloud probably is somewhat less than the 5–10 km/sec translational velocity of the clouds.

The observations may be supplemented by the following rather elementary theoretical considerations. The mean free path for collision of gas clouds is 20–40 psc. A random velocity of 5 km/sec implies a collision for a given cloud every $\frac{2}{3} \cdot 10^7$ years. We see, then, that in two revolutions of the galaxy (i e., $\frac{1}{10}$ the lifetime of the galaxy) an individual cloud will undergo approximately 60 collisions. Hence, in any study of the interstellar medium, we must consider its dynamic equilibrium state in the presence of these collisions.

---

* Now at the University of Utah.

[1] J. L. Greenstein, *Ap. J.*, **104**, 414, 1946.

[2] B. Strömgren, *Ap. J.*, **108**, 242, 1948.

[3] W. S. Adams, *Ap. J.*, **97**, 105, 1943.

[4] W. S. Adams, *Ap. J.*, **109**, 354, 1948.

[5] F. L. Whipple, *Harvard Obs. Mono.*, No. 7, *Centennial Symposia*.

If we take the collision radius of a neutral hydrogen atom as 10^{-8} cm and a density of 1 atom/cm^3, the mean free path of a hydrogen atom is $0.6 \cdot 10^{15}$ cm or 40 a.u. Thus we see that the clouds are very much larger than the mean free path of an individual atom, and hence we may use conventional kinetic theory. Rather more complex considerations are necessary to obtain information about the internal state of the clouds in the intervals between collisions.[6, 7, 8, 9] Spitzer's[9] theoretical results give θ, the equilibrium temperature due to the radiation field of the stars, as a function of the density, ρ. The polytrope relation

$$\theta = \theta_0 \left(\frac{\rho}{\rho_0}\right)^{\alpha - 1} \tag{1}$$

provides an approximate and very convenient representation of the result. α lies in the range (1.00–1.04) for H II regions and in (0.4–0.98) for H I regions. It is proper to use these equilibrium temperatures in the subsequent analysis, since the relaxation time, for the approach to thermal equilibrium after a disturbance, is considerably less in H I regions than the interval between collisions and usually somewhat less in H II regions. Between the clouds the density is so low that the relaxation time is long compared to the periods of the dynamical processes, and the variation is adiabatic, i.e., $\alpha = \gamma$. Classical polytrope theory indicates that when $\alpha < \frac{4}{3}$, a cloud is unstable and collapses. If one assumes a rotation of the cloud, the model becomes stable. In order to estimate the effect of turbulence, consider the formula for the viscosity and root-mean-square thermal velocities of atomic hydrogen, where

$$\mu = \frac{1}{6\sigma^2} \sqrt{\left(\frac{m_H k \theta}{\pi^3}\right)} \cong \tfrac{1}{2} 10^{-5} \theta^{1/2} = \tfrac{1}{2} 10^{-4} \text{ c.g.s.}, \quad \text{when} \quad \theta = 100^\circ \text{ K},$$

$$\sqrt{\overline{u^2}} = \sqrt{\left(\frac{3 k \theta}{m_H}\right)} = 1.58 \times 10^4 \theta^{1/2} = 1.6 \times 10^5 \text{ cm/sec}, \quad \text{when} \quad \theta = 100^\circ \text{ K}, \tag{2}$$

where σ, the effective collision radius, has been taken very approximately as 10^{-8} cm. The resulting value for the kinematic viscosity ν implies that the diameter of the smaller turbulent eddies expected to occur in a gas cloud is of the order of 0.01 psc. The relaxation time of the turbulent field is small compared to the time between collisions of a cloud, and, hence, turbulence will not be considered.

II. FORMATION OF CLOUDS FROM A HOMOGENEOUS MEDIUM

Jeans's criterion for stability of a homogeneous gas shows that a fluctuation in density is unstable against increasing inhomogeneity, provided that its wave length is greater than λ_c, where

$$\lambda_c = \left(\frac{\pi \alpha k \theta}{G \rho m_H}\right)^{1/2}. \tag{3}$$

If a fluctuation is longer than λ_c, it will increase in severity. The regions of increased density will collapse until stabilized by their angular momentum. If $\alpha > \frac{4}{3}$, a stable radius is reached, even if there is no angular momentum due, say, to initial turbulence. It is of interest to note that $\alpha = 1$, $\theta = 35^\circ$ K, and a density of 10^{-23} gm/cm^3 in the primordial homogeneous medium gives λ_c comparable to the observed cloud spacing. Chandrasekhar has shown that equation (3) is modified somewhat if the primordial homogeneous me-

---

[6] J. H. Oort and H. C. van de Hulst, *B.A.N.*, No. 376, 1946.

[7] H. I. Ewen and E. M. Purcell, *Nature*, **168**, 356, 1951.

[8] C. A. Muller and J. H. Oort, *Nature*, **168**, 357, 1951.

[9] M. Savedoff and L. Spitzer, Jr., *Ap. J.*, **111**, 593, 1950.

dium had turbulent velocities comparable to the speed of sound.[10] The result is, obviously, to increase λ_c.

III. DYNAMICS OF THE INTERSTELLAR GAS CLOUDS

We shall set up a simplified model of the interstellar gas structures and investigate its dynamical properties. It would be desirable, of course, to attempt the problem generally and thereby deduce from the properties of the interstellar gas its dynamical state. However, such a general approach is complex, and the problem will be attacked by investigating specific models. The shortcomings of each unsuccessful model, it is hoped, will guide us in future efforts.

Let us assume that the interstellar gas exists in discrete clouds. The regions between the clouds are assumed to have negligible density. The clouds are assumed to preserve, to a large degree, their identities, even though they may be undergoing collisions with one another. The clouds will, in general, be rotating and hence oblate. In order to treat the problem mathematically with any degree of conciseness, it is necessary to represent each individual cloud by a homogeneous sphere of gas, of variable radius and rotational angular momentum p_s, which obeys the polytrope law (eq. [1]). We will neglect the oblateness, which would tremendously complicate our mathematics and can be shown to change our final results only by factors of the order of unity. Thus the gravitational self-energy of the cloud is given by

$$V = -\frac{3}{5}\frac{GM^2}{a}, \tag{4}$$

where M is the cloud mass, a its radius, and G the gravitational constant. The kinetic energy of its rotation is

$$\frac{5p_s^2}{4Ma^2}, \qquad p_s = \tfrac{2}{5}Ma^2\dot{\varphi}. \tag{5}$$

The kinetic energy of the translational degrees of freedom of the gas is given by $3Mk\theta/2m_H$. We note that

$$\rho = \frac{3M}{4\pi a^3}, \tag{6}$$

so that the translational thermal kinetic energy may be written

$$\frac{3Mk\theta_0}{2m_H}\left(\frac{a_0}{a}\right)^{3(\alpha-1)}, \tag{7}$$

where we assume a temperature θ_0 for a cloud radius a_0. Finally, the kinetic energy in the radial oscillations of the cloud is

$$\tfrac{3}{10}M\dot{a}^2. \tag{8}$$

The total kinetic energy is the sum of these three terms, there being no cross-product terms.

Let us first investigate the dynamical equilibrium conditions for our cloud model. The virial is probably the clearest means of getting at the problem. If $\boldsymbol{p}_i$ and $\boldsymbol{r}_i$ are the momentum and position of the ith particle in the cloud, we have

$$\frac{d}{dt}\sum_i \boldsymbol{p}_i\cdot\boldsymbol{r}_i = 2T + V, \tag{9}$$

---

[10] S. Chandrasekhar, Proc. R. Soc. *London*, *A*, **210**, 18, 26, 1951.

where T is the kinetic energy of the internal motions of the cloud and V is the gravitational energy. Choosing the origin at the center of the cloud, it is readily seen that

$$\sum_i \boldsymbol{p}_i \cdot \boldsymbol{r}_i$$

represents a weighted mean of the rate of expansion of the cloud, and hence the left side of equation (9) has the same sign as the radial acceleration of the cloud. For statical equilibrium it must, of course, vanish. If the equilibrium is to be stable, then

$$\frac{d}{da}\left(\frac{d}{dt}\sum_i \boldsymbol{p}_i \cdot \boldsymbol{r}_i\right) < 0 , \tag{10}$$

evaluated at the equilibrium radius. In order to discuss the stability, let us first compute the equilibrium radii. Introducing equations (4), (5), (7), and (8) into equation (9) gives

$$\frac{1}{2}\frac{d}{dt}\sum_i \boldsymbol{p}_i \cdot \boldsymbol{r}_i = \frac{3Mk\theta_0}{2m_H}\left(\frac{a_0}{a}\right)^{3(\alpha-1)} + \frac{5p_s^2}{4Ma^2} + \tfrac{3}{10}M\dot{a}^2 - \frac{3GM^2}{10a} . \tag{11}$$

In the case of a stationary state, we make

$$\sum_i \boldsymbol{p}_i \cdot \boldsymbol{r}_i = 0$$

and obtain

$$0 = \frac{3Mk\theta_0}{2m_H}\left(\frac{a_0}{a}\right)^{3(\alpha-1)} + \frac{5p_s^2}{4Ma^2} - \frac{3GM^2}{10a} . \tag{12}$$

In order to obtain an explicit expression for a, we consider only the cases $\alpha = 1$ and $\alpha = \frac{2}{3}$, values which cover typical *H* I and *H* II regions. We obtain

$$\begin{aligned} a &= \frac{GMm_H}{10k\theta_0}\left[1 \pm \sqrt{\left(1 - \frac{250k\theta_0 p_s^2}{3m_H G^2 M^4}\right)}\right] \qquad \text{for} \qquad \alpha = 1 ; \\ 0 &= \frac{3Mk\theta_0}{2m_H}\frac{a^3}{a_0} - \frac{3GM^2}{10}a + \frac{5p_s^2}{4M} \qquad \text{for} \qquad \alpha = \tfrac{2}{3} . \end{aligned} \tag{13}$$

To obtain a picture of the equilibrium of a cloud, the left-hand side of equation (11), which represents the time rate of change of the expansion of the cloud, is shown schematically in Figure 1. Curve A represents a cloud with too large a rotation to be in equilibrium. It will simply expand indefinitely; B represents the critical value of p_s. According to equation (10), $a = a_2$ is not a stable equilibrium. Finally, C represents a cloud for which p_s is not too large to allow equilibrium. Equation (10) implies that a_1 is a stable equilibrium and a_3 is an unstable equilibrium. For $a > a_3$, the cloud expands indefinitely because its temperature is too large. If a cloud finds itself too far to the left of $a = a_1$, owing perhaps to a collision,

$$\sum_i \boldsymbol{p}_i \cdot \boldsymbol{r}_i$$

will become too large by the time $a = a_1$ is reached and will carry the cloud on out to $a = a_3$, where the temperature will cause the cloud to expand indefinitely.

The maximum p_s which a cloud may possess and still be in equilibrium is readily derived from equations (13). It corresponds to the curve B in Figure 1. We see that

$$\frac{d}{dt}\sum_i p_i \cdot r_i$$

has a double root at $a = a_2$ and we obtain the maximum p_s as

$$p_{sm} = \begin{cases} \dfrac{GM^2}{5}\sqrt{\left(\dfrac{3m_H}{10k\theta_0}\right)} & \text{for} \quad \alpha = 1 \\[2ex] \dfrac{2M^2}{5}\left(\dfrac{G^2 m_H a_0}{15Mk\theta_0}\right)^{1/4} & \text{for} \quad \alpha = \frac{2}{3}\,. \end{cases} \tag{14}$$

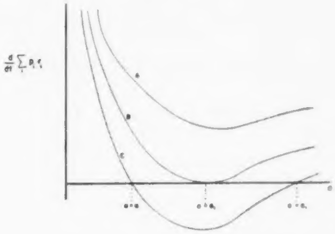

FIG. 1.—$\frac{d}{dt}\sum_i \rho_i r_i \, \alpha < \frac{4}{3}$

Introducing equation (14) into equation (13) gives us the maximum radius a_2 for a given mass or the minimum mass for a given radius:

$$a_2 = \begin{cases} \dfrac{Gm_H M}{10k\theta_0} & \text{for} \quad \alpha = 1 \\[2ex] \left(\dfrac{Gm_H M a_0}{15k\theta_0}\right)^{1/2} & \text{for} \quad \alpha = \frac{2}{3}\,. \end{cases} \tag{15}$$

Or, if we solve for M, we obtain the minimum cloud mass in the case of $\alpha = 1$ as

$$M = \frac{10a_2 k\theta_0}{Gm_H}\,, \tag{16}$$

and the density

$$\rho = \frac{15k\theta_0}{2\pi G m_H a_2^2}\,. \tag{17}$$

From equation (17) we find that the minimum density for a cloud at 40° K and a radius of 10 psc is about 100 hydrogen atoms/cm^3. Actually, the density should be somewhat greater than this, say 200 atoms/cm^3, in order that collisions may not disrupt the cloud. These densities are a little greater than the observed values and are the first indication of our coming difficulties with a purely gravitational model of the interstellar medium.

Let us now proceed with the final stage of our analysis by considering the effects of the collisions of clouds. With $\alpha < 1$, one sees from equation (1) that the collisions will be quite inelastic, i.e., the temperature will drop as the density increases. Hence a collision of two clouds initially moving with velocities greater than their escape velocity will probably only rarely succeed in disrupting the clouds. Or, in other words, the clouds will produce a minimum of splashing on collision, behaving somewhat like putty balls.

The first point of importance arises from a consideration of the conditions for statistical equilibrium between the translational and the rotational degrees of freedom. For equipartition of energy we expect that

$$\tfrac{1}{2}M\,\overline{v^2} = \frac{5p_s^2}{4Ma^2}, \tag{18}$$

where $\overline{v^2}$ is the mean square of the translational velocity of the clouds. We define

$$x = \frac{p_s}{p_{sm}}.$$

Then, for instance, for $\boldsymbol{\alpha} = 1$, we have, from equation (13),

$$\frac{p_s}{a} = \frac{p_{sm}}{a_2}\,\frac{x}{1-\sqrt{(1-x^2)}},$$

$$a = a_2\left[1-\sqrt{(1-x^2)}\right].$$

Thus

$$\frac{d}{dx}\left(\frac{a}{a_2}\right) = \frac{x}{\sqrt{1-x^2}} > 0,$$

$$\frac{d}{dx}\left(\frac{p_s}{a}\right) = -\frac{p_{sm}}{a_2}\,\frac{1}{\sqrt{(1-x^2)}\left[1-\sqrt{(1-x^2)}\right]} < 0.$$

The maximum value of x is unity, and this gives the minimum value of p_s/a, viz., p_{sm}/a_2. Therefore, it follows that, as the clouds collapse, their rotational energy increases. That this must be the case is physically obvious from the virial theorem. Thus the right-hand side of equation (18) exceeds the left, and energy will be fed from the internal energy to $\overline{v^2}$ upon collision. This produces further collapse, etc. If, on the other hand, we begin with the left-hand side of equation (18) the larger, then energy will be fed from $\overline{v^2}$ to the internal energy of the clouds, causing them to expand. In this case, it is clear $\frac{1}{2}M\overline{v^2}$ must not exceed the value of $5p_{sm}^2/4Ma_2^2$ when a_2 is reached, or else the clouds will simply expand to infinity. Thus

$$\overline{v^2} < \frac{5p_{sm}^2}{2M^2a_2^2}.$$

From equations (14) and (15), this becomes

$$\overline{v^2} < \left(\frac{k\theta_0}{m_H}\right)^{1/2} \times \begin{cases} \sqrt{3} & \text{for} \quad \alpha = 1 \\ \sqrt{6} & \text{for} \quad \alpha = \frac{2}{3}. \end{cases} \tag{19}$$

That is, $\sqrt{\overline{v^2}}$ is somewhat less than the thermal velocity of the molecules of which the cloud is composed. At 40° K, we then have $\sqrt{\overline{v^2}} < 1$ km/sec, which is 1 order of magnitude less than observed.[5]

If we assume, then, a statistical equilibrium between the rotational and translational degrees of freedom, it follows that the clouds have $a \ll a_2$, $p_s \ll p_{sm}$, since equation (19) is not satisfied. This immediately implies that the process of transferring energy from the internal energy of the cloud to its translational energy is well under way.

One may show this process more formally by considering the distribution of clouds over their internal states. This is given[11] by $\exp[-H/kT]$, where T is defined by

$$M\overline{v^2} = 3kT\ , \tag{20}$$

and H is the Hamiltonian for an isolated cloud. To compute the Hamiltonian, we first write the Lagrangian. We must include the potential energy of the gas itself, i.e.,

$$-\int_{a=a_0}^{a=a} p\,dV = -\frac{Mk\theta_0}{3m_H(1-\alpha)}\left[\left(\frac{a}{a_0}\right)^{3(1-\alpha)}-1\right]. \tag{21}$$

Using Euler's angles to describe the rotational state of the cloud, we have, from equations (4), (8), and (21),

$$\begin{aligned} L = \tfrac{1}{5}Ma^2(\dot\theta^2+\dot\psi^2+\dot\varphi^2+2\dot\psi\dot\varphi\cos\theta) + \tfrac{3}{10}M\dot a^2 + \frac{3GM^2}{5a} \\ + \frac{Mk\theta_0}{3m_H(1-\alpha)}\left[\left(\frac{a}{a_0}\right)^{3(1-\alpha)}-1\right]. \end{aligned} \tag{22}$$

The Hamiltonian is

$$\begin{aligned} H = \frac{5}{4Ma^2}\left[p_\theta^2+\frac{1}{\sin^2\theta}(p_\psi^2+p_\varphi^2-2p_\psi p_\varphi\cos\theta)\right]+\frac{5}{6M}p_a^2 \\ -\frac{3GM^2}{5a}-\frac{Mk\theta_0}{3m_H(1-\alpha)}\left[\left(\frac{a}{a_0}\right)^{3(1-\alpha)}-1\right]. \end{aligned} \tag{23}$$

If C is a normalization constant, the number in the radius range da is $A(a)da$, where

$$A(a) = C\int_0^{\pi}\int_{-\infty}^{+\infty}\int_{-\infty}^{+\infty}\int_0^{2\pi}\int_0^{2\pi}\int_{-\infty}^{+\infty}\int_{-\infty}^{+\infty}\exp\left(-\frac{H}{kT}\right)dp_a\,dp_\theta\,d\varphi\,d\psi\,dp_\psi\,dp_\varphi\,d\theta\ , \tag{24}$$

and the indicated order of integration is as convenient as any. One finds ultimately

$$\begin{aligned} A(a) = \frac{64\sqrt{6}\pi^4}{25}CM^2k^2T^2\exp\left(\frac{Mk\theta_0}{m_HkT(1-\alpha)}\right) \\ \Big\}a^3\exp\left[\frac{1}{kT}\left(\frac{3GM^2}{a}+\frac{Mk\theta_0}{m_H(1-\alpha)}\left[\frac{a}{a_0}\right]^{3(1-\alpha)}\right)\right]\Big\}. \end{aligned} \tag{25}$$

We see that for $\alpha < \frac{4}{3}$, $A(a)$ diverges at both $a = 0$ and $a = \infty$ to such an extent that

$$\int_0^\infty A(a)\,da$$

diverges at both ends. Therefore, the equilibrium configuration of the clouds is either with all clouds expanded to infinity or collapsed into points. We see, then, that, by allowing collisions between the clouds, a cloud may lose its angular momentum. The angular momentum is converted, on collision, to relative angular momentum of the colliding units. With the loss of the stabilizing effect of the angular momentum, the cloud may be expected to collapse.

It is of interest to consider the implications of the above calculations. Observationally, there is evidence for an approach to statistical equilibrium of the translational velocities. If we assume that this equilibrium extends to the rotational state of the clouds and recall that some 50 collisions have probably been suffered by each cloud, then we would find all the gas clouds either expanded to infinity or collapsed, presumably into stars or clusters of stars. The material in the clouds which expand to infinity may to a large extent be scavenged by Jeans's collapse mechanism and so is not permanently lost to the system of discrete clouds.

---

[11] R. C. Tolman, *The Principles of Statistical Mechanics* (Oxford: Clarendon Press, 1938).

If one feels that the collision rate of one collision every $\frac{2}{3} \cdot 10^7$ years would deplete the translational velocity of the clouds too seriously because of the inelasticity of such collisions; and, if one also expects statistical equilibrium of the internal states after 50 collisions, then one must look for modifications of the above simple randomly moving gravitational cloud model. This suggests magnetic fields, with their subsequent stabilizing effect. However, we shall limit ourselves here to a discussion of the purely dynamical possibilities. We may assume that the translational velocities are not random, as assumed above, but rather ordered, so that the collision rate falls well below 25 collisions per revolution of the galaxy. The idea has been suggested by J. L. Greenstein that the clouds do not exist separately but rather in groups or complexes such as are seen as spiral arms of dust and gas in extragalactic systems. The clouds within a given complex presumably follow semiregular orbits, with the result that the collision rate is greatly reduced. It is interesting to discuss the idea of complexes in light of Jeans's instability criterion. The existing clouds have masses of the order of $10^3\ M_\odot$. If we assume a primordial medium with a density of 10^{-1} hydrogen atoms/cm^3 and radiation conditions comparable to those assumed by Spitzer in his calculation of the temperature of the interstellar medium, then $\theta \sim 200°$ K and λ_c is 10^3 psc if the medium is quiescent; λ_c is more than 10^3 psc if the medium is turbulent. A cell will collapse until supported by its angular momentum, with, say, 50 hydrogen atoms/cm^3. The temperature will soon fall to $\sim 40°$ K, and, although Jeans's criterion does not apply rigorously to an isolated mass, one finds that the cell becomes internally unstable, and further collapse begins taking the single large cell into many small cells or clouds with masses $\sim 3 \cdot 10^3\ M_\odot$. We see, then, that a reasonable set of initial conditions leads to a complex of acceptable clouds. Thus complexes, not single clouds, are formed from the initially homogeneous medium. Thus the proposal seems quite plausible theoretically. Whether or not one accepts the above speculations on the ordering of translational velocities, the calculations indicate that there will be a tendency for at least some of the gas clouds to collapse, giving the possibility of forming star clusters.

I should like to express my gratitude to Professors H. P. Robertson, Leverett Davis, Jr., and J. L. Greenstein for much guidance during the progress of this work and to Professors Lyman Spitzer, Jr., and R. N. Thomas for their helpful discussion of much of the material.

MAGNETO-HYDRODYNAMIC SHOCK WAVES

H. LAWRENCE HELFER*
Yerkes Observatory

Received August 29, 1952

ABSTRACT

An interpretation of the de Hoffman-Teller shock-wave equations for an infinitely conducting medium is given analogous to the classical interpretation of the ordinary hydrodynamic shock-wave equations of Rankine and Hugoniot. Two cases of interest are considered as a consequence of this theory. It is shown that weak magnetic fields in interstellar clouds will be amplified, and, if external mechanisms are available to reduce the compressional effects of shock waves, the field will reach a value $H \sim (8\pi p)^{1/2}$, where p is the pressure. Also, some aspects of the internal motions of prominences are considered; it is shown that $H \sim 0.1$ gauss will yield results in accord with the observational material.

I. INTRODUCTION

The propagation of waves of infinitesimal amplitude in an incompressible conducting fluid in the presence of a magnetic field was first investigated by Alfvén.[1] Van de Hulst[2] and Herlofson[3] independently extended the theory for compressible fluids and showed that, in general, three different modes of motion were possible, each characterized by a different velocity. Furthermore, the velocities of propagation were found to be dependent not only upon the strength of the magnetic field but also upon the direction of propagation.

The study of waves of finite amplitude (i.e., shock waves) in such a fluid has not been carried out so carefully. In ordinary hydrodynamics the passage of a plane shock wave through a medium results in abrupt changes in the pressure, temperature, and density. The situation is then fully described by the equations of Rankine and Hugoniot. The interpretation of these equations is well known[4] and will not be discussed here. Recently, de Hoffman and Teller[5] have derived the analogues of the Rankine-Hugoniot equations for an infinitely conducting fluid. It is the purpose of this paper to provide a systematic interpretation of their results and to show that we can recover the results of van de Hulst[3] in the limits of weak shocks.

The problem of the generation of shock waves will be left open. It is known that shock waves will be produced by disturbances of finite amplitude or by causing a finite charge of momentum in a medium, as when a piston in a fluid is suddenly advanced. We may therefore expect that varying convection currents and turbulence will produce shock waves. There does not appear to be any good method, however, of estimating the strength of the shocks produced by such mechanisms in regions of astrophysical interest.

The effect of departures from the assumption of infinite conductivity will not be considered. The validity of this assumption for astrophysical phenomena has been discussed elsewhere,[5] and, in view of the large dimensions of interstellar clouds, on the one hand,

---

* National Science Foundation Predoctoral Fellow, 1952–1953.

[1] Cf., e.g., H. Alfvén, *Cosmical Electrodynamics* (London: Oxford University Press, 1950), chap. iv.

[2] *Symposium: Problems of Cosmical Aerodynamics* (Dayton, Ohio: Central Air Documents Office, 1951), chap. vi.

[3] N. Herlofson, *Nature*, **165**, 1020, 1950.

[4] Cf., e.g., Bleakney and Taub, *Rev. Mod. Phys.*, **21**, 584, 1949; Courant and Friedrichs, *Supersonic Flow and Shock Waves* (New York: Interscience Publishers, 1948).

[5] *Phys. Rev.*, **80**, 692, 1950.

and the large conductivities of stellar material, on the other,[6] it appears as if this is a reasonable assumption for many astrophysical problems.

II. THE BASIC FRAME OF REFERENCE

Consider a two-dimensional medium of infinite electrical conductivity, originally homogeneous, through which a plane shock front is passing. We shall distinguish the parameters describing the material in front of the advancing shock from those describing the matter behind the shock by subscripts 1 and 2, respectively; thus the velocities of the matter on the two sides of the shock will be denoted by V_1^0 and V_2^0. Let the velocity of the shock front in the direction of propagation be U. For convenience, we take $V_1^0 = 0$. The situation is then as in *A* in Figure 1.

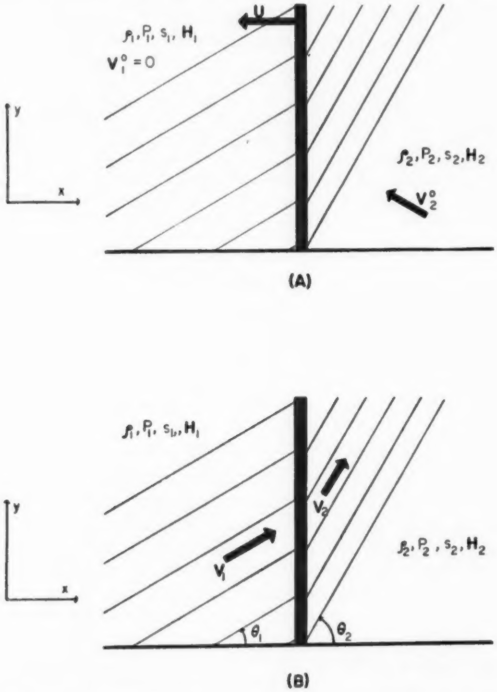

FIG. 1.—*A* refers to the initial co-ordinate system; *B* refers to the preferred co-ordinate system. The diagonal lines represent the lines of force; the heavy vertical line represents the shock front.

Following de Hoffman and Teller, we shall transform to a system of reference in which the shock is at rest and matter streams toward the shock front in a direction parallel to the lines of force (cf. *B*, Fig. 1). It may be shown[5] that, in such a system, matter will also stream away from the shock front in a direction parallel to the lines of force. Letting θ_1 be the angle between the lines of force on side 1 and the direction of propagation of the shock and

$$s_1 = \tan \theta_1 , \tag{1}$$

---

[6] D. E. Osterbrock, *Phys. Rev.*, **87**, 468, 1952.

we find that the transformation equations are:

$$V_{1x} = -U\,; \qquad V_{1y} = -s_1 U\,;$$
$$V_{2x} = V^0_{2x} - U\,; \qquad V_{2y} = V^0_{2y} - s_1 U\,. \tag{2}$$

The inverse transformation is:

$$V^0_{1x} = 0\,; \qquad V^0_{1y} = 0\,; \qquad U = -V_{1x}\,;$$
$$V^0_{2x} = V_{2x} - V_{1x}\,; \qquad V^0_{2y} = V_{2y} - V_{1y}\,. \tag{3}$$

The foregoing transformation is possible whenever the lines of force on side 1 are not parallel to the shock front.

In general, three cases may be distinguished: (1) $s_1 = 0$, (2) $0 < s_1 < \infty$, and (3) $s_1 = \infty$ (when transformation [2] is not possible). The first and third cases can be considered as limiting cases of (2); in view of the importance of these cases, it is of interest to examine them first.

III. PARALLEL AND PERPENDICULAR SHOCKS

When $s_1 = 0$, the magnetic field has no influence upon the hydrodynamic phenomena. Since it is unaltered by the passage of the shock, the situation may therefore be completely described by the classical Rankine-Hugoniot equations:

$$\rho_1 V_1 = \rho_2 V_2\,, \tag{4}$$

$$\rho_1 V_1^2 + p_1 = \rho_2 V_2^2 + p_2\,, \tag{5}$$

and

$$\rho_1 V_1 \mathfrak{U}_1 + p_1 V_1 + \tfrac{1}{2}\rho_1 V_1^3 = \rho_2 V_2 \mathfrak{U}_2 + p_2 V_2 + \tfrac{1}{2}\rho_2 V_2^3\,, \tag{6}$$

and the specification of a parameter such as, e.g., $Y = p_2/p_1$ or $\eta = \rho_2/\rho_1$. In equations (4)–(6) and in the following equations, V refers to the material stream velocity, ρ the density, and $\mathfrak{U}$ the internal energy. In cases when no ambiguity can arise, the subscript 1 will be omitted.

In the third case, the co-ordinate transformation (2) is not possible; in this case we may transform from the initial co-ordinate system into one in which the velocity vector $\boldsymbol{V}_1$ is perpendicular to the stationary shock front. The analogues to the Rankine-Hugoniot equations, then, are:

$$\rho_1 V_1 = \rho_2 V_2\,, \tag{7}$$

$$\rho_1 V_1^2 + p_1^* = \rho_2 V_2^2 + p_2^*\,, \tag{8}$$

$$\rho_1 V_1 \mathfrak{U}_1^* + p_1^* V_1 + \tfrac{1}{2}\rho_1 V_1^3 = \rho_2 V_2 \mathfrak{U}_2^* + p_2^* V_2 + \tfrac{1}{2}\rho_2 V_2^3\,, \tag{9}$$

where

$$p_i^* = p_i + \frac{H_i^2}{8\pi}\,, \qquad \mathfrak{U}_i^* = \mathfrak{U}_i + \frac{H_i^2}{8\pi\rho_i} \qquad (i = 1,\,2)\,, \tag{10}$$

and

$$H_1 V_1 = H_2 V_2\,. \tag{11}$$

Equations (7)–(9) have exactly the same forms as in the case already considered (cf. eqs. [4]–[6]), if one takes into account the magnetic pressure and energy by equations (10) and the coupling of the magnetic and velocity fields by equation (11). In fact, this last equation shows that the magnetic field acts as if glued to the matter and is compressed by the shock exactly to the same extent as the fluid:

$$\frac{H_2}{H_1} = \frac{\rho_2}{\rho_1} \equiv \eta \, . \tag{12}$$

In this case, the specification of two parameters is required: one giving a measure of the shock strength and the other expressing the importance of the magnetic field. For example, for a perfect gas $U = p/(\gamma - 1)\rho$, and we may introduce the quantities

$$Q_i = \frac{H_i^2}{8\pi p_i} \qquad (i = 1, 2) \, , \tag{13}$$

and use $Q \equiv Q_1$ as one of our parameters.

Since

$$Q = \frac{1}{\gamma - 1} \, \frac{H_1^2 / 8\pi \rho_1}{p_1 / (\gamma - 1) \rho_1} \, , \tag{14}$$

we note that $(\gamma - 1)Q$ is the ratio of the magnetic energy per unit mass to the internal energy per unit mass.

With the aid of substitutions (13), equations (7)–(11) may be brought into the form

$$\frac{V_2}{V_1} = \frac{1}{\eta} \qquad (V_1 \neq 0) \, , \tag{15}$$

$$\frac{Q_2}{Q_1} = \frac{\eta^2}{Y} \, , \tag{16}$$

$$\rho_1 V_1^2 \left[1 - \frac{1}{\eta} \right] + p_1 \left[(1 - Y) + Q (1 - \eta^2) \right] = 0 \, , \tag{17}$$

$$\tfrac{1}{2} \rho_1 V_1^2 \left[1 - \frac{1}{\eta^2} \right] + p_1 \left[\frac{\gamma}{\gamma - 1} \left(1 - \frac{Y}{\eta} \right) + 2Q (1 - \eta) \right] = 0 \, . \tag{18}$$

The secular equation resulting from equations (17) and (18) is

$$Q (\eta - 1)^3 + \left[\frac{2\gamma}{\gamma - 1} + (Y - 1) \right] (\eta - 1) - \frac{2}{\gamma - 1} (Y - 1) = 0 \, . \tag{19}$$

The condition $Y - 1 > 0$ requires η to assume values $\eta \geqslant 1$; furthermore, for a given Q and Y, η is determined uniquely. The presence of the magnetic field is seen to cause a decrease in the compression, η. Assignment of values to any two of the three quantities Q, Y, and η uniquely determines all the quantities of interest. The nature of the relation between Q, Y, and η for the monatomic perfect gas ($\gamma = \frac{5}{3}$) is essentially described by the solid-line curves in Figure 7, if x is interpeted as η.

We note that, since (cf. eq. [19])

$$Q = \frac{2 (Y - 1) - (\eta - 1) \left[2\gamma + (\gamma - 1)(Y - 1) \right]}{(\gamma - 1)(\eta - 1)^3} \, , \tag{20}$$

the requirement $Q \geqslant 0$ is equivalent to

$$\eta - 1 \leqslant \frac{2 (Y - 1)}{2\gamma + (\gamma - 1)(Y - 1)} \, ; \tag{21}$$

letting $Y \rightarrow \infty$ in the foregoing inequality, we conclude that

$$\eta - 1 \leqslant \frac{2}{\gamma - 1} \, , \tag{22}$$

which is a classical result.

Also, since equation (20) may be written as

$$(\eta - 1) = (\eta_0 - 1)\left[1 - \tfrac{1}{2}(\gamma - 1)\beta(\eta - 1)^3\right], \tag{23}$$

where

$$\eta_0 - 1 = \frac{2(Y - 1)}{2\gamma + (\gamma - 1)(Y - 1)}, \qquad \beta = \frac{Q}{Y - 1}, \tag{24}$$

it may be concluded that

$$\eta - 1 \leqslant \left[\frac{2}{(\gamma - 1)\beta}\right]^{1/3}, \tag{25}$$

a relation of particular interest for large values of β.

The solution of equations (17) and (18), taken in connection with equation (15) and subject to the restriction imposed by equation (19), gives expressions for the various velocities of interest:

$$\left(\frac{V_1}{c_1}\right)^2 = \frac{\eta}{\gamma}\,\frac{(Y - 1)}{(\eta - 1)}\left[1 + \beta(\eta^2 - 1)\right], \tag{26}$$

$$\left(\frac{V_2}{c_2}\right)^2 = \frac{1}{\gamma\eta}\,\frac{(Y - 1)}{(\eta - 1)}\left[1 + \beta(\eta^2 - 1)\right], \tag{27}$$

$$\left(\frac{c_2}{c_1}\right)^2 = \frac{Y}{\eta}, \tag{28}$$

where $c = \gamma p/\rho$ is the velocity of sound.

The presence of the magnetic field increases the values of quantities (26)→(28), compared to the classical hydrodynamic values, since the compression is decreased.

The same may be said of the quantity

$$\left(\frac{V_1 - V_2}{c_1}\right)^2 = \frac{1}{\gamma\eta}(Y - 1)(\eta - 1)\left[1 + \beta(\eta^2 - 1)\right], \tag{29}$$

although it is not so obvious in this case. This increase represents a transfer of kinetic into magnetic energy. If we write $\eta + \epsilon = \eta_0$, where η_0 is the compression with zero field present and ϵ is consequently the decrease in the compression due to the presence of the field, then $|(V_1 - V_2)/c_1|$ increases in the presence of a field if

$$\frac{1}{\eta}(\eta - 1)\left[1 + \beta(\eta^2 - 1)\right] - \frac{\eta + \epsilon - 1}{\eta + \epsilon} > 0, \tag{30}$$

i.e., if

$$(\eta - 1)(\eta^2 - 1)\beta - \frac{\epsilon}{\eta + \epsilon} > 0. \tag{31}$$

Since $\eta > 1$ and $(\eta - 1)^2 < \eta^2 - 1$, the inequality surely holds if

$$\frac{\eta(\eta - 1)^3\beta}{1 - (\eta - 1)^3\beta} > \epsilon. \tag{32}$$

On the other hand, equation (23) may be brought into the form

$$\epsilon = \frac{\frac{1}{2}(\gamma - 1)\beta(\eta - 1)^4}{1 - \frac{1}{2}(\gamma - 1)\beta(\eta - 1)^3}. \tag{33}$$

Therefore,

$$\epsilon < \frac{\frac{1}{2}(\gamma - 1)\beta(\eta - 1)^4}{1 - \beta(\eta - 1)^3}, \tag{34}$$

if $\gamma < 3$. Since $\eta > \frac{1}{2}(\gamma - 1)(\eta - 1)$, relation (32) must hold.

IV. OBLIQUE SHOCKS

For the case $0 \leqslant s_1 \leqslant \infty$, the situation becomes more complicated, the direction of the material streaming away from the shock front not being necessarily unique. The coupling between the magnetic and the hydrodynamic fields is intermediate between the two cases already considered, and, indeed, magnetic energy may be converted into kinetic or potential energy. As may be expected, three parameters are now needed to make the problem determinate: one measuring the shock strength, one measuring the importance of the magnetic field, and a third measuring the obliqueness of the lines of force with respect to the shock front. For this purpose, the quantities Q, Y, and s_1 will be used.

In the preferred co-ordinate system (cf. B, Fig. 1), $\boldsymbol{V}_1$ is parallel to $\boldsymbol{H}_1$ and $\boldsymbol{V}_2$ is parallel to $\boldsymbol{H}_2$, and consequently we can set the electric vectors $\boldsymbol{E}_1$ and $\boldsymbol{E}_2 = 0$. Then, for the perfect gas, the analogues of the Rankine-Hugoniot equations as derived by de Hoffman and Teller are

$$\rho_1 V_{1x}^2 + p_1 + \frac{1}{8\pi} H_{1y}^2 = \rho_2 V_{2x}^2 + p_2 + \frac{1}{8\pi} H_{2y}^2 ; \tag{35}$$

$$\rho_1 V_{1x} V_{1y} - \frac{1}{4\pi} H_{1x} H_{1y} = \rho_2 V_{2x} V_{2y} - \frac{1}{4\pi} H_{2x} H_{2y} ; \tag{36}$$

$$\frac{\gamma}{\gamma - 1} p_1 V_{1x} + \tfrac{1}{2} \rho_1 [V_{1x}^2 + V_{1y}^2] V_{1x} = \frac{\gamma}{\gamma - 1} p_2 V_{2x} + \tfrac{1}{2} \rho_2 [V_{2x}^2 + V_{2y}^2] V_{2x} . \tag{37}$$

To these equations may be added the conditions

$$\rho_1 V_{1x} = \rho_2 V_{2x} \qquad \text{and} \qquad H_{1x} = H_{2x} , \tag{38}$$

which follow from the equation of continuity and the condition div $\boldsymbol{H} = 0$, and the further conditions

$$\frac{H_{iy}}{H_{ix}} = \frac{V_{iy}}{V_{ix}} = s_i \qquad (i = 1, 2) , \tag{39}$$

which express the fact that the velocity and magnetic vectors are parallel.

It is convenient to introduce the dimensionless parameters D_1, D_2, and x, defined by

$$D_i \boldsymbol{H}_i = (4\pi \rho_i)^{1/2} \boldsymbol{V}_i \qquad (i = 1, 2) \tag{40}$$

and

$$s_2 = x s_1 . \tag{41}$$

The quantitites D_i^2 are the ratios of kinetic energy per unit volume to magnetic energy per unit volume on the two sides of the shock. The quantity x gives a measure of the amount of refraction of the lines of force when passing through the shock; we shall refer to it as the *bending factor*.

As a consequence of these definitions, we have the following identities:

$$V_i^2 = 2 D_i^2 Q_i \frac{p_i}{\rho_i} ; \qquad V_{ix}^2 = 2 D_i^2 Q_i \frac{p_i}{\rho_i (1 + s_i^2)} ; \qquad V_{ix} V_{iy} = s_i V_{ix}^2 \qquad (i = 1, 2) ; \tag{42}$$

$$H_{iy}^2 = Q_i p_i \frac{s_i^2}{1 + s_i^2} ; \qquad H_{ix} H_{iy} = \frac{1}{s_i} H_{iy}^2 \qquad (i = 1, 2) . \tag{43}$$

It then follows from equations (38), (39), and (41) that

$$H_{2y} = x H_{1y} ; \tag{44}$$

therefore,

$$\frac{Q_2}{Q_1}=\frac{T^2}{Y}\,,\qquad \frac{H_2^2}{H_1^2}=T^2\,, \tag{45}$$

where

$$T^2=\frac{1+s^2x^2}{1+s^2}\,. \tag{46}$$

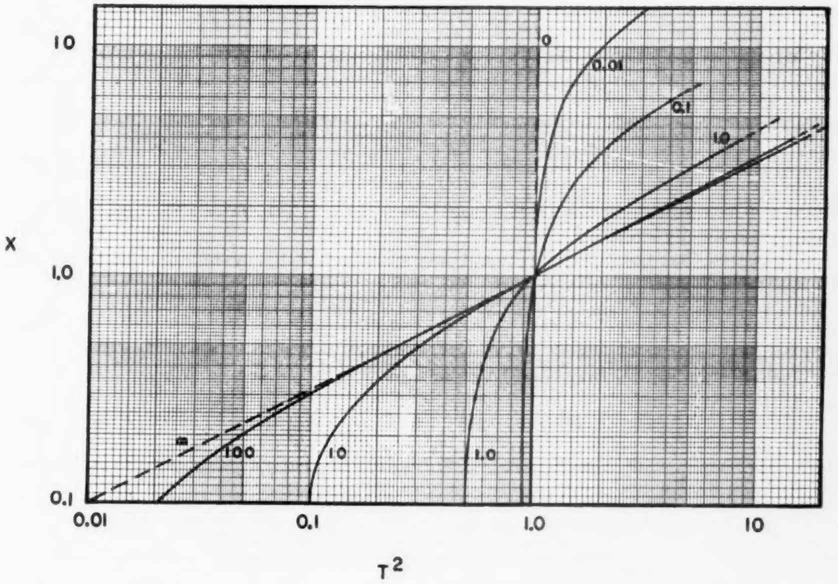

FIG. 2.—Graph of the amplification factor. Here x is to be regarded as being without sign; s^2 is the parameter differentiating the curves.

In view of equation (45), T^2 may be appropriately called the *amplification factor*. This amplification factor is illustrated in Figure 2; a discussion of its significance and limitations is postponed until Section IX.

Similarly, from equation (38), or its equivalent,

$$V_{2x}=\frac{1}{\eta}\,V_{1x}\,, \tag{47}$$

and equations (40), we have

$$D_2^2=\frac{1}{\eta}\,D_1^2\,. \tag{48}$$

Rewriting equations (35)–(37) in terms of the quantities introduced, we have, respectively,

$$\left[1+\frac{2}{1+s_1^2}\,D_1^2Q_1+\frac{s_1^2}{1+s_1^2}\,Q_1\right]=Y\left[1+\frac{2}{1+s_2^2}\,D_2^2Q_2+\frac{s_2^2}{1+s_2^2}\,Q_2\right], \tag{49}$$

$$\left[\frac{s_1}{1+s_1^2}\,D_1^2Q_1-\frac{s_1}{1+s_1^2}\,Q_1\right]=Y\left[\frac{s_2}{1+s_2^2}\,D_2^2Q_2-\frac{s_2}{1+s_2^2}\,Q_2\right], \tag{50}$$

$$\left[\frac{\gamma}{\gamma-1}+D_1^2Q_1\right]=\frac{Y}{\eta}\left[\frac{\gamma}{\gamma-1}+D_2^2Q_2\right]; \tag{51}$$

or, making use of transformations (41), (45), and (48), we have

$$Q_1=\frac{(1+s_1^2)\,(Y-1)}{2\,D_1^2\,(1-1/\eta)+s_1^2\,(1-x^2)}, \tag{52}$$

$$D_1^2=\frac{1-x}{1-x/\eta}, \tag{53}$$

$$Q_1D_1^2=\frac{\gamma}{\gamma-1}\;\frac{Y/\eta-1}{1-T^2/\eta^2}, \tag{54}$$

where $x=1$, resulting in the trivial case $Y=1$, $\eta=1$, and $T^2=1$ (cf. eqs. [50] and [51]), is specifically excluded.

It appeared that the most convenient way of reducing this system of equations is to introduce the quantity

$$A\equiv\frac{1-1/\eta}{1-x/\eta}, \qquad \eta=\frac{1-xA}{1-A}. \tag{55}$$

Equations (48) and (53) may then be replaced by

$$D_1^2=1-xA\,, \qquad D_2^2=1-A\,; \tag{56}$$

these expressions reveal the physical interpretation of A as a measure of the inequality between the kinetic and the magnetic energies per unit volume. Also, we note that

$$\eta=\frac{(\text{Kinetic energy per unit volume})_{\text{Side 1}}}{(\text{Kinetic energy per unit volume})_{\text{Side 2}}}\cdot\frac{(\text{Magnetic energy per unit volume})_{\text{Side 2}}}{(\text{Magnetic energy per unit volume})_{\text{Side 1}}}.$$

In terms of A, equation (52) becomes

$$A=\frac{1}{2\,(1-x)}\left[\,(1+s^2)\,\frac{Y-1}{Q}+s^2\,(x^2-1)\,\right], \tag{57}$$

an equation which may be regarded as an alternate definition of A in terms of Q, Y, and s. We may rewrite equation (57) in the form

$$Y-1=\frac{1-x}{1+s^2}\,[\,2A+(x+1)\,s^2\,]\,Q, \tag{58}$$

which serves to define the $(Q, Y-1)$ relation in terms of A, x, and s. An expression for Q may be found in terms of these same three parameters by means of equations (52), (54), and (55):

$$Q=\frac{\gamma\,(1+s^2)\,A}{A^2[\,(\gamma-1)\,x-(\gamma+1)\,]+A\,[\,2-\{\,(2-\gamma)\,x+\gamma\,\}\,s^2\,]+(x+1)\,s^2}. \tag{59}$$

For the case, $\gamma=\frac{5}{3}$, equation (62) becomes

$$Q=\frac{5\,(1+s^2)\,A}{2\,(x-4)\,A^2+[\,6-(x+5)\,s^2\,]\,A+3\,(x+1)\,s^2}. \tag{60}$$

In principle, one would like to determine the problem by specifying Q, V, and s. However, the mathematical formulation of the problem favors the utilization of s^2, x, and A as the parameters. Then $V - 1$ and Q may be determined from equations (58) and (59) or (60); the remaining quantities η, D_1, and D_2 then follow from equations (55) and (56). In order to help facilitate such calculations, Figures 3–7 have been prepared which give Q versus $V - 1$ as a function of the parameters x and s^2. Using these graphs for a given Q, V, and s, we may determine x; equation (57) then delivers A, and all the remaining quantitites follow as already explained. The representative values of s^2 chosen were 0.01, 0.1, 1, 10, and 100, corresponding, respectively, to values of 6°, $17\frac{1}{2}$°, 45°, $72\frac{1}{2}$°, and 84° for θ_1.

Interpolation between the various graphs may be accomplished to good approximation by

$$\begin{aligned} Q(s^2+\Delta s^2, x, A) &= Q(s^2, x, A) + \Delta s^2\left[\frac{\partial Q}{\partial(s^2)}\right]_{x,\ A\ \mathrm{const}} + \ldots, \\ \beta^{-1}(s^2+\Delta s^2, x, A) &= \beta^{-1}(s^2, x, A) + \Delta s^2\left[\frac{\partial \beta^{-1}}{\partial(s^2)}\right]_{x,\ A\ \mathrm{const}} + \ldots, \end{aligned} \tag{61}$$

where, for $\gamma = \frac{5}{3}$,

$$\begin{aligned} \left[\frac{\partial Q}{\partial(s^2)}\right]_{x,\ A\ \mathrm{const}} &= \frac{Q}{1+s^2}\left[1+\tfrac{1}{5}Q\left\{(x+5)-\frac{3(x+1)}{A}\right\}\right], \\ \left[\frac{\partial \beta^{-1}}{\partial(s^2)}\right]_{x,\ A\ \mathrm{const}} &= \frac{1}{1+s^2}\left[1-x^2-\beta^{-1}\right]. \end{aligned} \tag{62}$$

We shall resume the discussion of the solutions expressed in Figures 3–7 in Section IX.

The requirements $D_1^2 \geqslant 0$, $D_2^2 \geqslant 0$, $V - 1 \geqslant 0$, and $Q \geqslant 0$ impose restrictions upon the range of A. The latter two requirements are of particular value in numerically evaluating Q and $V - 1$: for $Q \geqslant 0$ requires the numerator and denominator of equation (60) to be of the same sign, and this result in general limits the range of A *qua* the roots of the quadratic denominator, and the requirement $V - 1 \geqslant 0$ implies, in accordance with equation (58), a further limitation on the range of A. As a guide to further calculations, we may give the *minimal* restrictions upon the range of A shown in Figure 8. The shaded regions are the permitted regions of A. In all cases $\eta \geqslant 1$.

V. WEAK SHOCKS

Several limiting cases are of interest. In the graphs the case of $V - 1 \leqslant 0.1$ has been neglected, for the shock strength in such cases is so low that, considering that dissipative processes are always present, it is most probable that such solutions act as ordinary magneto-hydrodynamic waves to a very good approximation.

Consider, then, solutions for which $V \cong 1$ and Q is arbitrary. Then, from equation (58), we must have: (a) $x - 1 \cong 0$ or (b) $2A + (x+1)s^2 \cong 0$.

We first treat case a. Put $1 - x = \epsilon$, where $|\epsilon| \ll 1$. Then equation (60) becomes

$$Q = \frac{5}{6}\,\frac{(1+s^2)A}{-A^2+(1-s^2)A+s^2}\left[1+O(\epsilon)+\ldots\right], \tag{63}$$

which, on neglecting second-order terms, becomes

$$A^2 + \left[(s^2-1)+(1+s^2)\delta\right]A - s^2 = 0 \tag{64}$$

where

$$\delta = \frac{5}{6Q}. \tag{65}$$

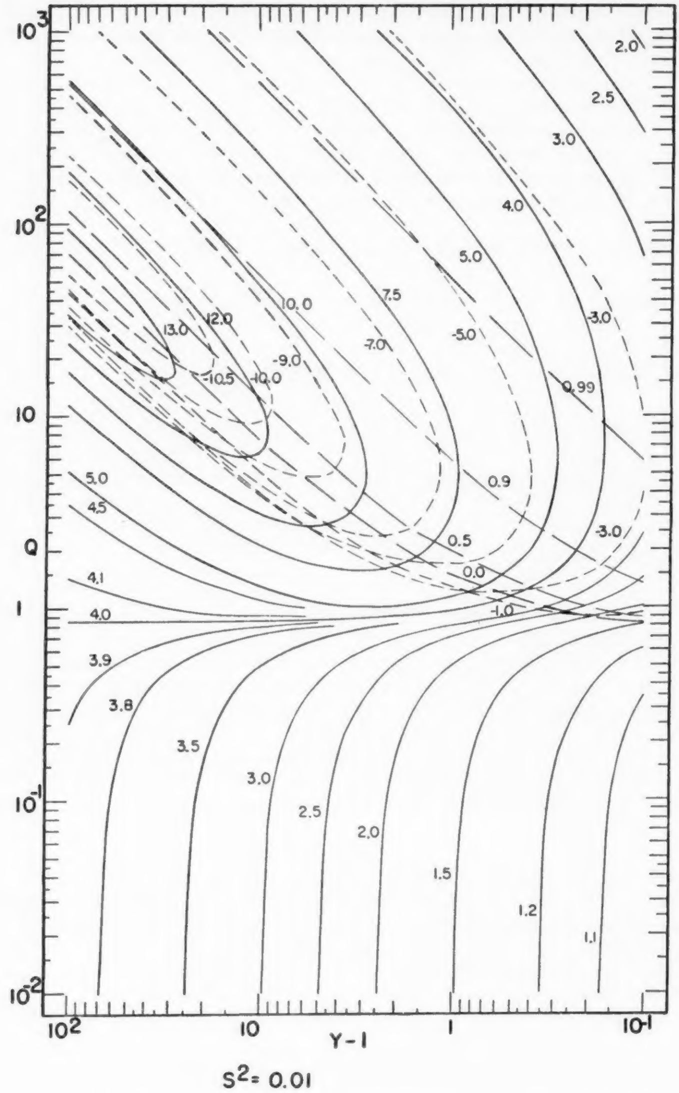

FIG. 3.—Graph of the (Q, $Y - 1$) relation for $s^2 = 0.01$. The parameter differentiating the curves is x. The solid-line curves represent solutions for which $x > 1$; the long-dashed-line curves represent solutions for which $1 > x \geqslant 0$; the short-dashed-lines curves represent solutions for which $0 > x$.

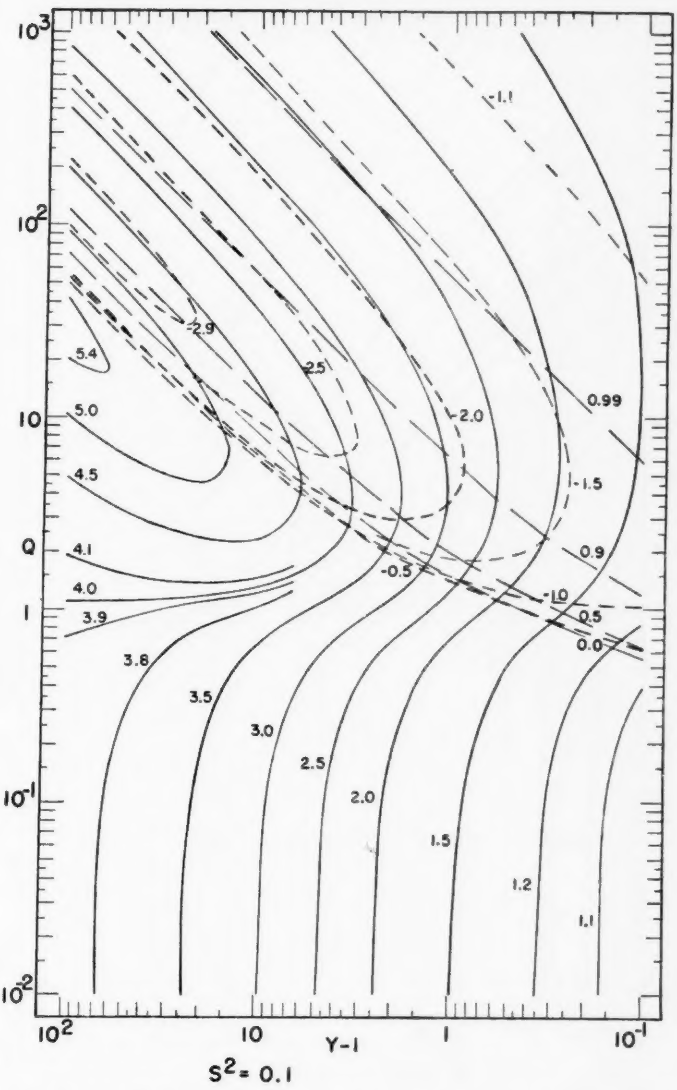

FIG. 4.—Graph of the $(Q, Y - 1)$ relation for $s^2 = 0.1$; the arrangement of the curves, otherwise, is the same as in Fig. 3.

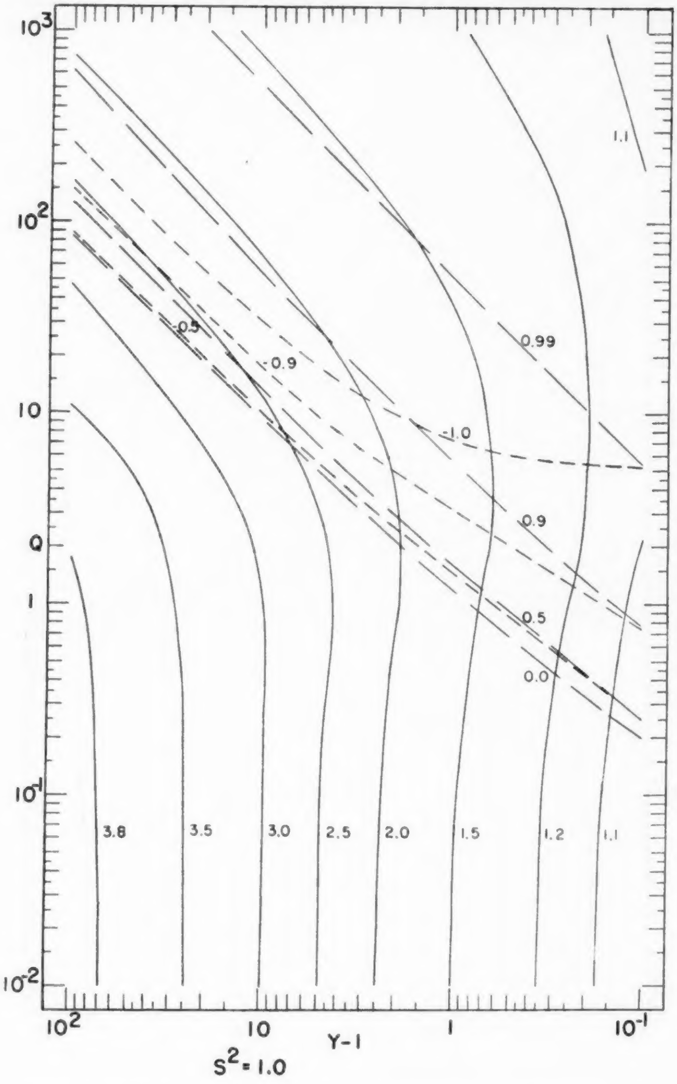

FIG. 5.—Graph of the $(Q, Y - 1)$ relation for $s^2 = 1$; the arrangement of the curves, otherwise, is the same as in Fig. 3.

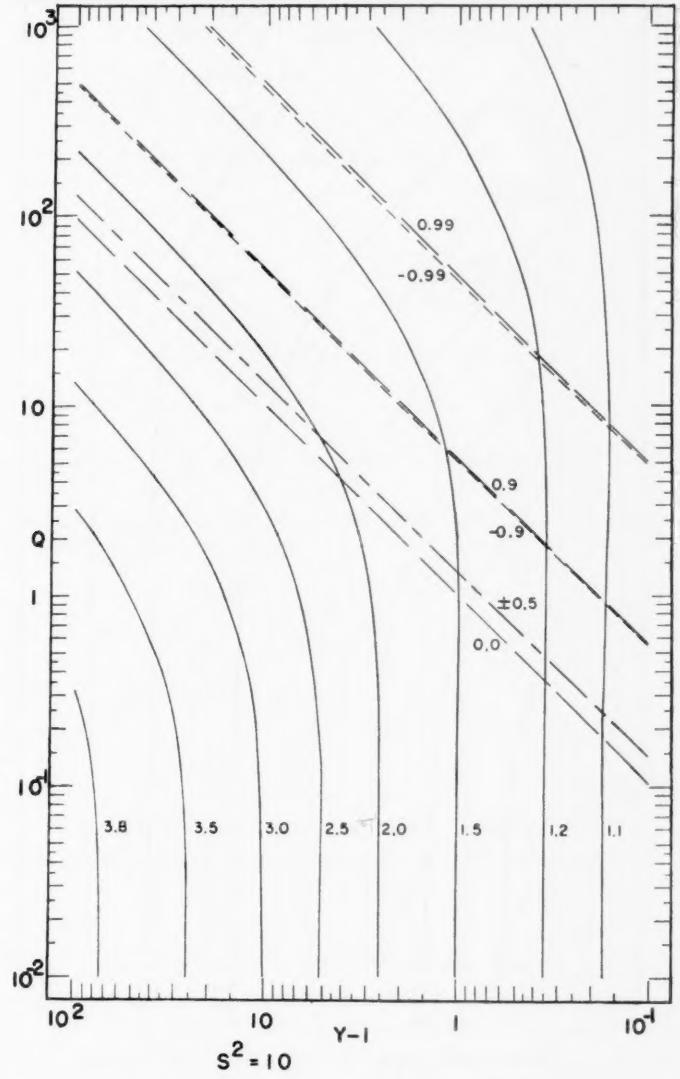

FIG. 6.—Graph of the (Q, $Y - 1$) relation for $s^2 = 10$. The curve of alternate long and short dashes is used to represent two solutions which coincide as far as the scale of these graphs is concerned; the other curves have the same significance as in Fig. 3.

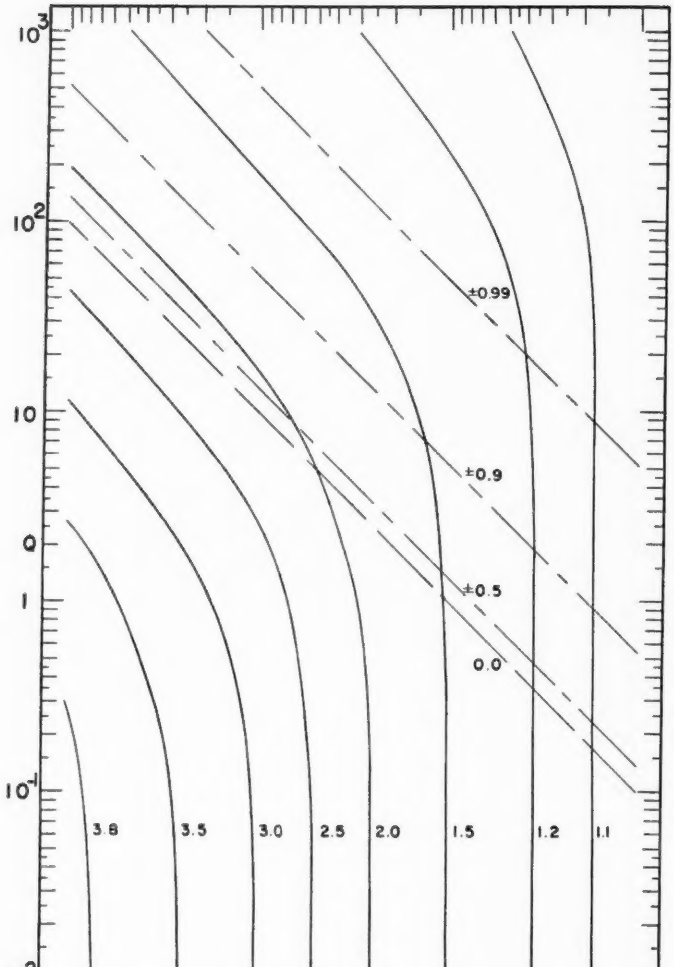

FIG. 7.—Graph of the $(Q, Y - 1)$ relation for $s^2 = 100$; the arrangement of the curves, otherwise, is the same as in Fig 6.

The solution of equation (64) is

$$A = \tfrac{1}{2}\left[1 - s^2 - \delta(s^2+1) \pm \{(s^2+1)^2 + 2\delta(s^4-1) + \delta^2(s^2+1)^2\}^{1/2}\right]. \tag{66}$$

For large Q values, the two solutions are

$$A_+ \cong 1 - \delta\,, \qquad A_- \cong -(1+\delta)\,s^2\,, \tag{67}$$

while, for small Q values, the corresponding solutions are

$$A_+ \cong 0\,, \qquad A_- \cong 1 - [s^2 + \delta(1+s^2)]\,. \tag{68}$$

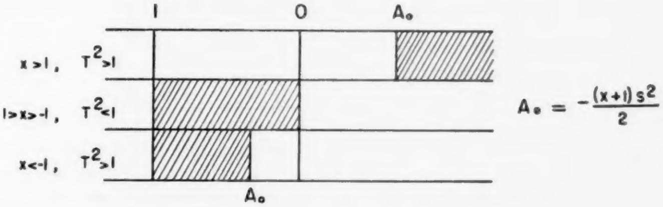

FIG. 8.—The boundary restrictions imposed upon A.

The foregoing solutions have a very simple interpretation. First, however, we may note that, for $x \to 1$, equations (56) give

$$D_1^2 = 1 - A_x \cong 1 - A = D_2^2\,. \tag{69}$$

Then, writing

$$V_a^2 \equiv \frac{H^2}{4\pi\rho} \tag{70}$$

and making use of the relations

$$V_1^2 = D_1^2 V_a^2 \tag{71}$$

and

$$\frac{c_1^2}{V_a^2} = \frac{\gamma}{2Q} = \delta \qquad \left(\text{for } \gamma = \tfrac{5}{3}\right), \tag{72}$$

we find that the solutions for large Q values (cf. eqs. [67]) correspond to

$$V_{1,+}^2 = c_1^2\,, \qquad V_{1,-}^2 = V_a^2 \sec^2\theta + c_1^2 \tan^2\theta\,, \tag{73}$$

with $V_a^2 \gg c_1^2$.

Similarly, for Q small (cf. eqs. [68]) we obtain the solutions

$$V_{1,+}^2 = V_a^2\,, \qquad V_{1,-}^2 = c_1^2 \sec^2\theta + V_a^2 \tan^2\theta\,, \tag{74}$$

with $V_a^2 \ll c_1^2$.

If we now transform back to the original co-ordinate system in which the matter on side 1 of the shock is stationary (cf. eqs. [3]), the velocity of the disturbance in the direction of propagation (at an angle θ with the lines of force) may be written as

$$\begin{aligned} U_+ &\to \left[\frac{H_x^2}{4\pi\rho}\right]^{1/2} && \text{for} \quad Q \to 0 \\ &\to c_1 \cos\theta && \text{for} \quad Q \to \infty\,, \end{aligned} \tag{75}$$

$$\begin{aligned} U_- &\rightarrow c_1 && \text{for} \quad Q \rightarrow 0 \\ &\rightarrow \left[\frac{H_x^2}{4\pi\rho}\right]^{1/2} \sec\theta && \text{for} \quad Q \rightarrow \infty \, , \end{aligned} \tag{76}$$

where H_x is the component of the magnetic field in the direction of propagation. These solutions therefore correspond precisely to two of the three modes of motion obtainable in the case of the corresponding magneto-hydrodynamic wave theory as developed by van de Hulst,[2] namely, the retarded sound wave and the modified Alfvén wave.

Next, we shall consider case *b*. Putting

$$2A + (x+1)\, s^2 = 2\epsilon \, , \qquad \text{where} \qquad |\epsilon| \ll 1 \, , \tag{77}$$

we may bring equation (60) into the form

$$Q = -\frac{5}{4} \frac{(1+s^2)\, A}{A\,(A+s^2)^2 - \frac{1}{2}\epsilon\,[\,2A^2 - (6-A)\, s^2]} \, . \tag{78}$$

If we now impose the condition that $Q \geqslant 0$ but arbitrary, we are left with two alternatives: (1) $A \cong -s^2$ or (2) $A \cong 0$. The former alternative, in virtue of equation (77), implies $x \cong 1$ and consequently, large Q values; we shall therefore recover the same solutions as we found previously (cf. solution A_-, eq. [67]).

However, when $A \cong 0$, we obtain a new solution, for then $x \cong -1$ and $V_1^2 \cong V_a^2$. The transformation (eqs. [3]) back to the original co-ordinate system gives

$$U_3 = \left[\frac{H_x^2}{4\pi\rho}\right]^{1/2} \qquad \text{for arbitrary } Q \, ; \tag{79}$$

further, the matter on side 2 of the shock streams in a direction parallel to the shock front itself. This corresponds to the third mode of van de Hulst and represents the true Alfvén wave.

VI. SMALL MAGNETIC FIELDS

We may now consider the case of Q small and $Y-1$ arbitrary. These solutions should lead in the limit $Q \rightarrow 0$ to the shocks of the ordinary hydrodynamic theory. They are of particular interest in view of the general weakness of the fields encountered in many astrophysical problems.

Inspection of equations (58) and (60) shows that Q is small whenever (*a*) $|A|$ is small and not nearly a root of the quadratic denominator of equation (60) or (*b*) $|A|$ is large.

In case *a* solutions (58) and (60) become

$$Q \cong \frac{5}{3} \frac{1+s^2}{(x+1)\, s^2}\, A \, ; \qquad Y - 1 = \tfrac{5}{3}(1-x)\, A \, . \tag{80}$$

The case $x \cong -1$ is specifically excluded. We see that this predicts $Y-1$ very small, and this case is merely a specialized duplication of our earlier results of Section V.

The second case, of $|A|$ very large, however, is more interesting. Then,

$$Q \cong \frac{\gamma\,(1+s^2)}{(\gamma-1)\,x - (\gamma+1)} \frac{1}{A} = \frac{5}{2} \frac{1+s^2}{x-4} \frac{1}{A} \qquad (\text{for } \gamma = \tfrac{5}{3}) \, , \tag{81}$$

and

$$Y - 1 \cong \frac{2\gamma\,(1-x)}{(\gamma-1)\,x - (\gamma+1)} = \frac{5}{6} \frac{1-x}{x-4} \qquad (\text{for } \gamma = \tfrac{5}{3}) \, . \tag{82}$$

Also, A is restricted to values $A < 0$ and x to values $4 < x \leqslant 1$; consequently, *for weak fields, the magnetic field is always amplified.*

It is particularly to be noted in this case that Y is independent of both s^2 and A or, alternatively, of Q. This accounts for the straight-line portions of the curves in the lower parts of Figures 3–7. The extent of the applicability of this limiting case may be judged, then, by the amount of deviation of these curves from the vertical straight lines. It appears that for ordinary applications we may use this limiting case whenever $Q \leqslant \sim 0.1$.

The dependence of the shock strength upon the bending factor essentially arises from the relation

$$\eta = \frac{1 - A x}{1 - A} \rightarrow x \qquad (A \rightarrow -\infty), \tag{83}$$

which expresses the equality of the bending with the compression in this approximation. Then, since,

$$Y - 1 \simeq \frac{2\gamma(1-\eta)}{(\gamma-1)\eta - (\gamma+1)}, \tag{84}$$

we have

$$\eta = \frac{(\gamma-1) + (\gamma+1) Y}{(\gamma-1) Y + (\gamma+1)} = \frac{1 + 4Y}{Y + 4} \qquad (\text{for } \gamma = \tfrac{5}{3}), \tag{85}$$

the usual form of the (η, Y) relation in ordinary hydrodynamic shock theory.

It appears reasonable, therefore, in dealing with weak field shocks, to use the results of classical shock theory to give, for example, the compression in dealing with collisions of shocks, etc., reserving equation (81) for the determination of A. The velocities, the magnetic field amplification, and the bending of the lines of force may subsequently be determined by means of equations (56), (45), and (85).

VII. LARGE MAGNETIC FIELDS

Finally, we shall consider the case of large Q, which arises when A has a value close to one of the roots of the quadratic denominator of equation (60). For this case, then, we may replace A by one of these root values in equation (58) and obtain $(Y - 1)/Q$ as a function of s^2 and x alone. This situation corresponds to the straight-line portions of the curves in the upper parts of Figures 3–7. As can be judged from these diagrams, this limiting case generally holds for $Q \geqslant \sim 100$.

VIII. LIMITATIONS ON x AND s^2

The requirement that the roots of the denominator be real imposes certain limitations upon x and s^2. We require, quite generally, that

$$[6 - (x+5) s^2]^2 \geqslant 24 (x+1)(x-4) s^2, \tag{86}$$

which always holds for $4 \geqslant x \geqslant -1$. For $x > 4$ or $x < -1$, however, the inequality need not, in general, be true; and, if one chooses the equality sign, one can solve for the maximum and minimum values of x compatible with an assigned s^2 value. Precaution is necessary, however, for the other boundary restrictions of the problem must be met. In particular, for $x > 4$, we must require that

$$2(x-4) A^2 + [6 - (x+5) s^2] A + 3(x+1) s^2 \leqslant 0; \tag{87}$$

or, writing $x = 4 + \epsilon$ in equation (87), we see that

$$3[2 - 3s^2] A + 15 s^2 + \epsilon [2A^2 + s^2(3 - A)] \leqslant 0. \tag{88}$$

A *minimal* condition for this to be satisfied is

$$s^2 < \tfrac{2}{3}. \tag{89}$$

Similarly, for $x < -1$, we require

$$2(x-4)A^2 + [6-(x+5)s^2]A + 3(x+1)s^2 \geqslant 0 . \tag{90}$$

If we put $x = -1 - \epsilon$, the expression becomes

$$-10A^2 + 2(3-2s^2) - \epsilon[2A^2 + s^2(3-A)] \geqslant 0 , \tag{91}$$

which demands as a *minimal* condition that

$$s^2 < \tfrac{3}{2} . \tag{92}$$

Table 1 lists some representative values of $x_{\max}$ and $x_{\min}$.

TABLE 1

VALUES OF $x_{\max}$ AND $x_{\min}$

s^2	$x_{\max}$	$x_{\min}$	s^2	$x_{\max}$	$x_{\min}$
0.01	13.4	-11.1	0.667	4.00	-1.14
0.05	7.03	-4.50	1.0	4.00^-	-1.04
0.10	5.57	-3.00	1.5	4.00^-	-1.00
0.25	4.41	-1.78	>1.5	4.00^-	-1.00^+
0.50	4.04	-1.28			

It is to be noted that it is the application of this theory which limits the maximum amplification of a magnetic field, given a specific s^2 value (cf. Fig. 2).

IX. DISCUSSION OF THE SOLUTION

In essence, the solution of the problem of the behavior of magneto-hydrodynamic shocks is given by Figures 3–7. The curves represented in them may be considered in three groupings: (1) $x > 1$, (2) $1 > x \geqslant 0$, and (3) $x \leqslant 0$, corresponding in the limiting case of $Y \rightarrow 1$ to the modified Alfvén wave, the retarded sound wave, and the undisturbed Alfvén wave. Of these three, only the first is always permitted, the other two modes not appearing until the magnetic energy is comparable with the internal energy ($Q \sim 1$). No more than three different modes of motion may arise for specified Q, Y, and s, and only upon limiting curves may two modes result. The more complex solutions appear only for small values of s^2, and, as s^2 increases, the solutions become rapidly simplified. This complexity of solutions at low s^2 values, resulting in rather high values permitted for $|x|$, may, in a sense, be considered offset by the lower value of the amplification factor obtainable in these cases.

As s^2 increases, the curves $x = +a$ and $x = -a$ tend to approach coincidence; this results essentially from the fact that, in this case,

$$(x+1)s^2 \gg 2A , \tag{93}$$

so that (cf. eq. [58])

$$Y - 1 \simeq \frac{s^2}{1+s^2}(1-x^2)Q , \tag{94}$$

which is independent of the sign of x.

In the limiting case, $s^2 \rightarrow \infty$, for the two modes for which A is positive, equations (58) and (60) become

$$Y - 1 \simeq (1-x^2)Q \tag{95}$$

and

$$A \simeq \frac{3(x+1)Q}{5+(x+5)Q} . \tag{96}$$

All three modes are still obtainable in general. A comparison between Figures 6 and 7 shows that the solutions for the various modes of motion are already well approximated by the limiting case, even for s^2 as low as 10.

The foregoing results on the multiplicity of solutions may appear contrary to the fact that only one solution was found in the treatment of perpendicular shocks (cf. Sec. III, the case $s_1 = \infty$). The contradiction is, however, resolved if we recall that the co-ordinate systems used in the two cases differ. In treating perpendicular shocks, we used a co-ordinate system in which the velocities were taken perpendicular to the magnetic field and the shock front; in the limiting case $s^2 \rightarrow \infty$, the co-ordinate system is one in which the velocity vectors are parallel to the lines of force. Consequently, only the solutions analogous to the modified Alfvén wave can be found in the former case, while in the latter case, in the limit $s^2 \rightarrow \infty$ (but excluding $A \cong -\infty$), only solutions analogous to the true Alfvén wave and the retarded sound wave can be found; for, even though x loses its physical meaning, it may still be defined by means of relation (95). For all practical purposes, the solutions represented in Figure 7 give the solutions in the case $s^2 \cong \infty$ to a high degree of approximation.

Perhaps the most significant result of this investigation from the astrophysical point of view is the fact that weak magnetic fields are always amplified by the passage of shock fronts. In general, this amplification is not sufficient to offset the decrease of the quantity Q, which always occurs, regardless of the shock strength. Indeed, we may consider an infinitely conducting medium in which a very weak magnetic field is present and consider a succession of shock waves passing through the medium. In the absence of any external mechanisms, the magnetic field will be successively amplified without limit, the situation being described most usefully as a descending series of points on our graphs of the $(Q, Y - 1)$ relation, reflecting the consequent increase of pressure, temperature, and density. However, it would be premature to attempt to explain the large fields required in the present theories of interstellar polarization[7] and the origin of cosmic rays[8] solely by a mechanism such as this, without examining the effects of external mechanisms, such as convection, turbulence, and radiative processes, on the extent of compression possible. This is a serious consideration when one recalls that the density of interstellar clouds is estimated to be only 10 to 100 times greater than that of ordinary interstellar matter, while the magnetic fields desired are at least of the order of 10^{10} times greater than the initial fields which Batchelor[9] and Schlüter and Biermann[10] have demonstrated could spontaneously arise in a turbulent conducting medium.

If, on the other hand, the shock waves in the picture we have described follow one another at fairly long time intervals, we may expect that the other forces which are operative will tend to restore the original values of pressure, density, and temperature. The most likely candidate for this role appears to be radiative processes, since, for a perfect gas,

$$\frac{T_2}{T_1} = \frac{Y}{\eta}, \tag{97}$$

where T is the temperature and the corresponding heating of the gas will be quite high for all except the weakest shocks. It is not by any means obvious, however, that such a process would limit the maximum density of interstellar matter to a value of $N \sim 10$–100 particles/cm³. Certainly, the amplification mechanism will exist in interstellar matter on a more modest scale, for turbulence and convection currents may be expected to give rise to shock waves.

---

[7] Spitzer and Tukey (*Ap. J.*, **114,** 187, 1951) require fields of 10^{-3}–10^{-5} gauss; Douis and Greenstein (*Ap. J.*, **119,** 206, 1951) require 10^{-4}–10^{-5} gauss fields at the very minimum.

[8] Fermi (*Phys. Rev.*, **75,** 1169, 1949) assumes fields of 5×10^{-6} gauss, while Richtmeyer and Teller (*Phys. Rev.*, **75,** 1729, 1949) require longer fields, $\sim 10^{-5}$ gauss.

[9] *Proc. R. Soc. London A*, **201,** 405, 1950.

[10] *Zs. f. Naturforsch.*, **5a,** 237, 1950.

If the other factors which are operative are reasonably efficacious in the model under consideration, the situation may be described by an ascending series of points on the graphs of the $(Q, Y - 1)$ relation. Eventually, a point must be reached for which only one mode of motion is possible, the following point falling in a region in which all three modes are possible. An examination of the graphs of the possible solutions shows that, in general, the region of three permissible modes is bounded below by curves of low $|x|$ values, corresponding to very strong de-amplification of the magnetic field. The magnetic field, then, will, in general, approach an "equilibrium" state in which $Q \sim 1$ within an order of magnitude or so. We may ask what fields the condition $Q \sim 1$ would imply for a perfect gas under astrophysical conditions. We find the results given in Table 2.

TABLE 2

VALUES OF THE MAGNETIC FIELD FOR $Q \sim 1$ FOR A PERFECT GAS

Region	Physical Conditions	H (Gauss)
H I regions	$T \sim 50°$ K; $N \sim 10$ atoms/cm^3*	10^{-6}
H II regions	$T \sim 10^4 °$ K; $N \sim 1$ ion/cm^3*	6×10^{-6}
Inner corona	$p \sim 10^{-3}$ dynes/cm^2	0.16
Stellar atmospheres	$p \sim 10^3$ dynes/cm^2	160
Stellar interiors	$p \sim 10^{16}$ dynes/cm^2	5×10^8

* We have used here the estimates given by L. Spitzer, Jr., *Symposium: Problems of Cosmical Aerodynamics* (Dayton, Ohio: Central Air Documents Office, 1951), p. 36.

Finally, in this connection, it is desirable to remember that the magnetic field amplification is essentially due to the compression of the matter, a fact which is hidden in any discussion of the amplification factor alone. For this reason it is perhaps more convenient to consider the charge in the magnetic energy per unit mass caused by the passage of a shock front. We may then introduce the quantity

$$R = \frac{T^2}{\eta}, \tag{98}$$

which, for weak fields, becomes,

$$R = \frac{1 + x^2 s^2}{x(1 + s^2)}, \tag{99}$$

a graph of which is shown in Figure 9.

The quantity R, then, is a measure of the amplification which is independent of the compressional effects. We note that only for rather large values of s^2 (for $\theta > \sim 45°$) do we get any appreciable "true" amplification; furthermore, this "true" amplification is nowhere nearly so great as the graph of T^2 would seem to imply. Also, the ratio of the Alfvén velocities on either side of the shock is given by the relation

$$\frac{V_{a2}^2}{V_{a1}^2} = R. \tag{100}$$

In discussions such as this, it would appear that R, rather than T^2, is the more fundamental quantity to consider.

As an application of the theory of magneto-hydrodynamic shocks, we may investigate the following problem. Consider a homogeneous perfect gas of density $N \sim 10^9$ particles/cm^3, temperature $T = 5 \times 10^4 - 5 \times 10^5 °$ K, and extremely high conductivity, and consider the passage of shock waves through the medium. For convenience, we shall assume that only shocks of "average" inclination ($s^2 = 1$) occur. Furthermore, we shall restrict our attention to shocks which do not heat up the medium appreciably, i.e., that $V/\eta \leqslant \sim 1.1$ (cf. eq. [97]). We then ask: Is it possible to contract a model, compatible with these temperature and density restrictions, which will result in velocity discontinuities of the order of 30–100 km/sec?

In other words, we are investigating a perfect gas at the density and temperature of the solar chromosphere and inner corona[11], and the question is posed as to whether the passage of shock waves through such a medium can result in the production of velocity discontinuities of the order of magnitude of those observed in prominence studies.[12] The fact that the spectra of prominences show no significant changes when the structures of prominences develop indicates that no significant temperature changes occur. Rather arbitrarily, we have selected the condition $T_2/T_1 \leqslant \sim 1.1$ as representing this observational fact and have imposed this as a subsidiary condition on the model.

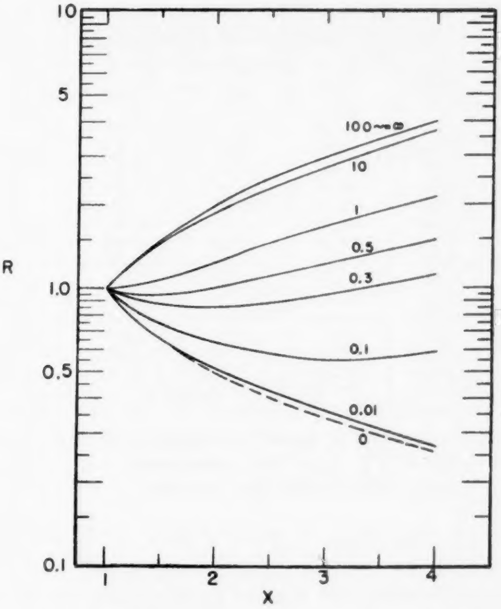

FIG. 9.—Values of the "true" amplification R in the case of weak fields, $Q \ll 1$. Here s^2 is the parameter differentiating the various curves.

The procedure used in this model investigation was as follows. The solutions $s^2 = 1$ alone were considered. First the curves for which $x < 1$ were examined, as this gives the maximum bending of the lines of force. Arbitrary values of $x = 0.5, 0.0, -0.5, -0.9$, and -1.0 and of $V = 1.1, 1.5, 2, 5$, and 10 were then chosen, and, for all possible combinations of these values of x and Y, Q was obtained from Figure 5. The case $x = -1.0$ was considered in a limiting sense, the permitted values of Q being all $Q \geqslant Q_c$, where Q_c is the value given by the $x = -1.0$ curve in the figure. All the calculations used Q_c, and the effect of using $Q \geqslant Q_c$ was estimated by remembering that A decreases as Q increases. The quantity A was then calculated by means of equation (57). The compression follows from equation (55), and then Y/η may be found. Application of the restriction $Y/\eta \leqslant 1.1$ eliminated all the solutions save those for $Y = 1.1$ (all x values) and $Y = 1.5$, $x = 0.0$. For the surviving solutions, the velocities were then calculated from equations (56) and (71), and the transformation (3) was then performed, so that the matter on side 1 of the shock will be at rest. The results were as given in Table 3.

---

[11] Van de Hulst, *A Course in Radio Astronomy* (Leiden, 1951), p. 61.

[12] The motions of prominences in general are discussed in Hynek, *Astrophysics* (New York: McGraw-Hill Book Co., Inc., 1951), chap. vi (by E. Pettit); E. Pettit, *Ap. J.*, **98**, 16, 1943. A detailed discussion of the abrupt velocity changes in prominences, so very suggestive of shock waves, is given in R. R. McMath and E. Pettit, *Ap. J.*, **88**, **244**, **1938**.

TABLE 3

THE $x < 1$ SOLUTIONS FOR $Y/\eta \leqslant 1.1$

x	0.5	0.0	−0.5	−0.9	−1.0	0.0
Y	1.1	1.1	1.1	1.1	1.1	1.5
Q	0.25	0.20	0.25	0.75	5.0	0.65
A	0.050	0.000	0.017	0.025	0.010	0.27
η	1.03	1.00	1.03	1.05	1.02	1.37
Y/η	1.07	1.10	1.07	1.05	1.08	1.10
T^2	0.63	0.50	0.63	0.91	1.00	0.50
R	0.61	0.50	0.61	0.86	0.98	0.37
V^0_{2x}	−0.18	−0.21	−0.18	−0.090	−0.025	−0.44
V^0_{2y}	−0.44	−0.71	−0.98	−1.27	−1.40	−0.71
V^0_2	0.48	0.74	0.99	1.28	1.40	0.83
ϕ	67°	74°	80°	86°	89°	58°
V^0_2/H (km/sec gauss)	330	510	680	880	970	580
p/H^2 (dynes/cm² gauss²)	0.16	0.20	0.16	0.050	0.0080	0.062
T/H^2 (° K/gauss²)	1.1×10^6	1.4×10^6	1.1×10^6	3.5×10^5	5.6×10^4	4.3×10^5

In this table the quantities V^0_{2x}, V^0_{2y}, and V^0_2 are measured in units of V_{a1} and ϕ is defined by the relation: $\tan\phi = |V^0_{2y}/V^0_{2x}|$. The values below the line in the table follow from the assumption that $N = 10^9$ particles/cm², for then:

$$\frac{V_{a1}}{H} = 690 \text{ km/sec gauss}; \qquad T = 7 \times 10^6 p; \qquad \frac{p}{H^2} = \frac{0.04}{Q}. \tag{101}$$

The velocities obtained indicate that $H \sim 0.1$ gauss would be satisfactory, and, with this choice, only the first three columns give sufficiently high temperatures. From this alone, we could conclude that $Y \cong 1.1$, $Q = 0.2$–0.4, and $0.5 \geqslant x \geqslant -0.5$ would yield a satisfactory model.

However, for the given Q and Y values, there also exists a solution $x > 1$, which must not be in discord with the desired pressures and temperatures. It is consequently necessary to investigate the solutions $x > 1$.

In order to cover a wide range of Q values, Y and Q were assumed assigned and x found from Figure 5. All possible combinations of $Y = 1.1$, 1.5, 2, 5, and 10 and of $Q = 0.01$, 0.1, 1, 10, 100, and 1000 were investigated. After x has been found, the procedure to be followed is the same as in the case we have already explained; the condition $Y/\eta \leqslant 1.1$ permitted acceptance of only the $Y = 1.1$ solutions. The results are given in Table 4.

The case of $Y \cong 1.1$, $Q = 0.2$–0.4, and $H \sim 0.1$ gauss yields an $x > 1$ solution with a very small velocity discontinuity, $V^0_2 \sim 5$ km/sec, which would be difficult to detect observationally. We then conclude that this case would represent the observational material fairly.

One may be tempted, after viewing the table of $x > 1$ solutions, to consider the case $Y \cong 1.1$, $Q = 10$–100, and $H \sim 1$ gauss. However, the $x < 1$ solution corresponding to such a case would yield (cf. the $x = -1.0$ solutions) quite high temperatures and enormous velocity discontinuities, on the order of 1000 km/sec. Since this is not permitted, this case must be excluded from further consideration.

The conclusion to be drawn from this discussion is that the model $Y \cong 1.1$, $Q = 0.2$–0.4, and $H \sim 0.1$ gauss, within the framework of this paper formally represents the observed velocity discontinuities in prominence motions. This model must not be taken too literally. In particular, the assumption of homogeneity would not, in general, be true, the medium being under the influence of an external gravitational field, of fluctuating internal motions and electric fields, and of mechanisms of ionization and excitation. Similarly, the assumption of plane shock fronts is an extreme idealization. Even the assumption that prominence material as a hydrodynamic fluid is subject to criticism; for, in order for the hydrodynamic model to be applicable, the shock front itself, of order of magnitude of the mean free path, must be small compared to the mean dimensions of the system. Attention, therefore, should be limited to those regions less than 50,000 km above the solar limb, at which height the mean free path is $\sim$1000 km and above which the hydrodynamic model begins to break down.

TABLE 4

THE $x > 1$ SOLUTIONS FOR $Y/\eta \leqslant 1.1$

Q	0.01	0.1	1	10	100	1000
Y	1.1	1.1	1.1	1.1	1.1	1.1
x	1.05	1.05	1.08	1.14	1.12	1.09
A	-201	-20.1	-2.29	-1.14	-1.07	-1.05
η	1.05	1.05	1.06	1.08	1.06	1.05
Y/η	1.05	1.05	1.04	1.03	1.04	1.05
T^2	1.05	1.05	1.08	1.15	1.13	1.09
R	1.00	1.00	1.03	1.07	1.06	1.05
V_{2x}^0	$-$ 0.0089	$-$ 0.073	-0.068	-0.075	-0.060	-0.045
V_{2y}^0	+ 0.51	+ 0.087	+0.030	+0.064	+0.057	+0.044
V_2^0	0.51	0.11	0.074	0.099	0.083	0.063
ϕ	89°	40°	24°	40°	44°	45°
V_2^0/H (km/sec gauss)	350	76	51	68	57	44
p/H^2 (dynes/cm^2 gauss^2)	4	0.4	4×10^{-2}	4×10^{-3}	4×10^{-4}	4×10^{-5}
T/H^2 (K/gauss^2)	3×10^7	3×10^6	3×10^5	3×10^4	3×10^3	3×10^2

Nevertheless, in small local regions in the lower parts of prominences, shock phenomena may occur under physical conditions reasonably similar to those assumed in earlier parts of the paper, and in this connection, the model constructed is highly suggestive.

In conclusion, I wish to express my gratitude to Dr. S. Chandrasekhar for suggesting this problem to me and for his constant encouragement at moments of severe trial.

A GRAVITATIONALLY CONTRACTING STELLAR MODEL

RICHARD D. LEVEE
Berkeley Astronomical Department, University of California*

Received August 4, 1952

ABSTRACT

A stellar configuration under homologous gravitational contraction is considered. The energy generation is given by $\epsilon = \epsilon_0 T$, radiation pressure is neglected, and the opacity is given by Kramers' law. The solution yields three eigenvalues: The central value of the polytropic index, the constant of the mass-luminosity equation, and the constant of the equation of energy generation. The distributions of ρ, T, $M(r)$, and $L(r)$ are almost identical to those of the standard model, although ρ_c and T_c are slightly higher, since the polytropic index varies from 2.97 at the center to 3.25 at the surface. The mass-luminosity equation shows that $L \propto R^{-0.5}$ for constant M and leads to a time scale of 5×10^7 years for the sun.

I. INTRODUCTION

The equations of equilibrium and the conditions for the stability of a gravitationally contracting gas sphere have been thoroughly investigated by L. H. Thomas.[1] H. Roth[2] has made an exact integration, including the effect of radiation pressure, for a central temperature of $5 \times 10^{6}\,^\circ$ K, and for a central pressure of 8.5917×10^{12} dynes/cm^2. The general problem, but where radiation pressure is neglected, has been considered by Mrs. Harrison.[3] However, for the model concerned, the procedure followed by Mrs. Harrison is incorrect,[4] and the present investigation has therefore been undertaken.

II. THE BASIC EQUATIONS

Since Roth[2] found, in his investigations, that no convective core occurs, it seems probable that the same might be true for the case where radiation pressure is neglected.[5] Therefore, our equations are the standard equations of radiative equilibrium:[6]

$$\frac{dM(r)}{dr} = 4\pi \rho r^2 , \qquad \frac{dL(r)}{dr} = 4\pi \rho r^2 \epsilon ,$$
$$\frac{dP}{dr} = -\frac{GM(r)\rho}{r^2} , \qquad \frac{dT}{dr} = -\frac{3\kappa L(r)\rho}{16\pi a c r^2 T^3} . \tag{1}$$

If the gas pressure is given by the perfect gas law,

$$P = \frac{k\rho T}{\mu H} , \tag{2}$$

---

* Now at Laws Observatory, University of Missouri.

[1] *M.N.*, **91**, 122 and 619, 1931.

[2] *Phys. Rev.*, **39**, 525, 1932.

[3] *Ap. J.*, **102**, 216, 1945.

[4] Since this investigation was begun, Mrs. Harrison has kindly informed the author of an independent discovery of her error by Öpik, *Contr. Baltic U.*, No. 35, 1947.

[5] Although Schatzman (*Ann. d'ap.*, **10**, 93, 1947) states that a convective core is necessary (see eq. [5.2]), a numerical error (replace 158 for 78 in this eq.) revises the whole argument.

[6] Chandrasekhar, *An Introduction to Stellar Structure* ("Astrophysical Monographs" [Chicago: University of Chicago Press, 1939]).

and the opacity follows Kramers' law,

$$\kappa = \kappa_0 \rho T^{-3.5} , \tag{3}$$

where κ_0 is a function of the chemical composition only, then the contraction may be homologous.[1] In this case the energy generation is given by

$$\epsilon = \epsilon_0 T , \tag{4}$$

where

$$\epsilon_0 = -\frac{3\gamma - 4}{\gamma - 1} \frac{1}{R} \frac{k}{\mu H} \frac{dR}{dt} . \tag{5}$$

III. TRANSFORMATION OF VARIABLES

Consider the homology-invariant functions, u, v, w, and x, defined by

$$u = \frac{d \log M(r)}{d \log r} , \qquad v = -\frac{d \log T}{d \log r} ,$$
$$w = \frac{d \log L(r)}{d \log r} , \qquad x = -\frac{d \log P}{d \log r} . \tag{6}$$

From equations (1), (2), (3), and (6), we get

$$u = \frac{4\pi r^3 \rho}{M(r)} , \qquad v = \frac{3 \kappa_0 L(r) \rho^2}{16 \pi a c r T^{7.5}} ,$$
$$w = \frac{4\pi \rho r^3 \epsilon_0 T}{L(r)} , \qquad x = \frac{G M(r) \rho}{r P} . \tag{7}$$

Taking the logarithmic derivatives of equations (7) and using equations (6), we have

$$\frac{d \log u}{d \log r} = 3 - x + v - u , \qquad \frac{d \log x}{d \log r} = u + v - 1 ,$$
$$\frac{d \log w}{d \log r} = 3 - x - w , \qquad \frac{d \log v}{d \log r} = w - 1 + 9.5 v - 2x . \tag{8}$$

Dividing the first, second, and fourth of equations (8) by the third, we obtain

$$\frac{du}{dw} = \frac{u(3 - u - x + v)}{w(3 - x - w)} , \qquad \frac{dx}{dw} = \frac{x(u + v - 1)}{w(3 - x - w)} ,$$
$$\frac{dv}{dw} = \frac{v(w - 1 - 2x + 9.5 v)}{w(3 - x - w)} . \tag{9}$$

Thus we have reduced the number of simultaneous differential equations from four to three. Equations (9) are now to be integrated numerically for u, v, and x as functions of the independent variable w.

IV. THE BOUNDARY CONDITIONS FOR THE NEW VARIABLES

A. AT THE SURFACE

In the general variables we have $\rho \rightarrow 0$, $T \rightarrow 0$, as $r \rightarrow R$. Then from equations (7) and (1) we have, at the surface,

$$u = 0 , \qquad w = 0 , \qquad v = \infty , \qquad x = \infty . \tag{10}$$

B. AT THE CENTER

In the general variables $T \rightarrow T_c$, $\rho \rightarrow \rho_c$, $M(r) \rightarrow 0$, and $L(r) \rightarrow 0$ as $r \rightarrow 0$. Then from equations (7) and (1) we have, at the center of the configuration,

$$u = 3\,, \qquad w = 3\,, \qquad v = 0\,, \qquad x = 0\,. \tag{11}$$

V. THE ASYMPTOTIC SERIES AT THE SURFACE

We now derive the general solution of equations (9) in asymptotic form. Writing (9) in symmetric form and making the transformation of variable $x = vm$, we have

$$\frac{du}{u(3-u-mv+v)} = \frac{dw}{w(3-mv-w)} = \frac{dv}{v(w-1-2mv+9.5v)} \tag{12}$$

$$= \frac{dm}{m(u-w-8.5v+2mv)}\,.$$

Examining this expression, we see that $u = 0, w = 0, v = \infty$, and $m = 4.25$ is a singular point of the equations. In particular, these are the values of the variables at the surface. If we now expand around this point, neglecting, in a first approximation, the small quantities u and w in the first three expressions, the equation (12) reduces to

$$\frac{du}{u(3-3.25v)} = \frac{dw}{w(3-4.25v)} = \frac{dv}{v(v-1)} = \frac{dm}{4.25(u-w-8.5v+2mv)}\,. \tag{13}$$

The solution of the equation formed by the first and third expressions of (13) is

$$u = \frac{C_1}{v^3(v-1)^{0.25}}\,. \tag{14}$$

The solution of the equation formed by the second and third expressions is

$$w = \frac{C_2}{v^3(v-1)^{1.25}}\,. \tag{15}$$

If we now replace u and w in the fourth expression of equations (13) by equations (14) and (15), respectively, we may solve the equation formed by the third and fourth expressions for $m = m(v)$. That is,

$$\frac{dv}{v(v-1)} = \frac{dm}{4.25\{C_1/[v^3(v-1)^{0.25}] - C_2/[v^3(v-1)^{1.25}] - 8.5v + 2mv\}} \tag{16}$$

or

$$\left[\frac{C_1}{v^4(v-1)^{1.25}} - \frac{C_2}{v^4(v-1)^{2.25}} + \frac{(2m-8.5)}{(v-1)}\right]dv = \frac{dm}{4.25}\,. \tag{17}$$

This expression can be solved by the use of the integrating factor[7] $(v-1)^{-8.5}$. Multiplying through equation (17) by $(v-1)^{-8.5}$ and integrating, we have

$$\frac{m-4.25}{4.25(v-1)^{8.5}} = C_1\int\frac{dv}{v^4(v-1)^{9.75}} - C_2\int\frac{dv}{v^4(v-1)^{10.75}} + C_3$$

or

$$m = 4.25 - \frac{(v-1)^{8.5}}{3v^{12.75}C_1} + \frac{(v-1)^{8.5}}{v^{13.75}}\left[\tfrac{17}{55}\left(C_2 - \tfrac{39}{4}C_1\right) + \frac{731}{236v}\left(C_2 - \tfrac{39}{8}C_1\right)\right. \tag{18}$$

$$\left. + \frac{34357}{2076v^2}\left(C_2 - \tfrac{39}{12}C_1\right) + \ldots\right] + 4.25C_3(v-1)^{8.5}\,.$$

---

[7] That an integrating factor is to be expected can be shown from a somewhat different development which leads to a linear equation of the first order.

Unfortunately, in the present numerical solution the series used was not so good as formula (18), since it was derived by using dv/v^2 in equation (17) instead of $dv/v(v-1)$.

Equations (14), (15), and (18) then constitute the leading terms of the general series solution at the surface. In our particular solution $m \to 4.25$ as $v \to \infty$ and therefore $C_3 = 0$.

VI. THE ARBITRARY CONSTANTS C_1 AND C_2

The arbitrary constants C_1 and C_2, which appear in equations (14), (15), and (18), are related to the mass, radius, and luminosity of the star in the following way. Consider the expression xw/u. From equations (7) we obtain

$$\frac{xw}{u} = \frac{G\mu H}{k} \frac{\epsilon_0}{L(r)} \frac{M(r)^2}{r} .$$

At the surface

$$\left(\frac{xw}{u}\right)_{r=R} = \frac{G\mu H}{k} \frac{\epsilon_0}{L} \frac{M^2}{R} . \tag{19}$$

Let us call this constant, C. From equations (14), (15), and (18) we have, remembering that $x = mv = 4.25v$,

$$C = \left(\frac{xw}{u}\right)_{r=R} = \frac{4.25C_2 v}{v^{4.25}} \frac{v^{3.25}}{C_1} = \frac{4.25C_2}{C_1} .$$

Hence

$$C = \frac{4.25C_2}{C_1} = \frac{G\mu H}{k} \frac{\epsilon_0}{L} \frac{M^2}{R} . \tag{20}$$

This is the equation of energy generation where C is an eigenvalue.[8] Consider also the expression $x^{7.5}u^2/v$. From equations (7) we have

$$\left(\frac{v}{x^{7.5}u^2}\right)_{r=R} = \frac{3k_0 L}{(4\pi)^3 4ac} \left(\frac{k}{G\mu H}\right)^{7.5} \frac{R^{0.5}}{M^{5.5}} . \tag{21}$$

Let us call this constant Q. Again from equations (14) and (18) we have

$$Q = \left(\frac{v}{x^{7.5}u^2}\right)_{r=R} = \frac{v^{7.5}}{v^{7.5}(4.25)^{7.5}C_1^2} = \frac{1}{(4.25)^{7.5}C_1^2} .$$

Hence

$$Q = \frac{1}{(4.25)^{7.5}C_1^2} = \frac{3k_0 L}{(4\pi)^3 4ac} \left(\frac{k}{G\mu H}\right)^{7.5} \frac{R^{0.5}}{M^{5.5}} . \tag{22}$$

This relation is recognized as the mass-luminosity equation where Q is a second eigenvalue of the problem.

VII. THE POWER SERIES REPRESENTATION AT THE CENTER

From equations (11) we have, at the center, $u = 3$, $w = 3$, $x = 0$, and $v = 0$. We may expand in a power series around $(w - 3)$. That is,

$$u = 3 + \sum_{i=1}^{\infty} a_i (w-3)^i , \qquad x = \sum_{i=1}^{\infty} b_i (w-3)^i , \qquad v = \sum_{i=1}^{\infty} c_i (w-3)^i .$$

---

[8] Mrs. Harrison takes $C = 1$ (*op. cit.*, p. 217, eqs. [10] and [8]).

Using equations (9) and expanding in the usual manner, we have

$$
\begin{aligned}
u &= 3+\frac{m_0-1}{m_0}(w-3)+\frac{1410.5-378m_0}{294m_0^2}(w-3)^2+\ldots,\\
x &= -\tfrac{5}{3}(w-3)+\frac{40-5m_0}{63m_0}(w-3)^2+\ldots, \qquad (23)\\
v &= -\frac{5}{3m_0}(w-3)+\frac{1462.5-360m_0}{126m_0^2}(w-3)^2+\ldots,
\end{aligned}
$$

where the arbitrary constant m_0 determines the solution.

VIII. THE ARBITRARY CONSTANT m_0

The effective polytropic index n is defined as

$$\frac{d\log P}{d\log T}-1=n\,.$$

From equation (6), we have

$$\frac{d\log P}{d\log T}=\frac{x}{v}=m\,.$$

Thus the quantity m is the effective polytropic index plus 1. At the center, from equations (23), $m = m_0$ and $n = m_0 - 1$. The arbitrary constant m_0 then is just the value at the center of the effective polytropic index plus 1. There exists, however, only one value of m_0 such that $m \to 4.25$, or $n \to 3.25$, as $w \to 0$. This value of m_0 is the third eigenvalue of our problem.

The presence of the three eigenvalues, Q, C, and m_0, is explained in the following way. Since $L(0) = 0$ and $M(0) = 0$, an integration from the surface will involve two constants of integration. These are the eigenvalues Q and C. However, since $\rho \to 0$ and $T \to 0$ simultaneously as $r \to R$, an integration from the center will involve only one constant of integration. This is the eigenvalue m_0.

IX. THE INTEGRATIONS

Since integrations from the center of the configuration require us to determine only one eigenvalue, whereas integrations from the surface inward require two eigenvalues, we shall start from the center.

Since integrations of other chemically homogeneous stellar models have shown that, in general, the polytropic index increases outward, we made a first estimate of m_0 by considering what value one would need for $(dm/dw)_{r=0} \le 0$ (since w decreases outward). Now

$$\frac{dm}{dw}=\frac{d}{dw}\left(\frac{x}{v}\right)=\frac{v(dx/dw)-x(dv/dw)}{v^2}\,.$$

Using equations (9), we have

$$\left(\frac{dm}{dw}\right)_{r=0}=\left[\frac{x}{vw}\left(\frac{u-8.5v-w-2x}{3-x-w}\right)\right]_{r=0}\le 0\,.$$

Our series expressions at the center, to first-order terms, gives

$$\left(\frac{dm}{dw}\right)_{r=0}=\frac{79}{6m_0}-\tfrac{10}{3}\le 0\,,$$

or $m_0 \geq 3.95$. Then $m \sim 3.95$ will serve as a first estimate of m_0 in equations (23).

Let us consider equation (18), where we have replaced v by w from equations (15). For very large v,

$$m = 4.25 - \frac{C_1}{3C_2} w + \ldots + \frac{C_4}{w^2},$$

where $C_4 = 4.25 C_3 C_2^2$.

From the above equation we see that, as one integrates outward in the independent variable w, the value of m will go either to plus infinity if C_4 is positive, or to minus infinity if C_4 is negative. If C_4 is zero, then $m \rightarrow 4.25$ as $w \rightarrow 0$, and we have the solution we are seeking.

One then chooses a value of m_0 and integrates outward until the curve of m as a function of w diverges. If the curve diverges to minus infinity, he takes a value of m_0 slightly larger and performs a second integration, carrying on the integration until this curve diverges. A plot of m as a function of w is shown in Figure 1. Since the particular curve we seek does not diverge, we may suppose the second derivative to be small in the region of divergence of the above curves. Therefore, to determine a new value of m_0, we interpolate in the accelerations, which may be taken to be the second differences at three equally spaced points. One then either starts again from the origin or interpolates in all variables and carries on the integration from the last interpolated points.

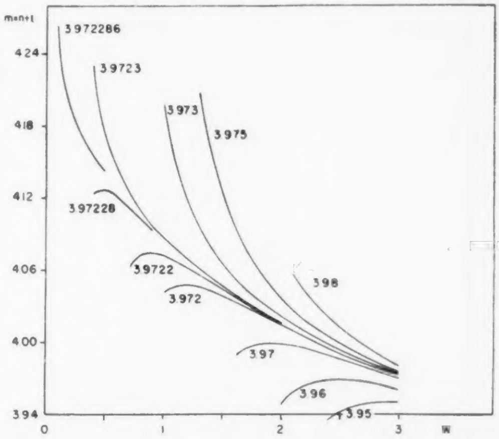

FIG. 1.—Curves in the m–w plane. The number associated with a curve represents the central value of m.

In the present problem several trials gave a value of $m_0 = 3.972286$, which carried our particular solution out to $v = 1.51$, $u = 0.69$, $w = 0.37$, and $x = 6.28$. At this point the outward integrations were stopped, and Q and C were estimated by equations (19) and (21). Using these values of Q and C, an integration was made inward, using equations (18) as a starting series. The values of Q and C were changed and further trials made until the inward integration fitted the outward one in all variables as functions of v. A plot of u and w against v is shown in Figure 2, and the run of all variables is given in Table 1. The eigenvalues arrived at were $Q = 1.882 \times 10^{-6}$ and $C = 1.898$.

We now have u, x, and w as functions of v throughout the configuration, but wish to find how T, ρ, L, and M vary with r. From equations (8), we have

$$\frac{d\log v}{d\log r}=w-1-2x+9.5\,v\,.$$

Then

$$\frac{dr}{r}=\frac{dv}{v\,(w-1-2x+9.5\,v)}\,,$$

and integration gives

$$\log r\,\Big|_r^R=\int_v^\infty\frac{dv}{v\,(w-1-2x+9.5\,v)}\,,$$

or

$$\log\xi=\log\frac{r}{R}=-\int_v^\infty\frac{dv}{v\,(w-1-2x+9.5\,v)}\,. \tag{24}$$

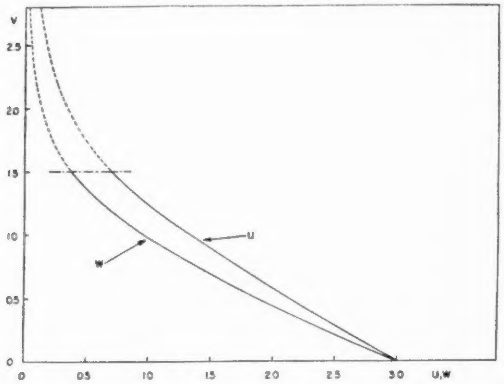

FIG. 2.—Curves in the u–v and w–v planes. The inward integration was fitted to the outward one at $v = 1.5$.

TABLE 1

DISTRIBUTIONS OF THE HOMOLOGY INVARIANT'S u, w, x, AND v

r/R	u	w	x	v
1.000	0.000	0.000		
0.900	0.002	0.000	42.5	10.0
0.800	0.018	0.002	21.2	4.99
0.698	0.071	0.014	14.0	3.29
0.597	0.190	0.055	10.3	2.43
0.499	0.400	0.165	7.94	1.89
0.402	0.755	0.420	6.02	1.45
0.300	1.30	0.931	4.17	1.02
0.201	1.99	1.71	2.34	0.580
0.098	2.72	2.62	0.638	0.160
0.000	3.00	3.00	0.000	0.000

Near the surface this integral is evaluated approximately by setting $w = 0$ and $x = 4.25v$. Equation (24) then leads to ξ as a function of v. Solving equations (7) for T, ρ, $M(r)$, and $L(r)$ and using equations (20) and (22), we have

$$\begin{aligned} \frac{T}{(GH/k)(\mu M/R)} &= \frac{T}{T_0} = \left(CQ\,\frac{1}{\xi^4}\,\frac{u^3x^3}{w\,v}\right)^{1/3.5}, \\ \frac{\rho}{M/4\pi R^3} &= \frac{\rho}{\rho_0} = \left(CQ\,\frac{1}{\xi^{11}}\,\frac{u^{6.5}x^{6.5}}{w\,v}\right)^{1/3.5}, \\ \frac{M(r)}{M} &= \left(CQ\,\frac{1}{\xi^{0.5}}\,\frac{u^3x^{6.5}}{w\,v}\right)^{1/3.5}, \\ \frac{L(r)}{L} &= C\,\frac{\xi^3}{w}\,\frac{T}{T_0}\,\frac{\rho}{\rho_0}. \end{aligned} \qquad (25)$$

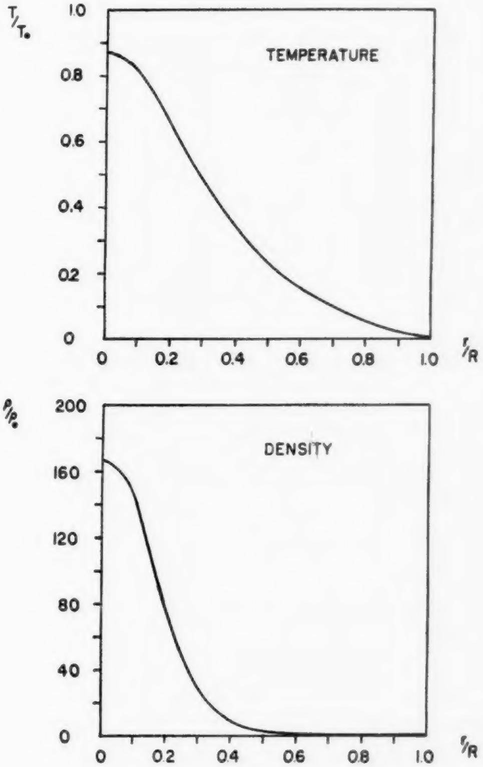

FIG. 3.—The temperature and density distributions in the gravitationally contracting stellar model

X. RESULTS

Equations (25) and the values of Q and C determined in Section IX allow us to determine the distributions of T, ρ, $L(r)$, and $M(r)$ with r/R. These are shown in Figures 3 and 4 and are listed in Table 2.

From Figure 3 we read off the central values of the temperature and density as

$$T_c = 0.871 \frac{\mu H}{k} \frac{GM}{R} \tag{26}$$

and

$$\rho_c = 167 \frac{M}{4\pi R^3}\,. \tag{27}$$

Expressing L, M, and R in solar units and evaluating the constants, equation (20), the equation of energy generation, becomes

$$L = 6.40 \times 10^6 \frac{\epsilon_0 \mu M^2}{R}\,, \tag{28}$$

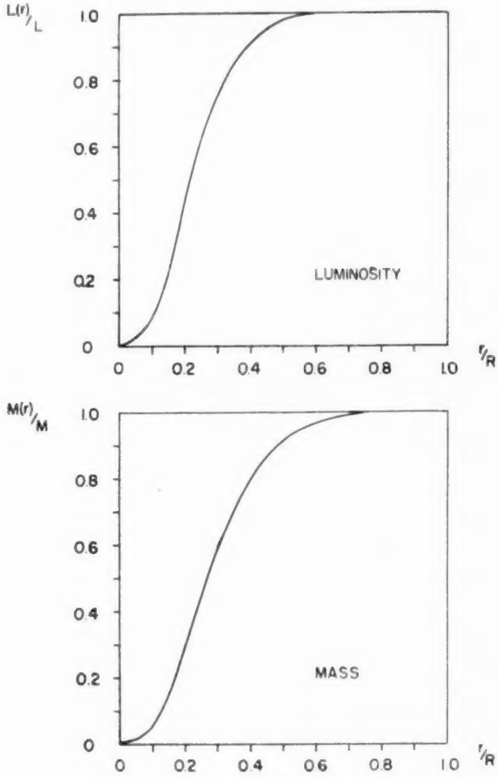

FIG. 4.—The luminosity and mass distributions in the gravitationally contracting stellar model

and equation (22), the mass-luminosity equation, becomes

$$L = 9.92 \times 10^{24} \frac{\mu^{7.5} M^{5.5}}{R^{0.5} \kappa_0} . \tag{29}$$

The polytropic index of a gravitationally contracting stellar model obeying Kramers' law of opacity is found to vary from 2.972 at the center to 3.25 at the surface.

XI. CONCLUSIONS

From equations (5) and (20), we obtain

$$\frac{dR}{dt} = \frac{1-\gamma}{3\gamma - 4} \frac{C}{G} \frac{LR^2}{M^2} .$$

TABLE 2

DISTRIBUTIONS OF TEMPERATURE, DENSITY, MASS, AND LUMINOSITY

r/R	T/T_0	ρ/ρ_0	$M(r)/M$	$L(r)/L$
1.000	0.000	0.000	1.000	1.000
0.900	.026	0.003	1.000	1.000
0.800	.059	0.035	0.996	1.000
0.698	.101	0.207	0.988	0.999
0.597	.158	0.864	0.968	0.997
0.499	.231	2.97	0.916	0.978
0.402	.332	9.33	0.804	0.910
0.300	.475	28.6	0.595	0.749
0.201	.652	75.4	0.306	0.441
0.098	.814	148	0.051	0.081
0.000	0.871	164	0.000	0.000

Evaluating the constants and expressing L, M, and R in solar units and t in years, we have

$$\frac{dR}{dt} = 5.98 \times 10^{-8} \frac{LR^2}{M^2} \frac{1-\gamma}{3\gamma - 4} . \tag{30}$$

This equation allows us to determine the Helmholtz-Kelvin time scale. For the sun, $L = 1$, $M = 1$, and, with $\gamma = \frac{5}{3}$,

$$\frac{dR}{R^2} = -3.98 \times 10^{-8} dt .$$

Then the time during which the sun can have existed while radiating at its present rate is

$$t = -2.52 \times 10^7 \int_{\infty}^{1} \frac{dR}{R^2} = 2.52 \times 10^7 \text{ years} . \tag{31}$$

This is in good agreement with the result given by Chandrasekhar.[9] He finds, with the assumption that the sun has a polytropic density distribution of index 3, $t = 2.4 \times 10^7$ years.

However, equation (29) shows us that the luminosity varies as $1/R^{0.5}$, and therefore we can write

---

[9] *Op. cit.*, p. 455.

$$\frac{dR}{R^{1.5}} = -3.98 \times 10^{-8} dt .$$

Then

$$t = -2.52 \times 10^{7} \int_{\infty}^{1} \frac{dR}{R^{1.5}} = 5.04 \times 10^{7} \text{ years} . \qquad (32)$$

The distributions of T, ρ, and $M(r)$ are almost identical with those given by Eddington for the standard model.[10] The values of T_c and ρ_c are slightly higher than those of a polytrope of index 3, since the value of the polytropic index in the gravitationally contracting model increases from almost 3 at the center to 3.25 at the surface.

The greater part of this work was carried out at the Leuschner Observatory of the University of California, Berkeley. The remainder, in particular the inward integration, was completed with the use of the IBM machines, during night hours, at the Forrestal Research Center of Princeton University.

In conclusion I wish to thank Dr. Louis G. Henyey for his valuable assistance and continued encouragement during the entire course of the problem.

---

[10] See Waldmeier, *Einführung in die Astrophysik* (Basel: Verlag Birkhauser, 1948), p. 88.

THE VARIATIONAL METHOD FOR PROBLEMS OF RADIATIVE TRANSFER

I. ISOTROPIC SCATTERING WITH A CONSTANT NET FLUX

Su-Shu Huang*
Berkeley Astronomical Department, University of California

Received August 15, 1952

ABSTRACT

The variational method for problems of radiative transfer is further simplified, so that it can be used easily for many problems encountered in astrophysics. In this first paper of the series we have applied this new method to the Milne problem and found an approximate solution for the source function. The approximate solution agrees extremely well with the exact solution at all points where the numerical evaluation for the latter has already been carried out. Unlike the exact solution, the approximate solution has a simple analytical form and is very easy to evaluate numerically at any point.

The variational method for certain inhomogeneous integral equations concerned with radiative-transfer problems was first formulated by R. E. Marshak[1] in dealing with neutron diffusion, which is governed by the same mathematical equation as the scattering of radiation. Marshak's method was later slightly modified by the present author[2] in such a way that the simultaneous equations which determine the parameters in the trial function are linearized. In this way we can easily obtain approximate solutions of certain inhomogeneous integral equations with high accuracy. In order to apply this variational method to the problem of isotropic scattering of radiation with a constant net flux, the Milne-Schwarzschild integral equation is first transformed into an inhomogeneous integral equation with a characteristic constant which represents the constant term in the expression for the source function. This characteristic constant can be expressed in terms of the parameters by a quadratic equation. Applying the variational method to his inhomogeneous integral equation, we finally get a set of algebraic equations, one of which is quadratic, while the rest are linear. The characteristic constant (i.e., the constant term in the source function) thus determined has a very high accuracy because of the stationary property of the functional.

Unlike the case of neutron diffusion, we are not required to have an especially high accuracy for the constant term and are interested only in the over-all accuracy of the source function in the whole range. (More specifically, we want a better approximation for the source function in a region near the surface, because the observed emergent radiation depends more upon the source function near the surface than upon that in the far interior of the atmosphere.) Then the previous method can be further simplified, so that the final equations all become linear. This can be seen in the following way.

Consider the Milne-Schwarzschild integral equation

$$J(\tau) = \frac{1}{2}\int_0^\infty J(\tau')E_1(|\tau-\tau'|)\,d\tau' , \tag{1}$$

with

$$E_n(x) = \int_1^\infty \frac{e^{-xv}}{v^n}\,dv . \tag{2}$$

---

* John Simon Guggenheim Foundation Fellow.

[1] *Phys. Rev.*, **71**, 688, 1947; B. Davison, *Phys. Rev.*, **71**, 694, 1947; J. LeCaine, *Phys. Rev.*, **72**, 564, 1947.

[2] *Phys. Rev.* **88**, 50, 1952.

Since the asymptotic form[3] for the source function at infinite depth is linear, we may write

$$J(\tau) = \tau + q(\tau)\,, \tag{3}$$

where $q(\tau)$ should approach a constant as $\tau \to \infty$. The integral equation for $q(\tau)$ can be obtained directly by substituting equation (3) in equation (1). Hence

$$q(\tau) = \frac{1}{2}\int_0^\infty q(\tau')E_1(|\tau - \tau'|)\,d\tau' + \tfrac{1}{2}E_3(\tau)\,. \tag{4}$$

The functional, defined as follows:[2]

$$\mathfrak{F}(q) = \int_0^\infty q(\tau)\left\{q(\tau) - \frac{1}{2}\int_0^\infty q(\tau')E_1(|\tau - \tau'|)\,d\tau'\right\}d\tau - \int^\infty q(\tau)E_3(\tau)\,d\tau\,, \tag{5}$$

will be stationary for the actual solution of equation (4).

Let us now choose a trial function,

$$q(\tau) = A_1 + A_2E_2(\tau) + A_3E_3(\tau) + A_4E_4(\tau) + A_5E_5(\tau)\,, \tag{6}$$

where $E_i(\tau)$ is defined in equation (2) and the A_i's are parameters to be determined. Evidently, equation (6) conforms to the required condition that $q(\tau) \to$ constant as $\tau \to \infty$. Substituting equation (6) in equation (5) and carrying out the integration, we find that

$$\begin{aligned}\mathfrak{F} = {} & \tfrac{1}{4}A_1^2 + \frac{1}{2}\left(1 - \frac{\pi^2}{12}\right)A_2^2 + \frac{1}{2}\left(-\tfrac{13}{72} - \tfrac{4}{9}\ln 2 + \frac{\pi^2}{18}\right)A_3^2 \\ & + \frac{1}{2}\left(\tfrac{23}{90} + \tfrac{4}{5}\ln 2 - \frac{\pi^2}{24}\right)A_4^2 + \frac{1}{2}\left(-\tfrac{10{,}419}{151{,}200} - \tfrac{552}{1575}\ln 2 + \frac{\pi^2}{30}\right)A_5^2 \\ & + \tfrac{2}{3}(1 - \ln 2)A_1A_2 + \tfrac{1}{8}A_1A_3 + \left(\tfrac{11}{30} - \tfrac{2}{5}\ln 2\right)A_1A_4 + \tfrac{5}{72}A_1A_5 \\ & + \tfrac{1}{3}(1 - \ln 2)A_2A_3 + \left(\tfrac{67}{144} + \tfrac{2}{9}\ln 2 - \frac{\pi^2}{18}\right)A_2A_4 + \left(\tfrac{111}{360} - \tfrac{11}{30}\ln 2\right)A_2A_5 \\ & + \tfrac{1}{24}A_3A_4 + \left(-\tfrac{49}{480} - \tfrac{2}{5}\ln 2 + \frac{\pi^2}{24}\right)A_3A_5 + \left(\tfrac{11}{120} - \tfrac{1}{10}\ln 2\right)A_4A_5 - \tfrac{1}{3}A_1 \\ & - \tfrac{1}{8}A_2 - \left(\tfrac{2}{5}\ln 2 - \tfrac{1}{5}\right)A_3 - \tfrac{1}{18}A_4 - \left(\tfrac{2}{7}\ln 2 - \tfrac{13}{84}\right)A_5\,.\end{aligned} \tag{7}$$

The determination of the A_i's follows in the usual way, by putting

$$\frac{\partial \mathfrak{F}}{\partial A_i} = 0 \qquad (i = 1, 2, 3, 4, 5)\,. \tag{8}$$

Equations (8) represent a set of five linear algebraic equations in five unknowns, A_1, A_2, . . . , A_5, and can be easily solved. The final result is

$$\begin{aligned}J(\tau) = {} & \tau + 0.71044067 - 0.27894936E_2(\tau) + 0.52805161E_3(\tau) \\ & - 0.61868635E_4(\tau) + 0.35260116E_5(\tau)\,,\end{aligned} \tag{9}$$

---

[3] G. Placzek and W. Seidel, *Phys. Rev.*, **72**, 550, 1947; also E. Hopf, *Mathematical Problems of Radiative Equilibrium* ("Cambridge Tracts," No. 31 [1934]).

as compared with

$$J(\tau) = \tau + 0.71044609 - 0.27891881E_2(\tau) + 0.52732328E_3(\tau) - 0.61602263E_4(\tau) + 0.35036496E_5(\tau) \tag{10}$$

by the previous method.[2] We have tabulated the source function in Table 1, where equations (9) and (10) are compared numerically with the results calculated by C. Mark[4] from the exact analytic solution.[3] We can therefore see that the two variational methods give nearly the same accuracy for the tabulated range. But the value of the constant term is better determined by the previous method (0.7104460894) than by the present one (0.7104406738), for this same quantity computed from the exact formula[3] is 0.71044609.

TABLE 1

EVALUATION OF $J(\tau)$

τ	Mark	Previous Method	Present Method
0	0.577350	0.577439	0.577439
0.01	0.5982	0.598240	0.598240
0.02	0.6154	0.615380	0.615380
0.03	0.6312	0.631227	0.631226
0.05	0.6607	0.660745	0.660744
0.1	0.7279	0.727918	0.727918
0.2	0.8495	0.849558	0.849557
0.3	0.9633	0.963372	0.963370
0.4	1.0731	1.073093	1.073092
0.5	1.1803	1.180292	1.180291
0.6	1.2858	1.285799	1.285798
0.8	1.4935	1.493532	1.493530
1.0	1.6985	1.698539	1.698538
1.5	2.2051	2.205135	2.205132
2.0	2.7079	2.707923	2.707920
3.0	3.7098	3.709812	3.709807
4.0	4.7102	4.710272	4.710278

It should be mentioned that, as the elimination of the A_i's is going on in the process of solving the simultaneous equations (8), we are continuously losing significant figures. Because of the limitation of the size (ten digits) of the available computing machine, we have restricted ourselves in the very beginning to ten figures for the coefficients of the A_i's in equations (8). After four unknowns ($A_1, \ldots, A_4$) have been eliminated, we are left with an equation for A_5 having only three significant figures, i.e.,

$$0.0000000346A_5 = 0.0000000122 ,$$

which gives $A_5 = 0.35260116$. If we start the equation with more than ten figures, the value of A_5, and consequently of A_4, A_3, A_2, and A_1, will be different, and the final result should give a better representation of the actual solution. As the solution we have obtained is already extremely good and also because larger computing machines are not available, we have not tried to solve the linear equations with more than ten decimals. The loss of significant figures in the process of solving the simultaneous equations occurs both in the previous method and in the present method. It occurs also in the cases considered in the two papers immediately following the present one.

The emergent intensity $I(0, \mu)$ follows directly from equation (9) or (10). Normalizing the solution $I(0, \mu)$ to yield a net flux πF, we have

---

[4] *Phys. Rev.*, **72**, 558, 1947.

$$\begin{aligned}\frac{I(0, \mu)}{F} &= 0.75\mu + 0.5328305 - 0.2092120 \frac{1}{\mu}\varphi_2\left(\frac{1}{\mu}\right) \\ &\quad + 0.3960387 \frac{1}{\mu}\varphi_3\left(\frac{1}{\mu}\right) - 0.4640147 \frac{1}{\mu}\varphi_4\left(\frac{1}{\mu}\right) + 0.2644509 \frac{1}{\mu}\varphi_5\left(\frac{1}{\mu}\right)\end{aligned} \tag{11}$$

from equation (9), or

$$\begin{aligned}\frac{I(0, \mu)}{F} &= 0.75\mu + 0.5328346 - 0.2091891 \frac{1}{\mu}\varphi_2\left(\frac{1}{\mu}\right) \\ &\quad + 0.3954925 \frac{1}{\mu}\varphi_3\left(\frac{1}{\mu}\right) - 0.4620170 \frac{1}{\mu}\varphi_4\left(\frac{1}{\mu}\right) + 0.2627738 \frac{1}{\mu}\varphi_5\left(\frac{1}{\mu}\right)\end{aligned} \tag{12}$$

from equation (10). The function $\varphi_n(\lambda)$ is defined as follows:

$$\varphi_n(\lambda) = \int_0^\infty e^{-\lambda t} E_n(t)\, dt = \int_1^\infty \frac{dx}{x^n (x + \lambda)} \qquad (\lambda > -1)\,, \tag{13}$$

which can be easily evaluated for integral values of n. Equations (11) and (12) give nearly the same numerical results. The emergent radiation has been computed by many authors with different methods. A recent review of the results by different authors is given by D. H. Menzel and H. K. Sen.[5] We have computed values of $I(0, \mu)$ according to equations (11) and (12) and compared them with the table[6] computed from the exact analytic expression.[3] The error is maximum (0.016 per cent) at $\mu = 0$ and decreases rapidly as μ increases. At $\mu = 0.01$ it is already reduced to 0.004 per cent. For the rest of the range the error involved in equation (11) or (12) is about one part in one million. The error will be further reduced if we solve equations (8) correctly to more than ten digits.

Finally, it should be mentioned that using the exponential integrals, $E_n(x)$,[7] in representing the source function has already been done by many authors.[1,5]

I wish to express my sincere thanks to Professor Otto Struve for his encouragement and for the conveniences which he has kindly rendered to me during the investigation of the problems presented in this and the two following papers.

[5] *Ap. J.*, **110**, 1, 1949.

[6] A complete table can be found in G. Placzek, *Phys. Rev.*, **72**, 556, 1947. See also S. Chandrasekhar, *Ap. J.*, **99**, 189, 1944. Note that we should multiply Placzek's $\varphi(\mu)$ by $(\sqrt{3})/2$ before comparing it with equation (11) or (12). This is due to different ways of normalization.

[7] Numerical tables for $E_n(x)$ can be found in G. Placzek, *The Function $E_n(x)$* (Ottawa, Canada: National Research Council of Canada, 1946).

THE VARIATIONAL METHOD FOR PROBLEMS OF RADIATIVE TRANSFER

II. THE FORMATION OF ABSORPTION LINES IN THE MILNE-EDDINGTON MODEL

SU-SHU HUANG*
Berkeley Astronomical Department, University of California

Received August 15, 1952

ABSTRACT

The variational method has been applied to the problem of the line formation in the M-E model. Making use of the asymptotic form of the source function first obtained by Menzel and Sen, we are able to derive, with one parameter in the trial function, a simple explicit formula for the profile, with an error of only about 0.2 per cent. A formula derived from a trial function having three parameters is also given. A numerical example shows that it agrees extremely well with the results obtained by the use of other methods. A correct asymptotic form is the main reason for the high accuracy in the final result without introduction of too many parameters in the trial function.

Following the notation used previously,[1] we write the Schwarzschild integral equation in the following form:

$$J(t) = [1-\Lambda(t)]B(t) + \tfrac{1}{2}\Lambda(t)\int_0^\infty J(t')E_1(|t-t'|)\,dt', \tag{1}$$

where t is the total optical depth in the absorption line, and

$$\Lambda(t) = \frac{\sigma_\nu}{r+l_\nu+\sigma_\nu}. \tag{2}$$

For the Milne-Eddington (M-E) model, $\Lambda(t) = \text{Constant} \equiv \Lambda_0$ and $B(t)$ becomes a linear function of t, i.e.,

$$B(t) = c_0 + c_1 t. \tag{3}$$

Equation (1) therefore assumes a simpler form:

$$J(t) = (1-\Lambda_0)(c_0+c_1 t) + \tfrac{1}{2}\Lambda_0\int_0^\infty J(t')E_1(|t-t'|)\,dt'. \tag{4}$$

The asymptotic form of $J(t)$ at great depth has been found by D. H. Menzel and H. K. Sen[2] to be

$$J(t) \to c_0 + c_1 t + A_1 e^{-mt}, \tag{5}$$

where A_1 is a constant to be determined and m is a positive root of the following equation:

$$m = \Lambda_0 \tanh^{-1} m. \tag{6}$$

This equation has been solved for certain values of Λ_0 by S. Chandrasekhar[3] and by Menzel and Sen.[2]

---

* John Simon Guggenheim Foundation Fellow.

[1] S. S. Huang, *Ann. d'ap.*, **15**, 169, 1952.

[2] *Ap. J.*, **113**, 482, 1951.

[3] *Radiative Transfer* (London: Oxford University Press, 1950).

Now let

$$J(t) = c_0 + c_1 t + q_0(t) . \tag{7}$$

From the asymptotic form given by equation (5), $q_0(t)$ must approach zero as $t \to \infty$. Substitute equation (7) in equation (4), and the following equation for $q_0(t)$ results:

$$q_0(t) = \tfrac{1}{2}\Lambda_0 \int_0^\infty q_0(t') E_1(|t-t'|)\, dt' + \tfrac{1}{2}\Lambda_0 [\, c_1 E_3(t) - c_0 E_2(t) \,] . \tag{8}$$

The required functional in the present case is[4]

$$\begin{aligned} \tilde{\mathfrak{F}}(q) = \int_0^\infty q(t) \Big\{ q(t) - \tfrac{1}{2}\Lambda_0 \int_0^\infty q(t') E_1(|t-t'|)\, dt' \Big\}\, dt & \\ - \Lambda_0 \int_0^\infty q(t) [\, c_1 E_3(t) - c_0 E_2(t) \,]\, dt . & \end{aligned} \tag{9}$$

It can be easily seen that $\tilde{\mathfrak{F}}$ is stationary when $q(t) = q_0(t)$. From equations (8) and (9) we have

$$\tilde{\mathfrak{F}} = \Lambda_0 (\tfrac{1}{8} c_1^2 - \tfrac{1}{4} c_0^2) + (\Lambda_0 - 1) \Big[c_0 \int_0^\infty q_0(t)\, dt + c_1 \int_0^\infty q_0(t)\, t\, dt \Big] . \tag{10}$$

In other words,

$$c_0 \int_0^\infty q_0(t)\, dt + c_1 \int_0^\infty q_0(t)\, t\, dt$$

is stationary and can be very accurately determined, although we shall not make use of this property.

Conforming with the asymptotic form given by equation (5), we assume a simple trial function as follows:

$$q_0(t) = A_1 e^{-mt} , \tag{11}$$

where A_1 is the only parameter to be determined. The corresponding $\tilde{\mathfrak{F}}$ then becomes

$$\tilde{\mathfrak{F}} = \frac{A_1^2}{2} \Big[\frac{1}{m} - \Lambda_0 \frac{\ln(1+m)}{m^2} \Big] - A_1 \Lambda_0 [\, c_1 \varphi_3(m) - c_0 \varphi_2(m) \,] , \tag{12}$$

where $\varphi_n(x)$ has already been defined in the previous paper. Because of relation (6), we may also write equation (12) as

$$\tilde{\mathfrak{F}} = \frac{A_1^2}{2} \Big[- \frac{\Lambda_0}{2m^2} \ln(1 - m^2) \Big] - A_1 \Lambda_0 [\, c_1 \varphi_3(m) - c_0 \varphi_2(m) \,] . \tag{13}$$

In deriving equation (12) or (13), the formula

$$\int_0^\infty e^{-\lambda t'} E_1(|t-t'|)\, dt' = \int_1^\infty \frac{e^{-tx} dx}{x(\lambda - x)} + e^{-\lambda t} \frac{2}{\lambda} \tanh^{-1} \lambda \tag{14}$$

has been used. Although the integral

$$\int_0^\infty e^{-\lambda t'} E_1(|t-t'|)\, dt'$$

is defined here for all positive values of λ, equation (14) holds only for $\lambda < 1$. Setting

---

[4] See references in Paper I.

$\partial\mathfrak{F}/\partial A_1 = 0$, we have

$$A_1 = K_0(m)\,c_0 - K_1(m)\,c_1\,, \tag{15}$$

where

$$K_0(m) = \frac{2m^2}{\ln(1-m^2)}\left[\frac{1}{m} - \frac{1}{m^2}\ln(1+m)\right] \tag{16}$$

and

$$K_1(m) = \frac{2m^2}{\ln(1-m^2)}\left[\frac{1}{2m} - \frac{1}{m^2} + \frac{1}{m^3}\ln(1+m)\right]. \tag{17}$$

Hence

$$J(t) = c_0 + c_1 t + [K_0(m)\,c_0 - K_1(m)\,c_1]\,e^{-mt}\,, \tag{18}$$

and

$$I_\nu(0,\mu) = c_0 + c_1\mu + [K_0(m)\,c_0 - K_1(m)\,c_1]\frac{1}{1+m\mu}\,. \tag{19}$$

In the continuous background we have

$$I_c(0,\mu) = B_0 + B_0\beta_0\mu\,,$$

where B_0 and β_0 are related to c_0 and c_1 in the following way:[1]

$$c_0 = B_0\,, \qquad c_1 = \frac{B_0\beta_0 r}{r + l_\nu + \sigma_\nu}\,.$$

We therefore have, for the residual intensity,

$$r_\mu = \frac{I_\nu(0,\mu)}{I_c(0,\mu)} = \frac{1}{1+\beta_0\mu}\left\{1 + \frac{K_0(m)}{1+m\mu} + \frac{\beta_0 r}{r + l_\nu + \sigma_\nu}\left[\mu - \frac{K_1(m)}{1+m\mu}\right]\right\}. \tag{20}$$

Similarly, we can derive a corresponding formula for the residual intensity from the flux, thus:

$$r_f = \frac{F_\nu(0)}{F_c(0)} = \frac{6}{3+2\beta_0}\left\{\tfrac{1}{2} + K_0(m)\,\varphi_2(m) + \frac{\beta_0 r}{r + l_\nu + \sigma_\nu}\left[\tfrac{1}{3} - K_1(m)\,\varphi_2(m)\right]\right\}. \tag{21}$$

Equations (20) and (21) give two simple analytical expressions for the absorption line in the M-E model. Moreover, the accuracy of these two formulae is very high; we shall give a numerical example here to illustrate it.

The case $\Lambda_0 = 0.8$ and $l_\nu = 0$ has been computed extensively by Menzel and Sen[2] both from their method and from Chandrasekhar's methods.[3] The value of m corresponding to $\Lambda_0 = 0.8$ is 0.7104117843.[2] Equations (20) and (21) become, for the present case (i.e., $\Lambda_0 = 0.8$),

$$r_\mu = \frac{1}{1+\beta_0\mu}\left[1 - \frac{0.4944130}{1+0.7104118\mu} + \frac{\beta_0 r}{r + l_\nu + \sigma_\nu}\left(\mu + \frac{0.3152217}{1+0.7104118\mu}\right)\right], \tag{22}$$

and

$$r_f = \frac{6}{3+2\beta_0}\left[0.3298572 + 0.4418108\,\frac{\beta_0 r}{r + l_\nu + \sigma_\nu}\right]. \tag{23}$$

Putting $\beta_0 = 3/(8x)$ and $l_\nu = 0$ in equation (23) in order to compare directly with Menzel and Sen's table, we obtain

$$r_f = \frac{3}{1+4x}\,[0.8796193x + 0.0883622]\,. \tag{24}$$

Equation (24) is numerically compared with others' results in Table 1. The error is about

0.2 per cent in all cases computed. Hence the present simple formula can be used for all practical purposes.

If higher approximations are required, we can take

$$q(t) = A_1 e^{-mt} + \sum_{n=2}^{N} A_n E_n(t) \tag{25}$$

as a trial function. Before we write down the final result for $\mathfrak{F}$ which corresponds to equation (25), it is profitable to introduce the following abbreviations:

$$\Phi_n(\lambda) = \int_1^\infty \frac{\ln(1+x)}{x^n(x+\lambda)}\, dx \qquad (\lambda > -1)$$

$$i_{ks} = i_{sk} = \int_0^\infty E_k(t) E\ (t)\, dt\,, \tag{26}$$

and

$$I_{ks} = I_{sk} = \int_0^\infty \int_0^\infty E_k(t) E_s(t') E_1(|t-t'|)\, dt dt'\,.$$

TABLE 1

A NUMERICAL EXAMPLE FOR THE EVALUATION OF THE RESIDUAL INTENSITY*

x	VARIATIONAL METHOD		EXPONENTIAL INTEGRAL METHOD	H-FUNCTION	GAUSSIAN QUADRATURE (3D APPROX.)
	1 Parameter Eq. (24)	3 Parameters Eq. (41)			
0.1	0.3778	0.377303	0.377303	0.377298	0.3794
$\frac{1}{6}$	.4229	.422236	.422236	.422231	.4248
0.25	.4624	.461552	.461552	.461547	.4645
$\frac{1}{3}$	.4906	.489635	.489635	.489630	.4928
0.35	0.4953	0.494316	0.494316	0.494310	0.4976

* The last three columns are taken from Menzel and Sen's paper.

The functional corresponding to equation (25) now becomes

$$\begin{aligned}\mathfrak{F} = -\tfrac{1}{2} A_1^2\left[\frac{\Lambda_0}{2}\frac{\ln(1-m^2)}{m^2}\right] + A_1\Lambda_0 \sum_{n=2}^{N} A_n \int_1^\infty \frac{dx}{x(x-m)}\,\varphi_n(x) \\ + \frac{1}{2}\sum_{k,\,s=2}^{N} A_k A_s (2 i_{ks} - \Lambda_0 I_{ks}) - \Lambda_0 \Big\{ A_1 [c_1\varphi_3(m) - c_0\varphi_2(m)] \\ + \sum_{n=2}^{N} A_n (c_1 i_{3n} - c_0 i_{2n}) \Big\}\,.\end{aligned} \tag{27}$$

Or if we take into account only three parameters, A_1, A_2, and A_3, in the trial function, we have

$$\begin{aligned}\tilde{\mathfrak{F}} = -\tfrac{1}{2}A_1^2\left[\frac{\Lambda_0}{2}\frac{\ln(1-m^2)}{m^2}\right] &+ \Lambda_0 A_1 A_2\,[\varphi_2(-m) - \Phi_3(-m)] \\ &+ \Lambda_0 A_1 A_3\,[\tfrac{1}{2}\varphi_2(-m) - \varphi_3(-m) + \Phi_4(-m)] + \tfrac{1}{2}A_2^2(2i_{22} - \Lambda_0 I_{22}) \\ &+ A_2 A_3(2i_{23} - \Lambda_0 I_{23}) + \tfrac{1}{2}A_3^2(2i_{33} - \Lambda_0 I_{33}) - \Lambda_0 A_1[c_1\varphi_3(m) - c_0\varphi_2(m)] \\ &- \Lambda_0 A_2(c_1 i_{23} - c_0 i_{22}) - \Lambda_0 A_3(c_1 i_{33} - c_0 i_{23})\,. \end{aligned} \tag{28}$$

Both the integrals i_{ks} and I_{ks} can be easily evaluated.[5]

Let us now consider briefly the evaluation of $\Phi_n(-m)$. Since $m < 1$, $\Phi_n(-m)$ is well defined. By the recurrence formula,

$$\Phi_n(-\lambda) = -\frac{1}{\lambda}\int_1^\infty \frac{dx}{x^n}\ln(1+x) + \frac{1}{\lambda}\Phi_{n-1}(-\lambda)\,, \tag{29}$$

we can express all $\Phi_n(-\lambda)$'s in terms of $\Phi_1(-\lambda)$, which can be evaluated by the series expansion; thus

$$\begin{aligned}\Phi_1(-\lambda) &= \int_1^\infty \frac{dx}{x(x-\lambda)}\ln(1+x) = \frac{1}{\lambda}\lim_{R\to\infty}\int_1^R\left[\frac{1}{x-\lambda} - \frac{1}{x}\right]\ln(1+x)\,dx \\ &= \frac{1}{\lambda}\left\{\tfrac{1}{2}[\ln(1+\lambda)]^2 - \ln(1+\lambda)\ln(1-\lambda) + \frac{\pi^2}{12} - S\left(\frac{1-\lambda}{1+\lambda}\right)\right\},\end{aligned} \tag{30}$$

where

$$S(x) \equiv x - \frac{1}{2^2}x^2 + \frac{1}{3^2}x^3 - \frac{1}{4^2}x^4 + \dots\,. \tag{31}$$

Three linear equations

$$\frac{\partial\tilde{\mathfrak{F}}}{\partial A_i} = 0 \qquad (i = 1, 2, 3)\,, \tag{32}$$

determine the three unknowns, A_1, A_2, and A_3 completely. The solution can be put into the usual determinant form:

$$A_1 = \frac{(\delta\beta\gamma)}{(\alpha\beta\gamma)}\,, \qquad A_2 = \frac{(\alpha\delta\gamma)}{(\alpha\beta\gamma)}\,, \qquad A_3 = \frac{(\alpha\beta\delta)}{(\alpha\beta\gamma)}\,, \tag{33}$$

where

$$\begin{aligned} &\alpha_1 = -\frac{\Lambda_0}{2}\frac{\ln(1-m^2)}{m^2}\,, \qquad \alpha_2 = \Lambda_0[\varphi_2(-m) - \Phi_3(-m)]\,, \\ &\alpha_3 = \Lambda_0[\tfrac{1}{2}\varphi_2(-m) - \varphi_3(-m) + \Phi_4(-m)]\,; \qquad \beta_1 = \alpha_2\,, \\ &\beta_2 = \tfrac{4}{3}(1 - \ln 2) - \Lambda_0\left(\tfrac{1}{3} - \tfrac{4}{3}\ln 2 + \frac{\pi^2}{12}\right), \\ &\beta_3 = \tfrac{1}{4} - \Lambda_0(\tfrac{1}{3}\ln 2 - \tfrac{1}{12})\,; \qquad \gamma_1 = \alpha_3\,, \\ &\gamma_2 = \beta_3\,, \qquad \gamma_3 = -\tfrac{2}{5} + \tfrac{4}{5}\ln 2 - \Lambda_0\left(-\tfrac{79}{360} + \tfrac{56}{45}\ln 2 - \frac{\pi^2}{18}\right); \\ &\delta_1 = \Lambda_0[c_1\varphi_3(m) - c_0\varphi_2(m)]\,, \\ &\delta_2 = \Lambda_0[\tfrac{1}{8}c_1 - \tfrac{2}{3}(1 - \ln 2)\,c_0]\,, \\ &\delta_3 = \Lambda_0[(-\tfrac{1}{5} + \tfrac{2}{5}\ln 2)\,c_1 - \tfrac{1}{8}c_0]\,. \end{aligned} \tag{34}$$

---

[5] J. LeCaine, *Phys. Rev.*, **72**, 564, 1947.

If $\Lambda_0 = 0$, we have $A_i = 0$ directly from equation (9), or $J(t) = c_0 + c_1 t$, which is the correct result.

For the emergent intensity and flux we have, from equations (7) and (23),

$$I_\nu(0, \mu) = c_0 + c_1\mu + \frac{A_1}{1 + m\mu} + \frac{1}{\mu}\sum_{n=2}^{N} A_n \varphi_n\left(\frac{1}{\mu}\right) \tag{35}$$

and

$$F_\nu(0) = c_0 + \tfrac{2}{3}c_1 + 2A_1\varphi_2(m) + 2\sum_{n=2}^{N} A_n i_{2n}\,. \tag{36}$$

For $N = 3$, equation (36) reduces simply to

$$F_\nu(0) = c_0 + \tfrac{2}{3}c_1 + 2\left[\frac{1}{m} - \frac{1}{m^2}\ln(1+m)\right]A_1 + \tfrac{4}{3}(1 - \ln 2)\,A_2 + \tfrac{1}{4}A_3\,. \tag{37}$$

For $\Lambda = 0.8$, we have, from equations (33),

$$\begin{aligned} A_1 &= 0.3198512\,c_1 - 0.4282012\,c_0\,, \\ A_2 &= -0.0972655\,c_1 - 0.1649612\,c_0\,, \\ A_3 &= 0.1448928\,c_1 + 0.0813576\,c_0\,. \end{aligned} \tag{38}$$

The corresponding formulae for the residual intensities are therefore ($\Lambda_0 = 0.8$)

$$\begin{aligned} r_\mu = \frac{I_\nu(0,\mu)}{I_c(0,\mu)} = \frac{1}{1+\beta_0\mu}\Bigg\{ 1 &- \frac{0.4282012}{1 + 0.7104118\mu} - 0.1649612\,\frac{1}{\mu}\varphi_2\left(\frac{1}{\mu}\right) \\ &+ 0.0813576\,\frac{1}{\mu}\varphi_3\left(\frac{1}{\mu}\right) + \beta_0\,\frac{r}{r + l_\nu + \sigma_\nu}\left[\mu + \frac{0.3198512}{1 + 0.7104118\mu}\right. \\ &\left. - 0.0972655\,\frac{1}{\mu}\varphi_2\left(\frac{1}{\mu}\right) + 0.1448928\,\frac{1}{\mu}\varphi_3\left(\frac{1}{\mu}\right)\right]\Bigg\} \end{aligned} \tag{39}$$

and

$$r_f = \frac{F_\nu(0)}{F_c(0)} = \frac{6}{3 + 2\beta_0}\left[0.3290666 + 0.4416182\,\frac{\beta_0 r}{r + l_\nu + \sigma_\nu}\right]. \tag{40}$$

In order to compare equation (40) with Menzel and Sen's table, we have, by putting $\beta_0 = 3/(8x)$ and $l_\nu = 0$ in equation (40),

$$r_f = \frac{3}{1 + 4x}(0.8775109x + 0.0883236)\,. \tag{41}$$

The values of r_f computed from equation (41) are listed in Table 1. We can see how well equation (41) agrees with others' results. We have also computed r_μ from equation (39) and compared with the tabulated values[2] obtained both from Menzel and Sen's and from Chandrasekhar's methods. The agreement here is also very good (four-figure agreement for all computed values except at $\mu = 0$, where a difference in the fourth figure happens for all values of x).

In concluding this paper we should mention that the present method has many merits. First, it is very easy to derive an accurate result; second, it gives simple formulae for the line profile (both for the intensity and for the flux) in terms of elementary functions; and, third, like Menzel and Sen's method, it gives an explicit form for the source function, which is very important in the understanding of the line formation at different depths in the stellar atmosphere.[6]

[6] S. S. Huang, *Ap. J.*, **115**, 529, 1952.

THE VARIATIONAL METHOD FOR PROBLEMS OF RADIATIVE TRANSFER

III. REFLECTION EFFECT

SU-SHU HUANG*
Berkeley Astronomical Department, University of California
Received August 15, 1952

ABSTRACT

The variational method has been applied to the problem of diffuse reflection by a plane-parallel atmosphere scattering radiation isotropically. Approximate expressions with five parameters have been derived both for the source function and for the emergent radiation. The numerical results are in good agreement with those computed by other methods.

The integral equation for the source function appropriate to the problem of diffuse reflection by a plane-parallel atmosphere scattering radiation isotropically was first obtained by E. A. Milne:[1]

$$J(t)=\frac{1}{2}\int_0^\infty J(t')E_1(|t-t'|)\,dt'+\tfrac{1}{4}F\,e^{-t/\mu_0}\,, \tag{1}$$

where μ_0 is the cosine of the angle of incidence on the boundary of the atmosphere of the reflecting star of a parallel beam of radiation of flux πF per unit area normal to itself. For large values of t the last term can be neglected, and we are left with an equation which has been fully investigated. The asymptotic behavior of that equation is $a+bt$, where a and b are two constants. But the constant b is proportional to the asymptotic diffuse flux; hence it vanishes in the present case.[2] Therefore, we can write a trial function for $J(t)$ in the following form:

$$J(t)=A_0+A_1e^{-t/\mu_0}+\sum_{n=2}^{N}A_nE_n(t)\,, \tag{2}$$

where A_0, A_1, A_2, etc., are constants to be determined by the variational method.

It is easy to see that the functional,

$$\mathfrak{F}=\int_0^\infty J(t)\left\{J(t)-\frac{1}{2}\int_0^\infty J(t')E_1(|t-t'|)\,dt'\right\}dt-\frac{F}{2}\int_0^\infty J(t)\,e^{-t/\mu_0}dt\,, \tag{3}$$

attains an extremal when $J(t)$ is a correct solution of equation (1). The calculation of $\mathfrak{F}$ for the trial function (2) is nearly the same as that in the previous paper. Only, in carrying out the integration involved in equation (3), we should use

---

* John Simon Guggenheim Foundation Fellow.

[1] *M.N.*, **87,** 43, 1926; also E. Hopf, *Mathematical Problems of Radiative Equilibrium* ("Cambridge Mathematical Tracts," No. 31 [1934]).

[2] D. H. Menzel and H. K. Sen, *Ap. J.*, **113,** 490, 1951.

$$\int_0^\infty e^{-\lambda t'} E_1(|t-t'|)\,dt' = \int_1^\infty \frac{e^{-\lambda t} - e^{-xt}}{x(x-\lambda)}\,dx + \frac{e^{-\lambda t}}{\lambda}\ln(1+\lambda) \tag{4}$$

instead of the simpler formula given by equation (14) in Paper II, because here $\lambda = 1/\mu_0 \geq 1$. Thus

$$\begin{aligned}\tilde{\aleph} = {} & \tfrac{1}{4}A_0^2 + A_0 A_1 \varphi_2\left(\frac{1}{\mu_0}\right) + \tfrac{1}{2}A_1^2\varphi_2\left(\frac{1}{\mu_0}\right) + A_0\sum_{n=2}^{N} A_n i_{2n} + A_1 \sum_{n=2}^{N} A_n G_n\left(\frac{1}{\mu_0}\right) \\ & + \frac{1}{2}\sum_{k,s=2}^{N} A_k A_s (2i_{ks} - I_{ks}) - \frac{F}{2}\left[A_0\mu_0 + \frac{A_1}{2}\mu_0 + \sum_{n=2}^{N} A_n\varphi_n\left(\frac{1}{\mu_0}\right)\right],\end{aligned} \tag{5}$$

where $\varphi_n(\lambda)$, i_{ks}, and I_{ks} have been defined in the previous paper, and

$$\begin{aligned}G_n(\lambda) &= 2\int_0^\infty e^{-\lambda t} E_n(t)\,dt - \int_0^\infty\int_0^\infty e^{-\lambda t'} E_n(t) E_1(|t-t'|)\,dt\,dt' \\ &= \varphi_n(\lambda)[1+\lambda\varphi_2(\lambda)] - \Phi_{n+1}(\lambda).\end{aligned} \tag{6}$$

$\Phi_n(\lambda)$ was also defined in the previous paper, and its explicit expression for $-1 < \lambda < 0$ is given there. For the positive argument we should have

$$\Phi_1(\lambda) = \frac{1}{\lambda}\left\{\frac{\pi^2}{12} + \tfrac{1}{2}[\ln(1+\lambda)]^2 - S\left(\frac{1-\lambda}{1+\lambda}\right)\right\}, \tag{7}$$

where

$$S(x) = x - \frac{1}{2^2}x^2 + \frac{1}{3^2}x^3 - \ldots . \tag{8}$$

The recurrence formula for $\Phi_n(\lambda)$ is the same for both positive and negative λ. Hence any $\Phi_n(\lambda)$ can be computed, once $\Phi_1(\lambda)$ is known. As far as I am aware, the infinite series $S(x)$ has not been tabulated, and we have to compute it for each case. If we take $N = 4$, equation (5) becomes

$$\begin{aligned}\tilde{\aleph} = {} & \tfrac{1}{4}A_0^2 + A_0A_1\varphi_2\left(\frac{1}{\mu_0}\right) + \tfrac{1}{2}A_1^2\varphi_2\left(\frac{1}{\mu_0}\right) + A_0A_2i_{22} + A_0A_3i_{23} + A_0A_4i_{24} \\ & + A_1A_2G_2\left(\frac{1}{\mu_0}\right) + A_1A_3G_3\left(\frac{1}{\mu_0}\right) + A_1A_4G_4\left(\frac{1}{\mu_0}\right) \\ & + \tfrac{1}{2}A_2^2(2i_{22} - I_{22}) + \tfrac{1}{2}A_3^2(2i_{33} - I_{33}) + \tfrac{1}{2}A_4^2(2i_{44} - I_{44}) \\ & + A_2A_3(2i_{23} - I_{23}) + A_2A_4(2i_{24} - I_{24}) + A_3A_4(2i_{34} - I_{34}) \\ & - \frac{F}{2}\left[A_0\mu_0 + \frac{A_1}{2}\mu_0 + A_2\varphi_2\left(\frac{1}{\mu_0}\right) + A_3\varphi_3\left(\frac{1}{\mu_0}\right) + A_4\varphi_4\left(\frac{1}{\mu_0}\right)\right].\end{aligned} \tag{9}$$

where

$$\varphi_2\left(\frac{1}{\mu}\right)=\mu-\mu^2\ \ln\left(\frac{1+\mu}{\mu}\right),$$

$$\varphi_3\left(\frac{1}{\mu}\right)=\tfrac{1}{2}\mu-\mu\varphi_2\left(\frac{1}{\mu}\right),$$

$$\varphi_4\left(\frac{1}{\mu}\right)=\tfrac{1}{3}\mu-\mu\varphi_3\left(\frac{1}{\mu}\right);$$

$$\begin{aligned}G_2\left(\frac{1}{\mu}\right)&=\tfrac{3}{2}\mu-3\mu^2\ \ln\left(\frac{1+\mu}{\mu}\right)+(2\ \ln\ 2)\,\mu^2-\mu^3\left\{\frac{\pi^2}{12}-\frac{1}{2}\left[\ln\left(\frac{1+\mu}{\mu}\right)\right]^2\right.\\&\qquad\left.-S\left(\frac{\mu-1}{\mu+1}\right)\right\},\\G_3\left(\frac{1}{\mu}\right)&=\mu\left[\tfrac{7}{6}-\tfrac{2}{3}\ \ln\ 2-\tfrac{1}{2}\mu\ \ln\left(\frac{1+\mu}{\mu}\right)-G_2\left(\frac{1}{\mu}\right)\right],\\G_4\left(\frac{1}{\mu}\right)&=\mu\left[\tfrac{11}{24}-\tfrac{1}{3}\mu\ \ln\left(\frac{1+\mu}{\mu}\right)-G_3\left(\frac{1}{\mu}\right)\right];\\i_{22}&=\tfrac{2}{3}(1-\ln\ 2),\qquad i_{23}=\tfrac{1}{8},\qquad i_{24}=\tfrac{11}{30}-\tfrac{2}{5}\ \ln\ 2,\\2i_{22}-I_{22}&=1-\frac{\pi^2}{12},\qquad 2i_{33}-I_{33}=-\tfrac{13}{72}-\tfrac{4}{9}\ \ln\ 2+\frac{\pi^2}{18},\\2i_{44}-I_{44}&=\tfrac{23}{90}+\tfrac{4}{15}\ \ln\ 2-\frac{\pi^2}{24},\qquad 2i_{23}-I_{23}=\tfrac{1}{3}(1-\ln\ 2),\\2i_{24}-I_{24}&=\tfrac{67}{144}+\tfrac{2}{9}\ \ln\ 2-\frac{\pi^2}{18},\qquad 2i_{34}-I_{34}=\tfrac{1}{24}.\end{aligned}\tag{10}$$

As usual, the five linear equations obtained from

$$\frac{\partial\widetilde{\mathfrak{F}}}{\partial A_i}=0\tag{11}$$

determine the five parameters A_i $(i=0,1,\ldots,4)$.

We have solved equations (11) for two cases, i.e., $\mu_0=1$ and $\mu_0=0.5$. For $\mu_0=1$, we have

$$\begin{aligned}A_0&=1.2591642F, & A_1&=-0.1526755F,\\A_2&=-0.3583104F, & A_3&=0.4095809F,\\A_4&=-0.6781485F.\end{aligned}\tag{12}$$

For $\mu_0=0.5$, we have

$$\begin{aligned}A_0&=0.4347856F, & A_1&=0.2806519F,\\A_2&=-0.0943005F, & A_3&=-2.1509711F,\\A_4&=2.8803468F.\end{aligned}\tag{13}$$

The emergent intensity is given by

$$I(0,\mu)=A_0+A_1\left(\frac{\mu_0}{\mu_0+\mu}\right)+\sum_{n=2}^{N}A_n\frac{1}{\mu}\varphi_n\left(\frac{1}{\mu}\right).\tag{14}$$

TABLE 1

INTENSITY OF REFLECTED RADIATION

μ	$I(0, \mu)/F$					
	$\mu_0 = 1$			$\mu_0 = 0.5$		
	Present	Chandra-sekhar's	Menzel and Sen's	Present	Chandra-sekhar's	Menzel and Sen's
0	0.726919	0.726950	0.727457	0.505767	0.503200	0.503209
0.1	0.824333	0.824361	0.829197	.523002	.523076	.523120
0.2	0.878615	0.878580	0.881379	.521299	.521279	.521698
0.3	0.918489	0.918473	0.919899	.516576	.516566	.516913
0.4	0.949855	0.949864	0.950439	.511380	.511391	.511596
0.5	0.975463	0.975467	0.975541	.506408	.506420	.506511
0.6	0.996894	0.996876	0.996657	.501851	.501851	.501863
0.7	1.015157	1.051643*	1.014724	.497738	.497749	.497681
0.8	1.030942	1.030936	1.030387	.494042	.494046	.493937
0.9	1.044741	1.044742	1.044117	.490721	.490728	.490583
1.0	1.056920	1.056913	1.056250	0.487731	0.487735	0.487572

* Using Chandrasekhar's table of $H(\mu)$ (*Radiative Transfer*, p. 125), we have computed the value to be 1.0152, which differs from the value given by Menzel and Sen.

and can be computed by substituting the suitable solution for $A_0, A_1, \ldots, A_4$ in the expression. For $\mu_0 = 1$ and $\mu_0 = 0.5$ we have tabulated the numerical results together with those computed by Menzel and Sen's[2] and Chandrasekhar's methods[3] (both are taken from Menzel and Sen's paper). The solution by the variational method for this problem is not so good as for that of the line formation, and we have to consider a trial function of five parameters in order to get an accurate result.

Application of the variational method to other problems in the theory of radiative transfer will be discussed later.

---

[3] S. Chandrasekhar, *Radiative Transfer* (London: Oxford University Press, 1950), pp. 80–87.

INFLUENCE OF DOPPLER EFFECT AND DAMPING ON LINE-ABSORPTION COEFFICIENT AND ATMOSPHERIC RADIATION TRANSFER*

GILBERT N. PLASS AND DANIEL I. FIVEL
Department of Physics, Johns Hopkins University

Received August 11, 1952

ABSTRACT

The general term is given for the Taylor series and asymptotic expansions of the line-absorption coefficient when both the Doppler effect and damping contribute to the line shape. The influence of the Doppler effect on the fractional absorption of a line as measured in the laboratory is calculated and compared with the usual expressions which assume a Lorentz line shape. The radiation transfer in a planetary atmosphere is calculated when both the Doppler effect and damping contribute to the line shape and when the change of half-width with height is taken into account. It is shown that for the earth's atmosphere the radiative transfer calculated from the Lorentz shape alone is not changed appreciably by the Doppler effect for either weak or strong lines at heights up to at least 50 km, even at altitudes where the Doppler width is somethat greater than the Lorentz width.

INTRODUCTION

When both the Doppler effect and Lorentz collision damping contribute to the line width, a knowledge of the line-absorption coefficient is needed for problems in such diverse fields as stellar radiation, laboratory absorption measurement, and atmospheric radiation transfer. As is well known, the expression for the line-absorption coefficient is[1]

$$k(\nu, a) = \frac{k_0 a}{\pi} \int_{-\infty}^{\infty} \frac{\exp(-x^2)}{a^2 + (\omega - x)^2}\, dx \tag{1}$$

$$= \frac{k_0}{\pi^{1/2}} \int_0^{\infty} \exp\left(-ax - \frac{x^2}{4}\right) \cos \omega x\, dx\,, \tag{2}$$

where $k_0 = (S/\Delta\nu_D)(\ln 2/\pi)^{1/2}$; $a = (\boldsymbol{a}/\Delta\nu_D)(\ln 2)^{1/2}$; $\omega = (\nu - \nu_0/\Delta\nu_D)(\ln 2)^{1/2}$; k is the absorption coefficient at the frequency ν; S is the total intensity of the line; $\Delta\nu_D$ is half the Doppler width at half-maximum; and $\boldsymbol{a}$ is half the Lorentz plus natural width at half-maximum.

The line-absorption coefficient given by equation (1) has been tabulated by a number of authors, including Mitchell and Zemansky,[1] Hjerting,[2] and Harris.[3] Here this work is extended to give the general term of the expansion of $k(\nu, a)$ in a Taylor series in powers of a and also in an asymptotic expansion in inverse powers of $\nu - \nu_0$.

In the second section we discuss the measurement of the fractional absorption from a beam of radiation in the laboratory when the Doppler effect makes an appreciable contribution to the line width. These results reduce in certain limiting cases to the well-known results of Ladenburg and Reiche[4] for the fractional absorption of a single line having the Lorentz shape.

The pressures and temperatures of a planetary atmosphere are such that both the Lorentz and the Doppler effects contribute to the line broadening. It was shown by Strong and Plass[5] that an isothermal atmosphere composed of radiating gases which have

---

* This work was supported by the ONR.

[1] Mitchell and Zemansky, *Resonance Radiation and Excited Atoms* (Cambridge: At the University Press, 1934), pp. 101 and 320.

[2] *Ap. J.*, **88**, 508, 1938.

[3] *Ap. J.*, **108**, 112, 1948.

[4] *Ann. d. Phys.*, **42**, 181, 1911.

[5] *Ap. J.*, **112**, 365, 1950.

Lorentz-broadened lines can emit very much more radiation from the lower layers than would be calculated from a model using a gray absorption coefficient. The radiation escaping to space from the lower layers of the atmosphere comes predominantly from the wings of the pressure-broadened lines, for, as the lines in the upper atmospheric layers are considerably narrower, they do not effectively absorb the radiation from the wings of the lines in the lower layers. The model of Strong and Plass assumed an isothermal atmosphere with a radiating gas having a constant fractional concentration. The absorption lines of this gas were assumed to have the Lorentz line shape and not to overlap appreciably at the atmospheric pressures considered. This model has been extended to include cases where the atmosphere is nonisothermal,[6] where the collision-broadened line shape is asymmetrical at frequencies far from the line center,[7, 8, 9] where the lines of the band overlap appreciably,[9, 10, 11, 12] and where the fractional concentration of the radiating gas varies with height.[6, 9, 10]

Although the above-mentioned calculations determine the radiation balance in the atmosphere from ground level to the middle stratosphere, they cannot be applied at higher altitudes without further consideration, since the collision-broadened line shape has been assumed. At higher altitudes the Doppler effect contributes appreciably to the half-width. The radiation balance under these conditions is examined in the last part of this paper.

LINE-ABSORPTION COEFFICIENT

The line-absorption coefficient can be evaluated as a power series in the parameter a if we expand the Reiche form of the integral as given by equation (2) in a Taylor series in a:

$$k(\nu, a) = \frac{k_0}{\pi^{1/2}} \sum_{n=0}^{\infty} \frac{(-1)^n 2^{n+1} a^n}{n!} \int_0^{\infty} x^n \exp(-x^2) \cos 2\omega x \, dx \, . \tag{3}$$

First we evaluate the integrals that occur in equation (3) for even integral values of n. We note that the Hermite polynomial of the nth degree, $H_n(x)$, is defined as

$$H_n(x) = (-1)^n \exp(x^2) \frac{d^n}{dx^n} \exp(-x^2) \, . \tag{4}$$

Let

$$A(\omega) = \int_0^{\infty} \exp(-x^2) \cos 2\omega x \, dx = \tfrac{1}{2}\pi^{1/2} \exp(-\omega^2) \, . \tag{5}$$

Differentiating this equation n times, where n is an even integer, we obtain

$$\begin{aligned} \frac{d^n}{d\omega^n} A(\omega) &= (-1)^{n/2} 2^n \int_0^{\infty} x^n \exp(-x^2) \cos 2\omega x \, dx \\ &= \tfrac{1}{2}\pi^{1/2} \frac{d^n}{d\omega^n} \exp(-\omega^2) \, . \end{aligned} \tag{6}$$

If we combine this expression with the definition of the Hermite polynomial, the nth term in the summation of equation (3) for even n is found to be

---

[6] J. I. King, *J. Meteorol.*, **9**, 311, 1952.

[7] G. N. Plass and D. Warner, *Phys. Rev.*, **86**, 138, 1952.

[8] G. N. Plass and D. Warner, *J. Meteorol.*, **9**, 333, 1952.

[9] G. N. Plass, *J. Opt. Soc.*, **42**, 677, 1952.

[10] G. N. Plass, *J. Meteorol.* (in press).

[11] L. D. Kaplan, *J. Meteorol.*, **9**, 1, 139, 1952.

[12] J. I. King, *Transfer Theory for Purely Pressure-broadened Band Spectra* (A.F.C.R.C. Rept. No. 5 [Salt Lake City: University of Utah, 1952]).

$$k_0 a^n (n!)^{-1} \exp(-\omega^2) H_n(\omega) \cos \tfrac{1}{2} n\pi .$$

The odd terms in the summation can be evaluated in a similar manner in terms of the function $F(\omega)$ defined by the equation[13]

$$F(\omega) = \int_0^\infty \exp(-x^2) \sin 2\omega x \, dx = \exp(-\omega^2) \int_0^\omega \exp(x^2) \, dx . \tag{7}$$

Now the nth derivative where n is an odd integer is

$$F^{(n)}(\omega) = (-1)^{(1/2)(n-1)} 2^n \int_0^\infty x^n \exp(-x^2) \cos 2\omega x \, dx . \tag{8}$$

Thus the nth term in the summation of equation (3) for odd n is found to be

$$-k_0 a^n (n!)^{-1} \frac{2}{\pi^{1/2}} F^{(n)}(\omega) \sin \tfrac{1}{2} n\pi .$$

The line-absorption coefficient can now be written as the sum of Hermite polynomials and derivatives of $F(\omega)$ in the form

$$k(\nu, a) = k_0 \sum_{n=0}^{\infty} \frac{a^n}{n!} [\exp(-\omega^2) H_n(\omega) \cos \tfrac{1}{2} n\pi - 2\pi^{-1/2} F^{(n)}(\omega) \sin \tfrac{1}{2} n\pi] . \tag{9}$$

This result agrees with the first five terms of the expansion as given by Harris.[3] However, the general term of the expansion is given here, and this result is used later.

It is interesting to note that the even terms in equation (9) can be summed exactly. The generating function of the Hermite polynomials is

$$\exp[-(t-\omega)^2] = \exp(-\omega^2) \sum_{n=0}^{\infty} (n!)^{-1} H_n(\omega) t^n . \tag{10}$$

In equation (10) replace t by it and add to this equation (10) with t replaced by $-it$. The resulting sum is the same as the sum over even n in equation (9), so that

$$k(\nu, a) = k_0 \left\{ \exp(a^2 - \omega^2) \cos 2\omega a - \frac{2}{\pi^{1/2}} \sum_{n=1}^{\infty} (n!)^{-1} F^{(n)}(\omega) a^n \sin \tfrac{1}{2} n\pi \right\} . \tag{11}$$

A similar procedure may be performed on the summation over odd n, but it does not lead to elementary functions. Equation (11) approaches the Doppler line shape as a approaches zero, as, of course, it should.

We shall also require the asymptotic expansion of $k(\nu, a)$ in inverse powers of ω. This can be obtained from an integral evaluated by Stokes:[14]

$$\int_0^v \exp(v^2 - t^2) \, dt = \frac{\pi^{1/2}}{2} \exp(v^2) - \frac{1}{2v} - \sum_{m=1}^{M} \frac{(-1)^m (2m-1)!}{2^{2m} (m-1)! \, v^{2m+1}} . \tag{12}$$

The substitution $v = -i\omega$ changes this integral into $-iF(\omega)$. Taking the nth derivative and evaluating the derivatives of the exponential in the same manner as described between equations (10) and (11), we obtain

---

[13] See, e.g., Mitchell and Zemansky, *op. cit.*, p. 321.

[14] E. T. Whittaker and G. N. Watson, *Modern Analysis* (4th ed.; Cambridge: At the University Press, 1940), p. 152.

$$k(\nu, a) = k_0 \Big\{ (\cos 2\omega a + \sin 2\omega a) \exp(a^2 - \omega^2) + \frac{1}{\pi^{1/2}} \sum_{n=1}^{\infty} \sum_{m=0}^{M} \frac{(2m+n)!\, \sin(\frac{1}{2} n\pi)\, a^n}{2^{2m} n!\, m!\, \omega^{2m+n+1}} \Big\} . \tag{13}$$

If $|\nu - \nu_0| \gg a$ and $|\nu - \nu_0| \gg \Delta\nu_D$, then the exponential term can be neglected, so that

$$k(\nu, a) = \frac{Sa}{\pi(\nu - \nu_0)^2} \Big\{ 1 + (\tfrac{3}{2} - a^2)\frac{1}{\omega^2} + (\tfrac{15}{4} - 5a^2 + a^4)\frac{1}{\omega^4} + \dots \Big\} . \tag{14}$$

The first three terms of equation (14) agree with those given by Harris.[3]

LABORATORY ABSORPTION

As an example of the application of these expressions for the line-absorption coefficient, the absorption measured in the laboratory over a finite frequency interval is calculated when the Doppler effect contributes to the width of the line. The assumption will be made that the lines in the band do not overlap to an appreciable extent at the pressures used in the experiment. This is usually the case under the conditions when the Doppler effect makes a contribution to the absorption. If the lines do not overlap appreciably, the total absorption from the lines in a band in a certain frequency interval is merely the sum of the absorptions from each of the individual lines.

For a single line the fractional absorption, A, is defined[15] as

$$A\Delta\nu = \int_{-\infty}^{\infty} [1 - \exp(-kw)]\, d\nu , \tag{15}$$

where $\Delta\nu$ is the frequency interval in which the absorption is measured and w is the optical thickness of the absorbing gas. The limits of integration are extended to infinity for convenience, since the interval $\Delta\nu$ is chosen sufficiently large so that the absorption from this particular line is negligible outside this interval. We consider the evaluation of the fractional absorption in three different cases.

Case I—weak-line approximation.—A line is called a weak line when $kw \ll 1$ at all frequencies, including the line center for a particular optical thickness w. Then, by expansion of equation (15) in powers of kw, we obtain

$$A\Delta\nu = w \int_{-\infty}^{\infty} k(\nu, a)\, d\nu . \tag{16}$$

If $k(\nu, a)$ is replaced by its expression from equation (11), the definite integral from the first term gives

$$A\Delta\nu = Sw . \tag{17}$$

All the terms from the summation in equation (11) vanish after integration, since, for large ω, $F(\omega) \cong (2\omega)^{-1}$ and therefore $F^{(n)}(\omega = \pm\infty) = 0$. If there are N nonoverlapping lines in the interval $\Delta\nu$, then

$$A\Delta\nu = w \sum_{j=1}^{N} S_j . \tag{18}$$

---

[15] See, e.g., W. M. Elsasser, *Heat Transfer by Infrared Radiation in the Atmosphere* (Cambridge: Harvard University Press, 1942).

Thus the fractional absorption varies linearly with w for a weak line, regardless of the value of a, i.e., of the relative contributions of the Doppler effect or natural and collision damping to the half-width. This result states that the total line intensity always determines the absorption from a weak line.

Case II—Doppler width alone.—At sufficiently low pressures, when the half-width due to damping is very small compared to the Doppler half-width, the fractional absorption can be calculated by substituting the first term of equation (9) in equation (15). The result has been given by Struve and Elvey.[16]

Case III—strong-line approximation.—A line is called a strong line when almost all the incident radiation is absorbed at frequencies within the total half-width of the line center for a particular optical thickness w. Obviously, when the optical thickness is increased sufficiently, a weak line becomes a strong line. The fractional absorption for a strong line is obtained from equation (14), since it accurately represents the line-absorption coefficient in the wings of the line. It is inaccurate only at frequencies inside the half-width, where both the approximate and exact expressions give the same virtually complete absorption. The result of the substitution of equation (14) in equation (15) is

$$A\Delta\nu = 2\left(\frac{Saw}{\pi}\right)^{1/2}\int_0^\infty \left\{1-\exp\left[-\frac{1}{x^2}\left(1+\frac{b}{x^2}+\frac{c}{x^4}+\dots\right)\right]\right\}dx\,, \tag{19}$$

where

$$b = \left(\tfrac{3}{2}-a^2\right)\beta\,, \qquad c = \left(\tfrac{15}{4}-5a^2+a^4\right)\beta^2\,, \qquad \beta = \frac{\pi\Delta\nu_D^2}{Saw\ \ln 2}\,.$$

This integral can be evaluated by expanding the $\exp(-b/x^4)$ and $\exp(-c/x^6)$ into a power series. The resulting integrals are all well known. The fractional absorption is thus found to be

$$A\Delta\nu = 2\,(Saw)^{1/2}\left\{1+\tfrac{1}{4}b+\tfrac{3}{8}c-\tfrac{15}{32}b^2-\tfrac{105}{8}bc-\tfrac{945}{128}c^2+\dots\right\}. \tag{20}$$

The fractional absorption for a line that is sufficiently strong so that $b \ll 1$ and $c \ll 1$ is given by the familiar square-root law, $A\Delta\nu = 2(Saw)^{1/2}$, usually derived from the Lorentz line shape.[4, 15] If $a \gg \Delta\nu_D$, the square-root law results when $Sw \gg a$, from the definitions of b, c, and β in equation (19). On the other hand, if $\Delta\nu_D \gg a$, the square-root law still results if $Saw \gg \Delta\nu_D^2$. In other cases the fractional absorption due to both Doppler and Lorentz widths can be calculated from equation (20). It is interesting to note that even when $\Delta\nu_D \gg a$ the main contribution to the absorption for a strong line comes from the wings of the Lorentz line shape and not from the Doppler shape, since the latter falls off exponentially from the line center.

ATMOSPHERIC RADIATION TRANSFER

In the calculation of radiation transfer in the atmosphere, the information usually desired is the amount of radiation transferred over a frequency interval large compared to the half-width of a particular line, rather than the amount transferred at a single particular frequency. It is well known[5, 6, 8, 9, 10, 11] that the transfer of radiation between any two atmospheric layers, between the ground and an atmospheric layer, and between an atmospheric layer and space can be calculated if the transmission function, $\tau(u_0, u_1)$, is known, where

$$\tau\,(u_0, u_1) = \exp\left\{-\sec\theta\int_{u_0}^{u_1} k\,(\nu, u, a)\,du\right\}, \tag{21}$$

θ being the angle included between the beam and the vertical. The optical thickness in the atmosphere, u, is defined as

---

[16] O. Struve and C. T. Elvey, *Ap. J.*, **79**, 409, 1934. The result for strong lines is their equation (6) and for weak lines is equation (5). In the latter equation the first factor 2 is incorrect and should be omitted.

$$u = \int_z^\infty c\,\rho\,d\,z = \int_z^\infty \rho_r\,d\,z\,, \tag{22}$$

where z is the vertical distance and the fractional concentration, c, is the ratio of the density of the radiating gas, ρ_r, to the total density, ρ. It should be noted that the optical thickness defined here decreases with height and is zero at the top of the atmosphere.

Consider the solution of Schwarzschild's equation for the intensity, I, of a beam directed upward at an angle θ to the vertical, at the height where the optical thickness has the value u_0

$$I\,(u_0) = I_0\,(u_1)\;\tau\,(u_0,\,u_1) + \sec\,\theta \int_{u_0}^{u_1} k\,(\nu,\,u,\,a)\;I_b\,(u)\;\tau\,(u_0,\,u)\;du\,, \tag{23}$$

where $I_0(u_1)$ is the incident intensity at the level u_1 and I_b is the black-body intensity, which is a function of u if the temperature varies with height. From equation (23) and a similar equation for radiation directed downward, expressions can be derived for the solution of any problem involving radiation exchange. Since all these expressions can be written in terms of the transmission function, $\tau(u_0,\,u_1)$, a knowledge of this function enables one to calculate the answer to any atmospheric radiation-transfer problem.

Here we calculate the contribution of the Doppler effect to the atmospheric radiation exchange. The Doppler width makes an appreciable contribution to the total line width for the absorbing bands in the atmosphere only at heights greater than 20 km. The overlapping of the lines in the band can be neglected for almost all lines at heights greater than 20 km because of the very low pressures. Therefore, we calculate the transmission function only for a single line. The contribution from the entire band is the sum of the contributions from each line when the lines do not overlap appreciably. In order to simplify the following calculations, we also assume that the atmosphere is isothermal. Since the Doppler width varies as the square root of the temperature, the width is only about 30 per cent greater at the temperature maximum near 60 km than it is at the temperature minimum in the stratosphere. The results below show that the atmospheric transmission in many cases would be very insensitive to a change of the Doppler width of this order of magnitude.

The integrated absorption for a line, Λ, defined by

$$\Lambda\,(u_0,\,u_1) = \int_{-\infty}^{\infty} [1 - \tau\,(u_0,\,u_1)]\;d\nu\,, \tag{24}$$

will be calculated for each of three cases. As discussed above, the radiation exchange over a frequency range large compared to the half-width can be calculated, once the integrated absorption, Λ, is known. As an example of the usefulness of Λ, the radiation loss to space, dR, into a solid angle $d\Omega$ at an angle θ to the vertical from an atmospheric layer between u_0 and u_1 is calculated under the assumptions of constant temperature with height and negligible overlapping of the absorption lines. Under these conditions, it has been shown that[6, 9]

$$dR = I_b \cos\,\theta\,[\Lambda\,(0,\,u_1) - \Lambda\,(0,\,u_0)]\;d\Omega\,. \tag{25}$$

According to kinetic theory, the Lorentz half-width is proportional to the total pressure, provided that the partial pressure of the absorbing gas is small compared to the total pressure. This condition is satisfied for all the absorbing gases in the earth's atmosphere. Therefore, the half-width,

$$a = \left(\frac{a_s}{p_s}\right) p\,, \tag{26}$$

where α_s is the half-width at the standard pressure p_s. A slightly more complicated equation applies if the absorbing gas is a major constituent of the atmosphere. The natural breadth is negligible for planetary atmospheres.

The dimensionless constant, γ, introduced by Strong and Plass[17] is defined by

$$\gamma = \frac{S c p_s}{2\pi \alpha_s g}. \tag{27}$$

When the Doppler width is negligible, the strong or weak-line approximation applies when γ is much greater or less than unity, respectively.[5]

Case I—weak-line approximation.—It will be assumed that the argument of the exponential in equation (21) is less than 1, even at the line center. In this case the exponential may be expanded, the order of integration reversed, and k replaced by the expression from equation (11). Then by an integration similar to that described in the section on laboratory absorption (case I), the result is obtained that

$$\Lambda(u_0, u_1) = S(u_1 - u_0) \sec \theta. \tag{28}$$

This result is valid even if the temperature varies with height (provided that S does not change appreciably over this temperature range) and even if the fractional concentration of the absorbing gas, c, varies with height.

If equation (28) is substituted in equation (25) and the result integrated over the hemisphere, the radiation loss to space from the layer between u_0 and u_1 for an isothermal atmosphere with constant c is found to be

$$R = 2 f_b S(u_1 - u_0) = 4\pi f_b \gamma (\alpha_1 - \alpha_0), \tag{29}$$

where f_b is the black-body flux, $f_b = \pi I_b$. Thus the radiation loss is the same as though there were only Lorentz and no Doppler broadening.

Case II—Doppler width alone.—The result of the substitution of the first term of equation (9) in equation (24) is

$$\Lambda(u_0, u_1) = 2\Delta\nu_D (\ln 2)^{-1/2} \int_0^\infty \{1 - \exp[-k_0(u_0 - u_1)\sec\theta \exp(-\omega^2)]\} d\omega. \tag{30}$$

This integral is similar in form to the one considered by Struve and Elvey.[16] By the use of this result, we find, for weak lines,

$$\Lambda(u_0, u_1) = S(u_0 - u_1)\sec\theta \sum_{n=0}^{\infty} \frac{(-1)^n [k_0(u_0 - u_1)\sec\theta]^n}{(n+1)!(n+1)^{1/2}} \tag{31}$$

and, for strong lines,

$$\Lambda(u_0, u_1) = \frac{2\Delta\nu_D}{(\ln 2)^{1/2}} \{\ln[k_0(u_0 - u_1)\sec\theta]\}^{1/2} \times \left\{1 + \frac{C}{2\ln[k_0(u_0 - u_1)\sec\theta} - \ldots\right\}, \tag{32}$$

where C is Euler's constant. The radiation loss to space into the solid angle $d\Omega$ can be obtained immediately from equation (25). The total radiation loss to space can be obtained by integrating equation (32) over the hemisphere. The radiation exchange between the highest layers of a planetary atmosphere can be calculated from these expressions for the integrated absorption.

Case III—strong-line approximation.—The majority of radiation is transferred by the strong lines of the radiating gases in the atmosphere.[5, 6] In order to calculate the influence of the Doppler effect on this radiation transfer when the change of the Lorentz half-width is taken into account, we substitute equation (14) in equation (21). With the help of equations (26) and (27) and after an elementary integration, the result is obtained that

---

[17] The constant, γ, defined here differs by a factor $\cos\theta$ from the constant used by Strong and Plass, *op. cit.*

$$\tau\,(u_0,\,u_1) = \exp\left\{-\frac{1}{x^2}\left[1+\frac{f\cos\theta}{x^2}+\frac{g\cos^2\theta}{x^4}+\ldots\right]\right\}, \tag{33}$$

where

$$x^2 = \frac{(\nu-\nu_0)^2}{\gamma\sec\theta\,(\alpha_1^2-\alpha_0^2)^2},$$

$$f = \frac{1}{\gamma\,(\alpha_1^2-\alpha_0^2)}\left[\frac{3\Delta\nu_D^2}{2\ln 2}-\frac{\alpha_1^2+\alpha_0^2}{2}\right],$$

$$g = \frac{1}{\gamma^2\,(\alpha_1^2-\alpha_0^2)^2}\left[\frac{15\Delta\nu_D^4}{4\,(\ln 2)^2}-\frac{5\,(\alpha_1^2+\alpha_0^2)\,\Delta\nu_D^2}{2\ln 2}+\frac{\alpha_1^4+\alpha_1^2\alpha_0^2+\alpha_0^4}{3}\right],$$

α_0 and α_1 being the Lorentz half-widths at the heights where the optical thicknesses are u_0 and u_1, respectively.

In this case the integrated absorption, Λ, from equation (24) is

$$\Lambda\,(u_0,\,u_1) = 2\gamma^{1/2}\,(\alpha_1^2-\alpha_0^2)^{1/2}\sec^{1/2}\theta\int_0^\infty[1-\tau\,(u_0,\,u_1)]\,dx\,. \tag{34}$$

Substituting for τ from equation (33), the resulting integral has the identical form of equation (19). From the previous evaluation of this integral as given by equation (20), the result in the present case can be immediately written as

$$\begin{aligned}\Lambda\,(u_0,\,u_1) = 2\pi^{1/2}\gamma^{1/2}\,(\alpha_1^2-\alpha_0^2)^{1/2}\sec^{1/2}\theta\,[1&+\tfrac{1}{4}f\cos\theta+\tfrac{3}{8}g\cos^2\theta\\ &-\tfrac{15}{32}f^2\cos^2\theta-\tfrac{105}{8}fg\cos^3\theta-\tfrac{945}{128}g^2\cos^4\theta+\ldots]\,.\end{aligned} \tag{35}$$

The radiation loss from an atmospheric layer to space in the solid angle $d\Omega$ is obtained by the substitution of this expression in equation (25). The total radiation loss from the top of the atmosphere down to the level $u = u_1$, obtained by integrating this expression over the hemisphere, is

$$R = \tfrac{8}{3}f_b\pi^{1/2}\gamma^{1/2}\alpha_1\,[1+\tfrac{3}{20}f_0+\tfrac{9}{56}g_0-\tfrac{45}{224}f_0^2-\tfrac{35}{8}f_0g_0-\tfrac{2835}{1408}g_0^2+\ldots]\,, \tag{36}$$

where f_0 and g_0 are the values of f and g when $\alpha_0 = 0$. Similarly, the radiation exchange between any two layers can be calculated from equation (35).

The terms outside the brackets in equations (35) and (36) are identical with the expressions for the radiation loss from a strong Lorentz-broadened line as derived by Strong and Plass.[5] This term is obtained for the Lorentz line shape if the line absorption at large distances from the line center is assumed to vary as $(\nu-\nu_0)^{-2}$. The terms inside the brackets of equations (35) and (36) represent the change in the radiation loss due to the fact that the actual line shape does not vary as $(\nu-\nu_0)^{-2}$ as the line center is approached. Again these terms agree with the result of Strong and Plass[5] when the Doppler width is zero.

The additional terms in equations (35) and (36) show clearly when the radiation loss is different from the loss calculated by the use of the Lorentz line shape alone. The radiation loss is clearly unchanged from the Lorentz result when $f_0 \ll 1$ and $g_0 \ll 1$. For these inequalities to be satisfied, it follows from the definitions of these quantities that it is sufficient that $(\Delta\nu_D^2/a_1^2) \ll \gamma$ and $\gamma \gg 1$. The major part of the atmospheric radiation is transferred by the very strong lines in the atmospheric bands. There are many lines in our atmosphere with $\gamma > 100$. For these most important lines, the Doppler width can become somewhat larger than the Lorentz width and still satisfy the above inequality. Therefore, we conclude that, *for the very strong atmospheric lines ($\gamma > 100$), the radiative transfer is the same as would be calculated from the Lorentz shape alone for heights up to 50 km.* The physical reason for this fact is that only the radiation transfer in the far wings is important for a very strong line. However, in the far wings the line shape is accurately represented by the Lorentz equation, even when the Doppler width is larger than the Lorentz width, since the Doppler line shape falls off exponentially. The results of case I show that, for a weak line, *the integrated absorption and radiation loss are the same, regardless of the relative contributions of the Lorentz and Doppler widths to the total width.* The physical reason for this result is that the total emission of a weak line determines the radiation loss, since the absorption by higher layers is very small.

The above results make possible an enormous simplification in the radiation calculations near the temperature maximum in the stratosphere (60 km). For a very strong line, the radiation is not influenced to any appreciable extent by the Doppler width. Thus the change in the Doppler width with temperature need not be taken into account. Similarly for the weak lines, the relative contributions of the Doppler and Lorentz widths to the total width need not concern us. It is only for the lines of intermediate strength at altitudes less than 50 km that the Doppler effect alters the radiative transfer calculated from the Lorentz shape alone.

In calculating the radiation transfer from an atmospheric band, the band is usually divided into several frequency intervals, each sufficiently large that it contains a number of individual lines. For the intervals at or near the center of the band, either the lines are all very strong lines, or the very strong lines completely dominate the weak lines in the radiation transferred. For such intervals the conclusions drawn above for very strong lines are valid. For the intervals near the edge of the band, all the lines usually satisfy the weak-line criterion. It is only intervals between the edge and center of the band that usually contain lines of intermediate strength and for which more elaborate calculations are necessary. However, since the frequency intervals may be chosen as large as desired, provided that the black-body intensity is approximately constant in the interval, it is usually possible to choose the intervals so that the majority of the lines in a given interval satisfy either the strong- or the weak-line criterion. When it is possible to divide the band into frequency intervals in this manner, the contribution of the Doppler effect to radiative transfer can be neglected for heights up to at least 50 km.

NOTES

RADIAL VELOCITIES OF FIVE SOUTHERN PROPER-MOTION STARS

Five dwarf objects in need of radial-velocity determination, included in Kuiper's list[1] of the "nearest stars," were observed by the writer at the suggestion of Dr. W. J. Luyten.[2] The spectrographic material was obtained through 1947, 1948, 1949, and 1952

TABLE 1

STELLAR WAVE LENGTHS

Fe I	3878.37	*Sr* II	4215.52
Ca II	3933.66	*Ca* I	4226.73
Al I	3961.52	*Cr* I	4254.35
Ca II	3968.47	*Fe* I	4260.48
Fe I	4005.25	*Fe* I	4325.76
Fe I, *Ti* I, *Mn* I	4030.64	*H*	4340.47
Fe I	4045.82	*Fe* I	4383.55
Fe I	4063.60	*Fe* I	4404.75
Fe I	4071.74	*Fe* I	4415.12
Fe I	4132.06	*Mg* II	4481.23*

* This line was measured only once.

TABLE 2

RADIAL VELOCITIES AND SPECTRA

CD	HD	Kuiper's Number	α_{1950}	δ_{1950}	m_v	Sp.	Velocity Absorption (Km/Sec)	P.E.	No. of Plates	Velocity Emission (Km/Sec)	P.E.	No. of Plates	Notes
−48°1011	22496	36	$3^h 33^m 4$	−48° 36′	9.3	K5e	+22	±1.1	9	+24	±2.7	6	1
−58°5564	125072	144	14 15.6	−59 8	6.7	K3	−14	±0.6	5	...	...	...	2
−45°13677	191849	212	20 10.3	−45 19	8.4	M0e	−32	±1.3	11	−41	±2.0	9	3
−49°13515	204961	229	21 30.2	−49 12	8.9	M3	+18	±1.1	3	...	...	...	4
−73°1672	222237	249	23 36.7	−72 59	7.36	K3	+64	±1.3	15	...	...	...	2

NOTES TO TABLE 2

1. The spectral type K5 is from the *Henry Draper Catalogue*. The Yerkes criteria indicate perhaps a somewhat later type. Our material shows the presence of central emission of *Ca* II, H and K.

2. The spectral type in the *Henry Draper Catalogue* is K0.

3. The spectral type M0 is Kuiper's. Our material shows the presence of central emission of *Ca* II, H and K.

4. The spectral type M3 is Kuiper's.

---

[1] *Ap. J.*, **95**, 201, 1942; *McDonald Contr.*, No. 44.

[2] Private communication of October 22, 1946.

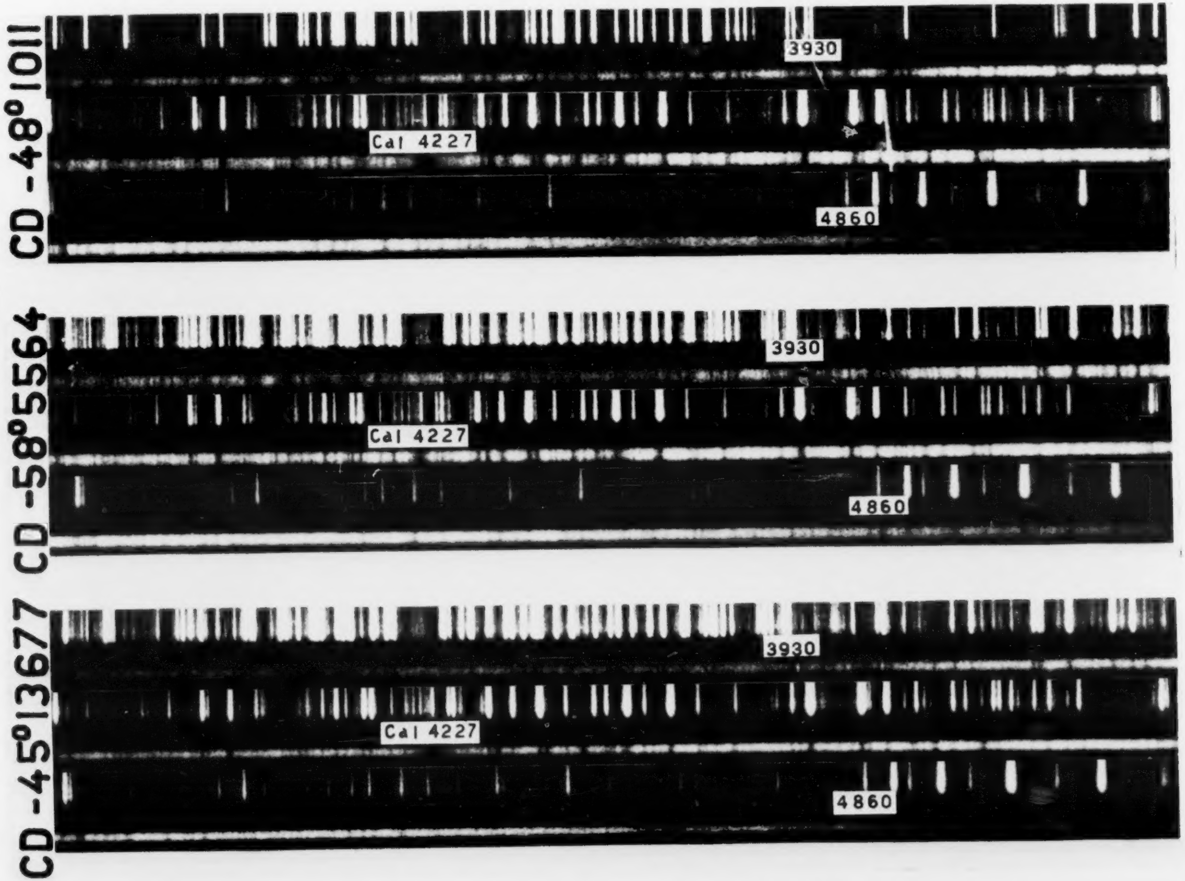
CD -48°1011
3930
Ca I 4227
4860
CD -58°5564
3930
Ca I 4227
4860
CD -45°13677
3930
Ca I 4227
4860

FIG. 1.—Positive enlargements of the spectra of southern proper-motion stars. The first strip of CD −48°1011 is an enlargement of a different plate

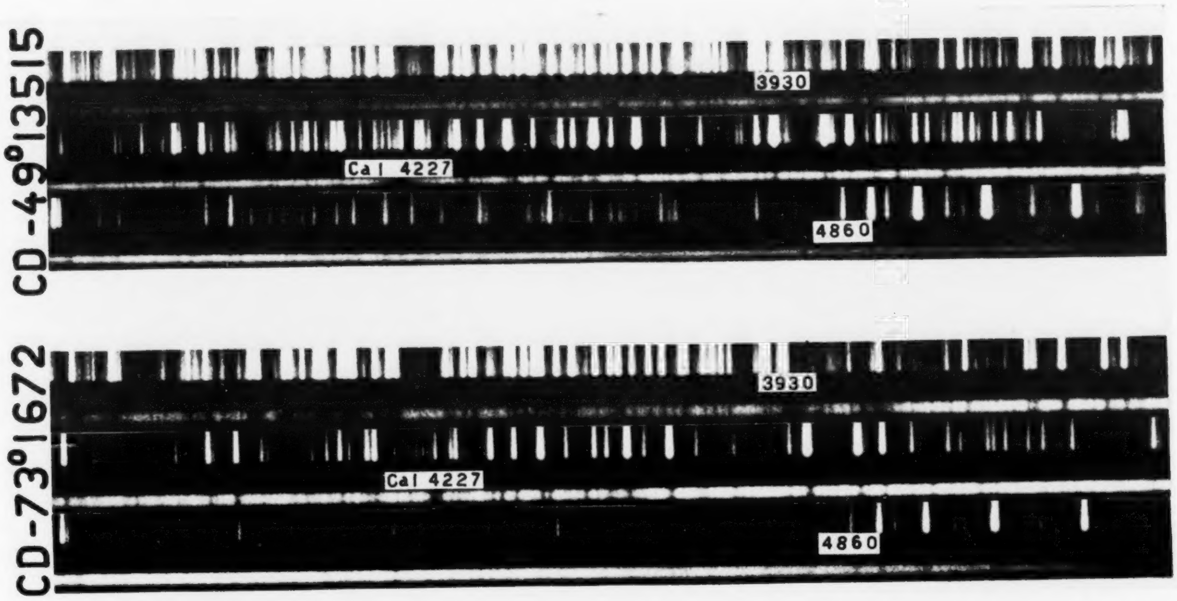
CD-49°13515
3930
Ca I 4227
4860
CD-73°1672
3930
Ca I 4227
4860

FIG. 2.—Positive enlargements of the spectra of southern proper-motion stars. The first strip of CD−48°1011 is an enlargement of a different plate

with the Bosque Alegre reflector and the Wood-grating spectrograph, which gives a dispersion of about 42 A/mm. Positive enlargements of the spectra of these stars are shown in Figures 1 and 2.

Table 1 lists the stellar wave lengths used in our work, and the results are presented in Table 2. The magnitudes are those given in Kuiper's paper.

I am indebted to Mr. Julio Albarracín for the reduction of the plates measurements.

JORGE SAHADE

OBSERVATORIO ASTRONÓMICO
CÓRDOBA, ARGENTINA
July 10, 1952

OBSERVATIONS OF HELIUM IN DIFFUSE NEBULAE

In the last fifteen years spectrographic observations of some galactic emission regions and nebulae[1,2,3,4] apparently detected helium only near the center of the Orion nebula, which is of the order of 1000 times brighter than the centers of ordinary nebulae.[5] The writer has recently found helium in several nebulae during a series of observations of emission regions and nebulae now in progress. The program is a systematic extension of the observations made with the nebular spectrograph[1,2] and B spectrograph[4] at the Yerkes and McDonald Observatories. Spectrophotometry of selected emission lines in a wide variety of emission regions is planned.

For the present work the B spectrograph is attached to the mounting of the 6-inch UV telescope on the roof of the Yerkes Observatory. Spectra are taken on Eastman 103*a*-F film using the spectrograph equipped with an object glass having a focal length of 41 mm and an aperture of 28 mm. Different parts of the aperture are used at different points along the slit to fill the $f/4$ collimator. The grating is set to center λ 5577 on the film, and emissions in the range $\lambda\lambda$ 3727–6870 may appear in a single exposure. The dispersion varies from about 335 A/mm at $H\alpha$ to about 400 A/mm at $H\gamma$. The slit is 0.10 mm wide and projects 0.016 mm wide on the emulsion, subtending an angle of $8'$ on the sky. About 10° along the length of the slit, which runs east-west, is not seriously vignetted. The accuracy of the setting in declination and of guiding the exposure of several hours is about $\pm 2'$ arc.

Star spectra are not well focused by the object glass in all wave lengths, and an attempt is made to exclude brighter stars from the slit. Their spectra may interfere with identifying *He* I 5876 or *He* I 6678 on the spectrograms. Such spectra may photographically enhance the *R* branch of the (8, 2) band of *OH* observed in the airglow by Cabannes, Dufay, and Dufay[6] at λ 5870, or the *Ne* I 6678 line arising from atmospheric scattering of terrestrial neon emission. Wave-length measures, which can be made to about ± 1A on a single line, separate *He* I 5876 from the *OH* near it, but they cannot separate *He* I 6678 and *Ne* I 6678. In the latter case the appearance of the line relative to other emissions and photographic enhancements of star spectra must be relied upon. No *Henry Draper Catalogue* stars with emission lines occur in the spectrograms used to identify interstellar helium.

Figure 1 is a $37\times$ enlargement of parts of Yerkes spectrograms B41, B48, and B69

---

[1] J. L. Greenstein and L. G. Henyey, *Ap. J.*, **86**, 620, 1937; **87**, 79, 1938; **89**, 653, 1939.

[2] O. Struve and C. T. Elvey, *Ap. J.*, **88**, 364, 1938; **89**, 119, 517, 1939; **90**, 301, 1939.

[3] A. B. Wyse, *Ap. J.*, **95**, 356, 1942.

[4] T. L. Page, *Ap. J.*, **108**, 157, 1948.

[5] B. Strömgren, *Problems of Cosmical Aerodynamics* (Dayton, Ohio: Central Air Documents Office, 1951), p. 7.

[6] *C.R.*, **230**, 1233, 1950.

of NGC 2237, NGC 1976 (the Orion Nebula for comparison) and NGC 6523, respectively. Some lines and bands originating in the nebulae, the airglow, and artificial terrestrial emissions are identified there. A faint line or band near λλ 6630–6635 may not reproduce in Figure 1 but appears on three spectrograms in Monoceros, including B41. It has not been identified. Table 1 gives further data on these spectrograms, including an estimate of the angular extent of the emissions in the nebulae.

TABLE 1

SPECTRA OF EMISSION NEBULAE WITH HELIUM

NGC No.	CENTER OF SLIT (1950)		EXPOSURE TIME	U.T. 1952	FILM B	ANGULAR EXTENT ON SLIT				
	α	δ				*H*α	[*N* II] 6584	[*S* II] 6717	*He* I 5876	*He* I 6678
2237...	6^h32^m	+ 5°00′	3^h22^m	Jan. 21	41	5°1	3°4	3°5	0°4	0°9
1976...	5 33	− 5 26	1 11	Jan. 31	48	2.8	0.8	0.6	0.4*	0.4*
6523...	17 56	−24 29	4 00	July 24	69	2.4†	2.4	0.6	0.4	......‡

* Approximately the width of the star spectrum.

† Larger section alone.

‡ Apparently not present.

The apparent change of the relative strengths of *He* I 6678 and *He* I 5876 in NGC 2237 and NGC 6523 must not be given much weight on the basis of these spectrograms alone. There is danger that HD 47240 spuriously enhances *Ne* I 6678 on exposure B41. In addition, the color excesses[7] of the stars apparently exciting NGC 2237 are slightly greater than those of the stars apparently in NGC 6523, and the atmospheric absorption affecting exposure B41 probably differs from that affecting exposure B69. The two helium lines have been suspected on other spectrograms in the series, but exposure B69 is the best new evidence to date. The determination of the *He*:*H* ratio in these nebulae must await future photometric work previously mentioned.

The writer wishes to thank Dr. B. Strömgren and Dr. A. B. Meinel for advice in the preparation of this note.

HUGH M. JOHNSON

YERKES OBSERVATORY
October 25, 1952

VIBRATION SPECTRUM OF $N^{14}N^{15}$

Some time ago Herzberg[1] drew attention to the possibility that the vibration spectrum of $N^{14}N^{15}$ may provide a means of detecting nitrogen in planetary or stellar atmospheres. Proper quantitative discussion was, however, prevented by lack of knowledge of the transition probabilities. The present note reports calculations on the fundamental band, λ 42894, which is the most intense member of the main progression.

---

[7] J. Stebbins, C. M. Huffer, and A. E. Whitford, *Ap. J.*, **91**, 20, 1940.

[1] *Ap. J.*, **57**, 428, 1938.

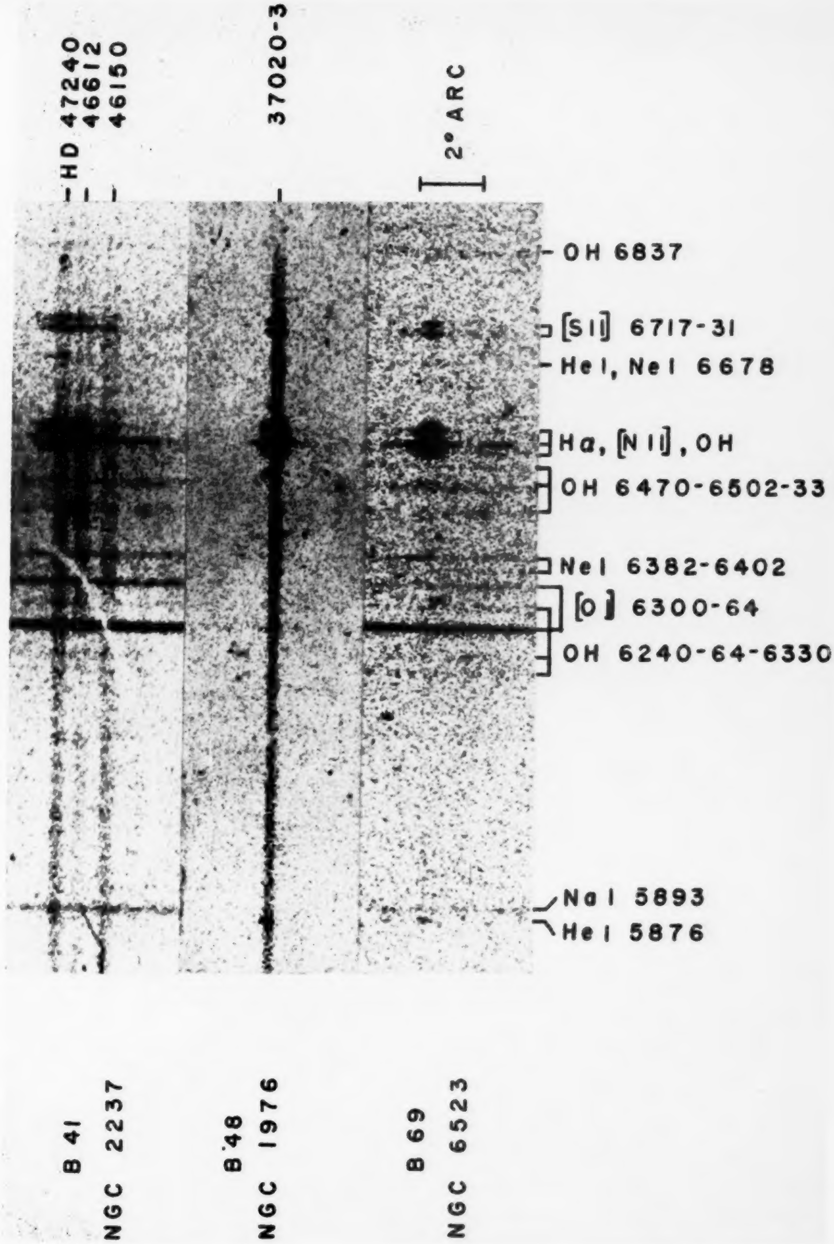
HD 47240
46612
46150
37020-3
2° ARC
OH 6837
[S II] 6717-31
He I, Ne I 6678
Hα, [N II], OH
OH 6470-6502-33
Ne I 6382-6402
[O I] 6300-64
OH 6240-64-6330
Na I 5893
He I 5876
B 41
NGC 2237
B 48
NGC 1976
B 69
NGC 6523

FIG. 1.—Spectra of three galactic emission nebulae showing helium

The Hamiltonian H_{het} of a heteronuclear molecule is given, to a high approximation, by

$$H_{\text{het}} = H_{\text{hom}} + \frac{h^2(\lambda_1 - \lambda_2)}{8\pi^2 M(\lambda_1 + \lambda_2)} \frac{\partial}{\partial R} \sum_i \frac{\partial}{\partial z_i}, \tag{1}$$

where H_{hom} is the Hamiltonian of the corresponding homonuclear molecule of the same total mass; h is Planck's constant; λ_1 and λ_2 are the ratios of the masses of the nuclei to the mass M of the proton; R is the internuclear separation; and z_i is the co-ordinate of the ith electron along the molecular axis. A simple expression for the dipole moment connecting the neighboring vibrational levels, v and $v+1$, may readily be obtained[2] by following the procedure described by Wick,[3] which involves treating the second term of H_{het} as a perturbation and neglecting the anharmonicity. From this expression it follows at once that the oscillator strength of the transition is given by

$$f(v,\ v+1) = \frac{4\pi^4 m^3 c^4}{3M e^4} \left\{ \frac{(v+1)(\lambda_1 - \lambda_2)^2}{\lambda_1 \lambda_2 (\lambda_1 + \lambda_2)} \right\} \alpha_P^2 \sigma^4, \tag{2}$$

where m and e are the electronic mass and charge; c is the velocity of light; α_P is the polarizability in the direction of the line joining the nuclei; and σ is the wave number of the radiation. Substitution of the values of the basic physical constants yields

$$f(v,\ v+1) = 8.9_0 \times 10^{23} \left\{ \frac{(v+1)(\lambda_1 - \lambda_2)^2}{\lambda_1 \lambda_2 (\lambda_1 + \lambda_2)} \right\} \alpha_P^2 \sigma^4, \tag{3}$$

α_P and σ being expressed in cm^3 and cm^{-1}, respectively.

In the case of $N^{14}N^{15}$, α_P is $2.3_8 \times 10^{-24}$ cm^3 and σ is 2331 cm^{-1} for the fundamental band.[4] Hence from equation (3) we obtain the oscillator strength,

$$f(0,\ 1) = 2.4 \times 10^{-14}. \tag{4}$$

It may be remarked that the oscillator strength of the fundamental band of H^1H^2 is almost 1,000 times greater.[3]

For a line on the linear part of the curve of growth, W, the equivalent width, and N, the number of absorbing molecules per unit area in the line of sight, are related by the well-known formula,

$$\frac{W}{N} = \frac{\pi e^2}{m c^2 \sigma^2} f. \tag{5}$$

It is convenient to replace N by L, the length of the equivalent path through *ordinary* nitrogen (in which the fraction of $N^{14}N^{15}$ may be taken as 3.8×10^{-3}). Using equation (4), we find that, for λ 42894, L is $(250W)$ atm-km, W being measured in angstroms and all the molecules being supposed in the lowest rotational level.[5]

D. R. Bates

Department of Applied Mathematics
Queen's University
Belfast, North Ireland

---

[2] D. R. Bates and G. Poots, *Proc. Phys. Soc. London* (in press).

[3] *Accad. Lincei Atti*, **21**, 708, 1935.

[4] Cf. *Landolt-Börnstein Zahlenwerte und Funktionen* (Berlin: Springer Verlag, 1952).

[5] If some of the molecules are in excited rotational levels, the expression for L is, of course, the same with W interpreted as the sum of the equivalent widths of the individual lines.

A NEW PHOTOGRAPH OF THE *Mg* II DOUBLET AT 2800 A IN THE SUN

A photograph showing the *Mg* II doublet, $3s^2S-3p^2P^\circ$, in emission and absorption in the solar spectrum was obtained on September 3, 1952, from an Aerobee rocket flown from the White Sands Proving Grounds, New Mexico. Considerably more detail was recorded than in spectra published previously.[1] In this flight the attempt was made to obtain especially intense exposures and also high resolution. A sun-following device was used to keep the spectrograph directed toward the sun in azimuth, and this succeeded in producing exposures several times more intense than the best obtained in earlier experiments.

The spectrograph was similar to that described by Johnson, Purcell, Tousey, and Watanabe[2] and employed a 40-cm grating radius, 15,000-line per inch, Bausch and Lomb grating blazed for the extreme ultraviolet. In order to obtain high resolution, the grating was used in the second order, and Eastman Kodak type IV-O film was employed.

The portion of the spectrum covering the *Mg* II doublet is shown in Figure 1 and was made between 77 and 85 km altitude above sea-level. Because of the intense exposure, a considerable amount of detail within the absorption lines was recorded. In Figure 1, *A* and *B* are the *Mg* II emission lines, 2795.523 A and 2802.698 A, respectively, and are the reversed cores of broad absorption lines; with the present resolution the density of the short-wave-length line is about the same as that of the spectrum outside the absorption lines. The contour of the absorption lines is given, approximately, by the shape of the upper edge of the spectrum. The wings clearly extend to the edges of the portion of the spectrum shown. The separation between the absorption lines and the width of each line were such that there was a broad region of less absorption between *C* and *D*. The short-wave-length member of the pair is the stronger in both emission and absorption, as expected from theory.

The *Mg* II absorption lines, $3p^2P^\circ-3d^2D$, 2797.989 A and 2790.768 A, each of intensity 40 as listed by Moore,[3] appear to be present, although both are blended with other lines. The longer of the pair lies at the absorption line marked *C* in Figure 1; this is blended with a line of the *Mn* I triplet, $a^6S-y^6P^\circ$, at 2798.270 A, intensity 8*R*, and possibly with a line of *Fe* II, intensity 5, at 2797.914 A, and one of *Fe* I, intensity 15, at 2797.775 A. The best value of observed wave length is 2798.0 A, agreeing most closely with the *Mg* II line. The other of this *Mg* II pair is not labeled in Figure 1 but can easily be seen as the first line on the short-wave-length side of *A* and lies at 2790.8 A. The line marked *D* lies at 2801.1 A and is in good agreement with another line of the same triplet of *Mn* I at 2801.084 A, intensity 6. Again, there is a possibility of blending with *Cr* II, 2800.77 A, intensity 85, and *Ti* II 2800.65 A, intensity 30. The third line of the *Mn* I triplet, 2794.817 A, was not detected, since it was too close to the very strong line of *Mg* II.

The width of the *Mg* II emission lines is 0.7–0.8 A and is instrumental in origin. Although the slit width corresponded to 0.3 A, in this grating arrangement only about 8,000 lines of the grating were illuminated at one time by the patch of sunlight streaming through the slit and diffracted by it. The resolution produced by the grating under these conditions, assuming an efficiency of 50 per cent of theoretical, would be 0.4 A. Therefore, the total line width expected for an intense exposure, as in the case of the *Mg* II

---

[1] E. Durand, J. J. Oberly, and R. Tousey, *Ap. J.*, **109**, 1–16, 1949; J. J. Hopfield and H. E. Clearman, Jr., *Phys. Rev.*, **73**, 877–884, 1948.

[2] F. S. Johnson, J. D. Purcell, R. Tousey, and K. Watanabe, *Jour. Geophys. Res.*, **57**, 157–176, 1952.

[3] Charlotte E. Moore, *An Ultraviolet Multiplet Table* (National Bureau of Standards, Circular 488 [Washington, D.C.]), Sec. I (1950); Sec. II (1952).

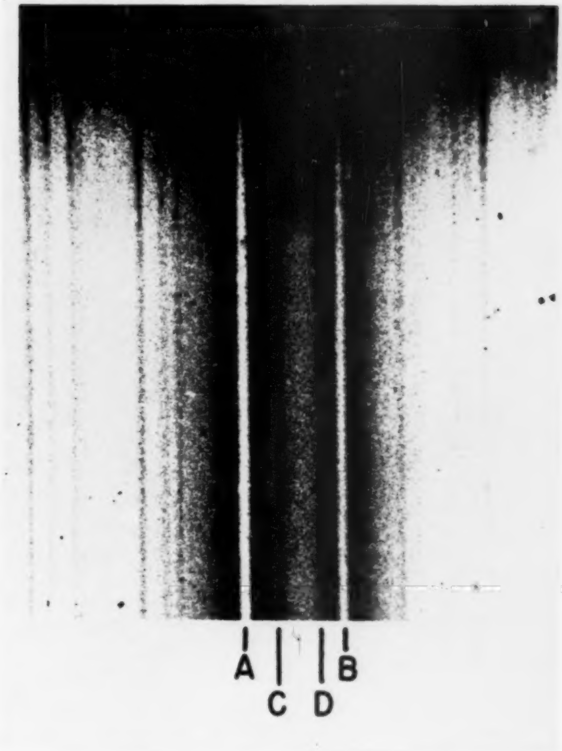

FIG. 1.—The solar spectrum near 2800 Å photographed from a rocket at an altitude of about 80 km on September 3, 1952. *A* and *B* are the *Mg* II lines at 2795.523 Å and 2802.698 Å, and are present as intense emission cores at the centers of broad absorption lines.

emission lines in Figure 1, was 1 A, or a little less. The lines tapered at the top edge of the spectrum because of the reduced exposures associated with the astigmatic nature of the spectrum.

F. S. JOHNSON
J. D. PURCELL
R. TOUSEY
N. WILSON

UNITED STATES NAVAL RESEARCH LABORATORY
WASHINGTON, D.C.

REVIEWS

Prism and Lens Making. By F. TWYMAN. 2d ed. London: Hilger & Watts, Ltd., 1952. Pp. 629.

Those who are acquainted with the first edition of this book by Twyman will scarcely recognize this new edition. It would be more appropriate to term this edition a completely new and different book. The first is a thin book of 178 pages dealing with topics of a rather limited interest, while the new edition is a sizable volume of 629 pages covering 16 topics of wider interest. The chapter on dioptric substances, as an example, has been greatly extended and includes a discussion of the new rare-earth glasses and synthetic optical crystals. Particularly noteworthy are the chapters dealing with the nature of the polishing process—molecular flow versus micro-grinding theories, nonspherical surfaces, and surface treatments.

This book is masterfully compiled and illustrated, and the information extremely up to date. This reference book will make a most valuable and useful addition to the libraries of all who have any interest in the field of optics.

A. B. MEINEL

Yerkes Observatory

Radio Astronomy. By BERNARD LOVELL and J. A. CLEGG. London: Chapman & Hall, Ltd., 1952. Pp. 238. $4.00.

In the years since the war particularly, the application of radio techniques to astronomical problems has opened a vital new field of research. Because of the fundamental differences between the observing techniques in the optical and the radio regions, many astronomers lack an appreciation of the problems involved in the use of radio waves, while, presumably, many physicists interested in radio technique lack an understanding of the astronomical problems which can be successfully attacked by the new methods. This book should help both groups to appreciate this important border-line field.

The book is written on an elementary level. An advanced amateur interested in either astronomy or radio should have no great difficulty reading the book, but the pace is rapid enough to hold the attention of a professional astronomer. The book opens with four chapters on the elementary astronomy and radio techniques needed for an understanding of the remainder of the book. Each of these chapters is self-contained and may be omitted by a reader familiar with the material covered. Nearly half of the remainder of the book is devoted to meteors. After a brief introduction to the results obtained from observations in the optical region, there follows a detailed account of the application of radar techniques to the problem of determining meteor orbits and a shorter discussion of the physical properties of meteors and meteor trails. The next four chapters survey the results of radio observations of the sun and briefly indicate some of the theoretical problems involved and some suggested solutions. Next is presented a similar survey of galactic radio emission, including a somewhat more detailed discussion of the "twinkling" of radio stars. An interesting account of radio observations of aurorae both by reflected and by emitted radiation follows. The final two chapters discuss the radio observations of the moon and the possible extension of similar observations to the nearer planets and asteroids. An explanation is given of the ways in which the necessary technique differs from that of either meteor observations or observations of stellar and galactic sources and of what might be gained from such observations.

In the effort to write a popular account, the authors make a few astronomical statements which are sufficiently vague to be misleading, but these are minor and do not detract from the usefulness of the book. The reviewer would like to have had a fuller discussion of the problems in radio astronomy other than those dealing with meteors, but the book presents sufficient detail that anyone interested in a particular field in greater detail should be able to follow the more specialized literature. The authors are to be commended both for the clear style in which they have presented the subject and for the use of many excellent diagrams. Another useful feature is the inclusion of a short bibliography at the end of each chapter.

N. G. ROMAN

Yerkes Observatory

The
FACE
of the
MOON

BY RALPH B. BALDWIN

An answer, in terms of the meteorite theory, to the question of how the moon came to exist in its present form.

The study of the moon—a mirror for the study of the earth.

256 pages. 6¼"×9¼". Illustrated. $5.00.

THE UNIVERSITY OF CHICAGO PRESS

New Model!

35-mm. EXAKTA "VX"

Single Lens Reflex Camera

One lens both for viewing and picture taking assures perfect sharpness, accurate exposure, maximum depth of field, and correct composition for color. You always see the exact image before you take the picture—whether the subject is an inch or a mile away, whether it is microscopic or gigantic, whether it is moving or stationary. Instantly interchangeable lenses permit telephoto, wide angle, close-up, copy and microscope photography. With f2.8 Zeiss Tessar "T" Coated Lens with Pre-Set Diaphragm Control.................$269.50 tax included

Write Dept. 1100 For Free Booklet "K"

NATURE PHOTOGRAPHY WITH MINIATURE CAMERAS by Alfred M. Bailey (Denver Museum of Natural History). This eminent explorer and scientist displays his finest Exakta photographs and others along with explanatory material. 35 full page photographs. 64 pages................50c

EXAKTA CAMERA COMPANY
46 W. 29th St. New York 1, N.Y.

A Completely Revised Edition

THE ATMOSPHERES OF THE EARTH AND PLANETS

By GERARD P. KUIPER

Important new material has been added to make this edition the most modern and complete monograph on planetary atmospheres.

Additions Include:

—Information recently obtained in V-2 flights about our upper air and the x-ray spectrum of the sun.

—Identification of the strong red and infrared emissions of the night sky.

—A new determination of the cosmic abundances of the chemical elements.

—A derivation of the ozone temperature in the upper stratosphere.

—A determination of the age of meteorites.

—A discussion of the presence of nitrous oxide in the lower atmosphere and its connection with the life-cycle.

—A reconstruction of the conditions leading to the escape of the "proto-atmosphere."

—A new section on Jovian planets.

—A development of the atmospheric conditions on Mars.

Paperbound $5.50 *Clothbound $8.50*

THE UNIVERSITY OF CHICAGO PRESS
5750 ELLIS AVENUE CHICAGO 37, ILLINOIS

Announcing . . .

Astrophysics

THE ATMOSPHERES OF THE SUN AND STARS

by LAWRENCE H. ALLER

Associate Professor of Astronomy, University of Michigan

A NEW WORK covering both the fundamentals and the major modern developments concerning the atmospheres of the sun and stars and solar-terrestrial relationships. A brief astronomical introduction is followed by a presentation of the background in physics necessary for a study of interstellar relationships—including atomic structure and spectra; gas laws and velocity distribution; ionization; excitation; dissociation of atoms and molecules; and selected aspects of radiation theory. In subsequent chapters these astrophysical principles are applied to the radiation of the sun and stars, to their continuous and dark-line spectra, to solar phenomena, and to solar-terrestrial relationships.

The book shows how each principle or important formula is put to use in solving some definite numerical problem concerned with the interpretation of the stars and nebulae.

CONTENTS:

SURVEY OF THE BASIC DATA. THE SPECTRA OF ATOMS AND MOLECULES. THE GAS LAWS AND THE EQUATIONS OF STATE; TURBULENCE. EXCITATION, IONIZATION, AND DISSOCIATION. THE EMISSION AND ABSORPTION OF RADIATION. THE RADIATION OF THE STARS. THE CONTINUOUS SPECTRA OF THE SUN AND STARS. THE FRAUNHOFER SPECTRUM. SOLAR PHENOMENA.

Approximately 450 pages, 117 illustrations, $12

PRE-PUBLICATION PRICE *(until April 15, 1953)*: **$10.50**

Order direct from

THE RONALD PRESS COMPANY 15 E. 26th St., New York 10